Revising emissions and climate scenarios with a compact Earth system model

Yann Quilcaille

université PARIS-SACLAY

UNIVERSITÉ DE VERSAILLES ST-QUENTIN-EN-YVELINES

université PARIS-SACLAY

NNT : 2018SACLVO41

Thèse de doctorat

Revisiting emissions and climate scenarios with a compact Earth system model

Thèse de doctorat de l'Université Paris-Saclay
préparée à Université de Versailles-Saint-Quentin-en-Yvelines

Ecole doctorale n°129 Sciences de l'Environnement d'Ile-de-France (SEIF)
Spécialité de doctorat : Océan, atmosphère, climat et observations spatiales

Thèse présentée et soutenue à Paris, le 5 Septembre 2018, par

YANN QUILCAILLE

Composition du Jury :

Philippe Bousquet Professeur, UVSQ (LSCE UMR8212)	Président du jury
Glen Peters Directeur de recherche, CICERO	Rapporteur
Joeri Rogelj Chargé de recherche, IIASA	Rapporteur
Céline Guivarch Directrice de recherche, ENPC (CIRED UMR8568)	Examinatrice
Greet Janssens-Maenhout Maître de Conférences, Ghent University (JRC)	Examinatrice
Philippe Ciais Directeur de recherche, CEA (LSCE UMR8212)	Directeur de thèse
Franck Lecocq Ingénieur en Chef des Ponts, des Eaux et des Forêts, ENPC (CIRED UMR8568)	Co-directeur de thèse
Thomas Gasser Chargé de recherche, IIASA	Co-directeur de thèse

Contents

Chapter 1

Introduction

Over the last decades, our understanding of the climate landscape has expanded and gained in complexity. This improvement responds to the growing awareness about climate change. Among other means, it has been achieved by a development of models and scenarios, to answer a wider and wider range of questions. This thesis contributes to this landscape by providing insights on socio-economic scenarios from an Earth system modelling point of view. To help every potential reader understanding the big picture, this introduction briefly explains the context of this thesis.

1.1 Basis of climate change

The properties of the matter to absorb and reemit electromagnetic radiation have been extensively studied in the 19^{th} century. In 1896, Svante Arrhenius was the first to try to calculate how the presence of "heat-absorbing gases" in the atmosphere may affect the mean temperature of the ground (Arrhenius, 1896). In the visible spectrum, these gases do not interfere with the electromagnetic radiation, but they do in the infrared spectrum. As such, the electromagnetic radiation directly emitted by the Sun arrives almost directly to the ground, warming the Earth surface and are reemitted in the infrared spectrum, following the black body law established few years before (Kirchhoff, 1860). Though, these infrared radiations are absorbed and reemitted by the "heat-absorbing gases", exactly like in a greenhouse. The most important greenhouse gases are H_2O, CO_2, CH_4 and N_2O. As such, Arrhenius was the first to show how the increase in the concentration of carbon dioxide (CO_2) in the atmosphere may increase the global mean surface temperature of the Earth. He also discussed the sources and sinks of CO_2, including the absorption by the ocean and the vegetation, and he noted that the industrial revolution introduces a new source, especially because of the combustion of coal. Finally, he also relates this influence of greenhouse gases to ice ages, for which different theories were debated.

1.2 Observations

Thanks to technological advances and changes in the geopolitical context, several initiatives were launched from the 1950s, especially during the International Geophysical Year, an international project that has lasted from July 1957 to December 1958. These initiatives were conducted to provide measurements that would be of concern for an ensemble of Earth sciences, such as solar activity, meteorology, oceanography, seismology, geomagnetism and ionospheric physics. The increase in the atmospheric concentration of CO_2 has been described from the late 1950s by Charles Keeling, using measurements at the observatories in Mauna Loa and in the South Pole (Keeling et al., 1976a,b). The capacities of measurements have continuously increased from this period, with more tools and successive improvements (Cubasch et al., 2013). Gaps in periods and countries without measurements were filled using different approaches, such as data assimilation. Previous observations conducted for instance with aircrafts and balloons have been used to extend backwards these analyses. These measurements have provided the evidence for an increase in the global surface temperature, that is to say for a global warming. From 1850-1900 to 1986-2005, the Earth surface has warmed by 0.61 °C (Hartmann et al., 2013). The evolution of the composition of the atmosphere is mostly responsible for this warming: the Earth's radiation balance, in other words the total radiative forcing, has increased between 1750 and 2011 by 1.6W/m^2 (Myhre et al., 2013).

Though, these measurements have shown other evolutions in the Earth system, caused by the anthropogenic influence. Climate change encompass increases in the temperatures of the air above land and above oceans, but also of the sea surface. The ocean heat content increases, absorbing most of the excess energy brought in the Earth system. It is responsible for the expansion of the oceans, and thus the increase of the sea level, with the help of the melting of glaciers and the snow covers. The sea-ice extents at the poles are also decreasing. The warmer air and the increased evapotranspiration cause the humidity of the atmosphere to rise. The emissions of other compounds are affecting the atmospheric composition in the lower layers of the atmosphere, the troposphere, but also in upper layers, the stratosphere. For instance, Molina and Rowland (1974) showed that several halogenated compounds may deplete atmospheric ozone. These results were highly debated, until the improvement in the satellite coverage established a developing "hole" in the stratospheric ozone layer above Antarctica. The emissions of several of those compounds were regulated through the Montreal protocol, and recent analysis show that this protocol is bearing fruits (WMO, 2006).

Additional measurements were performed using ice cores from the poles. The analysis of the air trapped in the ice over time allowed the reconstruction of the evolution of greenhouse gases atmospheric concentrations, global mean surface temperature, global mean sea level change. In the meantime, the comprehension of the orbital parameters of the Earth has improved, be it for their evolution or their impact on the Earth climate (Milankovictch, 1969). It results that, even though the

changes in the solar irradiance have affected the Earth climate, with the atmospheric concentrations of greenhouse gases, human activities are affecting the Earth system at an unprecedented rate.

1.3 The modelling of climate change

Another kind of tool in climate sciences is the model. As our comprehension of the Earth system improves, its mathematical representation refines. The model corresponds to the ensemble of equations required to answer to predefined questions. Depending on the complexity of the problem, the model may require numerical treatment. Thanks to the computer development and the increase in computing capacities, models have become widely used. Models can be classified depending on the region and time period evaluated, its resolutions and the interactions represented. Typically, for paleoclimate studies, models tend to have lower resolutions to allow calculations for longer time periods. For questions relative to current and future climate change, climate models may have high resolutions, with detailed interactions. Some may have even higher resolutions by focusing over a region. A last category of models is described as "simple" or "reduced-form", because they have lower resolutions, which are traded for a greater number of interactions. These simple models mimic the behavior of other models, and may be used to combine the strengths of different models. The lower computing costs of simple models allow the calculation over longer time periods, but also probabilistic projections of climate change.

The resolution and the complexity of models used in climate sciences have improved, as marked by the reports of the Intergovernmental Panel on Climate Change (IPCC). Until the First Assessment Report of the IPCC (IPCC, Working Group I, 1990), the climate change modelling was restricted to the atmosphere, the land surface, the ocean and eventually the sea ice. Modelling of aerosols were implemented in the climate models used in the Second Assessment Report (IPCC, Working Group I, 1996). The carbon cycle, and a dynamic vegetation, were added in the models used in the Third Assessment Report (IPCC, Working Group I, 2001). The modelling of atmospheric chemistry and land ice were added afterwards. From the Fourth Assessment Report (AR4, IPCC, Working Group I (2007)) to the Firth Assessment Report (AR5, IPCC, Working Group I (2013)), Atmosphere Ocean General Circulation Models have evolved to Earth System Models (ESM) thanks to other improvements and better couplings between these components. As a remark, because of uncertainties in the modelling of the Earth system, the models produced by different teams project different climate changes, although usually similar (Flato et al., 2013).

Here, we describe the major drivers for a climate model (Blanco et al., 2014; Myhre et al., 2013). The primary inputs are emissions, be it the inventories for the historical period, or the scenarios of emissions for the projections. These emissions can be attributed to anthropogenic activities, such as fossil-fuel consumptions, ag-

riculture and livestocks. The compounds emitted are CO_2, CH_4, N_2O, CO, SO_2, NO_X, NH_3, black carbon (BC), organic carbon (OC), non-methane volatile organic compounds and halogenated compounds. Some are greenhouse gases, other aerosols, and several have indirect effects through changes in the atmospheric chemistry. Gridded emissions may be required for ESMs, but the altitude of emissions may be of interest, especially because of the impact of aircraft emissions. The emissions from volcanoes also affect climate. The second inputs concern the land use. The change in the land cover introduces a radiative forcing, but the land use introduces as well other perturbations in the biogeochemical cycles, and ultimately in the composition of the atmosphere. The impacts of land use activities on the terrestrial biosphere are usually splitted in two components. On the first hand, emissions from land use change correspond to the direct anthropogenic perturbation, usually positive because of deforestation, and on the other hand, the land sink corresponds to the change in the absorption of CO_2 by the terrestrial biosphere, because of modifications in the atmospherical composition, local climate and soil properties. As a remark, the rigorous expressions for these fluxes may depend on the model, but both always sum up to the net CO_2 flux between the atmosphere and the terrestrial biosphere (Gasser and Ciais, 2013). Other drivers can be used, such as the change in the solar irradiance.

1.4 Development of scenarios

There are two categories of scenarios. The first are idealized scenarios, such as an increase in the partial pressure of CO_2 by 1% every year from the preindustrial for 140 years, leading a four-fold multiplication of the preindustrial CO_2. Pulses in emissions are also used to characterize the response of different aspects of the Earth system. A second category is usually produced by economic models. Under a set of socio-economic hypothesis, this economic model evaluates the economic activities, and ultimately the emissions and the land use.

Just like climate models, an ensemble of equations is used to describe socio-economic activities, and numerically solved. Overall, economic models can be classified depending on the approach (top-down or bottom-up), and the focus (long-term or short-term). On the first hand, computable general equilibrium models adopt very simplified representations of the sectors, but in a comprehensive macroeconomic framework. Bottom-up engineering models use detailed descriptions of the technical constraints and potentials of the sectors, but without the same robustness of the macroeconomic framework. On the other hand, growth models focus on key mechanisms for long-term projections, whereas models that are based on econometrical relations are more fitted for short-term projections. Hybrid models also exist, in-between these categories. Among all of these economic models, some have been developed to integrate a large number of interactions between human and natural systems. These Integrated Assessment Models (IAMs) usually integrate at least a macroeconomic core, using representations in regions, economic sectors, resources,

techniques and different categories of population, and a coupled land-use model. Most of the scenarios used in climate sciences are now produced using IAMs, under assumptions for demographic, economic and technological developments, behavioral changes, resource availabilities, policy settings, etc (Blanco et al., 2014; Clarke et al., 2014).

1.5 Contribution of this thesis

As said earlier, the climate landscape has become denser, with an increased complexity of the tools used, be it models or scenarios. This thesis is somewhat at the interface between the socio-economic community and the climate sciences community, although rooted in the latter one. Its goal is to put into perspective an ensemble of elements of socio-economic scenarios from an Earth system modelling point of view. Each one of these elements are of interest for the socio-economic and Earth system modelling teams.

The first element of this thesis (chapter 2) is a focus on the uncertainties in the calculation of the emissions. For the historical period, several inventories coexist. Depending on the sector responsible for the emissions and the compound, the disagreement in inventories may reach a factor 2, or be as low as 5% (IPCC, 2006; EEA, 2013). Uncertain activities and appropriate emission factors are responsible for these discrepancies. In socio-economic scenarios, uncertainties arise from emission factors. Though, we ignore how much the uncertainty in the emissions impact climate projections. We tackle this question for the fossil-fuel emissions, the main contributor to climate change. We identify the contributions of the different uncertainties (Earth system modelling, CO_2 emissions and coemissions) under three contrasted projections of fossil-fuel extractions.

The second element of this thesis (chapter 3) is a climate assessment of the recent Shared Socio-economic Pathways (IIASA, 2018c), an ensemble of socio-economic scenarios. Our purpose is to exhibit the gaps in the database, to evaluate the climate projections of these scenarios after having corrected those flaws, and finally deduce more general results.

The third element of this thesis (chapter 4) is an analysis of different aspects of Carbon Dioxide Removal (CDR) techniques. Most of the socio-economic scenarios that limit global warming well below 2°C above preindustrial levels, in other words that respect the Paris Agreement, use negative emissions (Fuss et al., 2014). It consists in the artificial carbon capture and storage and/or in the enhancement of natural carbon sinks, leading to a removal of CO_2 from the atmosphere. Though, these techniques are not yet feasible at a commercial scale, and their implications for the Earth system are not yet well understand. This element is an analysis of the reversibility of the Earth system and the implications for the afforestation/reforestation and enhanced oceanic weathering techniques. To do so, the protocols of the CDR-Model Intercomparison Project (Keller et al., 2017) are used, and developed.

As a remark, in the three chapter of this thesis, the reduced-form ESM OSCAR v2.2 (Gasser (2014) for v2.1, Gasser et al. (2017a) and v2.2) is used. It comes that these elements illustrate the potential of this model. OSCAR v2.2 has been developed for the last chapter, to include a representation of the total sea surface alkalinity. As another remark, although the three chapters may seem separated, several connections are showed. In the conclusion of this thesis (chapter 5), the major results are recalled, with the connections between the chapters.

Box 1: Brief description of OSCAR v2.2

OSCAR v2.2 is a reduced-form Earth system model, or a "simple" Earth system model, that we use throughout this thesis. Here, we provide a very short description of this model. More details on its components can be found in box 2. These descriptions are based on the description of OSCAR v2.2 (Gasser et al., 2017a). If necessary, details about the previous version (v2.1) can be found in Gasser (2014).

The purpose of this model is to reproduce the evolution of the perturbations of the Earth system stemming from a preindustrial equilibrium. All components of the Earth system necessary to simulate climate change are represented. The figure 1.1 provides the reader with an illustrative representation of the model, with only the synthetic parts of the models. The inputs of the models are land-use variables, emissions and complementary radiative forcings. These inputs can be provided at different levels of aggregation, be it regions or biomes (Gasser et al., 2017a). Every variable of the Earth system can be an output of the model, such as the increase in global mean surface temperature or the atmospheric composition.

Every one of these components is designed to reproduce the behavior of more specialized models, such as dynamical vegetation models, chemistry-transport models or global climate models. As such, OSCAR is not process-based like these models, but use adapted equations. The behaviors are emulated at lower spatial and temporal resolutions than the specialized models. The sensitivities of every aspect of the Earth system of every available model can be combined in OSCAR, forming about 10^{44} potential combinations. The low computing cost and its meta-modelling approach allows the model to run in a probabilistic framework, using a Monte-Carlo analysis, or to compute large ensembles of scenarios.

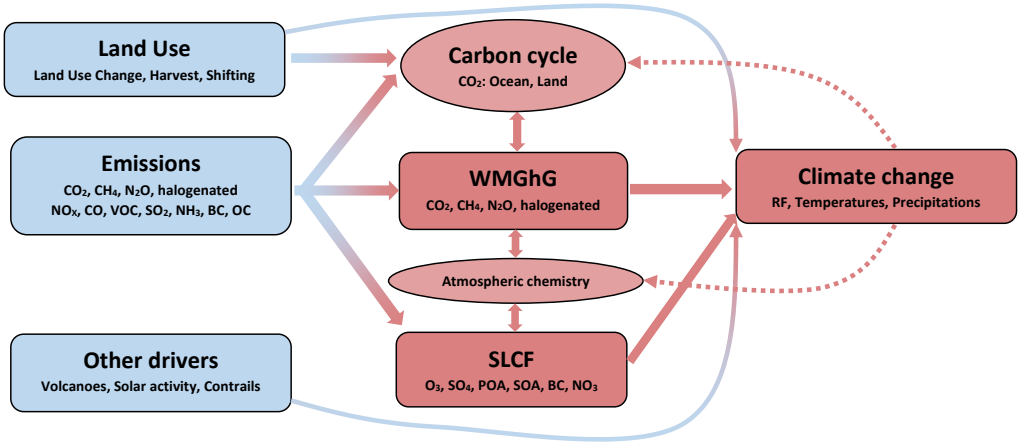

Figure 1.1: *Schematic description of the reduced-form Earth system model OSCAR v2.2. The full description of the model can be found in Gasser et al. (2017a).*

Box 2: description of the components of OSCAR v2.2

This box aims at providing few details about the modelling of the components of OSCAR v2.2, presented briefly in box 1. More details can be found in Gasser et al. (2017a).

The carbon cycle of the model is separated in two components: the ocean and the land. The oceanic carbon cycle is based on mixed-layer impulse response developed by Joos et al. (1996), with three modifications. The impulse response function is written as its equivalent box model. The carbonate chemisty integrates a dependency on sea surface temperature. The stratification of the ocean is included, using a mixed-layer depth varying with global sea surface temperature. The land carbon cycle encompasses the evolution of the carbon stocks (soil, litter and vegetation) and fluxes in a restricted number of regions and biomes. The net primary productivity, heterotrophic respiration, change in fire intensities or metabolization are accounted, with their dependency in temperature or precipitations. A book-keeping model is used to account for the extensive perturbations of the terrestrial biosphere, be it in terms of Land Use Change, shifting cultivations or harvested biomass. OSCAR integrates the computation of biomass burning emissions, but also of CH_4 emissions from wetlands.

The tropospheric and stratospheric chemistry are represented within OSCAR. The change in ozones, hydroxyl radical and equivalent effective stratospheric chlorine are accounted for, with the ensuing oxidations. Additional oxidations are also represented, be it those in the upper layers of the atmosphere, or even those in dry soils or in the oceanic boundary layer. 37 halogenated compounds are accounted through the atmospheric chemistry and their individual radiative forcings. Aerosols contribute to the atmospheric chemistry through their impact on the creation of ozone and hydroxyl radical.

The atmospheric composition of radiatively active species are used to calculate the individual radiative forcings. The effects of clouds on the radiative forcing are represented, using the semi-direct effect of absorbing aerosols, and the indirect effects of aerosols through the atmospheric burden of soluble aerosols. OSCAR represents the change in surface albedo through the change in the land-cover and the deposition of black carbon (BC) on snow. The contribution of volcanoes, of the solar activity and of contrails on the radiative forcing are direct inputs in OSCAR. All of these radiative forcings allow the computation of the evolution of the temperatures and precipitations in the Earth system.

Chapter 2

Uncertainty in projected climate change arising from uncertain fossil-fuel emission factors

2.1 Introduction

Sources of uncertainty in climate change projections are numerous (Cox and Stephenson, 2007; Hawkins and Sutton, 2009; Allen et al., 2000), ranging from the future evolution of anthropogenic drivers of climate change like future greenhouse gas and aerosol emissions, to the modeling of the Earth system's response. Scenarios based on contrasted socio-economic storylines and an ensemble of integrated assessment models (Moss et al., 2010; O'Neill et al., 2014) are used to explore the uncertainty in future human activities. For such a given emission scenario, the uncertainty in climate change is estimated by using different Earth system models (Flato et al., 2013) to translate emissions into changes in concentrations, radiative forcing and climate. However, the extent in which the uncertainty in emissions affects climate change projections is not well known.

Fossil fuel use is the largest anthropogenic driver of climate change. The burning of fossil fuels emits carbon dioxide (CO_2) to the atmosphere, and the fraction of CO_2 remaining airborne is the largest anthropogenic forcing of climate change. Other climate forcing agents such as carbon monoxide (CO), sulfur dioxide (SO_2) or nitrogen oxides (NO_X) are also co-emitted with the burning of fossil fuels, their use as feedstock in various industrial processes. During their extraction, fugitive emissions occur, in particular methane (CH_4) (Kirschke et al., 2013; EEA, 2013). The amount of each species emitted by these three activities related to fossil fuels is estimated via emission inventories, which combine activity data such as the mass of fuel used or the energy obtained from these fuels, with emission factors related to the carbon content of fuels and to technologies that produces co-emitted species (EEA, 2013).

Because of the various methodologies and input data they use, different emission inventories show differences in their estimates of fossil CO_2 emissions, such as Olivier (2002), Marland et al. (2009), Andres et al. (2012). The 2006 IPCC Guidelines for National GHG Inventories (IPCC, 2006) recommend to use a mean carbon content for lignite of 101 $kgCO_2/GJ$ with a range from 91 to 115 $kgCO_2/GJ$ (95% confidence interval); hence a 10% uncertainty in the CO_2 emissions from lignite. For co-emitted non-CO_2 species, the uncertainty is much larger because their emissions depend not only on the composition of each fuel (in carbon, sulfur, nitrogen) but also on technologies that determine the fuel-use efficiency in different sectors, on the presence, enforcement of use, and efficiency of emission control devices (e.g. stack desulfurization) and on operating conditions (EEA, 2013; IPCC, 2006; Granier et al., 2011). For instance, according to the EMEP/EEA Air Pollutant Emission Inventory Guidebook 2013 (EEA, 2013), the emission factor of CO for the burning of brown coal to produce electricity and heat is 8.7 gCO/GJ, but the associated 95% confidence interval ranges from 6.7 to 60.5 gCO/GJ. This means that a given amount of energy produced by the combustion of brown coal comes with a -20 to +600% uncertainty on CO emissions.

In this study, we investigate how uncertainty in emission factors for CO_2 and non-CO_2 emissions associated with the combustion of fossil-fuels and their use in industrial processes affects climate change projections. First, we calculate ranges of uncertainty in CO_2 and non-CO_2 fossil-fuel co-emissions for historical and for three contrasted future scenarios of fossil fuel extraction. Second, we translate this uncertainty into a range of radiative forcing and climate change using the OSCAR v2.2 Earth system model, using a Monte-Carlo approach. Finally, we analyze the variance of the system and compare the uncertainty from emission factors to the one on the temperature response to emissions through Earth system processes.

2.2 Methods

An overview of our method is described in figure 2.1. Extraction scenarios (section 2.2.1) are combined with carbon contents, net calorific values and fractions of oxidations (section 2.2.2) to produce fossil-fuel CO_2 projections. We calculate co-emission ratios (section 2.2.3) to evaluate the fossil-fuel co-emissions. We complete these projections with non-fossil-fuel emissions and other anthropogenic drivers (section 2.2.4). Finally, the reduced-form Earth system model OSCAR is used with these drivers through a Monte-Carlo setup (section 2.2.5) to evaluate all required uncertainties. 5th and 95th percentiles are calculated to obtain the confidence intervals, whereas variances are used to calculate each contribution to the total variance.

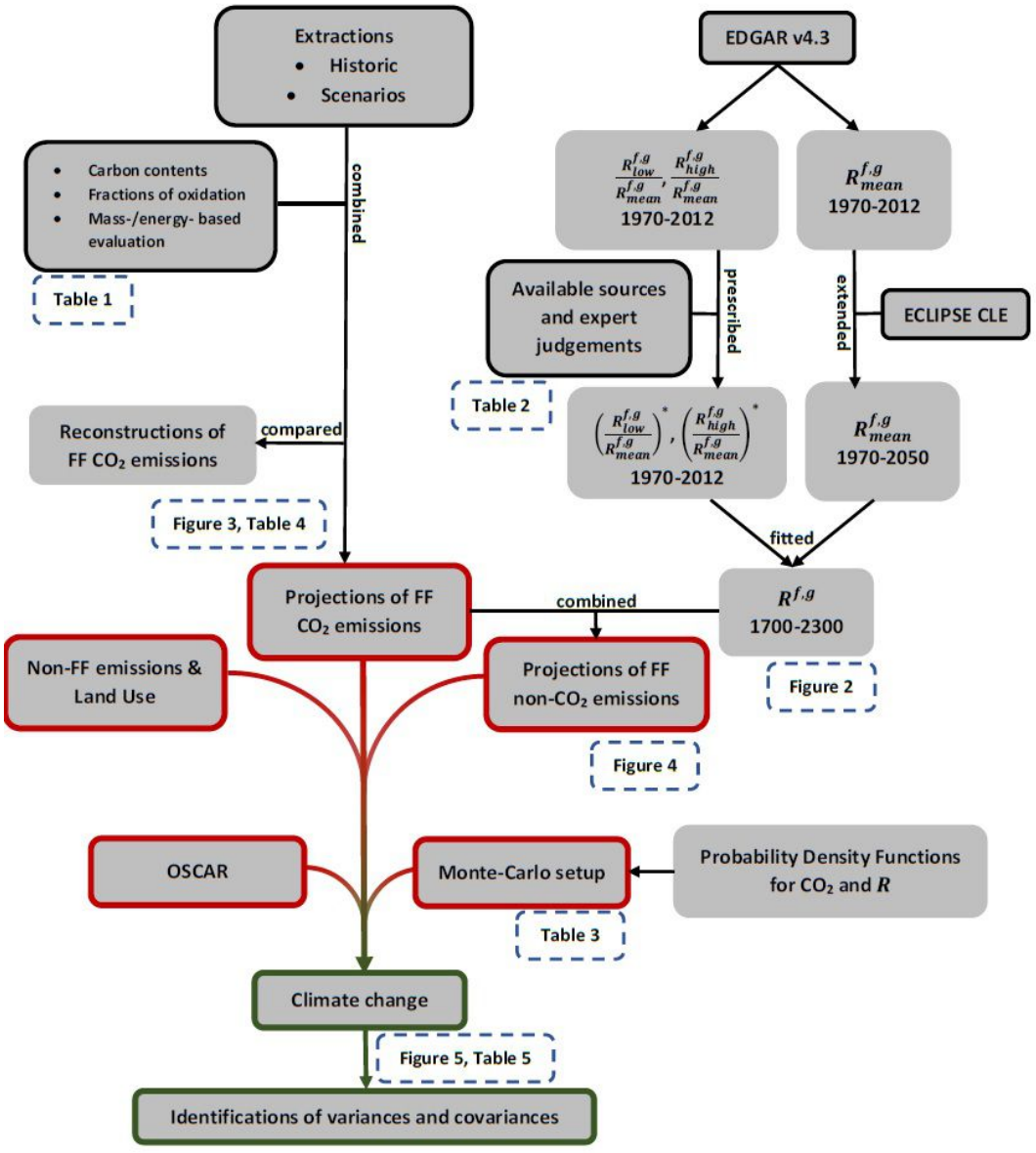

Figure 2.1: *Overview of the method used in this study. For different parts, we give references to the relevant tables and figures. "FF" stands here for Fossil-Fuel, and R corresponds to co-emission ratios.*

2.2.1 Extraction scenarios

We take the historical reconstruction of fossil-fuel extraction (1750-2012) and three future extraction scenarios (up to 2300) made by Mohr et al. (2015). Country-scale data is aggregated to the global scale for 8 types of coal, 5 types of oil and 5 types of gas. Peat extraction, flaring and cement production are not included. The three future extraction scenarios were produced with the GeRS-DeMo model (Mohr and Evans, 2010). Additionally, since conversion factors are provided by Mohr et al. (2015), historical reconstruction and scenarios can be expressed both in energy values and in mass of extracted fuels. The future abundance in fossil fuels remains uncertain (Ward et al., 2012), but this uncertainty is not included here. We use only three future scenarios, differing by their assumptions regarding ultimately recoverable resources, with a "Low", "Best Guess" (called "Medium" hereafter) and "High" case. For comparison, the Low scenario is between RCP2.6 and RCP4.5, the Medium close to RCP4.5 and the High near to RCP6.0 (van Vuuren et al., 2011a). These scenarios include no climate policy or transition to non-fossil energy sources -unlike transformation pathways (Clarke et al., 2014) or SSPs (Riahi et al., 2017)-, but this is not a limitation for our study since we focus on the climate change uncertainty induced by uncertain emission factors and for this purpose, we just need fossil-fuel scenarios comparable to those showed by the IPCC. The Mohr et al. scenarios have the advantage of documenting fuel extraction of various fuel types (allowing us to address uncertainty on carbon contents) and to be fully consistent regarding the different fuel types between the historical and future periods.

2.2.2 CO_2 emissions

2.2.2.1 Method used

The extraction scenarios are provided in terms of energy content. When calculated from energy-based fuel extraction data (superscript ene), CO_2 emissions in kgC/yr resulting from the use of a type f fuel are given by equation (2.1), where C_f is the fuel carbon content in kgC/J produced, FO_f the fraction oxidized of the extracted fuel (unitless) through combustions and uses, and e_f^{ene} the amount of fuel extracted in J/yr.

$$E_f^{CO_2} = FO_f C_f e_f^{ene} \tag{2.1}$$

However, the values used in Mohr et al. (2015) for the carbon contents and net calorific values are different from the literature, and may even lay out of the range of IPCC (2006). When calculating from mass-based fuel extraction data (superscript phy), we use the equation (2.2), with NCV_f the net calorific value of the fuel in J

per unit mass of extracted fuel and e_f^{phy} is the mass extracted per year.

$$E_f^{CO_2} = FO_f C_f NCV_f e_f^{phy} \tag{2.2}$$

To account for uncertain carbon contents or uncertain net calorific values – depending whether equation (2.1) or (2.2) is used – we use four different data sources to obtain six different sets of values: Mohr et al. (Mohr et al., 2015), CDIAC (Boden et al., 1995), IPCC (1996), the IPCC (2006) average, and its lower and upper bounds of the 95% confidence interval. The use of equation (2.1) or (2.2) is motivated by the differences observed in the sets of NCV and the associated uncertainties. The resulting different emission factors cause these two approaches not to be equivalent.

Regarding the uncertainty on oxidation fractions, we use the CDIAC values (Marland and Rotty, 1984) to produce three sets of oxidation fractions as shown in table 2.1. These values are also applied globally. Note that we do not use the oxidation fractions from other data sources, either because they are not explicitly reported, or because they are based on a different definition. Here, the oxidation fraction is defined as the fraction of the fuel oxidized during combustion in energy use and during non-energy use (Marland and Rotty, 1984). We do not use the confidence intervals from Marland and Rotty (1984) because the Tier 1 default oxidation fractions of IPCC (2006) lies out of this interval, all being equal to 100% in the case of lacking data. However, the intervals that we define at a global scale may still be underestimated, Liu et al. (2015) shows for the case of China a 92% oxidation rate.

Oxidation fractions	**100% oxidation**	**CDIAC**	**Lower**
Coal	1	0.982	0.964
Oil	1	0.918	0.836
Gas	1	0.98	0.96

Table 2.1: *Sets of oxidation fractions used. The lower case is built to be symmetrical to the 100% oxidation case with respect to the central CDIAC values (Marland and Rotty, 1984).*

The combination of the 4 carbon contents (one being a distribution), 3 oxidation fractions and 2 sources of fuel extraction data (energy-based or mass-based) provides us with a distribution of fossil-fuel CO_2 emission over the historical period and for each of the three future extraction scenarios.

2.2.2.2 Emission factors obtained

The IPCC (2006) NCV and carbon contents are both given with 95% asymmetric confidence intervals. Because the uncertainty on NCV and carbon contents are small enough compared to their mean, we can use Seijas-Macias and Oliveira (2012) to

evaluate the resulting asymmetric confidence intervals. We approximate the low asymmetry assuming both sides are normally distributed. This is represented in equations 2.3, where the carbon contents C and the NCV are expressed in terms of mean and in terms of 2.5th and 97.5th percentiles.

$$\sigma_{2.5\%} = \left(\frac{NCV_m - NCV_{2.5\%}}{1.96}\right)^2 C_m^2 + NCV_m^2 \left(\frac{C_m - C_{2.5\%}}{1.96}\right)^2 + \left(\frac{NCV_m - NCV_{2.5\%}}{1.96}\right)^2 \left(\frac{C_m - C_{2.5\%}}{1.96}\right)^2 \tag{2.3a}$$

$$\sigma_{97.5\%} = \left(\frac{NCV_m - NCV_{97.5\%}}{1.96}\right)^2 C_m^2 + NCV_m^2 \left(\frac{C_m - C_{97.5\%}}{1.96}\right)^2 + \left(\frac{NCV_m - NCV_{97.5\%}}{1.96}\right)^2 \left(\frac{C_m - C_{97.5\%}}{1.96}\right)^2 \tag{2.3b}$$

$$(CE)_m = C_m NCV_m \tag{2.3c}$$

$$(CE)_{2.5\%} = C_m NCV_m - 1.96\sqrt{\sigma_{2.5\%}} \tag{2.3d}$$

$$(CE)_{97.5\%} = C_m NCV_m + 1.96\sqrt{\sigma_{97.5\%}} \tag{2.3e}$$

The tables 2.2 and 2.3 summarize the resulting emission factors, oxidation fractions included, for the two approaches. For each one of the fuels extracted in the extraction scenarios, the fuel categories used in the different sets of values are given, with the resulting values. The fuel categories described in Mohr et al. (2015) are matched to those of Boden et al. (1995), IPCC (2006) and IPCC (1996).

Concerning coal, to the usual four categories (Anthracite, Bituminous, Sub-Bituminous and Lignite) and the usual two groups (Hard Coal, close to the black coal, and Brown Coal, close to soft coal) are added two intermediate categories. Boden et al. (1995) uses only two categories of coal, Hard coal and Soft coal. Thus, the fuel categories of Mohr et al. (2015) matched to Soft coal are only Brown coal and Lignite. Peat extraction is not included in the scenarios. IPCC (2006) and IPCC (1996) use the same coal categories. However, the Bituminous of Mohr et al. (2015) is considered as aggregating the categories Coking coal and Other Bituminous coal, because coking coal refers to high quality bituminous coal, that allows the production of a coke suitable to support a blast furnace charge. For the same reason, the aggregated category of Mohr et al. (2015) is taken as aggregating Coking coal, Other Bituminous coal and Sub-Bituminous coal. Semi-Anthracite is defined as an intermediary category between Anthracite and Coking coal.

Concerning gas, Mohr et al. (2015) consider 5 extraction sources, but one value. Similarly, Boden et al. (1995) uses only one value, independently of the extraction source of the gas. For the same reason, the sole value for Natural Gas is used for IPCC (2006) and IPCC (1996). We point out here that gases such as Gas Coke, Gas Works Gas, Coke Oven Gas, Blast Furnace Gas and Oxygen Steel Furnace Gas

are secondary products of coal, as shown in figure 2.3. Given the fact that we use extraction scenarios, the associated carbon contents and NCV are irrelevant.

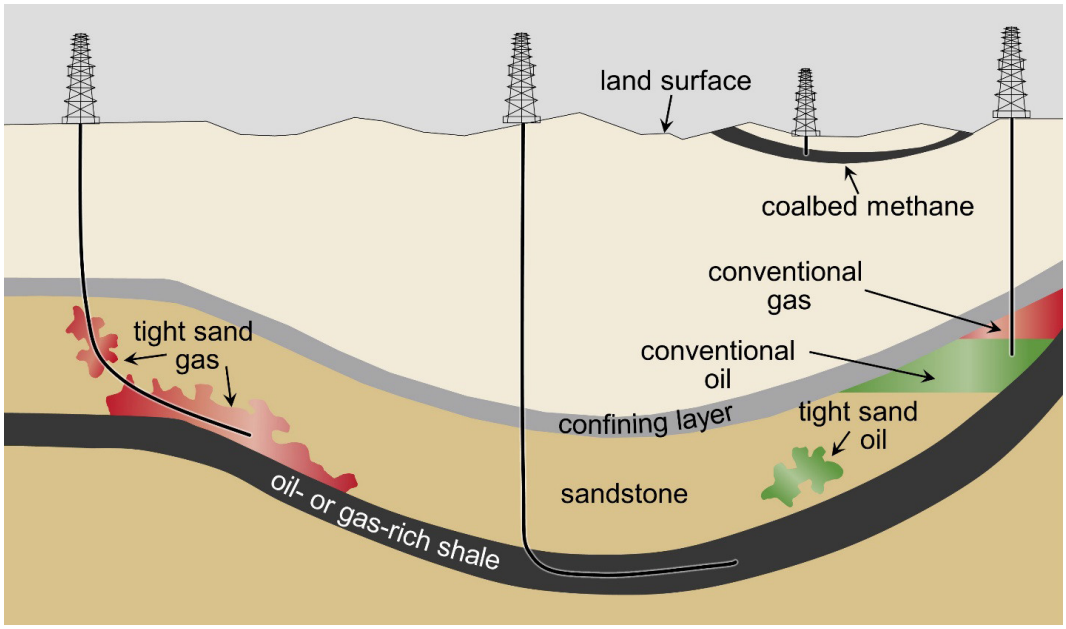

Figure 2.2: *Schematic cross-section of general types of oil and gas resources and the orientations of production wells used in hydraulic fracturing. Shown are conceptual illustrations of types of oil and gas wells. A vertical well is producing from a conventional oil and gas deposit (right). In this case, a gray confining layer serves to "trap" oil (green) or gas (red). Also shown are wells producing from unconventional formations: a vertical coalbed methane well (second from right); a horizontal well producing from a shale formation (center); and a well producing from a tight sand formation (left) (source: United States Environmental Protection Agency (2015)*

Concerning oil, the single value of Boden et al. (1995) for Conventional oil is used for all associated fuel categories of Mohr et al. (2015). Conventional oil flow freely from their reservoirs. However, hydraulic fracturing may be required to retrieve the fossil fuels within shales or tight formations (figure 2.2). Oil shales are organic-rich sources rocks, containing oil, gas or both within its pore space. Tight formations are low-permeability sedimentary formations, that can contain oil, gas or both within its pore space (United States Environmental Protection Agency, 2015). We point out that shale oil refers to the unconventional oil produced from oil shales. Thus, Tight oil from Mohr et al. (2015) refers to chemically conventional crude oil, but extracted from tight formations. For this reason, Tight oil is associated to the fuel category Shale oil from IPCC (2006). Kerogen oil is described as a synthetic crude oil created from kerogen-rich rocks, that is to say oil shales. Natural bitumen and extra heavy oils are both high-density oils, but with natural bitumen having a higher viscosity than extra heavy oils. Both can be extracted from tar sands. For these

reasons, these three oils are associated to the fuel category Oil Shale and Tar Sands from IPCC (2006).

We observe that the lignite of Mohr et al. (2015) lays out of the range of IPCC (2006) when using carbon contents (table 2.2), but not when combining carbon contents and net calorific values (table 2.3). This is explained by the increase in the relative uncertainty in the latter approach. Altogether, all values from Mohr et al. (2015) tend to be more in the range of the literature when combining both NCV and carbon contents. As a second remark, we point out that Boden et al. (1995) uses a single category of oil whereas non-conventional oils present different values, up to 45% of increase for kerogen oil. As a third remark, we note that a single gas category is used for all fuels, independently of its category. This is explained by the relatively similar composition of the treated gases, even though different techniques of extraction have been used. As a last remark, the category "Kerogen oil" in Mohr et al. (2015) has been associated to "Oil Shale and Tar Sands" in IPCC (2006) for its carbon contents, but not for its NCV. The NCV associated to "Oil Shale and Tar Sands" correspond to the content of the extracted material, and not to the oil extracted from this material. To match the energy content of this category in the extractions scenarios, the NCV of "Crude oil" of IPCC (2006) is used for "Kerogen Oil", but also the categories "Extra Heavy Oil" and "Natural Bitumen" for the same reason. Still, factors greater than 1 are observed for these three fuel categories using IPCC (2006) methodology, but also for "Kerogen Oil" using only Mohr et al. (2015) conversion factors. The lack of information about the correspondence of non-conventional fuels is responsible for these numbers, NCV and carbon contents more appropriate should be used.

For the carbon contents, it is important to note that the conversion factors in Mohr et al. (2015) are mass to CO_2 factors and not mass to CO_2e factors. For the NCV, it is also important to note that units are giga tonnes (Gt) only for coal, whereas they are in fact giga barrel (Gb) for oil, and trillion cubic feet (tcf) for gas. Given the fact that only the NCV ("mass conversion") from Mohr et al. (2015) are in EJ/Gt, EJ/Gb and EJ/tcf, whereas the literature provide us with EJ/Gt for coal, gas and oil. Thus, we calculate the mass equivalent of the extraction scenarios using NCV of Mohr et al. (2015) for coal and the mean NCV of IPCC (2006) of crude oil and conventional gas for others fuels.

Factors (kgC/GJ)	Mohr	CDIAC	IPCC2006	RevisedIPCC1996
Coal				
Anthracite		Hard	Anthracite	Anthracite
	18.94	24.71	26.33 [25.34 to 27.05]	26.32
Bitum.		Hard	Coking coal & Other Bitum. coal	Coking coal & Other Bitum. coal
	22.61	24.71	25.34 [23.68 to 26.88]	25.34
Sub-Bitum.		Hard	Sub-Bitum. coal	Sub-Bitum. coal
	24.51	24.71	25.74 [24.85 to 26.78]	25.73
Lignite		Soft	Lignite	Lignite
	31.74	25.75	27.05 [24.34 to 30.8]	27.1
Semi-Anthracite		Hard	Anthracite & Coking coal	Anthracite & Coking coal
	19.46	24.71	25.83 [24.36 to 27.05]	25.83
Bitum. and Sub-Bitum.		Hard	Coking coal & Other Bitum. coal & Sub-Bitum. coal	Coking coal & Other Bitum. coal & Sub-Bitum. coal
	23.68	24.71	25.47 [24.07 to 26.84]	25.47
Hard Coal		Hard	Anthracite & Coking coal & Other Bitum. coal	Anthracite & Coking coal & Other Bitum. coal
	21.7	24.71	25.67 [24.23 to 26.93]	25.66
Brown Coal		Soft	Lignite & Sub-Bitum. coal	Lignite & Sub-Bitum. coal
	27.15	25.75	26.39 [16.56 to 29.19]	26.42
Gas				
Conventional Gas		Gas	Natural Gas	Natural Gas
	13.9	13.43	14.99 [14.51 to 15.58]	14.99
Coal Bed Methane		Gas	Natural Gas	Natural Gas
	13.9	13.43	14.99 [14.51 to 15.58]	14.99
Shale Gas		Gas	Natural Gas	Natural Gas
	13.9	13.43	14.99 [14.51 to 15.58]	14.99
Tight Gas		Gas	Natural Gas	Natural Gas
	13.9	13.43	14.99 [14.51 to 15.58]	14.99
Hydrates		Gas	Natural Gas	Natural Gas
	13.9	13.43	14.99 [14.51 to 15.58]	14.99
Oil				
Conventional Oil		Oil	Crude Oil	Crude Oil
	18.97	18.64	18.35 [17.8 to 18.9]	18.36
Tight Oil		Oil	Shale Oil	Crude Oil
	18.97	18.64	18.35 [16.97 to 19.83]	18.36
Natural Bitumen		Oil	Oil Shale and Tar sands	Crude Oil
	18.97	18.64	26.79 [22.58 to 31.3]	18.36
Extra Heavy Oil		Oil	Oil Shale and Tar sands	Crude Oil
	18.97	18.64	26.79 [22.58 to 31.3]	18.36
Kerogen Oil		Oil	Oil Shale and Tar sands	Crude Oil
	26.65	18.64	26.79 [22.58 to 31.3]	18.36

Table 2.2: *Summary of the factors used from the extraction dataset used from energy (joules). These factors represent only the carbon content. Bitum. stands for Bituminous.*

Factors (tC/t)	Mohr	CDIAC	IPCC2006	RevisedIPCC1996
Coal				
Anthracite		Hard	Anthracite	Anthracite
	0.568	0.724	0.703 [0.566 to 0.849]	0.703
Bitum.		Hard	Coking coal & Other Bitum. coal	Coking coal & Other Bitum. coal
	0.543	0.724	0.684 [0.548 to 0.788]	0.684
Sub-Bitum.		Hard	Sub-Bitum. coal	Sub-Bitum. coal
	0.404	0.724	0.486 [0.295 to 0.67]	0.486
Lignite		Soft	Lignite	Lignite
	0.302	0.291	0.322 [0.146 to 0.589]	0.323
Semi-Anthracite		Hard	Anthracite & Coking coal	Anthracite & Coking coal
	0.564	0.724	0.709 [0.582 to 0.819]	0.709
Bitum. and Sub-Bitum.		Hard	Coking coal & Other Bitum. coal & Sub-Bitum. coal	Coking coal & Other Bitum. coal & Sub-Bitum. coal
	0.474	0.724	0.619 [0.466 to 0.747]	0.619
Hard Coal		Hard	Anthracite & Coking coal & Other Bitum. coal	Anthracite & Coking coal & Other Bitum. coal
	0.564	0.724	0.69 [0.555 to 0.807]	0.69
Brown Coal		Soft	Lignite & Sub-Bitum. coal	Lignite & Sub-Bitum. coal
	0.353	0.506	0.406 [0.222 to 0.631]	0.407
Gas				
Conventional Gas		Gas	Natural Gas	Natural Gas
	0.667	0.644	0.72 [0.687 to 0.765]	0.72
Coal Bed Methane		Gas	Natural Gas	Natural Gas
	0.667	0.644	0.72 [0.687 to 0.765]	0.72
Shale Gas		Gas	Natural Gas	Natural Gas
	0.667	0.644	0.72 [0.687 to 0.765]	0.72
Tight Gas		Gas	Natural Gas	Natural Gas
	0.667	0.644	0.72 [0.687 to 0.765]	0.72
Hydrates		Gas	Natural Gas	Natural Gas
	0.667	0.644	0.72 [0.687 to 0.765]	0.72
Oil				
Conventional Oil		Oil	Crude Oil	Crude Oil
	0.803	0.78	0.776 [0.73 to 0.828]	0.777
Tight Oil		Oil	Shale Oil	Crude Oil
	0.803	0.78	0.699 [0.577 to 0.841]	0.777
Natural Bitumen		Oil	Oil Shale and Tar sands	Crude Oil
	0.803	0.78	1.133 [0.946 to 1.335]	0.777
Extra Heavy Oil		Oil	Oil Shale and Tar sands	Crude Oil
	0.803	0.78	1.133 [0.946 to 1.335]	0.777
Kerogen Oil		Oil	Oil Shale and Tar sands	Crude Oil
	1.127	0.78	1.133 [0.946 to 1.335]	0.777

Table 2.3: *Summary of the factors used from the extraction dataset used with physical quantities (tons). These factors represent the product of the net carbon value and of the carbon content. Bitum. stands for Bituminous.*

2.2.3 Non-CO_2 co-emissions associated with the use of fossil fuels

2.2.3.1 Method used

Non-CO_2 species are co-emitted with CO_2 during fossil-fuel combustion and use in industrial processes because of non-carbon elements oxidized (e.g. sulfur giving SO_2), high temperature combustions oxidizing atmospheric nitrogen (N_2O and NO_X), or incomplete combustion processes (CH_4, CO, BC, OC and VOCs). We also consider ammonia (NH_3) emissions which occur through leaks during the production of coke where ammonia is used to reduce nitrogen oxides emissions (EEA, 2013). Methane (CH_4) produced during extraction, venting and flaring is however excluded. These species impact the climate system as greenhouse gases (CO_2, CH_4, N_2O), ozone precursors (CO, NO_X, VOCs), aerosols or aerosol precursors (SO_2, NH_3, NO_X, OC, and BC). In order to link the emissions of co-emitted species with those of CO_2, we define co-emission ratios ($R^{f,g}$) for each fuel f, and compound g:

$$E^{f,g} = R^{f,g} E^{f,CO_2} \tag{2.4}$$

Where $E^{f,g}$ is the co-emission of g for the fuel f. Since we derive CO_2 emissions from extraction and not consumption data (Davis et al., 2011), we have to use global and not regional co-emission ratios because we do not know where and through which technology each fuel is used. We evaluate global mean ratios ($R^{f,g}_{mean}$) for each co-emitted compound and for coal, oil and gas, using the EDGARv4.3.2 database (Olivier et al., 2015) over 1970-2012. The matching of fuels is described in figure 2.3.

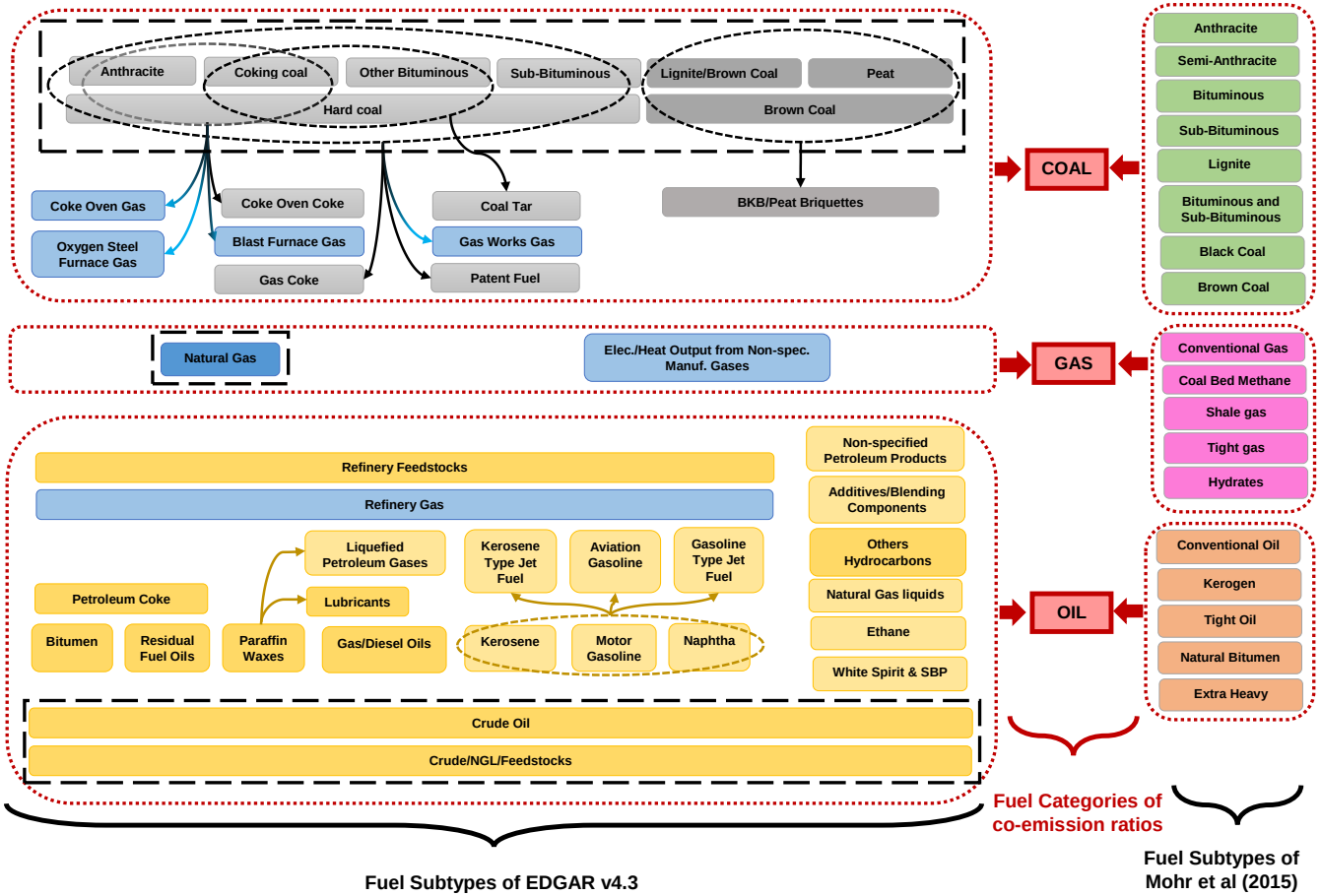

Figure 2.3: *Simplified representation of the sub-categories of fossil-fuels from EDGAR v4.3 and Mohr et al (2015). Each broad category of EDGARv4.3 is highlighted in different colors (e.g. dark yellow: heavy oils, light yellow: light oils)*

These ratios are extended to 2050 using the Current Legislation (CLE) scenario of ECLIPSEv5.0 (Stohl et al., 2015). This scenario integrates current and committed environmental laws, assuming known delays and failures. Among the three ECLIPSE scenarios, the CLE is deemed as closer to the "business as usual", compared to the two others: under the No Further Control scenario, committed legislations are not enforced, whereas under the Short Lived Climate Pollutants (SLCP) scenario, SLCP are strongly mitigated. Thus, the CLE scenario is relatively consistent with the absence of climate policies in our extraction scenarios (Mohr et al., 2015). To backcast and forecast these global ratios over the whole period (1750-2300), two different rules are created. The first rule is a constant extension of the average of the ratios over 1970-1975 to 1700-1970; and of that over 2007-2012 to 2012-2300 (Constant rule, equation 2.9). For the second rule we fit an S-shaped function over the 1970-2012 data from EDGARv4.3.2 and using the evolution to 2050 from ECLIPSEv5.0 as an additional constraint (Sigmoid rule, equation 2.10). These two rules are shown in the figures showing these ratios (figures 2.4 to 2.13).

To estimate the uncertainty in the co-emission ratios, we use an approach combining different elements. Relative uncertainty in global non-CO_2 emission is taken from the literature whenever possible, and we made assumptions for the remaining species for which we did not find literature data, as shown in table 2.4. We assume that the relative uncertainty in co-emission ratios is correlated to the inter-country spread in national co-emission ratios, weighted by national CO_2 emissions. Under this assumption, if the weighted spread in national co-emission ratios for species increases two-fold over a period, the uncertainty in the global co-emission ratios increases two-fold as well. The weighting by emissions is used to give less importance to countries that have less industrial activity. To do so, we extract from EDGARv4.3.2 the co-emission ratios for 113 world regions (most of them being individual countries, Narayanan and Walmsley (2008)), we weight each region's ratios by its CO_2 emissions. This is represented in equation 2.5, for the broad fuel category f (Oil, Coal or Gas), the world region r and the compound g, using EDGAR v4.3.2 emissions for the fuels $\{f_i \in f\}$ constituting the broad category.

$$E_{r,t}^{f,g} = \Sigma_{f_i \in f} E_{r,t}^{f_i,g} \tag{2.5a}$$

$$E_{r,t}^{f,CO_2} = \Sigma_{f_i \in f} E_{r,t}^{f_i,CO_2} \tag{2.5b}$$

$$R_{r,t}^{f,g} = \frac{E_{r,t}^{f,g}}{E_{r,t}^{f,CO_2}} \tag{2.5c}$$

We extract the resulting mean, 2.5th and 97.5th percentiles to define $\left(R_{mean}^{f,g}\right)^*$, $\left(R_{low}^{f,g}\right)^*$ and $\left(R_{high}^{f,g}\right)^*$, as showed in equations 2.6. $Q_r\left(X\left(t,r\right),E\left(t,r\right),p\right)$ is here

Compound	Relative uncertainty	Year(s) of application	Source
SO_2	± 12%	2000-2010	Smith et al. (2011)
BC	-32% to +118%	1996	Bond et al. (2004)
OC	-42% to +97%	1996	Bond et al. (2004)
NO_X	± 30%	2003-2013	Janssens-Maenhout et al. (2015)
CO	± 20%	2003-2013	Janssens-Maenhout et al. (2015)
CH_4	± 10%	1990-2010	IPCC (2006)
N_2O	± 10%	1990-2010	IPCC (2006)
VOC	± 20%	2003-2013	Assumed same as CO
NH_3	± 10%	1990-2010	Assumed same as N_2O

Table 2.4: *Relative uncertainty and period of time or date of rescaling used for co-emission ratios.*

the function returning the p-th percentile of $X(t,r)$ over r, weighted by $E(t,r)$.

$$\left(R^{f,g}_{mean,t}\right)^* = \frac{\Sigma_r E^{f,g}_{r,t}}{\Sigma_r E^{f,CO_2}_{r,t}} \tag{2.6a}$$

$$\left(R^{f,g}_{low,t}\right)^* = Q_r\left(R^{f,g}_{r,t}, 2.5\%\right) \tag{2.6b}$$

$$\left(R^{f,g}_{high,t}\right)^* = Q_r\left(R^{f,g}_{r,t}, 97.5\%\right) \tag{2.6c}$$

We extend $\left(R^{f,g}_{mean,t\in[1970,2012]}\right)^*$ to 2050 ($\left(R^{f,g}_{mean,t\in[1970,2050]}\right)^\times$) using the Current Legislation (CLE) scenario of ECLIPSEv5.0 (Stohl et al., 2015), as shown in equation 2.7. As a first remark, we precise that the emissions from ECLIPSE are aggregated along fuels. This forces us to assume the same trend for all fuels over 2012-2050. As a third remark, N_2O is not prescribed in ECLIPSE v5.0, and a sectoral inconsistency in CH_4 forces us not to use this trend neither for N_2O, nor for CH_4 (section 2.3.2). As a final remark, the CO_2 emissions used to produce the co-emissions ratios $R^{ECLIPSE,g}_t$ are those of RCP6.0 (Stohl et al., 2015).

$$\left(R^{f,g}_{mean,t\in[1970,2050]}\right)^\times = \begin{cases} \left(R^{f,g}_{mean,t\in[1970,2012]}\right)^* \\ \left(R^{f,g}_{mean,2012}\right)^* \frac{R^{ECLIPSE,g}_t}{R^{ECLIPSE,g}_{2012}} \end{cases} \tag{2.7}$$

We also rescale $\left(R^{f,g}_{low,t}\right)^*$ and $\left(R^{f,g}_{high,t}\right)^*$ using the low and high relative uncertainties ($\delta_{g,low}$ and $\delta_{g,high}$) and the period of time or year (T_g) shown in table

2.4. These rescales are showed in equation 2.8. They are produced over 1970-2012. $\langle X\,(t,y)\rangle_T$ designates the mean of X over the period T.

$$\left(R^{f,g}_{high,t}\right)^{\times} = \left(R^{f,g}_{mean,t}\right)^{*} + \left(\left(R^{f,g}_{high,t}\right)^{*} - \left(R^{f,g}_{mean,t}\right)^{*}\right) \frac{\delta_{g,high}}{\langle\left(R^{f,g}_{high,t}\right)^{*} - \left(R^{f,g}_{mean,t}\right)^{*}\rangle_{T_g}} \tag{2.8a}$$

$$\left(R^{f,g}_{low,t}\right)^{\times} = \left(R^{f,g}_{mean,t}\right)^{*} - \left(\left(R^{f,g}_{mean,t}\right)^{*} - \left(R^{f,g}_{low,t}\right)^{*}\right) \frac{\delta_{g,low}}{\langle\left(R^{f,g}_{mean,t}\right)^{*} - \left(R^{f,g}_{low,t}\right)^{*}\rangle_{T_g}} \tag{2.8b}$$

Finally, to extend these ratios to 1700-2300, we may apply the Constant extension rule for the three ratios to obtain the future uncertainties in the co-emission ratio of each species. The equation 2.9 illustrates this rule for the mean ratio, but is applied identically for the low and high ratios. In this case, the same extension to 2050 described in equation 2.7 is applied to $R^{f,g}_{low,t}$ and $R^{f,g}_{high,t}$. This allows a constant relative uncertainty before 1970 and after 2050, with reliable values over 1970-2050.

$$R^{f,g}_{mean,t\in[1700,2300]} = \left|\begin{array}{l} \langle\left(R^{f,g}_{mean,t}\right)^{\times}\rangle_{[1970,1974]} \\ \left(R^{f,g}_{mean,t\in[1970,2050]}\right)^{\times} \\ \langle\left(R^{f,g}_{mean,t}\right)^{\times}\rangle_{[2046,2050]} \end{array}\right. \tag{2.9}$$

We may also apply the Sigmoid extension rule (equation 2.10) for the three ratios. In this rule as well, the extension to 2050 described in equation 2.7 is not applied to $R^{f,g}_{low,t}$ and $R^{f,g}_{high,t}$. This would assume a constant relative uncertainty over 2012-2050. As mentioned before, we fit an S-shaped function on the mean, but also on the relative uncertainties, i.e. on their ratios. The mean co-emission ratio is characteristic of the average technologies, processes and fuels used in the fossil fuel sectors in the world. Assuming a S-shaped function for the mean co-emission ratio implies a single transition for the world co-emission ratio. The range in the relative co-emission ratios is characteristic of the relative heterogeneity of technologies, processes and fuels used in the fossil fuel sectors in the world. Assuming S-shaped functions for the relative uncertainties imply a single transition in this heterogeneity.

The assumption of S-shaped functions for low and high co-emission ratios are characteristic of the technologies, processes and fuels used for an undefined group of countries, accounting for their fossil fuel consumptions. Then, a better understanding can be obtained if dealing with assumptions regarding the shape of relative

high and low co-emissions ratios, rather than directly their values. Besides, fitting relative uncertainties also allows for a more accurate reproduction of low and high co-emission ratios presenting more than one transition. Finally, doing so allows to fit the three curves separately, instead of together to keep fits sorted. The latter point helps in facilitating the numerical calculations.

$$R^{f,g}_{mean,t\in[1700,2300]} = A^{f,g,mean} + \frac{B^{f,g,mean} - A^{f,g,mean}}{1 + exp\left(-(t - t_0^{f,g,mean})/\tau^{f,g,mean}\right)} \tag{2.10a}$$

$$R^{f,g}_{high,t\in[1700,2300]}/R^{f,g}_{mean,t\in[1700,2300]} = A^{f,g,high} + \frac{B^{f,g,high} - A^{f,g,high}}{1 + exp\left(-(t - t_0^{f,g,high})/\tau^{f,g,high}\right)} \tag{2.10b}$$

$$R^{f,g}_{low,t\in[1700,2300]}/R^{f,g}_{mean,t\in[1700,2300]} = A^{f,g,low} + \frac{B^{f,g,low} - A^{f,g,low}}{1 + exp\left(-(t - t_0^{f,g,low})/\tau^{f,g,low}\right)} \tag{2.10c}$$

2.2.3.2 Co-emission ratios obtained

The figure 2.4 shows the obtained co-emission ratios for SO_2. For coal, the evolution are correctly reproduced, in terms of mean and 95% confidence interval. However, the asymptotes for the mean and high ratio are lower than the ratio of ECLIPSE CLE for SO_2 after 2012. However, the Sigmoid extension follows correctly the ECLIPSE trend, as illustrated with the Constant extension. For oil and gas, the same observations after 2012 applies for the Sigmoid extension. However, before 1970, the Sigmoid extension is higher than the Constant extension. All fuels grouped show a correct reproduction of EDGAR v4.3.2 mean and confidence interval, and of ECLIPSE trend to 2025, but the fit for oil is responsible for an increasing difference after 2025.

ECLIPSE is here shown as the blue dashed line. This ratio is rescaled over the global ratio from EDGAR v4.3.2, because the underlying emissions of the ratio ECLIPSE CLE are hindered by the same sectoral inconsistency described later in this section. The rescaled ratio of ECLIPSE is not supposed to be equal to the extended mean ratio (black dashed line) after 2012, because the the trend of ECLIPSE has been identically applied to the mean co-emission ratios for oil, gas and coal, and the fuel mix is changing.

The figure 2.5 shows the obtained co-emission ratios for BC. For coal, the evolution are correctly reproduced, in terms of mean and 95% confidence interval. For coal, we observe strong variations of the 95% confidence interval around 2005, but not of the 67% confidence interval. This may be explained by incomplete datasets.

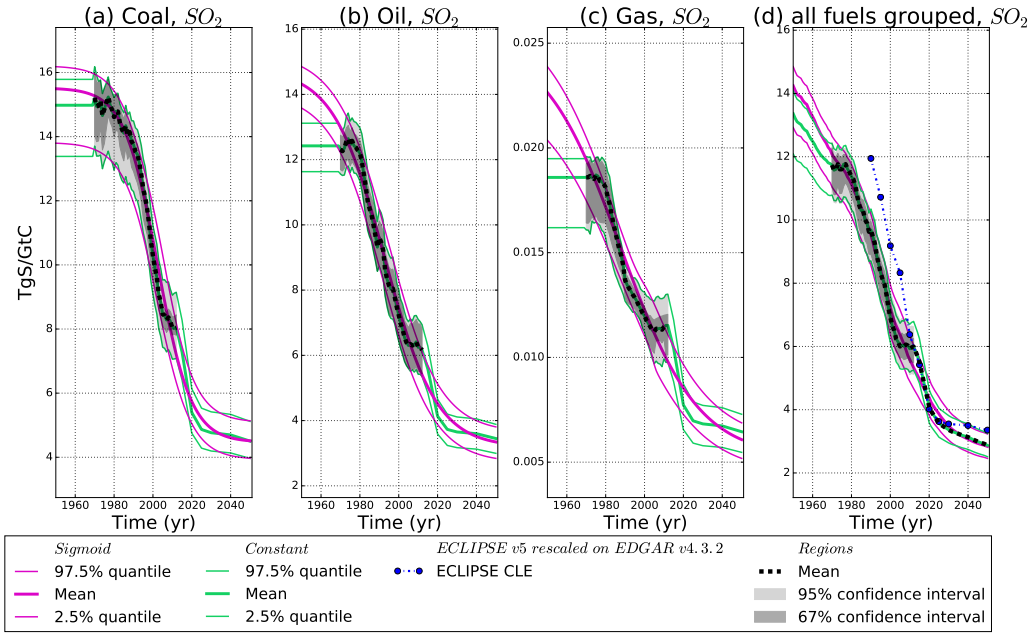

Figure 2.4: *Co-emission ratios for SO_2 and for coal (a), oil (b) and gas (c). The central black dashed line shows the global ratio taken from EDGAR v4.3.2 (Olivier et al., 2015). The histogram of co-emission ratios for GTAP regions (Narayanan and Walmsley, 2008) is represented, with its confidence intervals (shaded areas). Colored lines show the two extrapolation: Sigmoid (pink) and Constant (green).*

The same observation applies for gas. Besides, the decrease observed when grouping all fuels can be explained by the changing fuel mix, with an increasing share of oil and gas that have lower co-emission ratios. Finally, the oil and gas co-emission ratios are relatively constant over 1970-2012. However, the Sigmoid extension rule introduces strong variations over 1700-2300, especially for coal.

In figure 2.6, we represent an evaluation of the co-emission ratio over 1850-2000 using ACCMIP (Lamarque et al., 2010) and CDIAC (Boden et al., 2013). Note that the sectors associated with fossil-fuels in ACCMIP/RCP are slightly different from the sectors that we use. The co-emissions that we produce are those associated with the use of fossil-fuels in the sectors in bold in the column "IPCC-Code" of the tables 6.3 to 6.5, whereas the emissions associated with fossil-fuel sectors of ACCMIP/RCP are the total in each sector in bold in the column "CMIP5-Code". The difference lies in their aggregation. For instance, energy sector in ACCMIP/RCP include both fossil-fuels and biomass, whereas we excluded the latter in our analysis (table 6.1).

Thus, the co-emission ratio produced using ACCMIP and CDIAC sectors correspond to a ratio close but different from the ones that we produce. This ratio is higher over 1970-2000, because of the inclusion of biomass energy uses and flaring. Still, we observe that the co-emission ratios are relatively constant over 1970-2000,

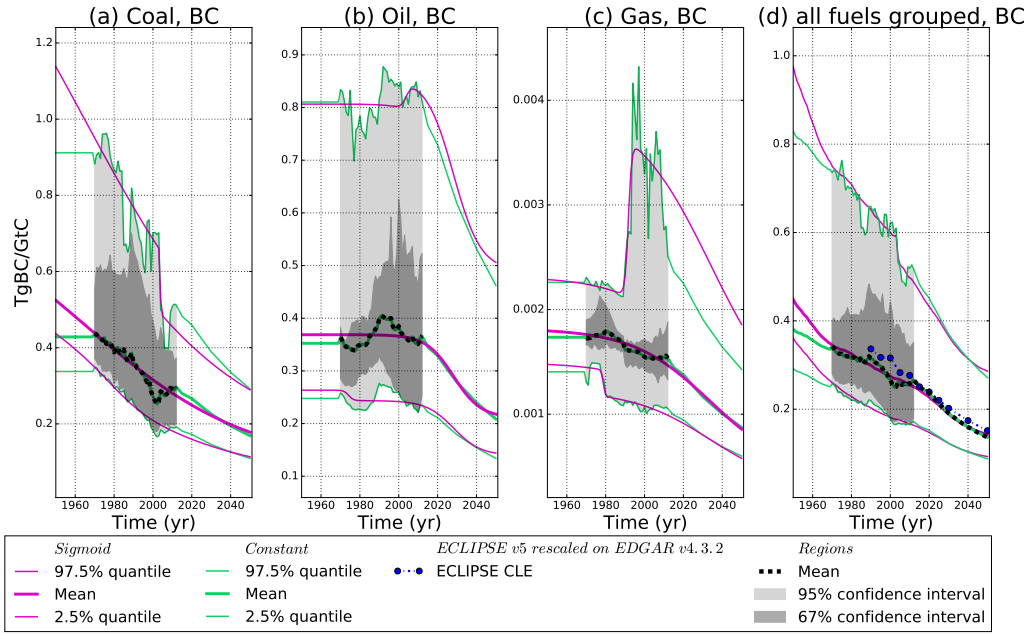

Figure 2.5: *Co-emission ratios for BC and for coal (a), oil (b) and gas (c). The central black dashed line shows the global ratio taken from EDGAR v4.3.2 (Olivier et al., 2015). The histogram of co-emission ratios for GTAP regions (Narayanan and Walmsley, 2008) is represented, with its confidence intervals (shaded areas). Colored lines show the two extrapolation: Sigmoid (pink) and Constant (green).*

but present an exponential decrease from 1850. Yet, this sectoral inconsistency and the fuel aggregation complicates the attribution of this decrease from 1850 to 1970-2000 level either to the evolution of co-emission ratios - that is to say change in technologies or quality of fuels - or the decrease of the share of biomass in energy mixes. We can only infer that the Constant extension rule may not be appropriate before 1970, and that the Sigmoid extension rule may be more representative of past higher level of co-emissions.

The figure 2.7 shows the obtained co-emission ratios for OC. For coal and gas, the evolution are correctly reproduced, in terms of mean and 95% confidence interval. For oil, the mean tends to be overestimated before 1985. A S-shaped function can hardly fit a three-level curve, with increasing levels of co-emissions of OC over 1970-2012, but sharp decrease because of the ECLIPSE trend. For lack of a better approach, the ECLIPSE trend is applied globally, which is equivalent to assuming a constant energy mix over 2012-2050. Yet, the ECLIPSE trend is based on RCP6.0 CO_2 emissions, and Masui et al. (2011) explains that in this RCP, the power sector shifts from coal fired production to gas fired production. For this reason, applying the ECLIPSE trend could lead to spurious evolution for some fuel categories. However, altogether, this trend still improves the production of the fit, avoiding the final asymptote to be too high. Note that like BC, ACCMIP and CDIAC may infer an

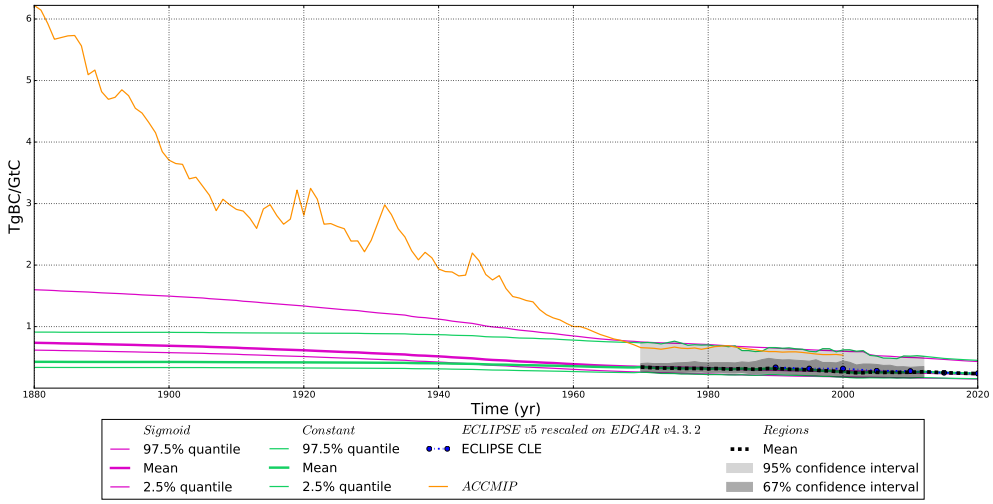

Figure 2.6: *Global co-emission ratios for BC. The central black dashed line shows the global ratio taken from EDGAR v4.3.2 (Olivier et al., 2015). The histogram of co-emission ratios for GTAP regions (Narayanan and Walmsley, 2008) is represented, with its confidence intervals (shaded areas). Colored lines show the two extrapolation: Sigmoid (pink) and Constant (green). An extended trend is produced using ACCMIP for BC and CDIAC for CO_2, but the underlying emissions correspond to different sectors.*

exponential decrease of the co-emission ratio for OC over 1850-2000. The decrease observed in the panel (d) of the figure 2.7 may even be underestimated, but as explained earlier, the sectoral inconsistency and the fuel aggregation do not allow for a more accurate statement.

The figure 2.8 shows the obtained co-emission ratios for NO_X. Coal is relatively well reproduced in terms of mean and confidence interval. Oil is also relatively well reproduced, but we observe that the mean is almost identical to the higher bound of the 67% confidence interval. This interval is particularly asymmetric, whereas the 95% confidence interval is much more symetric. It means that the majority of regions coemits NO_X less than the world average, which is balanced by some regions coemiting much more. Concerning gas, the same problem with the mean of the co-emission ratio for OC is observed. Besides, the higher bound of the 95% confidence interval is also imperfectly reproduced. The failure in the fit of the higher bound is caused by the failure of the mean, because of the choice of fitting the relative uncertainties. In this situation, fitting the absolute uncertainty with a S-shaped function may have lead better results.

The figure 2.9 shows the obtained co-emission ratios for CO. Coal and oil are relatively well reproduced in terms of mean and confidence interval. However, the fit of the higher bound of the confidence interval may be reducing too much. For gas, the same difficulty met in earlier cases (e.g. NO_X with gas) is observed. However,

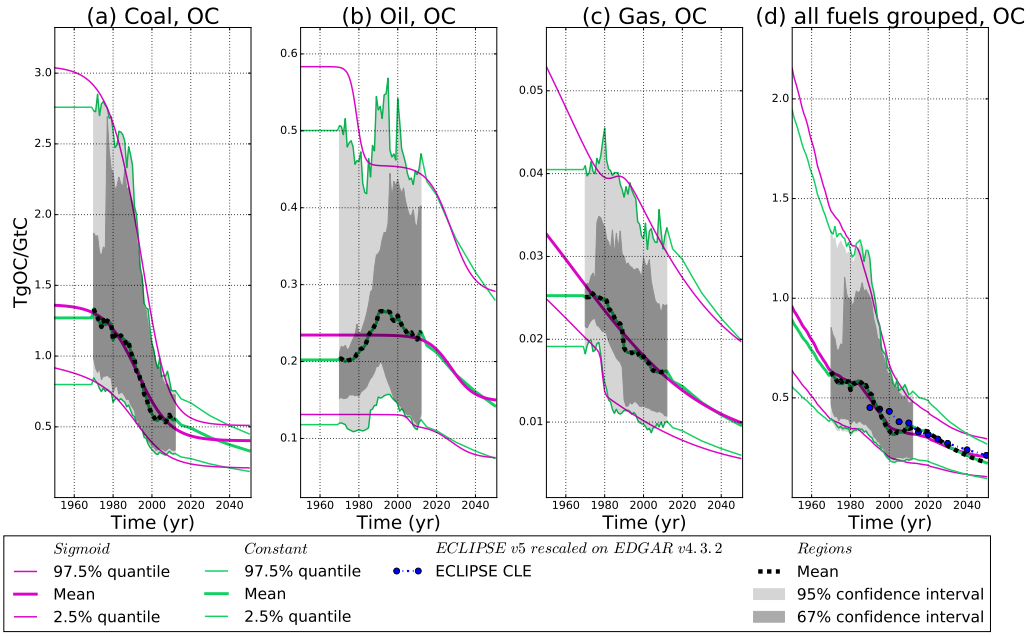

Figure 2.7: *Co-emission ratios for OC and for coal (a), oil (b) and gas (c). The central black dashed line shows the global ratio taken from EDGAR v4.3.2 (Olivier et al., 2015). The histogram of co-emission ratios for GTAP regions (Narayanan and Walmsley, 2008) is represented, with its confidence intervals (shaded areas). Colored lines show the two extrapolation: Sigmoid (pink) and Constant (green).*

it has a relatively low impact on the aggregated ratio, because gas is not the main contributor of CO emissions, compared to oil and coal.

The figure 2.10 shows the obtained co-emission ratios for CH_4. We remind the reader that the main contributions of CH_4 from the use of fossil-fuels is normally fugitive emissions during extraction, handling, transport and treatment of the fuels. Yet, this source is excluded here. What remains are CH_4 in combustion products of the fuel (IPCC, 2006). For coal and oil, mean and confidence intervals are correctly reproduced; for gas as well, but with a ratio increasing rapidly on 2000-2050. Yet, as shown in panel (d), it has a low impact on the aggregated results, because coal is more consumed and its co-emission ratio is the major contributor to the aggregated ratio.

The figure 2.11 shows the obtained co-emission ratios for N_2O. We remind here that agriculture is the main contributor of N_2O emissions, because of the use of synthetic fertilizers and animal waste, but also agricultural waste burning Olivier and Janssens-Maenhout (2014). Fuel combustion is only the second source (9% in 2010), followed by industrial processes (4% in 2010). In our case, emissions from the use of fossil fuels for the production of synthetic fertilizers are included, but not from the use of these fertilizers. Emissions from off-road machinery in agriculture and

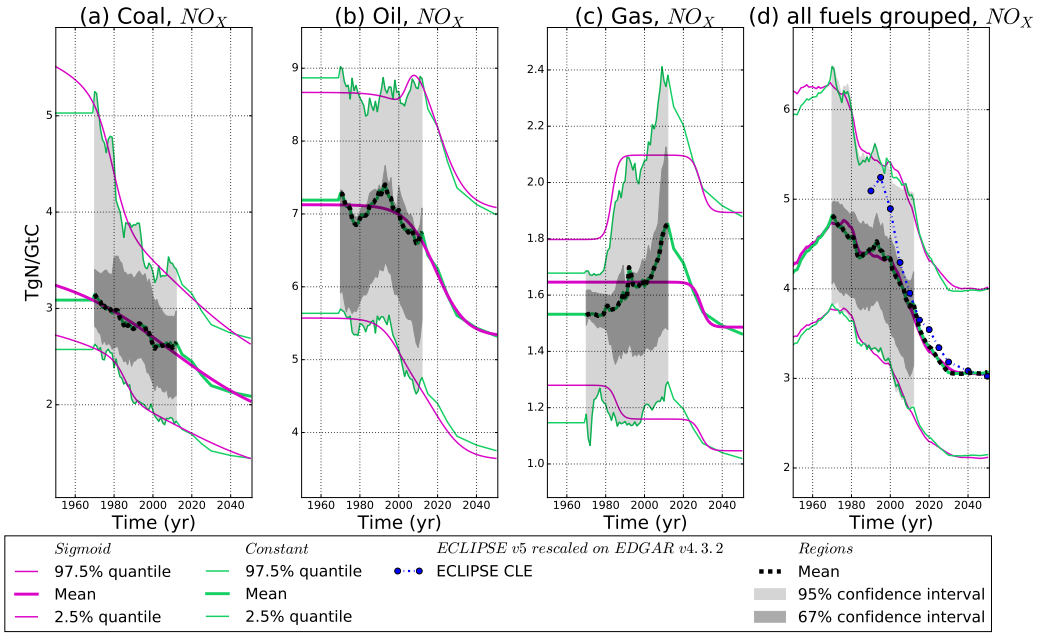

Figure 2.8: *Co-emission ratios for NO_x and for coal (a), oil (b) and gas (c). The central black dashed line shows the global ratio taken from EDGAR v4.3.2 (Olivier et al., 2015). The histogram of co-emission ratios for GTAP regions (Narayanan and Walmsley, 2008) is represented, with its confidence intervals (shaded areas). Colored lines show the two extrapolation: Sigmoid (pink) and Constant (green).*

forestry are included. For oil, a decrease is observed from 2000, that is imperfectly reproduced by the Sigmoid extension rule. The diminution in the mean co-emission ratio for oil since 2000 could be explained by two factors. On one hand, the CO_2 emissions keep increasing over 1970-2012. On the other hand, N_2O emissions from road transport (sector 1A3b) begin decreasing after 1999. We can trace this decrease back to the USA, that are the main emitters of N_2O in road transport. Yet, it is difficult to point precisely what is responsible for the latter change, for major source of N_2O emissions from road transport is reactions of the exhaust gas constituents of vehicles using post-combustion catalysts as emission control equipment. These reactions depend on several factors, such as the composition of the exhaust gases or their temperature, but there is still a need for additional research and testing (Barbour and Gillenwater, 2004). We do not know if the change observed in N_2O emissions are induced by regulation changes or by technological progress. For coal and gas, the means and the confidence intervals are correctly reproduced. Their contributions to the aggregated ratio is lower, and increasing because of the change in the processes leading to an overall slight increase of the oxidation of nitrogen from air.

For coal and oil, the means and the confidence intervals are correctly reproduced. For gas, both the mean and the confidence interval show a strong decrease to 2000

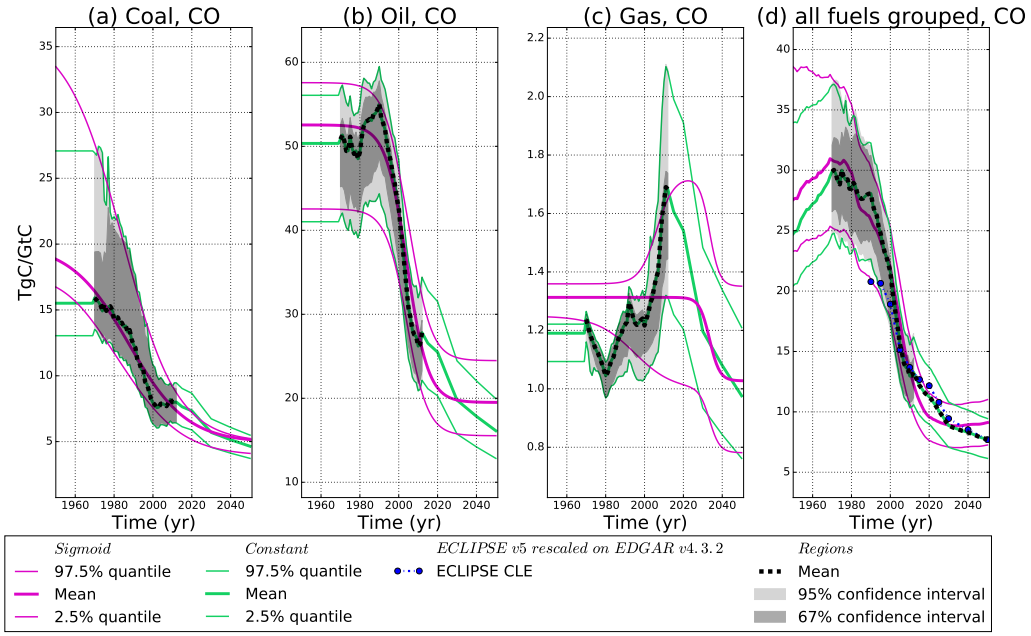

Figure 2.9: *Co-emission ratios for CO and for coal (a), oil (b) and gas (c). The central black dashed line shows the global ratio taken from EDGAR v4.3.2 (Olivier et al., 2015). The histogram of co-emission ratios for GTAP regions (Narayanan and Walmsley, 2008) is represented, with its confidence intervals (shaded areas). Colored lines show the two extrapolation: Sigmoid (pink) and Constant (green).*

followed by an increase on 2000-2012. Then, the ECLIPSE trend implies a decrease. Looking at the details of the sectors, most sectors studied here show VOC emissions slowly increasing, because of the strong increase of their activity, resulting in a decreasing co-emission ratio for each one of these sectors. However, from 2000, VOC emissions from road transport are increasing faster than their CO_2 emissions, especially in China. This can be related to the increase of the share of Natural Gas Vehicles in China (Hao et al., 2016).

The figure 2.13 shows the obtained co-emission ratios for NH_3. Coal and gas are relatively well reproduced in terms of mean and confidence interval, but are not the main contributors. The main contribution of NH_3 emissions during the use of fossil-fuels is the use of Selective Catalytic Reduction. During this process, NH_3 is used to reduce NO_X emissions, but with some NH_3 leaks (EEA, 2013). Regarding the observed evolutions in the mean co-emission ratio over 1970-2012, the beginning of NO_X emissions controls has started around 1970. In 1969, the first act in the world controlling NO_X emissions of industrial boilers has been implemented in California (Muzio et al., 1997), followed by the US Clean Air Act of 1970, regulating vehicle emissions (Greenstone, 2002). Since then, most industrialized countries have enacted such emissions controls, with the EU in 1988. This explains the sharp increase in NH_3 emissions. With the increased use of the second generation of catalysts,

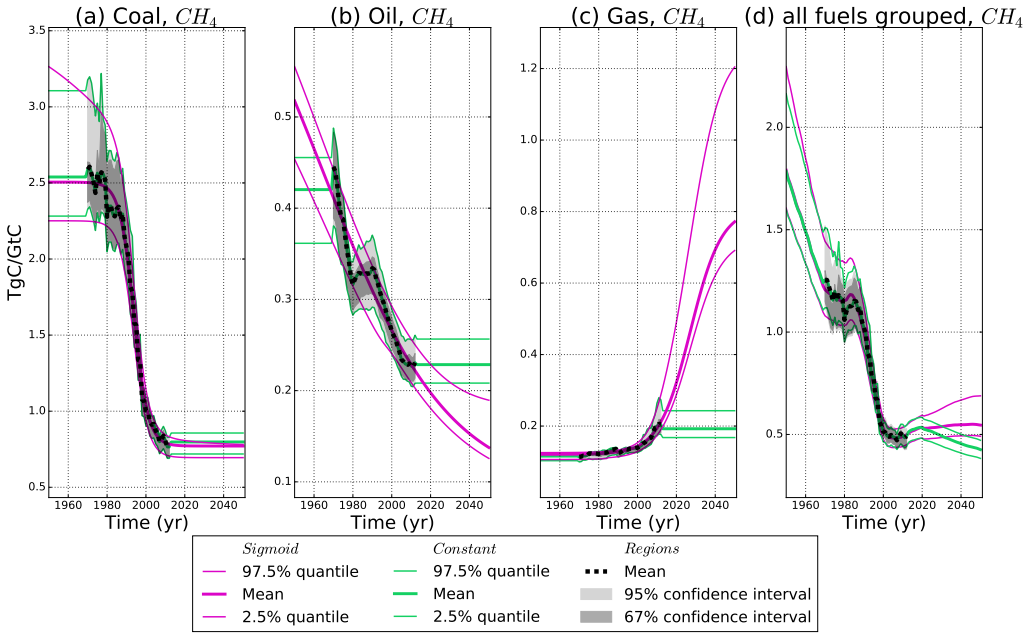

Figure 2.10: *Co-emission ratios for CH_4 and for coal (a), oil (b) and gas (c). The central black dashed line shows the global ratio taken from EDGAR v4.3.2 (Olivier et al., 2015). The histogram of co-emission ratios for GTAP regions (Narayanan and Walmsley, 2008) is represented, with its confidence intervals (shaded areas). Colored lines show the two extrapolation: Sigmoid (pink) and Constant (green).*

a stabilization then a reduction of the NH_3 emissions is observed (EEA, 2016). Regarding the fits for oil, ECLIPSE v5 dataset prescribe a reduction of the global co-emission ratio, that we apply also for oil. The historical increase in NH_3 co-emissions and the prescribed reduction render a S-shaped function not suited for the situation. However, we have chosen not to fit this kind of situation, for instance with double-S-shaped functions, for the sake of simplicity. Another approach would be to represent the NH_3/NO_X ratio for each fuel, to represent the relationship between the increase of NH_3 emissions occurring with the reduction of NO_X emissions. Yet, as represented in figure 2.8, NO_X has a single global decreasing trend, which will result in a co-emission ratio NH_3/NO_X with the same shape, thus not allowing to solve this difficulty.

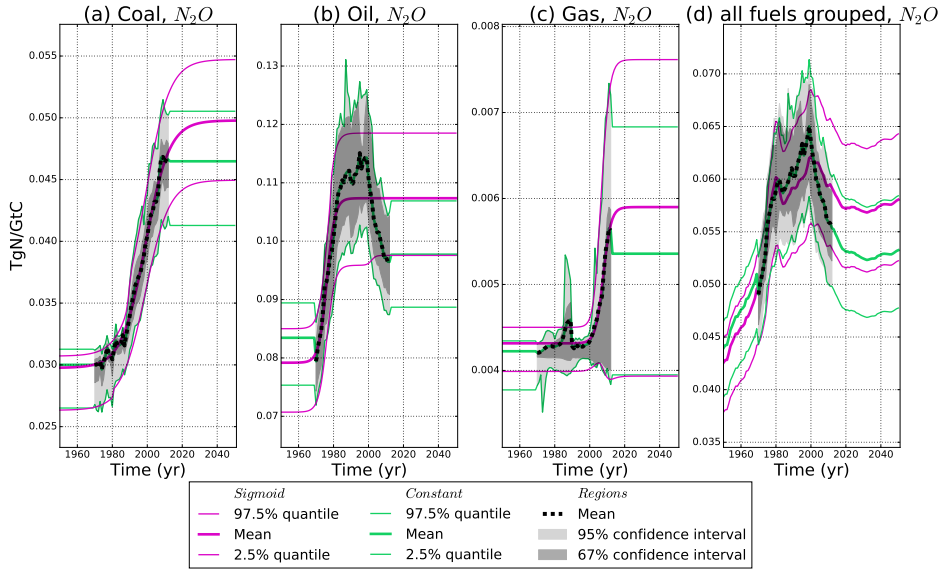

Figure 2.11: *Co-emission ratios for N_2O and for coal (a), oil (b) and gas (c). The central black dashed line shows the global ratio taken from EDGAR v4.3.2 (Olivier et al., 2015). The histogram of co-emission ratios for GTAP regions (Narayanan and Walmsley, 2008) is represented, with its confidence intervals (shaded areas). Colored lines show the two extrapolation: Sigmoid (pink) and Constant (green).*

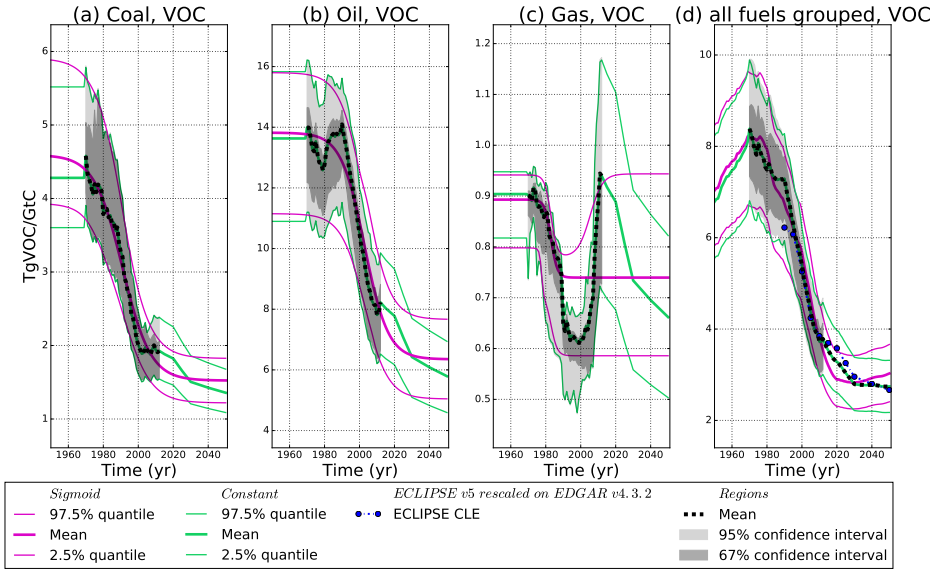

Figure 2.12: *Co-emission ratios for VOC and for coal (a), oil (b) and gas (c). The central black dashed line shows the global ratio taken from EDGAR v4.3.2 (Olivier et al., 2015). The histogram of co-emission ratios for GTAP regions (Narayanan and Walmsley, 2008) is represented, with its confidence intervals (shaded areas). Colored lines show the two extrapolation: Sigmoid (pink) and Constant (green).*

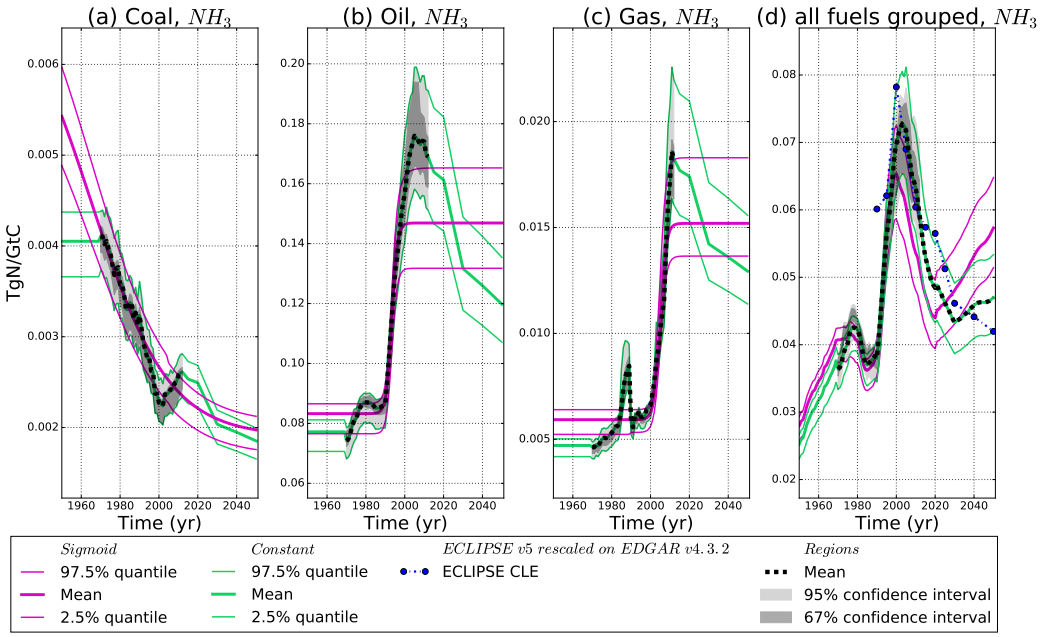

Figure 2.13: *Co-emission ratios for NH_3 and for coal (a), oil (b) and gas (c). The central black dashed line shows the global ratio taken from EDGAR v4.3.2 (Olivier et al., 2015). The histogram of co-emission ratios for GTAP regions (Narayanan and Walmsley, 2008) is represented, with its confidence intervals (shaded areas). Colored lines show the two extrapolation: Sigmoid (pink) and Constant (green).*

2.2.4 Non fossil-fuel emissions and other drivers

Past and future emissions from other sources than fossil-fuel (hereafter "background" emissions) are prescribed as follows. For the historical period, we take CO_2 emissions caused by cement production and flaring from CDIAC (Boden et al., 2013), and for other species we take existing inventories (EDGAR 4.2 Joint Research Centre (2011) and ACCMIP Lamarque et al. (2010)) of which we remove the fossil-fuel related sectors. For 2011-2100, we take emissions from the non-fossil-fuel sectors of the RCP6.0 (Meinshausen et al., 2011b; Lamarque et al., 2011). After 2100, we assume constant emissions at their levels of 2100.

As explained in section 2.2.3.2, the sectors associated with fossil-fuels in ACCMIP/RCP are slightly different from the sectors that we use. The difference lies in the sectoral disaggregations of the inventories or the RCP, that do not allow to remove only sectors associated with the use of fossil-fuels. For instance, we would also remove the production of heat and energy from biomass, as shown in tables 6.3 to 6.5. Because of these discrepancies, the non-fossil fuels emissions of these datasets added to our fossil-fuel emissions sum up to a slightly different total of the ones of the inventories. However, this inconsistency has no impact on our results, since we focus on the uncertainty caused by emissions from fossil-fuel alone.

Land-use and land-cover change data come from the LUH1.1 dataset (Hurtt et al., 2011) for 1750-2100. After 2100, land-cover is assumed constant, while harvest and shifting cultivations keep their 2100 levels.

2.2.5 Climate change projections

2.2.5.1 Principle of the method

We use the compact Earth system model OSCAR v2.2 (Gasser et al., 2017a; Arneth et al., 2017; Gasser et al., 2017b) to simulate climate change given uncertain fossil-fuel emissions and co-emissions. This model includes all the relevant components of the Earth system: the oceanic and terrestrial carbon cycles, the tropospheric and stratospheric chemistries of non-CO_2 greenhouse gases and ozone, and the direct and indirect climate effects of aerosols (Gasser et al., 2017a). For each Earth system process it features, OSCAR v2.2 is calibrated on more complex models to emulate their own range of sensitivity.

To estimate the uncertainty in projected climate change, a probabilistic Monte Carlo framework is used. The Monte Carlo ensemble is made of 1000 elements drawn by taking randomly: Earth system-related parameters (66 parameters of OSCAR v2.2, see table 3 of Gasser et al. (2017a)); the method through which fossil-fuel CO_2 emissions are calculated, energy-based or mass-based extractions (2 options), carbon contents or net calorific values (4 options since here we use the data of IPCC (2006) as a distribution), oxidation fractions (3 options); and non-CO_2 species co-emission ratios (27 distributions from since we have 9 species times 3 fuels).

When we have several distinct options, e.g. for the parameters of OSCAR or the choice of energy-based or mass-based fuel extraction data, each option is given the same probability. For variables related to CO_2 emissions and co-emission ratios, we fit a distribution over these probabilities and then draw a random value from this distribution. For CO_2 emissions, we use lognormal distributions, whereas lognormal or gamma distributions are used for co-emission ratios, depending on the quality of the fit (IPCC, 2006; Brown, 2013; EEA, 2013)). We assume the same drawn point in the distribution for all years, therefore we assume a 100% correlation of the uncertainty through time. More information over the production and handling of these probabilities can be found in section 2.2.5.2.

For each element of the ensemble, we produce 8 categories of simulations with OSCAR v2.2 in which the Earth system parameters, the parameters of fossil-fuel CO_2 emissions, and those of co-emitted species emissions are either the drawn value or kept constant (see table 2.5). The results of these simulations are used to analyze the uncertainty in projected climate change by attributing the variance of global temperature change to each one of the three sources of uncertainty, on the Earth system response, on CO_2 emissions, and on non-CO_2 co-emissions (their ratios to CO_2 emissions). More information over the production of the mean, confidence intervals, variances and covariances can be found in section 2.2.5.3. We point out however that the default configuration of OSCAR is used as a proxy of what would be a hypothetical (non-existing) "median" configuration. The small difference between these two causes a residual in the attribution of the variance – which we will show is negligible.

Experiment	Earth system	CO_2 emissions	Ratios	Decomposition
$\mathbf{EXP}_{0}$	default	median	median	Only median
$\mathbf{EXP}_{non-CO_2}$	default	median	*varying*	Var. from non-CO_2 emi.
$\mathbf{EXP}_{CO_2}$	default	*varying*	median	Var. from CO_2 emi.
$\mathbf{EXP}_{CO_2,non-CO_2}$	default	*varying*	*varying*	Var. and co-var. from CO_2 emi. & non-CO_2 emi.
$\mathbf{EXP}_{ES}$	*varying*	median	median	Var. from Earth system
$\mathbf{EXP}_{ES,non-CO_2}$	*varying*	median	*varying*	Var. and co-var. from Earth system & non-CO_2 emi.
$\mathbf{EXP}_{ES,CO_2}$	*varying*	*varying*	median	Var. and co-var. from CO_2 emi. & Earth system
$\mathbf{EXP}_{ES,CO_2,non-CO_2}$	*varying*	*varying*	*varying*	All var. and co-var.

Table 2.5: *Categories of simulations to attribute the uncertainty in projected climate change to Earth system response, CO_2 emissions and non-CO_2 species co-emissions. For each element of the Monte Carlo ensemble, the eight simulations of each line of the table are generated and used for the attribution to the variances and covariances. "var." stands for "variance" and "emi." for "emissions". "ES" refers to the source of uncertainty from the Earth system's response; "CO_2" to the source of uncertainty from the CO_2 emissions; and "non-CO_2" to the source of uncertainty from the non-CO_2 emissions.*

2.2.5.2 Focus over the production and use of probabilities

As said in section 2.2.5.1, all the Earth-sytem related parameters are assumed equiprobable, but not all parameters relative to the emissions. Equiprobability is also assumed when determining the use of oxidations fractions, mass- or energy- based evaluations or which set of NCVs and carbon contents to use between CDIAC, Mohr et al. (2015), IPCC (2006) and IPCC (1996). However, IPCC (2006) is given with confidence intervals, which implies the use of a probability density functions. Following IPCC (2006) guidance, we assume lognormal density function, because of the low asymmetry. Co-emission ratios are all prescribed with confidence intervals, which implies the use of probability density functions to choose a ratio for each compound and fuel using the three given. Following IPCC (2006) and EEA (2013) guidances, we assume gamma density functions, if possible, for its low-tails probability density function, and lognormal density functions otherwise.

For instance, we assume first for the co-emission ratios associated with the fuel f and the species g a gamma probability density function (PDF_{gamma}), having the location μ, the scale δ and the shape s for parameters. Our objective is to fit these parameters to reproduce the mean and the percentiles of the co-emissions ratios. Instead of fitting these parameters for each timestep, which would complicate the drawing of values for the Monte-Carlo framework, we fit the parameters over the whole trajectory. To do so, we calculate the average $\langle \Sigma_r E_{r,t}^{f,CO_2} \rangle_{traj}$ of our estimations of CO_2 emissions for this fuel (coal, gas or oil), and this mean trajectory is used to calculate the cumulative emissions over 1700-2300 of this gas g for this fuel f for the evolutions of the three characteristic ratios. First, the gamma distribution is fitted over these budgets using the appropriate percentile function (QF) and the mean function (M) (equations 2.11). In the case that the fit fails, the same task would be done assuming a lognormal density function ($PDF_{lognorm}$). Then, the distributions (gamma or lognormal) carrying the better results will be used.

$$PDF_{gamma}(x) = \frac{1}{\delta\Gamma(s)} \left(\frac{x-\mu}{\delta}\right)^{s-1} exp(-\frac{x-\mu}{\delta}) \tag{2.11a}$$

$$PDF_{lognorm}(x) = \frac{1}{s(x-\mu)\sqrt{2\pi}} exp\left(\frac{1}{2}\left(\frac{log\left(\frac{x-\mu}{\delta}\right)}{s}\right)^2\right) \tag{2.11b}$$

$$QF_{f,g}(97.5\%) = \Sigma_t \left(\left(R_{high,t}^{f,g}\right)^* \langle \Sigma_r E_{r,t}^{f,CO_2} \rangle_{traj}\right) = H \tag{2.11c}$$

$$M_{f,g} = \Sigma_t \left(\left(R_{mean,t}^{f,g}\right)^* \langle \Sigma_r E_{r,t}^{f,CO_2} \rangle_{traj}\right) = M \tag{2.11d}$$

$$QF_{f,g}(2.5\%) = \Sigma_t \left(\left(R_{low,t}^{f,g}\right)^* \langle \Sigma_r E_{r,t}^{f,CO_2} \rangle_{traj}\right) = L \tag{2.11e}$$

For negative asymmetry cases ($H - M \langle M - L$), we reverse the X axis. In this case, we use L^* defined as $-H$, M^* defined as $-M$ and H^* defined as $-L$.

To improve the prediction of the parameters, we have produced two functions approaching the ideal parameters for each distribution, as functions of the mean (M) and the percentiles at 2.5% and 97% (L and H). These first guesses are designed to accelerate the calculation and improve the quality of the fits. The third function is an exact relation between the parameters. Equation 2.12 is used for the gamma distribution. Equation 2.13 is used for the lognormal distribution.

$$s_0 = \left(\left(\frac{(H-M)^2 - (M-L)^2}{(H-L)^2} + 0.29123 \right) / 0.73342 \right)^{-4.49054} \tag{2.12a}$$

$$\delta_0 = \sqrt{\frac{(H-M)^2}{14.375|s_0|}} \tag{2.12b}$$

$$\mu_0 = M - s_0 * \delta_0 \tag{2.12c}$$

$$s_0 = \frac{H+L-2M}{M} \tag{2.13a}$$

$$\delta_0 = \frac{H-L}{2sinh\,(1.96 s_0)} \tag{2.13b}$$

$$\mu_0 = M - \delta_0 exp(\frac{1}{2} s_0^2) \tag{2.13c}$$

As explained in this section, probability density functions are fitted for the cumulative emissions over the period. For each compound g and fuel f, a random value V for the cumulative emissions is picked from this distribution. We get the time-evolution of the ratio matching this budget by assuming the 100% correlation over time, as illustrated in equation 2.14.

$$R_t^{f,g} = \begin{cases} R_{low,t}^{f,g} + \frac{V-L}{M-L} \left(R_{mean,t}^{f,g} - R_{low,t}^{f,g} \right) \; if \; V < M \\ R_{mean,t}^{f,g} + \frac{V-M}{H-M} \left(R_{high,t}^{f,g} - R_{mean,t}^{f,g} \right) \; if \; M \leq V \end{cases} \tag{2.14}$$

2.2.5.3 Treatment of the results

As shown in table 2.5, 8 experiments are conducted, depending whether or not each one of the 3 sources of uncertainty are taken into account or not. The experiment EXP_0 being independent of the configuration chosen. 1000 members for the Monte-Carlo are drawn. For each experiment, the mean and the 90% confidence interval are produced as shown in equation 2.15 for a variable $X_{m,EXP,t}$. m designates the member in the Monte-Carlo, EXP the experiment, and t the time step. $\langle . \rangle_m$

designates the mean over m and $Q_m(.,p\%)$ the percentile at p%. The mean $X^M_{EXP,t}$ and the percentiles $X^L_{EXP,t}$ and $X^H_{EXP,t}$ are produced with reference to 1986-2005.

$$X^M_{EXP,t} = \langle (X_{m,EXP,t} - \langle X_{m,EXP,t} \rangle_{1986-2005}) \rangle_m \tag{2.15a}$$
$$X^H_{EXP,t} = Q_m\left((X_{m,EXP,t} - \langle X_{m,EXP,t} \rangle_{1986-2005}), 95\%\right) \tag{2.15b}$$
$$X^L_{EXP,t} = Q_m\left((X_{m,EXP,t} - \langle X_{m,EXP,t} \rangle_{1986-2005}), 5\%\right) \tag{2.15c}$$

The variances and covariances evoked in table 2.5 are calculated as shown in equation 2.16. V_{ES} designates the variance associated with the Earth system's response, Cov_{ES,CO_2} the covariance associated with the Earth system's response and the CO_2 emissions, Res to the residual. We point out that variances and covariances are not estimated with reference to 1986-2005, but from the preindustrial reference year of the model, here 1700.

$$V_{tot} = V\left(X_{m,EXP_{ES,CO_2,non-CO_2},t}\right)_m \tag{2.16a}$$
$$V_{ES} = V\left(X_{m,EXP_{ES},t}\right)_m \tag{2.16b}$$
$$V_{CO_2} = V\left(X_{m,EXP_{CO_2},t}\right)_m \tag{2.16c}$$
$$V_{non-CO_2} = V\left(X_{m,EXP_{non-CO_2},t}\right)_m \tag{2.16d}$$
$$\begin{aligned} Cov_{ES,CO_2} = \frac{1}{2}\Big(&V\left(X_{m,EXP_{ES,CO_2},t}\right)_m - V\left(X_{m,EXP_{ES},t}\right)_m \\ &- V\left(X_{m,EXP_{CO_2},t}\right)_m\Big) \end{aligned} \tag{2.16e}$$
$$\begin{aligned} Cov_{ES,non-CO_2} = \frac{1}{2}\Big(&V\left(X_{m,EXP_{ES,non-CO_2},t}\right)_m - V\left(X_{m,EXP_{ES},t}\right)_m \\ &- V\left(X_{m,EXP_{non-CO_2},t}\right)_m\Big) \end{aligned} \tag{2.16f}$$
$$\begin{aligned} Cov_{CO_2,non-CO_2} = \frac{1}{2}\Big(&V\left(X_{m,EXP_{CO_2,non-CO_2},t}\right)_m - V\left(X_{m,EXP_{CO_2},t}\right)_m \\ &- V\left(X_{m,EXP_{non-CO_2},t}\right)_m\Big) \end{aligned} \tag{2.16g}$$
$$\begin{aligned} Res = V_{tot} &- V_{ES} - V_{CO_2} - V_{non-CO_2} \\ &- 2Cov_{ES,CO_2} - 2Cov_{ES,non-CO_2} - 2Cov_{CO_2,non-CO_2} \end{aligned} \tag{2.16h}$$

2.3 Results

2.3.1 CO_2 emissions

In figure 2.14 (left part) we compare the reconstructed trajectories of historical CO_2 emissions from fossil-fuel combustion and use in industrial processes (36 trajectories from varied emission parameters as in section 2.2.2) with those from the EDGAR v4.3.2 (Olivier et al., 2015) and CDIAC (Boden et al., 2017) inventories. These inventories do not use the same fuel extraction data than ours from Mohr et al., but their emission factors or oxidation fractions may coincide with some of our 36 estimates.

Over 1970-2008, the mean of our reconstructions (black) is 8% higher than EDGAR v4.3.2 (blue) and 5% higher than CDIAC (red). Before 1970, this relative difference with CDIAC decreases and the mean of our reconstructions is 10% lower than the CDIAC inventory in 1900 (not shown). This difference stabilizes to 5% in the period 1750-1800. Comparing our reconstructions of CO_2 emissions to EDGAR emissions point to stronger differences concerning non-conventional fuels. Still, part of the difference is likely explained by the different extraction datasets used. However, a detailed comparison is not possible, because the extractions per fuel type and region used by CDIAC and EDGAR are not openly available.

In table 2.6, we compare the range of reconstructed CO_2 emissions with other widely used inventories for the years 2005 and 2010. When considering only energy-based estimates, our range of historical emissions is representative of the dispersion in the inventories. When considering the mass-based method however, this range is doubled. It shows that net calorific values are a key source of uncertainty in our calculations.

	2005	**2010**
EDGAR4.3.2, IEA, CDIAC, EIA & BP	7.34-8.26 (± 6%)	8.14-9.13 (± 6%)
Energy-based reconstructions	7.23-8.30 (± 7%)	8.37-9.62 (± 7%)
Mass-based reconstructions	7.23-9.39 (± 13%)	8.37-10.32 (± 10%)

Table 2.6: *Total CO_2 fossil-fuel emissions. We show the 95% uncertainty ranges of our reconstructions over the historical period, compared to 5 inventories in 2005 and 2010 (EDGAR v4.3.2 (Olivier et al., 2015), IEA (IEA, 2018), CDIAC (Boden et al., 2013), EIA (EIA, 2018) and BP (BP, 2018)), depending on the use of energy- or mass-based reconstructions.*

Figure 2.14 (right part) shows the future trajectories of fossil-fuel CO_2 emissions based on the extraction scenarios from Mohr et al. (2015). High quality coals and conventional oil and gas are consumed first. As shown in figure 2.15, after 2050, non-conventional oils and gases are extracted. After 2100, the extractions of the different fuels are mostly decreasing. As exceptions, the extractions of lignite, kerogen oil, coal bed methane, shale gas, tight gas and hydrates tend to decrease only after 2150. For all scenarios, the relative range of uncertainty in emission tends to increase after

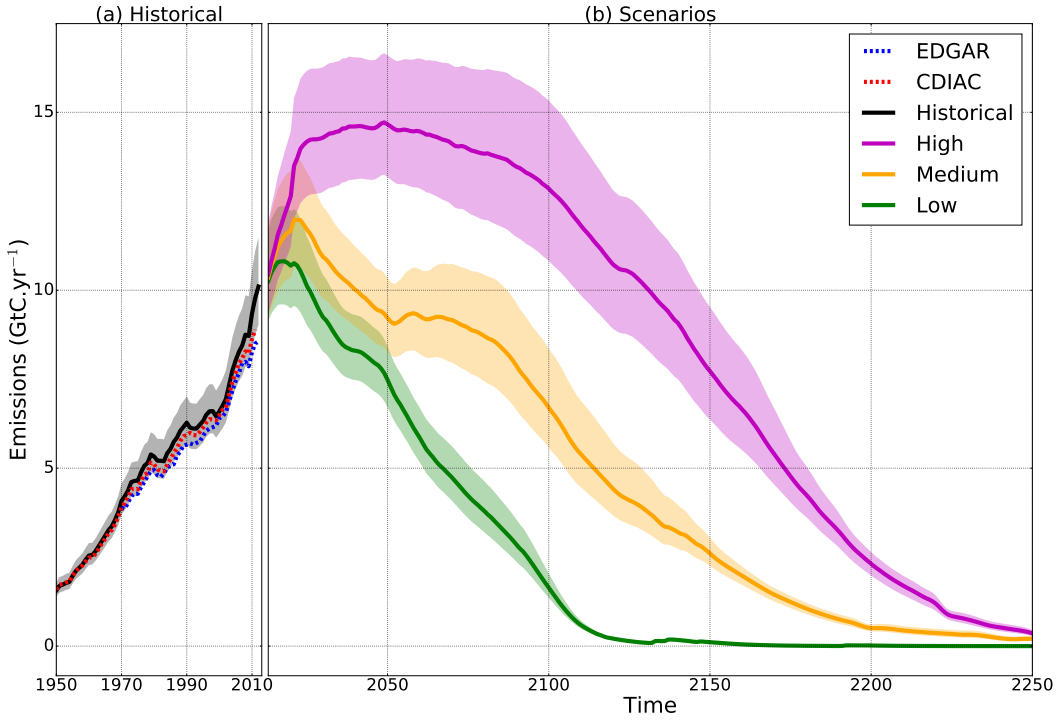

Figure 2.14: *Total CO_2 emissions from fossil-fuel, for the historical period and the three extraction scenarios of Mohr et al. (2015). We compare the median value of our reconstruction (black) to the inventories from CDIAC (red) and EDGAR v4.3.2 (blue) over the historical period. The uncertainty (gray shaded area) corresponds to the ensemble of the 36 trajectories of CO_2 emissions obtained by varying the method of inventory (energy-based or mass-based), the oxidation fractions, and the carbon contents or net calorific values (see section 2.2.2).*

2010, up to a ±24% uncertainty in the High scenario, ±36% in the Medium, and ±21% in the Low. This increase in uncertainty in the future (table 2.7) is caused by an increase in the share of non-conventional fuels being consumed in the future, these fuels having more uncertain carbon contents and net calorific values. For instance, in the Low scenario, the share of total emissions of natural bitumen increases to 40% around 2110, and the share of extra heavy oils increases to 20% around 2090, because of the increasing scarcity in conventional oil. In the Medium and High scenarios, resources in kerogen oil are enough that its emissions reach 100% in 2280 and 57% in 2248, respectively. For today's estimates, these non-conventional fuels have limited consequences because of their low level of consumption, but it is likely to change in the future.

	Peak of emissions	**Maximum of uncertainty**	**Cumulated on 2000-2300**
"High"	2049 (± 12%)	2248 (± 24%)	± 15%
"Medium"	2021 (± 13%)	2281 (± 36%)	± 15%
"Low"	2018 (± 13%)	2095 (± 21%)	± 13%

Table 2.7: *Ranges obtained in our three scenarios of extraction at the time of peak emission, of peak uncertainty, and cumulated over 2000-2300.*

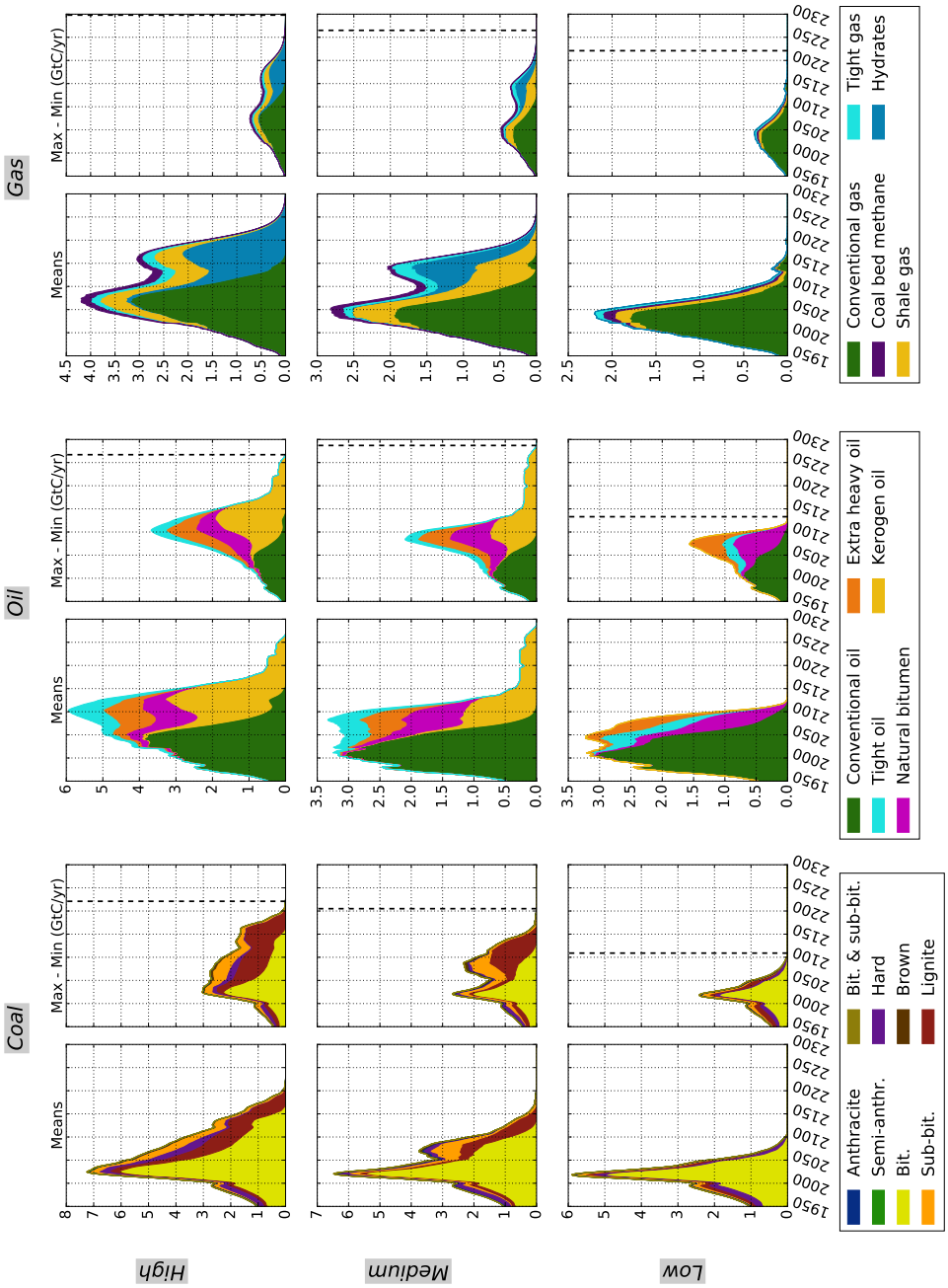

Figure 2.15: *Decomposition of the CO_2 emissions for each scenario of extraction over each line. Fuel categories are sorted in coal, oil and gas categories. For each subtype, the mean of all evaluations is represented (left panel), followed by their absolute ranges (right panel). The vertical black dashed line represents a threshold behind which CO_2 emissions for this group of fuel are too low to draw any meaningful conclusion. It is calculated as 0.1% of the maximum of these emissions over 1950-2300.*

2.3.2 Non-CO_2 emissions

Non-CO_2 co-emissions trajectories are presented in figure 2.16 for the scenario Medium. The sectoral inconsistency mentioned in section 2.2.4 requires a rescale of those emissions to be comparable to most existing inventories. Emissions are rescaled only in this figure, not in the simulations, using the average over 1970-2000 of EDGAR v4.3.2 emissions following our sectoral definition and that of the ACCMIP, RCP and ECLIPSEv5.0 datasets (Lamarque et al., 2010; Meinshausen et al., 2011b; Stohl et al., 2015)). Note that we do not compare our non-CO_2 emissions to EDGAR v4.3.2 itself, to avoid obvious matching. Fugitive emissions are included in the fossil-fuel sector of other inventories but not in ours: this means that the rescaling factor for the methane is too large to be meaningful. For this reason, methane is not compared in this figure.

As our CO_2 emission reconstruction lies in the range of other inventories (table 2.6, and as our co-emission ratios are based on EDGAR v4.3.2 (figures 2.4 to 2.13), with literature data to constrain the ranges of the ratios (table 2.4), we observe in figure 2.16 that our historical reconstructions of non-CO_2 emissions are also comparable to existing inventories such as Smith et al. (2011), but also Stern (2006) and Cofala et al. (2007). This is especially true in the case of SO_2 which is an important species because of its strong climate cooling effect. Around the years 2000 and 2010, our emissions of OC and BC follow values close to those of EDGARv4.3.2 per construction, and these are also comparable to Novakov et al. (2003) (which also use BC/CO_2 ratios), Ito and Penner (2005) and Junker and Liousse (2006). For BC, our estimate lies close to the ECLIPSEv5.0 present-day assessment (Stohl et al., 2015) and that of Bond et al. (2004). For OC, however, the difference is larger, especially in 2000, but each estimate remains within the uncertainty range of one another. For other species – that is CO, NO_X, VOCs, N_2O and NH_3 – our estimates are also comparable to the ACCMIP (Lamarque et al., 2010) and EDGAR v4.2 datasets (Joint Research Centre, 2011).

For the future projections, this Medium scenario is somewhat close to RCP4.5 in terms of extracted fossil fuels, but our co-emission ratios reach those of ECLIPSEv5.0 CLE in 2050 - by construction. The policy and technological assumptions underlying the RCPs and the CLE scenario of ECLIPSEv5.0 are different from our projections based on CO_2 emissions and a plausible evolution of co-emitted ratios, so that there is no reason for our non-CO_2 emissions future curves to match exactly the RCP ones. Still, our projections remain relatively consistent with the RCPs for all species, with the notable exception of NH_3 (figure 2.16). This difference is caused by the lower correlation of NH_3 emissions with CO_2 emissions. NH_3 emissions are especially caused by the use of catalysis to reduce NO_X emissions, and this advocate for the use of ratios of NH_3 emissions over NO_X emissions. However, when taking the ratio of NH_3 emissions over NO_X, the strong correlation between NH_3 and NO_X fades, which is a flaw of the approach through co-emission ratios based on CO_2 as reference gas.

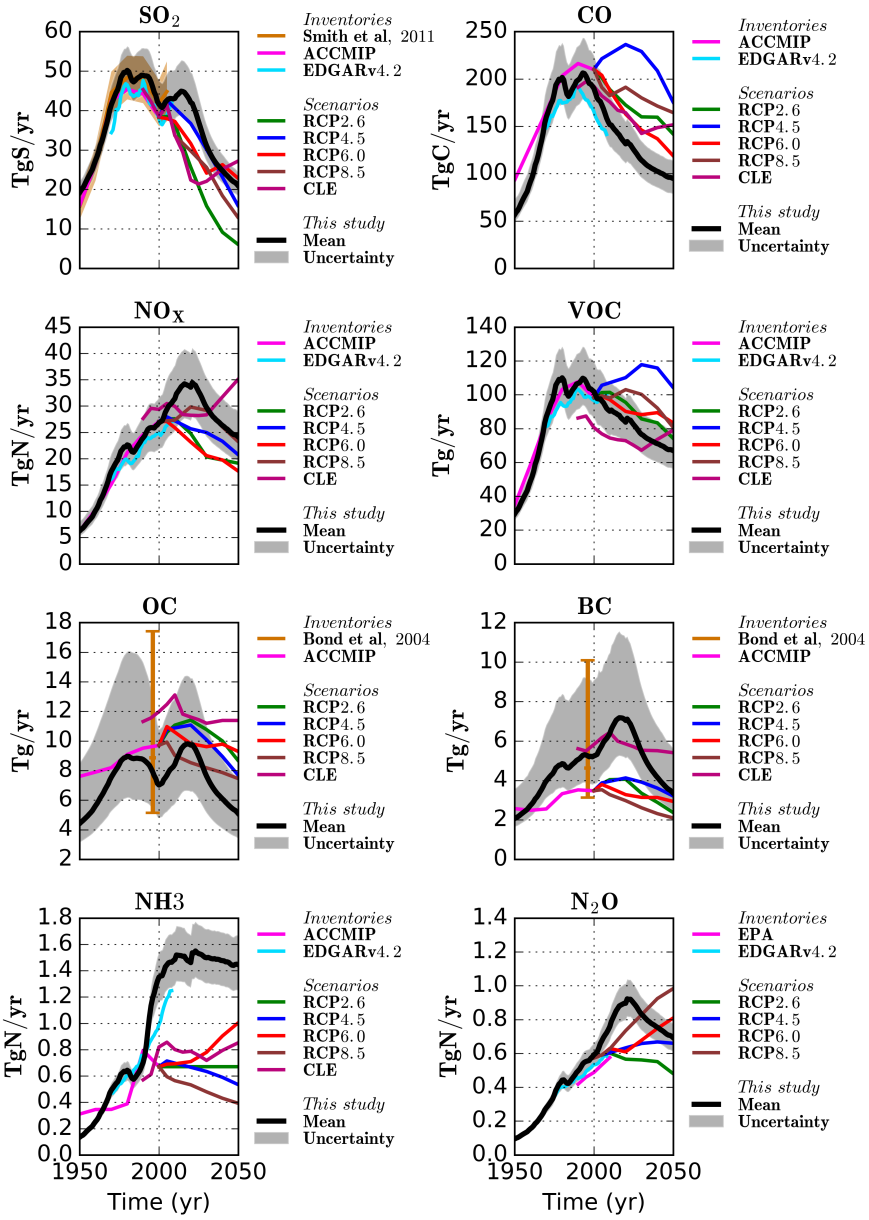

Figure 2.16: *Fossil-fuel emissions for the scenario of extraction "Medium". The black plain line is the median of trajectories, and in shaded gray is the 95% confidence interval evaluated from all trajectories. For comparison are represented the co-emissions associated with fossil-fuel sectors from ACCMIP (Lamarque et al., 2010), EDGAR 4.2 (Joint Research Centre, 2011), EPA (EPA, 2012), the RCP (Meinshausen et al., 2011b) and the scenario CLE of ECLIPSEv5.0 (Stohl et al., 2015). The 90% confidence interval from Smith et al. (2011) for total SO_2 emissions has been transformed into a 95% confidence interval assuming normal distribution. The 95% intervals from Bond et al. (2004) for fossil-fuel BC and OC emissions are also represented. The sectoral inconsistency (e.g. biomass energy not included in our analysis) mentioned in section 2.2.4 requires for the comparison a rescale. Only in this figure, our emissions are multiplied by the emissions of EDGAR v4.3.2 for the sectors matching ACCMIP & RCP sectors, and divided by the emissions of EDGAR v4.3.2 for the sectors corresponding to our analysis.*

To compare these non-CO_2 emissions to those of Rogelj et al. (2014), several assumptions have to be used. First, the consumption of fossil-fuels have to be relatively close. Here, we represent the non-CO_2 emissions under the scenario of extraction Medium, which is relatively close to the extractions of RCP4.5 (section 2.2.1). Then, the extraction scenarios assume no climate policies, and the coemission ratios follow the trend of the scenario ECLIPSEv5.0 Current Legislation (CLE). The emissions in 2050 in Current Legislation of RCP4.5 in Rogelj et al. (2014) can be compared to our mean estimates for SO_2, CO and OC. Concerning NO_X and BC, we calculate an increasing trend, followed by a decrease, whereas these emissions in Rogelj et al. (2014) decrease most of the time. On the other hand, we calculate higher VOC emissions, but decreasing faster. The ranges in 2050 from Current to Stringent Legislation in Rogelj et al. (2014) can be compared to our lower uncertainties in 2050 for SO_2, CO, NO_X and OC. For VOC, our estimates are smaller, whereas those for BC are bigger. Overall, our estimates are consistent with the Current Legislation emissions of Rogelj et al. (2014) in 2050, and our lower 95% confidence interval is equivalent to the Current to Stringent Legislation ranges.

We compare our non-CO_2 emissions to those of the Shared Socio-Economic Pathways (SSP) that target the RCP4.5 (Rao et al., 2017). Our mean SO_2 emissions in 2050 are relatively close to SSP2 estimates. The range spanned by the SSP marker scenarios is bigger than our 95% confidence interval, for our estimates have stronger implicit assumptions compared to those of the SSP scenarios. For NO_X and BC emissions, our mean estimates are higher compared to those of the SSP, but the range of SSP emissions in 2050 is equivalent to our 95% confidence interval, contrary to SO_2 emissions.

It comes from Rao et al. (2017) and Rogelj et al. (2014) that our estimates are compatible with current legislation scenarios, with a lower bound of our uncertainty range equivalent to stringent legislation scenarios. Yet, our range of BC emissions may be overestimated, and so might be the one for NO_X emissions.

2.3.3 Climate change projections

The upper panel of the figure 2.17 shows global surface temperature change with respect to the average of 1986-2005 (ΔT) simulated with OSCAR v2.2 and for the three future scenarios. In the Low, Medium and High scenarios, respectively, the 90% uncertainty range of ΔT in 2100 due to uncertain Earth system parameters only are 1.1-2.6 °C, 1.5–3.0 °C and 1.9-3.6°C, with median values of 1.8°C, 2.2°C and 2.7°C. For the uncertainty from fossil-fuel CO_2 and non-CO_2 emission parameters only, these ranges are 1.8-2.0°C, 2.1–2.4°C and 2.6-2.9°C around 2100, which is about 6 times smaller than the Earth system uncertainty. When both the Earth system parameters and the emission parameters vary, the total uncertainty range remains very close to the case with varying Earth system parameters only. This shows that the total uncertainty on ΔT is largely dominated by the Earth system uncertainty, despite an uncertainty of about 15% in cumulative CO_2 emission estimates (figure

2.14), and uncertainties of up to a factor 2 for some non-CO_2 emissions (figure 2.16).

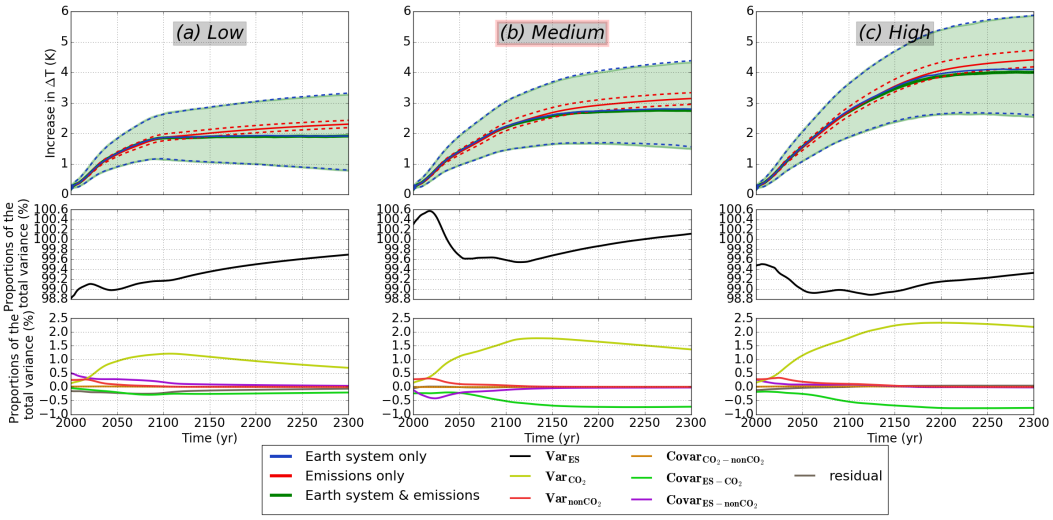

Figure 2.17: *Upper panel: global surface temperature changes (in K) with respect to the average of 1986-2005 for the three extraction scenarios in the upper panels. The median and the 90% uncertainty range are shown for three experiments: with Earth system parameters varying (blue intervals), CO_2 and non-CO_2 eission parameters varying (red intervals), and both varying at the same time (green plain line and shaded area). In the middle and lower panels, the variances and covariances identified are represented in terms of proportion of the total variance.*

These results, summarized in table 2.8, also holds for the years 2200 and 2300. Besides, the ΔT obtained from the Low scenario are very close to the results for RCP4.5 from ESM (Knutti and Sedláček, 2012; Collins et al., 2013), the Medium scenario to RCP6.0 and the High scenario somewhat between RCP6.0 and RCP8.5. Knowing the correspondence of the three scenarios of extraction with the ones of RCP (figure 11 of van Vuuren et al. (2011a)), and taking into account that the emissions from non-fossil fuels are prescribed here by RCP6.0, these projections in ΔT are consistent with the projections of RCP.

In figure 2.17, using our 8 factorial simulations we attribute the variance of temperature change with all sources of uncertainty varying (green in figure 2.17) to variances and co-variances specific to uncertainties in the Earth system, fossil-fuel CO_2 emissions and non-CO_2 co-emissions. It is confirmed that the Earth system uncertainty largely dominates, since its attributed variance stays around 100% of the total variance in the three scenarios.

The variance attributed to fossil-fuel CO_2 emissions peaks below 1.5%, 2% and 2.5% of the total variance in the Low, Medium and High scenarios, respectively; thus being quite negligible. The later CO_2 fossil-fuel emissions are peaking; the smaller the proportion of their associated variance peaks. Conversely, the co-variance attributed to the coupling of fossil-fuel CO_2 emissions and the Earth system does not

Scenarios	Simulations	2100	2200	2300
"Low"	EXP_3: Emi.	1.9 ±0.1 (±6%)	2.1 ±0.1 (±6%)	2.3 ±0.1 (±5%)
	EXP_4: ES	1.9 ±0.7 (±39%)	1.9 ±1.0 (±54%)	1.9 ±1.3 (±66%)
	EXP_7: Emi. & ES	1.8 ±0.8 (±41%)	1.9 ±1.0 (±54%)	1.9 ±1.2 (±65%)
"Medium"	EXP_3: Emi.	2.2 ±0.1 (±6%)	2.9 ±0.2 (±6%)	3.1 ±0.2 (±6%)
	EXP_4: ES	2.2 ±0.8 (±36%)	2.7 ±1.2 (±43%)	2.8 ±1.4 (±51%)
	EXP_7: Emi. & ES	2.2 ±0.8 (±36%)	2.7 ±1.2 (±43%)	2.7 ±1.4 (±52%)
"High"	EXP_3: Emi.	2.7 ±0.2 (±6%)	4.1 ±0.2 (±6%)	4.4 ±0.3 (±6%)
	EXP_4: ES	2.7 ±0.9 (±32%)	4.0 ±1.4 (±35%)	4.1 ±1.6 (±40%)
	EXP_7: Emi. & ES	2.7 ±0.9 (±33%)	3.9 ±1.4 (±36%)	4.0 ±1.7 (±42%)
RCP2.6		0.9 ±0.7 (±73%)		
RCP4.5		1.9 ±0.7 (±38%)		
RCP6.0		2.3 ±0.8 (±34%)		
RCP8.5		4.0 ±1.2 (±30%)		

Table 2.8: *Median and 90% ranges for the increase in global temperature with respect to the average of 1986-2005 (°C), for the three scenarios of extractions and for the simulations with variations of the parameters relative to the emissions ("Emi."), or to the Earth system ("ES"), or both ("Emi. & ES"). The relative uncertainties are given in parentheses. For comparison, the mean and ranges in 2100 of the RCP are given (based on a Gaussian assumption, by multiplying the multi-model standard deviation by 1.64, as in Collins et al. (2013).*

peak at all. It increases (in absolute value) in all three scenarios to reach respectively -0.2%, -0.7% and -0.8% by 2300. This negative co-variance reduces even further the importance of accounting for the uncertainty in fossil-fuel CO_2 emission estimates at the same time as that in the Earth system's response. The dampening effect of the carbon cycle, that removes roughly half of yearly anthropogenic emissions from the atmosphere (Le Quéré et al., 2016), can explain this negative sign of the covariance between fossil-fuel CO_2 emission uncertainty and Earth system uncertainty.

The variance attributed to non-CO_2 emissions present a similar profile in all three scenarios. It peaks at about 0.3% of the total variance, around 2025 – a time at which it becomes less in magnitude than the variance attributed to fossil-fuel CO_2 emissions. The shorter lifetimes for most of the non- CO_2 species explains this decrease with time. The co-variance attributed to the coupling of non-CO_2 emissions and the Earth system is the only one that appears to be scenario-dependent. In the Low and High scenarios, it decreases with time, starting with a positive value in 2000 of 0.5% and 0.3%, respectively, of the total variance. In the Medium scenario, it is negative and peaks at about -0.4%. These various behaviors show the complex interplay between all the non-CO_2 species, their timing of emission, and the Earth system's response, various couplings and feedbacks.

The co-variance attributed to the coupling of CO_2 and non-CO_2 emissions remains negligible (<0.1%) throughout all three scenarios. The residual term remains also negligible, except in the Low scenario. Because this scenario has less CO_2

emissions, it indicates that the default configuration of OSCAR differs more from a hypothetical median configuration for processes related to non-CO_2 species than for the carbon cycle.

2.4 Discussion

2.4.1 Sensitivity analysis

The first investigated key assumption of our study is the extension rule used to extrapolate the co-emission ratios (section 2.2.3). Using Constant extensions instead of Sigmoids extensions, with the Medium scenario, does not significantly alter our main quantitative result regarding the negligibility of emission factors when projecting climate change (figure 2.18). The only noticeable change is in the co-variance attributed to the coupling of non-CO_2 emissions and the Earth system which remains of the same order of magnitude but sees its sign changed. This emphasizes again the sensitivity of the Earth system's response to the timing and mixing of non-CO_2 species emission.

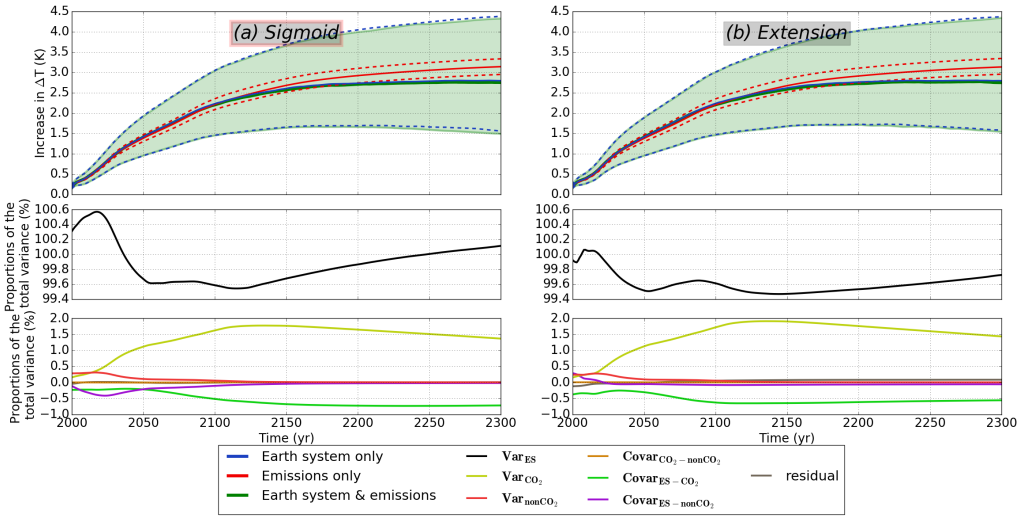

Figure 2.18: *Effect of the co-emission ratios extension rule on projected global temperature change and attributed variance. The case "sigmoid" is the one used in the main results section.*

The second investigated key assumption is the background of non-fossil emissions and land-use change (section 2.2.4). We repeat our simulations for the Medium scenario but with the other available RCPs (RCP2.6, RCP4.5 and RCP8.5) as background data. Again, our main conclusions remain valid (figure 2.19). The stronger change appears when using RCP8.5 – that is, a more positive background in terms of radiative forcing – in which case the variance attributed to emissions (CO_2 and non-CO_2 alike) is further reduced. The RCP2.6 and the RCP4.5 are

the backgrounds presenting the stronger variances and covariances. For RCP2.6, the variance associated with CO_2 emissions is lower than the one associated with the RCP4.5 that does not exceed 2%. However, the covariance associated with the coupling of CO_2 emissions and the Earth system are higher in absolute value in the RCP2.6, that does not exceed -0.5%. The influence of land use change in the covariances is relatively hard to discern, for the uncertainty in CO_2 emissions is here related to the uncertainty on CO_2 emissions from Fossil Fuels and not from Land Use Change. Yet, changes in land variables may affect the carbon sinks, affecting the variances and covariances related to the Earth system. We observe that the covariance of CO_2 emissions with the Earth system is much lower in the RCP4.5, even lower than the residual. Thus, it is possible that a mechanism of compensation of this covariance is occurring through the land carbon sink, but more information is required for a robust conclusion.

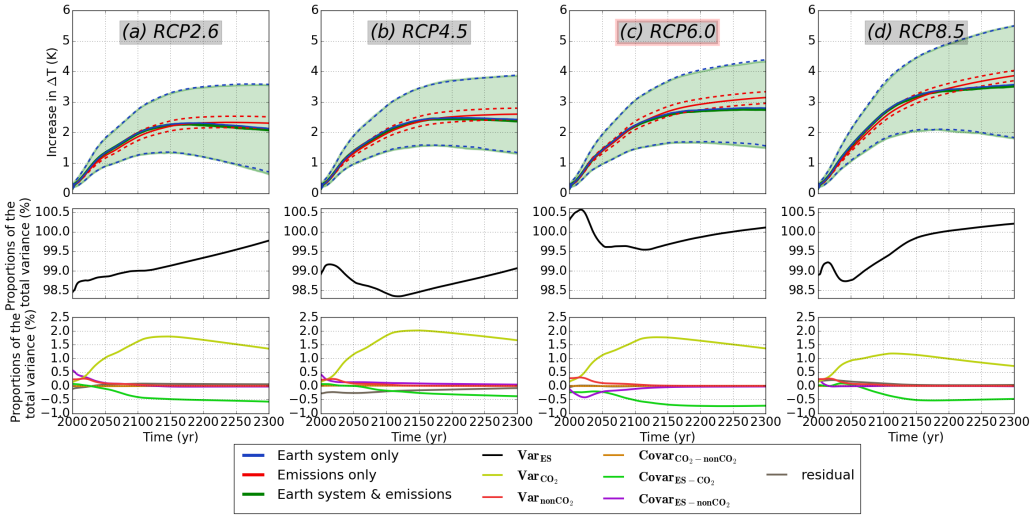

Figure 2.19: *Effect of the change in the non-fossil-fuel emissions. The case of "RCP6.0" is the reference.*

For completeness, we have also tried 500 and 2000 members for our Monte Carlo ensemble. 1000 members appears to be a good tradeoff between efficiency and accuracy (figure 2.20) to test the variances introduced by the uncertainty in fossil fuel emissions. The variances and covariances are relatively unchanged between 1000 and 2000 members, although these changes sum up to a reduction of the Earth system uncertainty by 1%.

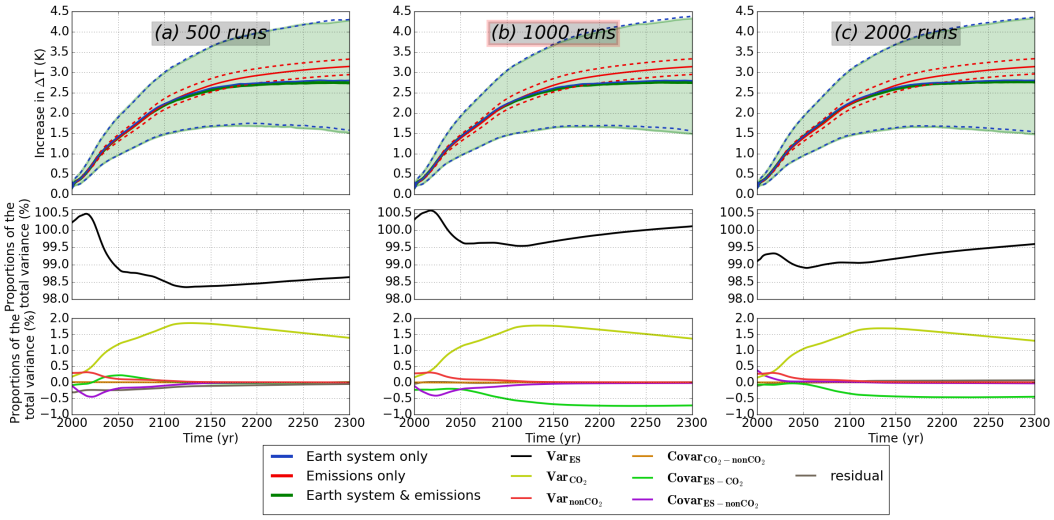

Figure 2.20: *Effect of the change in the number of runs in the Monte-Carlo. "1000 runs" is the reference.*

2.4.2 Limitations

2.4.2.1 Limitations induced by the methods

We use a global approach to estimate CO_2 emissions and non-CO_2 co-emissions trajectories based on global "emission factors", and this can be deemed a caveat of our study. The use of national data, both for CO_2 and co-emissions, would certainly provide more accurate estimates (Andres et al., 2012). However, in the dataset we use, the national data is expressed in terms of extraction, whereas the actual driver of emission in a country is fossil-fuel consumption (Davis et al., 2011). Going from the former to the latter requires trade data which is not available over distant periods in the past, nor is it for the future. Although datasets of national fossil-fuel consumption do exist, they are not openly available (Speirs et al., 2015). Similarly, we use global instead of national NCVs, carbon contents, and co-emission ratios, whereas these factors vary greatly among countries. Using national values for these factors would be possible, but it implies having a bottom-up approach based on fuel consumption data, for which fuels, emitting technologies and operating conditions should be distinguished, especially for non-CO_2 co-emissions (Peng et al., 2016). In this case, evaluating the resulting uncertainty would require a tremendous effort, in order to produce data that is not provided even by well-established inventories.

Our approach allows us to combine the uncertainty in key parameters (energy or mass-based inventory method; carbon contents; fractions of oxidations; co-emissions) in an efficient manner without the need of making assumptions as to e.g. future use of emitting technologies. As we have shown that our calculated CO_2 and non-CO_2 global emission trajectories and uncertainties are comparable to existing bottom-up data, we argue that our approach is good enough given the purpose of our investigation on the impact of uncertainty in fossil fuel emission estimates on projected climate change. Our study might overestimate the uncertainty in future non-CO_2 co-emissions, but this actually strengthens our conclusion regarding the negligibility of this source of uncertainty.

2.4.2.2 Validity for other climate variables

Up to this section, we have chosen to present only the uncertainty analysis for the global surface temperature as referred to in the UNFCCC. For the Earth's surface temperature, the total radiative forcing and total annual precipitation change, three global Earth system variables, which integrate the effect of various anthropogenic perturbations, we conclude that the emission-induced uncertainty is negligible. However, we will show here that this uncertainty is negligible for most variables, except the atmospheric partial pressure of CO_2 and the radiative forcing of tropospheric ozone.

The atmospheric partial pressure of CO_2 shows strong uncertainties (figure 2.21), because of its dependency to the CO_2 emissions. Though, the carbon sinks affect this atmospherical partial pressure. In the High scenario, the atmospheric concentration

of CO_2 in 2100 with respect to the average of 1986-2005 reaches 352 ppm, with a range of 321-390ppm. In terms of extrema of the confidence interval, this is about 42% of the total uncertainty. In terms of variances, this translates into 92% to the Earth system's response. The uncertainty in CO_2 emissions contributes with 8% to the total variance of atmospheric CO_2. The covariance of the uncertainty in CO_2 emissions and of the Earth system modelling partially offsets the CO_2 emissions induced uncertainty. Under a given background, the higher are CO_2 emissions, the higher are the absolute uncertainties on CO_2 emissions, and thus, the higher is the relative contribution of these uncertainties to the total variance of the system. As CO_2 emissions increase, the relative contribution of the covariance of CO_2 emissions to the Earth system, thus related to the carbon cycle, is increasing as a response of the uncertainty in the modelling of the carbon cycle. Finally, for the scenario of extraction "Low", the emissions-induced uncertainty increases the total variance by 2%, and 8% with the scenario "High".

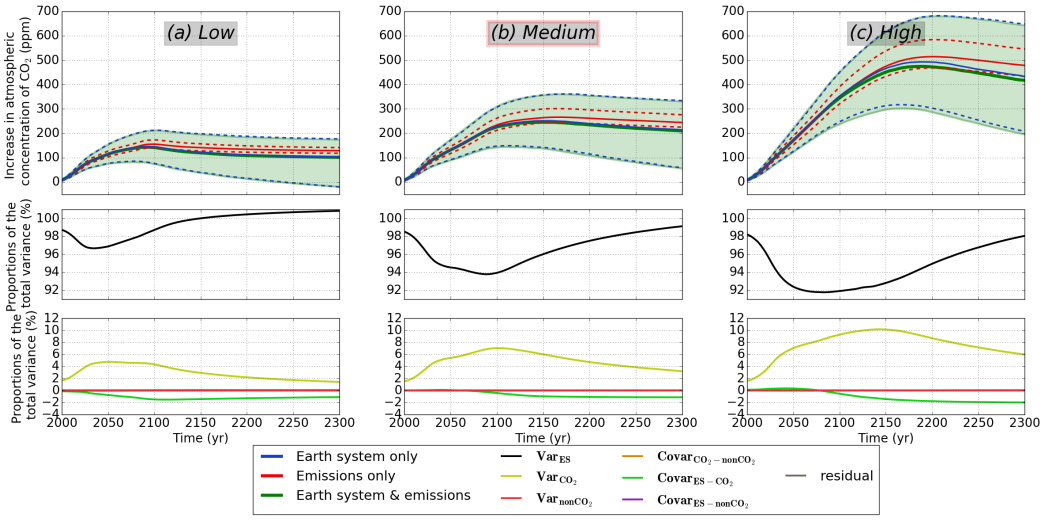

Figure 2.21: *Increase in atmospheric partial pressure of CO_2 (ppm) with reference to 1986-2005.*

For ocean surface pH, the emissions-induced uncertainty is comparable to those for atmospheric partial pressure (figure 2.22). An increase of the total variance by 3 to 6% can be expected. In terms of confidence interval, this translates in the highest scenario of extraction in 2100 as an acidification by 0.2 to 0.7 points for the Earth system response, compared to a 0.2 to 0.3 acidification for the emissions-induced uncertainty. We observe that a strong difference between the medians of those two experiments appear. In OSCAR, there is only two available options for the response of pH to the change in dissolved inorganic carbon, causing the medians to be very different. When using means and not medians, the result is closer to the response of the atmospheric concentration of CO_2 (figure 2.21). Regarding the sinks, the ocean sink has its total variance increased by 10%, whereas the land sink is relatively with

an decrease of the total variance by up to 2%, and a increase of the total variance by up to 3%. Although uncertainties in CO_2 emissions represent the major fraction of the change of the total variance, and ultimately the total uncertainty, it has a relatively low impact on the increase in global surface temperature and radiative forcing, but not for the atmospheric partial pressure.

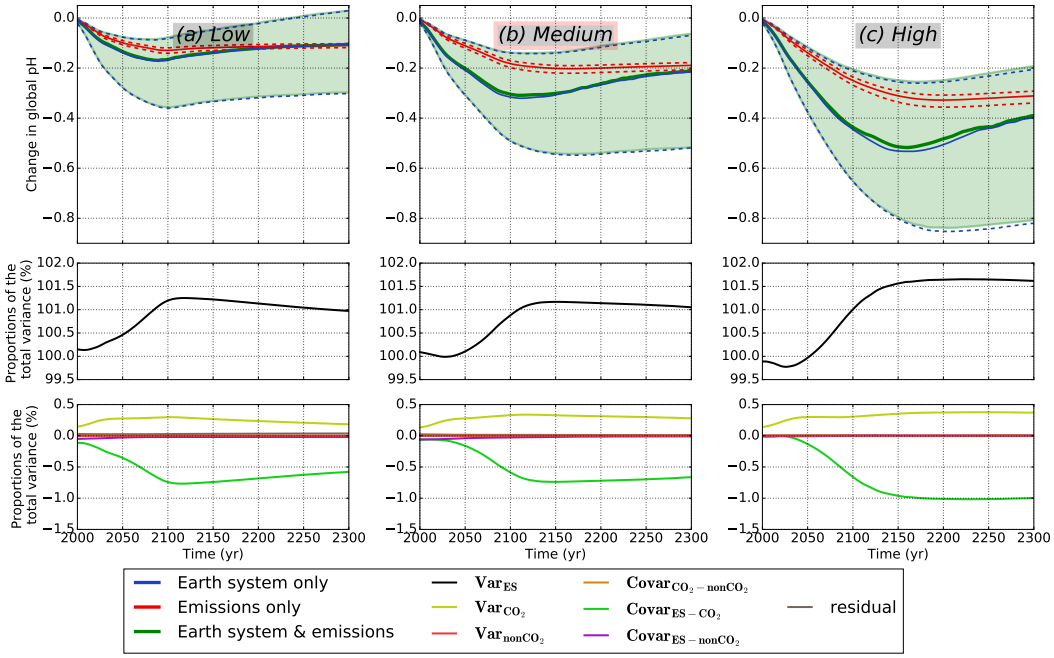

Figure 2.22: *Change in pH with reference to 1986-2005.*

Looking at the total radiative forcing (figure 2.23), emission-induced uncertainties sum up to to 2% for the scenario of extraction "Low", but 5% for the two others, principally because of the uncertainty in CO_2 emissions. The radiative forcing of CO_2 being the main contribution to the total radiative forcing, it explains the strong variances and covariances associated with CO_2 (figure 2.21). Looking at the radiative forcing associated with the aerosol-clous interaction, the emissions-induced uncertainty sum up to a maximum of 2%. However, this 2% is not high enough to be of interest, for instance for the prevision of the impact of climate change on the photovoltaic power generation (Jerez et al., 2015), because much higher uncertainties are involved.

Overall, other species tend to have smaller contributions to the total radiative forcing. The relative contributions of variances and covariances are affected by the fraction that co-emissions of a given compound represent in total emissions of this compound, and how uncertain are these co-emissions. The relative contributions are also affected by the sensitivities of these species to the increase in global surface temperature. Finally, biomass burning emissions are also affected by the uncertain-

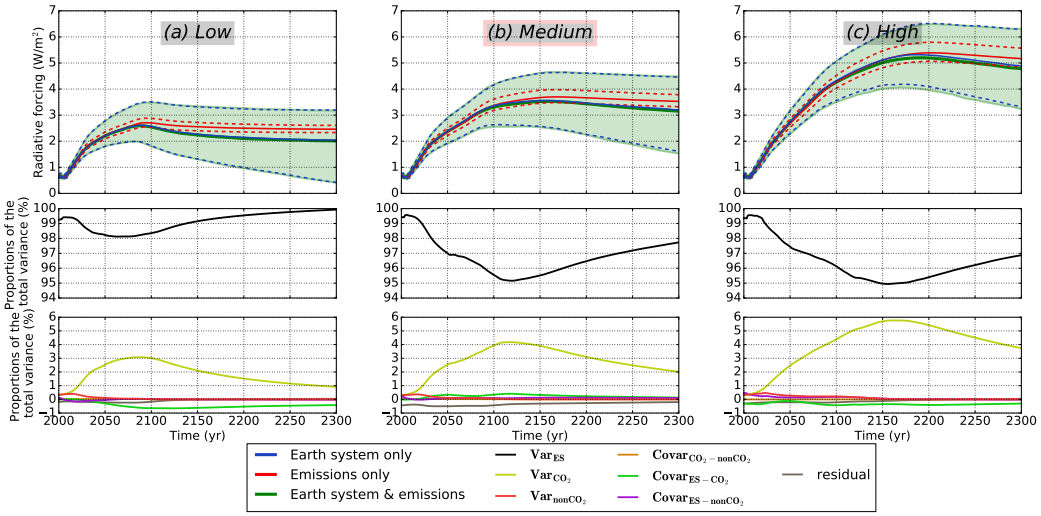

Figure 2.23: *Radiative forcing (W/m^2) with respect to 1986-2005.*

ties, be it in their modelling or in their drivers. Overall again, the co-variances of the Earth system modelling either to co-emissions or to CO_2 emissions are usually negative in the following individual radiative forcings, partially compensating the increase in the total variance caused by the variance from co-emissions.

Regarding BC, the emissions-induced uncertainty may contribute up to 9% of the total variance, occurring around 2025 in the highest scenario of extraction (figure 2.24). The stronger contribution is obviously the variance from non-CO_2 emissions, but as noted before, the covariance with the representation of the Earth system tend to compensate this variance. In the highest scenario of extraction, the variance from non-CO_2 emissions is higher, and its co-variance with the Earth system modelling is lower. We could not identify the exact origin of this change, because of the multiple interactions constituting the covariance between co-emissions and the Earth system modelling. We observe that the uncertainties in CO_2 emissions have an impact, partially through their sensitivity to global surface temperature, but especially through biomass burning emissions.

Regarding sulphated aerosols from SO_2 co-emissions, the uncertainty in their radiative forcing is changed by $\pm$ 2% because of the emissions-implied uncertainties, except in the highest scenario of extraction (figure 2.25). Here, the total variance is reduced by 2 to 6%, the covariance of CO_2 emissions with the Earth system modelling being more negative compared to other scenarios. It may be explained by the change in biomass burning emissions, or the sensitivity to global surface temperature, though, we could not identify more precisely the exact mechanism.

The total variance of the radiative forcing associated with primary organic aerosols is changed by about $\pm$ 1% when introducing the emissions-induced uncertainty (figure 2.26). Such a low contribution is caused by the strong compensation of the

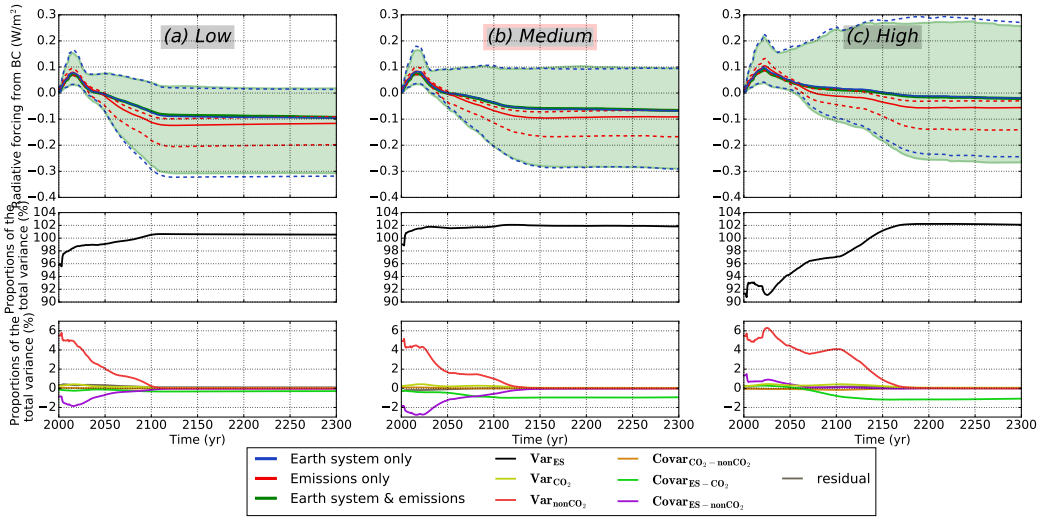

Figure 2.24: *Radiative forcing from black carbon (W/m^2) with respect to 1986-2005.*

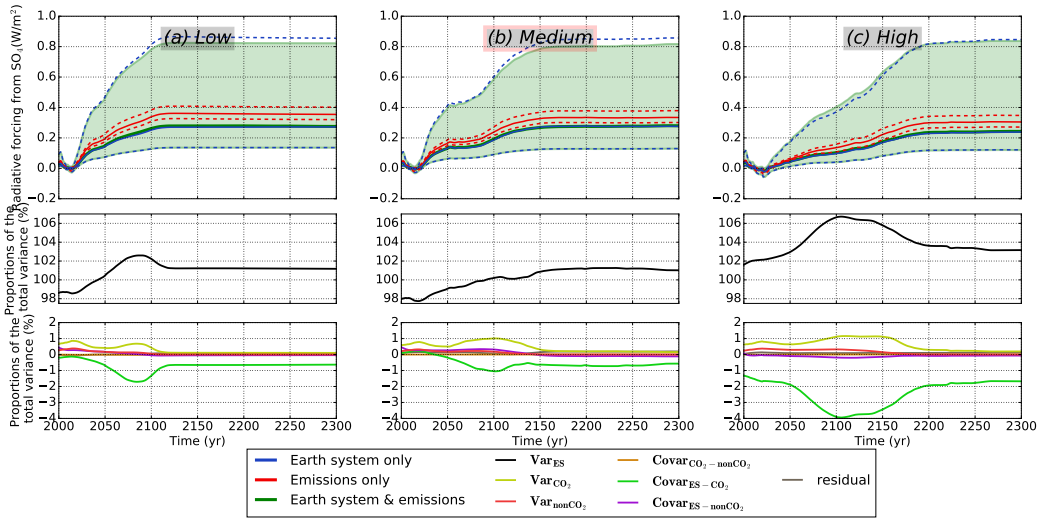

Figure 2.25: *Radiative forcing from sulphated aerosols (W/m^2) with respect to 1986-2005.*

introduced variances by the covariances.

The same results appear for the radiative forcing associated with nitrated aerosols (figure 2.27), the result of the atmospheric chemistry. In this case, the strong compensation by the covariance of CO_2 emissions with the Earth system modelling reduce the total contribution of emissions uncertainties to -0.8% to 0.4%. Like sulphated aerosols, this covariance is stronger for the higher scenario of extraction, though we could not identify the precise mechanism for this change.

For most others variables such as radiative forcings from N_2O, CH_4, secondary

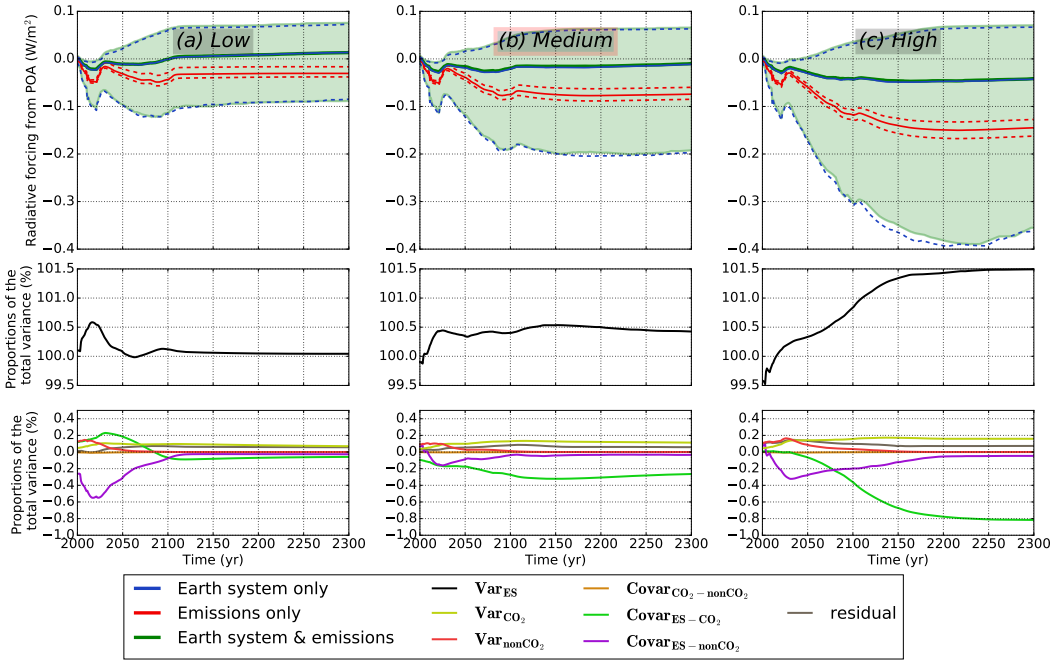

Figure 2.26: *Radiative forcing from primary organic aerosols (W/m^2) with respect to 1986-2005.*

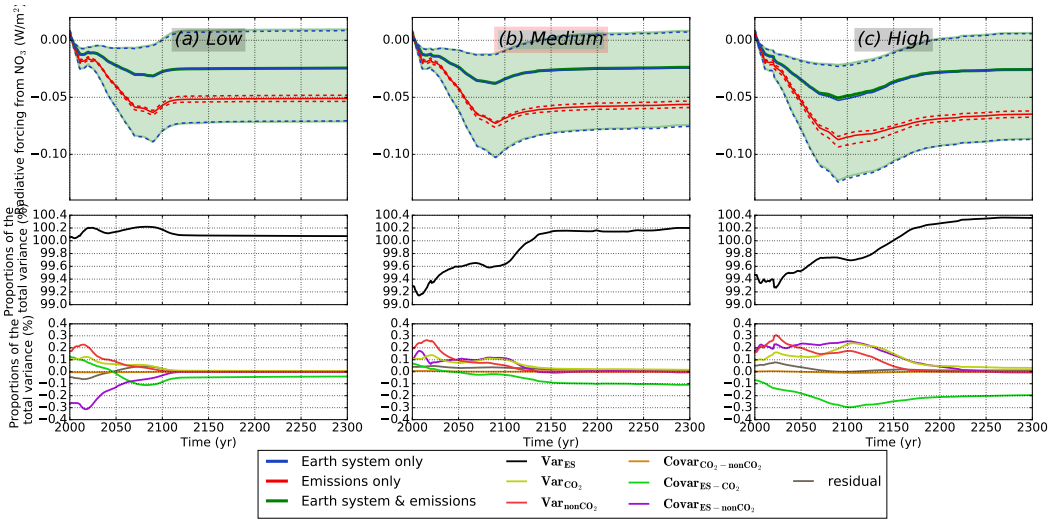

Figure 2.27: *Radiative forcing from nitrate aerosols (W/m^2) with respect to 1986-2005.*

organic aerosols, clouds, black carbon on snow and stratospheric ozone, the total contribution of the emissions-induced uncertainties is relatively weak, especially because of the compensation by covariances. The covariance of CO_2 emissions with the

Earth system representation is responsible for most of this compensation. Again, this compensation may be related to the change in the uncertainty in biomass burning emissions or in global surface temperature. Global precipitations show a relative low contribution for emissions-induced uncertainties. In terms of variance, the Earth system's response variance contributes almost to 100% to the uncertainty in global precipitations in 2100 with respect to the average for 1986-2005 (figure 2.28). In OSCAR v2.2, precipitations are written using two terms. The long term response of the hydrological cycle follows the evolution of the global surface temperature, whereas the local energy imbalance has a short term response, calculated using the atmospheric fraction of the radiative forcing (Gasser et al., 2017a). Usually, the second term partially compensates the first term. The uncertainties introduced in these two terms sum up to three main terms. The variance associated with the uncertainty in CO_2 emissions accumulates slowly over time with both the increase in global surface temperature and the radiative forcing from CO_2.Its covariance with the Earth system modelling more than compensates this variance. Finally, the covariance of the modelling of the Earth system and the non-CO_2 emissions reduces further the total variance of the system, thus its uncertainty, except in the highest scenario of extraction. Similarly, we could not identify what mechanism underlies such compensations.

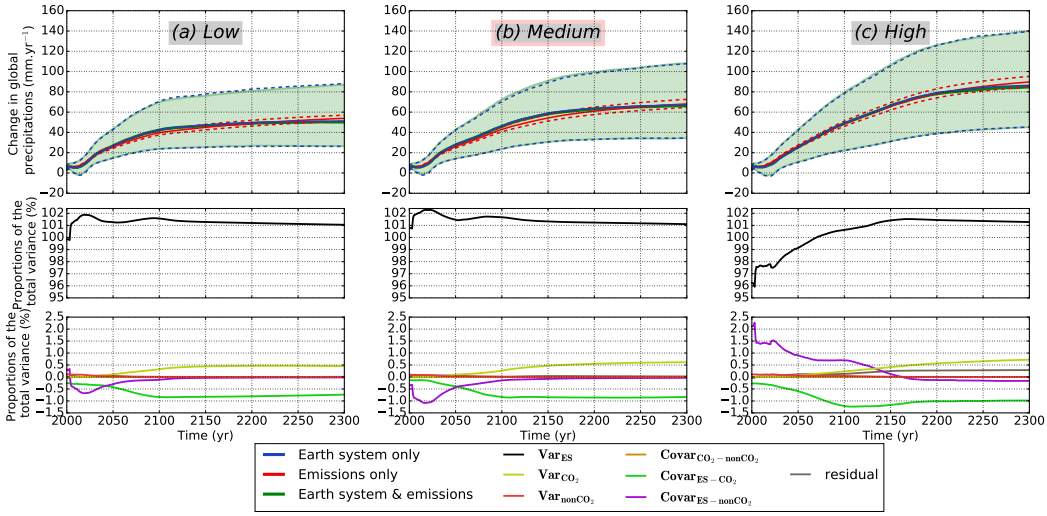

Figure 2.28: *Change in precipitations ($mm.yr^{-1}$) with respect to 1986-2005.*

The change of the radiative forcing of tropospheric ozone in 2100 with respect to the average of 1986-2005 shows as well an uncertainty less negligible. The total variance of the system is increased by up to 15%. For this variable, the emissions-implied uncertainty cannot be neglected. In terms of confidence intervals, it reaches 0.08 W/m^2, with an emissions-implied uncertainty of 0.05-0.14W/m^2 in the High scenario in 2100 (figure 2.29). It represents 43% of the uncertainty obtained with variations of all the parameters. At that time, the variance of the Earth system's

response reaches 86% of the total variance. The principal reasons for such an effect is caused by the strong variance in non-CO_2 emissions during the period where co-emissions are emitted, and then the variance in CO_2 emissions. This is due to both the change in the composition of the troposphere, and then the uncertainty in global surface temperature because of the CO_2 emissions-implied uncertainty. The radiative forcing of tropospheric ozone can be related to some extent to air quality issues (Crippa et al., 2016; West et al., 2013). As shown in Saikawa et al. (2017), uncertain emissions hamper air quality assessments. This calls for transparence and improvement of activity data and emission factors.

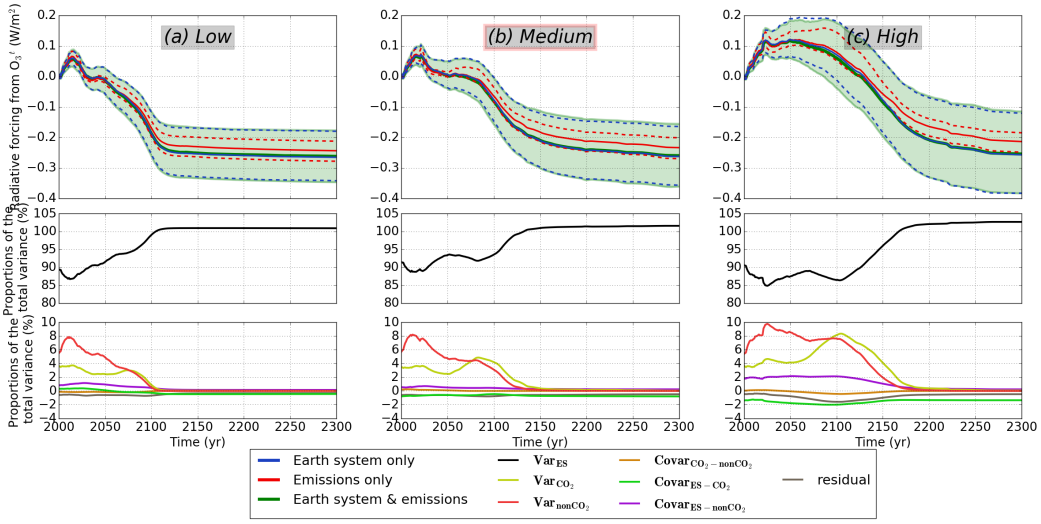

Figure 2.29: *Radiative forcing from tropospheric ozone (W/m^2) with respect to 1986-2005.*

The different contributions to the total variance of the global surface temperature ΔT show partially compensating effects between all the species and components of the Earth system. Even though we can conclude that the uncertainty of anthropogenic fossil fuel emissions does not have a significant impact on the global temperature change, this is not the case for the impacts on atmospheric CO_2, ocean acidification or air quality.

2.5 Conclusions

We produced a distribution of historical CO_2 emissions from fossil-fuels with a relative uncertainty range of $\pm 11\%$ (figure 2.14). Using broad fuel categories increase the uncertainty, because it masks the change in composition of its fuels (e.g. Hard coal, composed of anthracite, bituminous and sub-bituminous coals). Besides, the first resources depleted are conventional oil and gas and coals of good quality, leaving fossil fuels with stronger uncertainties on their carbon contents and net caloric values. Thus the relative uncertainty on fossil-fuel emissions is likely to increase with time, although the absolute uncertainty is likely to decrease with the consumptions of fossil-fuels (figure 2.15). We have also produced three distributions of emission scenarios whose uncertainty reaches 15% in 2300 for cumulative emissions, and which have been complemented with non-CO_2 co-emission scenarios calculated using top-down estimates of co-emission ratios.

With the compact Earth system model OSCAR and a Monte Carlo setup, we have projected the global temperature change induced by these scenarios (figure 2.17). The relative uncertainty in these projections ranges from 42% to 65%, and we have shown that the largest share is caused by the uncertainty in the Earth system representation and only 6% by the uncertainty of anthropogenic emissions from fossil fuel.

Our study shows that the global median temperature change induced by a given fossil fuel scenario is determined mainly by the uncertainty in the representation of the Earth system's physical processes, and only for an insignificant part by the uncertainty in the estimate of fossil fuel emissions. However, the uncertainty of the fossil fuel emissions has a significant impact on the total variance for other species-specific Earth system variables, such as the atmospheric concentration of CO_2 and the radiative forcing from tropospheric ozone. We also point out that this result may not apply locally, for variables such as precipitations.

Therefore, it remains important to keep improving the emission factors used in emission inventories. For each existing category of fuel, the carbon content and net calorific value have to be periodically updated, to account for the variation in the mix of the fuels that compose it. Factors about non-conventional fuels need particular attention; and so do non-CO_2 species (Li et al., 2017a, 2016).

Chapter 3

Climate assessment of the Shared Socio-economic Pathways scenarios

3.1 Introduction

With the Representative Concentration Pathways (RCP) and the Shared Socio-economic Pathways (SSP), a new generation of scenarios has been developed since 2010 (Moss et al., 2010). In this study, we identify gaps in the SSP public database that we fix in order to calculate the climate projections under the SSP scenarios.

Before the SSPs and RCPs, the main scenarios used by models were developed sequentially. With the SRES scenario family (Nakicenovic et al., 2000), 4 different storylines were developed, consisting in a set of hypotheses for the economic developments, populations and the technologies. One of the 4 scenarios families, the A1, was decomposed further, depending on the balance of fossil-fuel energy in the energy system. 6 Integrated Assessment Models (IAM) have used these storylines as inputs to evaluate the correspondent emissions, providing 40 scenarios. 4 of these scenarios were designated as "marker scenarios", deemed as characteristic of the 4 scenarios families. Climate models use them as inputs to calculate the climate projections under these scenarios. One of the key findings with the SRES scenarios were that equivalent levels of radiative forcing can be reached from different scenarios (IPCC, Working Group I, 2007; van Vuuren et al., 2014).

Using this result, a matrix of scenarios has been designed (van Vuuren et al., 2011a). Scenarios of land use, emissions and corresponding concentrations are designed (van Vuuren et al., 2011a). These 4 RCPs are representative of 4 levels of climate change, from the highest, the RCP8.5 (Riahi et al., 2011), to the lowest, the RCP2.6 (van Vuuren et al., 2011b). On one hand, the full extent of the climate change has already evaluated by the Climate Models (CMs) with concentrations or the Earth System Models (ESMs) with emissions (Collins et al., 2013; Meinshausen

et al., 2011b; Lamarque et al., 2011). On the other hand, the storylines SSPs were developed (O'Neill et al., 2014). Socio-economic scenarios were produced by IAMs for these storylines, and climate policies are implemented in these scenarios to reduce the emissions and reach the radiative forcings of the RCPs by 2100. The design of climate policies are harmonized using Shared Policy Assumptions (SPA, Kriegler et al. (2014)). 6 IAMs were used, 5 being marker for their SSP. The other IAMs and other economic models are used, leading to non-marker SSP scenarios (Riahi et al., 2017). Climate change and climate policies may affect the socio-economic development in the scenarios, which may lead to variations from the assumptions of the SSPs. To compute the SSP scenarios, the IAMs use the reduced-form ESM MAGICC v6 to calculate the increase in global surface temperature (van Vuuren et al., 2017; Fricko et al., 2017; Fujimori et al., 2017; Calvin et al., 2017; Kriegler et al., 2017). For the IAM IMAGE, the version of the model has been slightly adapted (van Vuuren et al., 2017). The new framework of RCPs and SSPs aims at overcoming several difficulties (van Vuuren et al., 2011a):

- The linear process of calculation of socio-economic, climate change and environmental impacts is time-consuming, which hinders their uses for climate research and policy-making. Such a parallel development is used to shorten the process.
- An increasing interest is given to adaptation strategies, which calls for their integration in the scenario families, then the storylines. Another interest is given to the evaluation of the long-term consequences of climate policies on the socio-economic system and the Earth system. It implies that for each storyline, different scenarios are developed.
- CMs have improved, not only in terms of resolution, but also in terms of modelling of the processes. The climate models have thus evolved into Earth system models, with improved projections, but with needs for more details in the scenarios.
- The junction from the historical period to the scenario had to be updated.

Thanks to this scenario matrix architecture, the socio-economic SSP scenarios converge to a limited set of radiative forcings by 2100. However, SSP scenarios have not necessarily followed the same radiative forcing pathways, leading to different evolutions of the Earth system. Besides, trades-off in the emissions could lead to equivalent total radiative forcing, but impact differently the Earth system. For these reasons, the consequences undergone by the Earth system under the SSP scenarios should be assessed. These scenarios are thus considered as a starting point for new climate change assessment (Riahi et al., 2017).

The objective of the study presented in this chapter was initially two-fold. Using the reduced-form ESM MAGICC v6, some climate insights have already been computed, namely the concentrations of the three main greenhouse gases (CO_2, N_2O

and CH_4), the radiative forcings of different agents (CO_2, N_2O, CH_4, F-gases, aerosols and others) and the increase in global surface temperature (Riahi et al., 2017; Meinshausen et al., 2011a). These climate insights may be used to relate the SSP scenarios to the climate projections under RCP scenarios produced by the ESMs. A subset of SSP scenarios is still meant to be used by the modelling teams of CMIP6 (Eyring et al., 2016a), especially through endorsed intercomparison exercises such as LUMIP (Lawrence et al., 2016) or ScenarioMIP (O'Neill et al., 2016). Yet, it is only a subset of scenarios, for the ESMs are too computation-intensive, and the SSP scenarios are too many for ESMs to calculate all of them. Just like MAGICC v6, the reduced-form ESM OSCAR v2.2 is also able to calculate the climate projections of the SSP scenarios. Furthermore, OSCAR can also provide an assessment of these scenarios for other aspects of the Earth system, that have not be provided in the SSP database. The associated uncertainties are not provided in the SSP database, but can be calculated by OSCAR. Thus, the primary objective was to propose an extensive assessment of the climate projections under SSP scenarios.

The second objective was to use the SSP scenarios as a basis to compare MAGICC v6 to OSCAR v2.2, and to identify any eventual biases in these two models. However, as described in this chapter (sections 3.2.2, 3.2.3 and 3.2.6), the SSP public database has turned out to be incomplete. Several variables that would be necessary for an accurate climate projections were missing, and the protocol used by MAGICC v6 is not detailed enough. Because of that, we have focused on the primary objective. Instead of the second objective, we propose an extension for the SSP public database. It allows an extensive assessment of the climate projections under these scenarios, helping in identifying mitigation and adaptation challenges.

We extent the scenario database concerning its land-use (section 3.2.3) and its halogenated compounds (section 3.2.2). From a more recent base year (section 3.2.6), we calculate the climate projections of these scenarios, using the reduced-form ESM OSCAR v2.2 and a Monte-Carlo setup. We account for the perturbations of the natural emissions by the climate change. Finally, we analyze the climate projections of these scenarios. We analyze the emissions of SSP scenarios (section 3.3.1), with a focus on CO_2 emissions from Land Use Change, comparing our calculations to those of the IAMs. We assess the increases in global surface temperature (section 3.3.2), the radiative forcings (section 3.3.3), the atmospheric compositions (section 3.3.4), the main features of the carbon cycle (section 3.3.5), Kaya decomposition (section 3.3.7), and the carbon budgets (section 3.3.8).

3.2 Method

3.2.1 Selection of the scenarios

The SSP scenarios are produced according to the matrix of the SSPs and the RCPs. On the first axis, 5 SSPs have been developed. On the other axis, 4 RCPs and a baseline are used. Each SSP consists in a storyline, that are presented in table

3.2. Under each storyline, each IAM produces a baseline, and produces other scenarios where the radiative forcing reaches the one of a RCP by 2100, as presented in table 3.1. To do so, the IAM implements climate policies following the Shared Policies Assumptions (SPAs, Kriegler et al. (2014)) associated with the SSP. Scenarios have been provided to the database by 6 IAMs: AIM-CGE, GCAM4, IMAGE, MESSAGE-GLOBIOM, REMIND-MagPie and WITCH-GLOBIOM. Other models (IIASA GDP, IIASA-WiC POP, NCAR, OEECD ENv-Growth, PIK GDP-32) have provided information to the database (IIASA, 2018c). We keep only the scenarios produced by the IAMs AIM-CGE, GCAM4, IMAGE, REMIND-MagPie, MESSAGE-GLOBIOM and WITCH-GLOBIOM (table 3.3). As a remark, these 6 IAMs have only partially covered the matrix of scenarios. Because the RCP8.5 already matches or exceeds the level of radiative forcing obtained for the baselines of the more pessimistic SSPs, this RCP was not an appropriate target. Another target was also introduced, called "RCP3.4" to fill the gap in-between RCP2.6 and RCP4.5. Just like other RCPs, 3.4 stands here for 3.4W/m^2 at the end of the 21st century. We retrieve a total of 103 scenarios, as summarized in table 3.1.

	AIM	GCAM4	IMAGE	MESSAGE	REMIND	WITCH
SSP1-Baseline	Y	Y	M	Y	Y	Y
SSP1-RCP6.0	NR	NR	NR	NR	NR	NR
SSP1-RCP4.5	Y	Y	M	Y	Y	Y
SSP1-"RCP3.4"	Y	Y	**M**	Y	**Y**	Y
SSP1-RCP2.6	**Y**	**Y**	**M**	**Y**	**Y**	Y
SSP2-Baseline	Y	Y	Y	M	Y	Y
SSP2-RCP6.0	Y	Y	Y	M	Y	Y
SSP2-RCP4.5	Y	Y	Y	M	Y	Y
SSP2-"RCP3.4"	Y	Y	Y	M	Y	Y
SSP2-RCP2.6	**Y**	**Y**	**Y**	M	**Y**	NR
SSP3-Baseline	M	Y	Y	Y	NR	Y
SSP3-RCP6.0	M	NR	Y	Y	NR	Y
SSP3-RCP4.5	M	NR	Y	Y	NR	Y
SSP3-"RCP3.4"	M	NR	Y	Y	NR	Y
SSP3-RCP2.6	N	NR	N	N	NR	N
SSP4-Baseline	Y	M	NR	NR	NR	Y
SSP4-RCP6.0	NR	M	NR	NR	NR	Y
SSP4-RCP4.5	Y	M	NR	NR	NR	Y
SSP4-"RCP3.4"	Y	M	NR	NR	NR	Y
SSP4-RCP2.6	**Y**	**M**	NR	NR	NR	Y
SSP5-Baseline	Y	Y	NR	NR	M	Y
SSP5-RCP6.0	Y	Y	NR	NR	M	Y
SSP5-RCP4.5	Y	Y	NR	NR	M	Y
SSP5-"RCP3.4"	Y	**Y**	NR	NR	**M**	Y
SSP5-RCP2.6	Y	**Y**	NR	NR	**M**	N

Table 3.1: *Scenarios retrieved from the 6 IAMs for the SSPs and RCPs. Available scenarios are in green and marked with Y. Available scenarios from the IAM marker are in blue and marked with M. Scenarios for which the IAM could not provide a solution are in red and marked with N. Scenarios that have not been run are in gray and marked with NR. If a scenario presents an overshoot greater or equal to 0.4W/m^2, the cell is* ***highlighted****. This table is inspired from the table 2 of the supplementary material of Riahi et al. (2017).*

SSP1	**Sustainability – Taking the Green Road (Low challenges to mitigation and adaptation)** The world shifts gradually, but pervasively, toward a more sustainable path, emphasizing more inclusive development that respects perceived environmental boundaries. Management of the global commons slowly improves, educational and health investments accelerate the demographic transition, and the emphasis on economic growth shifts toward a broader emphasis on human well-being. Driven by an increasing commitment to achieving development goals, inequality is reduced both across and within countries. Consumption is oriented toward low material growth and lower resource and energy intensity.
SSP2	**Middle of the Road (Medium challenges to mitigation and adaptation)** The world follows a path in which social, economic, and technological trends do not shift markedly from historical patterns. Development and income growth proceeds unevenly, with some countries making relatively good progress while others fall short of expectations. Global and national institutions work toward but make slow progress in achieving sustainable development goals. Environmental systems experience degradation, although there are some improvements and overall the intensity of resource and energy use declines. Global population growth is moderate and levels off in the second half of the century. Income inequality persists or improves only slowly and challenges to reducing vulnerability to societal and environmental changes remain.
SSP3	**Regional Rivalry – A Rocky Road (High challenges to mitigation and adaptation)** A resurgent nationalism, concerns about competitiveness and security, and regional conflicts push countries to increasingly focus on domestic or, at most, regional issues. Policies shift over time to become increasingly oriented toward national and regional security issues. Countries focus on achieving energy and food security goals within their own regions at the expense of broader-based development. Investments in education and technological development decline. Economic development is slow, consumption is material-intensive, and inequalities persist or worsen over time. Population growth is low in industrialized and high in developing countries. A low international priority for addressing environmental concerns leads to strong environmental degradation in some regions.
SSP4	**Inequality – A Road Divided (Low challenges to mitigation, high challenges to adaptation)** Highly unequal investments in human capital, combined with increasing disparities in economic opportunity and political power, lead to increasing inequalities and stratification both across and within countries. Over time, a gap widens between an internationally-connected society that contributes to knowledge- and capital-intensive sectors of the global economy, and a fragmented collection of lower-income, poorly educated societies that work in a labor intensive, low-tech economy. Social cohesion degrades and conflict and unrest become increasingly common. Technology development is high in the high-tech economy and sectors. The globally connected energy sector diversifies, with investments in both carbon-intensive fuels like coal and unconventional oil, but also low-carbon energy sources. Environmental policies focus on local issues around middle and high income areas.
SSP5	**Fossil-fueled Development – Taking the Highway (High challenges to mitigation, low challenges to adaptation)** This world places increasing faith in competitive markets, innovation and participatory societies to produce rapid technological progress and development of human capital as the path to sustainable development. Global markets are increasingly integrated. There are also strong investments in health, education, and institutions to enhance human and social capital. At the same time, the push for economic and social development is coupled with the exploitation of abundant fossil fuel resources and the adoption of resource and energy intensive lifestyles around the world. All these factors lead to rapid growth of the global economy, while global population peaks and declines in the 21st century. Local environmental problems like air pollution are successfuly managed. There is faith in the ability to effectively manage social and ecological systems, including by geo-engineering if necessary.

Table 3.2: *Summary of SSPs narratives, from Riahi et al. (2017).*

IAM	AIM-CGE	GCAM4	IMAGE	MESSAGE -GLOBIOM	REMIND -MagPIE	WITCH -GLOBIOM
Marker for	SSP3	SSP4	SSP1	SSP2	SSP5	
Emissions	yes	yes	yes	yes	yes	yes
Land Cover	yes	yes	yes	*no* (3.2.3.2)	yes	**no** (3.2.3.2)
Prim. bioenergies						
→ **Traditional**	**no** (3.2.3.4)	yes	yes	yes	yes	**no** (3.2.3.4)
→ **Without CCS**	yes	yes	yes	yes	yes	yes
→ **With CCS**	*yes*	yes	yes	yes	yes	yes

Table 3.3: *Availability of different categories of variables in the public SSP database (IIASA, 2018c). Where this category of variable is not available at all,* ***no*** *is written. Where it is only partially missing, no is written. In both cases, the refered section provides more information for the corresponding treatment. "Prim. bioenergies" stands for Primary biomass energies. CCS stands for Carbon Capture and Storage. Emissions are used within OSCAR, Land Cover is translated into net Land Use Change (section 3.2.3.1) and primary biomass energy are used to evaluate harvest and shifting cultivations (section 3.2.3.4 and 3.2.3.3).*

As a remark, all variables are provided in the SSP database with a 10 years step, except for the first time step (2005, 2010, 2020, 2030,... 2100). We use a linear interpolation for each one of the variables of each scenario to get an annual resolution. We acknowledge that the direct outputs of these IAMs, that may have annual resolutions, do not show linear evolution over these steps. Yet, other interpolation techniques (e.g. splines) would not ensure the consistency of the scenario, for instance concerning the carbon balance. For this reason, linear interpolations are likely to reduce biases in climate and atmospheric composition changes.

3.2.2 Halogenated compounds

Fluorinated gases are provided by the IAMs as a single category, called F-Gases, expressed in CO_2eq/yr. However, OSCAR uses 37 halogenated compounds, and their emissions need to be provided over the period of the scenarios. To do so, we assume that the list of fluorinated agents listed in the category F-Gases corresponds to the compounds containing fluorine provided in the RCPs emissions (Meinshausen et al., 2011b; IIASA, 2018b). Thus, we decompose these emissions into emissions of 7 hydrofluorocarbons (HFC), namely HFC-23, HFC-32, HFC-125, HFC-134a, HFC-143a, HFC-227ea and HFC-245fa ; three perfluorocarbons (PFC), namely CF_4, C_2F_6 and C_6F_14 ; and SF_6. Other compounds are taken either as the emissions of the RCP targeted or as zero if not provided by the RCPs. It concerns 4 HFCs, 5 PFCs, NF_3 and 16 ozone-depleting substances (ODS), as lumped below.

1. Emissions from the decomposition of the category F-Gases of SSPs scenario:
    - HFC: HFC-23, HFC-32, HFC-125, HFC-134a, HFC-143a, HFC-227ea, HFC-245fa

- PFC: CF_4, C_2F_6 and C_6F_14
- SF_6

2. Emissions dependent of the RCP, then applied according to the RCP targeted for each SSP scenario:
   - ODS: HCFC-22, HCFC-141b
3. Emissions independent of the RCP, applied identically for all SSP scenarios:
   - ODS: CFC-11, CFC-12, CFC-113, CFC-114, CFC-115, CCl_4, CH_3CCl_3, HCFC-142b, Halon-1211, Halon-1202, Halon-1301, Halon-2402, CH_3Br, CH_3Cl
4. Emissions not provided by the RCPs, set to 0:
   - HFC: HFC-152a, HFC-236fa, HFC-365mfc, HFC-43-10mee
   - PFC: C_3F_8, cC_4F_8, C_4F_10, C_5F_12, C_7F_16
   - NF_3

As a remark, HFC-43-10mee is provided by the RCPs according to Meinshausen et al. (2011b), but is not available in the RCP database (IIASA, 2018b).

Concerning the decomposition used for the first group of halogenated compounds, we use the Global Warming Potential (GWP) at 100 years of the AR5. For each scenario SSP, we calculate the CO_2eq for the F-gases of the corresponding RCP F^{RCP}. To do so, we use the emissions E_X^{RCP} of each fluorinated gas X (category 1 of the list above) and their GWP-100yrs g_X (equation 3.1). We decompose F^{SSP} using F^{RCP}, as illustrated in equation 3.2. In this equation, emissions are sum over the regions. Thus, the regional fractions of emissions follow those of the RCPs, and not those of the SSPs. Yet, it avoids to break the continuity in emissions at the transition. This treatment is a mere decomposition, and no rescale. The rescale of the resulted SSPs emissions of F-gases and other halogenated compounds is done as explained in section 3.2.6.

$$F^{RCP} = \Sigma_X g_X E_X^{RCP} \tag{3.1}$$

$$E_{X,t}^{SSP} = E_{X,t}^{RCP} \frac{F_t^{SSP}}{F_t^{RCP}} \tag{3.2}$$

As showed in the equation 3.2, the emissions of the first group of halogenated compounds are deduced from a decomposition of the emissions of a RCP scenario. The choice of the corresponding RCP scenario depends on the SSP scenario. For a scenario run by an IAM under SSP storyline targeting the radiative forcing of a RCP, we use this RCP as the reference for the decomposition of halogenated compounds.

For baselines, we use the total radiative forcing of the marker for this SSP-Baseline (Riahi et al., 2017) and deduce which RCP applies. For a scenario SSP1-Baseline, we use the mean of the RCP4.5 and RCP6.0. For a scenario SSP2-Baseline or SSP3-Baseline, we use the mean of the RCP6.0 and RCP8.5. For a SSP4-Baseline, we use the RCP6.0. For a SSP5-Baseline, we use the RCP8.5. For the second group of halogenated compounds, no decomposition is used, and we use directly the emissions of the corresponding RCP.

The emissions of fluorinated gases are represented in the results, section 3.3.1.6. For the sake of intelligibility, only the SSP scenarios under the storyline SSP1 are showed in the figure 3.15. The results under the other storylines are given in appendix (section 6.2.2).

3.2.3 Land Use

3.2.3.1 Principle of the treatment of Land Cover from SSPs

To begin with, the IAMs report land cover along with CO_2 emissions from Land Use Change (LUC). The climate insights reported in the SSP database have been produced with MAGICC v6, running directly the CO_2 emissions from LUC reported by the IAMs. It would be possible to use these inputs, but we highlight several obstacles here.

The terrestrial biosphere undergoes two perturbations. The first corresponds to extensive perturbations, driven by land use, land management change and forestry, shorten here in LUC. The second corresponds to the combination of intensive perturbations, affecting the local properties of the terrestrial biosphere, for instance through the increase in atmospheric CO_2, the increase of nitrogen deposition and the climate change (Ciais et al., 2013). It results from these perturbations carbon fluxes between the terrestrial biosphere and the atmosphere. Two terms are usually written for these fluxes: the first corresponds to the CO_2 emissions from LUC, and the second one corresponds to the land sink. Usually, they are respectively positive and negative from the biosphere to the atmosphere. However, the definitions may differ depending on the models used (Gasser and Ciais, 2013). If the CO_2 emissions from LUC used in a simple climate model such as MAGICC or OSCAR are calculated by an IAM under a definition that is not the one used in the climate model, the land sink has to be adapted. The modelling of the terrestrial carbon cycle remains uncertain, and so are the land carbon sink and the CO_2 emissions from LUC. Prescribing these emissions to the climate model implies an artificial reduction of the uncertainties of the Earth system.

We are unsure of what definition or calculation has been used for the CO_2 emissions from LUC in the IAMs. We are also unsure of the feedbacks from climate change that are effectively included in their calculation. As a non-exhaustive list of the feedbacks between the terrestrial biosphere and the climate system, the following effects can be enumerated:

1. increase of the net primary productivity (NPP) through fertilization by CO_2 (Friedlingstein et al., 1995)
2. increase of the NPP through nitrogen fertilization and impact of local climate (Thornton et al., 2007; Friedlingstein et al., 2006)
3. impact of local climate on the heterotrophic respiration in soils and litters (Tuomi et al., 2008)
4. impact of local climate on the mortality of living biomass (Anderegg et al., 2013)
5. change in fire intensities (Van Der Werf et al., 2010)
6. perturbation of the nitrogen cycle (Wieder et al., 2015) and the phosphorus cycle (Goll et al., 2012)
7. decrease of wetlands emissions because of the increase in sulfur deposition (Gauci et al., 2004)
8. decrease of the CO_2 uptake of vegetation because of the increase in tropospheric ozone (Sitch et al., 2007)
9. migration of biomes because of changes in local climate (Jones et al., 2009)

Other processes affect the CO_2 fluxes of the terrestrial biosphere, such as the agricultural practices (Pugh et al., 2015), which increase further the complexity of their evaluation. The perturbation of the net flux of CO_2 between the biosphere and the atmosphere is usually broken down into two components: the emissions from LUC and the land sink. Yet, several definitions coexist in the literature, which may lead to relative differences in estimates up to 20% (Gasser and Ciais, 2013). As such, CO_2 emissions from LUC and the land sink come with an uncertainty (Friedlingstein et al., 2014a; Arneth et al., 2017), either because of the definition or because of the uncertainty in the modelling. A robust evaluation of these fluxes requires an extensive assessment (Le Quéré et al., 2016).

We summarize the following analysis in table 3.4, based on the description papers of the SSP scenarios, on the short description of the models made available for SSPs (SSP, 2018), Popp et al. (2017), and on the available documentation for this model. As a remark, some IAMs may have capacities, that may not be implemented, for the sake of the SSP scenarios. For instance, IMAGE has cut off most of its feedbacks from climate change, with the exception of climate change and CO_2 concentration on natural vegetation. In this sense, IMAGE is inconsistent with the others IAMs. According to the literature, the CO_2 emissions from LUC calculated by the IAMs for the SSP scenarios are calculated either with models or integrated methods, such as GCAM4 or AIM-CGE. Some integrate feedbacks from CO_2 fertilization or the impact of climate change whereas others do not. As a remark, some IAMs distinguish

primary and secondary forests, or different sets of agricultural practices, whereas others use implicit representations.

We decide to use the calculation of CO_2 emissions from LUC by OSCAR rather than those of the IAMs. By using the calculation in OSCAR, we make sure that these emissions and the land sink are consistent in terms of definitions. It allows us as well to account for the uncertainty of the modelling of the terrestrial carbon cycle, but also for the feedbacks integrated in OSCAR v2.2 (Gasser et al., 2017a). The dependency in local surface temperatures, local precipitations and atmospheric CO_2 are accounted in an ensemble of mechanisms, using the net primary productivity, the mortality or the heterotrophic respiration, between different carbon pools (vegetation, litter, soil). OSCAR is calibrated on the latest intercomparison exercises (CMIP5, ACCMIP, TRENDY, CCMVal2, WETCHIMP). All details can be found in Gasser et al. (2017a).

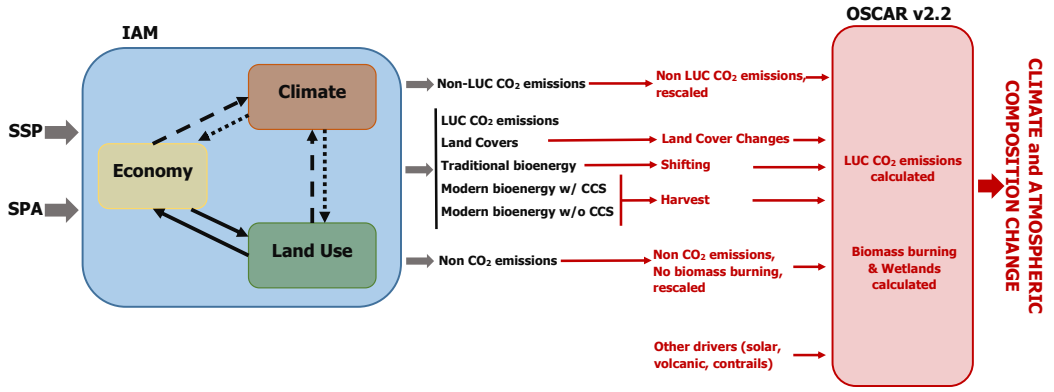

Figure 3.1: *Simplified representation of the treatment of the database, with a focus over land use variables. The SSPs narratives are combined to the SPAs in IAMs (left, blue box), producing the variables present in the SSPs database (middle, in black). These variables are treated (middle, in red) for use in OSCAR v2.2 (right, red box), for calculation of the climate projections. As a remark, these variables are provided at a regional scale in the SSP public database (table 6.6).*

For the reasons presented in this section, we use OSCAR to calculate the CO_2 emissions from LUC, using a reconstruction of the required land variables. As described in figure 3.1, land cover from IAMs are transformed into land cover changes as described in the section 3.2.3.2 ; area extents of shifting cultivations (simultaneous expansion and abandonment of pastures and croplands) are deduced for each SSP scenario as described in the section 3.2.3.4 ; harvested biomass are deduced for each SSP scenario as described in the section 3.2.3.3 ; CO_2 emissions from LUC are evaluated with OSCAR as described in the section 3.2.3.5. Wetlands and biomass burning emissions are then calculated with OSCAR, to ensure the internal consistency, as described in the section 3.2.6.

IAM	SSP	For SSP:	For IAM:	Used for LUC emissions	Climate feedbacks accounted?	Practices & Forests
IMAGE	1	van Vuuren et al. (2017)	Stehfest et al. (2014)	LPjML Bondeau et al. (2007) MAGNET Woltjer et al. (2014)	Yes van Vuuren et al. (2017)	Explicit Stehfest et al. (2014)
MESSAGE -GLOBIOM	2	Fricko et al. (2017)	Krey et al. (2016) MESSAGE (2018)	G4M Kindermann et al. (2006) GLOBIOM Havlík et al. (2011)	No Fricko et al. (2017)	Explicit MESSAGE (2018)
AIM-CGE	3	Fujimori et al. (2017)	AIM/CGE (2018)	Change in carbon density & forest area Fujimori et al. (2014)	No Fujimori et al. (2017) Hasegawa et al. (2017)	Agriculture: no Hasegawa et al. (2017) Forests: yes. AIM/CGE (2018)
GCAM4	4	Calvin et al. (2017)	Calvin et al. (2011) GCAM (2017)	Change in global terrestrial carbon stock Wise et al. (2014)	No? Calvin et al. (2017) Wise et al. (2014)	Implicit Calvin et al. (2011) Wise et al. (2014)
REMIND -MagPIE	5	Kriegler et al. (2017)	Luderer et al.	LPjML Bondeau et al. (2007) MagPIE Lotze-Campen et al. (2008)	No? Kriegler et al. (2017) Luderer et al.	Agriculture: no Lucas et al. (2007) Forests: yes Bondeau et al. (2007)
WITCH -GLOBIOM			Bosetti et al. (2006) Bosetti et al. (2009)	GLOBIOM Havlík et al. (2011)	No Bosetti et al. (2009)	Explicit Havlík et al. (2011)

Table 3.4: *Summary of our conclusions regarding the CO_2 emissions from LUC calculated by the IAMs involved in the SSP database. We provide as much as possible the sources that we have used, along with IIASA (2018d), SSP (2018) and Popp et al. (2017). CO_2 emissions from LUC may be calculated within IAMs either by models or using integrated methods, as in AIM-CGE and GCAM4. In the column "Climate change feedbacks", we report our conclusions for the SSP scenarios as much as possible given the information provided. Otherwise, our conclusions are based on the documentation of the model. The column "Practices & Forests" is here to inform about the modelling of agricultural practices and the differentiation made between primary and secondary forests.*

3.2.3.2 Land Use Change

The land cover of the SSP scenarios is provided for 5 land-cover classes (Popp et al., 2017), that we match to one of the compatible descriptions of biomes of OSCAR (Gasser et al., 2017a), as described in table 3.5. As a remark, OSCAR uses a limited number of biomes. The parameters relative to the terrestrial biosphere are calibrated on more complex models, with different representations of the terrestrial biosphere. Using a limited number of biomes and rules to bring the representations of these models to these biomes, it allows OSCAR to emulate their behavior (Gasser et al., 2017a). We acknowledge that aggregating biomes may introduce errors, for instance by grouping primary and secondary forest, yet OSCAR is calibrated using the TRENDY data (Sitch et al., 2015) and CMIP5 data (e.g. Friedlingstein et al. (2014b) and Arora et al. (2013)), and using an adequate weighting method for aggregating the plant functional types in biomes. This method improves the capacity of OSCAR to emulate the terrestrial biosphere, in spite of the aggregations.

The aggregation of the biomes of the IAMs into 5 broad categories also introduces errors as well. For instance, "Other Natural Lands" may include deserts, as done with REMIND-MagPIE (Kriegler et al., 2017). Thus, a fraction of this land cover, and thus its transitions, should be associated with the biome of OSCAR "Bare soils: deserts". Although identifying the fraction of the land cover is possible, we could not identify the transitions associated with deserts within "Other Natural Lands". We choose to associate this category as a whole to the biome "Grasslands and Shrublands" of OSCAR, for this solution is expected to have lower consequences.

Land Cover of IAMs in the SSPs	**Biomes of OSCAR v2.2**
Built-up	Bare soils: urban areas
	Bare soils: deserts
Forest	Forests
Cropland	Croplands
Pasture	Pastures
Other Natural Lands	Grasslands
	Shrublands

Table 3.5: *Matching of the 5 categories of land cover of SSPs to the biomes of OSCAR v2.2. Primary and secondary forests are both included in "Forest".*

The land cover of the biomes are provided for each one of the 5 world regions as detailed in table 6.6 in appendix (section 6.2.1).

As shown in table 3.3, MESSAGE-GLOBIOM does not provide the area extent for the biome Built-up & Desert. Because the total area of the other biomes remains constant along time in the scenarios produced using MESSAGE-GLOBIOM, it appears that this biome is not explicitly represented (Fricko et al., 2017) in MESSAGE-GLOBIOM. Even though this biome had been represented, the sum of the area extents of the other biomes remains constant. This is why we consider the change in

Land Cover for this biome to remain constant.

As mentioned in table 3.3, WITCH-GLOBIOM reports no land cover for any of its scenarios. To compensate for this lack of data, two solutions may be considered. This IAM uses the same land-use model than MESSAGE-GLOBIOM, thus the scenario SSP having for target a given RCP under MESSAGE-GLOBIOM could replace the missing land cover for WITCH-GLOBIOM for the same scenario. The other solution is to use the land cover of the IAM marker of the SSP for the land cover of WITCH-GLOBIOM. The second solution has been chosen, because WITCH-GLOBIOM has provided results for the scenario SSP4 and SSP5, whereas MESSAGE-GLOBIOM has provided none of the SSP4 and SSP5.

The figure 3.2 shows the change in land cover for the 5 biomes with reference to 2005 for the SSP scenarios over 2005-2100. For the sake of intelligibility, only scenarios using SSP1 are shown, and only at a global scale. The other SSP scenarios are represented at a regional scale in the figures in appendix (section 6.2.3). Over 2005-2010, the change in area extents of the biomes are comparable to those of the Land Use Harmonization dataset (LUH) v1.1 (Hurtt et al., 2011). The trends are relatively consistent over 1960-2005 and the beginning of the scenarios, except for the built-up area. The only IAM that does not present a constant area for this biome is IMAGE, independently of the scenario. Because the land cover of this IAM marker is used for WITCH-GLOBIOM, this IAM also shows variations in the land cover of the built-up area. Most of the scenarios show an increase in the afforested area. Middle-East and Africa tends to be much more scenario-dependent. In most of the scenarios and most of the regions, a global increase in the cropland area is projected, with a global decrease in the pasture area. The grassland & shrubland area shows trends more dependent of the scenarios and the regions. In this figure, we also notice that the scenarios can be grouped depending on the IAM used. In other words, under the SSP1, changes in area extents of the biomes depend primarily on the IAM used, and then on the forcing target of the scenario. Comparing to other SSPs (figures in appendix section 6.2.3), the major determinant is the SSP storyline, the second is the IAM and the third is the forcing target.

In OSCAR, variables related to the land cover and the land uses are used for the carbon cycle and the change in albedo from land-cover change. However, the sole area extents for the 5 biomes are not enough for an accurate estimate of the fluxes in the biosphere. Transitions between biomes are not equivalent in regard of the biogeochemical cycles (Ciais et al., 2013), implying that transitions in terms of land use change are required. Besides, the harvest of biomass in a biome does not affect the land cover, but affects the net primary productivity. Finally, reciprocal transitions between biomes affect also the biogeochemical cycles. For instance, transforming 10% of the area of a region from forest into croplands and pastures, but 10% of the same region from croplands and pastures to forest in the meantime, will affect the carbon stocks and fluxes in the region, that is to say, the carbon cycle. In OSCAR, three variables are required (Gasser et al., 2017a):

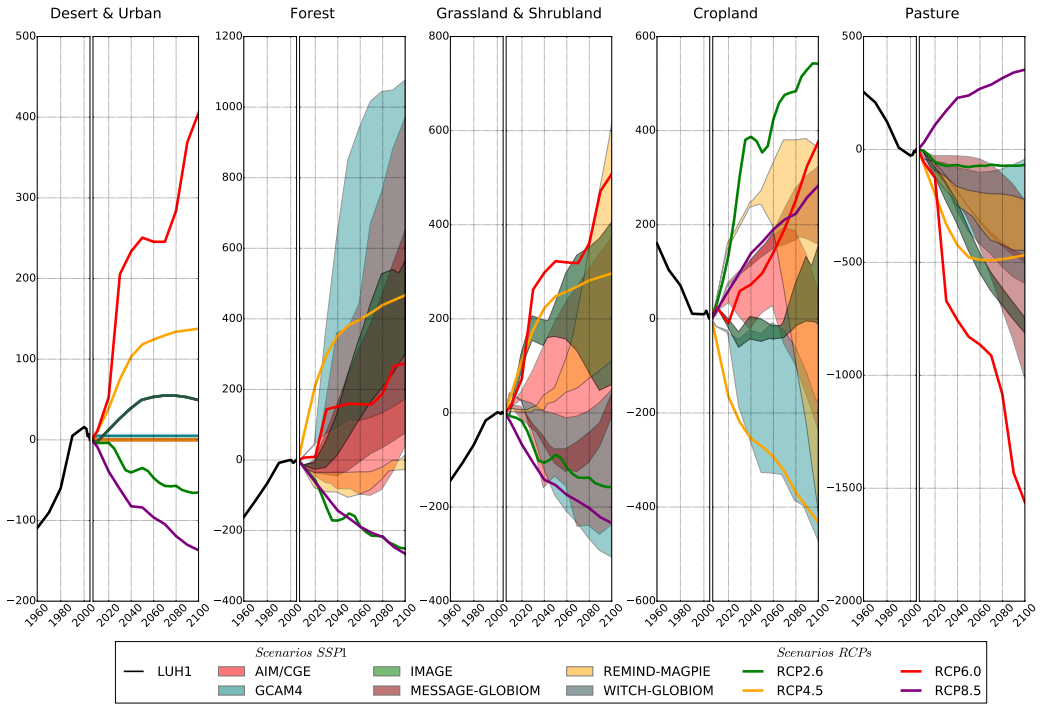

Figure 3.2: *Change in area extent of the 5 biomes (**Mha**) with reference to 2005 for the SSP scenarios under the storyline SSP1 over 2005-2100, and under different RCPs. For the sake of clarity, the area extents are summed over the regions, and given only for SSP1 scenarios. However, the regional detail is provided for each SSP in appendix (section 6.2.3). The area extents over 1960-2010 and for the RCPs scenarios are shown for comparison, prescribed by the Land Use Harmonization dataset v1.1 (Hurtt et al., 2011). For the SSP scenarios (shaded areas), the color corresponds to the IAM that has produced the corresponding scenario. For the RCPs scenarios (plain lines), similar colors may be used if and only if the IAM used to produce the RCP is the same: IMAGE has been used for RCP2.6, MiniCAM (now GCAM4) for RCP4.5, AIM for RCP6.0 and MESSAGE for RCP8.5 (IIASA, 2018b).*

- Land use change: matrix LUC of the gross human-induced transitions of areas between biomes $lcc^{b_1 \to b_2}$ (Mha/yr)
- Harvested biomass: vector H of the extractions of woody biomass from each biome h^{b_1}, without change in land cover (GtC/yr)
- Area extents for shifting cultivations: matrix S of the transitions between biomes occurring reciprocally $s^{b_1 \leftrightarrow b_2}$ (Mha/yr). Because of the simultaneous transitions, the land cover undergoes no net change.

We explain the way that shifting and harvest drivers are estimated for each

scenario SSP in the sections 3.2.3.4 and 3.2.3.3.

According to Popp et al. (2017), the assessment of gross land use change is planned in the future phases of the scenario development. The evaluation of these detailed transitions is meant to be included with the Land Use Harmonization 2 dataset (LUH2, LUH2 (2018)), along with the extension of LUH1 (Hurtt et al., 2011). In support of the Land Use Model Intercomparison Project (LUMIP, Lawrence et al. (2016)) and the Scenario Model Intercomparison Project (ScenarioMIP, O'Neill et al. (2016)), 6 SSP scenarios have been treated: SSP1-2.6 (IMAGE), SSP2-4.5 (MESSAGE-GLOBIOM), SSP3-7.0 (AIM-CGE), SSP4-3.4 (GCAM4), SSP4-6.0 (GCAM4) and SSP5-8.5 (REMIND-MagPIE). Because only 6 scenarios among the 103 selected are available, we cannot use this treatment in this chapter. Instead, we use the algorithm from Stocker et al. (2014) to transform land cover into net land use changes, and compare its results to the 6 SSP scenarios processed in LUH2 (section 3.4.2). This algorithm aims at reproducing net transitions between biomes using priorities in transitions. Ideally, land use changes should be studied through gross transitions, that is to say accounting for transitions from one biome to another and reciprocally (bidirectional), and not net transitions (unidirectional), that is to say accounting only for differences. The use of gross transitions is motivated by the impact on the net primary productivity of the biosphere (Li et al., 2017b). Yet, according to Stocker et al. (2014), traditional land use maps provide only net changes. For lack of a better alternative, we produce net land use change at the regional scale.

Following Stocker et al. (2014), we introduce the priorities of transition described in table 3.6. In our case, the first transition is from the biome Forest to the biome Cropland. At a given year, if either the land cover of the Cropland area decreases, or the land cover of the Forest increases, no net transition from Forest to Cropland is possible. If the land cover of Forest decreases whereas the land cover of the Cropland increases, the land cover change from Forest to Cropland would be equal to the minimal transition to bring one of these two to zero. For instance, if the Cropland area increases twice as much the Forest area decreases, the transition from Forest to Cropland is equal to the change in Forest area, but this transition does not fully explain the extent of the increase in Cropland area. The same process is repeated for each transition by order of priority.

From ↓ to →	**Urban & Desert**	**Forest**	**Grassland & Shrubland**	**Cropland**	**Pasture**
Urban & Desert	-	16	19	4	8
Forest	10	-	20	1	6
Grassland & Shrubland	9	13	-	2	5
Cropland	12	15	18	-	7
Pasture	11	14	17	3	-

Table 3.6: *Matrix of priority used for the production of net land use change transition from land cover. The same matrix is applied for all world regions.*

Using this method, we produce the net transitions in terms of land use change.

Because the transitions are available at a 10 years resolution (IIASA, 2018c), and converted to an annual resolution using a linear interpolation, the annual transitions are constant over the initial timesteps (2005-2010, 2010-2020, 2020-2030,... 2090-2100).

In figure 3.3, we represent the annual net transition from forest to croplands (Mha/yr), summed over all regions. To improve the intelligibility of the figure, we represent only the SSP1s scenarios, for a single transition. The ensemble of transitions under other storylines are provided in appendix (section 6.2.4). Over 1960-2010, the major transition are forests to croplands and pastures, that is to say deforestation. We notice also strong transitions from grassland & shrublands to croplands and pastures, and in a lesser extent, desert & urban areas to croplands and pastures. The algorithm (red plain lines) reproduces imperfectly the transitions from LUH1 (black plain lines). When considering the transitions at the regional scale, we observe that in several cases, transitions from a biome b_1 to a biome b_2 occur even if the land cover of b_1 is increasing or if the land cover of b_2 is decreasing. For instance, in the reforming countries over 1990-2010, the land cover of b_2 (grasslands & shrublands here) declines, implying no transitions to b_2 according to the used algorithm. Yet, a conversion of b_1 (croplands) to b_2 still occurs according to the LUH1. Besides, without this conversion, the change in land cover of b_2 is not enough to explain the transitions from b_2 to b_3 (pastures) according to LUH1. Whatsoever the priority matrix (table 3.6), this algorithm cannot handle these cases and reproduces perfectly the net transitions. Even though some transitions are not reproduced with their full extent, and some spurious transitions are produced (e.g. Desert & Urban to Forest), we will still use this algorithm, for lack of a better alternative. This method is discussed more extensively from a theoretical perspective in section 3.4.1. In section 3.4.2, we also discuss the quality of this reconstruction, using the new LUH2 dataset, that reevaluates the historical transitions, but also encompass 6 SSP scenarios.

Concerning the SSP1 scenarios, several transitions do not follow the historical trend in the projections. This is particularly important for transitions to the forest, in the line of the storyline SSP1 "Green Road", or "Sustainability", with an emphasis on environmental boundaries. Transitions from the Desert & Urban biomes are also reduced, in the line of constant Built-up areas for most of the scenarios. The direction of transitions between grasslands & shrublands and croplands depends very much on the regions and the scenarios. The scenarios can be grouped depending on the IAM used (section 6.2.4), although not as clear in the transitions compared to the change in land cover. For instance, the new afforested areas stem from grasslands & shrublands in AIM-CGE, pastures in MESSAGE and IMAGE, and pastures and croplands in GCAM4 and REMIND. WITCH-GLOBIOM shows the same trends as IMAGE, because WITCH-GLOBIOM did not report a land cover and we assume it uses the land cover of the marker, which is IMAGE for SSP1.

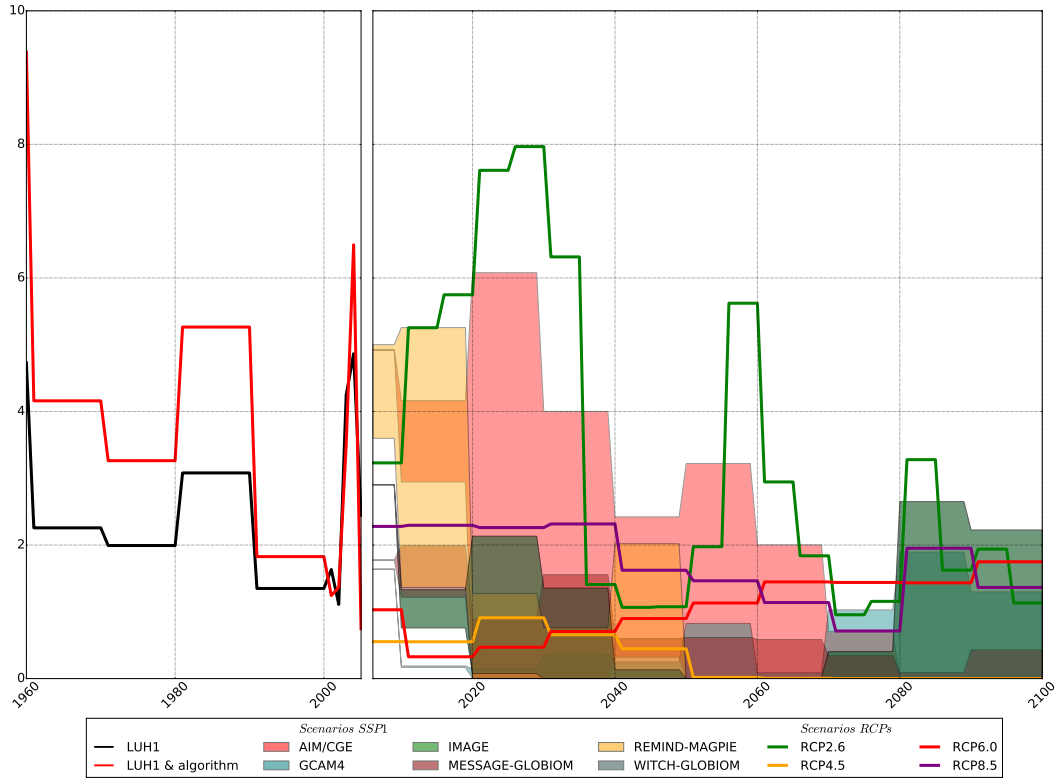

Figure 3.3: *Global annual net transition from forest to croplands (**Mha/yr**) for the SSP scenarios under the storyline SSP1 over 2005-2100, and for all RCPs. All other transitions, for all SSP scenarios, are provided in appendix (section 6.2.4). The land use changes for 1960-2010 and for RCPs scenarios are shown for comparison, prescribed by the Land Use Harmonization dataset v1.1 (Hurtt et al., 2011). For comparison, the reconstruction of the net transitions from LUH1 are done using its land cover changes and the algorithm from Stocker et al. (2014) (red plain line), for comparison with the original transitions of LUH1 (black plain lines). For the SSP scenarios (plain lines), the color corresponds to the IAM that has produced the corresponding scenario. For the RCPs scenarios (dashed lines), similar colors may be used if and only if the IAM used to produce the RCP is the same: IMAGE has been used for RCP2.6, MiniCAM (now GCAM4) for RCP4.5, AIM for RCP6.0 and MESSAGE for RCP8.5 (IIASA, 2018b).*

3.2.3.3 Harvested biomass

This driver corresponds to the sole extraction of biomass, without changing the land cover. The biomass is extracted principally from Forest, and then from Grassland & Shrublands. The LUH dataset provides estimates for the historical annual harvested biomass over the historical period (GtC/yr). In OSCAR, the biomass is assumed

to be harvested only from the living biomass, and that this withdrawn biomass will regrow with time. The carbon extracted from the vegetation is allocated to different carbon pools: fuel wood products, pulp-based products, hardwood-based products but also slash. The latter is directly allocated to the litter.

However, the SSP database does not provide us with detailed outputs for the different products of harvested biomass, and for the different biomes. Instead, the only related variables to harvest are: the land cover, primary energy from traditional biomass, from modern biomass with CCS or from modern biomass without CCS. In the lack of a better solution, we choose to assume that the prescribed harvest of LUH1 evolves over the period of the scenario proportionally to the production of primary energy from biomass energy with and without CCS in the corresponding region. We use both, with and without CCS, because carbon stocks and thus the dynamic of the biomes are affected by the harvested biomass, being used with or without CCS. This proportionality can actually be translated into the assumption that modern bioenergies use a constant fraction of harvested biomass from forests, and another constant fraction from grasslands & shrublands.

We acknowledge that this hypothesis is very likely to be wrong. Historically, harvested biomass concerned woody biomass, from forests and grasslands & shrublands. Yet, the development of modern bioenergy now includes more sources, but also more products (Rose et al., 2014a). In the SSP scenarios, bioenergy using CCS is strongly developed (Popp et al., 2017), in particularly for the most ambitious scenarios that usually require negative emissions (Fuss et al., 2014). For instance, under our assumption, no biomass is harvested from croplands, even though some are likely to be extracted. Yet, in OSCAR, harvest only concerns the woody biomass (Gasser et al., 2017a). Normally, only the fraction of bioenergies that is not provided by croplands, for instance for biofuels, should be accounted in our relation. Nevertheless, without more detailed variables in the SSP database, we are constrained to these hypotheses. In section 3.4.3, we discuss the sensitivity of our results. Besides, a comparison of the produced harvested biomass to those of LUH2 for the 6 available scenarios is given in section 3.4.2.

AIM-CGE does not report bioenergy with CCS for the baselines and the least ambitious forcing targets. We consider that in these scenarios, no bioenergy with CCS is required to reach these specific forcing targets, then no bioenergy with CCS is reported. Thus, we will consider that bioenergy with CCS for these scenarios will be zero.

In figure 3.4, we represent the annual harvested biomass that we produce for SSP scenarios, under the storyline SSP1. For the sake of clarity, we represent the total annual harvested biomass, summed over all regions and all biomes. The detail can be found in section 6.2.5, for all SSP scenarios. Historically, most of the harvested biomass comes from forests. In SSP scenarios, it remains true. Yet, we observe a very strong development of the development of the harvest from grasslands & shrublands in reforming countries, but also in Latin America (section 6.2.5). The major source of harvested biomass in the SSP1 scenarios still remains forest, and

regionally, it becomes reforming countries and Latin America, although those in OECD countries 1990 increase as well. As observed with the land cover (figure 3.2), scenarios may be grouped depending on the IAM, rather than the forcing target. Though, the SSP tends to remain the major driver.

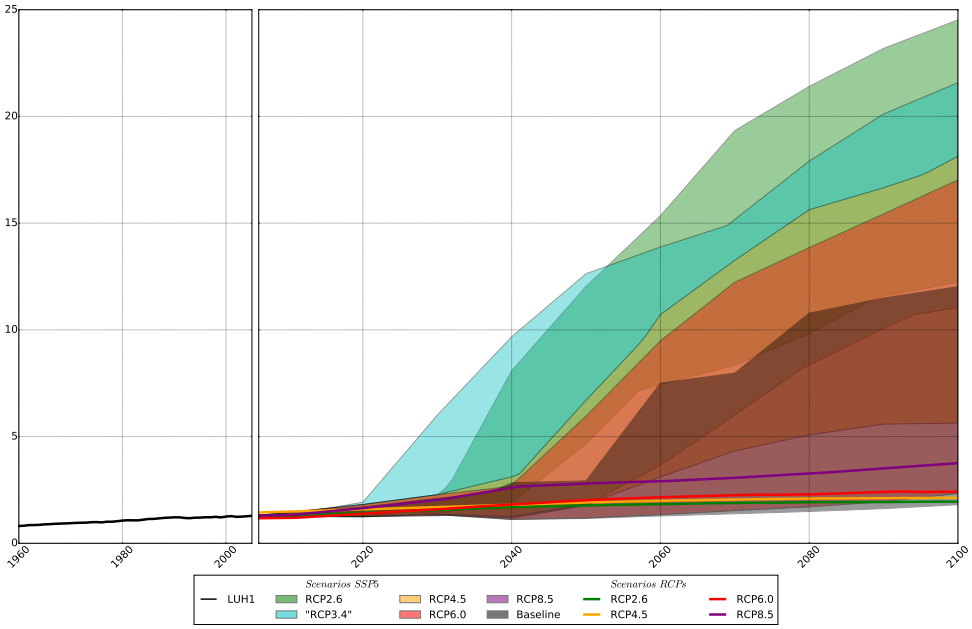

Figure 3.4: *Annual harvested biomass (**GtC/yr**) for the SSP scenarios under the storyline SSP5 over 2005-2100, summed over all regions and all biomes. The detail for all SSP scenarios can be found in appendix (section 6.2.5). The harvested biomass for 1960-2010 and for RCPs scenarios are shown for comparison, prescribed by the Land Use Harmonization dataset v1.1 (Hurtt et al., 2011). For the SSP scenarios, each color corresponds to the realizations by the ensemble of IAMs for sthis RCP under this SSP. For the RCPs scenarios (plain lines), similar colors may be used if and only if the IAM used to produce the RCP is the same: IMAGE has been used for RCP2.6, MiniCAM (now GCAM4) for RCP4.5, AIM for RCP6.0 and MESSAGE for RCP8.5 (IIASA, 2018b).*

3.2.3.4 Shifting cultivation

Shifting cultivations correspond to parallel expansion and abandonment of croplands and pastures with the other biomes, mostly forests. This is typical from the traditional "slash and burn" practice in the tropics (Heinimann et al., 2017). While an area is used for agriculture, others are fallowed. The area used for croplands and pastures is farmed until the not productive enough, and then abandoned for biomass regrowth. Eventually, a previous fallowed area will be cleared out, often using fire, and used anew for agriculture. While an area is fallowed, and if not with

fire, biomass may be extracted for timber, firewood and so on. The LUH dataset provides estimates for the historical annual areas used for shifting cultivations over the historical period (Mha/yr). In OSCAR, during a shifting turnover between two biomes (e.g. pastures and forests), biomass is harvested from the vegetation of both biomes under the assumption that its living biomass has grown only during the shifting turnover rate. The time associated with this turnover is assumed to be 15 years. The above-ground fraction of the harvested carbon is added to the same carbon pool for wood products as described in section 3.2.3.3, whereas the remaining fraction of the carbon withdrawn from the vegetation is allocated to the litter pool.

Given the available variables in the SSP database, we make the assumption that the area extents used for shifting cultivations evolve proportionally to the production of traditional biomass energy of the scenario in the corresponding region. This latter driver corresponds mainly to the use of biomass for cooking and heating, especially in developing countries because of low modernization of the energy system. We acknowledge that, because of the use of fire to clear the areas for shifting cultivations, most of the biomass is not used for traditional biomass energy. We acknowledge as well that traditional biomass energy is not fully provided by fallowed areas, thus shifting cultivations. Our assumption is hence equivalent to two assumptions:

1. The biomass energy extracted from fallowed areas is only a fraction of the biomass that was on the biome, the rest of this biomass being mostly burned for soil fertility. This fraction is assumed to remain constant. This assumption can be respected if fire is used in constant proportions when using shifting cultivations, even if the extent of this practice is reduced.

2. The traditional biomass energy uses a fraction from fallowed areas for shifting cultivations, and this fraction is assumed to remain constant. This assumption can be respected, if the mix of energy sources in traditional biomass energy remains unchanged, even if traditional biomass energy as a whole decreases in the global energy mix.

The forest management for traditional biomass energy in developed countries hampers these assumptions, because this practice cannot be related to shifting cultivations. It is likely that it may lead to overestimated extents for shifting cultivations. Furthermore, Heinimann et al. (2017) shows that estimates for area extents of shifting cultivations are probably overestimated. Still, in the lack of a better alternatives or more appropriate variables, we use these assumptions. In section 3.4.3, we calculate how sensitive are our results to these assumptions.

As mentioned in table 3.3, AIM-CGE does not report any primary energy from traditional biomass. The solution chosen here has been to use its primary energy from biomass without CCS as driver. We acknowledge that this solution is not appropriate. Another solution would have been to use the primary energy from traditional biomass of the marker for this scenario. Yet, for a given scenario under a SSP and a target in radiative forcing defined by a RCP, the realizations under differ-

ent IAMs are quite different, as shown in figure 3.5. Thus, we use our assumption, in the lack of a better option.

As mentioned in table 3.3, WITCH-GLOBIOM does not report primary energy from traditional biomass for the OECD90 countries and the reforming countries. Yet, this can be explained because this source is much lower in these countries than in Asia, Middle East & Africa and Latin America. Shifting cultivations are also very low in OECD90 and reforming countries. Thus, we assume that shifting cultivations keep the same level in these countries for all SSP scenarios. Yet, a better solution may be to prescribe shifting cultivations in OECD90 and reforming countries decreasing with the same rate than the global traditional biomass energy.

In figure 3.5, we represent the corresponding transitions for shifting cultivations that we produce for SSP scenarios, under the storyline SSP1. The figures for the scenarios under other storylines are given in appendix (section 6.2.6). For most of the scenarios under SSP1, primary energy from traditional biomass is decreasing, hence shifting cultivations. As illustrated with land cover (figure 3.2), the scenarios can be grouped depending on the IAM used. The evolution of shifting cultivations depends primarily on the storyline, then on the IAM and finally on the climate policy. REMIND-MagPIE uses the same traditional biomass energy for all scenarios, independently on the SSP and the forcing target. For MESSAGE-GLOBIOM, the trajectory for the traditional biomass energy depends only on the SSP, but is unaffected by the climate policy. AIM-CGE evaluates traditional biomass energy increasing faster than other IAMs, which remains true for other SSPs. This is likely to be related to our assumption, concerning its unreported traditional biomass energy. Comparing SSP, these evolutions are consistent with the storylines for land use change, that can be summarized as follow (Popp et al., 2017):

- SSP1: Land use is strongly regulated, and tropical deforestation rates decrease strongly. This leads to a strong decrease in traditional biomass energy.
- SSP2: Land use is partially regulated, and tropical deforestation rates slowly decrease. Incentives to avoid deforestation and to promote afforestation do not start before 2030. This leads to a slow decline in traditional biomass energy.
- SSP3: Land use regulation is very limited, and deforestation continues. This leads to a relatively constant traditional biomass energy.
- SSP4: The land use regulation is developing countries is very limited. This leads either to a relatively constant or to a increasing then decreasing traditional biomass energy.
- SSP5: Land use is partially regulated, and deforestation slowly decreases. This leads to a slow decline in traditional biomass energy.

As a remark, the LUH2 dataset does not prescribe anymore shifting cultivations (LUH2, 2018), because it has been showed that it may be lower than previously eval-

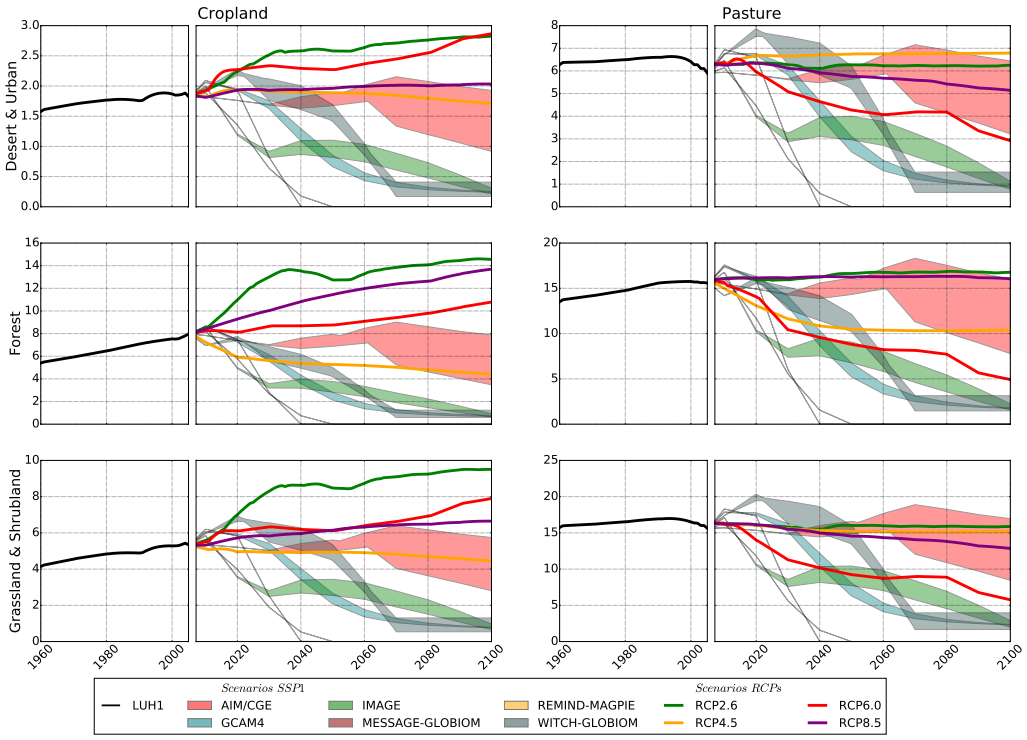

Figure 3.5: *Global annual gross bidirectional transitions for shifting cultivations (**Mha/yr**) for the SSP scenarios under the storyline SSP1 over 2005-2100. The transitions for shifting cultivations for 1960-2010 and for RCPs scenarios are shown for comparison, all being directly prescribed by the Land Use Harmonization dataset v1.1 (Hurtt et al., 2011). For the SSP scenarios (shaded areas), the color corresponds to the IAM that has produced the corresponding scenario. For the RCPs scenarios (plain lines), similar colors may be used if and only if the IAM used to produce the RCP is the same: IMAGE has been used for RCP2.6, MiniCAM (now GCAM4) for RCP4.5, AIM for RCP6.0 and MESSAGE for RCP8.5 (IIASA, 2018b).*

uated (Heinimann et al., 2017). For this reason, we cannot compare our evaluations for shifting cultivations to those of the 6 scenarios of LUH2 dataset.

3.2.3.5 Emissions from Land Use Change

Within the SSP public database, CO_2 emissions are grouped in two categories: Total Emissions and Emissions from LUC. The difference will be called thereafter Emissions from Fossil-Fuels & Industry, albeit it includes other emissions, such as bioenergies. As explained in the section 3.2.3.1, although emissions from Land Use Change are provided, no feedback of climate change is implemented on these emissions in most cases. We use instead the calculation in OSCAR (Gasser et al.,

2017a). The calculation of these emissions by OSCAR is compared to those of the IAM in section 3.3.1.2.

3.2.4 Other radiative forcings: solar, volcanic and contrails

For a robust assessment of the climate projections, we need not only the emissions and the land-use, but also other forcings. OSCARv2.3 uses three radiative forcings as direct inputs: solar, volcanic and contrails. We use the data from IPCC (2013) over 1750-2010. We show in figure 3.6 the corresponding values and their hypotheses. Concerning the solar radiative forcing, we set its forcing over 2010-2100 at $0.028 W/m^2$, the average over the last 11 years cycle. Concerning the volcanic radiative forcing, the activity is set from 2010 to that of an "average volcano". The volcanic radiative forcing shown in figure 3.6 is the change in the radiative budget induced by the volcanic activity. If this volcanic activity is higher than usually, the volcanic radiative forcing will be negative, leading to a cooling of the atmosphere, whereas a volcanic radiative forcing lower than usually will be positive, leading to a warming of the atmosphere. Thus, the "average volcano" leads to a zero radiative forcing. Concerning the contrails radiative forcing, we did not infer the evolution of the aviation sector in the SSPs, nor of its impact through the formation of contrails. For these reasons, we set this radiative forcing to 0.

The hypothesis of ignoring the contrails radiative introduces a sharp reduction in 2010 in the total radiative forcing of 0.048 W/m^2. However, this reduction can be neglected, compared to the reduction in the volcanic radiative forcing. In the last years, the volcanic activity has been lower than in previous decades, leading to a positive contribution to the radiative forcing, and the transition to the assumed average volcanic activity for the scenarios occurs in 2010. These reasons explain the sharp reduction of 0.306 W/m^2 in 2010. This transition can be seen as a discontinuity in the figures showing the radiative forcings (section 3.3.3). Though, this transition remains within past evolutions (Myhre et al., 2013), and projecting the SSP scenarios with an average volcanic activity rather than none is physically more appropriate.

3.2.5 Monte Carlo setup

To produce the uncertainties in the climate projections of the SSP scenarios, we use a Monte-Carlo setup as a probabilistic framework. We draw 1000 members, that are the parametrizations of OSCAR. Two groups of parameters can be distinguished. One corresponds to the driving datasets, as explained in section 3.2.6 concerning the emission datasets. The other corresponds to the ensemble of sensitivities of Earth system processes. More details about these parameters can be found in table 3 of Gasser et al. (2017a). Every scenario SSP is run under each parametrization drawn.

For every scenario SSP, we produce the median and the 90% confidence intervals of all required climate outputs. We emphasize that these uncertainties are not constrained using observations, and are representative of the range in modeling of

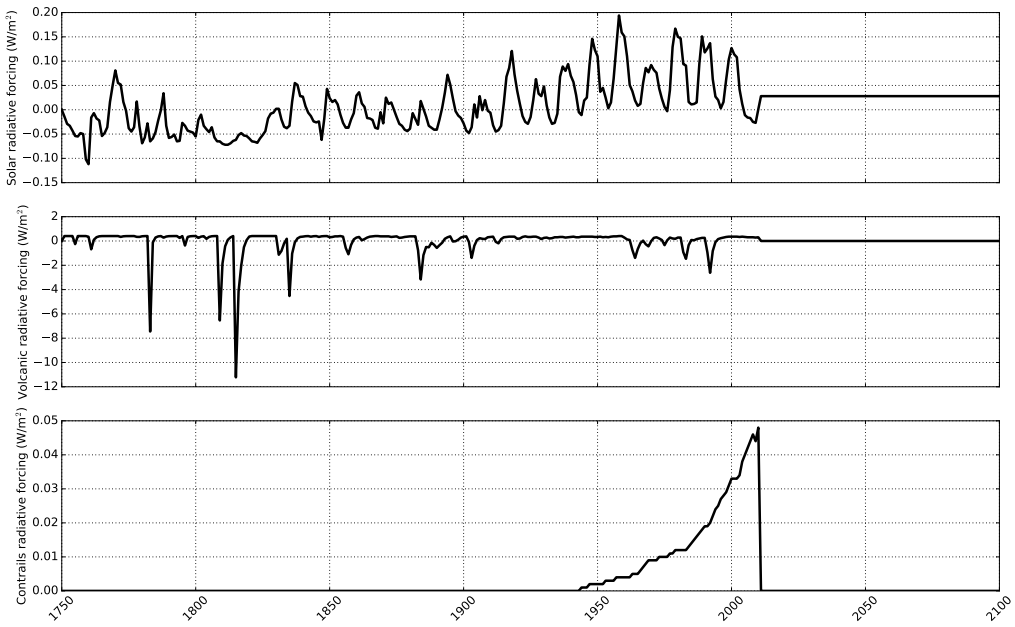

Figure 3.6: *Evolutions of the other radiative forcings prescribed in OSCAR v2.2. The upper panel corresponds to the solar radiative forcing, set to the mean of the last 11-year cycle for SSPs. The middle panel corresponds to the volcanic radiative forcing, set to the "average volcano" for SSPs. The lower panel corresponds to the contrails radiative forcing, set to zero for SSPs.*

the Earth system in OSCAR v2.3. We calculate the median and the 90% confidence interval for all emissions as well, not only LUC emissions, because different emissions datasets may be used over the historical period, leading to different emission pathways over the scenario period (section 3.2.6).

3.2.6 Harmonization of the emissions

As explained in the section 3.2.5, for each scenario SSP, a Monte-Carlo simulation is performed using OSCAR under different parametrizations. This study uses the approach OSCAR has been developed for (Gasser et al., 2017a). Each parametrization corresponds to a set of climate parameters, but also choices of inventories for the historical period. For each of these inventories, only anthropogenic emissions are taken into account.

Inventories present discrepancies. Particulary, they have different level of emissions in 2010. The selection of different inventories in the Monte-Carlo simulation provides a basic mean for accounting the uncertainties in the inventories, as illus-

trated in the chapter of this thesis on the uncertainties in fossil-fuels emissions. However, it also means that emissions have to be harmonized. A second argument for this harmonization is the presence of discrepancies inbetween the starting point of emissions in the SSP scenarios. The main reason for these discrepancies in the SSP emissions is the use of different inventories by the IAMs to calculate their emissions (IIASA, 2018e; SSP, 2018). There might be a secondary reason: it is unsure which contributions are included in the emissions, for instance, whether biomass burning emissions are included. Would biomass burning emissions be included, their calculation is likely not to include the impact of climate change and its uncertainties, as explained in section 3.2.3.1. Thus, we choose to extend the anthropogenic emissions using the SSP emissions, while biomass burning emissions and wetlands emissions are calculated by OSCAR over the complete simulation (figure 3.1).

In this study, the multiple inventories that have been integrated in OSCAR v2.2 (Gasser et al., 2017a) are used for the historical period in the Monte-Carlo setup. The emissions of the historical period are extended using the emissions of each scenario SSP. We choose as starting point for the extension 2010, and not 2005. The climate insights on the SSP scenarios computed by MAGICC were computed using a rescale in 2005 (IIASA, 2018e), although one of the objective of the RCPs & SSPs framework is to update the starting year of the scenario (van Vuuren et al., 2014). They are harmonized to the RCPs, except for N_2O and CH_4. The inventory ACCMIP shares the same emissions in 2005 with the RCPs. For N_2O and CH_4, the dataset EDGAR is used as starting point in 2005. Among the inventories used in our study, we use EDGAR v4.2 (Joint Research Centre, 2011) and ACCMIP (Lamarque et al., 2010).

Different harmonization methods can be used. Rogelj et al. (2011) describes three simple methods to harmonize a scenario to historical emissions. Under the assumption of aggregating the same sectors, and consistent mismatch of the sectoral emissions inbetween the two emission pathways, an uniform scaling can be applied using a mere proportionality. Assuming that the mistmatch of the sectoral emissions will decrease through time, for instance thanks to enhanced reporting and monitoring of the emissions, a tapered scaling can be applied. It consists in a proportionality defined from the harmonization year, that decrease to 1 over a prescribed period. Assuming that the discrepancies is instead due to a difference in the reported sectors, the difference at the hamonization year can be used to provide a constant offset for the scenario. For instance, tapered scaling has been used for AR5WG3 (Schaeffer et al., 2015; Clarke et al., 2014). It is unsure which harmonization method has been used for the climate insights under MAGICC (IIASA, 2018e; SSP, 2018; Riahi et al., 2017). Because the main reason for the discrepancies inbetween SSP scenarios is the use of different inventories, we choose to apply an uniform scaling, to which OSCAR adds the CO_2 LUC and the natural emissions.

Over the historical period, emissions of each species X can be decomposed into different categories, as described below. Some are drivers of OSCAR, such as $E^{hist}_{anth,X}$, whereas others are not drivers of the model, but calculated within OSCAR,

such as E_{LUC}^{OSCAR}, although they contribute to climate change.

- $E_{anth,X}^{hist}$ are emissions from inventories, not produced from natural sources
- E_{LUC}^{OSCAR} are CO_2 LUC emissions calculated by OSCAR, using land use changes, harvests, shifts and Earth system variables adapted from ESMs
- $E_{BB,X}^{OSCAR}$ are biomass burning emissions calculated by OSCAR
- $E_{bio,X}^{OSCAR}$ are other non-CO_2 natural emissions sources that are impacted by climate change, such as wetlands emissions, and calculated by OSCAR.

The emissions of a compound X of a given SSP scenario are noted here E_X^{SSP}, considered as the total anthropogenic emissions, except for CO_2 where the LU emissions E_{LUC}^{SSP} can be added. This component is provided in the SSP database, but as explained in section 3.2.3.1, we use E_{LUC}^{OSCAR} not only for the historical period, but also over the scenario period. Under the consideration that E_X^{SSP} corresponds to anthropogenic emissions, the biomass burning emissions $E_{BB,X}^{SSP}$ and other non-CO_2 natural emissions $E_{bio,X}^{SSP}$ still need to be added. We use OSCAR to evaluate these contributions over the period of the scenarios. Besides, we use the total anthropogenic emissions provided E_X^{SSP} to extend the anthropogenic emissions, as illustrated in equation 3.3.

$$E_{X,t\in[1700,2100]} = \begin{cases} \left(E_{anth,X}^{hist} + E_{BB,X}^{OSCAR} + E_{bio,X}^{OSCAR}\right)_{t\in[1700,2010]} \\ \left(E_{anth,X,2010}^{hist} \frac{E_X^{SSP}}{E_{X,2010}^{SSP}} + E_{BB,X}^{OSCAR} + E_{bio,X}^{OSCAR}\right)_{t\in[2010,2100]} \end{cases} \tag{3.3}$$

3.3 Results

In this section, we analyze successively the emissions prescribed (section 3.3.1), the increase in global surface temperature (section 3.3.2), the radiative forcings (section 3.3.3), the atmospheric concentrations (section 3.3.4), the variables relative to the carbon cycle (section 3.3.5), biomass burning emissions (section 3.3.6), an extended Kaya decomposition (section 3.3.7) and carbon budgets (section 3.3.8).

3.3.1 Emissions

Instead of presenting the results for all emissions (CO_2, CH_4, N_2O, halogenated compounds, SO_2, BC, OC, NO_X, CO, VOC, NH_3), we focus on the major species: the three major greenhouse gases (CO_2, N_2O, CH_4), SO_2 to represent other aerosols and F-Gases.

- CO_2 emissions from "Fossil Fuels & Industry" (the so-called difference between the Total CO_2 emissions and the CO_2 LUC emissions from the IAMs) in section 3.3.1.1. This category is different from the SSP database only in its rescale to the historical period (section 3.2.6).
- CO_2 emissions from LUC in section 3.3.1.2. These emissions are calculated by OSCAR as explained (section 3.2.3.5), and are compared here to the IAMs emissions provided in the SSP database.
- CH_4 emissions in section 3.3.1.3. We show here the anthropogenic CH_4 emissions, but also the perturbation in CH_4 emissions from wetlands and biomass burning. The fraction of the perturbed natural emissions in these emissions is also shown.
- N_2O emissions in section 3.3.1.3. Like CH_4, we show the anthropogenic N_2O emissions, and the perturbation in N_2O emissions from biomass burning. We also show how much these latter emissions represent in terms of fraction.
- SO_2 emissions in section 3.3.1.3. Like CH_4 and N_2O, we show the anthropogenic emissions, and the contribution of perturbed SO_2 biomass burning emissions.
- F-Gases emissions in section 3.3.1.6. It includes the specific treatment performed for these emissions (section 3.2.2).

3.3.1.1 CO_2 emissions from Energy & Industry

The SSPs CO_2 emissions from Energy & Industry are a direct result of IAMs, where only the rescale to CO_2 inventories takes action (section 3.2.6). These emissions are represented in figure 3.7. Here, each panel shows the emissions under different forcing targets. Another perspective can be found in figure 8 of Bauer et al. (2017), that shows panels for each forcing targets for the different SSPs.

SSP1 is the "Sustainability" scenario, with a reduction of the inequalities and with an energy transition. In the baseline, the growth rate of CO_2 emissions from Energy & Industry reduces in the first half of the century, to peak in 2040 at 11.7GtC/yr or to remain close to 14.0 GtC/yr from 2070. The introduction of climate policies reduces effectively the cumulated emissions, and shifts the peaks of emissions. The peak is around 2050 when targeting the RCP4.5, 2040 with RCP3.4 and 2030 with RCP2.6. To reach RCP2.6, by 2100, negative emissions are used, leading to CO_2 emissions from Energy & Industry ranging from -2.5 to 0.9GtC/yr.

SSP2 is the "Middle of the Road" scenario. The trend of the baseline is an increase in the emissions over the whole century, ranging in 2100 between 18.6 and 24.1 GtC/yr in 2100. For the RCP6.0 forcing target, emissions may stop increasing between 2040 and 2090, to reach between 9.8 and 16.6 GtC/yr in 2100. For all following targets, emissions begin to decrease after 2050. Negative emissions are

used to reach RCP2.6 by 2100, with CO_2 emissions from Energy & Industry ranging from -6.3GtC/yr to -0.9GtC/yr.

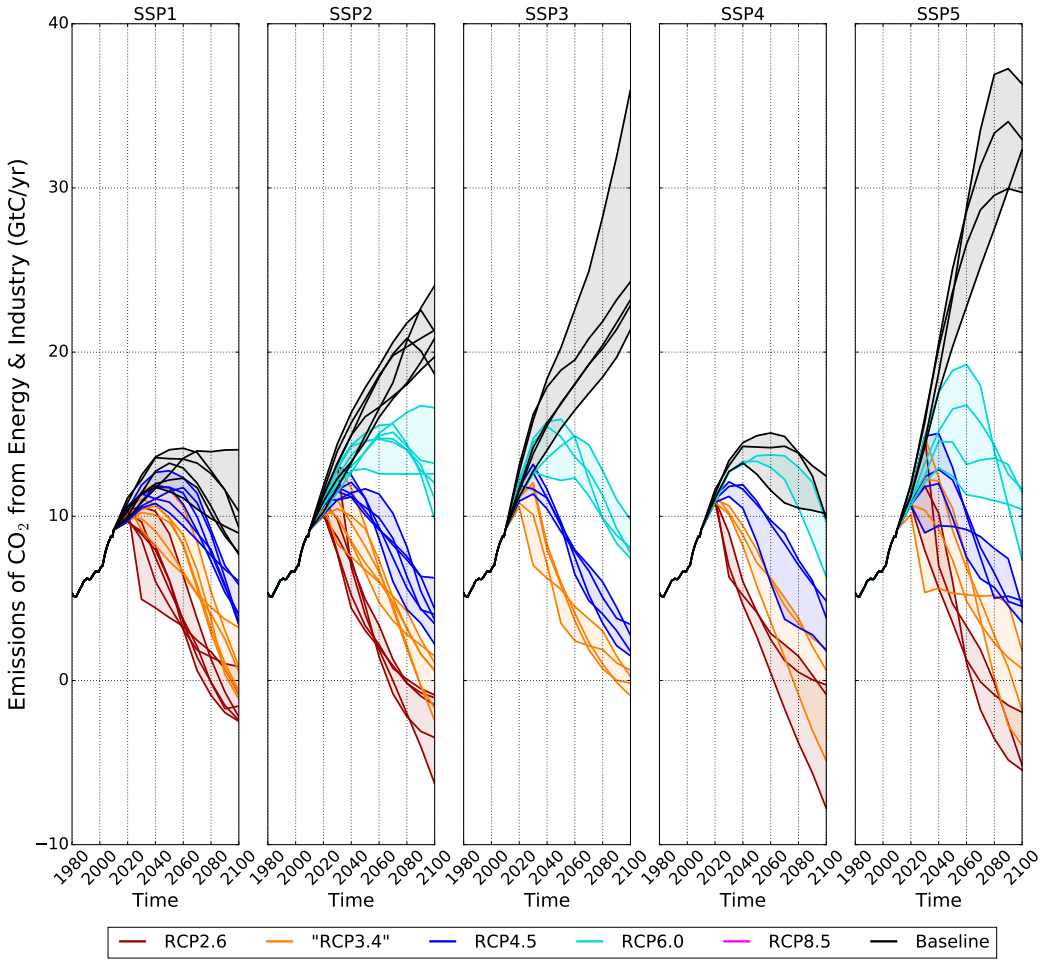

Figure 3.7: *CO_2 emissions from Energy & Industry from 1980 to 2100. The transition from the historical period and the scenario happens in 2010. Each subfigure details the results for a given SSP. The scenarios are also classified depending on the forcing target. Each line represents an IAM that has run this SSP and this forcing target, and in plain color is their ensemble.*

SSP3 is the "Regional Rivalry" scenario, with an emphasis on inequality and fossil fuels. Its emissions for the baseline increase to 21.4 to 36.0 GtC/yr in 2100. Implementing a climate policy to reach a RCP6.0 reduces the emissions to 7.4 to 9.8 GtC/yr. In other forcing targets, the peak of emissions happens before 2030. Negative emissions are used to reach reach RCP3.4 by 2100. CO_2 emissions from Energy & Industry range from -0.9 to 0.6GtC/yr. Under this storyline, no IAM could find solutions to reach RCP2.6.

SSP4 is the "Inequality" scenario, with high inequalities and investment in both fossil-fuels and low-carbon energy sources. The baselines reach between 9.9 and 12.5 GtC/yr in 2100. For the three IAMs that has run this scenario, emissions peak between 2040 and 2070. The peaks and levels of emissions decrease with the implementation of more stringent climate policies. To reach RCP2.6 under this scenario, negative emissions are used, with CO_2 emissions from Energy & Industry inbetween -7.8 and -0.3GtC/yr in 2100.

SSP5 is the "Fossil-Fuel Development" scenario, with an increased consumption of fossil fuel resources and an increased cooperation. Without climate policies, emissions are between 29.7 and 36.3 GtC/yr in 2100. Just like other SSPs, the implementation of a forcing target quickly decreases the peak and levels of emissions. Negative emissions are used to reach low climate changes. Under RCP3.4, CO_2 emissions from Energy & Industry range from -3.9 to 1.9 GtC/yr. Under RCP2.6, they range from -5.4 to -1.9GtC/yr.

In terms of baselines, SSP1 and SSP4 are relatively similar, whereas SSP3 and SSP5 are also relatively similar. This can be explained by the underlying assumptions in terms of consumptions of fossil fuel resources. Besides, across all SSPs, the patterns observed for the same forcing targets are also relatively close, although timings may vary. According to Bauer et al. (2017), the slow technological change and the concern over energy security are responsible in SSP3 for higher emissions. The low diffusion of technological options in SSP4 reduces the potential for mitigation. In terms of reduction in the emissions, the nuclear power has relatively low increasing demand in SSP3 and SSP4, while the assumption on its social acceptance in SSP5 does not allow for its development. Shares of bio-energy remain relatively small, albeit bio-energy with CCS contributes significantly to CDR. For these reasons, the reductions in Energy & Industry emissions are higher in SSP5 and SSP3, lower in SSP2 and much lower in SSP4 and SSP1.

3.3.1.2 CO_2 emissions from Land Use Change

Under the land use changes (section 3.2.3.2), the shifting cultivations (section 3.2.3.4) and the harvest (section 3.2.3.3) that we calculate for the SSP scenarios, we calculate the CO_2 emissions from LUC using OSCAR, with the impact of climate change included. These results are presented in figure 3.8 and table 3.7. In figure 3.8, we represent the evolutions as produced by OSCAR. In table 3.7, we focus on the comparison to the emissions calculated by OSCAR and the IAMs. These emissions are affected by an ensemble of drivers such as land use change regulation and land based mitigation policies (Smith et al., 2014), Land productivity growth (Weindl et al., 2015; Robinson et al., 2014)), food consumptions (Bajželj et al., 2014; Hiç et al., 2016)), international trade (Schmitz et al., 2012)) and globalization (Verburg et al., 2009). A description of these drivers for the SSPs can be found in table 1 of Popp et al. (2017).

In the figure 3.8, we notice that the pathways of CO_2 emissions from LUC can

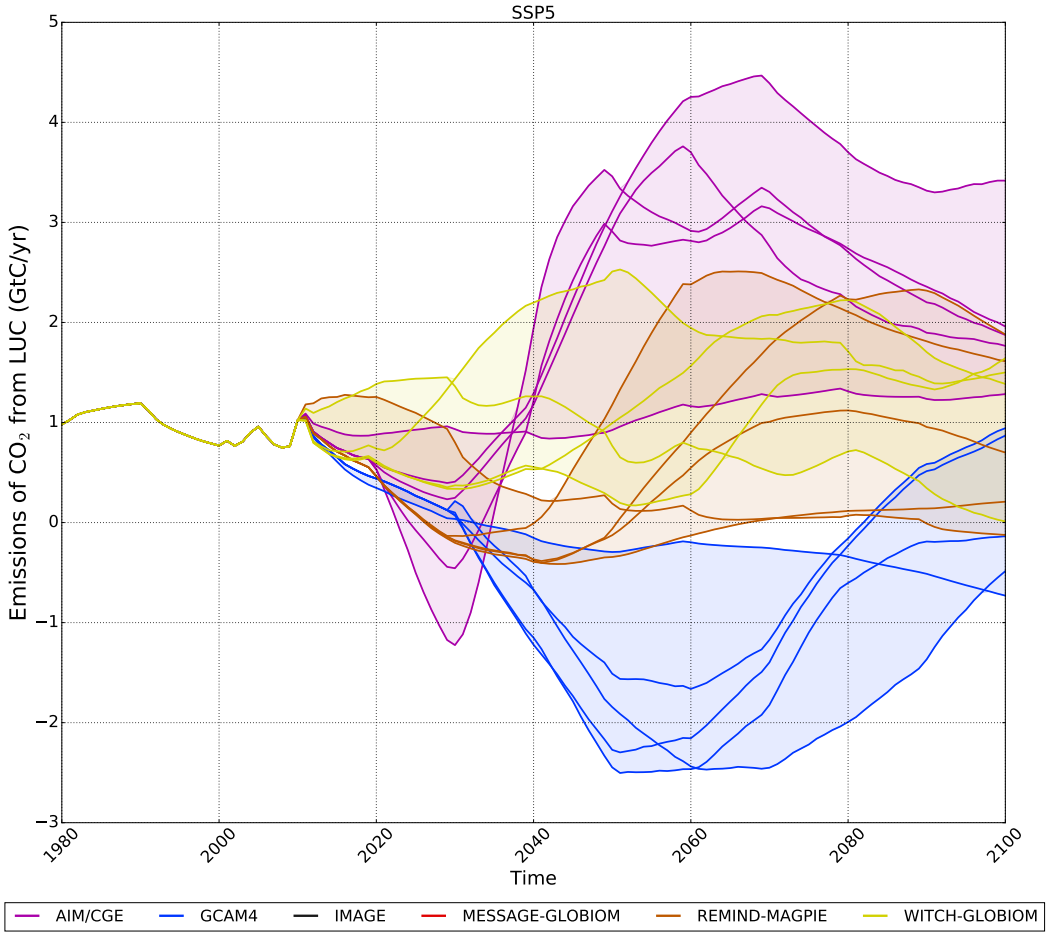

Figure 3.8: *CO_2 emissions from Land Use Change (GtC/yr) from 1980 to 2100. The transition from the historical period and the scenario happens in 2010. Each sub-figure details the results for a given SSP. The scenarios are also classified depending on the forcing target. Each line represents an IAM that has run this SSP and this forcing target, and in plain color is the ensemble of common scenarios to an IAM. For the sake of clarity, uncertainties are not represented here.*

be grouped depending on the IAM used, as shown with LUC (figure 3.2), shifting cultivations (figure 3.5) and harvest (figure 6.16). The differences between the groups tends to be more marked in SSP3, and in a lesser extent with SSP4 and SSP5. These effects can be related to the implementation of the assumptions for each storyline SSP in the different IAMs. By comparing globally these emissions between SSP, these emissions are the least reduced in SSP3, and a little more in SSP4 and SSP5, which can also be related to these storylines.

In the SSP1, its storyline states that the land use sector is strongly regulated and participates to mitigation policies without delays, with high improvements of

agriculture and diets. We observe that the emissions are reduced very rapidly under this SSP (figure 3.8). This is true for all IAMs. In AIM-CGE, two effects combine for a reduction of these emissions. The first one happens over 2010-2040 in the presence of a climate policy, whereas the second one happens from 2060, even in the absence of a climate policy. In GCAM4, the emissions decrease up to 2050, but increase afterwards, without exceeding 2010 level. It can be related to the increase of the area extent of forests in GCAM4 under SSP1 (figure 3.3), rapid over the first half of the SSP scenarios, then slower. In IMAGE, emissions are reduced rapidly up to 2030, then only tend to decrease up to 2070, to finally tend to increase. It may be explained by the increase of the area extent of forests and grasslands & shrublands, followed by an increase only of the area extent of forests (figure 3.3). In MESSAGE-GLOBIOM, emissions are reduced up to 2040, increase up to 2090, and then decrease anew. It might be explained by the simultaneous increase in the area extent of forests and grasslands & shrublands, the latter one slowing down to increase afterwards. In REMIND-MagPIE, emissions are reduced up to 2040, but the following directions of evolutions are very dependent on the climate policy. In WITCH-GLOBIOM, emissions are reduced up to 2070, with several interruptions, and increase after 2070. Such a late increase is due to two effects. First, WITCH-GLOBIOM uses the land variables of IMAGE, because WITCH did not report them to the SSP public database, and IMAGE is the marker for SSP1. Then, contrary to IMAGE, WITCH-GLOBIOM calculates a late increase of the primary energy associated with bioenergies without CCS. Other evolutions of the land variables or bioenergies are relatively comparable. Because of this late increase in modern bioenergies without CCS, the harvested biomass of WITCH-GLOBIOM has only a late catch-up with the one of IMAGE, and so does the CO_2 emissions from LUC. Also, the more stringent is the forcing target, and the lower are negative emissions. Emissions tend to be more negative under GCAM4 compared to other IAMs. According to IAMs (IIASA, 2018c), emissions are also relatively unchanged between 2060-2070 and 2090-2100, but not according to OSCAR.

In the SSP2, mean assumptions are made for the regulation, the participation, the improvements and the food consumption. Groups of scenarios by IAM tend to overlap, especially because those using AIM-CGE or GCAM4 span a larger range. Globally, the emissions of this SSP are reduced relatively slowly (figure 3.8). Those under AIM-CGE span a larger range, from an increasing up to three times 2010 levels in 2070 followed by a decrease, to emissions over the full period up to 0.08 GtC/yr in 2100. Scenarios under GCAM4 span an even larger range, from the baseline decreasing then increasing up to two times 2010 levels in 2100, to negative emissions as low as -1.46 GtC/yr in 2100. On the contrary, scenarios under IMAGE follow similar trends, with a decrease over the whole period, reaching a 0.00 to 0.56 GtC/yr in 2100. For MESSAGE-GLOBIOM as well, the pathways are more grouped, with a decrease up to 2070-2090, followed by an increase, reaching -0.28 to -0.84 GtC/yr. Under REMIND-MagPIE, the evolutions are relatively common up to 2040, but then depend on the forcing target. Under WITCH-GLOBIOM,

the baseline tends to oscillate, whereas other scenarios show a decrease followed by an increase, even above the baseline after 2080. Compared to SSP1, the fossil-fuel consumption tends to be higher, leading higher needs for negative emissions. However, the SSP2 presents negative emissions from LUC that are not as negative as those from SSP1, because of the assumptions of this storyline for the LUC sector.

The SSP3 is the worst case for the LUC sector, with limited regulation and participation to the climate policies, continued deforestation, low improvement of agriculture and resource-intensive consumption. LUC emissions are positive over the whole period, with an increase over the first part of the century, followed by a decrease (figure 3.8). The scenarios under AIM-CGE present the higher LUC emissions for this SSP, increasing by a factor 3 to 4 by 2100. The only scenario for SSP3 under GCAM4 is the baseline and presents a doubling of these emissions with a decrease from 2080. Scenarios under IMAGE present the lower LUC emissions for this SSP, with a fast doubling and a fast decrease from 2050, almost to 2005 levels. In MESSAGE-GLOBIOM, the increase is slower, remaining around a doubling of 2005 levels. WITCH-GLOBIOM provide scenarios spanning a large range, from 3 times the 2005 levels by 2100 to a return to these levels. Also, all IAMs calculate LUC emissions that are lower than those of OSCAR (IIASA (2018c) & table 3.7).

In the SSP4, the developed countries regulate their LUC sector, cooperate and have high consumption lifestyles. The opposite behaviors stand for the other countries, with high deforestation rates. Under this storyline, the higher ranges are obtained for the scenarios (figure 3.8). Under AIM-CGE, LUC emissions decrease only after 2060 to 2080, to reach 1.72 to 0.00 GtC/yr in 2100. In GCAM4, evolutions depend very much on the forcing targets, with emissions ranging from 3.97 to -0.11 GtC/yr. Under WITCH-GLOBIOM, emissions increase significantly in all scenarios, reaching 4.44 to 2.42 GtC/yr in 2100. For this SSP as well, LUC emissions from IAMs are lower than those of OSCAR (table 3.7). In several cases, LUC emissions are positive, even though the IAM evaluates them as negative.

In the SSP5, the LUC sector is regulated, resource-intensive, with high increase in productivity and a slow decline in rate of deforestation. Finally, the cooperation to climate policies is delayed, albeit with full participation of the LUC sector. This SSP present the most different evolutions across all SSPs (figure 3.8). The scenarios produced with the same IAM have very contrasted evolutions. Without climate policy, LUC emissions evolve relatively steadily. A climate policy targeting RCP6.0 induce high variations in LUC emissions. Then, the more ambitious are the forcing targets, the slower are the decrease and the increase: LUC emissions peak lower and sooner, both in minima and maxima. For AIM-CGE, the LUC emissions are relatively constant. Yet, its SSP5-RCP6.0 decrease rapidly, up to -1.22 GtC/yr in 2030. For GCAM4 also presents contrasted evolutions between its baseline, a monotonous decrease up to -0.73 GtC/yr, and the LUC emissions for scenarios with climate policies first decrease, up to about 2060, then increase. For its SSP5-RCP2.6, emissions have decreased to -1.66 GtC/yr and increase back to 0.94 GtC/yr. With REMIND-MagPIE, its baseline globally decreases to 0.21 GtC/yr.

Between the SSPs, the forcing target and the IAMs, the major factor determining the pattern of LUC emissions tends to be the SSPs, and the second the IAMs. In most SSP scenarios, the implementation of the basic level of the climate policy, that is to say when leaving the SSP-baseline for SSP-RCP6.0 or SSP-RCP4.5, leads to a pattern different from that of the baseline. As forcing targets become more ambitious, patterns are changed with earlier peaks. Often, LUC emissions tend to be slower, but not systematically.

We remind that the calculation of LUC emissions and carbon stocks by IAMs should not integrate feedbacks such as CO_2 fertilization or impact of climate change on different aspects of the terrestrial biosphere (NPP, heterotrophic respirations, carbon stocks,...). IMAGE is the only exception. In our study, LUC emissions integrate these feedbacks. Here, because of the lack of data in the SSP public database, these emissions are calculated from drivers derived from the database. Thus, we acknowledge that the comparison of these two calculations of LUC emissions may integrate the treatment of the database.

To go further, we compare the CO_2 emissions from LUC that OSCAR v2.2 calculates for the reconstructed land variables of the SSP scenarios to those calculated by the IAMs. First of all, all the CO_2 emissions from LUC calculated by the IAMs remain in the 90% confidence interval of those calculated by OSCAR. However, most of the CO_2 emissions from LUC calculated by the IAMs are lower than those calculated by OSCAR. We summarize in table 3.7 the differences in the cumulative LUC emissions over 2010-2100. We acknowledge that the results presented in these paragraphs are based on this criterion, the difference in cumulative CO_2 emissions from LUC, and this criterion is not perfect. A difference close to zero could mask positive differences during a first period, balanced by negative differences during a second period. As such, this table remains a mere summary of this comparison, albeit we deem it as representative of the evolutions of the differences.

- The differences are lower for some IAMs. For instance, REMIND-MagPIE calculates cumulative CO_2 emissions that are often within 20 GtC of those calculated by OSCAR. The differences to the cumulative CO_2 emissions of MESSAGE-GLOBIOM or IMAGE tend to be higher. Finally, AIM-CGE, GCAM4 and WITCH-GLOBIOM are the IAMs for which the differences are the strongest.

- The cumulative LUC emissions tend to be more different from the baseline to the strongest climate policies, targeting RCP2.6. This effect tends to be stronger for GCAM4, although it remains true for other IAMs.

- The stronger differences (greater than 200 GtC) that we calculate are obtained for scenarios under SSP3 for most IAMs, SSP4 for WITCH-GLOBIOM and in a lesser extent, SSP5 under AIM-CGE.

		AIM-CGE	GCAM4	IMAGE	MESSAGE	REMIND	WITCH
	SSP1	-78 < -20	-101 > -182	6 > -32	-26 > -43	41 > 24	17 > -10
	SSP2	49 > 9	87 > -91	74 > 25	11 > -21	95 > 51	
RCP2.6	**SSP3**						
	SSP4	110 > 27	271 > 53				263 > -5
	SSP5	181 > 8	-24 > -151			117 > 51	
	SSP1	-6 < 2	-124 > -173	-2 > -41	-30 > -31	16 > 14	-3 > -11
	SSP2	90 > 36	40 > -92	85 > 44	17 > -6	66 > 45	91 > -4
"RCP3.4"	**SSP3**	263 > 68		180 > 107	187 > 32		217 > 31
	SSP4	173 > 52	216 > 49				223 > -5
	SSP5	175 > 26	-46 > -156			86 > 40	155 > 8
	SSP1	15 < 21	-111 > -145	-9 > -25	-26 < -8	-11 < 0	-25 < -6
	SSP2	156 > 54	7 > -98	102 > 69	12 > 7	20 < 33	83 > -1
RCP4.5	**SSP3**	266 > 84		163 > 100	188 > 41		214 > 26
	SSP4	187 > 64	113 > 10				112 > -3
	SSP5	174 > 37	-71 > -156			44 > 24	120 > 2
	SSP1						
	SSP2	187 > 78	-10 > -66	91 > 63	19 < 30	18 < 29	52 > 2
RCP6.0	**SSP3**	317 > 106		151 > 94	168 > 54		179 > 21
	SSP4		83 > 17				102 > 8
	SSP5	240 > 51	-92 > -146			5 < 18	84 > 4
	SSP1	36 > 35	-16 > -36	6 > -6	0 < 45	-17 < -17	-15 < 8
	SSP2	111 > 79	49 > 15	90 > 62	35 < 62	29 < 44	71 > 14
Baseline	**SSP3**	240 > 108	177 > 116	152 > 94	157 > 89		158 > 20
	SSP4	199 > 82	104 > 50				133 > 9
	SSP5	98 > 53	-11 > -23			34 < 48	87 > 23
Legend		± 20 GtC	± 50 GtC	± 100 GtC	± 150 GtC	± 200 GtC	± 300 GtC

Table 3.7: *Comparison of the median cumulative CO_2 emissions from LUC over 2010-2100 of OSCAR to those of the IAM. Each colored cell corresponds to a SSP scenario. Within each cell, the left number corresponds to the cumulative CO_2 emissions from LUC over 2010-2100 calculated by OSCAR, whereas the right number corresponds to the cumulative emissions calculated by the IAM. Each cell is colored after the absolute difference of the scenario, the thresholds being given in the legend (lower line). All cumulative emissions are given in GtC.*

The latter point can be related to our hypothesis for the evolution of shifting cultivations. With the exception of SSP5 under AIM-CGE, SSP3 and SSP4-WTICH-GLOBIOM scenarios are the only scenarios for which the primary traditional bioenergy increases. AIM-CGE did not report any traditional bioenergy for these scenario, and we have assumed an evolution of the primary modern bioenergy without CCS, in the lack of a better driver for shifting cultivations. Because of these assumptions, the area extent of shifting cultivations increases, whereas it decreases for all other scenarios. Heinimann et al. (2017) shows that the area extent of shifting cultivations may be overestimated in LUH1, and we extent these shifting cultivations with an ad hoc assumption. We discuss this method in section 3.4.3.2. The sensibility analysis shows a reduction of the difference, especially stronger for scenarios under AIM-CGE, but still, the cumulative CO_2 emissions from LUC calculated by IAMs remain lower than those calculated by OSCAR. The dependency of the differences with IAMs could point out that the method used in the IAM for calculating LUC emissions still participate to these differences. The dependency with climate policies could be explained by the impact of our assumptions regarding shifting cultivations, that decreases with the decrease in traditional bioenergy, but also harvested biomass, that increases with the increase of modern bioenergies. Yet, the dependency with climate policies could also be explained by the impact of CO_2 fertilization and climate change on LUC emissions, and thus the method used to calculate LUC emissions.

These differences stem either from the use of different methods for the calculation of the CO_2 emissions from LUC, or even the use of different definitions of these emissions, or from the treatment of the land variables. Such differences represent a critical problem: the climate policies are designed to match different levels of radiative forcing, and the climate insights of these scenarios were calculated with MAGICC v6 using directly the CO_2 emissions from LUC calculated by the IAMs, and not those calculated by MAGICC (section 3.2.3.1). The consistency of the calculation of LUC emissions by IAMs and of the climate outputs by MAGICC determine the robustness of the climate policies.

Here, the CO_2 emissions from LUC that we calculate with OSCAR are dependent on the assumptions for harvested biomass and shifting cultivations (section 3.4.3.2). Our reproduction of the transitions in LUC are theoretically biased (section 3.4.1). The algorithm that we use for LUC does not reconstruct perfectly the transitions, be it the historical period from LUH1 or the 6 SSP scenarios provided by LUH2 (section 3.4.2). Nevertheless, all of the differences in CO_2 emissions from LUC between OSCAR and the IAMs cannot be explained only by the treatment of the land variables. The sensitivity analysis to our assumptions regarding shifting and harvest (section 3.4.3.2) shows that a difference still remains, but the major reason is that we have performed several experiments of the third chapter of this thesis with the land variables of SSP scenarios from LUH2, and differences remain, again. Different modellings or even different definitions of CO_2 emissions from LUC (Gasser and Ciais, 2013) could explain the remaining differences. The impact of climate change

feedbacks in these differences could be tested, for instance by turning off climate change feedbacks in OSCAR. Nevertheless, these sources of differences may be investigated for the 6 SSP scenarios treated in LUH2, thanks to the LUMIP project (Lawrence et al., 2016). Finally, as illustrated in section 3.3.5.3, the CO_2 emissions from Land Use Change and the land sink of OSCAR is lower than those of Le Quéré et al. (2016). It hinders the results from this section, and further development of OSCAR, for instance with regard to the modelling of the preindustrial land cover maps and carbon densities may help to solve this problem.

3.3.1.3 Methane emissions

Principal anthropogenic sources of CH_4 are the agriculture, fugitive emissions (oil, coal and gas) and waste. Wetlands and biomass burning emissions are natural and significative contributions to the emissions (O'Connor et al., 2010). Yet, under climate change and through land use, these emissions are perturbed. In figure 3.9, the total CH_4 emissions is calculated as the sum of anthropogenic emissions, the perturbation of wetlands emissions and biomass burning emissions with reference to the preindustrial equilibrium. The lower baseline CH_4 emissions occur with the SSP1, with 189 to 333 MtC/yr in 2100, whereas the higher occur with the SSP3, with 441 to 665 MtC/yr in 2100. Introducing climate policies impact clearly and quickly the emissions, especially with SSP1 and SSP5 scenarios. Broader ranges are obtained under SSP3 and SSP4, that might be an effect from increased inequalities and lower transfers of technologies translated into more uncertain estimates. Scenarios sharing the same forcing target have relatively similar CH_4 emissions, except for scenarios under SSP1. Even though the baseline of SSP1 is relative equivalent to the RCP6.0 of another SSP, the SSP1 scenarios for a given RCP are below in CH_4 emissions to the scenarios for the same RCP and for other SSPs.

We insist on the point that the emissions that we show in figure 3.9 correspond to the sum of the anthropogenic emissions and the perturbation of natural emissions, as described in section 3.2.6. This sum does not correspond exactly to the total CH_4 emissions, for unperturbed natural emissions are not included. It does not affect our climate projection, because OSCAR is based on the modelling of the perturbations from an assumed preindustrial equilibrium. It comes that unperturbed biomass burning and wetlands emissions are assumed to be in equilibrium with the other components of the Earth system. What is represented here is the perturbation in terms of CH_4 emissions, be it from anthropogenic sources, or from the perturbed natural sources. Over 2000-2009, wetlands emissions contributed to about 133-213 MtC/yr (Ciais et al., 2013; O'Connor et al., 2010). The change in 2000-2009 wetlands emissions with reference to the preindustrial equilibrium as calculated by OSCAR is 5.5 MtC/yr (Gasser et al., 2017a). This is only half of the evaluated change evaluated in the WETCHIMP project (Melton et al., 2013), because the capacity of OSCAR to reproduce regional climate changes, and thus local precipitations, is limited. Concerning CH_4 emissions from biomass burning, OSCAR calculates an

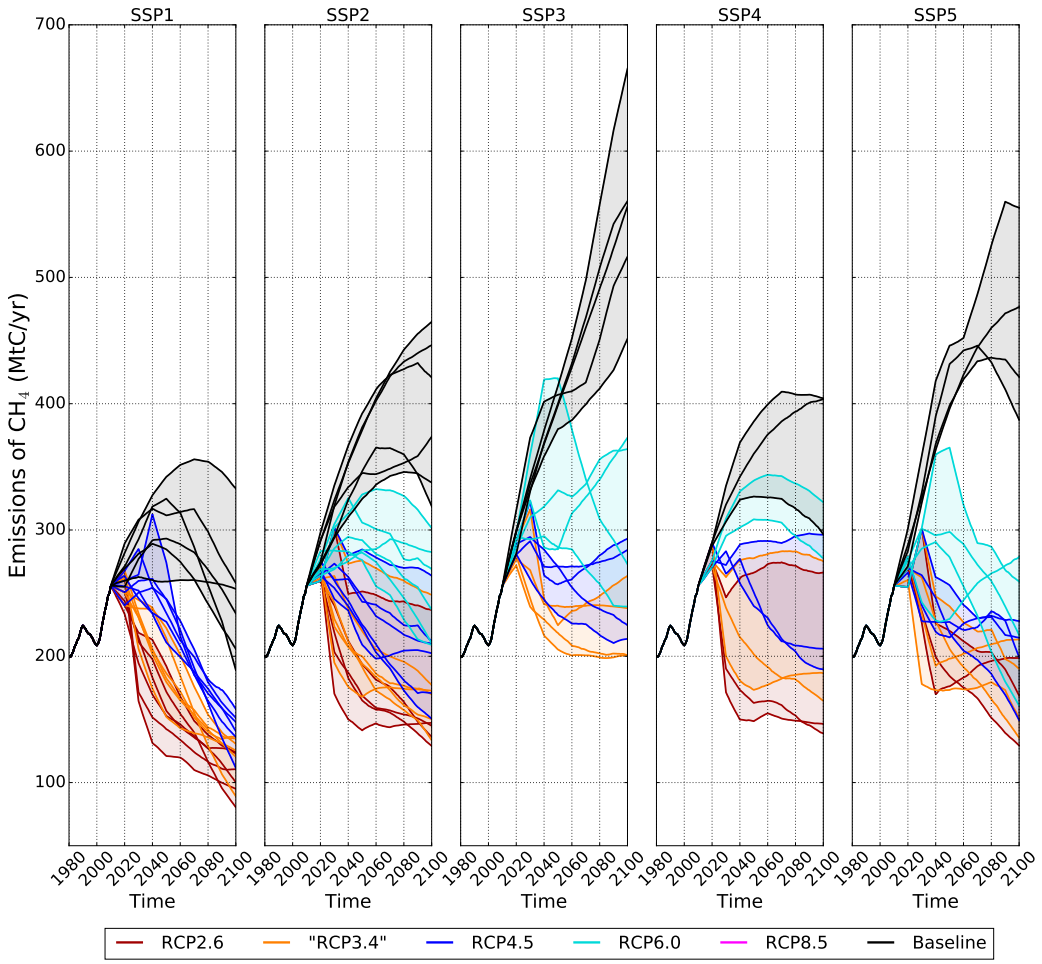

Figure 3.9: *Total CH_4 emissions from 1980 to 2100. The contributions from the perturbation of wetlands emissions and biomass burning emissions with reference to the preindustrial equilibrium are included in this figure. The transition from the historical period and the scenario happens in 2010. Each subfigure details the results for a given SSP. The scenarios are also classified depending on the forcing target. Each line represents an IAM that has run this SSP and this forcing target, and in plain color is their ensemble. For the sake of clarity, uncertainties are not represented here.*

increase for the mean of 1990-2000 with reference to the preindustrial equilibrium by 13.3 MtC/yr, which is comparable to Lamarque et al. (2010), although lower, and with a different temporal profile (Gasser et al., 2017a). Figures for the perturbation of wetlands emissions and biomass burning emissions are available in appendix (section 6.2.7).

We represent in figure 3.10 the fraction of anthropogenic emissions in total CH_4

emissions, that is to say the fraction of direct CH_4 emissions caused by the anthropogenic activity. As a remark, we define the fraction of anthropogenic emissions in total CH_4 emissions R_{anth,CH_4} using equation 3.4, with M_{MC} being the median over the Monte-Carlo members. We insist on the aforementioned point that unperturbed natural emissions are not included here, only anthropogenic emissions and perturbed natural emissions. The 90% confidence interval has also been calculated, but not shown in figure 3.10 in a sake of clarity. Here, this fraction corresponds to the direct anthropogenic emissions, although CH_4 emissions are also indirectly emitted through biomass burning and wetland emissions. The change in these natural emissions is caused by both extensive perturbations, through anthropogenic land use change, and intensive perturbations, for instance through changes in temperatures and precipitations. We choose not to include the change in natural emissions caused by the anthropogenic land use change, to ease the analysis.

$$R_{anth,CH_4} = M\left(\frac{E_{anth,CH_4}}{E_{anth,CH_4} + E_{BB,CH_4} + E_{WET,CH_4}}\right)_{MC} \tag{3.4}$$

In 2010, anthropogenic emissions account for 91.6% of total CH_4 emissions. We observe that by the end of the century, this fraction has decreased for all scenarios, even for the baselines of SSP3, where anthropogenic CH_4 emissions increase along the whole scenario. In 2100, this fraction has reduced from 90% to 50.2%. For scenarios with relative low diminishing fractions, this is due to the increase of all emissions (figures of the appendix, section 6.2.7), although anthropogenic emissions increase faster. According to OSCAR, for scenarios with highly diminishing fractions, anthropogenic emissions decrease, but emissions from biomass burning keep increasing over the whole period. First, wetlands emissions increase, but decrease afterwards. This is due to the stabilization of the increase in global surface temperature (section 3.3.2). This stabilization followed by change in precipitations and land cover induces the reduction in wetlands emissions from as late as 2090, to 2070 for scenarios with highly diminishing fractions. Because of the combination of these effects, scenarios sharing the same SSP and forcing target tend to group, but these groups tend to overlap, especially in SSP2 and SSP5. As a result, this diminishing fraction shows that, in these scenarios, although anthropogenic CH_4 emissions are reduced, the ongoing climate change increase natural emissions, cancelling partially the reductions in these emissions. Instead of partially cancelling the effect of the reductions in CH_4 emissions, it is possible to reduce their emissions, for instance by controlling their water table (Turetsky et al., 2014), and even improve carbon sequestration in this soils, for instance in coastal wetlands (Crooks et al., 2011).

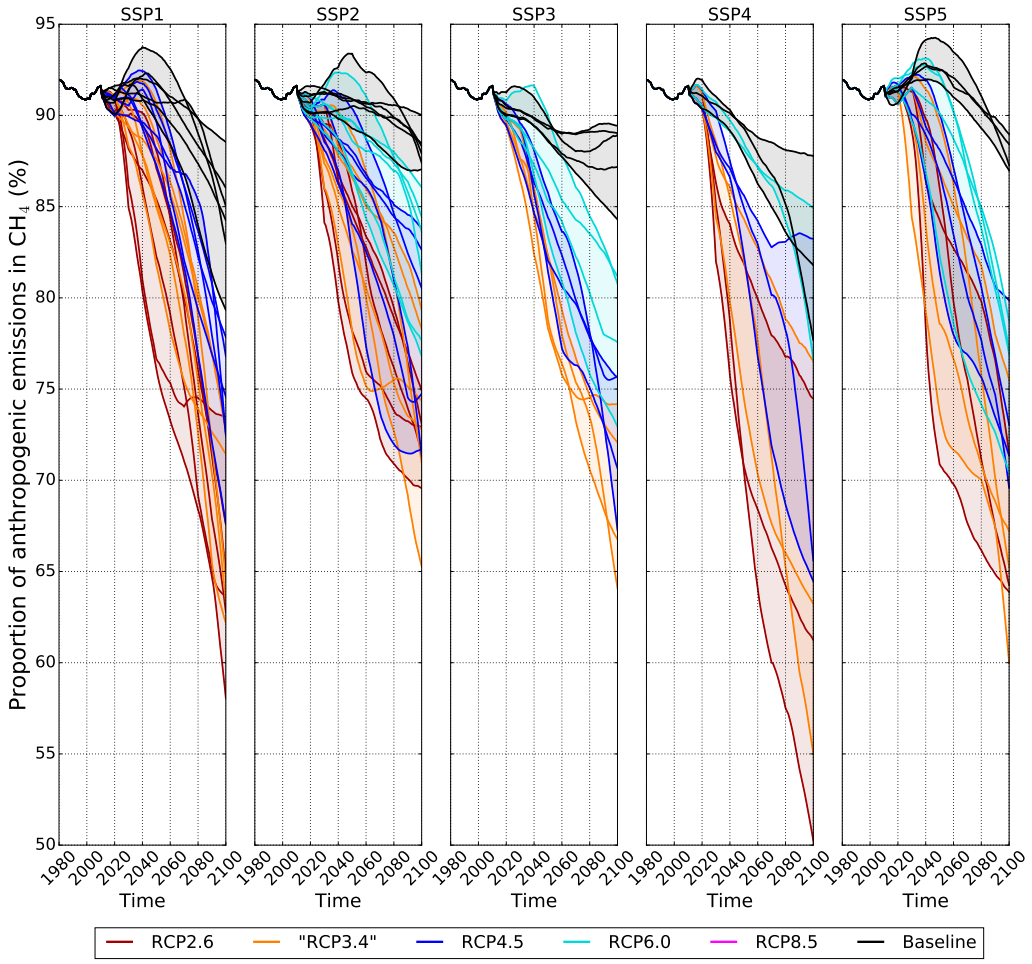

Figure 3.10: *Fraction of anthropogenic emissions in the total CH_4 emissions from 1980 to 2100. The transition from the historical period and the scenario happens in 2010. Each subfigure details the results for a given SSP. The scenarios are also classified depending on the forcing target. Each line represents an IAM that has run this SSP and this forcing target, and in plain color is their ensemble. For the sake of clarity, uncertainties are not represented here.*

3.3.1.4 Nitrous oxide emissions

Principal sources of N_2O are the use of manure and synthetic fertilizers in agriculture, industrial processes and fossil fuel combustion. The perturbation of the nitrogen cycle contributes to the N_2O emissions, for instance through the emissions from aquatic systems (Seitzinger et al., 2000) and biomass burning emissions (Lamarque et al., 2010). In OSCAR v2.2, the only natural contribution to N_2O emissions are biomass burning emissions, for the N_2O emissions from wetlands are not yet implemented in its modelling.

We represent in figure 3.11 the sum of anthropogenic N_2O emissions to the perturbation of N_2O emissions from biomass burning. The SSP1 scenarios have the lower baseline N_2O emissions, ranging from 5.1 to 8.8 MtN/yr in 2100, and the higher occurring with the SSP3 scenarios, ranging from 10.4 to 16.2 MtN/yr in 2100 (figure 3.11). Introducing climate policies has also for effect to reduce these emissions, by reducing their time of peaking and their growth rate. Yet, some scenarios that include climate policies still do not peak before 2100, as shown with SSP3. across SSPs, the emissions associated with scenarios of similar forcing target have relatively different N_2O emissions. Besides, SSP4 and SSP5 show larger ranges for similar radiative forcings.

As for methane, we have represented in figure 3.11 the sum of anthropogenic N_2O emissions and the perturbed N_2O biomass burning emissions, this perturbation being induced mainly by anthropogenic activity. In appendix is represented N_2O emissions from biomass burning (section 6.2.8) We represent in figure 3.12 the fraction of direct anthropogenic emissions in total N_2O emissions, that is to say the fraction of direct N_2O emissions caused by the anthropogenic influence. In 2010, anthropogenic emissions account for 90.3% of total N_2O emissions. We observe that by the end of the century, this fraction has decreased for most scenarios. In 2100, this fraction has reduced to 93.7% to 59.4%. The fraction does not decrease only in baselines, because of anthropogenic N_2O emissions increasing faster than N_2O emissions from biomass burning. In the others scenarios, the same explanation for CH_4 emissions stands: anthropogenic N_2O emissions decrease, but N_2O emissions from biomass burning keep increasing. The same result showed with methane stands here: this diminishing fraction shows that, in these scenarios, although anthropogenic N_2O emissions are reduced, the ongoing climate change increase natural emissions, cancelling partially the reductions in these emissions.

Figures for LUC emissions, N_2O and CH_4 emissions (figures 3.8, 3.9 and 3.11) emphasize that under full participation of the Land Use sector (SSP1 and SSP5), more negative LUC emissions are reached and the reduction in CH_4 emissions are reached faster. Besides, cooperation between countries tend to reduce the range in these emissions calculated by the IAMs: in SSP1 (high cooperation, low fossil-fuels), the ranges are minimal, slightly higher in SSP5 (high cooperation, high fossil-fuels) and higher in SSP4 and SSP5 (low cooperation). Finally, the patterns of N_2O and CH_4 emissions leading to a given forcing target tend to be relatively robust, albeit

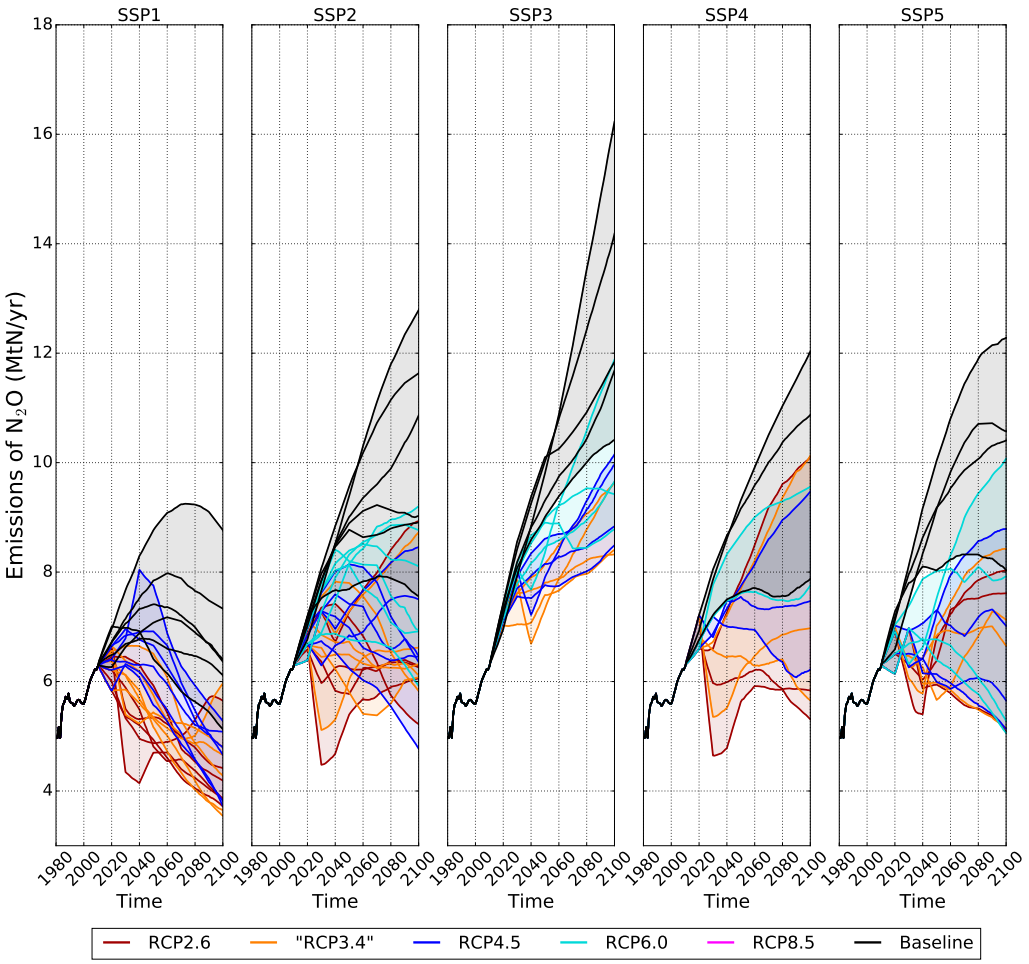

Figure 3.11: *Total N_2O emissions from 1980 to 2100. The contributions from the perturbation of biomass burning emissions with reference to the preindustrial equilibrium are included in this figure. The transition from the historical period and the scenario happens in 2010. Each subfigure details the results for a given SSP. The scenarios are also classified depending on the forcing target. Each line represents an IAM that has run this SSP and this forcing target, and in plain color is their ensemble. For the sake of clarity, uncertainties are not represented here.*

less for the SSP1 and SSP3, and less for N_2O.

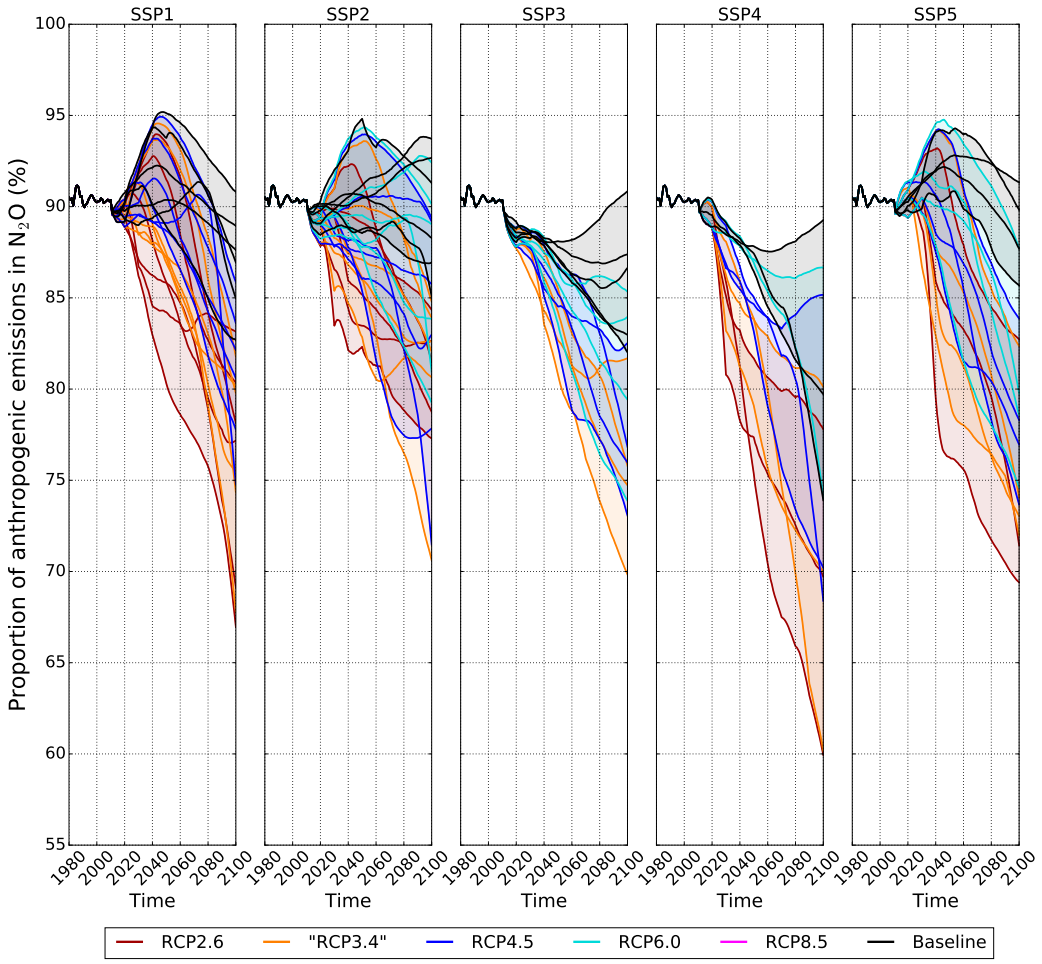

Figure 3.12: *Fraction of anthropogenic emissions in the total N_2O emissions from 1980 to 2100. The transition from the historical period and the scenario happens in 2010. Each subfigure details the results for a given SSP. The scenarios are also classified depending on the forcing target. Each line represents an IAM that has run this SSP and this forcing target, and in plain color is their ensemble. For the sake of clarity, uncertainties are not represented here.*

3.3.1.5 Sulfur dioxide emissions

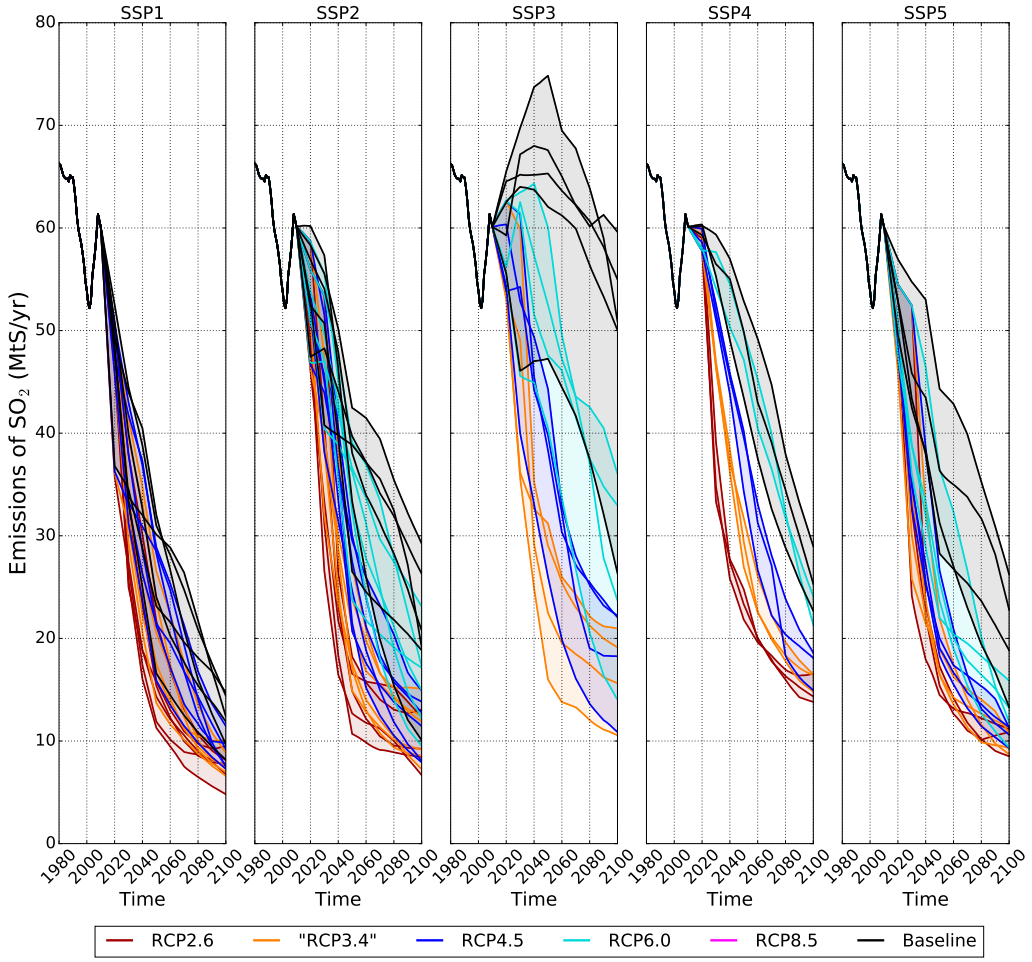

Figure 3.13: *Total SO_2 emissions from 1980 to 2100. The contributions from the perturbation of biomass burning emissions with reference to the preindustrial equilibrium are included in this figure. The transition from the historical period and the scenario happens in 2010. Each subfigure details the results for a given SSP. The scenarios are also classified depending on the forcing target. Each line represents an IAM that has run this SSP and this forcing target, and in plain color is their ensemble. For the sake of clarity, uncertainties are not represented here.*

We also show here the emissions for SO_2. We do not represent other aerosol emissions, to lighten the presentation of these results. The principal sources of SO_2 are through oil and coal combustion, from energy and transport. We represent in figure 3.13 the sum of anthropogenic SO_2 emissions to the perturbation of SO_2 emissions from biomass burning. across SSPs, these emissions are relatively similar, although SSP3 shows the larger emissions. This may be related to the hypotheses

of the scenarios regarding the fossil fuel consumption, although SO_2 emissions from SSP5 are in the range of other SSPs. A complementary reason may be the rapid technological progress and the successful resolution of local environmental problems in SSP5.

As for methane and nitrous oxide, the fraction of direct anthropogenic SO_2 emissions may be represented. In appendix, we show the SO_2 emissions from biomass burning and the fraction of anthropogenic SO_2 emissions (section 6.2.9). The same results for methane stand: this fraction is reduced, even in baselines. Even if anthropogenic SO_2 emissions are reduced, the contribution of biomass burning keep growing, representing in the most extreme cases (SSP5-2.6) 55.5% of the emissions. It means that, in this case, in 2100, perturbed SO_2 emissions from biomass burning may represent as much as SO_2 emissions directly emitted by anthropogenic sources.

3.3.1.6 Fluorinated gases emissions

The F-gases emissions evaluated by the IAMs show extremely rapid increase in their emissions, as shown in figure 3.14. The difference of the emissions that we represent to those of the SSP public database are only caused by the rescale of F-Gases emissions. When considering raw F-gases emissions from IAMs, that is to say without decomposition (section 3.2.2) and rescale (section 3.2.6), the SSP scenarios provides estimates for F-Gases emissions in 2005 that range from 532 to 757 to $MtCO_2eq/yr$. All baseline scenarios present high emissions at the end of the century. For comparison, with the same gases, the F-Gases emissions in the RCPs rises up to 2276 $MtCO_2eq/yr$ with the RCP8.5. AIM-CGE present the lowest baseline emissions with 1910 to 3179 $MtCO_2eq/yr$ in 2100, whereas GCAM4 present the highest baseline emissions with 3506 to 7167 $MtCO_2eq/yr$ in 2100. Under WITCH, the baseline emissions for the whole period do not depend on the SSP, all being equal to 3423 $MtCO_2eq/yr$ in 2100.

Contrary to baselines scenarios, most scenarios implementing a climate policy present a decrease in 2100 F-Gases emissions compared to 2005. However, there are some exceptions. In MESSAGE, the decrease in F-Gases emissions starts between 2020 and 2060, but without going under 2015 levels of emissions. The same observation applies for the SSP2-RCP6.0 under REMIND. WITCH also provides for 2100 F-gases emissions 2481 $MtCO_2eq/yr$ for the SSP1-RCP6.0 and 2217 $MtCO_2eq/yr$ for the SSP4-RCP6.0. For comparison with Velders et al. (2015), in terms of global emissions for the fluorinated gases, its upper range scenarios by 2050, about 5.2 $GtCO_2eq/yr$ is reached only by baselines of SSP5.

As explained in section 3.2.2, we decompose the F-Gases category in several fluorinated gases, but we also deduce other halogenated compounds such as SF_6. These halogenated compounds contributes by up to 1392 $MtCO_2eq/yr$ in 2005, but only up to 17 $MtCO_2eq/yr$ in 2100. We represent the result of our decomposition of the F-Gases for SSP1s scenarios in the figure 3.15. The detail of the results under the other storylines are given in appendix (section 6.2.2). The most emitted

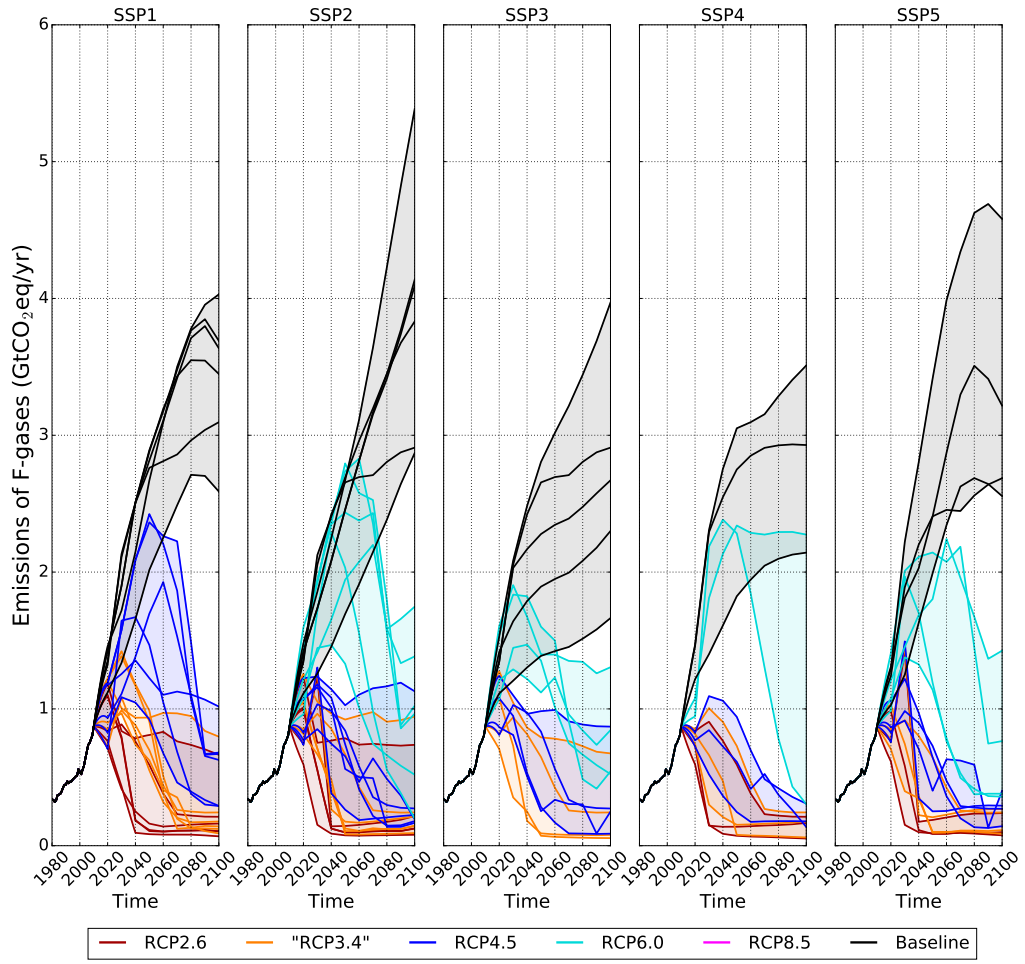

Figure 3.14: *Emissions of the category Fluorinated gases of the SSP scenarios from 1980 to 2100. The transition from the historical period and the scenario happens in 2010. Each subfigure details the results for a given SSP. The scenarios are also classified depending on the forcing target. Each line represents an IAM that has run this SSP and this forcing target, and in plain color is their ensemble. For the sake of clarity, uncertainties are not represented here.*

compound is the HFC-134a. Yet, other fluorinated gases must not be neglected, because of their impact on radiative forcing. For instance, compared to HFC-134a, HFC-143a has 10 times smaller emissions, but its GWP is 3.7 bigger. We observe that the implementation of a climate policy reduces as well the emissions of all fluorinated gases. This effect is particularly visible for SF_6. Besides, the stronger change in fluorinated emissions concerns the first implementation of a climate policy: strengthening the policy for reaching more ambitious forcing targets tends to have a weaker effect for the reduction of these specific emissions.

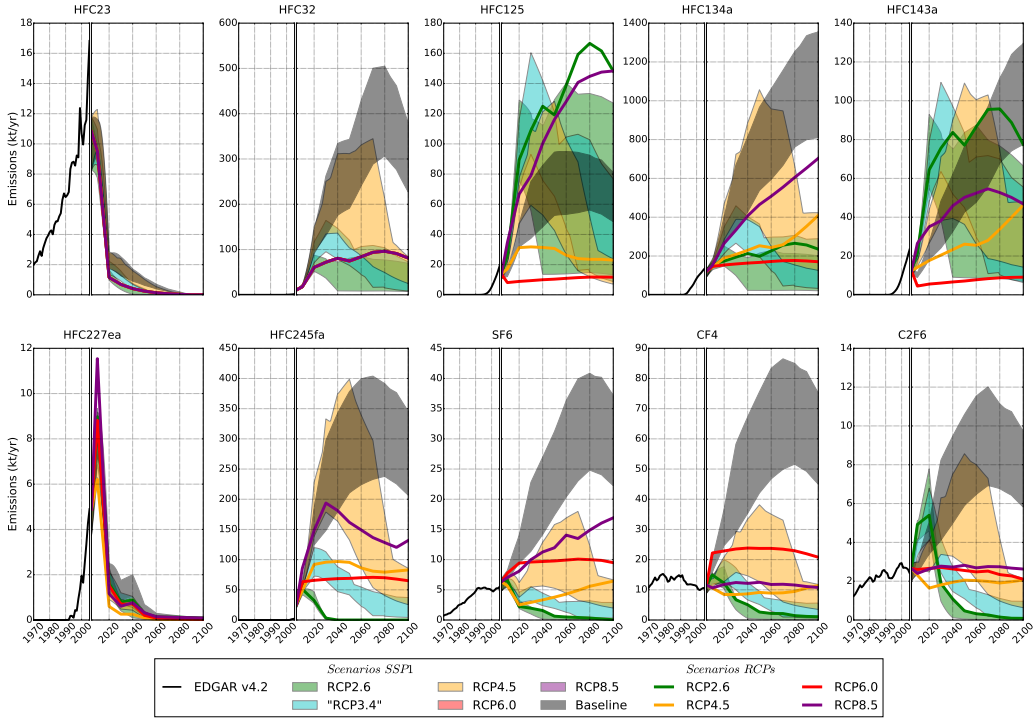

Figure 3.15: *Decomposition of the emissions of the category Fluorinated gases of the SSP scenarios illustrated with SSP1. For comparison, the emissions over 1970-2005 are given, prescribed by EDGAR v4.2 (Joint Research Centre, 2011). We also represent for comparison the emissions from RCPs (Meinshausen et al., 2011b). The color of lines corresponds either to the RCP targeted in the SSP scenarios (shaded areas), or to the RCP itself (plain lines). Similar figures for the other SSPs are given in appendix.*

3.3.2 Increase in global surface temperature

Using OSCAR, we calculate the projected increase in global surface temperature with reference to 1986-2005 (ΔT) for the 103 SSP scenarios selected (figure 3.16). In the same figure, we compare our results to the RCP climate projections calculated by the ESMs, representing the median ΔT and the 90% confidence intervals of their ensembles.

- All SSP-RCP scenarios are within the range of RCPs calculated by ESMs. The baselines of SSP1 and SSP4 are between RCP6.0 and RCP8.5, SSP2 principally in RCP8.5, SSP3 close to RCP8.5 and SSP5 is very close to RCP8.5.
- Even though SSP scenarios are not meant to follow the RCPs, but to reach it by the end of the century, we can observe that SSP scenarios tend to follow the ΔT of the RCPs. In other words, SSPs-RCP4.5 follow relatively well

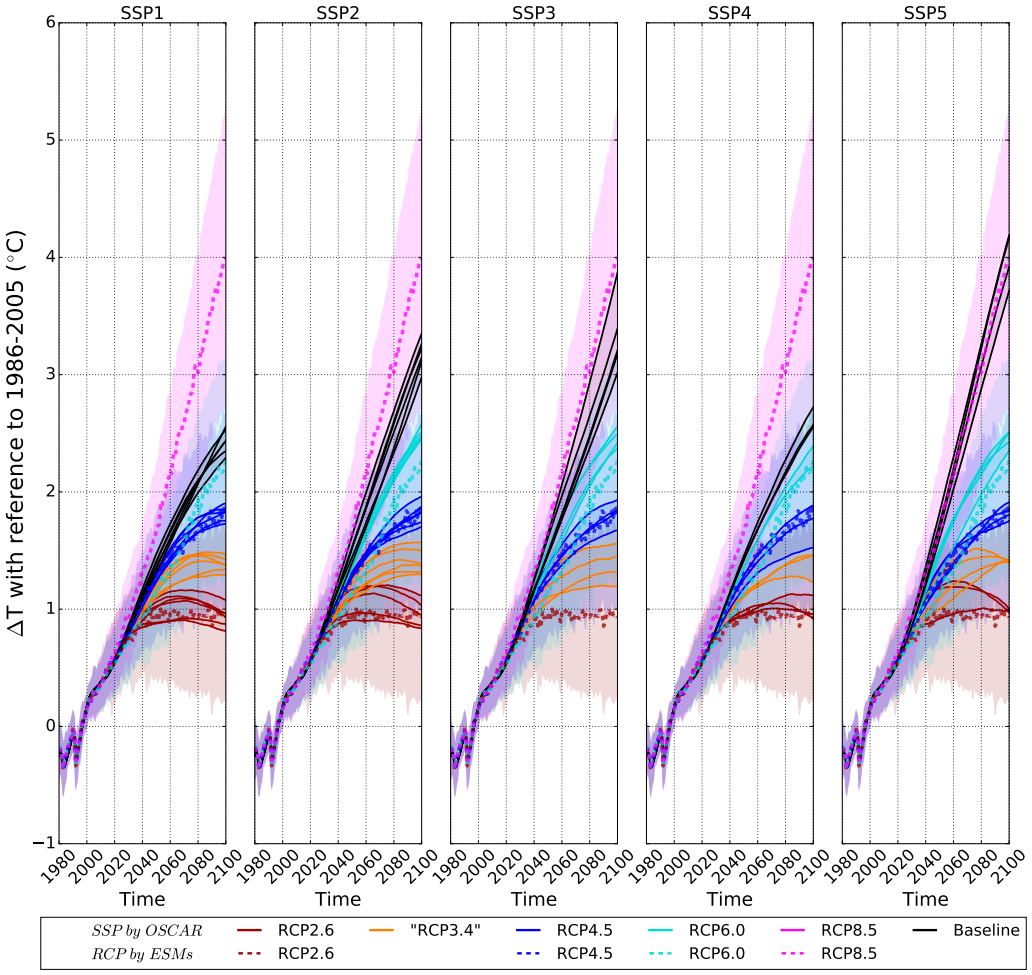

Figure 3.16: *Increase in global surface temperature with reference to 1986-2005 calculated by OSCAR for the SSP scenarios. Each subfigure details the results for a given SSP. The scenarios are also colored depending on their RCP. Each plain line represents an IAM that has run this SSP-RCP. For comparison, the increase in global surface temperature calculated by the ESMs for the RCPs are represented in terms of median and 90% confidence interval. For the sake of clarity, uncertainties on SSP-RCP climate projections are not represented here.*

ESMs-RCP4.5, but SSPs-RCP2.6 do not follow as well ESMs-RCP2.6. For SSPs-RCP6.0, most of the ΔT are above those of the RCP6.0 itself.

- We observe that in general, the more ambitious is the forcing target, the bigger is the range of the estimates. This dispersion can be as high as 0.36°C (SSP3-RCP3.4 and SSP4-RCP4.5).

- We note that, before 2100, scenarios with an low climate forcing target may

still have higher ΔT than scenarios a higher climate forcing target. After a given date, the scenarios with the low climate forcing target show sharp decrease in ΔT. For instance, some scenarios SSP5-RCP2.6 show a smaller ΔT than SSP5-"RCP"3.4 only after 2068.

- We observe that the SSP5 present the scenarios with the longest times to mitigate climate change, causing overshoots as high as 0.27°C. The assumptions of this storyline regarding fossil-fuel development and low international cooperation may be responsible for this inertia.

In the precedent figure, uncertainties are not represented, For the sake of clarity. Yet, these uncertainties may help to shed light on several aspects regarding forcing targets, especially in the frame of the Paris Agreement. Yet, two important points have to be precised first.

- For each scenario SSP-RCP-IAM, we produce the probability distributions, assuming lognormal distributions. We assume that for a given SSP-RCP, all IAMs are equiprobable, to aggregate the distributions of each SSP-RCP into a single one. We acknowledge that our method may introduce a bias: the coverage in terms of IAMs is not identical from a SSP-RCP to another. As described in table 3.1, some SSP-RCP-IAM are not available because the IAM could not find a solution (e.g. all SSP3-RCP2.6) or because the IAM did not report this scenario (e.g. all SSP4 under IMAGE). Yet, we choose to proceed with this bias. We deduce the probability density functions for the ΔT since the preindustrial equilibrium.

- OSCAR v2.2 assumes that the preindustrial equilibrium is in 1700 (Gasser et al., 2017a). Yet, the period 1850-1900 is often used as a reference for the global surface temperature (Hartmann et al., 2013), albeit evolutions in land cover changes, volcanic eruptions and the beginning of the industrial revolution responsible for fossil-fuel emissions. As a remark, 1720-1800 may be more appropriate as a reference for a preindustrial equilibrium (Hawkins et al., 2017). According to Hartmann et al. (2013), global surface temperature has increased by 0.61 °C from 1850-1900 to 1986-2005. Our method is then to calculate the probability density functions for the increase in global surface temperature in 2100 with reference to 1986-2005, and then add 0.61 °C to comply to 1850-1900 as preindustrial equilibrium. For information, OSCAR calculates an increase in global surface temperature of 0.94 °C from 1700 to 1986-2005.

For comparison, the increased in global surface temperature provided by MAGICC to the SSP database is 0.91 °C in 2005 (IIASA, 2018c). As far as we know (IIASA, 2018e; SSP, 2018; van Vuuren et al., 2017; Fricko et al., 2017; Fujimori et al., 2017; Calvin et al., 2017; Kriegler et al., 2017), we are unsure if the increase in global

surface temperature in the SSP database includes a rescale, eventually on 1986-2005, or if it is directly the outputs of the model.

We represent the global probability density functions for the ΔT, with reference to 1850-1900, obtained in 2100 for each SSP-RCP in figure 3.17. SSP3-RCP2.6 is empty, because IAMs did not find a solution to reach this target from SSP3 conditions. The SSP1-RCP6.0 is not represented, because the baseline is similar in terms of forcing target. Across SSP, common targets (RCP) show obviously relatively close appearances. Only baselines differ, for that they can only be related to the storyline, and not to a forcing target.

- The SSP5 presents the higher median ΔT, with 4.6°C of median ΔT.
- SSP3 and SSP2 are relatively close with respectively 3.9 and 3.8°C of median ΔT.
- SSP4 and SSP1 are also relatively close with respectively 3.2 and 2.9 °C of median ΔT.

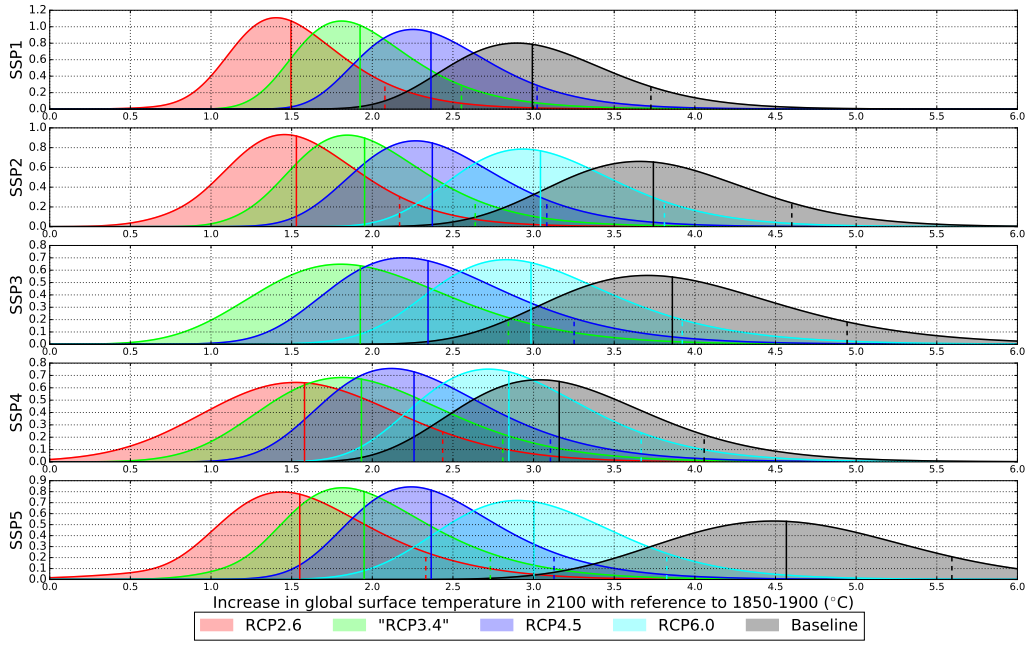

Figure 3.17: *Global probability density functions of the ΔT in 2100 with reference to the preindustrial equilibrium defined as 1850-1900. Each pannel corresponds to a storyline SSP. Each shaded area corresponds to a forcing target RCP. Each vertical plain line correspond to the median of the distribution. Each vertical dashed line correspond to the 90th percentile of the distribution (probability of 90% to stay below this temperature). The probability density functions of each scenario SSP-RCP-IAM are aggregated for each SSP-RCP assuming all IAMs are equiprobables.*

These relations can directly be related to the fossil-fuels consumption (Riahi et al., 2017). In SSP5, the CO_2 emissions from Energy & Industry are the highest compared to the baselines of other storylines. Those of SSP4 and SSP1 are the lowest ones.

We observe that distributions are very similar across SSPs when the forcing target is ambitious, either with RCP2.6 (1.5 to 1.6°C) or with RCP3.4 (1.9 to 2.0°C). Climate policies targeting RCP6.0 show a stronger variability across SSPs with median ΔT of 2.8 to 3.0°C

We have also represented in figure 3.17 the 90th percentile with vertical dashed lines. In other words, for each distribution, there is a probability of 90% to stay below this ΔT. In IAMs, climate policies are built to reach a given forcing target. If the median of the distribution is targeted, it means that there is 50% of chance to limit the global warming below this target, but also 50% of chance to exceed it. In the baseline of SSP5, there is a 90% probability not to exceed 5.6°C, whereas the median is at 4.6°C. In the most optimistic scenario, the SSP1-RCP2.6, there is 90% of probability not to exceed 2.08°C, whereas the median is at 1.5°C. Using either the 90th percentile instead of the median ΔT increase by 40% the odds, and increase by about 0.5 to 1°C the ΔT.

These global probability density functions can also be used to calculate the chance not to exceed the 2°C target of the Paris Agreement (table 3.8). We acknowledge that these scenarios are not build to respect the Paris Agreement (below 2 or even 1.5°C), but to reach the radiative forcing of the RCPs. For a given RCP, we observe differences in the distributions accross SSP scenarios. This is due to the use of different socio-economic assumptions in different sets of models. The 2°C target of the Paris Agreement is then used as a marker, to compare the chances of the sets of pathways at this point. For instance, under the target RCP2.6, the 2°C target is exceeded with a probability that range from 13 to 26%. Even though each group of SSP-RCP scenarios targets the same RCP, and then approximately the same ΔT, the probabilities to respect the 2°C still depend on the SSP.

	RCP2.6	**"RCP3.4"**	**RCP4.5**	**RCP6.0**	**Baseline**
SSP1	13	43	83		99
SSP2	16	46	81	100	100
SSP3		45	74	98	100
SSP4	26	46	69	97	99
SSP5	22	46	80	98	100

Table 3.8: *Probabilities of exceeding the 2.0 °C (%) temperature goal under the 5 storylines of the SSPs under the different forcing targets. The probability distributions of all the scenarios from the 6 IAMs and the 5 forcing targets are used to produce these estimates.*

We observe that the 2°C is exceeded with 26% in SSP4 but with 22% in SSP5: the risk would then be higher in SSP4. Aiming at RCP2.6, the weight of the lower

tail of the distribution of SSP4 is higher than the one of SSP5. It stands as well for the weight of the higher tail: SSP5 is more centred compared to SSP4. According to their storylines (table 3.2), SSP5 embodies a development based on competitive markets, innovation and participatory societies, whereas SSP4 embodies an unequal development using both carbon-intensive fuels and low-carbon energies. A possible explanation would be the larger differences in SSP4 compared to SSP5 (section 3.3.1). It would mean that increasing the inequalities in development flatten the distribution of emissions and thus climate change. One could evaluate the distributions in all emissions to compare them inbetween SSP4 and SSP5, but evaluating the distributions in ΔT is more efficient although less direct. These results are consistent with the literature (e.g. Swart et al. (2003), Blanco et al. (2014), Haraway (2015)).

We remind that these uncertainties are only representative of the modeling in OSCAR (section 3.2.6). OSCARv2.3 is not constrained using observations. Future development will allow to do so, bringing critical changes to these distributions. Besides, a robustness analysis shows a relatively low impact on the distributions. For information, the probabilities presented in table 3.8 may vary by 1 to 6%.

3.3.3 Radiative forcings

3.3.3.1 Total radiative forcing

We also produce the total radiative forcings (figure 3.18).

Over the historic, strong variations in radiative forcing occur in 1982 and 1991. Several volcanic eruptions are responsible for this evolution, the principals being El Chichon in 1982 and the Pinatubo in 1991 (Myhre et al., 2013). Besides, the sudden decrease in radiative forcing in 2010 is caused by our assumptions regarding contrails, volcanic and solar radiative forcing (section 3.2.4).

Because of the method used for calibrating climate policies in SSP-RCP scenarios, these scenarios do not reach exactly their target of radiative forcing, or exceed it, as illustrated with a range of 3.12 to 3.75W/m^2 for the SSP3-RCP3.4. Yet, the SSP scenarios aim at the same 2100 radiative forcings, and using the same compact climate model MAGICC v6.8 and the same harmonization process (IIASA, 2018e). This range in the final radiative forcing is the result of several effects. First, depending whether the IAM calibrate its climate policy using a hard coupling with MAGICC, or any other climate model, or using an ex-post calculation, or using carbon budgets, the forcing target is not reached with the same accuracy. This effect is supported by the range in the total radiative forcing of the SSP scenarios, as provided in the SSP database (IIASA, 2018c). A second explanation lies in our treatment of the land variables (section 3.2.3), which may lead to different CO_2 emissions from LUC, as discussed in section 3.4.2. Finally, differences in the modelling of MAGICC v6.8 and OSCAR v2.2 may cause additional biases. Though, a robust assessment of such biases requires the comparison of scenarios produced by

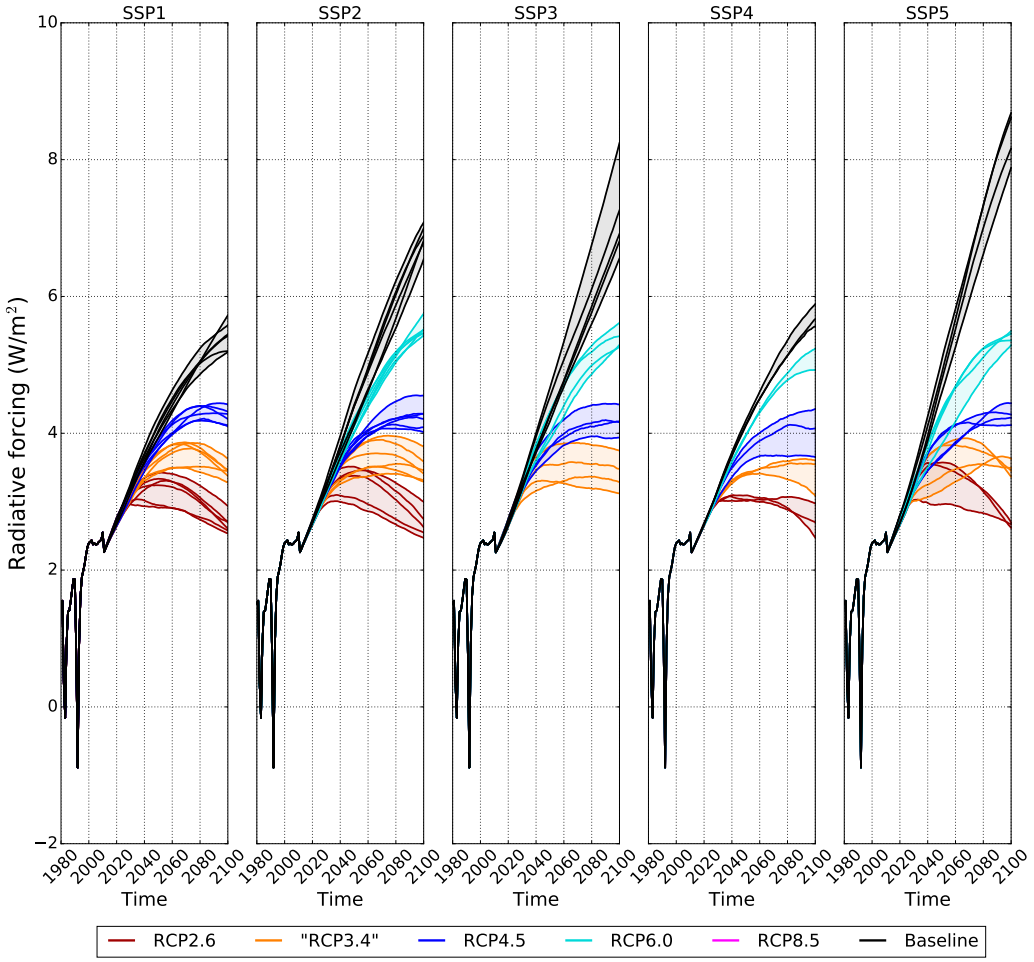

Figure 3.18: *Radiative forcing (W/m^2). Each subfigure details the results for a given SSP. The scenarios are also classified depending on the forcing target. Each plain line represents an IAM that has run this SSP and this forcing target. For comparison, the radiative forcing of 2011 with reference to 1750 is estimated at 2.3 W/m^2 (Myhre et al., 2013). For the sake of clarity, uncertainties on SSP climate projections are not represented here.*

both MAGICC and OSCAR, with full transparency. The climate insights of the SSP scenarios produced with MAGICC still lacks transparency (section 3.2.3), hindering the comparison for these scenarios.

Most of the scenarios targeting RCP2.6 have overshoots greater than $0.4W/m^2$, as detailed with the highlighted cells in table 3.1. WITCH-GLOBIOM tends to produce scenarios without overshoots, even for ambitious targets. We observe that the scenarios under SSP4 follow relatively similar patterns of radiative forcing in the first half of the century, especially when targeting RCP2.6 and RCP3.4. Fossil-

fuel CO_2 emissions are relatively similar, but the differences in patterns for other emissions tend to compensate altogether. Under SSP5, the scenarios that share the same forcing target tend to converge, even though these scenarios are different in terms of patterns of emissions. Over 2080-2100, the radiative forcing decreases with a rate of about -2.65.10^{-2} W.m^{-2}.yr^{-1} in SSP5-RCP2.6-REMIND-MagPIE, but only -8.06.10^{-3} W.m^{-2}.yr^{-1} in SSP5-RCP2.6-AIM-CGE. Although these two scenarios reach the same objective, their following evolutions in terms of radiative forcing differ by a factor of about 3. Such a quick mitigation of climate change in the late 21st century in REMIND-MagPIE may lead to socioeconomic implications very different to those of the slower mitigation represented in AIM-CGE.

3.3.3.2 Individual radiative forcings

OSCAR evaluates also all individual radiative forcings. We represent a synthesis in figure 3.19.

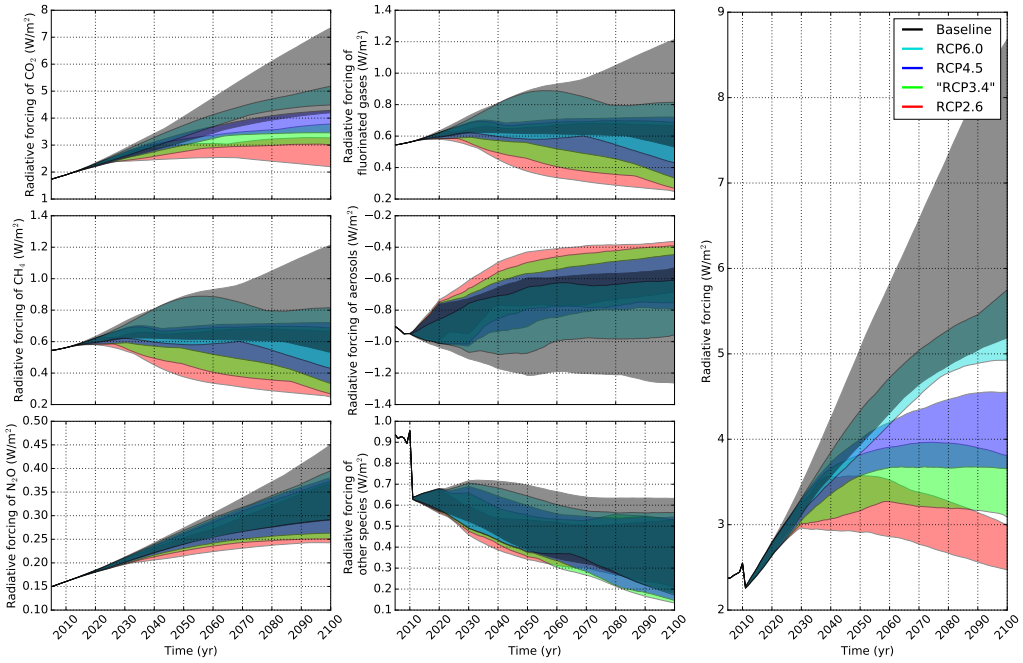

Figure 3.19: *Individual radiative forcings (W/m^2). On the first column are those of CO_2, CH_4, N_2O. On the second column are those of F-Gases, aerosols and others. On the last one is the total radiative forcing. Scenarios can be distinguished according to their forcing target. For comparison, the radiative forcing of 2011 with reference to 1750 is estimated at 2.3 W/m^2 (Myhre et al., 2013).*

- The major component of radiative forcing is CO_2, ranging from 2.20 to 7.35 W/m^2 in 2100. Thus, no scenario returns to, or under, the level of 2010 in

terms of radiative forcing of CO_2, which is of 1.90 W/m^2. Scenarios can very well be grouped depending on their forcing target, for this contribution of the radiative forcing is the major one (Ciais et al., 2013), and represents the primary object of most climate policies.

- To the radiative forcing of CH_4, we include the contribution of stratospheric water vapor, because of the impact of the concentration of CH_4 on the formation of stratospheric water vapor. This radiative forcing of CH_4 ranges from 0.25 to 1.21 W/m^2 in 2100. Out of 103 scenarios, 58 have their median radiative forcing of CH_4 decreasing below the 2010 level (0.56 W/m^2) before 2100. For CH_4, cenarios sharing the same forcing target still form group, although the groups by forcing targets tend to overlap.

- The radiative forcing of N_2O ranges from 0.24 to 0.45 W/m^2 in 2100. As observed with CH_4, scenarios sharing the same forcing target still form group, although the groups by forcing targets tend to overlap.

- The radiative forcing of fluorinated gases includes here only the contributions of HFC-23, HFC-32, HFC-125, HFC-134a, HFC-143a, HFC-227ea, HFC-245fa, CF_4, C_2F_6, C_6F_14 and SF_6, as described in section 3.2.2. Their radiative forcing starts at 0.03 W/m^2 in 2010, but finishes between 0.03 and 0.70 W/m^2 in 2100. The baselines correspond to the upper group of scenarios, whereas scenarios assuming a climate policy tend to have lower radiative forcing for F-Gases. As explained in section 3.3.1.6, different groups can be formed depending on the forcing target.

- In the radiative forcing of aerosols, we include the effects of primary and secondary organic aerosols, black carbon, sulphated aerosols, nitrates and clouds. These effects tend to reduce the radiative forcing by 0.95 W/m^2 in 2010, and by 0.36 to 1.26 W/m^2 in 2100. The only scenarios for which the cooling effect of aerosols is not reduced in 2100 compared to 2010 are the baselines of SSP3 under AIM-CGE, GCAM4, MESSAGE-GLOBIOM and WITCH-GLOBIOM, plus the SSP3-RCP6.0 of MESSAGE-GLOBIOM. According to 10 scenarios, this cooling effect is more than halved. This concerns in SSP1 the scenarios targeting RCP2.6, RCP3.4 and RCP4.5 for REMIND-MagPie and MESSAGE-GLOBIOM, RCP2.6 and RCP3.4 for AIM-CGE and RCP2.6 for IMAGE. In SSP2, this concerns only MESSAGE-GLOBIOM for RCP2.6. These scenarios illustrate a case. The mitigation of climate change leads to the reduction of all anthropogenic emissions, greenhouse gases and aerosols. Yet, the radiative forcing of aerosols is negative, and reduces climate change (Rose et al., 2014b). Thus, their reduction leads to an increase of the total radiative forcing. Nevertheless, their reduction is required for public health and environmental issues (Nemet et al., 2010). For the radiative forcing of aerosols, groups of scenarios sharing the same forcing target overlap too much, because of the dependency of all its contributions primarily to the IAM, and then to the SSP.

- The radiative forcing of other agents corresponds to all other contributions not included in others: volcanic, solar, contrails, stratospheric and tropospheric ozone, albedo of Land Cover Changes, deposition of black carbon on snow and halogenated compounds that are not F-Gases. As explained with the figure 3.18, the sudden decrease in 2010 can be explained by the hypotheses regarding the solar, volcanic and contrails radiative forcings (section 3.2.4). These other effects have contributions of 0.95 W/m^2 in 2010, and 0.65 W/m^2 in 2011. In 2100, all these contributions range from 0.13 W/m^2 to 0.65 W/m^2. All scenarios present an overall decrease of these effects. For this radiative forcing as well, groups of scenarios sharing the same forcing target overlap too much, because of the dependency of all its contributions primarily to the IAM, and then to the SSP.

From the observations of overlapping groups of scenarios sharing the same forcing target, we deduce the existence of compensating effects between the different forcing agents. This result is more detailed in section 3.3.4.1 with CO_2, in section 3.3.4.2 with CH_4 and in section 3.3.4.3 with N_2O.

3.3.4 Atmospheric concentrations

3.3.4.1 Carbon dioxide

We represent the variation of the atmospheric concentrations of CO_2 with reference to 2005 for the SSP scenarios in figure 3.20. As a preliminary remark, the land sink, the ocean sink and the carbon fractions are analyzed in section 3.3.5.

Very different CO_2 concentrations are obtained for the SSPs, even when considering only their baselines. The median values for the baselines range from 601 to 660 ppm for SSP1, but from 967 to 1094 ppm for SSP5, which would represent more than doubling of the current atmospheric concentration. The highest projection would be 3.94 times larger than the preindustrial concentration of 278 ppm.

Yet, introducing climate policies effectively reduces CH_4 emissions and thus its atmospheric concentrations. In SSP1, SSP2 and SSP3, the pathways of each climate policies are clearly distinguished, whereas those of SSP4 and SSP5 tend to overlap. As introduced in section 3.3.3.1, this points at compensating effects between the different radiative forcings. For instance, for SSP4 targeting RCP4.5, GCAM4 proposes a scenario reaching 523 ppm in 2100, whereas for SSP4 targeting RCP3.4, WITCH-GLOBIOM proposes a scenario reaching 556 ppm in 2100, and AIM-CGE proposes 539 ppm in 2100. In this case, the compensation is caused by much lower emissions for CH_4 for the two latter scenarios compared to the ones of GCAM4 under SSP4 targeting RCP4.5. Although Fossil-Fuel & Industry emissions for SSP5 tend to converge by group of forcing targets (section 3.3.1.1), LUC emissions tend to introduce differences (section 3.3.1.2) between the atmospheric concentrations of CO_2 by group of climate forcing as illustrated in figure 3.20. Besides, in SSP2, the concentrations tend to converge although they did not in terms of Fossil-Fuel

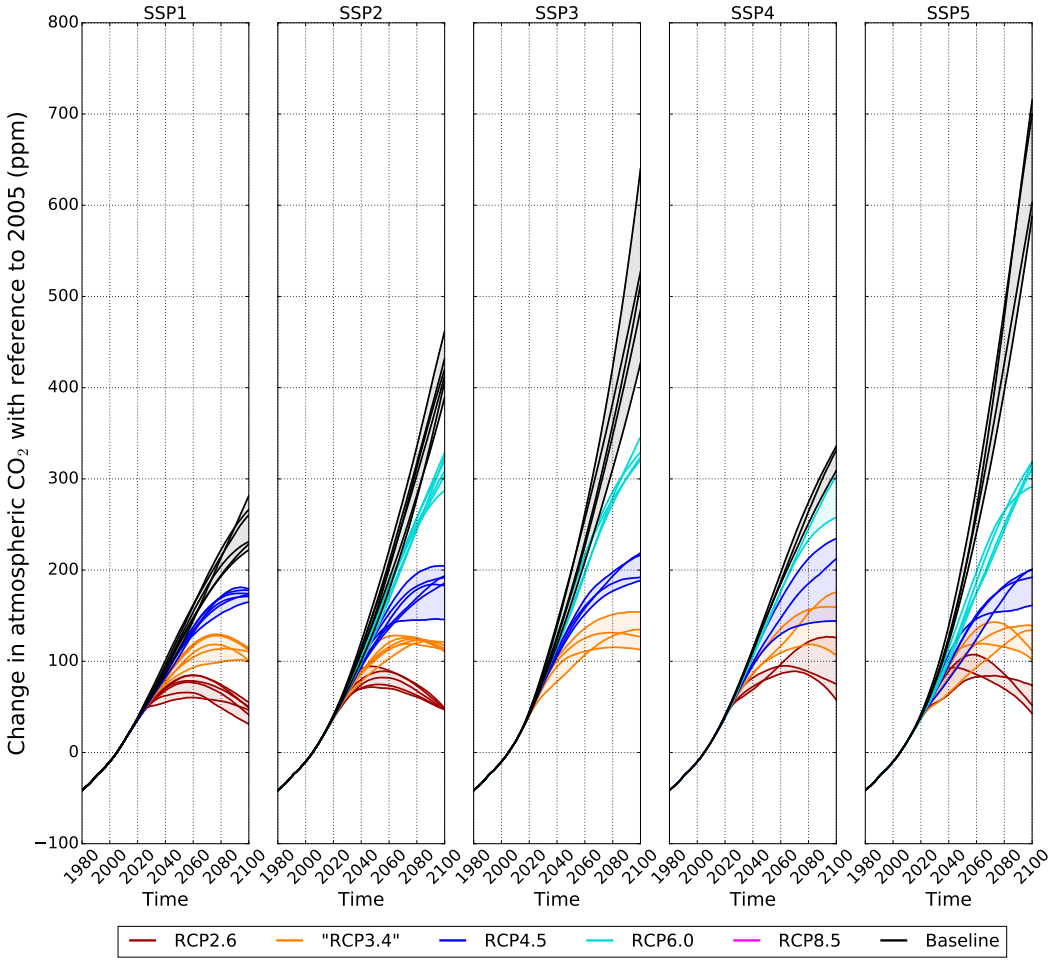

Figure 3.20: *Atmospheric concentrations of CO_2 with reference to 2005. Each subfigure details the results for a given SSP. The scenarios are also classified depending on the forcing target. Each plain line represents an IAM that has run this SSP and this forcing target. For comparison, the atmospheric concentration of CO_2 in 2005 was 378.8 ppm (Hartmann et al., 2013). For the sake of clarity, uncertainties on SSP climate projections are not represented here.*

& Industry emissions and LUC emissions. These compensating effects are stronger for SSP4, which is the storyline where the differences between the world regions are intensified. This might be a reason for the strength of these effects.

across SSPs, the patterns of the scenarios that lead to specific forcing targets are relatively similar, baselines excluded. Yet, there are some differences in timing, principally due to the assumptions made in the storylines for the delays in participation to climate policies.

3.3.4.2 Methane

We represent the variation of atmospheric concentrations of CH_4 with reference to 2005 for the SSP scenarios in figure 3.21. This concentration depends on the anthropogenic and natural emissions. As shown in section 3.3.1.3, even though anthropogenic emissions are affected by climate policies, the contribution of the perturbation of natural emissions (wetlands, biomass burning) increase. In SSP1, anthropogenic emissions may represent only 50.2% of these emissions (figure 3.10). Besides, this concentration depends as well on the stratospheric chemistry, affected by an ensemble of emissions.

First, very different CH_4 concentrations are obtained for the SSPs, even when considering only their baselines. The median values for the baselines range from 1774 to 2393 ppb in 2100 for SSP1, but from 2849 to 3768 ppb in 2100 for SSP3. Thus, only with baselines, CH_4 concentrations are between more than double or slightly lower than the 2010 level.

Then, all scenarios that introduce a climate policy show a reduction in CH_4 concentrations. The most effective reductions occur in SSP1 and SSP5, for which the land use sector completely participates to climate change mitigation. This could be attributed to a reduction of the emissions from livestock and agriculture. In SSP2 and SSP4, the land use sector has only a partial participation. In SSP3, it has a limited participation, but the food demand and the agriculture productivity are lower than those of SSP2 and SSP4. In SSP1, all scenarios including climate policy lead to a reduction of CH_4 concentrations compared to 2010. In SSP5, most of them do. In SSP3, only 3 out of 11 scenarios succeed in a reduction of CH_4 concentrations compared to 2010.

Finally, the scenarios sharing the same forcing targets and the same SSP tend to overlap, and these groups are very different across SSPs in terms of atmospheric concentrations of CH_4. For instance, in SSP4, GCAM4 proposes CH_4 emissions pathways for target RCP4.5 and RCP3.4 that are both significantly greater than those of AIM-CGE and WITCH-GLOBIOM for the same forcing target. In 2100, GCAM4 proposes 2145 ppb for RCP3.4, whereas AIM-CGE and WITCH-GLOBIOM proposes respectively 1714 and 1648 ppb for RCP4.5. As shown in the section 3.3.3.2, the same compensating effect in radiative forcing can be seen through atmospheric concentrations. In other words, it shows the existence of trade-offs not only between sectors, but also between greenhouse gases, in order to reach a specific forcing target.

3.3.4.3 Nitrous oxide

We represent the variation of atmospheric concentrations of N_2O with reference to 2005 for the SSP scenarios in figure 3.22.

Just like methane, this concentration depends on the anthropogenic and natural emissions. As shown in section 3.3.1.4, even though anthropogenic emissions are affected by climate policies, the contribution of the perturbation of natural emis-

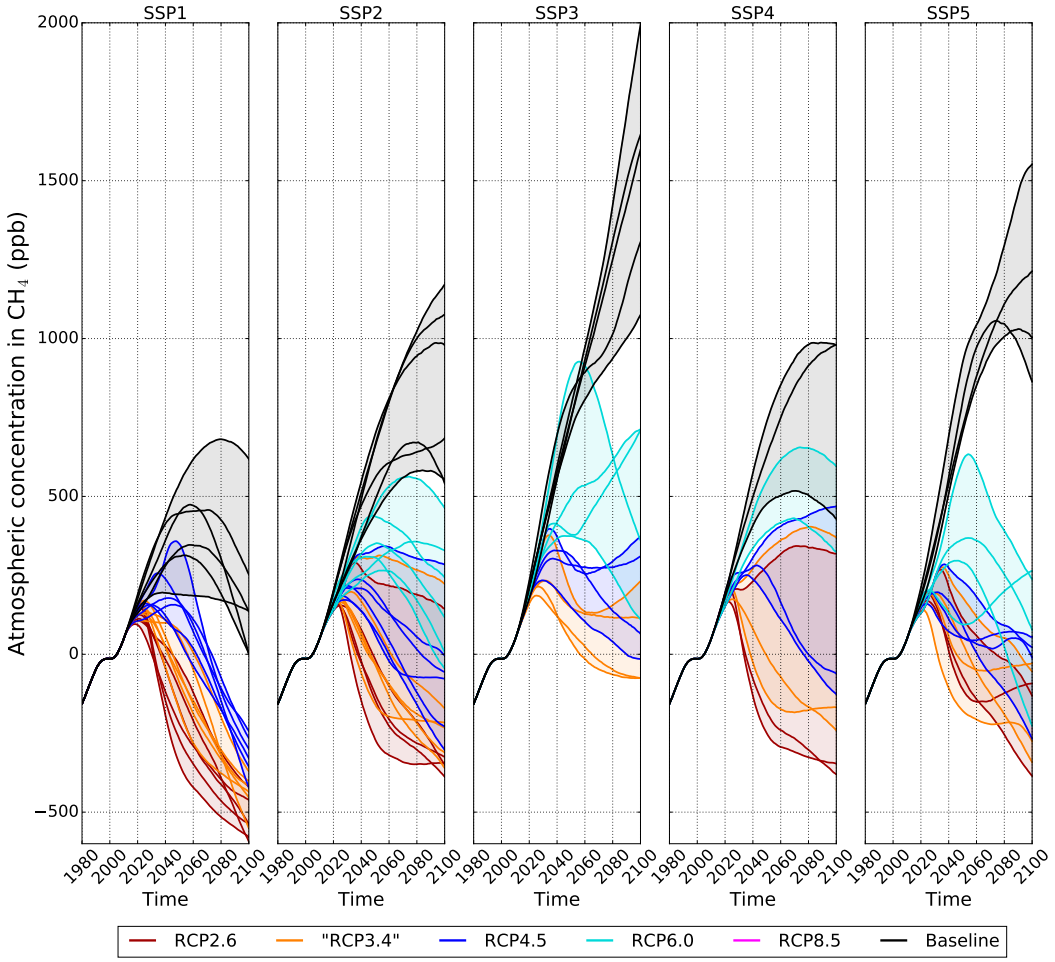

Figure 3.21: *Atmospheric concentrations of CH_4 with reference to 2005. Each subfigure details the results for a given SSP. The scenarios are also classified depending on the forcing target. Each plain line represents an IAM that has run this SSP and this forcing target. For comparison, the atmospheric concentration of CO_2 in 2005 was 1774.4 ppb (Hartmann et al., 2013). For the sake of clarity, uncertainties on SSP climate projections are not represented here.*

sions (biomass burning in OSCAR) increase. In SSP1, anthropogenic emissions may represent only 59.4% of these emissions (figure 3.12). Besides, this concentration depends as well on the stratospheric chemistry, affected by an ensemble of emissions.

First, the median values for the baselines range from 367 to 399 ppb in 2100 for SSP1, and from 408 to 435 ppb in 2100 for SSP5. For all baselines, but also for all SSP scenarios, N_2O concentrations have risen compared to 2100 levels.

Then, concerning the other scenarios, for all IAMs, the emissions in 2100 are lower for their scenarios with climate policies when comparing to their baselines

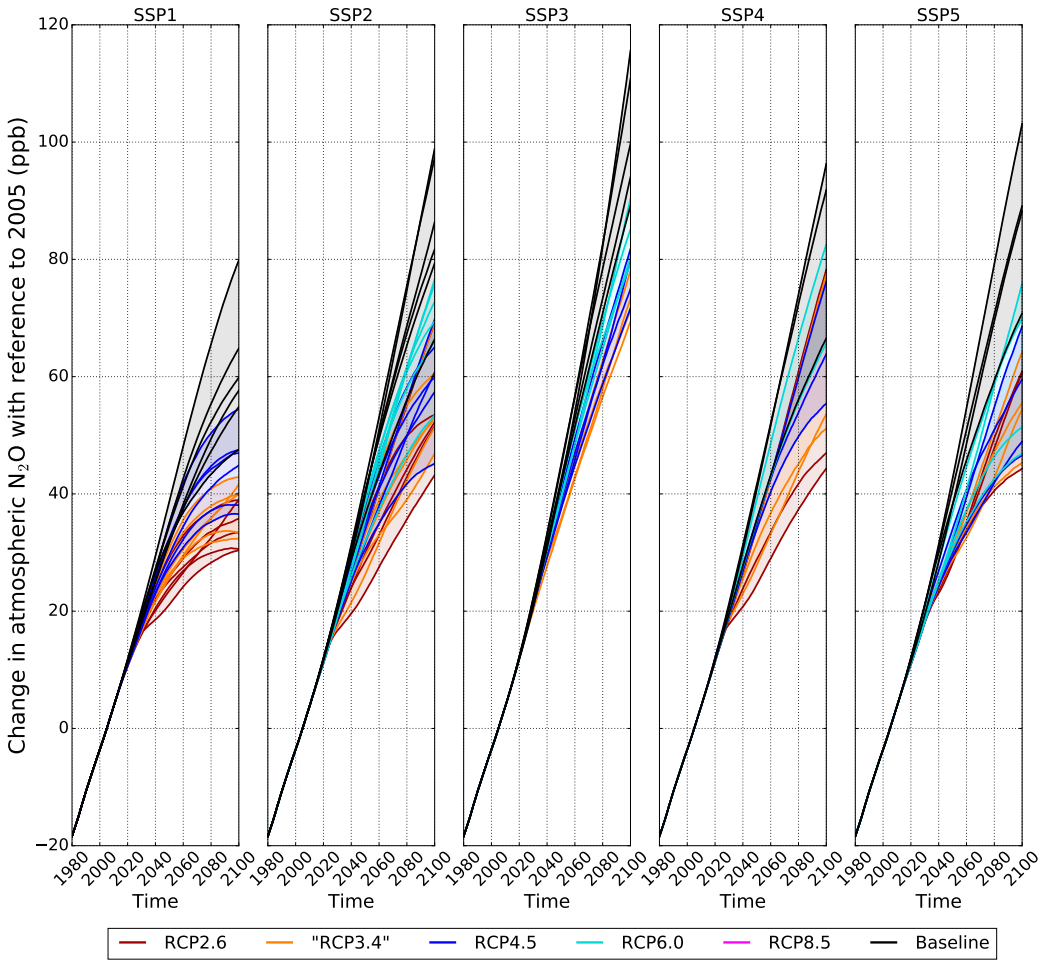

Figure 3.22: *Atmospheric concentrations of N_2O with reference to 2005. Each subfigure details the results for a given SSP. The scenarios are also classified depending on the forcing target. Each plain line represents an IAM that has run this SSP and this forcing target. For comparison, the atmospheric concentration of CO_2 in 2005 was 319.3 ppb (Hartmann et al., 2013). For the sake of clarity, uncertainties on SSP climate projections are not represented here.*

scenarios. Between 2010 and 2100, the SSP4-RCP3.4 and SSP4-RCP2.6 of GCAM4 are the only scenarios that are above their baselines, up to 2021 for SSP4-RCP3.4. However, climate policies tend to have a lower effect on N_2O concentrations compared to the effects on CO_2 or CH_4 concentrations. We observe even cases where strengthening the climate policy lead to an increase in N_2O concentrations in 2100. For instance in SSP5, REMIND-MagPie proposes respectively from the RCP6.0 to the RCP2.6 targets 366, 368, 374 and 380 ppb. A possible explanation could be the increase in N_2O emissions from croplands for the production for biofuels. Veri-

fying this possibility could be done by using emissions at sector level, which is not provided in the SSP public database.

Finally, as shown with individual radiative forcings (section 3.3.3.2) and with the atmospheric concentration of methane (section 3.3.4.2), scenarios sharing the same SSP and same forcing target form groups, but these groups overlap. It leads to a compensation of the different radiative forcings, finally reaching the forcing target. Yet, it could also be explained by an uncertainty in the calculation of these emissions greater than for CO_2.

3.3.5 Carbon cycle

3.3.5.1 Ocean carbon sink

We represent the variations of the ocean carbon sink (figure 3.23). This sink follows globally the variation of the CO_2 emissions from Fossil-Fuels & Industry and from LUC. As these emissions increase, the ocean remove more and more carbon because of the increase in the atmospherical concentration (figure 3.20). As emissions decrease, the atmospherical concentration stabilizes. However, the increase in ΔT decreases the capacity of the ocean to absorb and store carbon. It reduces the amount of carbon absorbed by the ocean, as illustrated in section 3.3.5.3.

In 2100, the ocean sink has been amplified to -2.71 to -3.70 GtC/yr in 2100 in the baselines of SSP1, and to -4.79 to -6.46 GtC/yr in 2100 in the baselines of SSP5. For comparison, the ocean sink of CO_2 in 2000 was 2.0 $\pm$ 1.0 GtC/yr (Takahashi et al., 2009). With the implementation of climate policies, CO_2 emissions are reduced leading to a decrease in the sink. According to OSCAR, there is no scenario in which the ocean sink becomes a net source of carbon.

Baselines excluded, climate policies effectively reduce CO_2 emissions, thus decrease the ocean sink. For each forcing target, the patterns are relatively similar across SSPs. Yet, the SSP4 shows some overlaping groups of scenarios, principally because of the trade-offs between CO_2, CH_4 and N_2O (sections 3.3.4.1, 3.3.4.2 and 3.3.4.3).

3.3.5.2 Land carbon sink

We represent the variations of the land carbon sink (figure 3.24). This sink follows the variation of the CO_2 emissions from Fossil-Fuels & Industry and from LUC. The patterns are relatively similar to those of the ocean carbon sink (figure 3.23). Similarly to the ocean carbon sink, we observe that the land sink decrease before stabilization of atmospherical CO_2. The capacity of the ocean to absorb and store carbon has degraded before, as illustrated in section 3.3.5.3.

In 2100, the land sink has changed to -1.91 to -2.94 GtC/yr in the baselines of SSP1, and to -3.38 to -4.68 GtC/yr in 2100 in the baselines of SSP5. For comparison, the land sink of CO_2 in 2000 was 2.6 $\pm$ 1.2 GtC/yr (Ciais et al., 2013). For the

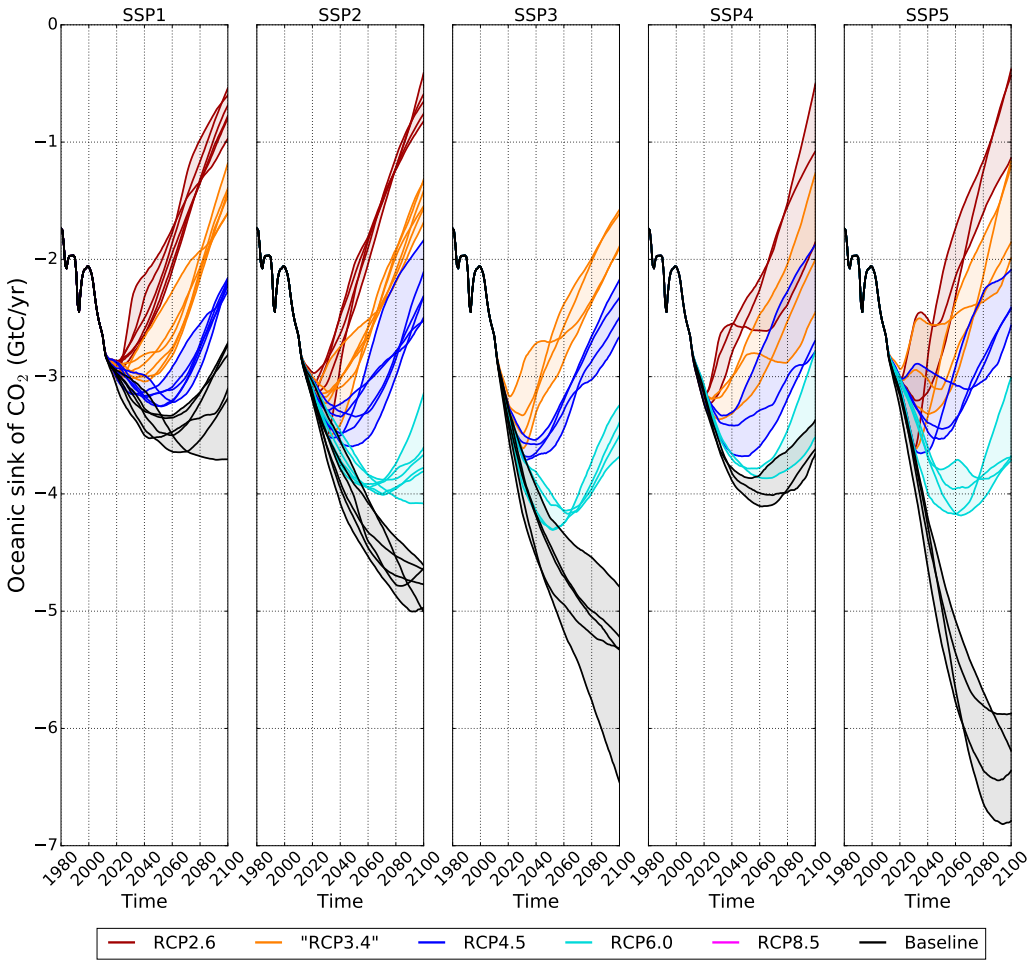

Figure 3.23: *Ocean sink of CO_2. Each subfigure details the results for a given SSP. The scenarios are also classified depending on the forcing target. Each plain line represents an IAM that has run this SSP and this forcing target. For the sake of clarity, uncertainties on SSP climate projections are not represented here.*

baselines of the SSP3 and SSP5, the increase in the land sink is not as fast as the ocean sink. This phenomenon appears in a lesser extent in all scenarios, and can be seen in the early evolutions. Over 2000-2020, the median ocean carbon sink has decreased by 1.03 GtC/yr, but by 0.89 GtC/yr for the land carbon cycle. This result indicates that the land sink tends to be more degraded than the ocean carbon sink, especially with high ΔT.

By 2100, several land sinks have become net sources. It occurs only in scenarios targeting RCP2.6, because of the strong decrease in the atmospherical concentration, leading to the land reservoir returning its stored carbon. It concerns principally SSP2 and SSP5, because of higher CO_2 emissions followed by a strong decrease in

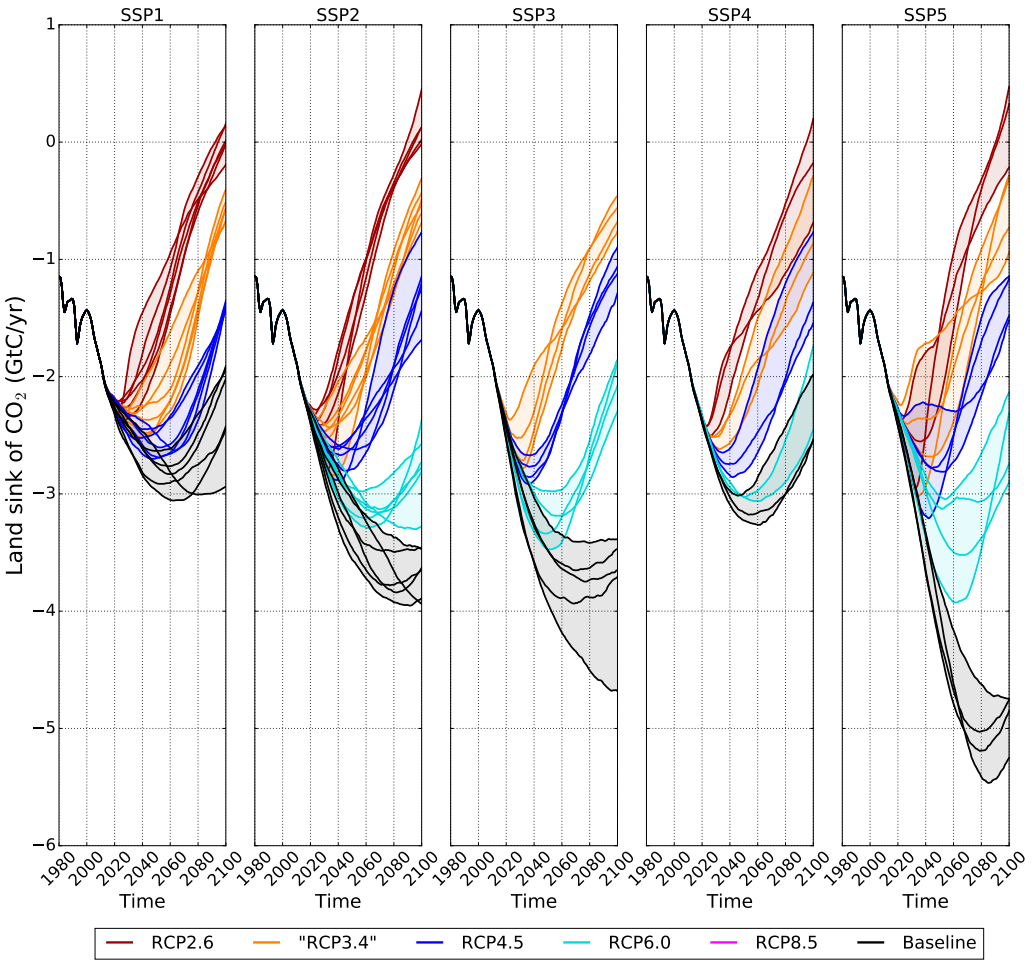

Figure 3.24: *Land sink of CO_2. Each subfigure details the results for a given SSP. The scenarios are also classified depending on the forcing target. Each plain line represents an IAM that has run this SSP and this forcing target. For the sake of clarity, uncertainties on SSP climate projections are not represented here.*

these emissions. In SSP2-RCP2.6 and in 2100, the median land sink is 0.45 GtC/yr under GCAM4, 0.13 GtC/yr under AIM-CGE and MESSAGE-GLOBIOM and only 0.02 GtC/yr under IMAGE. In SSP5-RCP2.6 and in 2100, the median land sink is 0.47 GtC/yr under GCAM4 and 0.32 GtC/yr under REMIND-MagPIE. In SSP4-RCP2.6, emissions are reduced fast enough to reduce this effect, leading to only 0.20 GtC/yr under GCAM4. In SSP1-RCP2.6, emissions are reduced fast enough as well: the median land sink is 0.16 GtC/yr under MESSAGE-GLOBIOM, 0.14 GtC/yr under AIM-CGE and only 0.01 GtC/yr under REMIND-MagPIE. This phenomenon of reversal of the land sink may affect the long term climate consequences of transformation pathways.

Yet, as illustrated in section 3.3.5.3, the land sink of OSCAR is lower than the one calculated in Le Quéré et al. (2016). This difference hinders the results from this section, and further development of OSCAR with regard to the modelling of the preindustrial land cover maps and carbon densities may help to solve this problem.

3.3.5.3 Carbon fractions

The CO_2 emissions from energy and industry (the usual category "Fossil Fuels & Industry", section 3.3.1.1) and from Land Use Change (section 3.3.1.2) are partially absorbed by the ocean carbon sink (section 3.3.5.1) and the land carbon sink (section 3.3.5.2). Here, we compare the partioning for the historical period (2006-2015) before calculating the cumulative carbon fractions for the scenarios.

According to the latest Global Carbon Budget (Le Quéré et al., 2016), 26% of the carbon emitted over 2006-2015 has been absorbed by the ocean, 30% by the land, and the other 44% of the carbon has remained in the atmosphere. For the climate projections of the SSP scenarios, we start the scenario from 2010: the period 2010-2015 introduces a variation. Under the CO_2 emissions from energy and industry $E_{FF\&I}$ (sections 3.2.6 and 3.3.1.1) and the CO_2 emissions from Land Use Change E_{LUC} (sections 3.2.3.5 and 3.3.1.2), and using its ocean sink $\Delta F_{\downarrow,ocean}$ and its land sink $\Delta F_{\downarrow,land}$, we calculate for each scenario the median of the carbon fractions (C) along the Monte-Carlo members ($M\left(X\right)_{MC}$). This operation is written in equation 3.5. Normalization to 100% is executed over the three fractions altogether.

$$C_{ocean} = M\left(\frac{\int_{2006-2015}\Delta F_{\downarrow,ocean}dt'}{\int_{2006-2015}\left(E_{FF\&I}+E_{LUC}\right)dt'}\right)_{MC} \tag{3.5a}$$

$$C_{land} = M\left(\frac{\int_{2006-2015}\Delta F_{\downarrow,land}dt'}{\int_{2006-2015}\left(E_{FF\&I}+E_{LUC}\right)dt'}\right)_{MC} \tag{3.5b}$$

$$C_{atmosphere} = M\left(\frac{\int_{2006-2015}\left(E_{FF\&I}+E_{LUC}-\Delta F_{\downarrow,ocean}-\Delta F_{\downarrow,land}\right)dt'}{\int_{2006-2015}\left(E_{FF\&I}+E_{LUC}\right)dt'}\right)_{MC} \tag{3.5c}$$

Over 2006-2015, the mean of these fractions over all scenarios is 52.8% for the atmosphere, 27.2% for the ocean and 20.0% for the land. The carbon fraction for the land is underestimated by 10 %, leaving the atmosphere with 8.8% more carbon. Even though the partioning depends on the scenario through the 2010-2015 period, the mean of the airborne fraction on all these scenarios is 52.8%, and ranges from 51.7 to 54.5%. This difference in the airborne fraction could be explained either by the period 2010-2015 or by the modelling in OSCAR. According to Le Quéré et al. (2016), $E_{FF\&I}$ has an average of 9.3 GtC/yr over 2006-2015, and E_{LUC} has an average of 1.30 GtC/yr over 2006-2015. With the SSP scenarios, the mean of the average of $E_{FF\&I}$ over 2006-2015 across scenarios is 9.20 GtC/yr, but it ranges from 9.02 to 9.54 GtC/yr. Concerning E_{LUC}, its mean is 0.96 GtC/yr and it ranges

from 0.81 to 1.21 GtC/yr across scenarios. Yet, these difference in the emissions are not enough to explain the difference in the airborne fraction. Even under the scenario that lead to the closer conditions to Le Quéré et al. (2016) (AIM-CGE in the baseline of SSP3), we obtain 9.30 GtC/yr for Fossil Fuels & Industry, and 1.21 GtC/yr for Land Use Change, but still 54% for the airborne fraction. As noticed in Gasser et al. (2017a), CO_2 emissions from Land Use Change from OSCAR are lower on 1959-2010 compared to Le Quéré et al. (2015), because of the biome-specific preindustrial carbon densities. Gasser et al. (2017a) notices as well that the land sink is also lower on 1959-2010 compared to Le Quéré et al. (2015), because of 4 specific preindustrial land cover maps, but also because of the difference in the spatial and temporal variability of the ΔT. For these reasons, it calls the results of sections 3.3.5.2 and 3.3.1.2 into question. Further development of OSCAR with regard to the modelling of the preindustrial land cover maps and carbon densities may help to solve this problem.

Keeping in mind that the airbone fraction should be lower, and the land carbon fraction higher, we turn to the SSP scenarios. The assessment of an annual partioning in all scenarios interferes with the fact that several transformation pathways have their total CO_2 emissions becoming zero. To overcome this difficulty, we calculate the cumulative carbon fraction for each one of the scenarios, as described in equations 3.6. The cumulative emissions and sinks are used, and the median over the members of the Monte-Carlo setup is calculated, along the 90% confidence interval. Normalization to 100% is applied to the three domain. The results are represented in figure 3.25.

$$C_{ocean}\left(t\right) = M\left(\frac{\int_{1700}^{t}\Delta F_{\downarrow,ocean}dt'}{\int_{1700}^{t}\left(E_{FF\&I}+E_{LUC}\right)d't}\right)_{MC} \tag{3.6a}$$

$$C_{land}\left(t\right) = M\left(\frac{\int_{1700}^{t}\Delta F_{\downarrow,land}dt'}{\int_{1700}^{t}\left(E_{FF\&I}+E_{LUC}\right)dt'}\right)_{MC} \tag{3.6b}$$

$$C_{atmosphere}\left(t\right) = M\left(\frac{\int_{1700}^{t}\left(E_{FF\&I}+E_{LUC}-\Delta F_{\downarrow,ocean}-\Delta F_{\downarrow,land}\right)dt'}{\int_{1700}^{t}\left(E_{FF\&I}+E_{LUC}\right)dt'}\right)_{MC} \tag{3.6c}$$

According to OSCAR, of all the CO_2 emissions from 1700 to 2010, 47.8% have remained in the atmosphere, 30.1% have been absorbed by the ocean, and 22.0% have been absorbed by the land. The SSP scenarios that implement climate policies reduce the cumulative airborne fraction. This is due to the reduction of the emissions, that allows the sinks to absorb more of the already emitted CO_2, but also to negative emissions that enhance this reduction of the airbone fraction. The carbon remaining in the atmosphere from 1700-2100 emissions may represent only 33.2%, but also as high as 61.1% in the worst cases. The scenarios with ambitious climate policies lead to an increase of the carbon sequestration in the land, that may be as

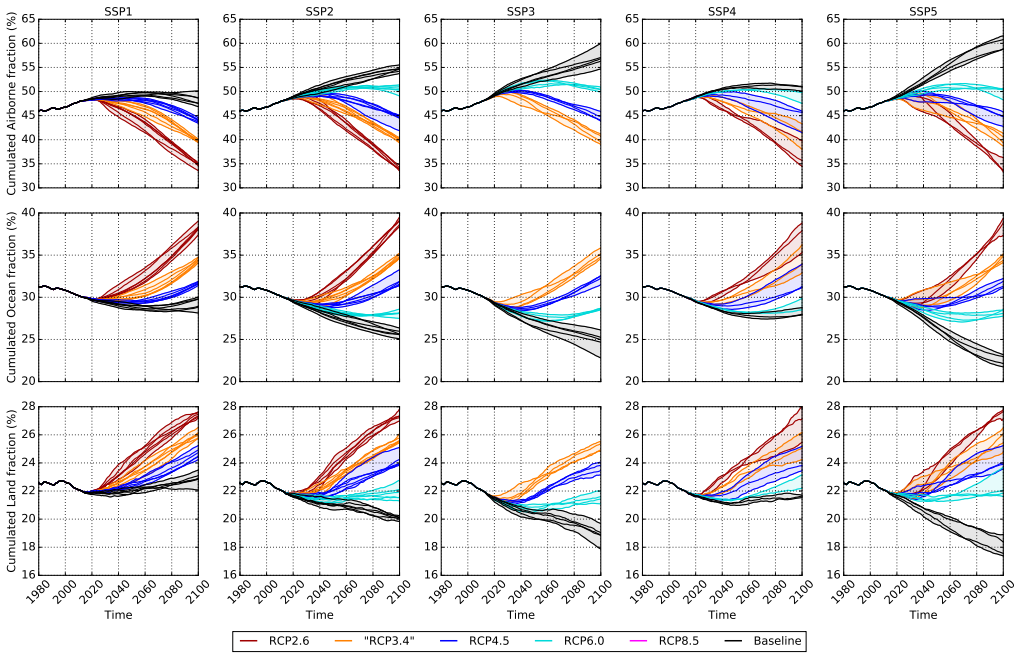

Figure 3.25: *Cumulative carbon fraction as described in equations 3.6. The lower line corresponds to the fraction of the carbon emitted since 1700 that has been absorbed by the land ; the middle line to the fraction absorbed by the ocean ; the upper line to the fraction remaining in the atmosphere. Each column details the results for a given SSP. The scenarios are also classified depending on the forcing target. Each plain line represents an IAM that has run this SSP and this forcing target.*

high as 27.7% of the total CO_2 emissions. Yet, land may be degraded in the worst cases, reducing the capacity of the land to store carbon, leaving only 17.3% of the total carbon in the land. As noticed in sections 3.3.5.1 and 3.3.5.2, degradation of the capacity of the ocean occurs not as fast as the one from land. The emitted CO_2 over 1700-2100 remains at 39.2% in the ocean under the scenario with the strongest mitigation, but reduced to 21.6% under the scenario with the highest CO_2 emissions.

The evolution of these fractions over 2010-2100 may be related to the cumulative total CO_2 emissions over the period, which explains why fractions of scenarios sharing the same forcing target are relatively similar, even across SSPs. Yet, within scenarios sharing the same forcing target, the evolution of these fractions depend as well on the eventual trade-offs in the reductions of the emissions of CO_2 and other forcing agents. It depends as well on the temporal patterns of these reductions. For instance, scenarios with overshoots have their sinks sooner degraded. Finally, the other biogeochemical cycles, such as the one of nitrogen, are affected by their corresponding emissions, such as N_2O or NO_X, introducing another feedback. However, this latter effect is not included yet in OSCAR v2.2.

3.3.6 Biomass burning emissions

As explained in section 3.2.6 and through equation 3.3, the variation of natural emissions, such as wetlands, and the variation in biomass burning emissions are not included in the emissions provided in most cases, if not all. Thus, OSCAR is used to calculate these emissions during the projections of the SSP scenarios.

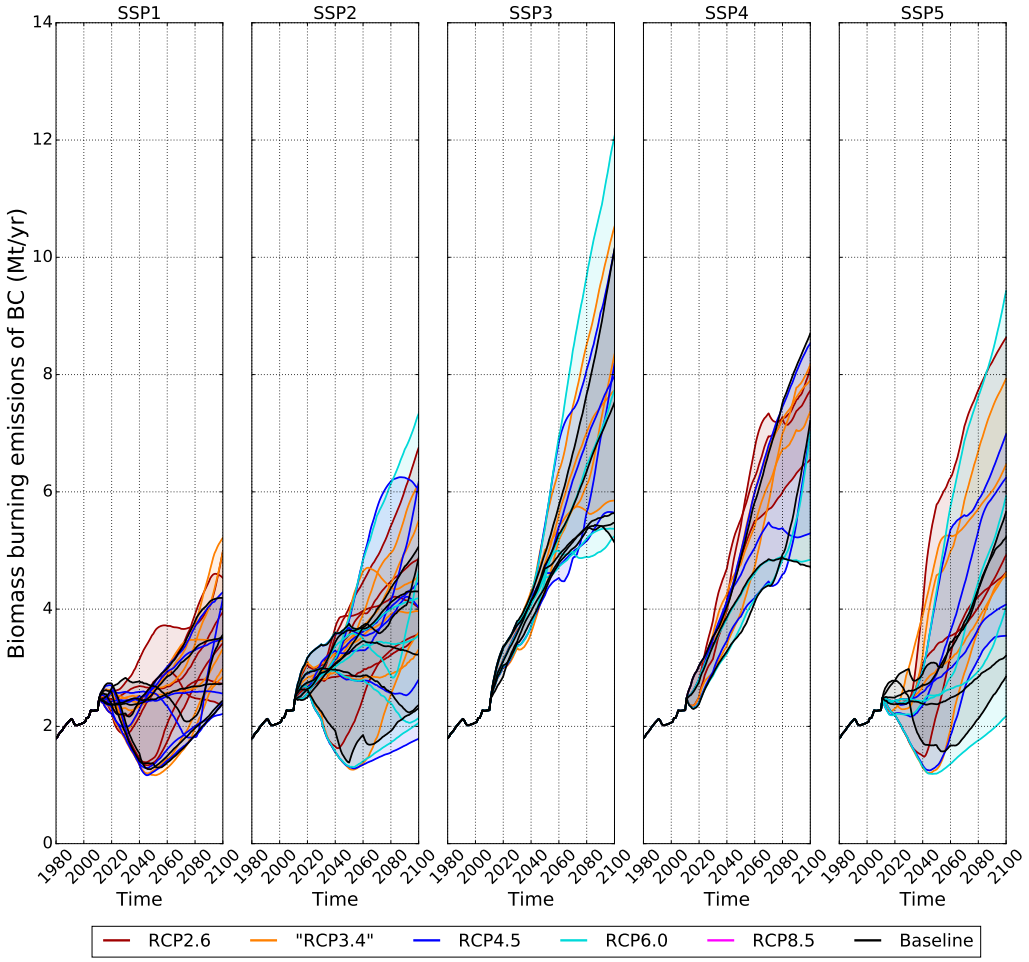

Figure 3.26: *Change in BC emissions from biomass burning since the preindustrial equilibrium from 1980 to 2100. The scenarios are classified depending on the forcing target. Each plain line represents an IAM that has run this SSP and this forcing target. For the sake of clarity, uncertainties on SSP climate projections are not represented here.*

OSCAR v2.2 assumes that the biomass burning emissions of all species are proportional to those of CO_2. The CO_2 biomass burning emissions are calculated using the CO_2 fluxes from changes in areal fire intensities and in land cover or in living biomass densities (Gasser et al., 2017a). As such, these emissions depend on the

carbon stocks in the vegetation and the local conditions of temperatures and precipitations. Here, we represent the BC emissions from biomass burning (figure 3.26). Because of the proportionality between biomass burning emissions, the same result shown here applies for other emissions from biomass burning (CH_4, N_2O, CO, NO_X, OC, SO_2, VOC, and NH_3).

In 2010, 2.3 Mt/yr of BC are emitted from perturbed biomass burning according to OSCAR. In SSP1, these emissions show a relative limited increase, up to 5.2 Mt/yr. In SSP3, BC emissions from biomass burning increase up to 12.1 Mt/yr. Although biomass burning depend on ΔT, it also depends on the precipitations, thus on the composition of the atmosphere, but the land use changes play an important role. In SSP1, the total area of croplands increases slowly or even decreases, whereas the total area of forests increases. In SSP3, the total area of croplands increases rapidly, whereas deforestation continues. Because of the importance of both the atmospheric composition (temperature, aerosols, clouds,...) and land use policies, the effects of different climate policies cannot be distinguished as easily as for other variables. Nevertheless, all SSP scenarios prescribe reductions in BC emissions. For instance, they are divided between 2005 and 2100 by a factor 4 in SSP1 and by a factor 2 in SSP3.

These reductions and the evolution of the Earth system lead to an increase of the relative importance of BC emissions from biomass burning. According to OSCAR, biomass burning weights for 30% of BC emissions in 2010, but for 85% in 2100 in SSP1 and 77% in SSP3. The lowest fraction in 2100 occurs in SSP2 with 44% of relative importance. This is consistent with the evolution of the share of perturbed natural emissions in "total" emissions (anthropogenic and perturbed natural emissions) showed in sections 3.3.1.3, 3.3.1.4 and 3.3.1.5. Biomass burning may account up to 41% in CH_4 emissions in 2100, up to 39% in N_2O emissions in 2100, but also up to 96% in CO emissions in 2100. This result accentuates the importance of land use policies for the mitigation of climate change.

3.3.7 Kaya decomposition

The Kaya identity is vastly used. To our knowledge, only Marangoni et al. (2017) has calculated this decomposition of CO_2 emissions for several IAMs in a broader framework, but also for the SSP scenarios. Yet, it concerns only the SSP1, SSP2 and SSP3, and only the Fossil Fuels & Industry CO_2 emissions. Here, we calculate this decomposition for the scenarios selected (table 3.1) across the 5 SSPs, and grouping Fossil Fuels & Industry and LUC emissions (figure 3.27). To facilitate the comparison, relative variations are used as described in equation 3.7. P stands for the global population, N for the global primary energy and E for global CO_2 emissions from both Fossil Fuels & Industry and LUC.

$$\frac{E}{E_{2005}} = \frac{P}{P_{2005}} \frac{GDP/P}{GDP_{2005}/P_{2005}} \frac{N/GDP}{N_{2005}/GDP_{2005}} \frac{CO_2/N}{CO_{2}{}_{2005}/N_{2005}} \tag{3.7}$$

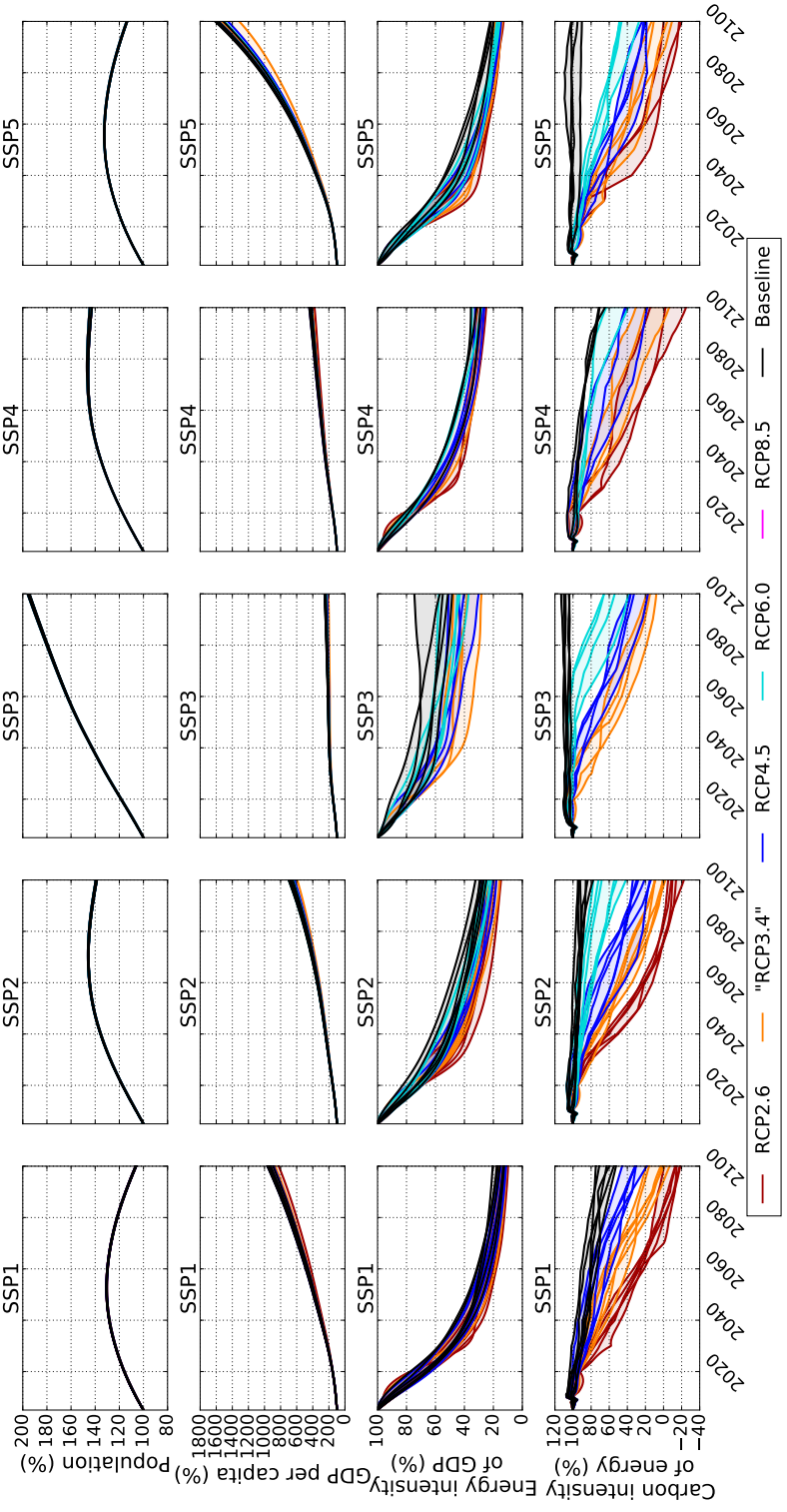

Figure 3.27: *Decomposition of the CO_2 emissions from Fossil-Fuels & Industry and of LUC into its main drivers. To each line corresponds the relative variation of the driver to 2005. For the sake of clarity, uncertainties on LUC emissions are not represented for the carbon intensity of energy.*

The population is prescribed in each scenario, according to its SSP. The lowest population growth in 2100 corresponds to SSP1 (+6%, 6.9 billion), and the highest to SSP3 (+85%, 12.7 billion). SSP5 is relatively close to SSP1. SSP2 and SSP4 are also relatively close, although SSP4 includes more assumptions concerning the populations per group of income levels.

The GDP per capita is multiplied in average by 9.3 in SSP1, 6.8 in SSP2, 2.4 in SSP3, 4.3 in SSP4 and 15.5 in SSP5. The lowest growth occur in SSP3 and in SSP4, that are the scenarios that assume the less cooperation, compared to SSP1, SSP2 and in SSP5 (Bauer et al., 2017). Markets are more regional in SSP4, whereas in SSP3, projects focus on national food and energy security rather than education and technological development (Riahi et al., 2017).

The evolutions of energy intensities are more different across scenarios of a SSP than they are for the previous drivers. In SSP1, energy intensities are reduced by 80 to 90 % in 2100. In this storyline, strong technological development and concerns with respect to environmental impacts are assumed, leading to such reduction of the energy intensities (van Vuuren et al., 2017). Climate policies does not markedly improve further the energy intensities. In SSP2, reductions by 68 to 85 % are achieved. Current trends are extrapolated for this storyline (Fricko et al., 2017). Climate policies have a limited impact on these reductions. This impact has the same order of magnitude than the dispersion in projections for each forcing target. In SSP3, energy intensities are reduced by 25 to 72%. Assumption of lower technological development and environmental concerns explain these lower reductions (Fujimori et al., 2017). Yet, the stronger are climate policies, the stronger tend to be the improvement in energy intensities. In SSP4, reductions by 75 to 85% are achieved. High disparities are assumed between high, medium and low income countries, but the overall improvement may be explained by the diversification of energy sources (Calvin et al., 2017). Climate policies do not distinctly affect these reductions. In SSP5, the energy intensities are reduced by 78 to 87%. Rapid technological development towars Fossil Fuel sources explains these reductions, that are however relatively not affected by climate policies.

In this Kaya decomposition, the carbon intensity of the energy is the driver with the most significant variations. For scenarios targeting the same RCPs, patterns of carbon intensities are relatively similar across SSPs, although the primary energy productions of the SSPs shift patterns. By 2100, the carbon intensities of the baselines are reduced in average by 38% in SSP1, 12% in SSP2, 37% in SSP4 and 1% in SSP5. In SSP3, the carbon intensity is in average increased by 6%. All climate policies of SSP1 and SSP2 lead to effective decrease in carbon intensities. In SSP3 and SSP5, climate policies are very effective at reducing the carbon intensity of the energy for low forcing targets, but the gains in carbon intensity of more ambitious climate policies are inferior than the gain of the initial climate policy. In these scenarios, fossil-fuels are largely used, and incentives to shift to other energy sources are created with climate policies. In SSP4, climate policies have impacts comparable to SSP1, although the differences between income groups of countries lead to less

differentiated impacts.

As a summary, the reduction of the carbon intensity is the major source of reduction of CO_2 emissions in the SSPs, and energy intensity of the GDP plays a secondary role. This result is consistent with Riahi et al. (2017). For the least ambitious climate policies, the reduction in the carbon intensity of the energy is stronger in the storylines with large fossil fuels consumptions, but the importance of fossil-fuel consumptions in the storyline tends to fade as the climate policy intensifies.

A Kaya decomposition can also be written for non-CO_2 emissions. Actually, such a decomposition leads to the use of a "co-emission ratio", as illustrated in equation 3.8. The last term of this equation links the emissions X of another compound to CO_2 emissions using its co-emission ratio X/E.

$$X = P\frac{GDP}{P}\frac{N}{GDP}\frac{E}{N}\frac{X}{E} \tag{3.8}$$

Here, total CO_2 emissions (E) and total X emissions can be used to evaluate this term for each SSP storyline, RCP forcing target and IAM model. We have used total emissions here, in a sake of simplicity. Co-emission ratios are easier to analyze if its calculation is based on the emissions of a given sector, and not total emissions. With SSP scenarios, this is critical because of negative CO_2 emissions, leading to zero emissions, and then net negative CO_2 emissions. However, the SSP public database does not provide enough the details of emissions for negative and non-negative CO_2 emissions. In a lack of a better option, we are forced to use total emissions. We represent in figure 3.28 the evolution of these ratios in the case of SO_2. Co-emission ratios for BC, OC, NO_X, N_2O, NH_3, CH_4 and VOC are also provided, but in appendix 6.2.10.

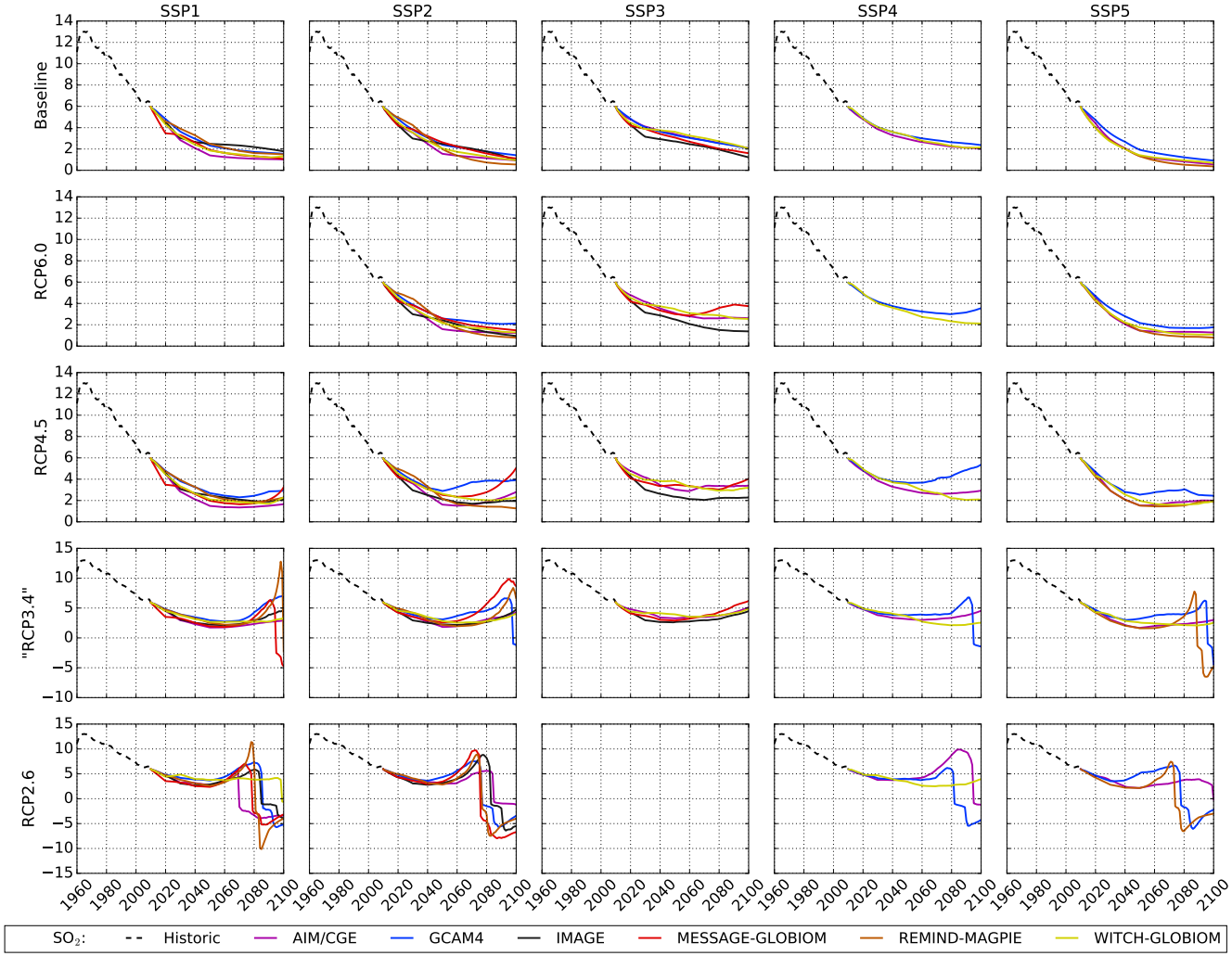

Figure 3.28: *Co-emissions ratios for SO_2, for extension of the Kaya decomposition (TgS/GtC). For the sake of clarity, uncertainties are not represented for the ratios. As a remark, the SSP1-RCP6.0 is empty, because the baseline is already similar to a RCP6.0. The SSP3-RCP2.6 is also empty, for no IAM could find a solution.*

To begin with, IAMs tend to show consistent relation for the co-emission ratios for similar forcing targets. Baselines and RCP6.0 are also relatively similar: mitigation of climate change leads to a reduction of CO_2 emissions and SO_2 emissions in the same proportions. It can be related to a reduced consumption of fossil fuels and constant emission factors, in spite of the differences in the sulfur contents of the different fuels, conventional and non-conventional (EEA, 2016). As the forcing target gets more ambitious, CO_2 emissions are reduced more than SO_2 emissions, leading to an uplifting of the ratio. It can be related to the unreduced SO_2 emissions from biomass burning, as explained in section 3.3.1.5. This is due to the use of global CO_2 and SO_2 emissions here. Going further, as CO_2 emissions become negative, the ratios stabilize around a new value around a value comparable to the one before CO_2 emissions becoming negative.

For other species, the SSP holds a stronger importance in the evolution of the coemission ratios, compared to SO_2. It can be related to the hypotheses regarding technological change and fossil-fuel development in each storyline.

As a remark, in the chapter of this thesis about the uncertainty of fossil-fuel emissions, co-emission ratios have been used. Though, these ratios were related only to fossil-fuel emissions. In the case of SO_2, most of its emissions are caused by the use of fossil fuels derived from coals and oils in the energy, industry and domestic sectors (Joint Research Centre, 2011; EEA, 2016). In the chapter about fossil-fuels, co-emission ratios were extended using S-shaped functions, leading to a global co-emission ratio decreasing from 13.5 TgS/GtC in 1960 to 3.0 TgS/GtC in 2050. All scenarios were produced assuming that no climate policy were implemented. Here, using the baselines of the SSP scenarios, we observe that the co-emission ratios decrease from 13 TgS/GtC in 1960 to 1.3 to 3.6 TgS/GtC in 2050, with similar evolutions. It comes that in the case of SO_2 under baselines scenarios, S-shaped functions can effectively be used to approximate the evolution of the co-emission ratios. For the other species, the contribution from the fossil-fuel sector is not as high, which renders the comparison not as appropriate.

3.3.8 Carbon budget

3.3.8.1 Mathematical basis

The fact that CO_2 emissions is the main driver of climate change (Myhre et al., 2013) has lead to the evaluation of a carbon budget, the amount of CO_2 emissions that has not to be reached in order to limit increase in ΔT to a threshold with a fixed probability. Several definitions, and then methods of evaluations, coexist (Rogelj et al., 2016b). For instance, the transient climate response to cumulative emissions (TCRE), defined as the ratio of ΔT to cumulative CO_2 emissions, may be used to evaluate a CO_2-only carbon budget. Until temperature peaks and if cumulative emissions evolve smoothly, this ratio has been shown to remain relatively constant (e.g Meinshausen et al. (2009), Matthews and Caldeira (2008), Gillett et al. (2013)).

This relatively linear relationship is due to the combined effects of the logarithmic dependency of the radiative forcing from CO_2 with its atmospheric concentration and the decreasing efficiency of the sinks with climate change, leading to a higher airborne fraction left in the atmosphere (Ciais et al., 2013). According to expert judgements based on the literature, the AR5 reports a likely range of 0.8 to 2.5 °C per 1000 GtC, if cumulative emissions are less than 2000 GtC, and until the time temperature peaks (Collins et al., 2013). Yet, as CO_2 emissions slow down, temperature peaks. Because of the inertias of the Earth system, be it in the carbon sinks or in the increase in ΔT, the balance in the processes that were causing this linear relationship is not respected anymore. The range in the carbon budgets may include an uncertainty in ΔT, but also the influence of the inertias of the Earth system, depending on the pattern of CO_2 emissions. This influence can only be evaluated using an ensemble of scenarios. Other emissions still contribute to global warming, causing the range in carbon budgets to depend on the emissions of other forcing agents (Rogelj et al., 2015). This latter contribution to the range of the carbon budgets can also be evaluated using an ensemble of scenarios.

The SSP database has the advantage to provide us with an ensemble of scenarios reaching different forcing targets, with different patterns of CO_2 and non-CO_2 emissions, and thus, with different evolutions in ΔT. Following Rogelj et al. (2016b), our goal is here to calculate two types of carbon budget, that account for non-CO_2 emissions:

- Threshold exceedance budget (TEB): cumulative CO_2 emissions at the time the scenario exceeds a threshold in ΔT (e.g. 2°C) with a fixed probability (e.g. 66%).

  ↪ Take into account the impact in ΔT of non-CO_2 emissions at the time of exceeding the threshold.

- Threshold avoidance budget (TAB): cumulative CO_2 emissions of a scenario up to its peak of ΔT, that remains below the threshold (e.g. 2°C) with a fixed probability (e.g. 66%).

  ↪ Take into account the impact in ΔT of non-CO_2 emissions at the time of the peak. As a remark, the TAB can also be calculated not up to the peak, but over a predefined period (2005-2050, 2050-2100) (e.g. Clarke et al. (2014)). Though, for a given scenario, the non-CO_2 emissions at the peak warming has a greater importance than at an arbitrary date such as 2050.

These definitions of the carbon budget are complementary. For a given threshold, TEBs are calculated only for scenarios that exceed the threshold, whereas TABs are calculated only for scenarios that do not. To improve the comparison to Rogelj et al. (2016b) and to Friedlingstein et al. (2014a), cumulative CO_2 emissions are calculated from 2015, regardless of the scenario. In our study, 2010-2015 is part of

the scenario, but total CO_2 emissions over 2010-2015 vary between 60.9 GtC and 68.6 GtC.

Because of the modeling of the terrestrial biosphere, the CO_2 emissions from Land Use Change are uncertain. If not accounting for this source of uncertainty, one can relatively simply use an ensemble of scenarios to provide an ensemble of values for the carbon budgets, and ultimately a range in the carbon budget. Given the literature (Friedlingstein et al., 2014a; Clarke et al., 2014; van Vuuren et al., 2016; Rogelj et al., 2016b), it seems that this source of uncertainty is not taken into account. If not accounted for, calculating the cumulative CO_2 emissions at the time of peaking or exceeding requires careful calculations. Here, we establish mathematical definitions for the carbon budgets, with increasing robustness. Once we have rigorously defined the budgets, we use the SSP database to calculate the carbon budgets, and show that these definitions lead to different ranges in carbon budgets.

We write here the definitions with the TAB. For the TEB, the same definitions stand although times of peaking are replaced with times of exceeding. We use the figure 3.29 to illustrate the definitions while we provide them.

We use an ensemble of scenarios $\{S\}$, such as the SSP database. For each scenario S for which the ΔT does not exceed the threshold ΔT_{lim} with a probability of $p\%$, we calculate its TAB, that is to say the cumulative CO_2 emissions at the time of peaking (or exceeding for the TEB). For each scenario S, we assume that a Monte-Carlo is used to calculate for each member i the ΔT ($\Delta T^{S,i}$) and the CO_2 emissions from LUC ($E^{S,i}_{LUC}$). Eventually, the CO_2 emissions from Fossil-Fuels & Industry may also depend on the member ($E^{S,i}_{FF\&I}$), as in our framework (section 3.2.6). We introduce the following notations: $P_{p\%}(V)$ is the p percentile of a variable V. $\left[V^X\right]^{X,90\%}$ corresponds to the 90% range of a variable V across an ensemble of trajectories X, that may include both scenarios and Monte-Carlo members. t_{init} and t^S_{peak} correspond respectively to the years from which emissions are cumulated to the maximum in ΔT of S.

Even though a Monte Carlo cannot be performed, we can still write the CO_2 emissions and the ΔT^S as calculated with a single member, represented here with the index 0. We assume that the $\Delta T^{S,0}$ and the $E^{S,0}_{LUC}$ are calculated in terms of median, which implies that the TAB can only be evaluated with a probability of 50%. We emphasize that it is assumed in the lack of a better option, for it cannot be respected for all scenarios. In other words, a climate model, be it an ESM or a simple climate model, may project the median climate change for one scenario. But by changing the scenario, such as its emissions, the same model under the same parametrization is likely not to project the median climate change anymore. The non-linear interactions (Murphy et al., 2004) are causing this dependency of the "median" model and parametrization to the scenario itself. In our case, using an ensemble of scenarios to calculate the carbon budget and its range, each scenario should be run with a "median" model and parametrization, but it cannot be the

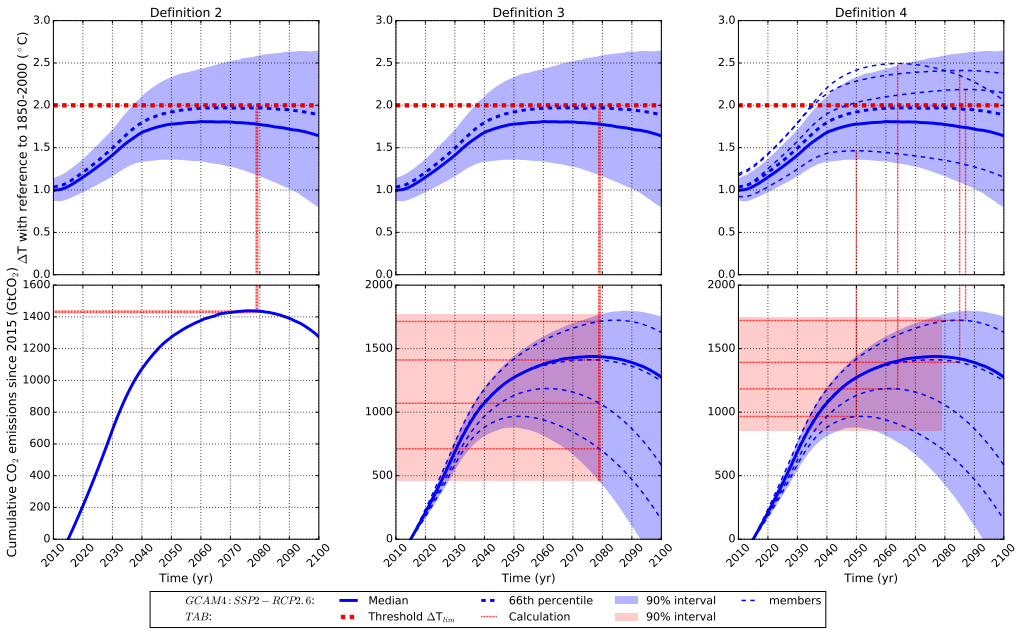

Figure 3.29: *Illustration of the calculation of the Threshold Avoidance Budget (TAB) for a scenario under the three main definitions. The higher panels correspond to the ΔT whereas the lower ones correspond to the cumulative CO_2 emissions since 2015. A single scenario is represented here (SSP2-RCP2.6 under GCAM4), in blue. Everything that concerns the calculation of its TAB is in red, under a threshold ΔT_{lim}, at 2°C here, for a probability not to exceed the threshold of 66%.*

same for all scenarios. Under this definition of the carbon budget, each scenario for which $\Delta T^{S,0}$ does not exceed ΔT_{lim} provides us with a single value of the carbon budget. The range TAB_1 of this ensemble of trajectories is calculated in terms of 90% confidence interval (equation 3.9), in order to exclude extreme scenarios (Clarke et al., 2014). This definition is not represented in figure 3.29, for this definition is very close to the 2nd definition. The only difference in this figure is that the 66th percentile cannot be used: in the best situation, only the median of ΔT and CO_2 emissions are calculated in the 1st definition.

$$TAB_1 = \left[\int_{t_{init}}^{t^S_{peak}} E^{S,0}_{LUC} + E^{S,0}_{FF\&I} dt \right]^{S,90\%} \tag{3.9a}$$

$$\Delta T^S_{50\%} = \Delta T^{S,0} \quad \text{maximum in} \quad t^S_{peak} \tag{3.9b}$$

$$\forall t, \Delta T^S_{50\%}(t) \leq \Delta T_{lim} \tag{3.9c}$$

The 2nd definition is different from the 1st, in that the climate projections of S are assessed in a Monte Carlo setup. For each scenario S, the $\Delta T^{S,i}$ is then

calculated for each member i of the Monte-Carlo. For this reason, the TAB can be calculated for probabilities p different of 50%. Yet, we assume in this definition that the the emissions are still calculated without uncertainties, and only the median (index 0) is used. Under this definition, each scenario S for which the p-percentile of the temperature ($\Delta T^S_{p\%}$) does not exceed the threshold ΔT_{lim} provides us again with a single value of the carbon budget. The range TAB_2 is calculated as well with a 90% confidence interval, as illustrated in equation 3.10. It differs from equation 3.9, in that any probability p% is used, but the median (index 0) is still used. In figure 3.29, the left panel illustrates this definition for ΔT_{lim}=2°C and p=66%. From this definition, a single value of the TAB is drawn for each scenario used. A range in the TAB is only obtained through an ensemble of scenarios.

$$TAB_2 = \left[\int_{t_{init}}^{t^S_{peak}} E^{S,0}_{LUC} + E^{S,0}_{FF\&I} dt\right]^{S,90\%} \tag{3.10a}$$

$$\Delta T^S_{p\%} = P_{p\%}\left(\Delta T^{S,i}\right) \quad \text{maximum in} \quad t^S_{peak} \tag{3.10b}$$

$$\forall t, \Delta T^S_{p\%}(t) \leq \Delta T_{lim} \tag{3.10c}$$

The 3rd definition is different from the 2nd, in that the emissions are calculated with uncertainties. Each member has its own CO_2 emissions from Land Use Change $E^{S,i}_{LUC}$, and eventually its own CO_2 emissions from Fossil Fuels & Industry $E^{S,i}_{FF\&I}$. In this case, a more robust definition can be used (equation 3.11). The range of the TAB is the "full range of cumulative emissions associated with the time of global average temperature increase exceeding the warming levels" (Friedlingstein et al., 2014a). Under this definition, each scenario for which $\Delta T^S_{p\%}$ does not exceed ΔT_{lim} provides us with as many values of the carbon budget as there are members in the Monte Carlo. Each value are the cumulative CO_2 emissions for this member from t_{init} to the time of peaking of the scenario t^S_{peak}. The range is written as the 90% confidence interval of the values of the selected scenarios with all their members. The middle panel of figure 3.29 illustrates this definition for ΔT_{lim}=2°C and p=66%. From this definition, a range in TAB can be obtained for each scenario, and is thus equal to the range in cumulative CO_2 emissions from t_{init} to t^S_{peak}. For an ensemble of scenarios, the range of the ensemble of values is calculated from both members and scenarios.

$$TAB_3 = \left[\int_{t_{init}}^{t^S_{peak}} E^{S,i}_{LUC} + E^{S,i}_{FF\&I} dt\right]^{S,i,90\%} \tag{3.11a}$$

$$\Delta T^S_{p\%} = P_{p\%}\left(\Delta T^{S,i}\right) \quad \text{maximum in} \quad t^S_{peak} \tag{3.11b}$$

$$\forall t, \Delta T^S_{p\%}(t) \leq \Delta T_{lim} \tag{3.11c}$$

In the precedent definition, for each scenario S, the cumulative emissions of all members are calculated up to a common date t^S_{peak}. However, the inertias of the

Earth system are different in-between the members, and different dates should be used. The 4th definition is different from the 3rd, in that the cumulative emissions of each member i and scenario S are calculated to the date of peaking of its temperature $\Delta T^{S,i}$ (equation 3.12). Each scenario for which $\Delta T^{S}_{p\%}$ does not exceed ΔT_{lim} provides with as many values of the cumulative CO_2 emissions as there are members. The range TAB_4 is calculated as the 90% confidence interval of all values from the scenarios S and their members i. In figure 3.29, the right panel illustrates the 4th definition for ΔT_{lim}=2°C and p=66%. For each scenario, a range in TAB is provided, and it is different from the one in the 3rd definition (middle panel). The times of peaking are effectively different in-between members, explaining these different ranges. The range in TAB calculated under the 3rd definition is not systematically higher than those calculated under the 4th definition. Finally, using an ensemble of scenarios, the range in TAB is calculated as the 90% confidence interval of values from both scenarios and members.

$$TAB_4 = \left[\int_{t_{init}}^{t^{S,i}_{peak}} E^{S,i}_{LUC} + E^{S,i}_{FF\&I} dt \right]^{S,i,90\%} \tag{3.12a}$$

$$\Delta T^{S,i} \quad \text{maximum in} \quad t^{S,i}_{peak} \tag{3.12b}$$

$$\forall t, \Delta T^{S}_{p\%}(t) = P_{p\%}\left(\Delta T^{S,i}\right) \leq \Delta T_{lim} \tag{3.12c}$$

To our knowledge of the literature, previous estimates do not provide mathematical definitions of the carbon budgets. In our understanding, the carbon budgets calculated by IAMs would be given by the 2nd definition, whereas those from Friedlingstein et al. (2014a), Rogelj et al. (2015) and Rogelj et al. (2016b) would follow the 3rd definition. The 4th definition accounts for a more realistic timing of the cumulative CO_2 emissions. For this reason, we deem the 4th definition (equation 3.12) to be more robust than the three others definitions (equations 3.9, 3.10 and 3.11). Yet, we emphasize that although more robust than the three others, this latter definition remains biased because of the coverage of scenarios. The use of scenarios with low ΔT introduces a bias for carbon budget for higher ΔT.

For comparison of our results to the literature such as Clarke et al. (2014) or Friedlingstein et al. (2014a), we ignore this bias to begin with. The results of these different definitions for the assessment of the mean and 90% ranges of the TEBs and TABs are summarized in table 3.9, for different thresholds ΔT_{lim} avoided/exceeded with probability of p%. The histograms of the values used to asses these budgets are showed in figure 3.30. All budgets are rounded to the nearest 10. The 1st definition (equation 3.9) is not represented, as it is a particular case of the 2nd definition (equation 3.10 , with p=50). Then, in table 3.10, we show the influence of this bias on the carbon budgets.

3.3.8.2 Carbon budgets biased by the coverage in scenarios

As explained in previous paragraphes, the use of scenarios with low ΔT bias the carbon budgets for higher ΔT. Yet, this bias is present also in other evaluation. To compare our method to the literature, we include this bias here.

	1.5°C		2.0°C		3.0°C		4.0°C	
	66%	50%	66%	50%	66%	50%	66%	50%
TAB_2			1340 1140-1600	1570 1070-2110	2260 1170-3250	2370 1160-3470	2870 1260-4570	3060 1290-5420
TAB_3			1240 430-1810	1460 620-2390	2120 750-3420	2230 840-3710	2730 920-4750	2930 970-5420
TAB_4			1240 610-1790	1470 650-2460	2110 850-3400	2230 870-3700	2720 960-4740	2930 980-5420
AR5 WG3			470-1020	800-1270				
TEB_2	640 540-740	800 690-930	1510 1310-1710	1800 1550-2170	3380 2980-3760	3930 3470-4310	5440 5180-5870	6270 6080-6530
TEB_3	630 470-790	780 590-980	1470 1110-1840	1750 1330-2250	3300 2620-3980	3830 3030-4620	5340 4500-6240	6180 5380-6960
TEB_4	800 350-1460	800 350-1460	1690 940-2770	1700 950-2800	3480 2260-5130	3510 2270-5200	5270 3770-7270	5600 3910-7610
AR5 WG1			850	960				
Friedlingstein et al., 2014			1200 900-1600	1500 1100-1900	2900 2500-3700	3300 3000-4200	4400 4100-5700	5100 5000-6500

Table 3.9: *Threshold Exceedance Budgets (TEBs) and Threshold Avoidance Budgets (TABs) from 2015 ($GtCO_2$), for different increases in global surface temperature with reference to 1850-1900 to exceed or avoid with a defined probability. For each budget, 3 assessments are provided, depending on the definition used (equations 3.10, 3.11 and 3.12). In each case, the mean (upper line) and the 90% range (lower line) is given. For comparison, carbon budgets from the IPCC AR5 WG1 (Ciais et al., 2013) and WG3 (Clarke et al., 2014), as written in Rogelj et al. (2016b), and Friedlingstein et al. (2014a) are provided. As a remark, the range for the TABs of IPCC AR5 WG3 are 10 to 90% range, not 5 to 95 % range like the others. We emphasize that these carbon budgets include the bias of coverage in scenarios.*

Few results can be deduced from figure 3.30 and table 3.9.

- Obviously, higher threshold temperatures lead to higher budgets. Lower probability, thus lower chances to avoid or not to exceed this temperature, lead as well to more permissive budgets (table 3.9).
- The budgets using the 2nd definition (equation 3.10) are calculated using a much lower sampling compared to the 3rd and 4th definitions (figure 3.30). The underlying histogram of the budgets under the 4th definition is more asymmetric than the one of the 3rd definition.
- Concerning TABs, no SSP scenarios could avoid 1.5°C, be it with a 50 or 66% probability. It does not mean that the target cannot be reached, but it informs us about the coverage in scenarios. We calculate TEBs for 1.5°C that

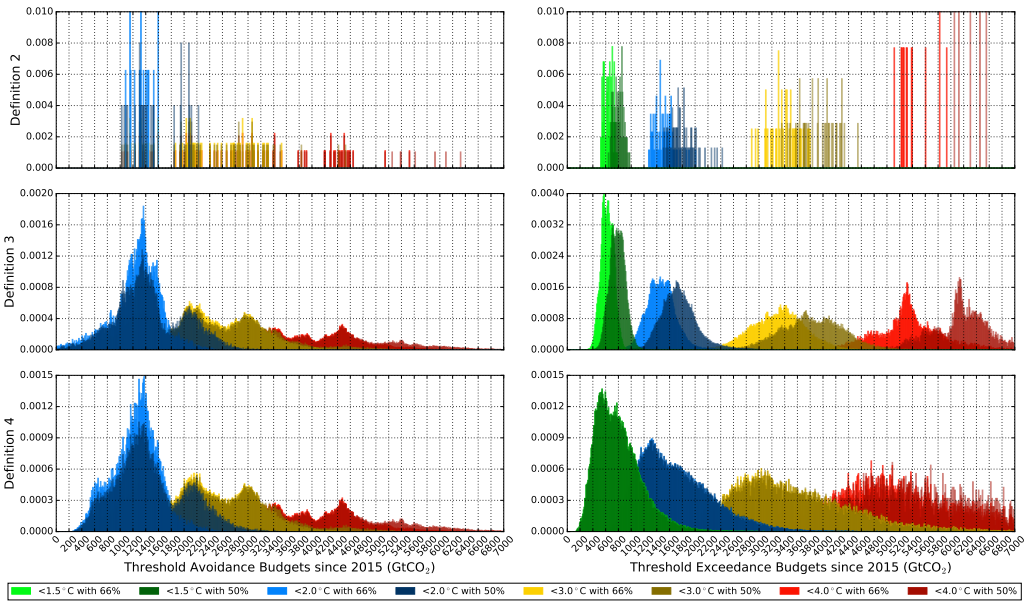

Figure 3.30: *Assessment of the TABs (left column) and of the TEBs (right column), depending on the equation used: equation 3.10 (upper line), equation 3.11 (middle line), equation 3.12 (lower line). In each case, and for each threshold in temperature ΔT_{lim} avoided/exceeded with a probability p%, the histogram of the values used to assess the mean and the 90% ranges are represented. We emphasize that these carbon budgets include the bias of coverage in scenarios.*

are higher than those arising from Millar et al. (2017). The difference in this TEBs can be explained by the difference in the framework, with a continuous adjusment over time to limit global warming at 1.5°C.

- Switching from the evaluation of TABs with the ensemble of cumulative median emissions for each scenario (2nd definition, equation 3.10) to the ensemble of cumulative emissions for each scenario and member of the Monte Carlo (3rd definition, equation 3.11) decrease the mean TAB by 100 to 140 $GtCO_2$. The 5th percentile of the TABs is decreased by 320 to 710 $GtCO_2$, whereas the 95th percentile is increased by 0 to 280 $GtCO_2$ (table 3.9). These differences tend to be lower for more ambitious targets. As a remark, the same SSP scenarios are used in the two definitions. The evolutions in the range are a direct effect of the increased sampling in the 3rd definition (figure 3.30). The fact that the mean cumulative emissions at the peak in t^S_{peak} are lower than the cumulative median emissions at the peak in t^S_{peak} can be related to the asymmetry of the CO_2 emissions from LUC.

- Switching from the evaluation of TABs with the ensemble of cumulative emissions for each scenario and member at the date of peak warming in the pth

percentile of ΔT^S (3rd definition, equation 3.11) to the ensemble of cumulative emissions for each scenario and member at the date of peak warming in each $\Delta T^{S,i}$ (4th definition, equation 3.12) change the mean TAB by only ±10 $GtCO_2$. The median TAB is then affected by less than 1%. Though, as shown in table 3.9, the 5th percentile of the TABs is increased by 10 to 180 $GtCO_2$ (up to +42%), whereas the 95th percentile is changed by 0 to 70 $GtCO_2$ (up to 3%). These differences are relatively weak in comparison of the values of the TABs, except for the 5% percentile. The stronger change is the increase of the 5th percentile of the TABs at 2°C with 66% probability: using the 3rd definition, their budget is estimated to a date too early for this pathway. Given the uncertainty in both climate change and carbon cycle, thus the effect of this uncertainty on cumulative CO_2 emissions from LUC, and thus on the date where ΔT peaks, we deem the 4th definition more accurate.

- Switching from the evaluation of TEBs with the ensemble of cumulative median emissions for each scenario (2nd definition, equation 3.10) to the ensemble of cumulative emissions for each scenario and member of the Monte Carlo (3rd definition, equation 3.11) decrease the mean TEB by 10 to 100 $GtCO_2$. The 5th percentile of the TEBs is decreased by 70 to 700 $GtCO_2$, whereas the 95th percentile is increased by 50 to 430 $GtCO_2$ (table 3.9). These differences tend to be lower for more ambitious targets. The increased sampling of scenarios exceeding a given temperature improve the assessment of the range of TEBs.

- Switching from the evaluation of TEBs with the ensemble of cumulative emissions for each scenario and member at the date of peak warming in the p percentile of ΔT^S (3rd definition, equation 3.11) to the ensemble of cumulative emissions for each scenario and member at the date of peak warming in each $\Delta T^{S,i}$ (4th definition, equation 3.12) change the mean TEB by -580 to 220 $GtCO_2$ (-9 to +27%). The more ambitious is the forcing target, and the more the mean TEB_4 is superior to the mean TEB_3. As with TABs, this change is an effect of the correction of spurious budgets. In the 3rd definition, the carbon budgets are gathered at the date where the ΔT exceeds the threshold with a probability p%. Though, for each member of the Monte Carlo, the carbon budget does not necessarily lead to the exceedance of the threshold in ΔT with p%. Going to the date where the p percentile of ΔT exceeds the threshold, and not to the date where the *Delta*T of the member exceeds the threshold, implies the inclusion of budgets abnormally low or high. For the more ambitious targets (below 2°C with 50%), the correction of the histogram of TEBs leads to a heavier higher tail, otherwise the lower tail tends to get a higher weight, causing this reduction in the mean TEBs. Histograms under the 4th definition tend to be wider compared to those under the 3rd definition. As shown in table 3.9, the 5th percentile of the TEBs is decreased by 120 to 1470 $GtCO_2$, up to -41%, whereas the 95th percentile is increased by 480 to 1150 $GtCO_2$, up to +85%. The widening of the histogram, and thus of the

range, is stronger in absolute values for higher targets, because of the increasing uncertainties in the system. Yet, in terms of relative values, this widening is higher for lower carbon budgets. can be related to the fact that the carbon budgets are affected by the parameters ruling the CO_2 emissions from LUC, and the same parameters also ruling the land sink of carbon, and thus the ΔT.

Ultimately, the widening of the range of the carbon budget when accounting for the correct timing of CO_2 emissions (4^{th} definition) is related to the parameters ruling the terrestrial biosphere. We observe that parameters that lead to CO_2 emissions from LUC higher than the median tend to have land sinks of carbon higher than the median, but not as much, leading to cumulative CO_2 emissions from LUC higher at the date where the threshold in temperature is exceeded. Because of that, it increases the weight of the upper tail of the distribution of carbon budgets. The same explanation applies for parameters with CO_2 emissions from LUC and land sinks lower than the median.

Summarized further, it shows that calculating the range of the carbon budgets, TEBs or TABs, is not as straightforward as it seems. Establishing rigorous definitions has shown differences in the resulting ranges.

- The 2^{nd} definition (equation 3.10) of the carbon budgets should not be used only, because of the poor sampling implied by the method.
- The 3^{rd} definition (equation 3.11) of the carbon budgets should not be used for the calculation of the TEBs. The correction of the dates of integration of the carbon budgets has a strong relative effect in this case. This correction is much lower for the TABs. Depending on the sensibility of the Earth system, peak warmings occur at relatively similar dates, whereas exceedances of specific temperatures occur at very different dates.
- For the same target, a temperature with a given probability, TABs are lower than TEBs. This is due to the stabilization of the ΔT after last emissions. If emitting up to the TEB, the threshold will be reached, but $Delta$T will keep increasing afterwards.
- To avoid a ΔT above 2°C with a probability of 66%, a maximum of 1240 $GtCO_2$ (610 to 1790) can be emitted from 2015. To exceed a ΔT of 2°C with a probability of 66%, 1690 $GtCO_2$ (940 to 2770) have to be emitted from 2015.

These values are comparable, though higher than those of Clarke et al. (2014) and Friedlingstein et al. (2014a), be it for the TABs or the TEBs. The ranges of our estimates are also wider, but it may be related to the set of scenarios used. The SSP scenarios are constrained to reach specific levels of radiative forcing, and it remains unclear how such a selection of scenarios affect the range of the carbon budgets, even if we compare our results to those from AR5 WG3 database (Clarke et al., 2014). TEBs and TABs are complementary, which leads to disjoint distributions of

scenarios in CO_2 emissions and in non-CO_2 emissions, and it remains also unclear how it may bias the range of the carbon budgets (Rogelj et al., 2016b).

3.3.8.3 Carbon budgets unbiased by the coverage in scenarios

As explained ealier, the use of scenarios with low ΔT bias the carbon budgets for higher ΔT. It concerns TABs for high ΔT. We have reproduced these carbon budgets by adding a lower bound in ΔT to the scenarios used to calculate the carbon budgets. Indeed, it does not change the TEBs. But for TABs, the scenarios used to calculate the carbon budgets at ΔT_{lim} are those for which the peak remain inbetween ΔT_{lim} and $\Delta T_{lim} - 1°C$. In table 3.10, we reproduce the equivalent of the table 3.9.

With bias	<2.0°C		<3.0°C		<4.0°C	
	66%	50%	66%	50%	66%	50%
TAB_2	1340 1140-1600	1570 1070-2110	2260 1170-3250	2370 1160-3470	2870 1260-4570	3060 1290-5420
TAB_3	1240 430-1810	1460 620-2390	2120 750-3420	2230 840-3710	2730 920-4750	2930 970-5420
TAB_4	1240 610-1790	1470 650-2460	2110 850-3400	2230 870-3700	2720 960-4740	2930 980-5420
Without bias	**1.0-2.0°C**		**2.0-3.0°C**		**3.0-4.0°C**	
	66%	50%	66%	50%	66%	50%
TAB_2	1340 1140 - 1600	1570 1070 - 2110	2580 1990 - 3280	2830 2010 - 3800	4300 3410 - 5000	4700 3820 - 6030
TAB_3	1240 430 - 1810	1460 620 - 2390	2420 1040 - 3500	2680 1380 - 3950	4160 2980 - 5260	4570 3220 - 6110
TAB_4	1240 610 - 1790	1470 650 - 2460	2410 1180 - 3480	2670 1450 - 3950	4150 2980 - 5260	4570 3220 - 6110
AR5 WG3	470-1020	800-1270				

Table 3.10: *Threshold Avoidance Budgets (TABs) from 2015 ($GtCO_2$), for different increases in global surface temperature with reference to 1850-1900 to exceed or avoid with a defined probability. For each budget, 3 assessments are provided, depending on the definition used (equations 3.10, 3.11 and 3.12). In each case, the mean (upper line) and the 90% range (lower line) is given. In the first half of the table, the carbon budgets are those including the bias of the coverage in scenarios, whereas in the second half of the table, it corresponds to those not including the bias. For comparison, carbon budgets from WG3 (Clarke et al., 2014), as written in Rogelj et al. (2016b), and Friedlingstein et al. (2014a) are provided. As a remark, the range for the TABs of IPCC AR5 WG3 are 10 to 90% range, not 5 to 95 % range like the others.*

With the correction of this bias, we observe an increase of the TABs, especially for the higher thresholds in ΔT. In our case, this bias has no effect for scenarios that limit the ΔT to 2°C, because no SSP scenarios reach ΔT lower the lower bound of 1°C. The TABs for limiting ΔT to 2.0-3.0°C with 50% of chances are about 300$GtCO_2$ (+14%) than those for limiting ΔT to 3.0°C with 50% of chances. Respectively, over the following thresholds presented in the columns 5 to 7 of table

3.10, this bias increases to 440 (+16%), 1430 (+53%) and 1670 $GtCO_2$ (+56%).

In the meantime, the 95% percentile increases as well, but with smaller relative variations, ranging from 2 to 13% for the carbon budgets targeting 3 and 4°C (with or without bias). Yet, the lower range of the carbon budget is obviously the most affected. The 5% percentile remain relatively constant without correction of the bias, but increase when constraining a lower bound for the ΔT. The stronger relative increase is obtained for the highest carbon budget, with an increase by 229% of the 5% percentile.

3.3.8.4 Differences between TEBs and TABs

Rogelj et al. (2016b) hypothetized that the difference between TEBs and TABs is not due to non-CO_2 warming, but due to the timescales of CO_2 emissions after their emissions. These assumptions are relatively intuitive, for the TABs are evaluated at the time of peaking in temperature, and inertias in the carbon cycle have to be accounted. The calculation of TEBs are evaluated at the time of exceedance, then not accounting for these inertias. However, these assumptions have not been proven yet. Here, we aim at testing this hypothesis.

We focus on the differences on TEBs and TABs at 2.0 °C, with 66% of probability, because it is one of the most discussed. We use the 4^{th} definition, because it accounts for a more accurate timescale of the carbon budgets. Finally, we include the correction of the bias of the coverage in scenarios, with a lower bound of 1.0°C. We obtain a set of values for TEBs and TABs, providing by scenarios and members of the Monte-Carlo. We emphasize that these sets are disjoint, because of the definitions of TEBs and TABs.

We aim at testing the dependency of the difference TEB-TAB to the non-CO_2 warming, taken as the difference in radiative forcing of all agents, except CO_2 (ΔRF_{non-CO_2}). We aim also at testing the dependency to the differences in timescales of CO_2 emissions after their emissions: we choose to summarize this quantity by the radiative forcing of CO_2 (ΔRF_{CO_2}). Because the radiative forcing of CO_2 accounts for an ensemble of timescales relative to CO_2 emissions after their emissions, this variable could be appropriate. We represent in figure 3.31 the frequencies of encounted values in the Monte-Carlo members of the SSP scenarios run by OSCAR. In the left panel, we observe an eventual correlation between the difference TEB-TAB and the difference between their radiative forcing of CO_2. In the right panel, we observe no specific trend.

To test these hypothesis, we pick up 1000 random values of TABs and 1000 random values of TEBs, so that each TAB is compared to each TEB. This sampling is meant to facilitate the calculation, for the full sample would be too big for calculation. We observe that the sampling changes affect the values of the tests that we will run with a relative impact of 2%.

We look for a correlation between ΔRF_{non-CO_2} and TEB-TAB on one hand, and

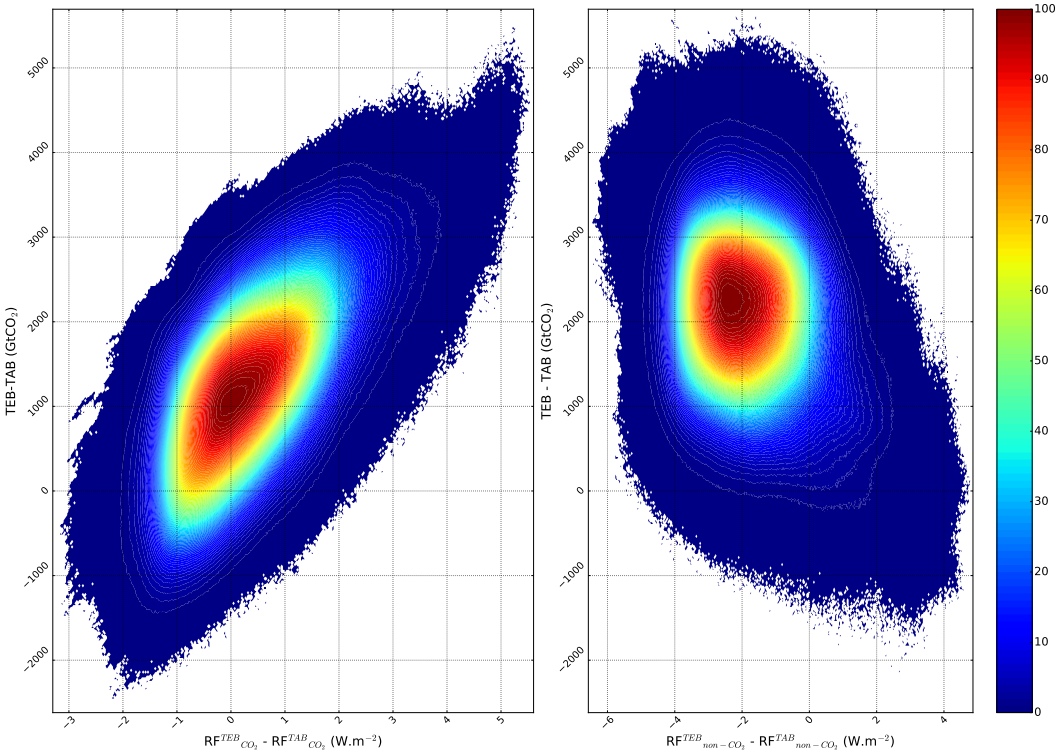

Figure 3.31: *Normalized frequencies of encounted differences in carbon budget and radiative forcings among the ensemble of runs of the SSP scenarios by OSCARv2.2. The X-axis of the left panel is the difference in radiative forcing of CO_2. The X-axis of the right panel is the difference in radiative forcing of non-CO_2 agents.*

ΔRF_{CO_2} and TEB-TAB on the other hand. We use the Kendall's rank correlation coefficient and Spearman's rank correlation coefficient to do so. We choose these tests, for they do not assume linear relationship, normal distributions. The Kendall's τ coefficient informs us about the statistical dependency of the two observations, wheras Spearman's ρ coefficient informs us about the monotony of the eventual relationship. The results obtained are summarized in table 3.11

Hypothesis tested	Kendall's rank correlation		Spearman's rank correlation	
	τ	p-value	ρ	p-value
ΔRF_{non-CO_2} and TEB-TAB?	-0.03	0.0	-0.05	0.0
ΔRF_{CO_2} and TEB-TAB?	0.36	0.0	0.50	0.0

Table 3.11: *Tests performed to evaluate the quality of the correlation of CO_2 warming or and non-CO_2 warming to the difference of carbon budgets.*

According to these tests, we obtain significant values for no correlation between non-CO_2 warming and the difference between TEBs and TABs. Yet, we obtain significant values for a monotonous correlation between CO_2 warming and the dif-

ference in carbon budgets. The assumptions of Rogelj et al. (2016b) are then correct. As explained at the beginning of this section, the differences inbetween TEBs and TABs can be related to the inertias of the carbon cycle. These inertias are accounted in TABs, but not in TEBs. We emphasize that our results are based on the SSP scenarios and the Monte-Carlo members, and then a subset of all possible emission pathways. Even though our results are robust given this data, using other scenarios may lead to different results. We also emphasize that our results do not show the carbon budgets are independent on the non-CO_2 emissions, but only that the differences between these emissions do not have a significant impact between TEBs and TABs.

3.3.8.5 Conclusion for carbon budgets

We have shown in section 3.3.8.1 different mathematical definitions for the carbon budgets. In section 3.3.8.2, we show that the 4^{th} definition is more robust compared to the three others, thanks to a better accounting of the time of exceedance or avoidance of the carbon budgets. In section 3.3.8.3, we show the influence of the bias of the coverage of scenarios: by using a lower bound in temperature, it corrects a strong spurious widening of the range of TABs, especially at high temperature targets. In section 3.3.8.4, we confirm the hypothesis of Rogelj et al. (2016b), assuming that the differences between TABs and TEBs are due to the timescales of CO_2 emissions after their emissions, and not their non-CO_2 warming.

According to OSCAR, CO_2 emissions are equal to 37.8 $GtCO_2$/yr in 2015 (37.4 according to Le Quéré et al. (2016)). Using the TABs, at this rate, our carbon budget to avoid 2°C with a probability of 66% is exceeded in 32 years (16-46). Using the TEBs, at this rate, 44 years (24-71) are required to exceed 2°C with a probability of 66%. We remind that the temperature will increase beyond afterwards, even without emitting further (Frölicher et al., 2014). It calls for a reduction of the emissions and for a rapid development of low carbon technologies (van Vuuren et al., 2016).

Yet, as emphasized in Peters (2018), there are no "magic number" for the carbon budgets, that could directly quantify the mitigation challenge. The carbon budget is just a tool, that helps explaining this challenge, and what it requires. Because of the uncertainty of the Earth system, the importance of CO_2 and non-CO_2 emission pathways and the method of calculation, this quantity can be highly debated. Here, we have proposed a robust and systematic framework to evaluate this budget, but it can still be debated. The most important values are the 1240 $GtCO_2$ to avoid 2°C with a probability of 66%, and 1690 to exceed it.

3.4 Limits of the land-use treatment

This section focus on the limits of our study, especially concerning the treatment of land variables. First, from a theoretical perspective, the algorithm that we use to

evaluate the net land use changes from the land cover can be shown to be imperfect (section 3.4.1). Then, we can use the LUH2 dataset to discuss our approach (section 3.4.2). Over the historical period, the net transitions are effectively imperfectly reproduced, but there are also reevaluations of transitions from the LUH1 dataset to the LUH2 dataset (section 3.4.2.1). Still, the net transitions calculated for 6 SSP scenarios in LUH2 are also imperfectly reproduced with our treatment. We also highlight that our assumptions for the harvested biomass may also be improved (section 3.4.2.2). However, more inputs from the SSP database or more SSP scenarios in the LUH2 dataset would be required to improve the treatment of the whole database. Finally, we show that our assumptions regarding the harvested biomass and the area extents of shifting cultivations have only a limited impact, especially in terms of ΔT (section 3.4.3).

3.4.1 Reconstruction of the transitions in land use change

As explained in section 3.2.3.2, we have used the algorithm of Stocker et al. (2014) to transform the land cover of the SSP scenarios into net land use changes. Here, we evaluate the theoretical outcome of this algorithm, and what it implies for its use to calculate the net land use changes of the SSP database.

Here, we want to transform the land cover $(LC_1, ..., LC_5)$ into net transitions $[LCC_{i,j}]$. For a vector $(LC_1, ..., LC_5)$, we are looking for the matrix of the transitions $[LCC_{i,j}]$, such that all elements are positive. For 5 biomes, a maximum of 10 transitions have to be found. Because the total variation of land area is zero, we have only 4 available equations. The algorithm of Stocker et al. (2014) provides us with one solution in a space of dimension 6, that corresponds to the minimum changes to match required changes in land cover. However, as observed with the historical conversions (section 6.2.4), minimum changes may not be enough. Some conversions from a biome i to a biome j even though $LC_i > 0$ or $LC_j < 0$.

Going further, using the LUH1 dataset, we observe that 7 net land cover changes occur over 1751-2010 and for all regions. Following Stocker et al. (2014) algorithm, there is a positive transition from the biome i to the biome j if and only if $LC_i < 0$ and $LC_j > 0$. Out of $(LC_1, ..., LC_5)$, there is at least LC_i positive and and at least one LC_j negative. By anti-symmetry, considering the case with a single LC_i positive is equivalent to considering the case with a single LC_i negative, we will consider only two cases: with one LC_i positive and with two LC_i positives. As shown in table 3.12, this algorithm can provide us with a maximum of 6 net land cover changes. It comes that this algorithm will never produce the 7 transitions calculated by LUH1, and then never be able to reconstruct perfectly the required patterns of LUC transitions.

Using the LUH1 dataset, we observe that several transitions are always zero for all regions. For instance, between deserts & urban areas, forest and grasslands & shrublands, no transition occurs. Any change in this biome is first transformed either to croplands or pastures. This is due to the hypotheses used for the construction of the dataset (Hurtt et al., 2006). It explains why we do not observe the maximum of

		1 ≥ 0	**2** ≤ 0 $\Downarrow$	**3** ≤ 0 $\Downarrow$	**4** ≤ 0 $\Downarrow$	**5** ≤ 0 $\Downarrow$
1	$\geq 0 \Rightarrow$	-	0	0	0	0
2	≤ 0	$LC_{1,2}$	-	0	0	0
3	≤ 0	$LC_{1,3}$	0	-	0	0
4	≤ 0	$LC_{1,4}$	0	0	-	0
5	≤ 0	$LC_{1,5}$	0	0	0	-

		1 ≥ 0	**2** ≥ 0	**3** ≤ 0 $\Downarrow$	**4** ≤ 0 $\Downarrow$	**5** ≤ 0 $\Downarrow$
1	$\geq 0 \Rightarrow$	-	0	0	0	0
2	$\geq 0 \Rightarrow$	0	-	0	0	0
3	≤ 0	$LC_{1,3}$	$LC_{2,3}$	-	0	0
4	≤ 0	$LC_{1,4}$	$LC_{2,4}$	0	-	0
5	≤ 0	$LC_{1,5}$	$LC_{2,5}$	0	0	-

Table 3.12: *Possible land cover changes deduced from Stocker et al. (2014) under the two representative cases: one positive LC_i (on the left) and two positives LC_i (on the right). In this table, columns and lines are shifted by decreasing change in area extent of land cover, in order to be representative of more cases.*

10 transitions occurring, but only 7.

As a summary, we know that this algorithm is limited, and will never reproduce perfectly the required patterns. LUC emissions are likely to be biased (Ramankutty et al., 2007). Yet, it provides us with relatively good land cover changes, that we use for lack of any better solutions. Nevertheless, transportation theory might be a better approach for this problem. Under Monge-Kantorovitch formulation, optimal land cover changes solving changes in the areas of the different biomes can be found when minimizing the ensemble of the costs of the transitions (Rachev, 1985). Different formulations for these costs have been tried, but the gain in reconstruction of the historical land cover changes are not satisfactory enough. Yet, it does not exclude the existence of an adapted formulation.

3.4.2 Comparison to LUH2

As seen in section 3.3.1.2, the CO_2 emissions from LUC calculated by OSCAR are very different from those of the IAMs. As explained at the end of section 3.3.1.2, it may be because of different definitions of these emissions, modelling of processes, or the land variables used. Our treatment of the land variables may bias the CO_2 emissions from LUC. In the LUH2 dataset (LUH2, 2018), 6 of these SSP scenarios have been recently treated and included for use in LUMIP (Lawrence et al., 2016) and (O'Neill et al., 2016), and thus in CMIP6 (Eyring et al., 2016b). It provides a mean to evaluate our treatment for the land variables used in this chapter.

The calculation of the CO_2 emissions from LUC using the land variables from LUH2 shows differences to those of the IAMs (section 4.2.3.3). For this reason, our treatment of land variables for the SSP scenarios cannot explain alone the differences observed in CO_2 emissions from LUC. Calculation of these emissions by other teams may help investigate why such differences are observed, and it may be obtained under the LUMIP project. Besides, by turning off climate change feedbacks in OSCAR or other models, the contribution of climate change feedbacks to these differences could be evaluated. Still, our purpose in this section is to investigate the differences in land

variables between the LUH1 dataset, the LUH2 dataset and our reconstructions, be it for the historical period or the SSP scenarios.

We remind that our estimates are based on the land cover provided in the SSP database, that aggregate the biomes of the IAMs, as explained in section 3.2.3.2. We have processed the net LUC transitions using the land cover of the SSP scenarios and an algorithm, that we have already shown to imperfectly reproduce the transitions over the historical period (section 3.2.3.1). We have estimated the harvested biomass of the SSP scenarios using those of LUH1 and assumptions (section 3.2.3.3). In the chapter concerning the participation of OSCAR to the Carbon Dioxide Removal Model Intercomparison Project, we describe our treatment of the LUH2 database for use in OSCAR. In order to assess the quality of our evaluations for net LUC transitions and harvested biomass, we compare our estimates for the 6 SSP scenarios to those of the LUH2 dataset, deemed as more consistent with the initial SSP scenarios.

3.4.2.1 Comparison to the land use change of LUH2

We represent in figure 3.32 global annual net land use changes from our different sources: the LUH1 dataset, the LUH2 dataset and the reconstruction of LUH1 using its change in land cover and the algorithm of Stocker et al. (2014). As a remark, a range appears around LUH1, and its reconstruction, in this figure. As explained in Gasser et al. (2017a), the calibration of the terrestrial biosphere uses the TRENDY (Sitch et al., 2015) and CMIP5 exercises (e.g. Arora et al. (2013), Friedlingstein et al. (2014a)). Yet, none of these exercises provide biome-specific outputs, which require an additional treatment for matching to the biomes of LUH1. Thus, depending on the land-cover map used to calibrate the preindustrial carbon fluxes and pools, the land use transitions are slightly affected (Gasser et al., 2017a). It implies a change in the reconstructions of these transitions by the algorithm described in Stocker et al. (2014). In this figure, we represent the LUH1 using the additional treatment for the land-cover map adapted for the mean of TRENDY models (black dash-dotted line) and the minimum to maximum range of the 13 other land-cover maps used in OSCAR v2.2 (Gasser et al., 2017a). Out of this section, for the sake of intelligibility, all figures were represented only with the land-cover map adapted for the mean of TRENDY models.

Concerning the comparison over 1980-2015 of LUH1 (black dash-dotted line) to LUH2 (black dashed line), all transitions are reevaluated within LUH2, the sign of the change depending on the transition considered. The major changes on this period at a global scale concern pastures: from LUH1 to LUH2, more areas are converted from pastures to urban & desert areas, whereas less are converted from pastures to forests. Similarly, from LUH1 to LUH2, more croplands are converted to grasslands & shrublands, whereas less are converted from croplands to forests. Over 2005-2015, transitions from both LUH1 and LUH2 exhibit higher variations. The variations in the transitions between croplands and pastures are reduced from LUH1

to LUH2. Yet, the variations in the transitions from either croplands or pastures to either Desert & Urban, Forests or Grasslands & Shrublands are increased from LUH1 to LUH2.

Then, comparing the transitions over the 6 SSP scenarios, we provide them over 2005-2100 based on the algorithm of Stocker et al. (2014) and the original SSP database (IIASA, 2018c). The evaluation of these transitions by LUH2 is meant to smoothly connect the projections of IAMs to the historical reconstructions of land-use. In LUH2, the annual transitions are meant to smoothen the link of the reconstruction of the historical period (850-2015) to the scenarios (2015-2100), and to preserve the changes prescribed by the IAM (LUH2, 2018). As such, it accounts for the differences in historical ending conditions and the IAMs initial conditions.

Considering the reconstruction of LUH1 (black plain line), as showed in section 3.2.3.1, the algorithm of Stocker et al. (2014) cannot reproduce perfectly the transitions of LUH1. Here, the annual net land use changes summed over all regions of the 6 SSP scenarios and the reconstruction following Stocker et al. (2014) are overall very different (figure 3.32). Several transitions may be evaluated by LUH2, but not in our study, such as transitions between deserts & urban areas on one hand, and on the other hand, either cropland or pasture. Some other transitions may be evaluated in our study, but not in LUH2, such as between forest on one hand, and on the other hand, grasslands & shrublands. Out of these specific transitions, the pattern of other transitions are reproduced for all scenarios, albeit only in terms of shape. The overestimation or underestimation of our estimates tends to be relatively constant along time (e.g. Forests to Pastures), although depending on the scenario and the given transition. Thus, as shown before, this algorithm does not reproduce correctly the transitions, although the general shape of transitions is broadly respected.

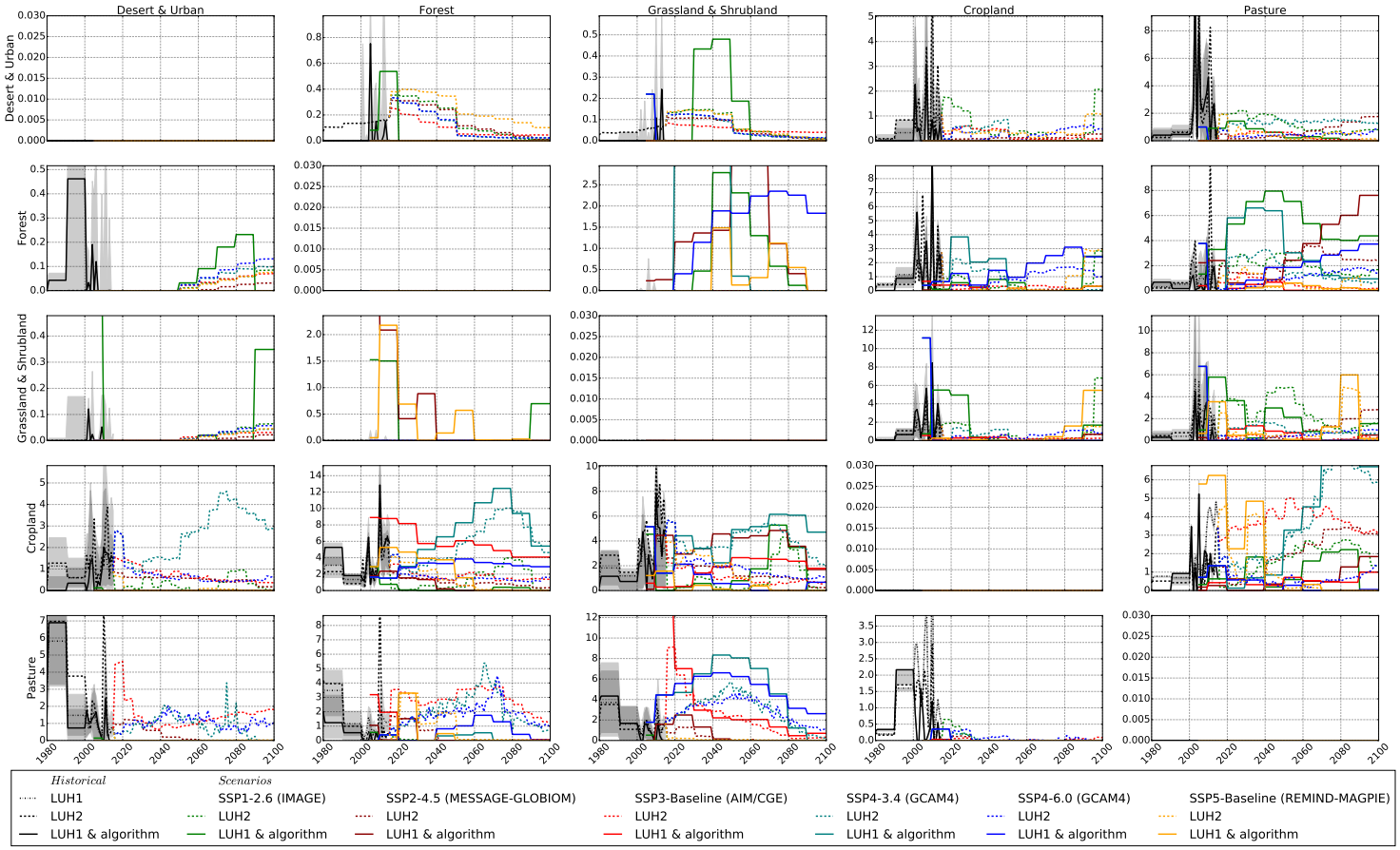

Figure 3.32: *Comparison of the global annual net land use changes (Mha/yr) for the 6 SSP scenarios. In dashed lines, the 6 SSP scenarios treated in the LUH2 dataset (LUH2, 2018) are provided over 2015-2100. In plain lines, we represent the 6 corresponding scenarios using the SSP original database (IIASA, 2018c) and the algorithm of Stocker et al. (2014), over 2005-2100. For comparison, the period 1980-2015 is shown, prescribed by the LUH2 dataset (black dashed line), the LUH1 dataset (black dash-dotted line, Hurtt et al. (2011)) and our reconstruction using the same algorithm (black plain line).*

The observation of this relatively constant overestimation/underestimation, thus a relatively constant ratio, between the two evaluations may be used to rescale the evaluation for all SSP scenarios through the algorithm of Stocker et al. (2014). However, two main obstacles limit this improvement. First, this ratio depends on the scenario. Yet, going further, by considering the SSP4-3.4 by GCAM4 and the SSP4-6.0 by GCAM4, the ratios are relatively equivalent, meaning that these ratios may not depend on the forcing target, but on the SSP and the IAM used. Because these 6 SSP scenarios are not enough to provide ratios for the correction of this algorithm under the 5 SSPs and the 6 IAMs, additional hypotheses would be required. The second obstacle is that these ratios would need to depend on the transitions. For the spurious transitions created by the algorithm, this ratio would be zero. Yet, for transitions where the algorithm implies a zero transfer, no ratio may help, although the introduction of a ratio implies a change in the implied change in land cover, thus eventual transfers for transitions with lower priority. Nevertheless, this is not necessarily enough to generate the appropriate transitions, as illustrated in section 3.2.3.1: some transitions from b_1 to b_2 may take place even though the change in land cover of b_1 increase or if the change in land cover of b_2, and this situation is not envisaged in Stocker et al. (2014). Because of these obstacles, the evaluation of these 6 SSP scenarios may only be of little help to improve the evaluation of all SSP scenarios after use of Stocker et al. (2014), especially because its algorithm does not account for transitions from biomes for which the area extent increases, or to biomes for which the area extent decreases.

3.4.2.2 Comparison to the harvested biomass of LUH2

We represent in figure 3.33 this comparison on global annual net land use changes first. To begin with, on 1980-2015, we compare LUH1 and LUH2. As explained in this section concerning the range in net transitions, harvested biomass shows a similar range. Over 1980-2015, the harvested biomass from forests in Middle-East & Africa and in Asia is reduced from LUH1 to LUH2, two regions where the shifting cultivations of LUH1 were strong (Hurtt et al., 2011). It may be related to Heinimann et al. (2017), that concluded in a previous overestimation of the extent of shifting cultivations. In LUH1, the transitions related to shifting cultivations were included, whereas they are not anymore in LUH2. Yet, the harvested biomass in Latin America is relatively unaffected. Concerning the harvested biomass from grasslands & shrublands, it is globally reduced from LUH1 to LUH2.

Concerning the scenarios, as explained in section 3.2.3.3, our treatment is an extension of the harvested biomass from LUH1 starting from 2005, under the assumption of proportionality to primary bioenergy with and without CCS. We observe that we overestimate the harvested biomass from forests, in most cases, except for the SSP5-Baseline under REMIND-MagPIE. Because of relatively strong increases in the harvested biomass from grasslands & shrublands over 2005-2015, we underestimate these harvested biomass over the 2005-2100. Proportionalities to either

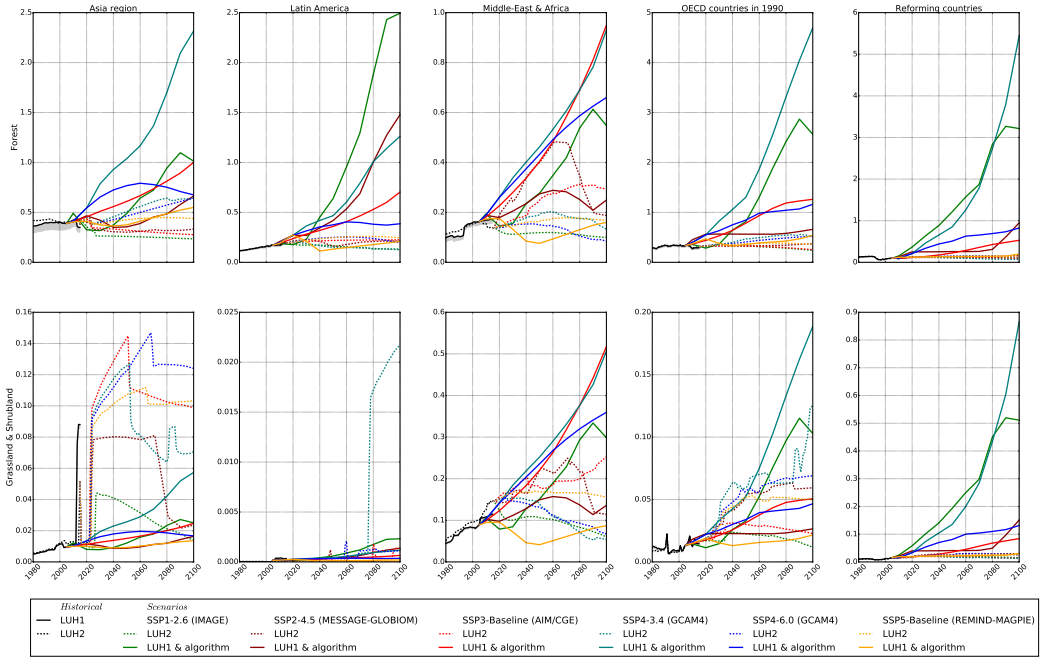

Figure 3.33: *Comparison of the annual harvested biomass (GtC/yr) for the 6 SSP scenarios. In dashed lines, the 6 SSP scenarios treated in the LUH2 dataset (LUH2, 2018) are provided over 2015-2100. In plain lines, we represent the 6 corresponding scenarios using the SSP original database (IIASA, 2018c) and the algorithm of Stocker et al. (2014), over 2005-2100. For comparison, the period 1980-2015 is shown, prescribed by the LUH2 dataset (black dashed line) and the LUH1 dataset (black dash-dotted line, Hurtt et al. (2011)).*

primary bioenergy without CCS or primary bioenergy with CCS does not improve these evaluations. Yet, we observe that a linear combination of these two drivers improve the evaluations, but the combination depends on the scenario, the biome and the region. Because the correction of the harvested biomass to bring to our method is depending heavily on the scenario, these 6 SSP scenarios are not enough to calibrate the correction for the full set of scenarios.

The treatment of the SSP scenarios in the LUH2 dataset for LUMIP and ScenarioMIP highlights the limits of our treatment, both concerning the use of the algorithm of Stocker et al. (2014) for the evaluation of the net land use changes and concerning the assumptions made for the evaluation of harvested biomass. Yet, without any additional outputs in the public SSP database, these limits cannot be overcome.

3.4.3 Assumptions for shifting cultivations and harvested biomass

3.4.3.1 Uncertainties regarding the evaluation of shifting cultivations and harvested biomass

The SSP public database is more complete than the RCPs public database, the land cover being not provided in the latter. Yet, the SSP public database is still not complete enough for accurate evaluation of climate change outputs. In the present study, land variables (land use change, shifting and harvest) have been evaluated from different drivers. Yet, some IAMs may have produced them, but not provided them in the public database, for they were not required.

The association of shifting cultivations with traditional bioenergy is assumed in the lack of a better solution (section 3.2.3.4). Besides, OSCAR uses the LUH v1.1 database (Hurtt et al., 2011) but using the most recent version of this dataset may have an impact on the projections. As explained in section 3.2.3.4, other recent evaluations show that shifting may be much lower than evaluated (Heinimann et al., 2017), and the LUH2 dataset does not prescribe anymore shifting cultivations (LUH2 (2018), section 3.4.2). The area extents for shifting cultivations is expected to decrease in the next decades (Heinimann et al., 2017): under our assumptions, their extents may increase, for instance in SSP5.

Another major problem with harvest concerns bioenergies with CCS. To begin with, we observe that several SSP scenarios provide scenarios with negative emissions in Total CO_2, that cannot be attributed only to CO_2 emissions from Land Use, but also to the difference between the two categories, the so-called CO_2 emissions from "Fossil Fuels & Industry". In the SSP scenarios, negative total emissions are obtained using CCS, mostly using bioenergies, and afforestation/reforestation (van Vuuren et al., 2017; Fricko et al., 2017; Fujimori et al., 2017; Calvin et al., 2017; Kriegler et al., 2017)). The mitigation through afforestation/reforestation, and more generally land use policies, are effectively included in the CO_2 emissions from Land Use Change, that we have reevaluated with OSCAR. The negative emissions observed in the so-called CO_2 emissions from Fossil Fuels & Industry can be related to the bionergies with CCS. However, it comes that:

- Negative emissions from bioenergies with CCS consist in biomass harvested from the terrestrial biosphere, and the carbon released during the combustion is stored in a separated carbon pool, such as geological reservoirs underground (Kemper, 2015). It corresponds to a carbon flux from the biosphere to this separated carbon pool, causing another carbon flux from the atmosphere to the biosphere. This latter flux is the one responsible for the emissions from bioenergies with CCS to be negative.

- However, the contribution of bioenergies with CCS is included within the category "Total Emissions", and by removing the emissions from LUC, it is within the emissions from "Fossil-Fuels & Industry". As such, the flux from the bio-

sphere to the reservoir, and then from atmosphere to the biosphere, is shorten in a flux from the atmosphere to the reservoir.

- Yet, the harvest of biomass affects the productivity of the biome, and thus the land carbon sink and the emissions from Land Use Change as well. Then, there are two modelling choices:

  1. If the harvest of biomass from biomes is not accounted, the carbon stocks will not be correctly estimated, thus introducing a bias in the land carbon sink and the Land Use Change emissions.
  2. If the harvest of biomass from biomes is accounted, the carbon stocks are correctly accounted. Yet, CO_2 will be withdrawn from the atmosphere a first time the year of the harvest because of its inclusion in the category "Total Emissions", and a second time in the years following the harvest through the change in the carbon stocks. As a remark, these two fluxes are not meant to be equal.

- Though, bioenergies can be provided by a large panel of sources, such as crops, residues of forestry processes, waste streams and algae, crops being the major source (Daioglou, 2016; Daioglou et al., 2016).

- In this study, the second modelling choice has been made. In OSCAR v2.2, the NPP of the crops is reduced by 80%, already assuming that this fraction is harvested and oxidized (Gasser et al., 2017a). The harvest prescribed concerns only the woody biomass, and should not include the harvest of biomass from crops.

↪ It comes that the evolution of the harvest prescribed in this study includes a supplementary harvest, which can be seen by comparison to the SSP scenarios treated in the LUH2 dataset (section 3.4.2). Reducing this bias may be done if prescribing in OSCAR the harvest of biomass only from forestry processes, then using only this fraction in primary bioenergies. Though, this fraction is not available in the SSP database.

- The ΔT of the SSP scenarios have been calculated using MAGICC6. The anthropogenic direct removal of carbon from the biosphere is prescribed in this model only through the global driver "Gross-deforestation" (Meinshausen et al., 2011a). We ignore what modelling choice has been made regarding the harvest of biomass for bioenergies with CCS.

↪ More information is required concerning both the the negative emissions from bioenergies with CCS and the accounting of the associated harvest for the evaluation of the ΔT in the SSP database.

3.4.3.2 Sensibilities of the evaluation of shifting cultivations and harvested biomass

Because of our uncertainties regarding a correct modelling of the shifting cultivations and the harvest, two other experiments were performed to evaluate the sensitivity of our analysis to shifting and harvest. In each case, we compare the difference in cumulative CO_2 emissions from LUC and in ΔT.

In the first experiment, we turn off only the mechanism for prescription of shifting cultivations. Thus, shifting remains equal to the 2010 level prescribed by LUH1 (Hurtt et al., 2011), and traditional bioenergy does not impact the area extents of shifting cultivations anymore. The cumulative CO_2 emissions from LUC since 2010 are affected by this change in shifting cultivations, and generally decreased. Although it depends on the scenario, this change is relatively stronger for scenarios with ambitious forcing targets. As shifting cultivations remain at 2010 level, the maximal reduction in cumulative CO_2 emissions from LUC since 2010 and for scenarios targeting RCP2.6 is from 110 GtC to 53 GtC. For this scenario, it corresponds to a 11% of relative decrease in the 394 GtC of cumulative total CO_2 emissions since 2010. For baseline scenarios, the maximal reduction in cumulative CO_2 emissions from LUC is now 240 GtC to 148 GtC. Its relative impact in cumulative total CO_2 emissions is reduced to 5% of the 1551 GtC for this scenario. The sensitivity in terms of CO_2 emissions from LUC to our assumptions regarding the area extents of shifting cultivations is higher for baseline scenarios, because traditional bioenergies are overall more used in these scenarios, just as shifting cultivations are less affected without land use policies. This change in LUC emissions has a relatively low impact when considering the increase in global surface temperature with reference to 1986-2005: using no evolution of the shifting cultivation instead of our hypothesis tends to reduce by less than 0.1°C the ΔT.

In the second experiment, we turn off only the mechanism for prescription of harvest (dashed lines). Thus, harvest remains equal to 2010 level prescribed by Hurtt et al. (2011), and modern bioenergies does not impact the harvest anymore. In all scenarios, the cumulative CO_2 emissions from LUC since 2010 are decreased. For scenarios targeting RCP2.6, the maximal decrease is from 181 GtC to 21 GtC. This strong absolute difference translates into 33% of decrease of the 486 GtC of the cumulative total CO_2 emissions since 2010. For baseline scenarios, the maximal decrease is reduced to 133 GtC to 75 GtC. It translates to 4% of relative decrease in the 1317 GtC in the cumulative total CO_2 emissions since 2010. This evolution from RCP2.6 scenarios to baseline scenarios is due to higher uses of bioenergies in the most ambitious scenarios, increasing our evaluation of the harvest. However, using no evolution of the harvest instead of our hypothesis has less than 0.2°C of impact on ΔT. As a remark, for the scenario SSP5-2.6 under AIM-CGE, its change in ΔT by 0.16°C still represents 17% of the increase with reference to 1986-2005.

As a remark, our assumptions regarding the harvested biomass and the area extents of shifting cultivations also impact biomass burning emissions. Yet, these

two experiments show relatively low impacts, which does not change our previous conclusions regarding biomass burning emissions (section 3.3.6). For instance, our conclusions regarding the increasing share of biomass burning emissions in total emissions (section 3.3.4) are not changed.

We deduce that the biases that we have shown affect strongly the CO_2 emissions from LUC, reducing cumulative total CO_2 emissions since 2010 by a third. It translates in terms of ΔT to 0.2 °C. More accurate evaluations would be possible if the details of the harvested biomass depending on the biomes (forests, crops,...) would be provided, but also the details of the CO_2 emissions: Land Use Change, bioenergies with CCS, bioenergies without CCS, Fossil-Fuels & Industry with CCS and Fossil-Fuels & Industry without CCS. Ideally, the distinction between the different sources of bioenergies should also be made, especially if forestry residues take a stronger share of the harvested biomass (Vaughan et al., 2018).

3.5 Conclusions

In this study, we assess the climate projections of the SSP scenarios. Yet, the SSP database does not provide all the anthropogenic drivers of climate change, and scenarios have to be completed to do so. Here is a summary of the different actions performed on the SSP public database.

1. Selection of 103 scenarios, from 5 SSPs, 6 IAMs and 5 categories of climate policies (section 3.2.2, table 3.1)

2. Decomposition of the global category "Emissions from Fluorinated Gases" into emissions of the 10 relevant gases, that we have completed with 27 halogenated compounds (section 3.2.2)

3. Transformation of the land cover (vector of the area extents) into net land use changes (matrix of the conversions, consistent with the biomes of OSCAR) using an algorithm (section 3.2.3.2)

4. Evaluation of the harvest of biomass using a simple rule (section 3.2.3.3)

5. Evaluation of the area extents of shifting cultivations using a simple rule (section 3.2.3.4)

6. Recalculation of the CO_2 emissions from Land Use Change using OSCAR v2.2 (section 3.2.3.5)

7. Adaption of the emissions to account for the perturbation of natural emissions, here, biomass burning and wetlands (section 3.2.6)

8. Assessment of the climate projections using OSCAR v2.2 and a Monte Carlo setup (section 3.2.5)

Using this assessment, we draw several conclusions, that we summarize here. All numbers are the median results, except when explicitly specified.

1. Increase in global surface temperature

   (a) Although SSP scenarios may share the same forcing target, they can present a range, for instance in the ΔT (section 3.3.2). This range can be as high as 0.36°C. In general, this range tends to increase as the forcing target is more ambitious.

   (b) We calculate the probability density functions for the ΔT with respect to the preindustrial equilibrium 1850-1900 for each SSP-RCP, aggregating the scenarios from different IAMs. SSP-RCPs sharing the same RCP obviously lead to close radiative forcings, and ultimately to close median ΔT, but the distributions depend on the SSP. Then, using the probability density functions, we show that the 90th percentiles of the ΔT are different. We note that the ΔT that has a 90% probability not to be exceeded is 0.5 to 1°C higher that the target (section 3.3.2).

   (c) Using the same probability density functions, we deduce the probabilities of exceeding the 2°C temperature goal under the different SSP-RCP (section 3.3.2).

2. Radiative forcings

   (a) Even if SSP scenarios share the same forcing target, and even the same SSP storyline, their dynamics may be very different depending on the IAM. The decrease in total radiative forcing over 2080-2100 in SSP5-RCP2.6 vary with a factor 3 (section 3.3.3.1). Because their target is in 2100, the consequences for climate change after 2100 are likely to be very different under these scenarios.

   (b) The effects of the implementation of climate policies can clearly be seen through the reduction of the radiative forcings from CO_2 and fluorinated gases, but not as clearly in those from CH_4, N_2O and aerosols (3.3.3.2).

   (c) With the reduction of the anthropogenic emissions, the cooling effect of aerosols is not as strong as it is baseline scenarios, which hampers mitigation (3.3.3.2). As a remark, the reductions of the associated emissions may have benefits concerning public health and environmental issues.

3. Atmospheric concentrations & anthropogenic emissions

   (a) Trade-offs are observed in the reduction of emissions. In terms of atmospheric concentrations or radiative forcings, the range of these trade-offs may be greater than the range induced by different climate policies. Reduction in the atmospheric concentration of CO_2 (section 3.3.4.1) may be compensated by a reduction in the atmospheric concentration of CH_4

(section 3.3.4.2) or N_2O (section 3.3.4.3). For instance, SSP4-RCP4.5-GCAM4 has 523 ppm of CO_2 but 2145 ppb of CH_4 in 2100. On the other hand, SSP4-"RCP3.4"-WITCH-GLOBIOM reaches a lower radiative forcing even though it has a higher CO_2 concentration (556 ppm), but a much lower CH_4 concentration (1645 ppb).

(b) According to all IAMs, in all SSPs, the implementation of a climate policy leads to a reduction of anthropogenic greenhouse gases emissions in 2100 (section 3.3.1). Yet, the effect of the implementation of climate policy in the emissions of other forcing agents such as CO, NO_X, BC, OC, VOC or NH_3 is not as clear: in multiple cases, these emissions are actually increased.

(c) As said in conclusion 3b, comparing to the baseline, implementing the basic level of a climate policy leads in all cases to a reduction of all greenhouse gases emissions in 2100. It can be seen through atmospheric concentrations of these greenhouse gases (section 3.3.4). However, we note that moving from the first level of a climate policy to the second does not necessary reduce the atmospheric concentrations of all greenhouse gases. For instance, in SSP5, the N_2O concentrations in 2010 from REMIND-MagPie increase from 366 to 380 ppb as the forcing target moves from RCP6.0 to RCP2.6. It may be explained by the increase in N_2O emissions from croplands for the production for biofuels.

(d) Although anthropogenic emissions tend to be reduced, the perturbation of natural emissions (wetlands and biomass burning) is increased with change in land cover and in climatic conditions. By 2100, anthropogenic emissions may represent as low as 50.2% of CH_4 emissions (section 3.3.1.3), 59.4% of N_2O emissions (section 3.3.1.4) and 55.5% of SO_2 emissions (section 3.3.1.5). Yet, instead of partially cancelling the effect of the reductions in CH_4 emissions, different opportunities are possible with wetlands, to reduce their emissions and improve their carbon sequestration (Crooks et al., 2011; Turetsky et al., 2014).

4. Emissions from Land Use Change

(a) The determinants for the trajectories of CO_2 emissions from Land Use Change are primarily the SSP, then the IAM and finally the forcing target (section 3.3.1.2). This is caused by similarities in the drivers: Land Use Changes (section 3.2.3.2), harvest of biomass (section 3.2.3.3) and area extents of shifting cultivations (section 3.2.3.4).

(b) In most scenarios of the 5 SSPs, the shape of CO_2 emissions from Land Use Change that we observe in the baseline are different from those that we observe for the first level of the climate policy. As forcing targets become more ambitious, the pattern of CO_2 emissions from Land Use Change are changed with sooner peaks (section 3.3.1.2). Often, Land Use Change emissions tend to be slower, but not systematically.

(c) The CO_2 emissions from Land Use Change from OSCAR are higher than those of the IAMs. This difference depends primarily on the IAM, and in a lesser extent on the SSP and the forcing target. A summary of these differences is presented in table 3.7, with differences in cumulative CO_2 emissions ranging from 0 to 268 GtC.

(d) Analyzing our calculation of CO_2 emissions from Land Use Change (section 3.3.1.2), using comparisons to LUH2 (section 3.4.2) and sensitivity analyses (section 3.4.3), we show that these differences can be partly related to our assumptions for the evolution of the area extents of shifting cultivations. Yet, SSP scenarios with the Land-Use variables from LUH2 have been used in the following chapter, and strong differences remain (sections 4.3.3 to 4.3.6). As such, the differences can be attributed to the methods used to calculate these emissions. Bearing in mind that MAGICC calculates climate projections for the SSP scenarios with the Land Use Change emissions of the IAMs, complementary evaluations are required to ensure that these emissions are consistent with those calculated by the Earth system models.

5. Carbon cycle

(a) Thanks to climate policies, the total CO_2 emissions are reduced, and it can be seen through the reduction of the absorption by the ocean sink (section 3.3.5.1) and the land sink (section 3.3.5.2). Besides, the capacities of the sinks to store and remove the carbon are degraded with climate change, the land sink being more affected than the ocean sink.

(b) According to OSCAR, several scenarios targeting the RCP2.6 have their land sink becoming a source of carbon by 2100 (section 3.3.5.2). It concerns principally the SSP5 and the SSP2, with high CO_2 emissions in the beginning of the scenario that are compensated later. In these cases, the land sink returns the carbon previously stored, with a rate as high as 0.47 GtC/yr.

(c) The comparison of the carbon fractions of OSCAR over 2006-2015 to those of Le Quéré et al. (2016) show that the land carbon fraction is underestimated by 10%, whereas the airborne fraction is overestimated by 8.8% (section 3.3.5.3). Yet, CO_2 emissions from Land Use Change are also underestimated compared to those of Le Quéré et al. (2016). Further development of OSCAR with regard to the modelling of the preindustrial land cover maps and carbon densities may help to solve this problem.

(d) Bearing in mind that OSCAR underestimate the land carbon fraction, and overestimate the ocean carbon fraction, we observe that the cumulative airborne fraction over 1700-2100, that is to say the fraction of the emissions over that period that remains in the atmosphere, range from 33.2% to 61.1% (section 3.3.5.3). The cumulative land carbon fraction

may be as low as 17.3% whereas the cumulative ocean carbon fraction may reach 21.6%.

(e) We have calculated the carbon budgets in terms of Threshold Exceedance Budgets (TEBs) and Threshold Avoidance Budgets (TABs) for different temperatures and probabilities (section 3.3.8). We have compared the assessments using different definitions of these budgets. It comes that to avoid a ΔT above 2°C with a probability of 66%, a maximum of 1240 $GtCO_2$ (610 to 1790) can be emitted from 2015. To exceed a ΔT of 2°C with a probability of 66%, 1690 $GtCO_2$ (940 to 2770) have to be emitted from 2015.

(f) With 37.8 $GtCO_2$/yr of CO_2 emissions in 2015 and assuming a similar rate, the carbon budget to avoid 2°C with a probability of 66% is reached in 32 years (16-46) (section 3.3.8). To exceed this level at this rate, 44 years (24-71) are required, but we remind that the temperature will increase beyond afterwards, even without emitting further. Bearing in mind that emissions are still increasing, and faster than in earlier decades (Le Quéré et al., 2016), it calls for urgent reductions of the emissions and rapid development of low carbon technologies (van Vuuren et al., 2016).

6. Using a Kaya decomposition for the SSP database, we observe that the reduction of the carbon intensity of the energy is the major source of reduction of CO_2 emissions in the SSPs, and energy intensity of the GDP plays a secondary role (section 3.3.7).

7. We extend the Kaya decomposition using global co-emission ratios. For SO_2, we show that IAMs tend to show consistent relations for the co-emission ratios for similar forcing targets. Besides, in the early mitigation (least ambitious forcing targets), reduction in SO_2 and CO_2 emission occur in similar proportions. For other species, the technological assumptions of each storyline SSP takes a stronger importance, compared to SO_2. For forcing targets, typically RCP2.6 and RCP3.4, CO_2 emissions are decreased more than the other emissions, because of negative CO_2 emissions and difficulties in the other emissions. For these targets, biomass burning emissions account for a greater share of the emissions (section 3.3.1).

Even though the SSP database (IIASA, 2018c) has showed to be a valuable resource, even of higher value than the RCP database (IIASA, 2018b) or the AR5WG3 database (IIASA, 2018a), missing variables have hindered this study. An accurate assessment of climate change require several variables, and the replacement of each missing variable implies a reduction in the accuracy of the assessment.

1. Land Cover were provided, but Land Use Changes are required. The algorithm of Stocker et al. (2014) has been used, for this is the best solution available with the provided variables. Even though this algorithm provides us with relatively close land use changes, we show that it is limited, and cannot reproduce

perfectly the required patterns (section 3.4.1). It may have an incidence on the calculation of CO_2 emissions from Land Use Changes. Monge-Kantorovitch theory may be a better approach for the evaluation of all transitions, but it still requires assumptions regarding the costs of the transitions (Rachev, 1985).

2. The harvest of biomass and the area extents of shifting cultivations were not provided, in spite of their importance for the carbon cycle. We have shown that the sensibility over our assumptions (sections 3.2.3.3 and 3.2.3.4) lead to a maximal change in ΔT of about 0.2 °C (section 3.4.3).

3. Nevertheless, most information regarding the climate assessment of SSP scenarios using MAGICC are missing, especially concerning the land variables. Until more information are given, it remains possible that the absorption of atmospheric CO_2 from bioenergies with CCS using forestry residues may be counted once through the harvest of biomass (counted directly in CO_2 emissions) and another time through the absorption by the terrestrial biosphere. It is also possible that the harvest is not counted in MAGICC, with the risk of biasing the carbon cycle.

4. In the planned 2nd stage of the SSP database, several variables of interest for this study will be released. For instance, the CH_4 and N_2O emissions from agriculture, forestry and other land use, but also the total CO_2 emissions captured and stored in geological deposits, be it with bioenergies or fossil fuels. The latter variables will be of great help to solve the previous point.

5. The Land Use Harmonization (LUH2, 2018) provides the land variables for 6 SSP scenarios. The comparison of these estimates to ours confirm the bias in Land Use Changes and harvest of biomass. Unfortunately, the LUH2 dataset cannot be used directly to calibrate the transitions and the harvests of the 103 SSP scenarios.

Overall, our assessment provides several key features and numbers for issues relative to climate change and mitigation challenges. Yet, we show that the SSP public database is not complete enough for accurate projections, for information are missing, even though ad-hoc assumptions are possible. In particularly, the Land-Use components provided on the database would need more details.

Besides, a comparison of the climate projections from OSCAR and MAGICC would have been very valuable. To date, several information about the precise method used for MAGICC, for instance for the land variables or the Land Use Change emissions, are missing, with just hints here and there (IIASA, 2018e), van Vuuren et al. (2017), Fricko et al. (2017), Fujimori et al. (2017), Calvin et al. (2017), Kriegler et al. (2017), SSP (2018)). Bearing in mind that the climate assessment of the scenarios, and thus the design of climate policies, currently rests on MAGICC (Clarke et al., 2014), a comparison of MAGICC to OSCAR would be of great help to look for any eventual bias both in MAGICC and in OSCAR, or in the treatment

of the scenarios. For this reason, more information on the precise treatments of the scenarios are required.

Chapter 4

Evaluation of implications of Carbon Dioxide Removal technologies for the Earth system

4.1 Introduction

Even though climate change awareness has grown over last decades, CO_2 emissions keep increasing (Boden et al., 2017; Myhre et al., 2013). The emissions of most short-lived climate forcers and other greenhouse gases keep increasing as well (Olivier and Janssens-Maenhout, 2014). This pace diminish our chances to mitigate climate change under 2, 3, or 4°C (Friedlingstein et al., 2014a). During the COP21, the Paris Agreement has confirmed the international target to limit climate change well below 2°C above preindustrial level, and to pursue efforts to limit the global warming to 1.5°C. Evaluations of the first intended nationally determined contributions show that these targets are very likely not to be respected (Rogelj et al., 2016a; Sanderson et al., 2016). Because of delays in mitigation, net negative emissions may become a requirement to keep climate change below 2°C by the end of the century (Peters et al., 2013). Besides, the more mitigation is delayed, and the less feasible will be the socio-economic pathways that lead to 2°C (Strefler et al., 2018), between high economic costs from transitions and large-scale development of carbon dioxide removal (CDR).

For the Fifth Assessment Report of IPCC (AR5), the Working Group 3 (WG3) gathered an ensemble of scenarios (Clarke et al., 2014). Out of the 116 scenarios limiting global warming in 2100 below 2°C, 101 use negative emissions (Fuss et al., 2014), that is to say, the intentional removal of CO_2 from the atmosphere using different technologies such as direct air capture (DAC) and bioenergy with carbon capture and storage (BECCS). Afforestation and reforestation may also be used to

enhance the land sink. Enhancement of the ocean sink may also be obtained by altering the sea surface alkalinity or increasing the biological pump. However, these technical means are not necessarily a solution to climate change, because their feasibility, their potential and their hazards are still subject to debate. These technologies are not ready yet for large scale development and have inherent limits (Smith et al., 2016). In the current state of knowledge, focusing on negative emissions is a risky gamble (Fuss et al., 2014; Anderson and Peters, 2016). Conventional mitigation remains a necessary part of any climate policy targeting a maximum global warming of 2°C by 2100 (Gasser et al., 2015).

The evaluation of the potential efficiency of these approaches is one goal of the Carbon Dioxide Removal Model Intercomparison Project (CDR-MIP, Keller et al. (2017)). It makes use of scenarios from the Scenario Model Intercomparison Project (ScenarioMIP, O'Neill et al. (2016)), the Land Use Model Intercomparison Project (LUMIP, Lawrence et al. (2016)) and the Coupled Climate-Carbon Cycle Model Intercomparison Project (C4MIP, Jones et al. (2016b)). These MIPs are within the scope of the latest Coupled Model Intercomparison Project Phase 6 (CMIP6, Eyring et al. (2016b)), which is composed of a set of common experiments (Diagnostic, Evaluation and Characterization of Klima, DECK), CMIP historical simulations and 21 endorsed-MIPs. The scenarios shared by CDR-MIP and these endorsed MIPs are scenarios developed from the recent framework of Representative Concentration Pathways (RCPs) and Shared Socio-economic Pathways (SSPs) (van Vuuren et al., 2014). In this framework, the different major climate targets, the RCPs, are reached by 2100 under the different socio-economic storylines represented by the SSPs. One reason for such a scenario matrix (van Vuuren and Riahi, 2011) is that it allows the study of negative emissions under different assumptions of technological development and social acceptance. As a remark, CDR-MIP focuses on the study of negative emissions, and not on other geoengineering techniques, such as Solar Radiative Management (SRM), albeit a joint experiment with the Geoengineering Model Intercomparison Project (GeoMIP, Kravitz et al. (2017)) is considered.

CDR-MIP aims at evaluating the potential and the risks of negative emissions (Kiel Earth Institute, 2018). Four experiments are planned: the reversibility of the Earth system, its response to direct atmospheric CO_2 removal, impacts of afforestation/reforestation and ocean alkalinization. The potential and the risks of CDR for the Earth system only are evaluated in a first time, with the expectation of evaluating the consequences for the society in a second time. Different categories of models are invited to participate, like Earth System Models (ESMs) for their resolution, but also models that trades a lower resolution for longer timescales and probabilistic framework. Yet, the coupling of the climate system with the carbon cycle is required, in order to account for the expected reduction of the potential of negative emissions with climate change (Jones et al., 2016a). This chapter represents the preliminary contribution of OSCAR v2.2 (Gasser et al., 2017a) to CDR-MIP. The methods used for these experiments will be explained, concerning the extension of OSCAR, the representation of the different experiments and the probabilistic

framework. The results of OSCAR will be used to assess the feasibility, potential and hazards of negative emissions through the four group of experiments of CDR-MIP. The limits of our study will be discussed, leading to our conclusions.

4.2 Methods

For the participation of OSCAR to this model intercomparison project, OSCAR has been updated to include the modelling of alkalinity. We explain in section 4.2.1 how alkalinity is represented, and how new functions for the calculation of the oceanic partial pressure of CO_2 and the pH are produced. Besides, the use of the land variables from LUH2 for several experiments require this database to be treated for OSCAR, as explained in section 4.2.2. Finally, the probabilistic framework used for the experiments of this project is detailed in section 4.2.4.

4.2.1 Extension of OSCAR v2.2 for alkalinity

4.2.1.1 OSCAR v2.2 and total alkalinity

Among the different techniques of negative emissions, the enhancement of oceanic weathering is discussed. The principle is to artificially increase the total alkalinity of sea water by dissolving alkilizing agents such as calcium hydroxide ($Ca(OH)_2$), forsterite (Mg_2SiO_4) or olivine ($(Mg,Fe)_2SiO_4$). The total alkalinity characterizes the excess of bases over acids in a solution, but is different from its basicity (Dickson, 1981; Sarmiento and Gruber, 2006). The total alkalinity (TA) in typical sea water solutions can be written as the sum of concentrations shown in equations 4.1 (Millero et al., 2002), with CA being the carbonate alkalinity.

$$TA = CA + \left[B\left(OH\right)_4^-\right] + \left[HPO_4^{2-}\right] + 2\left[PO_4^{3-}\right] + \left[Si\left(OH\right)_3O^-\right] + \left[H^+\right] - \left[OH^-\right] \tag{4.1a}$$

$$CA = \left[HCO_3^-\right] + 2\left[CO_3^{2-}\right] \tag{4.1b}$$

The increase of the total alkalinity is expected to decrease the acidity of sea water, and then to increase the capacity of the ocean to stock carbon (Kheshgi, 1995). The CO_2 absorbed in sea water is dissolved into H_2CO_3, which is a diacid, as represented through the equilibriums 4.2. The Dissolved Inorganic Carbon (DIC) is then defined as the sum of the concentrations of the three anions. As a remark, the equilibrium 4.2a merges two equilibriums. The gas CO_2 in sea water ($CO_{2(g)}$) dissolves in sea water into an aqueous form ($CO_{2(aq)}$), which is analytically equivalent to H_2CO_3 (Millero, 1995). For this reason, H_2CO_3 groups here these two forms. Besides, we approximate the activities of the different forms by their concentrations, and the

fugacity of CO_2 by its partial pressure pCO_2.

$$CO_{2(g)} + H_2O \Leftrightarrow H_2CO_3 \tag{4.2a}$$
$$H_2CO_3 \Leftrightarrow HCO_3^- + H^+ \tag{4.2b}$$
$$HCO_3^- \Leftrightarrow CO_3^{2-} + H^+ \tag{4.2c}$$
$$DIC = [H_2CO_3] + \left[HCO_3^-\right] + \left[CO_3^{2-}\right] \tag{4.2d}$$

In OSCAR v2.2 (Gasser et al., 2017a), the alkalinity is not represented. The ocean carbon-cycle is based on a mixed-layer IRF (Joos et al., 1996), used in others reduced-form ESMs such as MAGICC6 (Meinshausen et al., 2011a; Raupach et al., 2011). However, there are three modifications to this method already implemented in OSCAR v2.2. The function is written as its equivalent box model, as done in Harman and Al. (2011). To each one of the exponential terms of the IRF corresponds a box. Besides, the carbonate chemistry function has been updated to include the dependency on global sea surface temperature. Finally, an evolution of the mixed-layer depth of Joos et al. (1996) with the global sea surface temperature is introduced, to account for the stratification of the ocean. For this study, we have extended the carbonate chemistry function to a third variable, the total alkalinity. We have also extended the same mixed-layer IRF for the total alkalinity. Finally, we have also produced a new function for the pH, to account for changes in total alkalinity.

The carbon flux from the atmosphere to the ocean F_{in} is written using the atmospheric partial pressure of carbon CO_2 (expressed in ppm), the previously introduced atmospheric conversion factor α^{CO_2} from ppm to GtC and a gas exchange factor ν_{fg}. The carbon flux from ocean to the atmosphere F_{out} uses the new function f_{pCO_2} to evaluate the sea surface partial pressure of CO_2 using the DIC dic, the sea surface temperature T_S and the total alkalinity TA alk (equations 4.3).

$$\Delta F_{in} = \nu_{fg}\alpha^{CO_2}\Delta CO_2 \tag{4.3a}$$
$$\Delta F_{out} = \nu_{fg}\alpha^{CO_2} f_{pCO_2}\left(\Delta dic, T_{S,0} + \Delta T_S, \Delta alk\right) \tag{4.3b}$$

The DIC and the TA are deduced from the surface stocks in carbon C_{surf} (expressed in GtC) and alkalinity A_{surf} (expressed in mol), using equations 4.4. The ocean is assumed to have a global area A_{ocean} and a mixed-layer depth h_{mld}. A conversion factor α_{sol} is used for DIC to convert ppm.m^{-3} to $\mu mol.kgsol^{-1}$, and a conversion factor α_{alk} is introduced, to convert mol to $\mu mol.kgsol^{-1}$. The dependency of the mixed-layer depth is unchanged compared to Gasser et al. (2017a), using an exponential function parametrized with a relative intensity of the stratification

and its sensitivity to the sea surface temperature change.

$$\Delta dic = \frac{\alpha_{sol}}{\alpha^{CO_2}} \frac{\Delta C_{surf}}{A_{ocean} h_{mld,0} \left(1 + \frac{\Delta h_{mld}}{h_{mld,0}}\right)} \tag{4.4a}$$

$$\Delta alk = \alpha_{alk} \frac{\Delta A_{surf}}{A_{ocean} h_{mld,0} \left(1 + \frac{\Delta h_{mld}}{h_{mld,0}}\right)} \tag{4.4b}$$

The oceanic circulation and the mixing fluxes introduce fluxes from the sea surface stocks of DIC (F_{circ}) and TA ($F_{circ,A}$) to an implicit deep reservoir. To evaluate these fluxes, the sea surface is subdivided into several boxes (superscript oc), using the terms of the mixed-layer IRF. The stocks are splitted into C^{oc}_{surf} and A^{oc}_{surf} using the fractions π^{oc}_{circ}, such that $\Sigma_{oc}\pi^{oc}_{circ} = 1$. The pertubation of the stocks within each box decrease with associated turnover rates τ^{oc}_{circ}. We make the assumption that the oceanic circulation and the mixing fluxes affect the alkalinity stock in the same way as it does with the carbon stock. This implies that the same IRF can be used for the alkalinity stock (equation 4.5).

$$\Delta F^{oc}_{circ} = \Delta C^{oc}_{surf} / \tau^{oc}_{circ} \tag{4.5a}$$

$$\Delta F^{oc}_{circ,A} = \Delta C^{oc}_{surf} / \tau^{oc}_{circ} \tag{4.5b}$$

With the dissolution of CO_2 in sea water, the TA does not change because as many negative charges as $H+$ are added to the solution. Yet, TA can be artificially modified using a flux $F_{A,exo}$, that follows the same decomposition into boxes as the other surface input fluxes. These boxes are no geographical subdivision of the sea surface, but a symbolic decomposition of the stock into reservoirs corresponding to the different timescales of the IRF. This is why the artificial alkalinization cannot be regionalized here. The fluxes are summed for each box to form the variations in the stocks of each box, and the stocks of each box are used to estimate the surface stocks (equations 4.6).

$$\frac{d}{dt}\Delta C^{oc}_{surf} = \pi^{oc}_{circ}\Delta F_{in} - \pi^{oc}_{circ}\Delta F_{out} - F^{oc}_{circ} \tag{4.6a}$$

$$\frac{d}{dt}\Delta A^{oc}_{surf} = \pi^{oc}_{circ}\Delta F_{A,exo} - F^{oc}_{circ,A} \tag{4.6b}$$

$$\Delta C_{surf} = \Sigma_{oc}\Delta C^{oc}_{surf} \tag{4.6c}$$

$$\Delta A_{surf} = \Sigma_{oc}\Delta A^{oc}_{surf} \tag{4.6d}$$

As in Gasser et al. (2017a), the biological pump is assumed unaffected. Yet, this carbon export depends on sea surface temperature, nutrient availability and surface acidity (Ciais et al., 2013). In this preliminary contribution, this process is not added yet. A future development could be the introduction of a flux, corresponding to the increase of the biological export of organic and inorganic carbon from the sea surface to the deep ocean, at a global scale, since the preindustrial state. The biological export of alkalinity is proportional to the biological export of total carbon with the factor $2R/(1+R)$, where R is the rain ratio, defined as the ratio between the particulate organic carbon and the particulate inorganic carbon (Yamanaka and Tajika, 1996; Lima et al., 2014). In this project, only enhanced weathering by alkalinization is used. Yet, an increase of the biological pump may be achieved using fertilization (Joos et al., 1991; Eggleston and Galbraith, 2017). Other stages of a future development may be the implementation of the phosphorus and sulfur cycles and the effects of iron deposition (Fujii et al., 2005).

4.2.1.2 New functions for the oceanic pCO_2

The calculation of the oceanic partial pressure pressure of CO_2 is possible using DIC and CA, but it requires the thermodynamic constants of the equilibriums represented in equilibrium 4.2. Fits for these constants exist (Millero, 1995; Millero et al., 2002). However, we have chosen another approach, because total alkalinity can be increased, without changing the carbonate alkalinity, by adding other elements (equation 4.1). The two initial formulations for the function f_{pCO_2} have been kept, being either a Padé approximant (equation 4.7a) or a Power law fit (equation 4.7b), from Harman and Al. (2011). Their dependency in DIC follow these equations:

$$pCO_2^{Pade} = 380 \frac{x_0^{Pade} - x_1^{Pade} dic + \sqrt{((x_0^{Pade} - x_1^{Pade} dic)^2 - 4 x_2^{Pade} dic)}}{2 x_2^{Pade} dic} \tag{4.7a}$$

$$pCO_2^{Power} = 380 \left(x_2^{Power} + \left(dic / x_0^{Power} \right)^{1/x_1^{Power}} \right) \tag{4.7b}$$

For both formulations, each one of the coefficients x_i ($i \in [0,1,2]$) integrates a dependency in temperature, using three coefficients as described in equation 4.8a. These dependency is written as a second order polynomial function around a sea surface temperature T_S^* (equal to 15°C). The three coefficients $x_{i,j}$ of this polynomial functions are written using the index j ($j \in [0,1,2]$). These coefficients have been fitted as such in Harman and Al. (2011). We introduce for each one of the coefficients $x_{i,j}$ of these functions a new dependency in alkalinity. We assume also a second order polynomial function, as described in equation 4.8b, and the new set of coefficients will be fitted as well. The three coefficients that we introduce use the index k, leading to the coefficients $x_{i,j,k}$, i corresponding to the term in dic, j to the term in

T_S and k to the term in TA.

$$\forall i \in \{0,1,2\}, x_i = x_{i,0}\left(1 + x_{i,1}\left(T_S - T_S^*\right) + x_{i,2}\left(T_S - T_S^*\right)^2\right) \tag{4.8a}$$

$$\forall\,(i,j) \in \{0,1,2\}^2, x_{i,j} = x_{i,j,0}\left(1 + x_{i,j,1}TA + x_{i,j,2}TA^2\right) \tag{4.8b}$$

The 27 coefficients for the formulations Padé and Approximant used in this study are given in table 4.1. The fit is based on outputs from MOCSY v2.0 (Orr and Epitalon, 2014; MOCSY, 2018), an analytical solver of the exact equations of the chemical system. The pCO_2 has been produced with global values for silica (7.237 μmol.kgsol^{-1}), phosphate (0.515 μmol.kgsol^{-1}) and sea water density of 1025kg.m^{-3} provided by the World Ocean Database (Boyer et al., 2013). The boundaries and resolution of the domains of calibration are as follows:

- Domain of DIC: 1750 to 2350 μmol.kgsol^{-1}, with a resolution of 2 μmol.kgsol^{-1}
- Domain of TA: 2250 to 2450 μmol.kgsol^{-1}, with a resolution of 2 μmol.kgsol^{-1}
- Domain of T_S: 0 to 30°C, with a resolution of 0.2 °C
- Restriction to pCO_2 between 180 ppm and 1120 ppm (4 times the preindustrial pCO_2).

However, these fits are not fully optimized yet. The number of coefficients and sizes of the domains lead to long calculations, with successive improvements of the fits. The table 4.1 shows intermediary version of these fits, and improved versions will be used for the final contribution of OSCAR to CDR-MIP. Yet, these fits already provides pCO_2 with a relative precision of -5.1% to 5.3% for the Padé Approximant (figure 4.1) and -4.1% to 4.0% for the Power law fit (figure 4.2) for oceanic pCO_2 between 180 ppm and 1120 ppm. The previous versions of these fits were produced for an alkalinity of 2350 μmol.kgsol^{-1}, 35 PSU of salinity with 0 μmol.kgsol^{-1} of silicate and phosphate (Harman and Al., 2011). We compare the previous versions of these fits to the results from those of MOCSY using 2350 μmol.kgsol^{-1} as well, but 7.237 μmol.kgsol^{-1} of silica, 0.515 μmol.kgsol^{-1} of phosphate (Boyer et al., 2013) and 33.5 PSU. The previous Power Law fit reproduces MOCSY results with -4% to +15% of relative error, and the previous Padé Approximant fit performs with 0 to 13% of relative error. In order to reproduce the global oceanic pCO_2 in a large domain of alkalinity, the new versions of these fits will provided more accurate results. As a remark, 34.6 PSU of salinity may be more appropriate.

Padé Approximant				Power law fit			
$x_{i,j,k}$		$x_{i,j}$	x_i	$x_{i,j,k}$		$x_{i,j}$	x_i
$x_{0,0,0}$	$1.98486659.10^{4}$			$x_{0,0,0}$	$1.68598612.10^{3}$		
$x_{0,0,1}$	$1.28605763.10^{-5}$	$x_{0,0}$		$x_{0,0,1}$	$-2.88295755.10^{-4}$	$x_{0,0}$	
$x_{0,0,2}$	$1.04350753.10^{-7}$			$x_{0,0,2}$	$1.73892004.10^{-7}$		
$x_{0,1,0}$	$-1.85531718.10^{-2}$			$x_{0,1,0}$	$-2.62528013.10^{-3}$		
$x_{0,1,1}$	$1.56060449.10^{-4}$	$x_{0,1}$	x_0	$x_{0,1,1}$	$6.71163020.10^{-5}$	$x_{0,1}$	x_0
$x_{0,1,2}$	$-2.29819431.10^{-8}$			$x_{0,1,2}$	$1.85254584.10^{-8}$		
$x_{0,2,0}$	$2.56749116.10^{-4}$			$x_{0,2,0}$	$-4.28140612.10^{-3}$		
$x_{0,2,1}$	$-3.72010444.10^{-3}$	$x_{0,2}$		$x_{0,2,1}$	$-8.76234064.10^{-4}$	$x_{0,2}$	
$x_{0,2,2}$	$1.54584437.10^{-6}$			$x_{0,2,2}$	$1.92708160.10^{-7}$		
$x_{1,0,0}$	$1.61487548.10^{1}$			$x_{1,0,0}$	$2.15147425.10^{-2}$		
$x_{1,0,1}$	$-1.79046802.10^{-5}$	$x_{1,0}$		$x_{1,0,1}$	$1.51692922.10^{-3}$	$x_{1,0}$	
$x_{1,0,2}$	$-1.33971009.10^{-8}$			$x_{1,0,2}$	$-3.28031621.10^{-7}$		
$x_{1,1,0}$	$-1.70016804.10^{-2}$			$x_{1,1,0}$	$5.06919161.10^{-3}$		
$x_{1,1,1}$	$1.52813838.10^{-4}$	$x_{1,1}$	x_1	$x_{1,1,1}$	$2.59579956.10^{-3}$	$x_{1,1}$	x_1
$x_{1,1,2}$	$-2.82985747.10^{-8}$			$x_{1,1,2}$	$-6.04382859.10^{-7}$		
$x_{1,2,0}$	$7.75161156.10^{-4}$			$x_{1,2,0}$	$8.88087020.10^{-5}$		
$x_{1,2,1}$	$-1.98536342.10^{-3}$	$x_{1,2}$		$x_{1,2,1}$	$-1.90538980.10^{-2}$	$x_{1,2}$	
$x_{1,2,2}$	$7.00002932.10^{-7}$			$x_{1,2,2}$	$8.44651974.10^{-6}$		
$x_{2,0,0}$	$-7.31241101.10^{-1}$			$x_{2,0,0}$	$2.78720568.10^{-1}$		
$x_{2,0,1}$	$1.60313046.10^{-3}$	$x_{2,0}$		$x_{2,0,1}$	$-3.04427186.10^{-4}$	$x_{2,0}$	
$x_{2,0,2}$	$-2.58349114.10^{-7}$			$x_{2,0,2}$	$1.34443185.10^{-7}$		
$x_{2,1,0}$	$-5.79963711.10^{-3}$			$x_{2,1,0}$	$2.01869896.10^{-6}$		
$x_{2,1,1}$	$-1.74265789.10^{-3}$	$x_{2,1}$	x_2	$x_{2,1,1}$	$-3.23629116.10^{0}$	$x_{2,1}$	x_2
$x_{2,1,2}$	$6.92448437.10^{-7}$			$x_{2,1,2}$	$1.27516553.10^{-3}$		
$x_{2,2,0}$	$-2.26989340.10^{-4}$			$x_{2,2,0}$	$3.77489227.10^{-7}$		
$x_{2,2,1}$	$1.23965226.10^{-2}$	$x_{2,2}$		$x_{2,2,1}$	$1.30297516.10^{1}$	$x_{2,2}$	
$x_{2,2,2}$	$-5.24302528.10^{-6}$			$x_{2,2,2}$	$-5.71001766.10^{-3}$		

Table 4.1: *Coefficients for the function f_{pCO_2} using the Padé Approximant and the Power law fit. Each coefficient $x_{i,j,k}$ is identified through i for the term in DIC, j for the term in temperature and k for the term in TA. In the equations 4.7 and 4.8, temperatures are expressed in $^\circ C$, and DIC and TA are expressed in $\mu mol.kgsol^{-1}$. Coefficients are divided into groups depending on their use in the fit.*

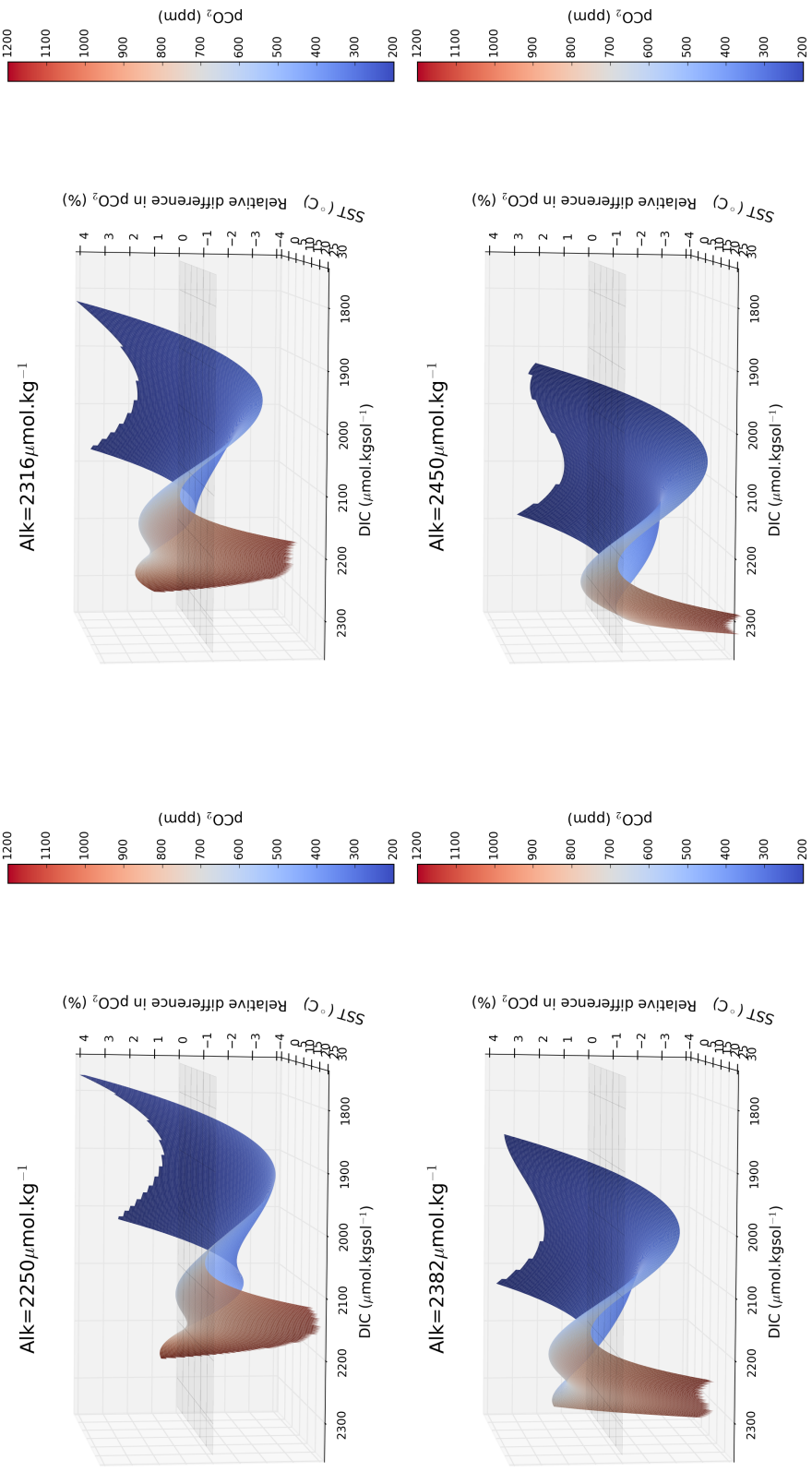

Figure 4.1: *Relative error for the Padé Approximant (%) for 4 values of alkalinity over the domain of the fit in DIC and sea surface temperature. The color of the surface patches corresponds to the value of the oceanic pCO_2 for this DIC, sea surface temperature and alkanity.*

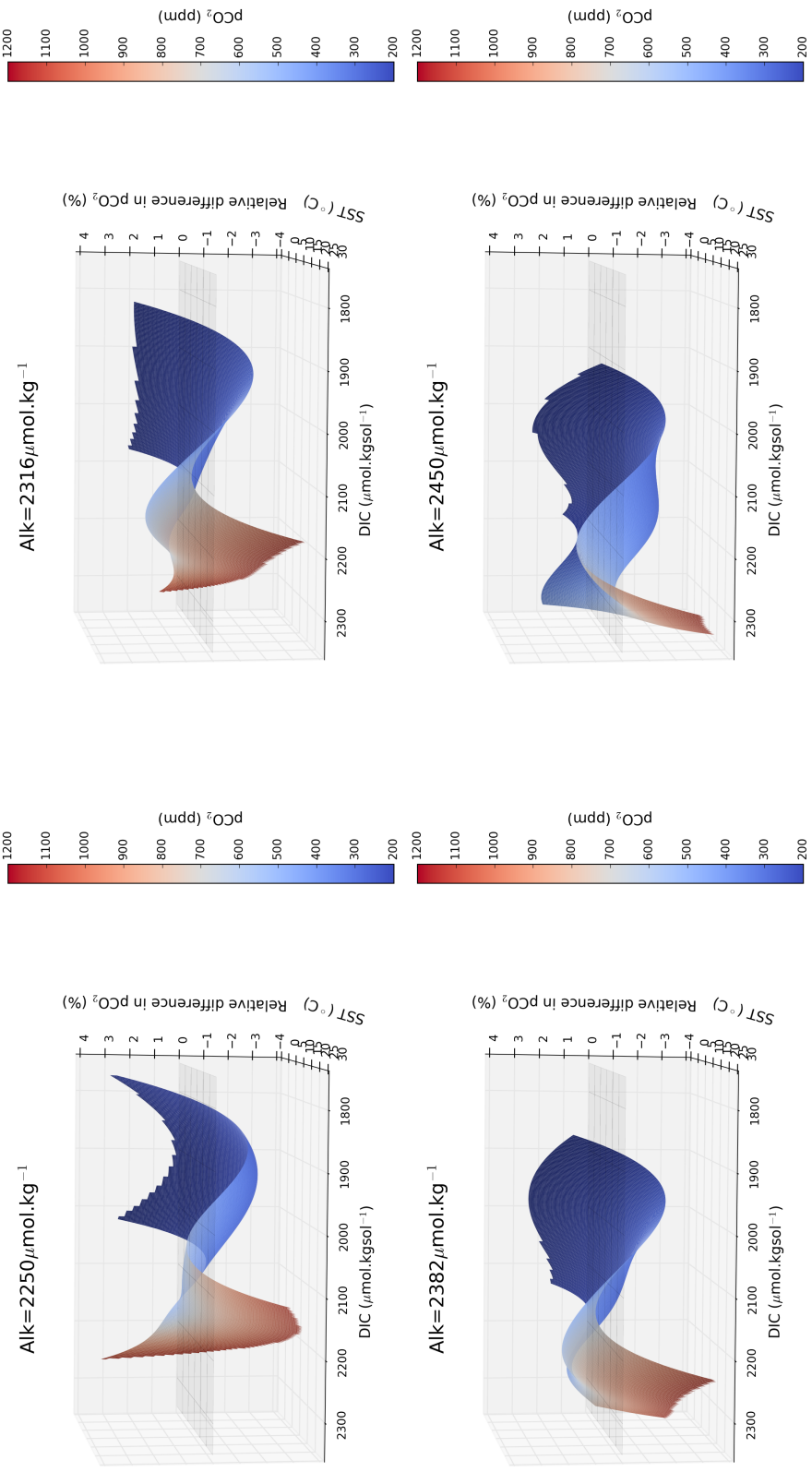

Figure 4.2: *Relative error for the Power law fit (%) for 4 values of alkalinity over the domain of the fit in DIC and sea surface temperature. The color of the surface patches corresponds to the value of the oceanic pCO_2 for this DIC, sea surface temperature and alkanity.*

4.2.1.3 New function for the oceanic pH

In OSCAR v2.2, two parametrizations for the evaluation of pH are used. Both are functions of the atmospherical pCO_2, as shown in equation 4.9a for Tans (2009) and in equation 4.9b for Bernie et al. (2010).

$$\Delta pH = -0.85 log\left(1 + \frac{\Delta CO_2}{CO_{2_0}}\right) \tag{4.9a}$$

$$\Delta pH = -0.00173\Delta CO_2 + 1.3264.10^{-6}(2CO_{2_0}\Delta CO_2 + \Delta CO_2^2) \tag{4.9b}$$

$$- 4.4943.10^{-10}(3\Delta CO_2 CO_{2_0}^2 + 3CO_{2_0}\Delta CO_2^2 + \Delta CO_2^3) \tag{4.9c}$$

To calculate pH from DIC and TA, we have chosen to base our calculations on the equilibrium 4.2. Knowing the DIC and the TA, two methods are possible. We call K_0, K_1 and K_2 the thermodynamic constants of the successive reactions for the CO_2 in sea water (equilibrium 4.2). It is possible to write the pH either using the DIC and and the atmospherical partial pressure CO_2 (equation 4.10a), or using the DIC and the CA (equation 4.10b, demonstrations in appendix).

$$\left[H^+\right] = \frac{K_0K_1 + \sqrt{K_0^2K_1^2 - 4K_1K_2(CO_2K_0 - DIC)}}{2(DIC - CO_2K_0)} \tag{4.10a}$$

$$\left[H^+\right] = \frac{(DIC - CA)K_1 + \sqrt{(CA - DIC)^2 K_1^2 - 4CA(CA - 2DIC)K_1K_2)}}{2CA} \tag{4.10b}$$

The equation 4.10a uses fits for K_0 (Weiss, 1974), K_1 and K_2 (Millero, 2010), whereas the equation 4.10b uses only those for K_1 and K_2: the second may be more accurate. The thermodynamic constants that we use are the same used in MOCSY, for internal consistency. By comparing the quality of the calculation of pH by these two methods on the database produced with MOCSY v2.0, we note that the second effectively presents better results. Finally, applying the first method in OSCAR v2.2 would require to calculate the atmospheric partial pressure using a fit. Even though this fit performs relatively well, it introduces another uncertainty. For these reasons, we evaluate the pH using the equation 4.10b. In this study, we use for K_1 and K_2 only the expressions of Millero (2010). Others expressions could be used (Millero, 1995; Millero et al., 2002; Lueker et al., 2000) to account for the uncertainty in this sensitivity, however Millero (2010) extends the other mentioned sources.

In this study, to use the carbonate alkalinity in equation 4.10b, we make the assumption that the difference to the total alkalinity (equation 4.1) remains constant. Yet, we acknowledge that the change in sea surface temperature and pH will affect the equilibrium of the others bases. We neglect phosphate and sulfate because their

contributions are well below one percent Sarmiento and Gruber (2006). Concentrations in $\left[B\left(OH\right)_4^-\right]$, $\left[H^+\right]$ and $[OH^-]$ are likely to change. Though, the coefficients of K_1 and K_2 could be the object of a fit using the database produced with MOCSY v2, in order to include the effect of borate and the dissociation constant of water.

4.2.2 Treatment of the LUH2 database

4.2.2.1 Principle of the treatment

OSCAR v2.2 uses LUH1 (Hurtt et al., 2011) for the land variables: the LUC transitions, the harvest of biomass and the shifting cultivations. With the scenarios of LUMIP and ScenarioMIP, the LUH2 has been developed to provide the historical LUC and harvest of biomass over 850-2015. The scenarios SSP1-2.6, SSP2-4.5, SSP3-7.0, SSP4-3.4, SSP4-6.0 and SSP5-8.5 over 2015-2100 have also been developed (LUH2, 2018). To comply with the CDR-MIP project, we have used the LUH2 as driving data for OSCAR v2.2.

To begin with, the LUH2 provides past and future data on a grid with a 0.25° x 0.25° resolution with ice-water fractions, the area of gridcells, the current country associated with this gridcell and the potential biomass density of natural vegetation. The latter variable is used in the model of LUH to calculate the biomass density and its growth (Hurtt et al., 2006, 2011). These maps are independent of time. The LUH2 also provides us with the fractions of 12 land-use states in each gridcell, the land-use transitions, the harvest from these biomes and management variables such as irrigation or biofuel crops. OSCAR may use up to 7 biomes (desert, urban, forest, grassland, shrubland, cropland and pasture). The biomes of LUH2 have been matched to those of OSCAR as described in figure 4.3.

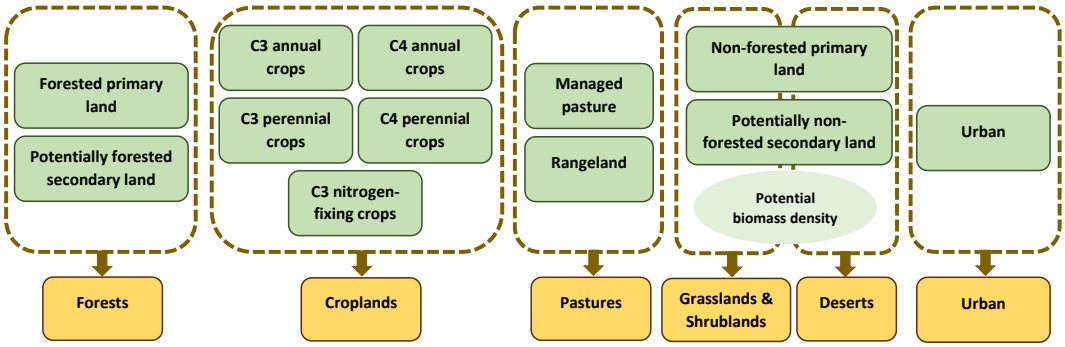

Figure 4.3: *Schematic description of the matching of land-use states of LUH2 (green) to the biomes used in this version of OSCAR v2.2 (yellow). The matching to Grasslands & Shrublands or to Deserts depends on the potential biomass density of the grid cell.*

In the cells where the fraction of non-forested primary land or potentially non-

forested secondary land are not zero, we use the potential biomass density (PD_{bio}) of natural vegetation, provided by LUH2. If the potential biomass density of this cell is above a threshold PD^*_{bio}, the fraction of this biome in this cell is treated as Grasslands & Shrublands. If its potential biomass density is under this threshold, only PD_{bio}/PD^*_{bio} of the fraction of this biome in this cell is treated as Grasslands & Shrublands. In this case, the rest of the fraction of this biome in this cell is considered as Deserts.

We acknowledge that this matching introduces biases. For instance, primary and secondary forests have different impacts on the carbon cycle: primary land has been impacted by human activities, whereas secondary lands recover from human disturbances. The LUH2 dataset allows the improvement of this aspect in OSCAR, for instance by using directly the LUH2 land-use states. For the time of this thesis, the method presented in figure 4.3 is used. The potential biomass density is already being used as a criterion in Hurtt et al. (2006) and Hurtt et al. (2011), which supports its use here.

		Desert & Urban	**Forest**	**Grassland & Shrubland**	**Cropland**	**Pasture**
OSCAR v2.2	Area (Mha)	3697 [1548, 6095]	4301 [2461, 5791]	3671 [557, 5532]	354 [328, 358]	870 [842, 874]
	Stock (GtC)	91 [2, 558]	1181 [476, 2900]	647 [51, 2345]	11 [4, 23]	123 [31, 417]
LU2 for OSCAR	Area (Mha)	3654	4536	3562	285	658
	Stock (GtC)	95 [10, 322]	1247 [870, 2254]	604 [287, 1434]	9 [4, 18]	85 [24, 272]

Table 4.2: *Preindustrial area (Mha) and carbon stock (GtC) for each one of the biomes used. "PI" stands for "Preindustrial". The means and the ranges of the preindustrial areas and carbon stocks of OSCAR v2.2 are given, for comparison to those as using the single preindustrial map produced using the LUH2 dataset, with a threshold of 1.8 kg/m^2 for the potential biomass density of natural vegetation and the sets of preindustrial carbon densities of OSCAR v2.2.*

To evaluate this threshold, we compare the obtained preindustrial areas extents and carbon stocks to those of OSCAR v2.2. In OSCAR v2.2, 9 calibrations for preindustrial carbon fluxes and pools are available, based on 9 dynamic global vegetation models used in TRENDY v2 (Sitch et al., 2015). Preindustrial area extents are produced by combining two categories of maps. The first corresponds to the anthropogenic biomes, with the preindustrial land-use map associated with land variables (LUC, harvest, shifting). The second corresponds to a vegetation map, chosen among 13: 2 being observations of land cover (MODIS, 2018; ESA-CCI, 2018), 2 being potential natural vegetation maps (et al. Ramankutty, 1999; Levavasseur et al., 2012), and 9 being the land-cover maps of the TRENDY models used to calibrate the preindustrial carbon fluxes and pools. For this reason, an ensemble of values are obtained for the preindustrial areas and their carbon stocks in OSCAR v2.2, but also for the carbon stocks produced using the preindustrial areas produced using the LUH2. We evaluate PD^*_{bio} to 1.8 kg/m^2 by comparing the obtained stocks of

carbon in the different biomes of these different preindustrial area extents to those of OSCAR (table 4.2). Although preindustrial area extents for Desert & Urban and Grassland & Shrubland are higher with LUH2, the preindustrial carbon stocks are slightly lower. This is due to a reevaluation of the forests in LUH2.

As another check, we represent the preindustrial areal fraction of desert under this threshold (figure 4.4). Subtropical deserts are correctly represented, although the Kalahari desert should be more centered to the East, on Bostwana, rather than on Namibia and South Africa. Cold deserts are also correctly represented. Finally, polar deserts do not appear here, because they are covered with ice. As such, their fractions from non-forested primary land and potentially non-forested secondary land are not relevant. Yet, this is consistent with OSCAR v2.2, and these lands do not affect directly the carbon cycle.

Finally, the maps are aggregated to OSCAR regions. As a result, the LUH2 is used to produce for the biomes Desert & Urban, Forest, Grassland & Shrubland, Cropland and Pasture:

- Preindustrial area extents, taken either in 1700 or 1850
- Historical LUC (Mha/yr) and harvest (GtC/yr), over 1700-2015
- Scenarios SSP1-2.6,SSP2-4.5, SSP3-7.0, SSP4-3.4, SSP4-6.0 and SSP5-8.5, for LUC (Mha/yr) and harvest (GtC/yr) over 2015-2100

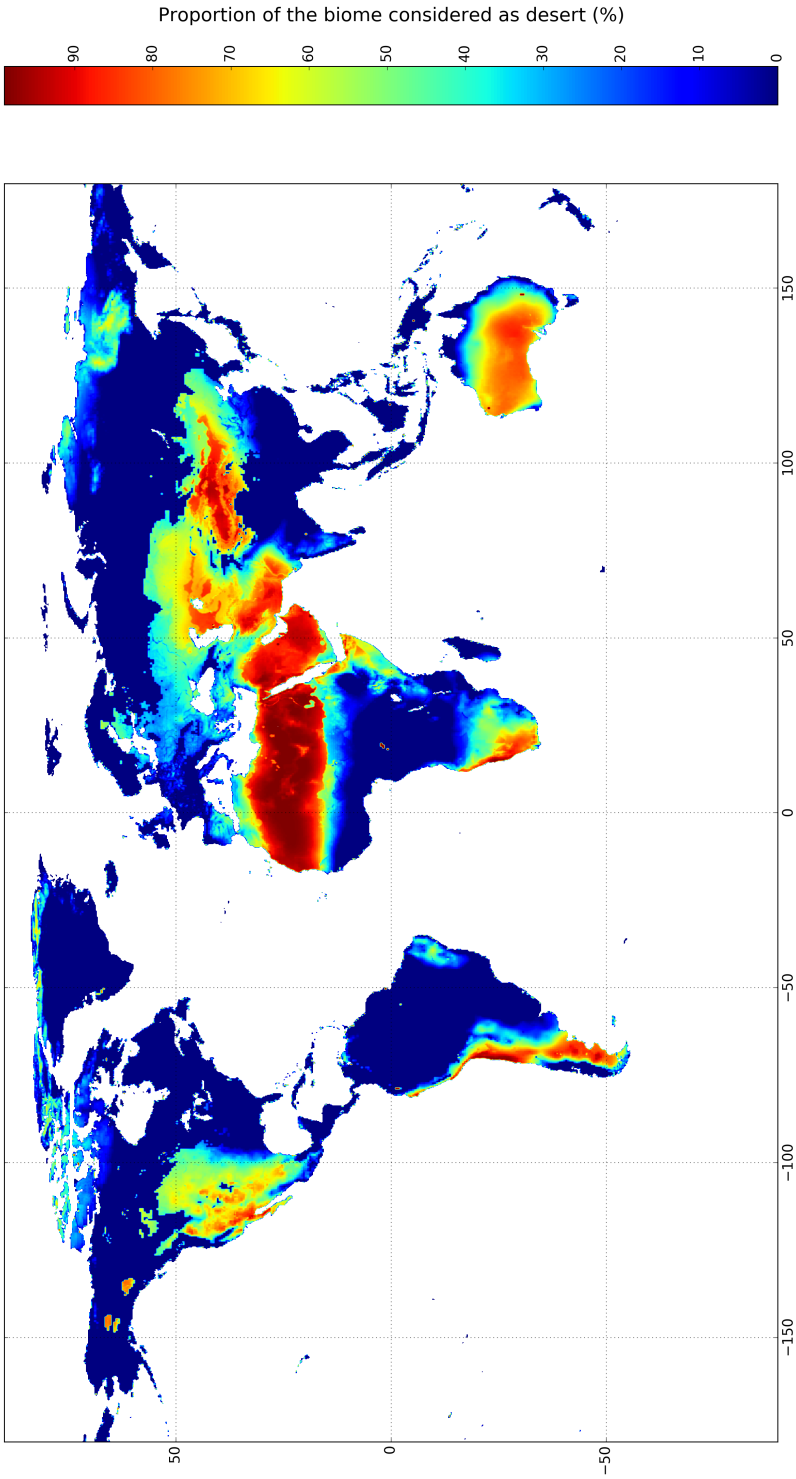

Figure 4.4: *Map of the areal fraction of deserts in 1700, using the threshold of 1.8 kg/m^2 for the potential biomass density of natural vegetation.*

4.2.2.2 Comparison of treated data from LUH2 to LUH1

We compare the obtained harvest from LUH2 (LUH2, 2018) to the one of LUH1 (Hurtt et al., 2011) in figure 4.5. From LUH1 (plain blue line) to LUH2 (dashed red line), the harvest has been strongly reduced by an averaged factor of 2 over 1850-2015. This reduction can be seen in all regions. We ignore the reason for such a decrease from LUH1 to LUH2. In the meantime, the harvest from grasslands and shrublands has been slightly increased, especially before 1920. This can be attributed to an increase harvest from this biome in the OECD countries in 1990.

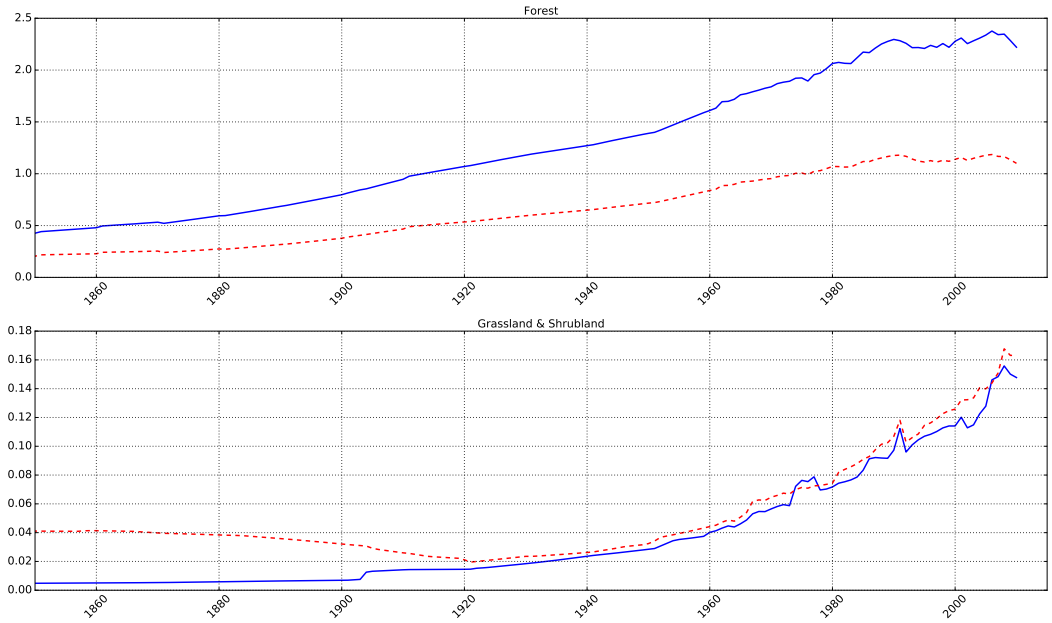

Figure 4.5: *Global evolution of harvest (GtC/yr) over 1850-2015. The evolution from LUH1 is in plain blue line, whereas the evolution from LUH2 is in dashed red line.*

We compare the obtained transitions in LUC from LUH2 (LUH2, 2018) to the one of LUH1 (Hurtt et al., 2011) in figure 4.6. From LUH1 (plain blue line) to LUH2 (dashed red line), almost all transitions have been reduced, with some exceptions. The most significative exceptions concern those between Grassland & Shrubland and Cropland. This increase may be related to the fact that LUH2 does not provide shifting cultivations, contrary to LUH1.

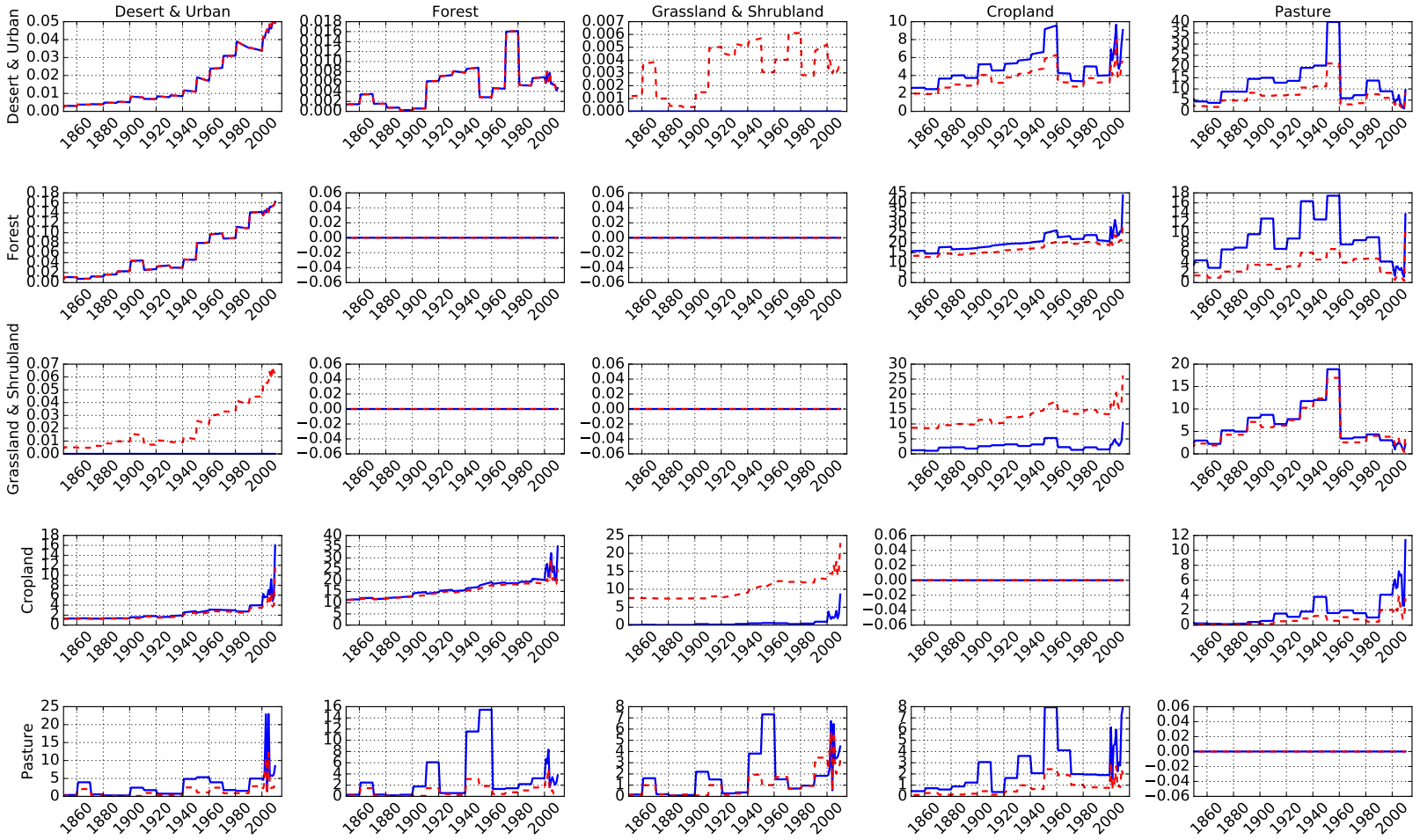

Figure 4.6: *Global evolution of LUC (Mha/yr) over 1850-2015. The evolution from LUH1 is in plain blue line, whereas the evolution from LUH2 is in dashed red line.*

4.2.3 Representation of the experiments

The project CDR-MIP consists in four experiments, each consisting in several scenarios, eventually with extensions. All available extensions of the scenarios will be used. Some scenarios are in common between the four experiments. The four experiments are:

- C1: Climate and carbon cycle reversibility
- C2: Direct CO_2 air capture with permanent storage
- C3: Afforestation/reforestation
- C4: Ocean alkalinization

For each experiment, we describe shortly the principle of the experiment and the protocol of each one of its scenarios. In several cases, it was necessary to adapt the protocol to the specificities of OSCAR, or OSCAR to the protocol. For instance, OSCAR v2.2 assumes that the preindustrial equilibrium is in 1700 (Gasser et al., 2017a). Because of land cover changes, volcanic eruptions and the beginning of the industrial revolution responsible for fossil-fuel emissions, the Earth system is not at the equilibrium in 1850 (Matthews et al., 2004). As a remark, 1720-1800 may be more appropriate as a reference for a preindustrial equilibrium (Hawkins et al., 2017). However, all protocols assume that the preindustrial equilibrium is in 1850. To comply with these protocols, OSCAR has been adapted in all scenarios to assume that 1850 is the preindustrial equilibrium. The modifications made to the protocols are gathered and then discussed in section 4.4.

4.2.3.1 Climate and carbon cycle reversibility

The objective of this experiment is to evaluate the reversibility of the different components of the Earth system. After an increase in the atmospheric partial pressure of CO_2, a decrease has to be prescribed. The DECK run *1pctCO2* is adapted for this use. Starting a preindustrial equilibrium in 1850, the atmospheric partial pressure of CO_2 increases by 1% every year, up to a four-fold increase of the 1850 level, reached 140 years after. Other drivers remain constant to their 1850 values. This experiment is extended in *1pctCO2-cdr*, by prescribing a decrease by 1%/year of the CO_2 level, up to the 1850 level. After, the CO_2 level is kept constant for 1000 years for OSCAR v2.2. The performed scenarios for this experiment are described in table 4.3. The reversibility of the components of the Earth system has already studied under such a study in Boucher et al. (2012), and show hysteresis behavior for instance for low-level clouds and the ocean stratification in the Southern Ocean. This hysteresis appears also in the Transient Climate Response to cumulated CO_2 emissions (TCRE) as showed in Zickfeld et al. (2016).

The *1pctCO2-cdr* scenario does not assume the form of the CDR technology used, but only the impacts of such negative emissions on the Earth system. Albeit

Name of the scenario	Description of the scenario
piControl	Concentrations driven run with all forcings kept constant to their 1850 values.
1pctCO2-cdr	Concentrations driven run with 1% increase of CO_2 only from 1850 to 1990, followed by 1% decrease of CO_2 only from 1991 to 2131, followed by 1000 years of stabilization.
1pctCO2	The first 140 years of *1pctCO2-cdr* corresponds to the scenario *1pctCO2*.

Table 4.3: *Descriptions of the scenarios used in the experiment C1.*

the reduction in CO_2 level represents an enormous challenge (Keller et al., 2017), such a fast evolution would still be informative because of the high signal-to-noise ratio.

As a remark, the preindustral land covers are computed using the database Land-Use Harmonization 2 (LUH2, LUH2 (2018)), as described in section 4.2.2. This state remains constant along all the scenarios of the experiment C1.

4.2.3.2 Direct CO_2 air capture with permanent storage

Small-scale studies and pilot plants have shown that several methods can be used for the capture of atmospheric CO_2 (DAC) (Lackner et al., 2012; Sanz-Pérez et al., 2016). Other technologies have been developed to store this carbon into permanent reservoirs (CCS) (Scott et al., 2013). Yet, the cost of these technologies still represent a barrier to their deployment. Assuming an idealized large scale deployment of DAC and CCS, this experiment aims at evaluating its response of the Earth system. The first part of this experiment is based on simulations driven by pulse perturbations. Emission pulses can be used to compute impulse response functions (IRF), that can in turn be used to compute metrics for the Earth system (Joos et al., 2013; Gasser et al., 2017b). From the 1850 state, the responses to a positive and a negative emission pulse are evaluated, to check any differences in the responses. The same calculation is produced from the 2010 conditions. The objective is the evaluation of a new emission metric: the global cooling potential (GCP). The use of the 1850 state and of the 2010 conditions is motivated by the expected dependency of the IRF in the initial conditions (Joos et al., 2013). All of these experiments are described in table 4.4.

The second part of this experiment uses the scenario SSP5-3.4 and its extension. This scenario has the advantage for the study to propose high emissions followed by high negative emissions. Although BECCS are used in this study (Muratori et al., 2016), negative emissions are here assumed to be induced from DAC and CCS. It violates the economic assumptions of the scenario (Keller et al., 2017). Besides, it may also not be fully consistent regarding the land use, and thus the carbon cycle.

Sub-group of the experiment Name of the scenario	Description of the scenario
C2_pi-pulse	
esm-piControl	Emissions driven run with all forcings kept constant to their 1850 values.
esm-pi-cdr-pulse	Emissions driven run with all forcings kept constant to their 1850 values, with the exception of a pulse of -100 GtC occurring 10 years after the start of the scenario. The scenario runs for 1000 years for long-term evolutions.
esm-pi-co2pulse	Emissions driven run with all forcings kept constant to their 1850 values, with the exception of a pulse of +100 GtC occurring 10 years after the start of the scenario. The scenario runs for 1000 years for long-term evolutions.
C2_yr2010-pulse	
yr2010co2	Concentrations driven run over the historical period, using CMIP6 inputs. From 2010, all forcings are kept constant to their 2010 values for 1000 years. Over the whole scenario, compatible emissions are calculated, to be used in the other experiments of this sub-group up to the year 3010.
esm-hist-yr2010co2-control	Emissions driven run using compatibles emissions of *yr2010co2*. This run is used to check the consistency of the evaluated compatible emissions.
esm-yr2010co2-noemit	Emissions driven run using compatibles emissions of *yr2010co2*. From 2010, CO_2 emissions are forced to zero.
esm-yr2010co2-cdr-pulse	Emissions driven run using compatibles emissions of *yr2010co2*. In 2015, a pulse of -100 GtC occurs.
esm-yr2010co2-co2pulse	Emissions driven run using compatibles emissions of *yr2010co2*. In 2015, a pulse of +100 GtC occurs.
C2_overshoot	
esm-ssp534-over-ext	Emissions driven run. Over 1850-2010, the scenario *esm-hist* is used to reproduce the historical climate change. Over 2010-2100, the scenario *esm-ssp534-over*, based on the scenario SSP5-3.4, is used. This scenario exhibits a strong overshoot. Over 2100-2300, its extension *esm-ssp534-over-ext* is used. Over 2300-3300, the scenario is extended using 2300 levels.
ssp534-over-bgcExt	Emissions driven run. This run is similar to *esm-ssp534-over-ext*, with one exception. Along the run, the CO_2 radiative forcing is calculated using the preindustrial CO_2 concentration, and not the one of the year.

Table 4.4: *Descriptions of the scenarios used in the experiment C2.*

Finally, the climate change projection for this SSP is different, precisely because of the use of BECCS (Muri, 2018). Nevertheless, this scenario remains an opportunity to evaluate issues of reversibility. The performed scenarios for this experiment are also described in table 4.4.

The prescribed concentrations for CO_2, CH_4, N_2O and all halogenated compounds are provided by Meinshausen et al. (2017), whereas the emissions of NO_X, CO, VOC, SO_2 , NH_3, OC, BC are prescribed using CMIP6 emissions (Hoesly et al., 2017). The calculation of the compatible emissions for these compounds follow the equations 4.11, deduced from the evolutions of the atmospherical concentrations in response to their sources and sinks.

$$E^*_{FF} = \alpha^{CO_2}\frac{d}{dt}\Delta CO_2 - E_{LUC} - \Delta F_{\downarrow ocean} - \Delta F_{\downarrow land} \tag{4.11a}$$

$$E^*_{CH_4} = \alpha^{CH_4}\frac{d}{dt}\Delta CH_4 - \Delta E^{BB}_{CH_4} - \Delta E^{WET}_{CH_4} - \Delta F^{\downarrow,OH}_{CH_4} - \Delta F^{\downarrow,h\nu}_{CH_4} - \Delta F^{\downarrow,X}_{CH_4} \tag{4.11b}$$

$$E^*_{N_2O} = \alpha^{N_2O}\frac{d}{dt}\Delta N_2O - \Delta E^{BB}_{N_2O} - \Delta F^{\downarrow,h\nu}_{N_2O} \tag{4.11c}$$

$$E^*_{HFC} = \alpha^{HFC}\frac{d}{dt}\Delta HFC - \Delta F^{\downarrow,OH}_{HFC} - \Delta F^{\downarrow,h\nu}_{HFC} - \Delta F^{\downarrow,X}_{HFC} \tag{4.11d}$$

$$E^*_{PFC} = \alpha^{PFC}\frac{d}{dt}\Delta PFC - \Delta F^{\downarrow,OH}_{PFC} - \Delta F^{\downarrow,h\nu}_{PFC} - \Delta F^{\downarrow,X}_{PFC} \tag{4.11e}$$

$$E^*_{ODS} = \alpha^{ODS}\frac{d}{dt}\Delta ODS - \Delta F^{\downarrow,OH}_{ODS} - \Delta F^{\downarrow,h\nu}_{ODS} - \Delta F^{\downarrow,X}_{ODS} \tag{4.11f}$$

Using the same notations as in Gasser et al. (2017a), each variable X of the model is the perturbation ΔX to a preindustrial state X_0. For instance, ΔCO_2 stands for the perturbation of the atmospherical partial pressure of CO_2. Compatibles emissions are marked with a star (E^*) and atmospheric conversion factors are used for each compound: α^{CO_2} from ppm to GtC; α^{CH_4} from ppb to MtC; α^{N_2O} from ppb to MtN; α^{HFC}, α^{PFC} and α^{ODS} from ppt to kt. E_{FF} corresponds to the fossil-fuels emissions, E_{LUC} to the land-use emissions, $\Delta F_{\downarrow ocean}$ to the ocean sink and $\Delta F_{\downarrow land}$ to the land sink. E^{BB}_C stands for the emissions of the compound C by biomass burning and $E^{WET}_{CH_4}$ for the wetlands emissions of CH_4. Finally, $F^{\downarrow,OH}_C$ corresponds to the sink of the compound C because of the troposherical oxidation by the hydroxyl radical OH. $F^{\downarrow,h\nu}_C$ corresponds to the sink because of the stratospherical oxidation $h\nu$. $F^{\downarrow,X}_C$ corresponds to the sink because of other processes such as oxidation in dry soils and in the oceanic boundary layer.

In the sub-group "C2_yr2010-pulse", all forcings but CO_2 are kept to their 2010 levels. Yet, we note the following points.

- Concerning aerosol emissions, anthropogenic emissions are kept at their 2010 levels. Yet, change in temperatures will affect biomass burning emissions,

which will result in a change in aerosol emissions.

- Concerning land use, two forcings could be identified, either the LUC emissions or the land use state. We choose to hold the land use state at 2010 level. In other words, the land use change, shifting cultivations and harvest are assumed to stop in 2010. This choice is made to serve the objective of this sub-group of the experiment, which is the evaluation the IRF starting from 2010 conditions. Keeping land variables (LUC, harvest and shifting) at their 2010 values would not imply constant LUC emissions because of variations in the other variables, such as global mean surface temperature. Because the CO_2 concentration is forced at a constant level in *yr2010*, the change in LUC emissions will not affect the CO_2 concentrations, and the compatible emissions will include the change in LUC emissions. Other land use variables would change, such as the radiative forcing induced by change in albedo. Besides, it is very likely that some LUC cannot be held over 1000 years: for instance, deforestation at 2010 pace over 1000 years would not be possible.

- OSCAR v2.2 uses several external radiative forcings as inputs, such as the change in solar irradiance, the radiative forcing from volcanic aerosols and the radiative forcing induced by contrails. All are kept to their 2010 values. Although these radiative forcing will evolve, keeping them at 2010 levels will avoid unwanted changes that may affect the calculation of the IRFs.

Concerning the sub-group "C2_overshoot", we note four major points on the implementation of the protocols, all of which being additional reasons for this study to be only a preliminary contribution of OSCAR v2.2 to CDR-MIP.

- The emissions over 1850-2010 are not those prescribed by *input4MIPs*, but those of OSCAR v2.2. We use CDIAC emissions (Boden et al., 2013) for fossil-fuels emissions, EDGAR v4.2 (Joint Research Centre, 2011) for N_2O and halogenated compounds and ACCMIP for CH_4, NO_X, CO, VOC, SO_2, NH_3, OC and BC (Lamarque et al., 2010). This choice is made for simplicity in the preparation of the protocols, taking into account that the inventories used are relatively closed to those of *input4MIPs*.

- The delivery of the emissions data for the scenarios of ScenarioMIP is expected for Mid-March 2018 (ScenarioMIP), but is not available yet (ESGF (2018), 23/06/2018). For this reason, we have chosen to use the SSP database (IIASA, 2018c), with the treatment described in the chapter 3. The treatment of this chapter covers the production of individual fluorinated gases instead of a merged category, the transformation of land cover data into net LUC and the spatial adaptation to OSCAR v2.2. The chosen scenario is the SSP5-3.4 produced using the marker IAM REMIND-MagPie (Kriegler et al., 2017).

- The land use forcings should be available (ScenarioMIP). Yet, the only scenarios available in terms of land state are the SSP1-2.6, SSP2-4.5, SSP3-7.0,

SSP4-3.4, SSP4-6.0 and SSP5-8.5 (ESGF, 2018; LUH2, 2018). For this reason, we have chosen to use the net LUC of the SSP5-3.4 under REMIND-MagPie produced by our treatment of the SSP database.

- The extension of the SSP5-3.4 (O'Neill et al., 2016) is built to lead this scenario to a 2.6W.m^{-2} level during the first half of the 22^{nd} century. CO_2 emissions from fossil-fuels - negative in 2100 - remains constant over 2100-2140, then increases linearly up to 0 in 2190, to remain constant afterwards. CO_2 emissions from LUC are assumed to be linearly reduced to the SSP1-2.6 level from 2100 to 2120, to remain constant afterwards. Other emissions are kept to their 2100 levels. However, LUC emissions for this SSP evaluated by the IAM marker, here REMIND-MagPie, are different from those calculated by OSCAR v2.2, as illustrated with the chapter 3. For the sake of internal consistency and simplicity, we have adapted this assumption: we use a linear transition of the land variables from the SSP5-3.4 level in 2100 to the SSP1-2.6 level in 2120. The land variables used for the SSP1-2.6 are those of LUH2 (LUH2, 2018), treated for this study as described in section 4.2.2.

As in C1, the preindustral land covers are computed using LUH2 (LUH2, 2018). In the scenarios of the subgroup C2_pi-pulse, the land cover remains constant. In the scenarios of the subgroup C2_yr2010-pulse, the land cover variables are prescribed by the LUH2 data in terms of LUC and harvest over 1700-2010 as described in section 4.2.2. As a remark, the LUH2 dataset does not include shifting, and it is assumed as zero in OSCAR for this study. The 2010 levels remain constant onwards. For the subgroup C2_overshoot, we also use the LUH2 data for the preindustrial land cover and land variables over 1700-2010. As described in this section concerning the implementation of the protocols of this subgroup, the land variables of our treatment for the SSP5-3.4 by REMIND-MagPie are used over 2010-2100, because of the lack of existing data for the corresponding scenario. After the transition over 2100-2120, the LUH2 for the SSP1-2.6 is used for the land variables.

4.2.3.3 Afforestation/reforestation

Over 2006-2015, 30% of CO_2 emissions have been absorbed by the land sink (Le Quéré et al., 2016). The principle of this method is to enhance this fraction of sequestered carbon by increasing the actual forest cover and managing these forests. Deforested areas may be reforested, and previously non-forested lands may be used to plant additional forest. Dynamic global vegetation models suggest that this method may have a substantial potential, even greater than initially expected (Arneth et al., 2017). Besides, climate change reduces the carbon sinks efficiency, and altered biogeochemical cycles (e.g. nitrogen, phosphor) may reduce further the potential for this method (Ciais et al., 2013). particularly for this experiment, a large panel of models to investigate this CDR method is very useful because of the different inherent uncertainties, such as the partioning and evolution of carbon stocks

Name of the scenario	Description of the scenario
esm-ssp585ext	Emissions driven run of the scenario *esm-ssp585* over 2010-2100, with its extension *esm-ssp585ext* over 2100-2300. 2300 levels are kept for another 1000 years. Scenario identic in C4.
esm-ssp585-ssp126Lu-ext	Emissions driven run of the scenario *esm-ssp585* over 2010-2100, using the SSP1-2.6 land use, with its extensions over 2100-2300. 2300 levels are kept for another 1000 years.

Table 4.5: *Descriptions of the scenarios used in the experiment C3.*

(Ramankutty et al., 2007), land mappings (Peng et al., 2016) or sub-grid processes (Yue et al., 2017). In this case, OSCAR v2.2 may be of interest especially for the evaluation of the long-term consequences of afforestation/reforestation: ecosystems may not recover back to their initial state, even centuries after CO_2 stabilization (Jones et al., 2010).

This experiment uses two scenarios (table 4.5). The SSP5 is a scenario assuming a fossil-fuel development, leading to high emissions especially in the baseline SSP5-8.5 (Kriegler et al., 2017). In the baseline, no climate policy affects the land use, and deforestation declines slowly. On the contrary, the SSP1 is a "green" scenario, assuming a development concerned about environmental boundaries (van Vuuren et al., 2017). In the SSP1-2.6, the land use is strongly regulated, with a strong reduction of tropical deforestation rates (Popp et al., 2017). The potential of afforestation/reforestation may be evaluated by comparing on one hand the climate change under the scenario *esm-ssp585* from C4MIP (Jones et al., 2016b), with emissions and land variables from SSP5-8.5, and on the other hand, the climate change under the scenario *esm-ssp585-ssp126Lu* from LUMIP (Lawrence et al., 2016), with emissions from SSP5-8.5 but land variables from SSP1-2.6.

We note one major adaptation of the protocols, which forms an additional reason for this study being only a preliminary contribution of OSCAR v2.2 to CDR-MIP. Just like the scenario SSP5-3.4 of the sub-group C2_overshoot, the emissions data for this scenario is expected for Mid-March 2018 (ScenarioMIP). For this reason, we have chosen to use the SSP database (IIASA, 2018c), with the treatment described in the chapter 3. The treatment of this chapter covers the production of individual fluorinated gases instead of a merged category, the transformation of land cover data into net LUC and the rescale of emissions to the inventories used in OSCAR v2.2 (Gasser et al., 2017a). The chosen scenarios of emissions chosen are the SSP5-8.5, produced using the marker IAM REMIND-MagPie (Kriegler et al., 2017), and the SSP1-2.6, produced using the marker IMAGE (van Vuuren et al., 2017).

The extension for the emissions of *esm-ssp585-ssp126Lu-ext* and *esm-ssp585ext* are the same : fossil-fuels CO_2 emissions are reduced linearly over 2100-2250 to "less than 10 GtC.yr^{-1}" (O'Neill et al., 2016). Not knowing exactly the value for 2250

CO_2 emissions, 10 GtC.yr^{-1} is assumed. After 2250, this level is kept constant. Concerning all others emissions, the 2100 levels are extended after 2100.

As in C1, the preindustral land cover is computed using LUH2 (LUH2, 2018), and so are the land variables for the historical period over 1700-2010 and the scenarios SSP5-8.5 and SSP1-2.6 over 2010-2100. Their extensions up to 2300 are taken constants onwards.

4.2.3.4 Ocean alkalinization

Over 2006-2015, 24% of the anthropogenic CO_2 emissions have been absorbed by the ocean sink (Le Quéré et al., 2016). The principle of the ocean alkalinization CDR method is to dissolve silicate or carbonate minerals in the oceans, to increase the total alkalinity, which reduces the acidity of seawater and increase the capacity of the ocean to store carbon. Total alkalinity measures the excess of bases over acids (Dickson, 1981). According to theoretical work, enhanced weathering seems to be an effective CDR method (Kohler et al., 2010; González and Ilyina, 2016; Ilyina et al., 2013), but limited by logistic constraints, such as the mining, transport and processing of the minerals (Strefler et al., 2018). The benefits in terms of mitigation may remain even after termination of the alkalinization (Ilyina et al., 2013). However, even though acidification of the oceans impacts the marine biology (Kroeker et al., 2013), the alkalinization of the oceans has also an impact on the marine biota (Köhler et al., 2013; Cripps et al., 2013). Other side effects of this method are related to the composition of the minerals. For instance, minerals could also bring nutrients, such as iron, to the biota, fertilizing the oceans, and increasing further the effects of the method. Yet, the benefits of fertilization decrease after stoppage with the consumption of nutrients by the biota, while the benefits from enhanced weathering remain longer after stoppage (Hauck et al., 2016). On the other hand, the dissolved minerals may also content toxic heavy metals.

This experiment is based on the scenario SSP5-8.5, and is designed to evaluate the response of the Earth system to ocean alkalinization. The prescribed amount of alkalinity has been calculated though exploratory simulations conducted with the CSIRO-Mk3L-COAL model, and is expected to lead an absorption of about 100 GtC. This implies that this experiment will be compared to the scenarios of the subgroup C2_yr2010-pulse. For this reason, the maximum extent of the potential of this method will not be evaluated in this experiment, but the experiment will rather be a comparison of the responses of the different models. This choice responds to the current resolution of models and the modelling of ocean carbonate chemistry (Keller et al., 2017). The scenarios of this experiment are described in table 4.6.

For this experiment as well, the use of a large panels of models is useful to investigate the range of the potential and the side effects of enhanced weathering. The high resolutions of ESMs may help to investigate local features, whereas models with lower resolutions such as OSCAR v2.2 may help to investigate long term trends. As explained in section 4.2.1, ocean modelling of OSCAR v2.2 has been adapted to

Name of the scenario	Description of the scenario
esm-ssp585ext	Emissions driven run of the scenario *esm-ssp585* over 2010-2100, with its extension *esm-ssp585ext* over 2100-2300. 2300 levels are kept for another 1000 years. Scenario identic in C3.
esm-ssp585-ocean-alk-ext	Emissions driven run of the scenario *esm-ssp585* over 2010-2100. Since 2020, 0.14 Pmol.yr^{-1} of total alkalinity is added, causing this part of the scenario to be named *esm-ssp585-ocean-alk*. The scenario are extended over 2100-2300, using *esm-ssp585ext* extension for the emissions. The 2300 levels are kept for another 1000 years.
esm-ssp585-ocean-alk-stop	Emissions driven run of the scenario *esm-ssp585* over 2010-2100. Over 2020-2070, 0.14 Pmol.yr^{-1} of total alkalinity is added. The scenario are extended over 2100-2300, using *esm-ssp585ext* extension for the emissions. The 2300 levels are kept for another 1000 years.

Table 4.6: *Descriptions of the scenarios used in the experiment C4.*

integrate alkalinity.

The effects of the addition of other nutrients, such as iron or silicate, on the marine biota are not considered in this experiment. The biologic pump of OSCAR v2.2 is assumed constant (Gasser et al., 2017a), despite climate change actually affecting the biologic pump (Arora et al., 2013; Ciais et al., 2013). In this study as well, we assume that the biologic pump remains unchanged. Besides, Keller et al. (2017) explains that 0.14 of total alkalinity Pmol.yr^{-1} are equivalent to 5.19 Pg.yr^{-1} of $Ca(OH)_2$ or 4.92 Pg.yr^{-1} of Mg_2SiO_4), assuming net instant dissolution reactions, adding respectively 2 or 4 moles of carbon (Ilyina et al., 2013). For the sake of simplicity, the dissolution of alkalinizing agents is considered only through the global flux 0.14 of total alkalinity Pmol.yr^{-1}.

4.2.4 Probabilistic framework

Using OSCAR v2.2 under a probabilistic Monte Carlo framework, we produce the uncertainties over the full period, for each scenario of each experiment. The Monte Carlo ensemble is made of 500 elements drawn by taking randomly, with equiprobability, Earth system-related parameters (64 parameters of OSCAR v2.2, see table 3 of Gasser et al. (2017a)). Each drawn configuration of OSCAR v2.2 is used for all the scenarios.

As a remark, the different elements of OSCAR v2.2 are built separately, to combine their different sensitivities. With prescribed driving datasets, 10^{41} parametriz-

ations are available. Yet, some members are inconsistent, which sometimes leads to divergent simulations. In OSCAR v2.2, it can usually be solved using thresholds for the ocean and land sinks. In our case, the length of the simulations and the high climate change calculated lead to a higher fraction of divergent runs. Thus, 1500 members are performed in the Monte Carlo, and only the 1000 first members that lead to non-divergent simulations with ocean and land sinks under 20 GtC/yr for all scenarios are kept. We observe that the new fits for pCO_2 tend to improve the stability of OSCAR v2.2.

4.3 Results

4.3.1 C1: Climate and carbon cycle reversibility

The first experiment consists in evaluating the reversibility of the different components of the Earth system in response of a 1% increase in atmospherical partial pressure of CO_2 over a quadrupling of the preindustrial CO_2, followed by a 1% decrease up to the preindustrial CO_2. We represent several variables of the system in figure 4.7.

In the period of the 1% increase, DIC increases by 220 μmol.kg^{-1} (209 to 225), and the acidity of sea surface water is increased by 0.62 (0.61-0.63). The evolutions of DIC and pH over the decrease are relatively symmetrical to their evolution over the increase.

In the first period, the ocean removes CO_2 up to 6.4 GtC/yr, with a 4.0 to 7.5 GtC/yr 90% confidence interval. The land sink remove CO_2 in a lesser but more uncertain manner, rising up to 5.5 GtC/yr (1.4 to 10.7). Then, even though atmospheric CO_2 is decreasing, the ocean and the land keep absorbing CO_2, although at a decreasing rate. The ocean begins emitting CO_2 in 2034, 44 years after the beginning of the decrease (40 to 49). It occurs earlier with the land sink, in 2017, 27 years after the beginning of the decrease (26 to 44). This scenario was described as difficult to achieve (Keller et al., 2017), and as a mere test, we compute the compatible emissions. For the period of 1% increase in CO_2, compatible emissions increase up to 35.3 GtC/yr (30.7 to 41.2). Over the period of 1% decrease, compatible emissions become negative, but not symmetrical to those of the period of 1% increase. Over this period, the compatible emissions decrease to -17.7 GtC/yr, reached in 2000, that is to say 10 years after the beginning of the period of 1% decrease. We represent the cumulative oceanic sink since the beginning of the experiment. At the end of this simulation, the ocean has stored 100.6 GtC (77.5 to 121.6). The carbon sequestered in the terrestrial biosphere is lost faster, for the cumulative land sink tends to zero. At the end of this simulation, still 1.9 GtC (-0.1 to 44.1) is stored in the land reservoir. We also represent the cumulative airbone fraction, that is to say the fraction of the carbon added since the beginning of the experiment that remains in the atmosphere. Over the period of the 1% increase, the CO_2 concentration increases faster and faster, and the carbon sinks are less and less efficient because of

climate change. For these reasons, the cumulative airborne fraction first decreases, because of the carbon uptake by the sinks, then stabilizes and then increases slowly as the carbon sinks are perturbed. On the period of the 1% decrease, this fraction decreases, because the atmospheric CO_2 is forced to decrease to zero, whereas the carbon sinks keep absorbing before reemitting.

In the period of the 1% increase, radiative forcing increases up to 7.2 $W.m^{-2}$ (6.4 to 7.6), decreasing almost symmetrically, because of the logarithmic dependency radiative forcing from CO_2 with the atmospherical CO_2. Note that, here, the radiative forcing includes CO_2 atmospheric changes, but also other compounds that are changed because of feedbacks internal to the system (e.g. atmospheric CH_4 changes caused by natural wetland emissions changes). The median increase in global surface temperature (ΔT) reaches its maximum 5 years after the end of the period of 1% increase (4.3 °C, 3.1 to 5.4) because of the inertia of the climate system, and in this model, in particular because of the inertia of the deep ocean. The median of the increase in global precipitations reaches its maximum 30 years later (54.1 $mm.yr^{-1}$, 9.5 to 97.2).

These different variables return to their preindustrial equilibrium within different timescales. Thanks to the fast equilibrium between the oceanic and the atmospheric pCO_2, surface DIC returns almost immediately to equilibrium, just as pH. Yet, the inertia in ΔT is responsible for a median increase of 1.0 °C at the end of the 1% decrease. The increase in ΔT is reduced under 0.1 °C only 334 years (196 to 575) after the return to preindustrial CO_2. This slow return is also responsible for the increase in global precipitations reduced to below 5 $mm.yr^{-1}$ after 238 years (140 to 430). We observe that 1000 years after the return to preindustrial CO_2, the ocean keeps outgasing CO_2 with a pace of 0.1 GtC/yr, while the land sink is almost zero, which implies a small but continued negative flux of compatible emissions of -0.1 GtC/yr.

To evaluate the reversibility of the different components of the Earth system, we represent the evolution of a set of variables describing the Earth system along the atmospherical CO_2 of this experiment (figure 4.8, red for the 1% increase, green for the 1% decrease, blue for the following 1000 years). We also evaluate the maximal perturbation reached by the variable during the experiment, and we indicate the time required to return to 5% of this level or below. The Earth system exhibits several hysteresis.

- We note that the ocean sink and the land sink present such hysteresis. As the atmospheric CO_2 increase, the carbon sinks absorb more and more, though with a decreasing efficiency. The land sink reaches an asymptote, corresponding the equilibrium between its decreasing efficiency and the increasing "emissions", that is to say the atmospheric CO_2 increasing by 1% every year. As the atmospheric CO_2 decreases, the carbon sinks absorb less and less, as illustrated in figure 4.7. The sinks peak at the end of the period of 1% increase: the terrestrial biosphere absorbs up to 5.5 GtC/yr (1.4 to 10.4) whereas the

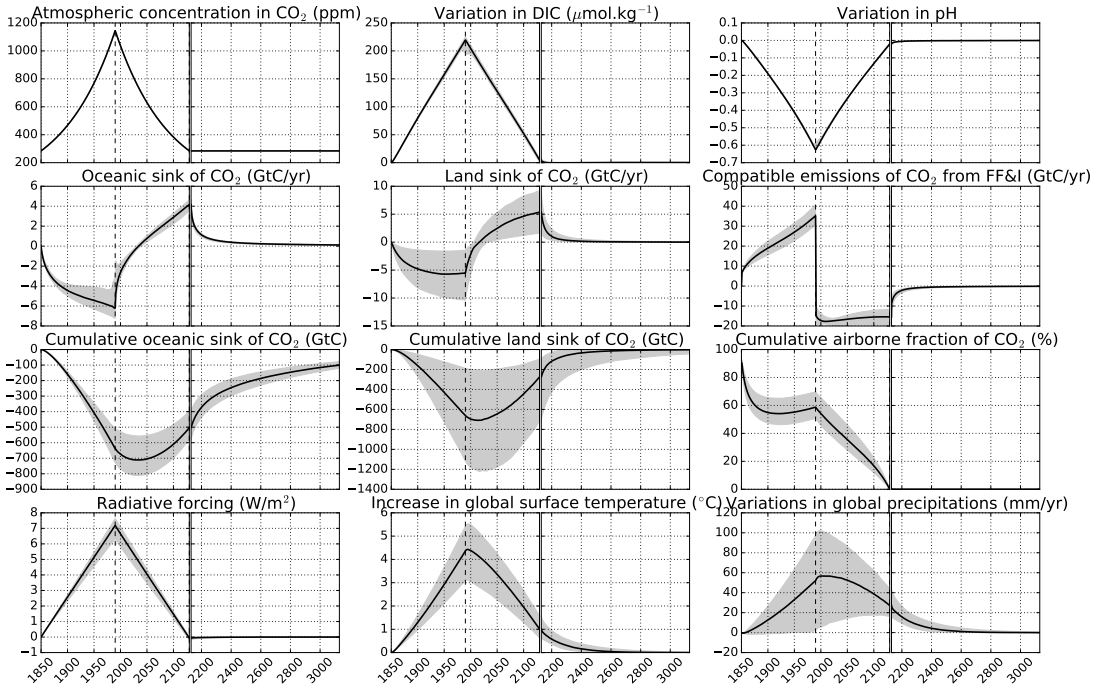

Figure 4.7: *Median and 90 % confidence interval under the scenario 1pctCO2-cdr. The first 140 years corresponds to the scenario 1pctCO2, whereas the variables under piControl remain zero. The evolution of each variable is respresented in two panels: the first 280 years on the left panel, the 1000 years of stabilization on the right panel. The vertical dashed line corresponds to the limit between the 1% increase and the 1% decrease in CO_2.*

ocean absorbs up to 6.2 GtC/yr (3.1 to 7.2).

- During the 1% decrease in atmospheric CO_2, the carbon sinks become sources, reemitting the carbon stored in their reservoir. As the atmospheric CO_2 returns to 284.3 ppm, the "preindustrial" level of 1850, the land sink is still reemetting 5.4 GtC/yr (1.6 to 9.2), and the ocean reemits 4.2 GtC/yr (3.5 to 4.6). The ocean requires 345 years to return within 5% of its maximal perturbation over the experiment, whereas the land requires only 190 years. These inertias are due to the multiple processess involved in the carbon cycle.

- Not all variables related to the carbon cycle present a hysteresis. This is the case for the DIC and the pH. This is due to the fast equilibrium of the atmospheric CO_2 with the CO_2 in the surfaces of the oceans. The radiative forcing from CO_2 is also directly linked to the atmospheric CO_2. CO_2 being the only direct change in this experiment, the radiative forcing is by far the major component of the total radiative forcing. For this reason, there is no hysteresis in the total radiative forcing.

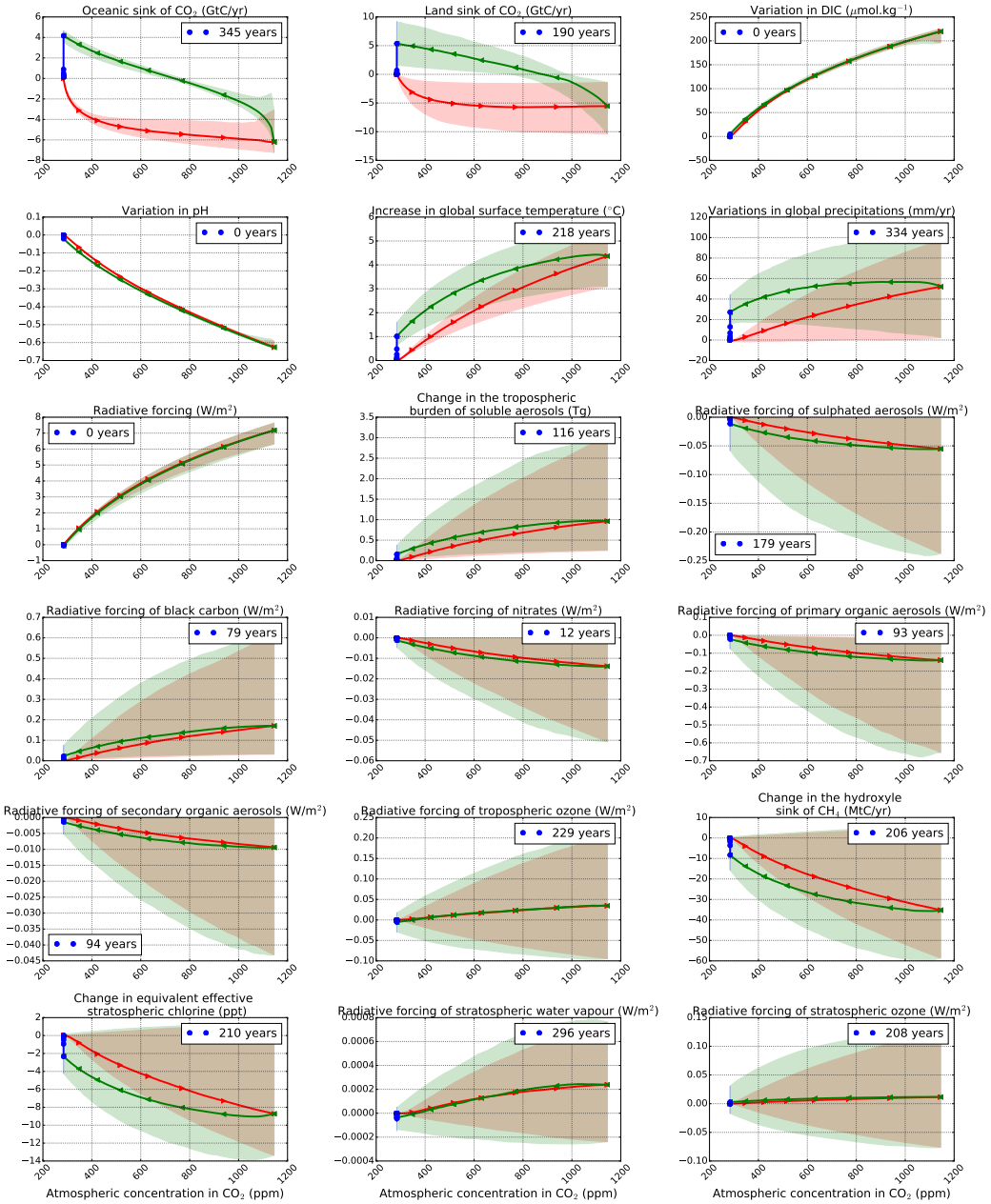

Figure 4.8: *Reversibility of the Earth system. Each panel corresponds to the evolution of a variable along the atmospheric partial pressure of CO_2 (ppm). The evolution of the variable is showed over the 1% increase in CO_2 in red, over the 1% decrease in CO_2 in green and over the following 1000 years in blue. The time required for the variable to return below 5% of the maximum value during the scenario is indicated in the white box.*

- The increase in the radiative forcing causes an increase in global surface temperature (ΔT). As the atmospheric CO_2 peaks, the ΔT has increased to 4.4°C (3.1 to 5.4). The maximal perturbation in ΔT is reached 4 years after the peak in CO_2, and is virtually equal. Over the period of 1% decrease in CO_2, the ΔT decreases slower compared to its increase, because of the perturbations in the climate system initiated over the first period. After the atmospheric CO_2 returns to the preindustrial level, 218 years are required for ΔT to return within 5% of its maximal perturbation (0.2°C) of the preindustrial level. This is due to the inertia of the climate system.

- Because of climate change, both in ΔT and precipitations, we note changes in natural emissions, from wetlands and biomass burning, that are responsible for additional perturbations in several radiative forcings. These perturbations in individual radiative forcings are relatively weak, as the emissions are relatively weak as well. The tropospheric burden of soluble aerosols that encompass sulphated aerosols, primary and secondary organic aerosols, nitrated aerosols and black carbon is affected by the changes in natural emissions. Its perturbation increases up to 1.0 Tg (0.25 to 3.0) as the atmospheric CO_2 peaks. As the atmospheric CO_2 decreases, the ΔT decreases as well, natural emissions return to their preindustrial level, and so does the tropospheric burden of soluble aerosols, thus the radiative forcing of clouds. The relatively long time to return within 5% of the preindustrial level (116 years) for this burden is caused by the inertia in ΔT, because of the inertia in the climate system.

- The radiative forcings associated with these natural emissions (sulphated aerosols, black carbon, nitrated aerosols, primary and secondary organic aerosols) show similar patterns, although the extent of their perturbations and the time to return within 5% of the preindustrial level are different. In OSCAR, biomass burning emissions of species are all proportional to the biomass burning emissions of CO_2, but the response of the atmospheric concentrations of the aerosols also depend on their climate sensibility.

- In OSCAR v2.2, the change in yearly precipitations in response of climate change is written using two terms (Gasser et al., 2017a). A long term response of the hydrological cycle is parametrized using the ΔT, whereas a short term response of the local energy imbalance is parametrized using the atmospheric fraction of the radiative forcing. The second term is negative, and partially compensates the first term. Bearing this modelling in mind, the increase in both radiative forcing (mostly CO_2) and ΔT, global precipitations increases by up to 52 mm/yr (2 to 97) over the period of 1% increase in CO_2. As the atmospheric CO_2 decreases, at first, the ΔT is relatively constant because of the inertias, whereas the radiative forcing (mostly from CO_2) decreases, causing an increase in global precipitations. The reduction of the energy imbalance causes an increase in water condensation. For this reason, the peak in the perturbation of global precipitations is reached 12 years after the beginning of

the period of the 1% decrease, reaching 57 mm/yr (6 to 102). However, even though the radiative forcing is decreasing, the ΔT begin to decrease, causing the change in global precipitations to finally decrease. Besides, the change in natural emissions affect the atmospheric concentrations of several species such as sulphates. The change of global precipitations returns slower to the preindustrial level as well because of the dependency of its short term to the radiative forcing of these species. As the atmospheric CO_2 has returned to the preindustrial level, global precipitations are still increased by 27 mm/yr (16 to 44) compared to the preindustrial. For global perturbations to return below 5% of the maximal perturbation to the preindustrial level, 334 years are required. Such a long time can be explained by the first term, the long term response of the hydrological cycle through the ΔT. This time is longer than the returning time for the ΔT, because the maximal perturbation of the global precipitations is reduced by the second term, depending on the radiative forcing, and this second term is almost zero after CO_2 has returned to the preindustrial level.

- The atmospheric chemistry undergoes a perturbation as well, but in a lesser extent. Even though the atmospheric concentrations of CH_4 and N_2O are kept constant along the simulation, the ΔT causes a first perturbation of the stratospheric chemistry. A second perturbation is caused by increase in wetlands emissions and biomass burning emissions, because of changes in ΔT and global precipitations. For these reasons, the stronger perturbation appears in the hydroxyle sink of CH_4 that compensates for the increase in wetlands emissions. At the end of the period of the 1% increase in CO_2, the hydroxyle sink of CH_4 absorbs 35 MtC/yr (5 to 59) more compared to the preindustrial level. The major perturbation being the increase in ΔT, these sinks return about as fast to the preindustrial level as ΔT. The change in the hydroxyle concentration affects as well the hydroxyle sinks for halogenated compounds, that can be seen through the change in the equivalent effective stratospheric chlorine, that also returns about as fast to the preindustrial level as does the ΔT, and thus the hydroxyle concentration. The change in the equivalent effective stratospheric chlorine affects in return the concentration of stratospheric ozone, as marked with its radiative forcing. Finally, stratospheric water vapour is also affected by the changed in the lagged atmospheric concentration of methane (Gasser et al., 2017a).

As a summary, the carbon cycle show strong hysteresis, with long lasting perturbations even after return of the atmospheric CO_2 to preindustrial level. For instance, the ocean sink requires 345 years to return within 5%. The ΔT peaks at 4.4°C (3.1 to 5.4), and inertias in the climate system are responsible for a return within 0.2°C of the preindustrial level 218 years after the atmospheric CO_2 is back to preindustrial level. The perturbation of precipitations at the peak in atmospheric CO_2 is compensated by local energy imbalance, but not at the end of the 1% de-

crease, causing this perturbation to last 334 years. Changes in biomass burning cause relatively weak perturbations in the aspects of the atmosphere related to aerosols. Changes in hydroxyle concentrations are also noted, mostly because of ΔT, causing a perturbation of the stratospheric chemistry that returns within 5% of the preindustrial level within 200 to 300 years depending on the aspect.

The hysteresis in the carbon cycle that we identify include feedbacks from the climate system. The protocol could be extended by adding a scenario with a 1% increase and 1% decrease in the atmospheric CO_2, but by turning off climate feedbacks on the carbon cycle. It would allow the quantification of how much CO_2 direct variations and climate change contribute to these hysteresis. Furthermore, the modelling of the carbon cycle and of the climate system are both sources of uncertainty for the responses of the Earth system. The protocol of this experiment requires concentration-driven scenarios. Yet, emissions-driven scenarios would have lead to different ranges of uncertainties. Emissions-driven scenarios could be calculated, using the CO_2 emissions that are compatible with a 1% increase and a 1% decrease in atmospheric CO_2, and that would be calculated by a single model for all models running this scenario.

4.3.2 C2: Direct CO_2 air capture with permanent storage

4.3.2.1 Pulse experiments

As explained in table 4.4, the first part of this experiment aims at evaluating IRF for two pulses from preindustrial conditions: a positive pulse (*esm-pi-co2pulse*) and a negative pulse (*esm-pi-cdr-pulse*). The second part aims at reproducing these scenarios, but from present-day state, 2010, be it for the positive pulse (*esm-yr2010-co2pulse*) and the negative pulse (*esm-yr2010-cdr-pulse*). We represent the evolution of the scenarios of the experiments C2_pi-pulse and C2_yr2010-pulse in figure 4.9.

To begin with, the concentrations driven scenario *yr2010co2* is used to evaluate compatible emissions for the other emissions driven scenarios of the experiment C2_yr2010-pulse. We use the scenario *esm-hist-yr2010co2-control* to check that these compatible emissions are correct: the difference in atmospheric CO_2 between these two scenarios remains below 0.3 ppm, then only 1% of the CO_2. Concerning the experiment C2_pi-pulse, the positive pulse of 100 GtC increases the preindustrial CO_2 by 7.3 ppm (5.5 to 8.7), whereas the negative pulse reduces the CO_2 by 7 ppm (5.3 to 7.2), thus to a lesser extent than the positive pulse. In the experiment C2_yr2010-pulse, the positive pulse of 100 GtC increases the CO_2 of 2010 by 11.9 ppm (8.3 to 14.8), whereas the negative pulse reduces the CO_2 by 11.5 ppm (8.2 to 14.0), thus to a lesser extent as well. The carbon sinks partially compensates the effects of the pulses, but this compensation is more effective in the preindustrial state, where the land and ocean sinks are not saturated yet. Concerning the increase in ΔT, the pulses induce a maximal difference of 0.3 °C from preindustrial conditions, and 0.2 °C from present-day conditions. At the end of the simulations, the differences

are reduced in both conditions to 0.1°C.

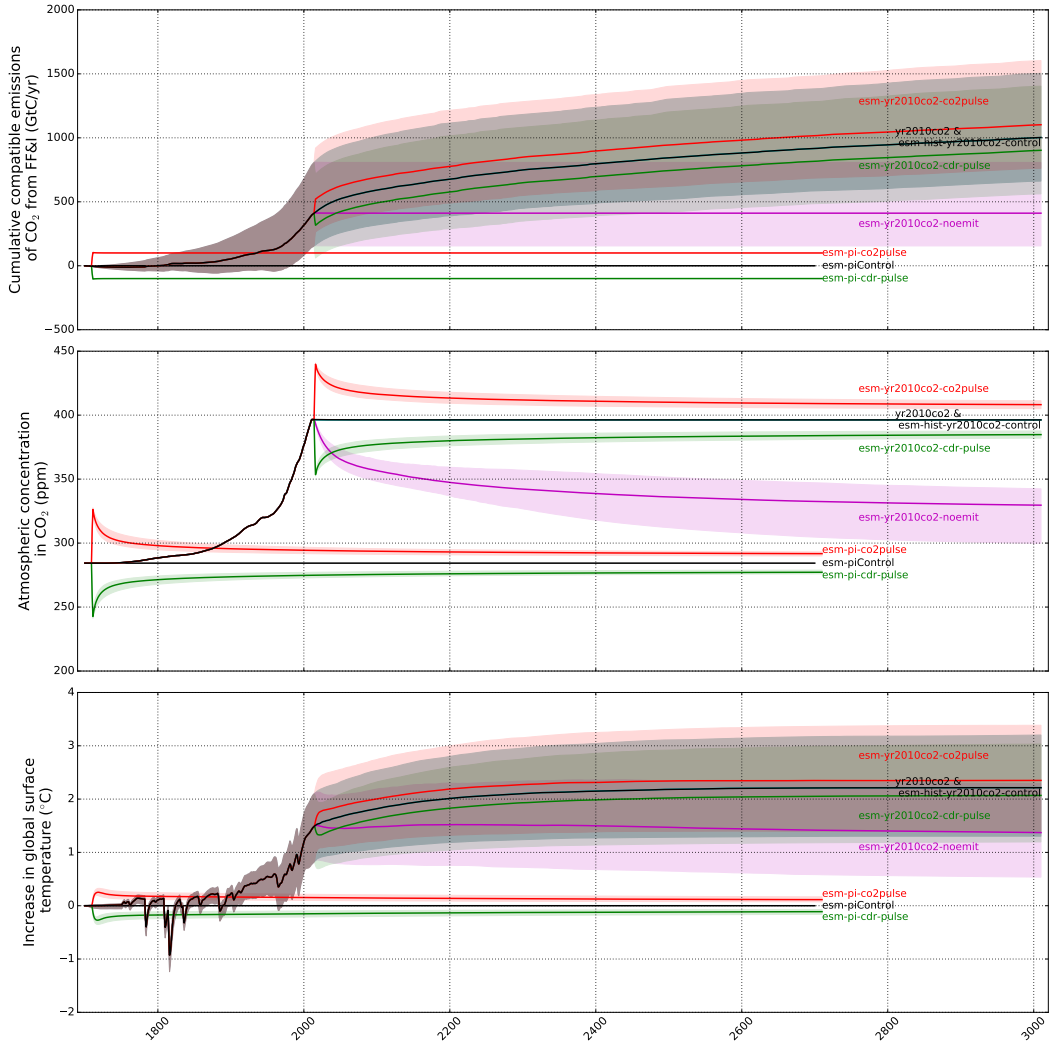

Figure 4.9: *Median and 90% confidence intervals for the scenarios of the experiments C2_pi-pulse and C2_yr2010-pulse. The upper panel corresponds to the cumulative compatible CO_2 emissions from Fossil Fuels & Industry (GtC). In the middle panel are represented the atmospheric CO_2 (ppm) of the scenarios.The lower panel corresponds to the increase in ΔT (°C).*

4.3.2.2 Impulse response functions

We evaluate four IRFs, that we fit to reproduce the evolutions under the four pulses scenarios (*esm-pi-cdr-pulse*, *esm-pi-co2pulse*, *esm-yr2010co2-cdr-pulse*, *esm-yr2010co2-co2pulse*). The results of this fit are showed in figure 4.10. First, as showed in Joos et al. (2013), the background affects the shape of the IRF, as represented with the difference between the group of IRFs from a disturbed state (plain lines) and those from a preindustrial lines (dashed lines). A higher fraction of the emitted CO_2 remains airborne in 2010 conditions compared to 1850 conditions. This is due to the deterioration of the carbon sinks under 2010 conditions. For the same reason, a negative pulse tends to be more effective at removing carbon than a positive pulse is at adding carbon.

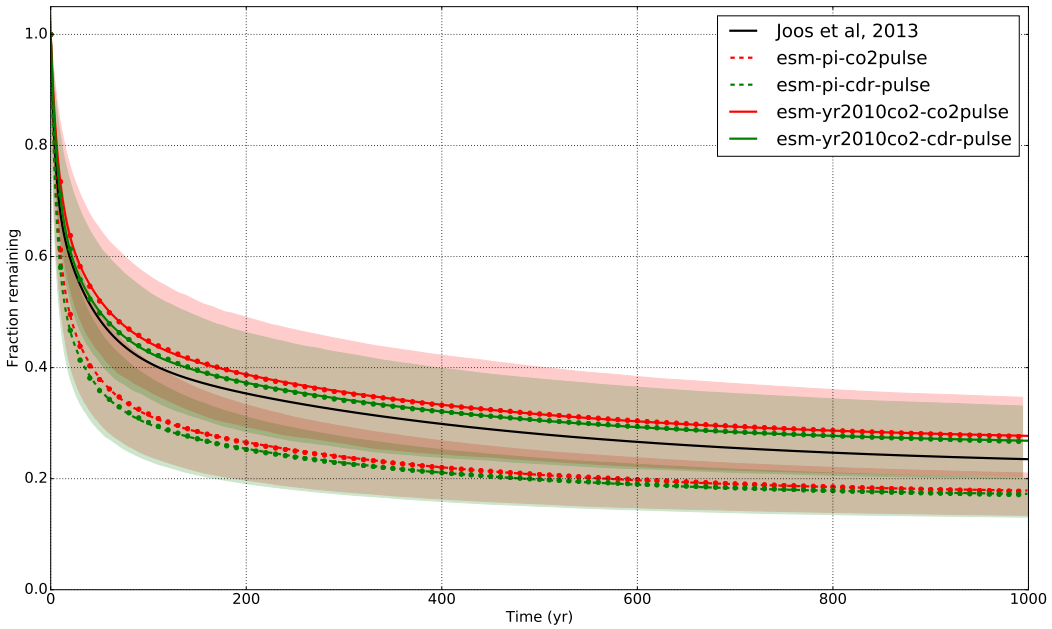

Figure 4.10: *Fractions of the CO_2 pulses remaining for positive pulses (red) and negative pulses (green), from the preindustrial conditions (dashed lines) and 2010 conditions (plain lines). The markers represent the outputs of OSCAR v2.2 whereas the lines represent fits. The shaded area corresponds to the 90% confidence interval of the IRF. The black plain line corresponds to the IRF from Joos et al. (2013).*

The median of each one of these pulses are fitted, using equation 4.12, similar to the equation (11) of Joos et al. (2013). The results of these fits are represented in table 4.7. Considering the coefficients a_0 which is the long term limit of the IRF, we confirm what we noticed in figure 4.9: using Joos et al. (2013), 21.7% of the carbon remains in the long term, but a positive pulse from 2010 conditions remains at 26.5% in the atmosphere, but only 17.1% of a positive pulse from 1850 conditions remains in the atmosphere. We observe as well that shorter timescales tend to have

a stronger weight in 1850 conditions compared to 2010 conditions.

$$IRF\,(t) = a_0 + \Sigma_{i=1}^{3} a_i exp\left(\frac{-t}{\tau_i}\right) \tag{4.12}$$

Conditions	Sign of the pulse	τ_1	τ_2	τ_3	$\mathbf{a}_0$	$\mathbf{a}_1$	$\mathbf{a}_2$	$\mathbf{a}_3$
Joos et al, 2013		394.4	36.54	4.304	0.217	0.224	0.282	0.276
2010	**+100 GtC**	346.4	38.65	6.618	0.265	0.215	0.257	0.262
	-100 GtC	343.3	37.69	6.228	0.257	0.204	0.252	0.285
1850	**+100 GtC**	308.2	33.42	5.813	0.171	0.178	0.257	0.391
	-100 GtC	295.9	31.60	5.336	0.166	0.170	0.244	0.417

Table 4.7: *Coefficients of the IRF for each pulse, using equation 4.12. The coefficients τ_i are in years, whereas the coefficients a_i are dimensionless.*

The scenario *esm-yr2010co2-noemit* is used to check the IRF. From 2010 onward, emissions from fossil fuel become zero. The IRF (figure 4.10 and table 4.7) are used on these compatible emissions, produced with the scenario *yr2010co2*. The results are represented in figure 4.11. The IRF produced from a 1850 background with a positive pulse calculates the CO_2 with a maximum of 1.5% of relative error over 1850-2010. The one using a negative pulse is within 1.3% over 1850-2010. IRFs produced from present-day conditions do not perform as well over 1850-2010. The IRF using a positive pulse from present-day conditions remains within 7.7% of the CO_2 of *esm-yr2010co2-noemit*, whereas the one using a negative pulse remains within 6.3%. The lower performance for pulses produced from present-day conditions is caused by their use for a period where the carbon cycle is not yet perturbed, while they should be used for a perturbed system. Over 2010-3010, the performance of IRFs from preindustrial conditions decrease respectively to 1.7% and 2.7% for the positive and negative pulses. IRFs from present-day conditions conserve their relative error, that has been accumulated over 1850-2010.

To improve the reproduction of *esm-yr2010co2-noemit*, IRF produced from a 1850 background should be used not be used after 2010, whereas IRF produced from present-day conditions should not be used before 2010. One could try to improve the reconstruction by applying successively the IRFs. If reconstructing using the IRF with a positive (respectively negative) pulse from preindustrial conditions before 2010, and using the value of 2010 as starting point for the reconstruction using the IRF with a positive (respectively negative) pulse from present-day conditions, the relative error is increased to 4.0 % (respectively 4.7%). Therefore, this method of successive application worsen the reconstruction of atmospheric CO_2, compared to the application of only the IRF from preindustrial conditions. Even though the performances up to 2010 are similar, the long term consequences of emissions over 1850-2010 are not similar if using an IRF from present-day or from preindustrial conditions. One could also try to improve the reconstruction by applying the IRF from preindustrial conditions to emissions up to a given year, the IRF from present-day

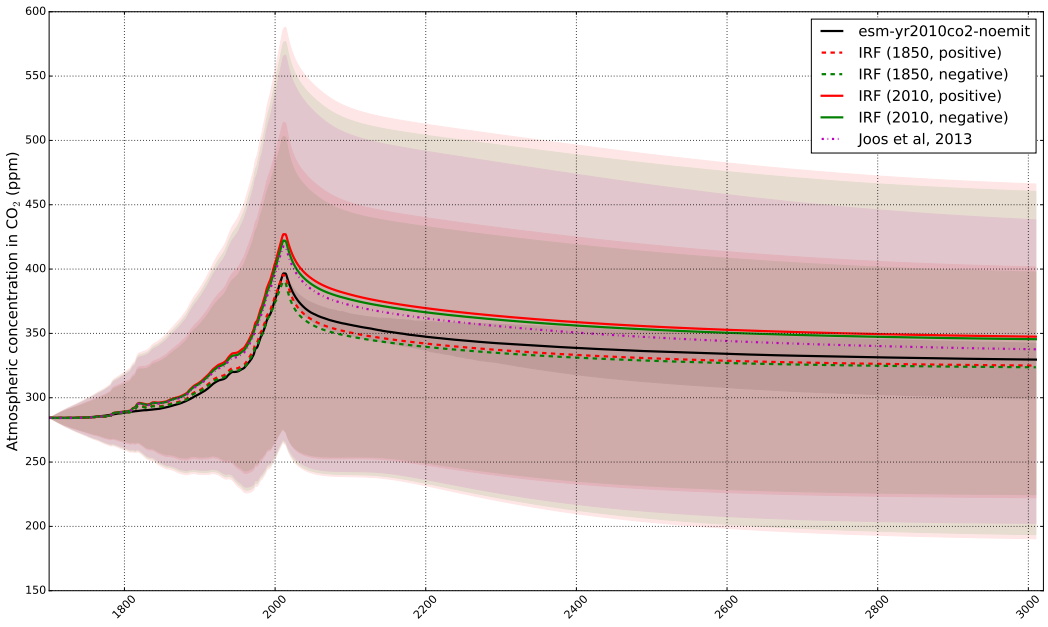

Figure 4.11: *Atmospheric concentration of CO_2 (ppm) from the scenario esm-yr2010co2-noemit (black plain line), and from reconstructions of these scenarios using the IRF (figure 4.10 and table 4.7) and the compatible emissions of this scenario. The shaded areas correspond to the reconstructions using the 90% confidence interval of the compatible emissions.*

conditions to emissions after this given year, and add the contributions. Depending on the year and the type of pulses, performances are not improved in all cases. Though, we observe that applying the IRF using preindustrial conditions and positive (respectively negative) pulse to emissions committed up to 1990, and the IRF using present-day conditions to emissions committed after 1990, the relative error after 2010 is slightly increased to 1.8% (respectively reduced to 0.6%). The strong reduction of the relative error when using the IRF from negative pulse and present-day conditions is due to the negative compatible emissions after 2010, in order to keep the atmospheric CO_2 concentration constant. It shows the importance of using the appropriate IRF depending on the conditions.

4.3.2.3 Global Cooling Potentials

The objective of the positive and negative pulses is to evaluate Global Cooling Potentials (GCP) (Keller et al., 2017). It is meant to be related to Global Warming Potentials (GWPs) and Global Temperature Potentials (GTPs).

The Absolute Global Warming Potential (AGWP) is the total energy added to the climate system by adding a unit of CO_2 over a defined period (Myhre et al., 2013). AGWPs are commonly used to evaluate GWPs, the ratio of the AGWP of a given

compound to the AGWP of CO_2. These GWPs can be used to aggregate emissions of multiple species into CO_2 equivalent. However, AGWP is subject to debates. The AGWP is not directly related to a climate response (O'Neill, 2000; Shine, 2009), and its name can be somewhat misleading (Myhre et al., 2013). The time horizons used for the definition of these metrics are also "candidates for discussion [that have] no special significance" (Houghton et al., 1990): a 100-years time horizon for the definition of GWP is based on no scientific reason (Shine, 2009). Yet, the time horizon, but also the size of the emission pulse and the background used to evaluate these AGWPs, all of these parameters matter (Joos et al., 2013). Because of the accuracy of GWP, they should rather used for short-term horizons (Smith and Wigley, 2000). Besides, grouping emissions of different species using GWP into a single basket for use in climate policy may put at risk the short-term success of the policy, because of trade-offs between emissions (Daniel et al., 2012). Finally, the inclusion or not of indirect effects is not systematic (Myhre et al., 2013; Boucher and Reddy, 2008). For these reasons, another metric was introduced: the Absolute Global Temperature change Potential (AGTP) and the GTP (Shine et al., 2005). Although AGTPs and GTPs still depend on the time horizon, the size of the pulse and the integration of different processes in the modelling, its interpretation tends to be easier (Joos et al., 2013; Peters et al., 2011; Azar and Johansson, 2012).

The objective of Keller et al. (2017) is to develop the Global Cooling Potential of CO_2. As such, it should rather be called Absolute Global Cooling Potential, and we choose to calculate the AGWPs and AGTPs associated with pulses of negative emissions to calculate the associated cooling. The global cooling potential of other species, that we can define as the ratio of their absolute global cooling potential to the one of CO_2 is not explored here. To comply to Keller et al. (2017), the absolute global cooling potential, be it an AGWP or an AGTP, will be called from now a global cooling potential.

The first definition of a GCP is here as an AGWP. As represented in equation 4.13a, we use here the time-integrated change in the total radiative forcing RF implied by a CO_2 emission pulse E at a time t_0 over a time horizon T, and not the CO_2 radiative forcing implied the IRF (section 4.3.2.2). We choose to represent the AGWP using the total radiative forcing to account for the full extent of the processes implied by such a pulse in the framework of OSCAR v2.2 (Gasser et al., 2017b). The second definition of a GCP is here as an AGTP, as represented in equation 4.13b. The AGWPs and AGTPs for the positive (+100 GtC) and negative pulses (-100 GtC) from a preindustrial state (1850) and a present-day state (2010) are represented in figure 4.12 and summarized in table 4.8. We emphasize that the AGWPs and AGTPs from negative pulses are taken in absolute value for comparison to those of positive pulses in the figure 4.12: a negative pulse in carbon emissions effectively leads to a reduction in radiative forcing or ΔT with respect to the control

experiment, as represented in the lower panel of figure 4.9 and in table 4.8.

$$AGWP_{CO_2}(T) = \frac{1}{E}\int_{t_0}^{t_0+T} (RF_{pulse} - RF_{control})(t)\,dt \tag{4.13a}$$

$$AGTP_{CO_2}(T) = \frac{(\Delta T_{pulse} - \Delta T_{control})(t_0 + T)}{E} \tag{4.13b}$$

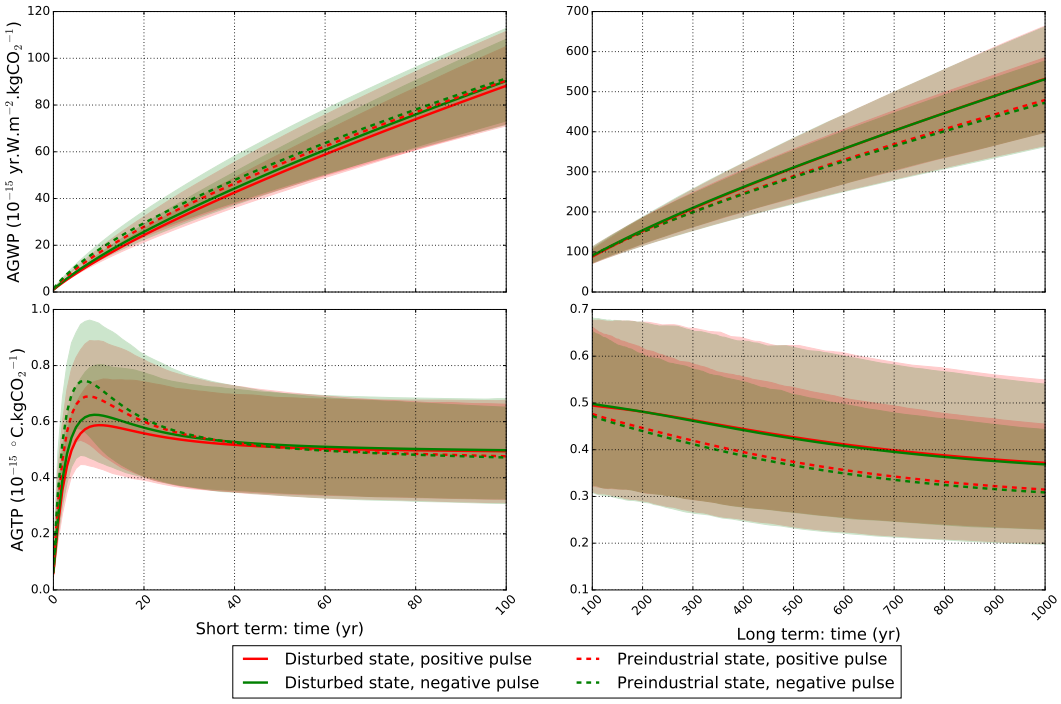

Figure 4.12: *AGWPs (upper panels) and the AGTPs (lower panels) for a positive pulse of +100 GtC (red) and a negative pulse of -100 GtC (green), from the preindustrial state, here 1850 (dashed lines) and a present-day state, here 2010 (plain lines). The mean (lines) and the 90 % confidence interval (shaded areas) are produced for each. For the sake of clarity, the time horizons of the AGWPs and AGTPs are separated between short term (<100 years, left panels) and long term (>100 years, right panels). For an easier comparison, the absolute values of AGWPs and AGTPs of negative pulses are given here.*

Different backgrounds or signs of the pulse introduce relative differences in AGWP and AGTP, that are lower for time horizons for 100 years, a little higher for time horizons for 50 years, and still higher for other time horizons (20, 500 and 1000 years). We observe that over short term, typically with a time horizon of 20 years, an additional unit of CO_2 added to a present-day state increases less the global surface temperature than does the same unit added to the preindustrial state. This is due

to the logarithmic relationship of the radiative forcing of CO_2 with its atmospheric concentration. The carbon cycle is already disturbed at present-day conditions, and the difference in airborne fractions of CO_2 for such a short timescale to compensate this logarithmic response. The opposite stands for the long term, typically more than 100 years, where an additional unit of CO_2 added to a present-day state increases more the global surface temperature than does the same unit added to the preindustrial state. The carbon cycle is already disturbed, and the airborne fraction of CO_2 is higher compared to a preindustrial state, and higher enough to compensate for the reduction of the warming efficiency because of the logarithmic relationship of the radiative forcing of CO_2 with its atmospheric concentration. In the long term, the cooling of negative emissions is inferior to the warming of positive emissions.

We compare in table 4.8 the AGWPs and AGWTPs that we produce, using negative and positive pulses of 100 GtC, from present-day and preindustrial conditions, to the best estimates from the multi-model of Joos et al. (2013). The AGWPs and AGTPs produced with 2010 conditions are much closer to those of Joos et al. (2013), because of the similarities in the conditions. The mean of AGWPs from positive emissions in 2010 conditions are inferior to the mean of Joos et al. (2013) by a maximum of 4.8%. For negative emissions, using its absolute values, this relative difference is reduced to 3.1%. The confidence intervals produced with OSCAR v2.2 are reduced by 20 to 30%. The mean of AGTPs tends to be more different from Joos et al. (2013) for time horizons of 20 years or 1000 years. Starting from 2010 conditions, AGTPs at a 20-year time horizon are relatively different by 11%, and up to 2.7% for other time horizons. The ranges of AGTPs are reduced by 30 to 40% comparing to those of Joos et al. (2013). Yet, the range of the AGTP at 100 years of Joos et al. (2013) presents a strong increase compared to those at 50 and 500 years. For this reason, we deem our range as more representative. We discuss the issue of the differences in ranges in section 4.4.

		20 yr	50 yr	100 yr	500 yr	1000 yr
AGWP of CO_2 (10^{-15} yr.W.m^{-2}.kgCO_2^{-1})						
Joos et al, 2013		25.2 (20.7 to 29.6)	53.5 (41.1 to 65.8)	92.5 (67.9 to 117)	324 (228 to 421)	548 (380 to 716)
2010	**positive**	24.3 (21.4 to 27.1)	50.9 (42.7 to 59.0)	88.2 (71.9 to 105.0)	310.0 (234.9 to 382.8)	531.9 (398.2 to 663.6)
	negative	-25.7 (-22.4 to -29.0)	-52.7 (-43.8 to -61.7)	-90.3 (-73.2 to -108.2)	-310.8 (-236.6 to -383.8)	-530.8 (-398.5 to -661.6)
1850	**positive**	27.9 (23.6 to 32.3)	54.6 (43.9 to 66.0)	90.4 (71.1 to 111.5)	289.2 (221.6 to 356.4)	479.1 (365.5 to 585.0)
	negative	-29.5 (-24.5 to -34.6)	-56.1 (-44.6 to -68.4)	-91.4 (-71.7 to -112.8)	-286.3 (-220.0 to -353.1)	-472.4 (-362.7 to -576.8)
AGTP of CO_2 (10^{-15} °C.kgCO_2^{-1})						
Joos et al, 2013		0.52 (0.27 to 0.76)	0.51 (0.24 to 0.81)	0.49 (0.05 to 0.92)	0.4 (0.13 to 0.7)	0.38 (0.19 to 0.57)
2010	**positive**	0.56 (0.39 to 0.74)	0.51 (0.34 to 0.69)	0.49 (0.32 to 0.68)	0.43 (0.27 to 0.62)	0.37 (0.23 to 0.55)
	negative	-0.58 (-0.4 to -0.77)	-0.52 (-0.35 to -0.7)	-0.5 (-0.32 to -0.68)	-0.42 (-0.27 to -0.62)	-0.37 (-0.23 to -0.54)
1850	**positive**	0.6 (0.4 to 0.82)	0.51 (0.34 to 0.71)	0.48 (0.31 to 0.66)	0.37 (0.24 to 0.53)	0.31 (0.2 to 0.45)
	negative	-0.61 (-0.41 to -0.84)	-0.51 (-0.34 to -0.7)	-0.47 (-0.31 to -0.65)	-0.37 (-0.23 to -0.52)	-0.31 (-0.2 to -0.44)

Table 4.8: *AGWP (upper part) and the AGTP (lower part) for positive and negative emissions, from the preindustrial state (1850) and a present-day state (2010). The mean and the 90 % confidence interval are produced for each. For comparison, mean and 90% confidence intervals from Joos et al. (2013) are also given.*

4.3.2.4 Overshoot experiments

The second part of the C2 experiment corresponds to the experiment C2_overshoot. It is based on the scenario SSP5-3.4 (Kriegler et al., 2017): mitigation of climate change is delayed, emissions are close to the baseline up to 2040, then CO_2 emissions decrease rapidly. The two scenarios used are *esm-ssp534-over-ext* and *ssp534-over-bgcExt*. Contrary to the scenario *esm-ssp534-over-ext*, the scenario *ssp534-over-bgcExt* requires the radiative forcing from CO_2 to be evaluated using the atmospheric partial pressure in CO_2 of 1850, and not the actual one. We group the climate variables simulated by OSCAR under these two scenarios into three figures. Figure 4.13 concerns the carbon cycle, figure 4.14 is a focus on the atmospheric chemistry of methane, nitrous oxide and ozone, and figure 4.15 regroups results regarding short-lived climate forcers. In the following paragraphs, we focus on the description of the impact of *esm-ssp534-over-ext*, before explaining the differences to *ssp534-over-bgcExt*.

As shown in figure 4.13, the carbon cycle shows a stabilization after 2300. Going more into details, we note the following points.

- Mitigation is delayed, CO_2 emissions from Fossil Fuels & Industry peaks at about 12 GtC/yr, then decreases to about -4 GtC/yr. In the extension of this scenario (O'Neill et al., 2016), the overshoot is emphasized: CO_2 emissions from Fossil Fuels & Industry increases only over 2140-2190, up to zero, and remain equal to zero afterward.

- In the meantime, LUC emissions from OSCAR decrease in the first half over 2000-2040, but increase up to 2090. These evolutions are relatively close to the SSP5-3.4 LUC emissions from REMIND-MagPie (IIASA, 2018c). They can be explained by the increasing development of bioenergies with CCS (Kriegler et al., 2017). Yet, LUC emissions from OSCAR are greater, especially concerning the emissions in 2100: REMIND-MagPie prescribes 0.07 GtC/yr, whereas OSCAR calculates 1.58 GtC/yr (-4.06 to 3.19). As explained in the chapter 3, the CO_2 emissions from LUC calculated by OSCAR and by the IAM REMIND-MagPIE are different for this SSP because of difference in modelling assumptions, but also because of the treatment of the SSP database. As explained in section 4.2.3.2, we have used our own evaluation of the LUC transitions, for these transitions are not available yet. Evaluation by other frameworks would be of interest to investigate this difference.

- O'Neill et al. (2016) assumes a linear transition over 2100-2120 in LUC emissions, from SSP5-3.4 level to SSP1-2.6 level. For the sake of internal consistency and simplicity, the linear transition is applied over LUC variables and not LUC emissions. We observe an almost linear reduction in LUC emissions, followed by a relative stabilization. The SSP1-2.6 from IMAGE prescribes -0.90 GtC/yr in 2100 (van Vuuren et al., 2017), but the CO_2 emissions from LUC of OSCAR have relatively stabilized in 2300 around -1.54 GtC/yr (-2.67

to -0.84). The land variables used over 2120-2300 are effectively those of the LUH2 database, that aim at a correct reproduction of the transitions of the initial SSP scenario. Even though climate change has an impact on these emissions, evaluation by other frameworks would also be of interest to investigate this difference in LUC emissions. Besides, this difference represents another reason for not prescribing LUC emissions while evaluating CDR experiments, but rather LUC variables.

- From 2300, the harvest of biomass remains equal to the level of the SSP1-RCP2.6 (0.90 GtC/yr). However, from 2120, the same land cover is kept, to avoid negative area extents if transitions occur for too long. This choice is one of the explanations for the reduction in LUC emissions.

- Under these CO_2 emissions, the land sink absorbs more and more carbon, up to about 2040, even though atmospheric CO_2 keeps increasing. The same result applies for the ocean sink. This reduction of the sinks is due to the strong reduction in CO_2 emissions. In 2040, the land and the ocean absorb respectively 2.56 GtC/yr (0.95 to 4.21) and 3.11 GtC/yr (2.54 to 3.76). It corresponds respectively to absorptions of 22.5% and 29.5% of the total CO_2 emissions in 2040. Yet, with negative emissions, atmospheric CO_2 begins decreasing from 2070. Land and ocean sinks are still absorbing carbon at this point. The land and ocean become sources of carbon respectively from 2107 (2088 to 2127) and from 2122 (2093 to 2141). The transition from negative emissions to carbon neutrality ends in 2190, causing a reduction of the land source of carbon, and only a temporary reduction of the ocean source of carbon. From 2300, the reduction in LUC emissions causes to a slow reduction of the reemissions by the ocean and the biosphere. Though, the reduction in LUC emissions is faster, because of the inertia specific to the ocean and the biosphere.

- The ΔCO_2 decrease from about 2070, but not below preindustrial level: in 3300, ΔCO_2 has stabilized at 330.3 ppm (215.5 to 351.0). The radiative forcing of CO_2 has stabilized at 1.37 $W.m^{-2}$ (-0.78 to 2.02) in 3300.

- In the ocean, the perturbation in pH stabilizes at -0.06 (-0.08 to 0.11), whereas the perturbation in DIC stabilizes at 24.2μmol.kgsol^{-1} (-59.4 to 33.1).

- According to the preliminary study using MAGICCv6, this scenario is expected to increase to 2.4°C and then to stabilize at 1.25°C above preindustrial levels from 2200. Here, ΔT peaks at 2.46°C (1.50 to 3.69) in 2077, but in 2200, ΔT is equal to 1.60°C (0.24 to 2.85) and keep decreasing, reaching in 3300 a ΔT of 1.05°C (-0.63 to 1.98). It raises the question why such a difference can be observed between MAGICCv6 and OSCAR v2.2 projections. It emphasizes the need for a comparison of these models.

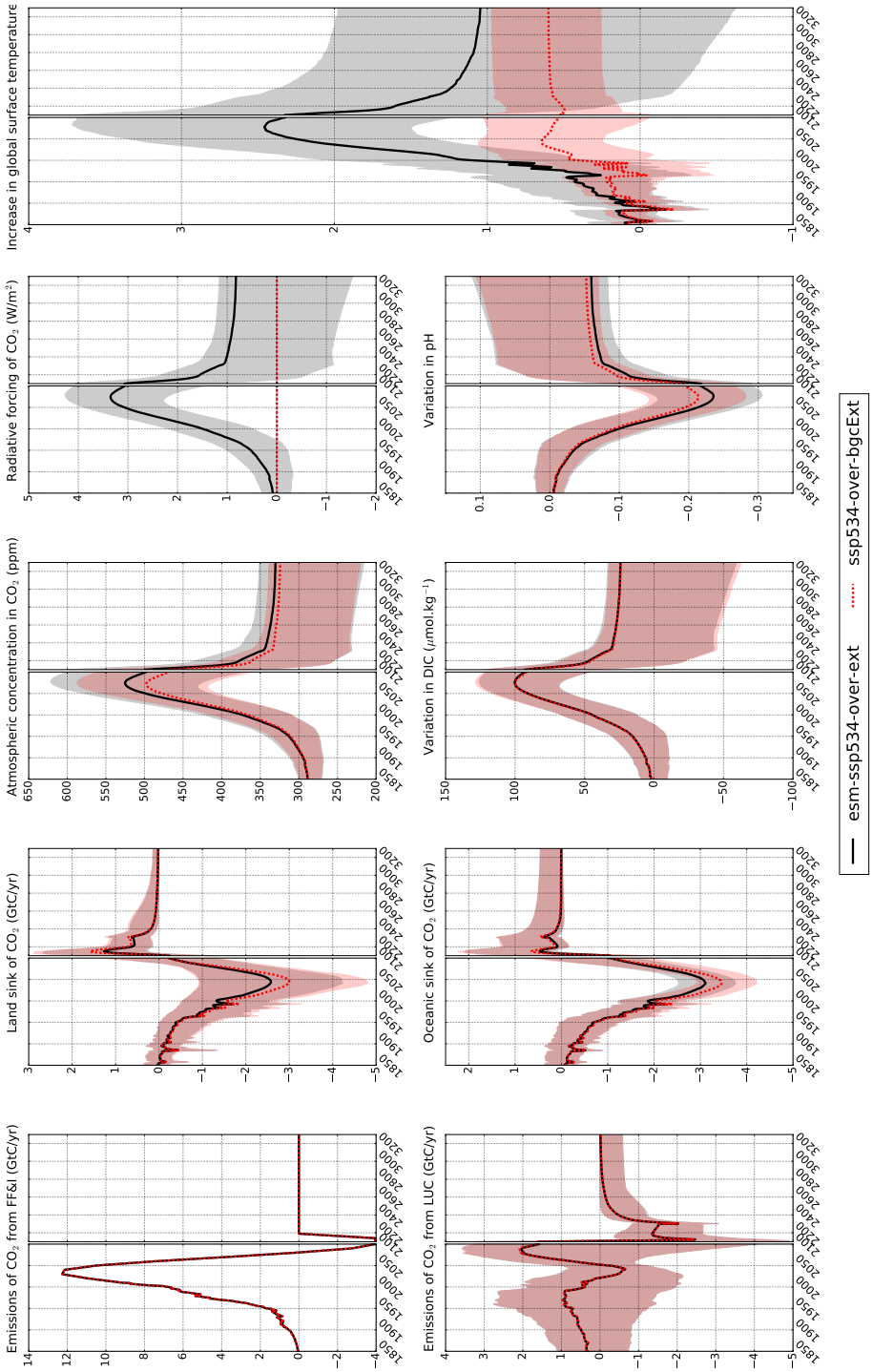

Figure 4.13: *Consequences of the scenarios esm-ssp534-over-ext and ssp534-over-bgcExt for the carbon cycle. Their median and 90% confidence interval are represented in black for the esm-ssp534-over-ext and in red for the ssp534-over-bgcExt.*

The scenario *ssp534-over-bgcExt* is different because of its forced zero radiative forcing for CO_2. Over short to long timescales, it implies a lower climate change. The difference in the carbon cycle, sinks and concentrations, is stronger when the difference in ΔT is the strongest, that is to say around 2070. Concerning ΔT, this scenario stabilizes in 3300 at 0.60°C (0.26 to 0.98), thus 1.86°C lower compared to the scenario *ssp534-over-ext*.

In figure 4.14, the atmospheric chemistry stabilizes even faster than the carbon cycle. We note the following points.

- CH_4 anthropogenic emissions increase to 254.0 MtC/yr in 2020, then decrease to 95.2 MtC/yr from 2100. In 2100, CH_4 emissions from biomass burning have increased by 28.8 MtC/yr (-5.5 to 54.6) and wetlands emissions have increased by 14.1 MtC/yr (0 to 37.3). Over 2100-2120, the linear change to LUC transitions causes a reduction in biomass burning emissions. After 2300, biomass burning emissions and wetlands emissions stabilize respectively to 4.67 MtC/yr (-3.12 to 10.3) and -0.52 MtC/yr (-16.3 to 6.59) because of the constant land cover and the stabilizations in the climate system.

- N_2O anthropogenic emissions increase to 5.22 MtN/yr in 2100. N_2O emissions from biomass burning follow the same evolution than those of CH_4. With anthropogenic emissions of CH_4 and N_2O constant from 2100, their sinks stabilize.

- The hydroxyle sink of CH_4 stabilizes on a relatively longer timescale compared to the dry soils & oceanic sink and the stratospheric sink, because of its dependency to the atmospheric partial pressure of CH_4. In 3300, CH_4 and N_2O have stabilized respectively to 1259 ppb (1152 to 1421) and 394.3 ppb (380.9 to 413.7).

- Tropospheric ozone takes longer to stabilize, which may be explained by the changes in natural emissions from 2300, because of the stopping of LUC transitions.

Regarding the scenario *ssp534-over-bgcExt*, the difference in CO_2 radiative forcing, thus ΔT, is responsible for relatively higher wetland emissions, partially compensated by the dry soils & oceanic and the stratospheric sinks. Though, after 2300, these differences fade.

In figure 4.15, we note that all perturbations also fade after 2300. We observe the following points.

- The anthropogenic emissions of these scenarios peak around 2020. Biomass burning emissions of these aerosols follow the same evolutions as described earlier for biomass burning emissions from CH_4 and N_2O. The sharp decrease over 2100-2120 is caused by the linear change in LUC transitions, and the second sharp decrease in 2300 is caused by the stopping in LUC transitions.

- After 2300, global warming stabilize, and so do the biomass burning emissions, and thus their individual radiative forcings.
- The stronger perturbation is in the tropospheric burden of soluble aerosols, stabilizing at 1.06 Tg (0.56 to 1.77) in 3300, with a radiative forcing of clouds at -0.27 W/m^2 (-0.62 to -0.07).

Under the scenario *ssp534-over-bgcExt*, differences can be explained by the differences in ΔT and precipitations. Though, in 3300, these differences can be neglected in the face of the perturbation.

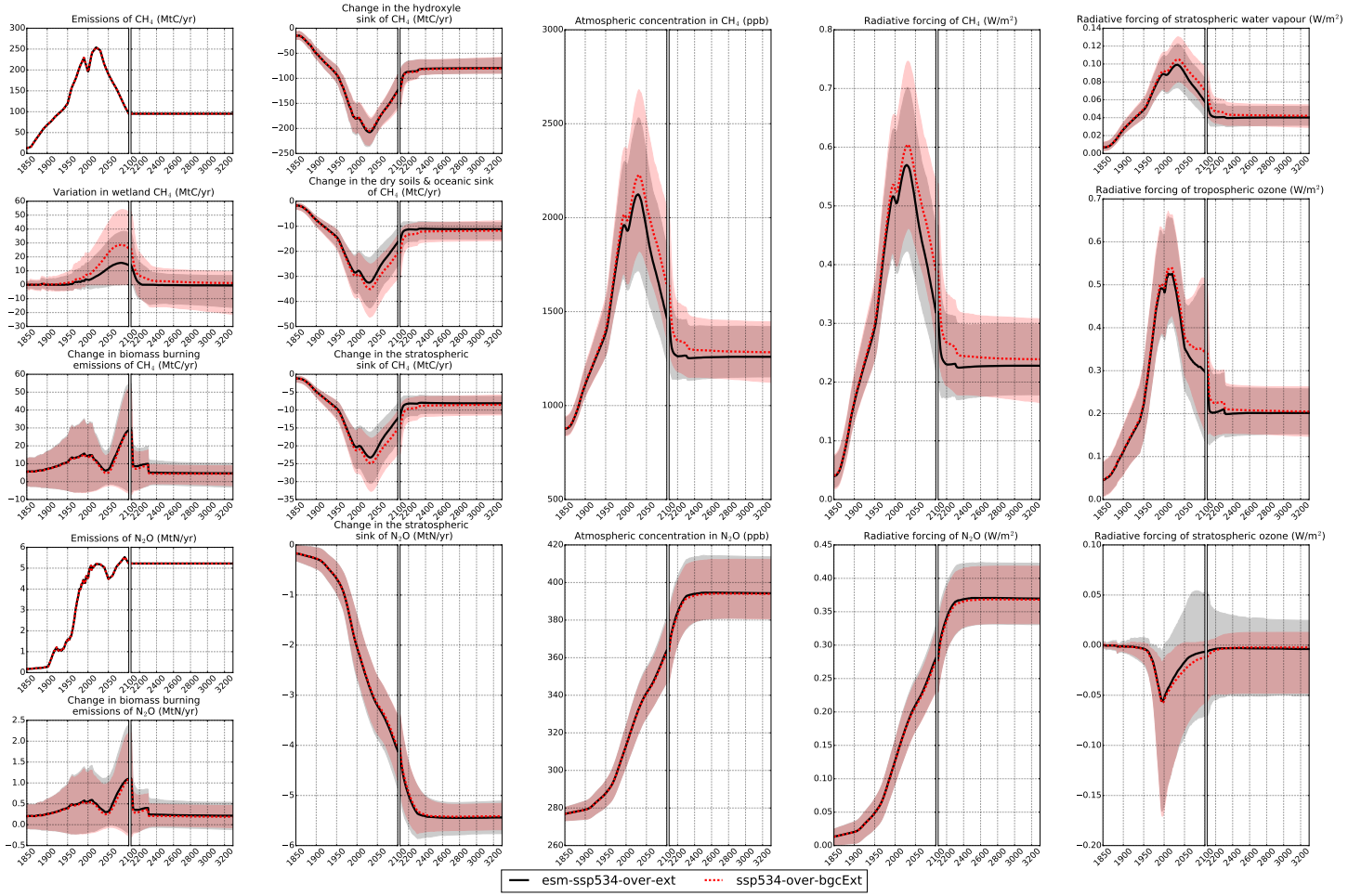

Figure 4.14: *Consequences of the scenarios esm-ssp534-over-ext and ssp534-over-bgcExt for methane, nitrous oxide and ozone. Their median and 90% confidence interval are represented in black for the esm-ssp534-over-ext and in red for the ssp534-over-bgcExt.*

4.3.3 C3: Afforestation/reforestation

This experiment aims at evaluating the consequences for the Earth system of afforestation and reforestation, but not the full potential of this method. The two scenarios used are *esm-ssp585ext* (SSP5-8.5 in emissions and LU) and *esm-ssp585-ssp126Lu-ext* (SSP5-8.5 in emissions and SSP1-2.6 in land use and land cover). We group the climate system variables of these two scenarios into three figures. Figure 4.16 concerns the carbon cycle, figure 4.17 is a focus on the atmospheric chemistry of methane, nitrous oxide and ozones, and figure 4.18 regroups results regarding short-lived climate forcers.

Concerning the carbon cycle, we note that the emissions of SSP5-8.5, with its extension to 2300 and beyond, lead to an extreme global warming (figure 4.16), that is not realistic in terms of fossil fuel resources and too high to remain within the domain of validity of OSCAR or other Earth system models. This is why alternative scenarios are developed in section 4.3.4. Though, we analyze these scenarios here using the climate variables provided by OSCAR.

- Emissions from Fossil-Fuels & Industry peak in 2090 at 37.3 GtC/yr, and are reduced to 10 GtC/yr from 2250 onwards. These emissions are responsible for the extreme climate change of these scenarios.
- LUC emissions decrease faster in *esm-ssp585-ssp126Lu-ext*, compared to *esm-ssp585ext*. Yet, we simulate an increase in LUC emissions of *esm-ssp585-ssp126Lu-ext*, that cause its emissions to exceed those of *esm-ssp585ext* over 2075-2115. Evaluations for these scenarios by the IAM markers do not show this evolution in SSP1-2.6 (van Vuuren et al., 2017; IIASA, 2018c). In 2100, IMAGE prescribes for LUC emissions for SSP1-2.6 -0.90 GtC/yr, whereas OSCAR evaluates them at -0.36 GtC/yr (-2.45 to 1.44). For comparison, in 2100, REMIND-MagPie prescribes for LUC emissions for SSP5-8.5 -0.42 GtC/yr, whereas OSCAR evaluates them at -0.61 GtC/yr (-2.96 to 0.25). However, even though the LUC emissions prescribed by IMAGE are within the confidence interval of OSCAR, the evolution of LUC emissions over 2000-2100 for SSP1-2.6 and SSP5-8.5 remain surprising, and will require others evaluations.
- Over 2100-2300, all other emissions have to remain constant, thus LUC transitions have been assumed constant over 2100-2300. Yet, CO_2 emissions from LUC keep decreasing over this period. In 2300, the stopping in LUC transitions cause a brutal reduction of these emissions. This stopping is done to avoid an inconsistent afforestation/reforestation over 1000 years. Afterwards, LUC emissions stabilize, but LUC emissions using SSP1-2.6 land use remain more negative than the ones under SSP5-8.5 land use.
- For the median results, the ocean and the land remain sinks over the complete period of the scenarios. The land sink tends to converge to zero, whereas the ocean sink compensates with a slow increase.

- In 3300, the land sink has stabilized respectively for *esm-ssp585ext* and *esm-ssp585-ssp126Lu-ext* to -0.14 GtC/yr (-4.49 to 0.34) and -0.14 GtC/yr (-4.39 to 0.37). In 3300, the ocean sink reaches respectively for *esm-ssp585ext* and *esm-ssp585-ssp126Lu-ext* -4.38 GtC/yr (-5.27 to -2.39) and -4.47 GtC/yr (-5.28 to -2.51). The difference in the land sink has faded after 2300, and is relatively weak in the ocean sink. This difference is due to differences in the ΔT.

- In terms of proportions, in *esm-ssp585ext*, the land has absorbed about 8% of the total carbon emitted over 1700-3300, but about 14% of the total carbon emitted over 1700-2300. This is due to the reduced efficiency of this sink. In the meantime, the ocean has absorbed about 34% of the carbon over 1700-3300, but 24% of the carbon over 1700-2300. This is due to first to the reduced efficiency of the oceanic carbon sink, and then, as the land sink deteriorates, the oceanic carbon sink has a higher carbon fraction to absorb.

- Comparing to *esm-ssp585-ssp126Lu-ext*, the differences are relatively small, and the only differences that can not be neglected is an increase of the carbon absorbed by land over 1700-2300, increasing from 14% to 15%. Otherwise, sinks are virtually unchanged.

- The atmospheric partial pressure of CO_2 reaches 4477 ppm (3223 to 5228) in *esm-ssp585ext*, and 4502 (3176 to 5218) in *esm-ssp585-ssp126Lu-ext*. Using SSP1-2.6 variables leads to a reduction in atmospheric partial pressure of CO_2 by only 0.5% in 3300.

- In 2100, both scenarios lead to a ΔT of 5.14°C (3.66 to 6.72). In 3300, the continued trend leads to an extreme ΔT of 13.8°C (10.0 to 19.3) for *esm-ssp585ext* and 13.9°C (10.1 to 19.4) for *esm-ssp585-ssp126Lu-ext*. Surprisingly, using SSP1-2.6 variables in such a scenario leads to an increase of ΔT by 0.1°C. Although the CO_2 radiative forcing is effectively reduced, its difference is too small to compensate for the additional 0.3W/m^2 introduced by the radiative forcing from Land Cover Change. For this reason, change in albedo may represent a limit for the potential of this method.

In figure 4.17 for atmospheric chemistry of CH_4, N_2O and ozone, and figure 4.18 for aerosols, we observe that *esm-ssp585ext* and *esm-ssp585-ssp126Lu-ext* lead to virtually indistinguishable evolutions in these variables.

Here, using SSP1-2.6 land use variables instead of SSP5-8.5 land use variables reduces only slightly the LUC emissions and the land sink, and ultimately the entire climate system is relatively unchanged. Though we note that that the cooling induced by land cover change may be reduced, and even become a warming under strong afforestation/reforestation. It would mean that climate policies that heavily relies on afforestation/reforestation are likely not to mitigate climate change. Though, we highlight major limits right away. First, the protocol of this experiment

leads to extreme climate change. Uncertainties have grown stronger and stronger, and a 0.1°C difference on a 9.3°C range can be neglected. Besides, a global warming by about 14°C is extrem, even for the ESMs that OSCAR emulates. For this reason, the validity of these results are subject to debates. We have developed alternative scenarios (section 4.3.4), as an improvement of the protocol. Then, this is the result from OSCAR, which may not be appropriate to answer this question. ESMs may provide more accurate results, albeit without their uncertainties. Finally, the difference in CO_2 emissions from LUC that we have already observed may play a crucial part in these results. It requires assessments from other models for comparison.

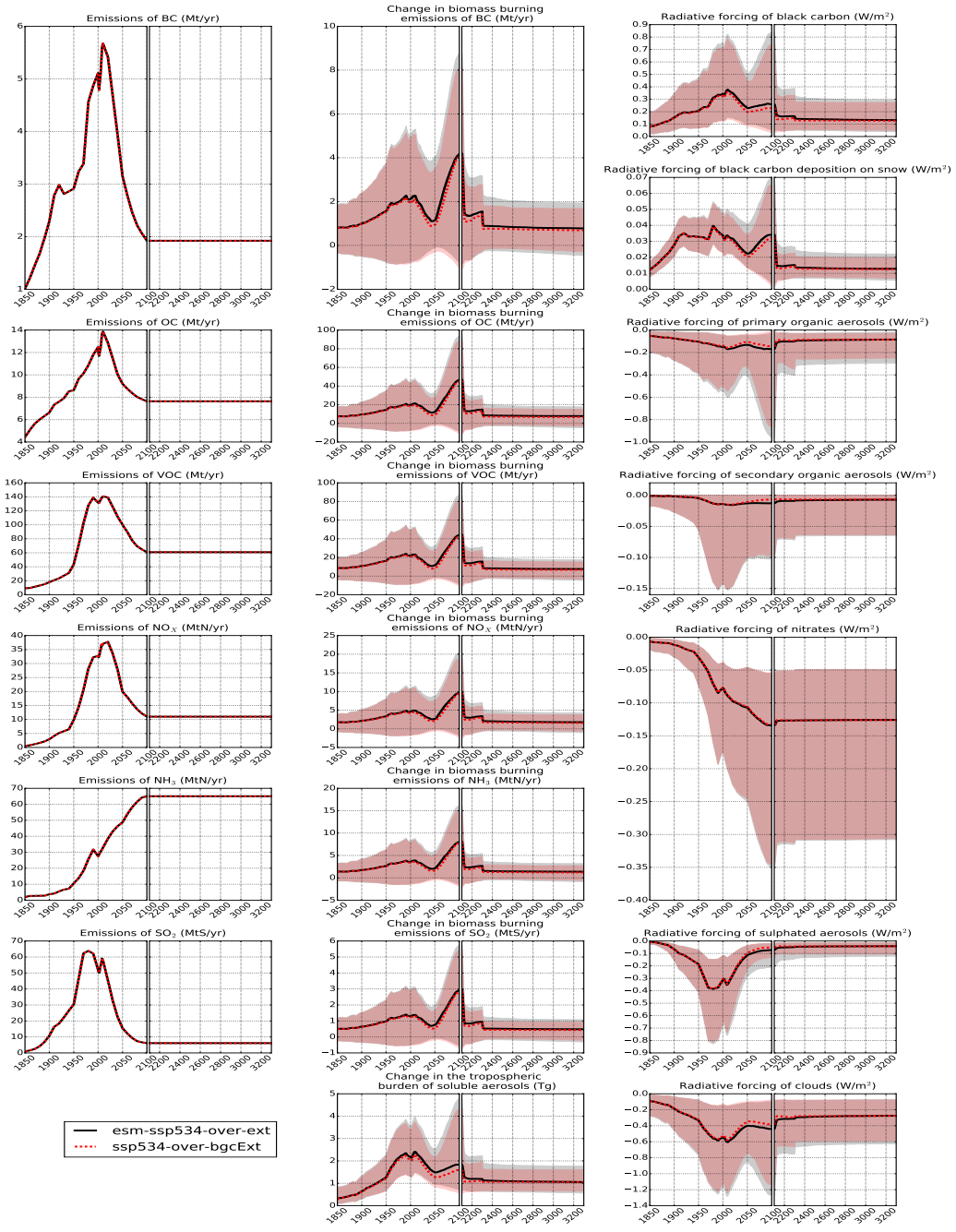

Figure 4.15: *Consequences of the scenarios esm-ssp534-over-ext and ssp534-over-bgcExt regarding aerosols. Their median and 90% confidence interval are represented in black for the esm-ssp534-over-ext and in red for the ssp534-over-bgcExt.*

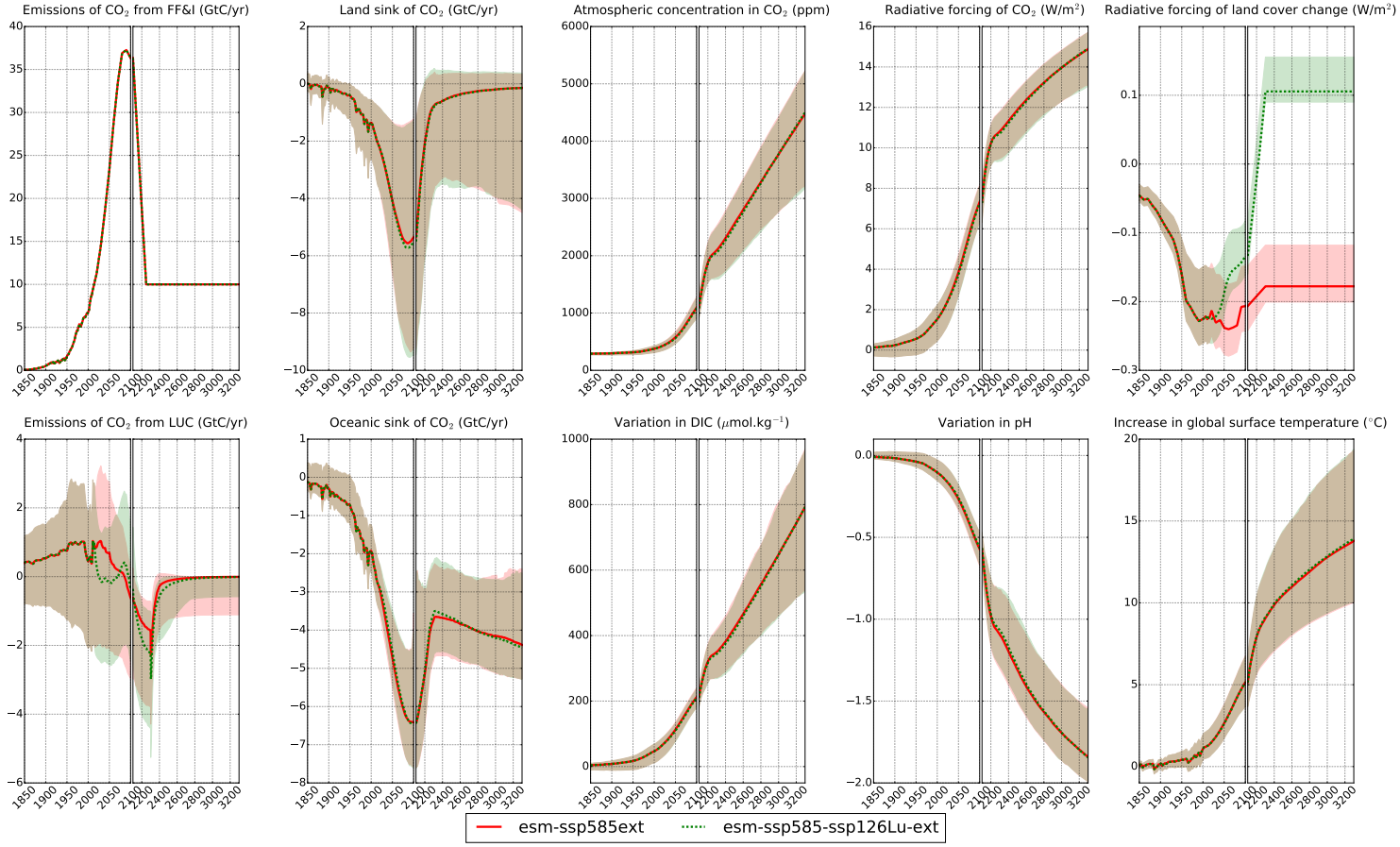

Figure 4.16: *Consequences of the scenarios esm-ssp585ext and esm-ssp585-ssp126Lu-ext for the carbon cycle. Their median and 90% confidence interval are represented in red for the esm-ssp585ext and in green for the esm-ssp585-ssp126Lu-ext.*

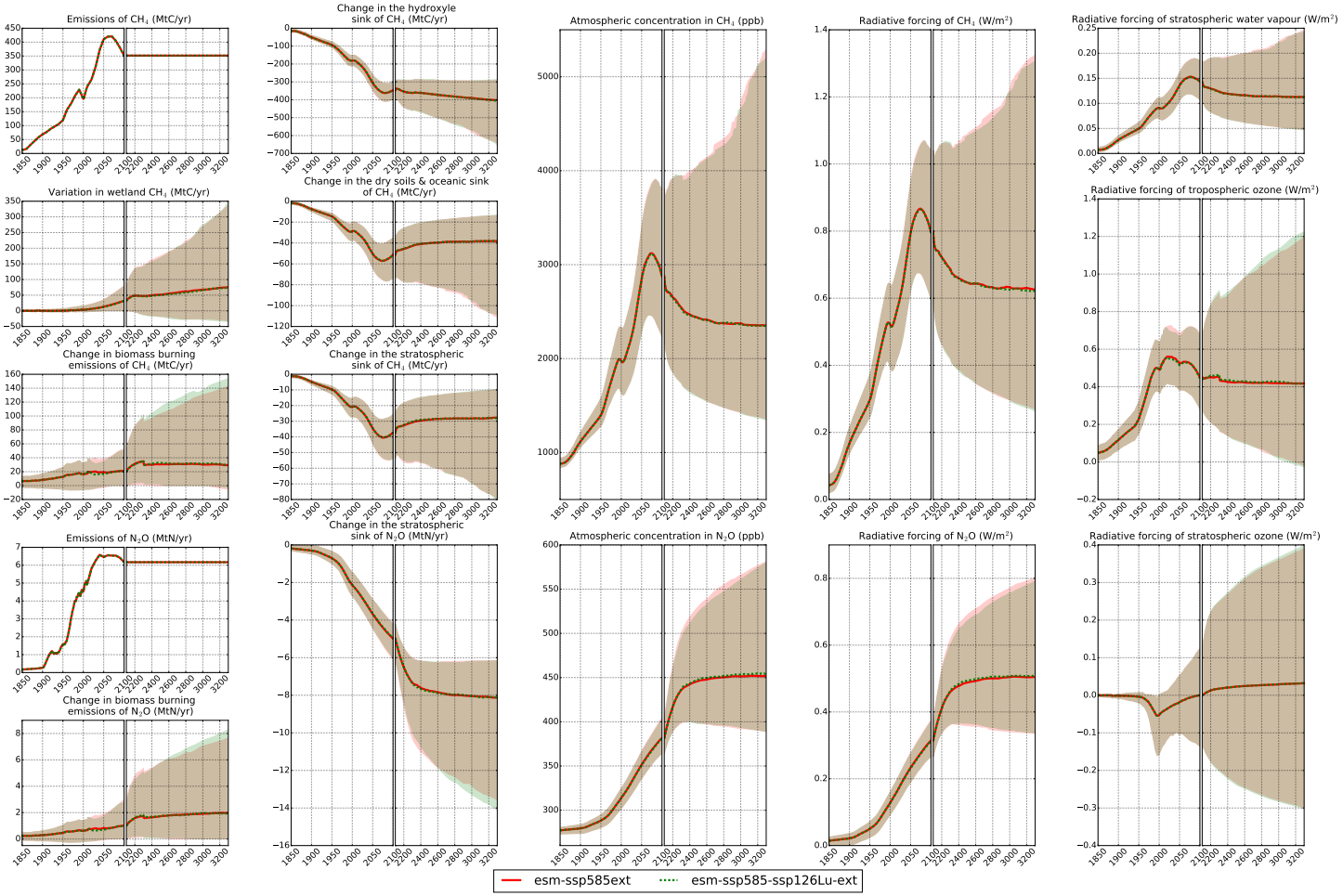

Figure 4.17: *Consequences of the scenarios esm-ssp585ext and esm-ssp585-ssp126Lu-ext for methane, nitrous oxide and ozone. Their median and 90% confidence interval are represented in red for the esm-ssp585ext and in green for the esm-ssp585-ssp126Lu-ext.*

4.3.4 C3, alternative: Afforestation/reforestation

As explained in sections 4.2.3.3 and 4.3.3, CO_2 emissions from Fossil Fuels & Industry follow the SSP5-8.5 up to 2100, to be reduced to 10 GtC/yr in 2250, and to remain constant onward. Yet, we choose to develop alternative scenarios, for two reasons.

- As explained in section 4.3.3, for such climate change, the results from OSCAR or other models are too uncertain, and several tipping elements have been very probably activated by then (Lenton et al., 2008). Thus, models may be too wrong to be of any support in this domain (David, 2014). As a remark, as explained in section 4.2.4, some inconsistent parametrizations of OSCAR may cause the model to diverge during the Monte Carlo simulation. Because of this experiment, the number of divergent simulations increases significantly.
- Even though this protocol does not aim at evaluating the potential of afforestation/reforestation measures, that high cumulative CO_2 emissions obliterate completely its potential, rendering this potential almost useless.
- The total emissions cannot be achieved with available fossil fuel resources:
  - The category "Emissions from Fossil Fuels & Industry" has obviously for main source fossil fuels. Among other sources, cement can be cited, with a fraction of emissions from Fossil Fuels & Industry increasing from about 1% to about 4% over 1750-2010 (Boden et al., 2013). In this reasoning, we neglect this fraction.
  - Although the notion of "available" fossil fuel resources depends on the demand, different estimates for ultimately recoverable resources can be estimated, including both conventional and unconventional resources. In the chapter 3, we have calculated the CO_2 emissions associated with the highest values for ultimately recoverable resources of Mohr et al. (2015). Using different approaches, we have identified the source of uncertainties in these emissions. Here, for the sake of clarity, we choose the calculation of emissions using the mean carbon contents and net calorific values from IPCC (2006), oxidation fractions from Boden et al. (1995) and the highest estimates of ultimately recoverable resources of Mohr et al. (2015), but the reasoning is independent of this choice.
  - Under these estimates of ultimately recoverable resources, the total emissions that can be emitted from fossil fuels are 2461 GtC, ranging from 2120 to 2827 GtC.
  - In SSP5-8.5, over 1700-2100, 2650 GtC are emitted by the category Fossil Fuels & Industry, already reaching the total that can be emitted. The extension to 2300 increases the total emissions over 1700-2300 to 6612 GtC. Adding 1000 years at 10 GtC/yr add again 10000 GtC to the total.

  - As recalled in Bauer et al. (2017) from Blanco et al. (2014), over 1750-2010, 368 GtC have been emitted from fossil fuels (362 with our estimates), with 177 from coal (176), 128 from oil (133) and 49 from gas (53). Figure 6 of Bauer et al. (2017) shows that, in the baseline of SSP5 (SSP5-8.5), the IAMs calculate cumulative resource extraction over 2010-2100 that are about twice the conventional and unconventional reserves for coal and oil, and about as much as the reserves for gas. New reserves have to be opened to fulfill these requirements.

Because the available fossil-fuel resources are already reached in 2100, we choose to produce scenarios in which emissions from Fossil Fuels & Industry are zero from 2100 onward. We acknowledge that such a reduction in these alternative scenarios are not plausible from a socio-economic perspective, but the previous scenarios are nor plausible from a geological perspective. Here, these alternative scenarios aim at providing a contrasted evolution. We acknowledge as well that a fraction of non-CO_2 emissions of SSP5-8.5 after 2100 may be emitted by the use of fossil-fuels, though we ignore the value of this fraction. We choose to keep the same non-CO_2 emissions that were described in the previous protocol. Like section 4.3.3, figure 4.19 represents features about the carbon cycle, figure 4.20 is a focus on the atmospheric chemistry of methane, nitrous oxide and ozones, and figure 4.21 regroups results regarding short-lived climate forcers.

Concerning the carbon cycle, we note that the emissions of SSP5-8.5, stopping after 2100, lead to a lower global warming, nonetheless high (figure 4.19).

- Emissions from Fossil-Fuels & Industry peak as well in 2090 at 37.3 GtC/yr, but become zero from 2100.
- LUC emissions follow an evolution very similar to those of original scenarios.
- For the median results, the ocean remain a sink over the complete period of the scenarios. Yet, the land sink become a source from 2220. Though, as emissions decrease, so do the sinks.
- In 3300, the land sink has stabilized respectively for *esm-ssp585ext* and *esm-ssp585-ssp126Lu-ext* to 0.08 GtC/yr (0.01 to 0.35) and 0.07 GtC/yr (0.01 to 0.23). In 3300, the ocean sink has stabilized respectively for *esm-ssp585ext* and *esm-ssp585-ssp126Lu-ext* -0.09 GtC/yr (-0.17 to 0.62) and -0.07 GtC/yr (-0.16 to 0.27).
- In terms of proportions, in *esm-ssp585ext*, the land has absorbed about 16% of the total carbon emitted over 1700-3300, but about 21% of the total carbon emitted over 1700-2300. Even though emissions and thus global warming are reduced in this alternative scenario, the land sink has still its efficiency reduced. In the meantime, the ocean has absorbed about 50% of the carbon over 1700-3300, but 35% of the carbon over 1700-2300. As with the original scenarios,

this is due to to the reduced efficiency of the oceanic carbon sink, and then, to the higher deterioration of the land sink that leaving more carbon to the ocean sink.

- The atmospheric partial pressure of CO_2 reaches 590.2 ppm (309.0 to 780.9) in *esm-ssp585ext*, and 564.4 (368.6 to 746.3) in *esm-ssp585-ssp126Lu-ext*. Using SSP1-2.6 land use variables leads to a reduction in atmospheric partial pressure of CO_2 by 4.4% in 3300. Though, comparing to the original scenarios, the decrease in atmospheric CO_2 is very close, but the relative difference in 3300 is higher in the alternative scenarios, for the asymptote in atmospheric CO_2 is lower.

- In 2100, both *esm-ssp585-ssp126Lu-ext* and *esm-ssp585ext* lead to a ΔT of 5.24°C (3.65 to 6.93), whereas the initial scenarios lead to 5.14°C (3.66 to 6.72). The difference at this date can be explained by the decreased number of members in the previous experiment, because of higher losses from divergent simulations.

- In 3300, the ΔT now stabilizes at 4.99°C (2.38 to 8.09) for *esm-ssp585ext* and 5.15°C (3.05 to 8.09) for *esm-ssp585-ssp126Lu-ext*. The same conclusion obtained from the original scenario stands here. Using SSP1-2.6 land variables in this scenario leads to an increase of ΔT by 0.1 to 0.2°C. Again, change in albedo may represent a limit for the potential of this method.

In figure 4.20 for atmospheric chemistry of CH_4, N_2O and ozone, and figure 4.21 for aerosols, we observe that *esm-ssp585ext* and *esm-ssp585-ssp126Lu-ext* are very close in term of climate outputs. Though, biomass burning emissions tend to be a little higher in *esm-ssp585-ssp126Lu-ext*, because of the change in the land cover, but also in a higher ΔT in the long term.

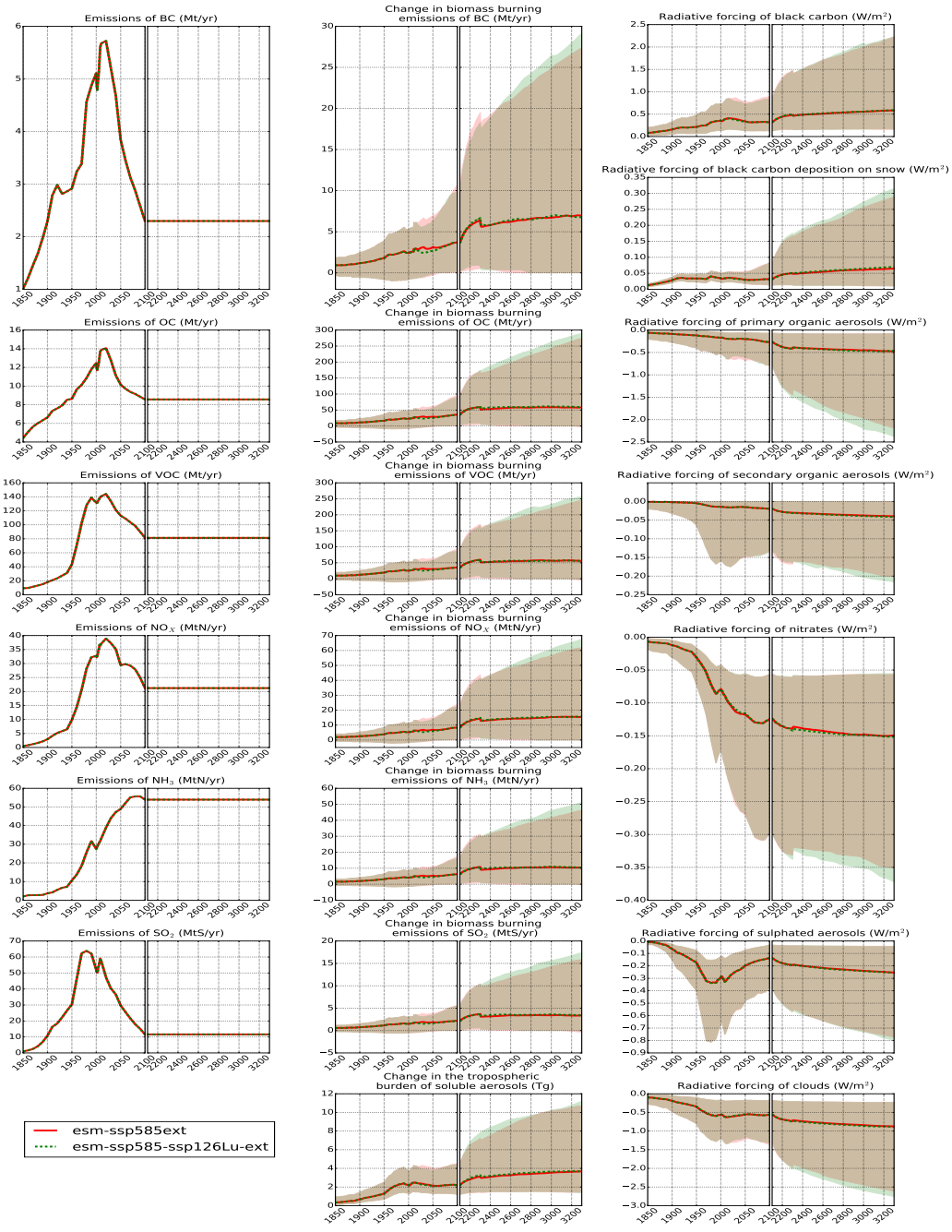

Figure 4.18: *Consequences of the scenarios esm-ssp585ext and esm-ssp585-ssp126Lu-ext regarding aerosols. Their median and 90% confidence interval are represented in red for the esm-ssp585ext and in green for the esm-ssp585-ssp126Lu-ext.*

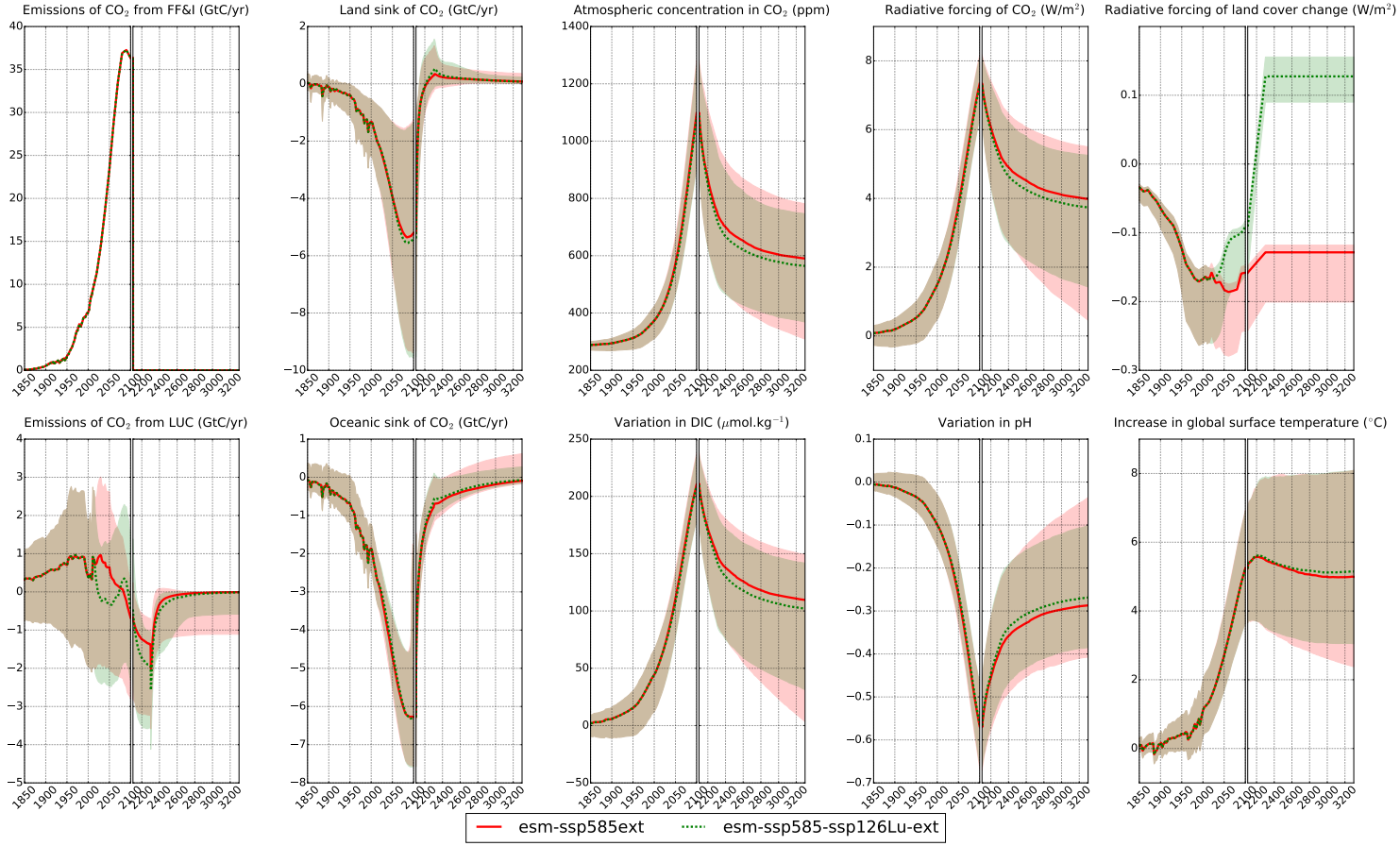

Figure 4.19: *Consequences of the alternative scenarios esm-ssp585ext and esm-ssp585-ssp126Lu-ext for the carbon cycle. Their median and 90% confidence interval are represented in red for the esm-ssp585ext and in green for the esm-ssp585-ssp126Lu-ext.*

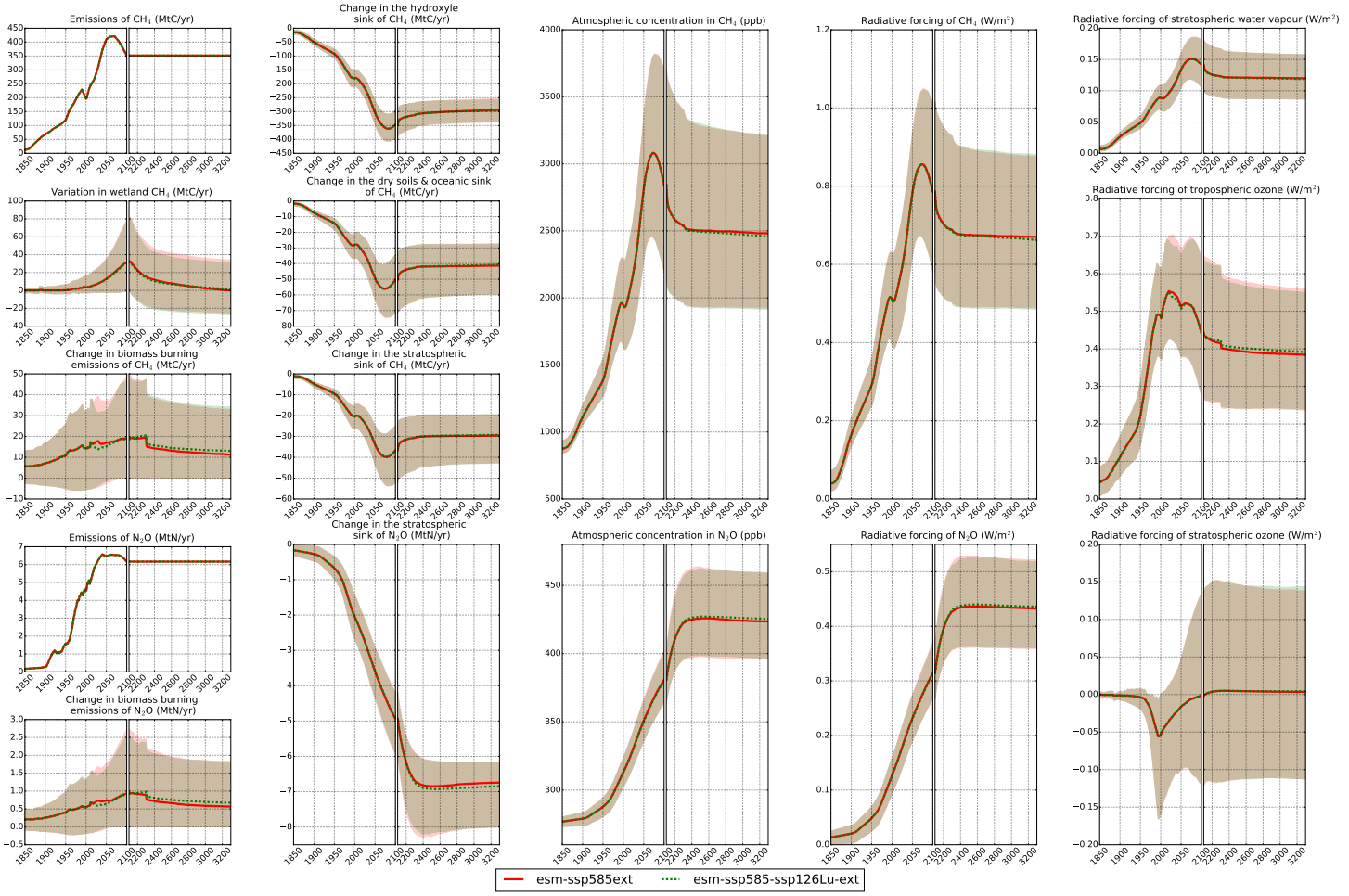

Figure 4.20: *Consequences of the alternative scenarios esm-ssp585ext and esm-ssp585-ssp126Lu-ext for methane, nitrous oxide and ozone. Their median and 90% confidence interval are represented in red for the esm-ssp585ext and in green for the esm-ssp585-ssp126Lu-ext.*

In the initial protocol, afforesting/reforesting lead to a virtually equivalent radiative forcing from CO_2, whereas it is reduced by from 3.98 W/m^2 to 3.74 in 3300 in the alternative protocol. With this measure, in 3300, the radiative forcing induced by changes in land cover increases from -0.18 W/m^2 to 0.11 in the initial protocol, but from -0.13 to 0.13 in the alternative protocol. From these results, be it with the initial protocol (section 4.3.3) or the alternative one (section 4.3.4), we deduce that afforesting/reforesting may not be an appropriate measure to mitigate climate change, because of the change of the albedo of the Earth. However, we recall that these results need to be compared to those of other models, especially ESMs. The modelling of how surface albedo changes affect climate change is difficult in simple models such as OSCAR or MAGICC, because it involves local processes (Gasser et al., 2017a). Albeit ESMs will not be able to calculate the associated uncertainties, their spatial resolution would help provide a more accurate answer to these effects, be it the CO_2 fluxes and the change in land cover.

4.3.5 C4: Ocean alkalinization

The objective of this experiment is to evaluate the consequences of alkalinization, and not its maximum potential. The control scenario is *esm-ssp585ext*, with emissions and land variables from SSP5-8.5, whereas alkalinization is experimented in *esm-ssp585-ocean-alk-ext* with 0.14 Pmol.yr^{-1} from 2020. TA termination experiment is also experimented with *esm-ssp585-ocean-alk-stop*, ending alkalinization in 2070.

In figure 4.22, we group the result of these three scenarios for the carbon cycle. Again, the extreme climate change simulated by SSP5-8.5 and its extensions has motivated us to create alternative scenarios, as detailed in section 4.3.6.

- Fossil Fuels & Industry and LUC emissions are those of *esm-ssp585ext*, as in experiment C3 (section 4.3.3). The LUC emissions and the land sink remain similar in the three scenarios.
- In 2070, the ocean sink of *esm-ssp585ext* absorbs 5.83 GtC/yr (4.28 to 6.81), whereas the ocean sinks of *esm-ssp585-ocean-alk-stop* and *esm-ssp585-ocean-alk-ext* absorbs 6.06 GtC/yr (4.51 to 7.03). Adding 0.14Pmol TA.yr^{-1} increase by 3.77% the ocean sink. After 2070, the ocean sink of *esm-ssp585-ocean-alk-stop* returns to the level of *esm-ssp585-ocean-alk-ext* in less than 5 years.
- In 2300, the ocean sink of *esm-ssp585-ocean-alk-ext* has absorbed 25.5% of the emitted carbon over 1700-2300, whereas those of *esm-ssp585-ocean-alk-stop* and *esm-ssp585ext* absorb respectively 24.6 and 24.4% of the emitted carbon.
- Concerning the termination of alkalinization, we have made the assumption that the oceanic circulation and the mixing fluxes affect similarly DIC and TA (section 4.2.1). The added TA is partially withdrawn from the surface ocean to the deep ocean. The addition over 2020-2070 has increased the TA

by only 6.88 μmol.kg^{-1} (5.93 to 8.89). By 3300, TA has decreased to 1.34 μmol.kg^{-1} (1.05 to 1.78) in *esm-ssp585-ocean-alk-stop*, but it has increased up to 51.1 μmol.kg^{-1} (39.5 to 68.2) in *esm-ssp585-ocean-alk-ext*. For comparison, adding 0.14 Pmol of TA to the sea surface waters up to the mixed layer depth correspond to a direct increase of its concentration by about 5 μmol.kg^{-1} before it is exported to the deep ocean. It means that most of the TA added in one year is exported to the deeper layers of the ocean.

- The reduction of acidity is almost negligible by 3300 (about 0.04).
- In 3300, the increase of the ocean sink has decreased the atmospheric partial pressure of CO_2 from 4477 ppm (3224 to 5218) to 4384 ppm (3154 to 5140), reducing radiative forcing by 0.06W.m^{-2} and ΔT by 0.12°C. With such a small difference in ΔT, the other components of the Earth system remain relatively unchanged.
- By 2100, the partial pressure of CO_2 is reduced from 1098 ppm (912.5 to 1281) in *esm-ssp585ext* to 1091 ppm (906.6 to 1273.7) in *esm-ssp585-ocean-alk-ext*. It corresponds to the withdrawal of about 14.5 GtC over 2020-2100. The level of 0.14Pmol.xyr^{-1} was fixed using exploratory simulations with the CSIRO-Mk3L-COAL model, in order to prescribe over 2020-2100 a 100 GtC removal from the atmosphere (Keller et al., 2017). The removal that we have calculated is 6 to 7 times less important than the one estimated, which calls for other assessments, be it from other teams or by adapting our modelling.

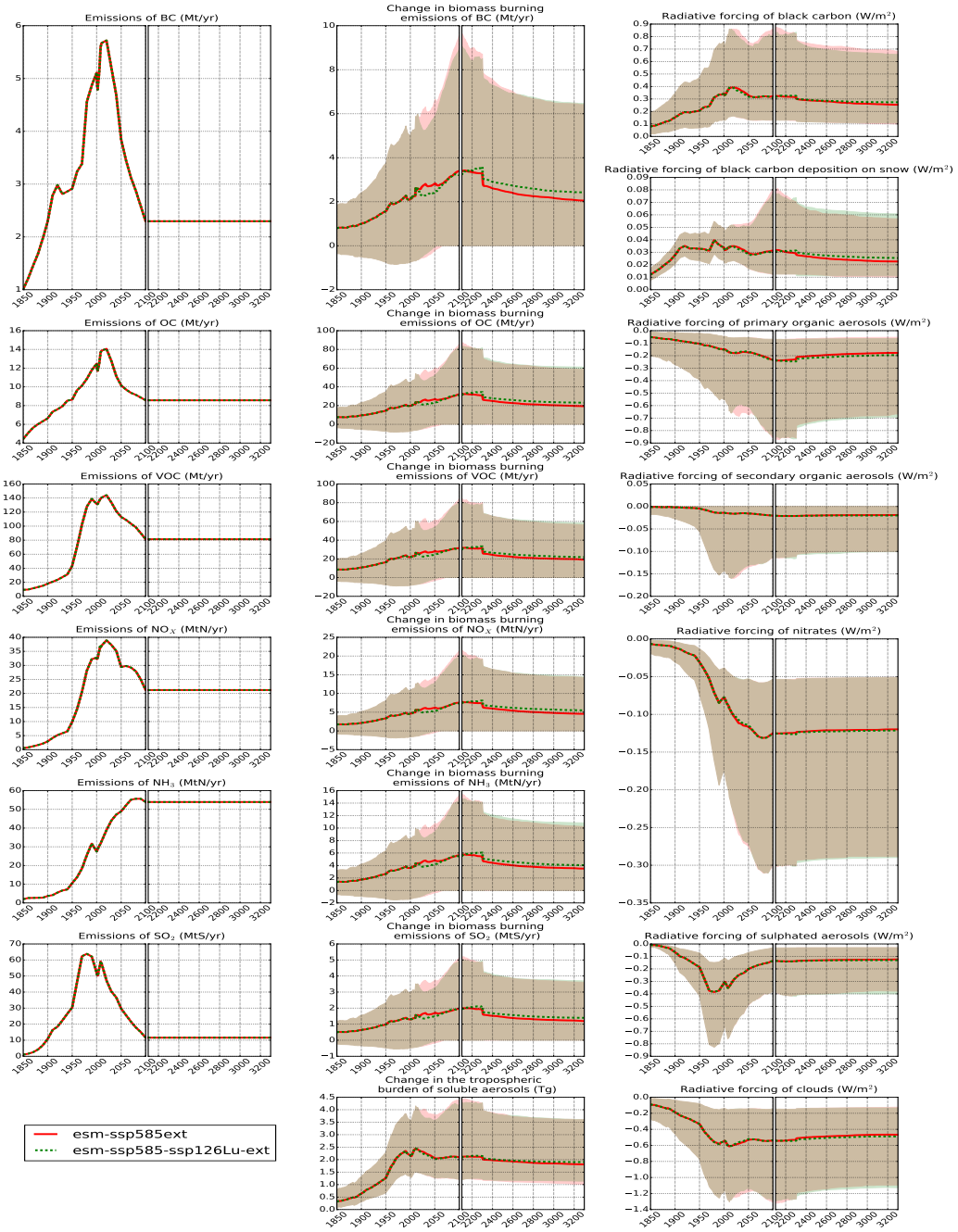

Figure 4.21: *Consequences of the alternative scenarios esm-ssp585ext and esm-ssp585-ssp126Lu-ext regarding aerosols. Their median and 90% confidence interval are represented in red for the esm-ssp585ext and in green for the esm-ssp585-ssp126Lu-ext.*

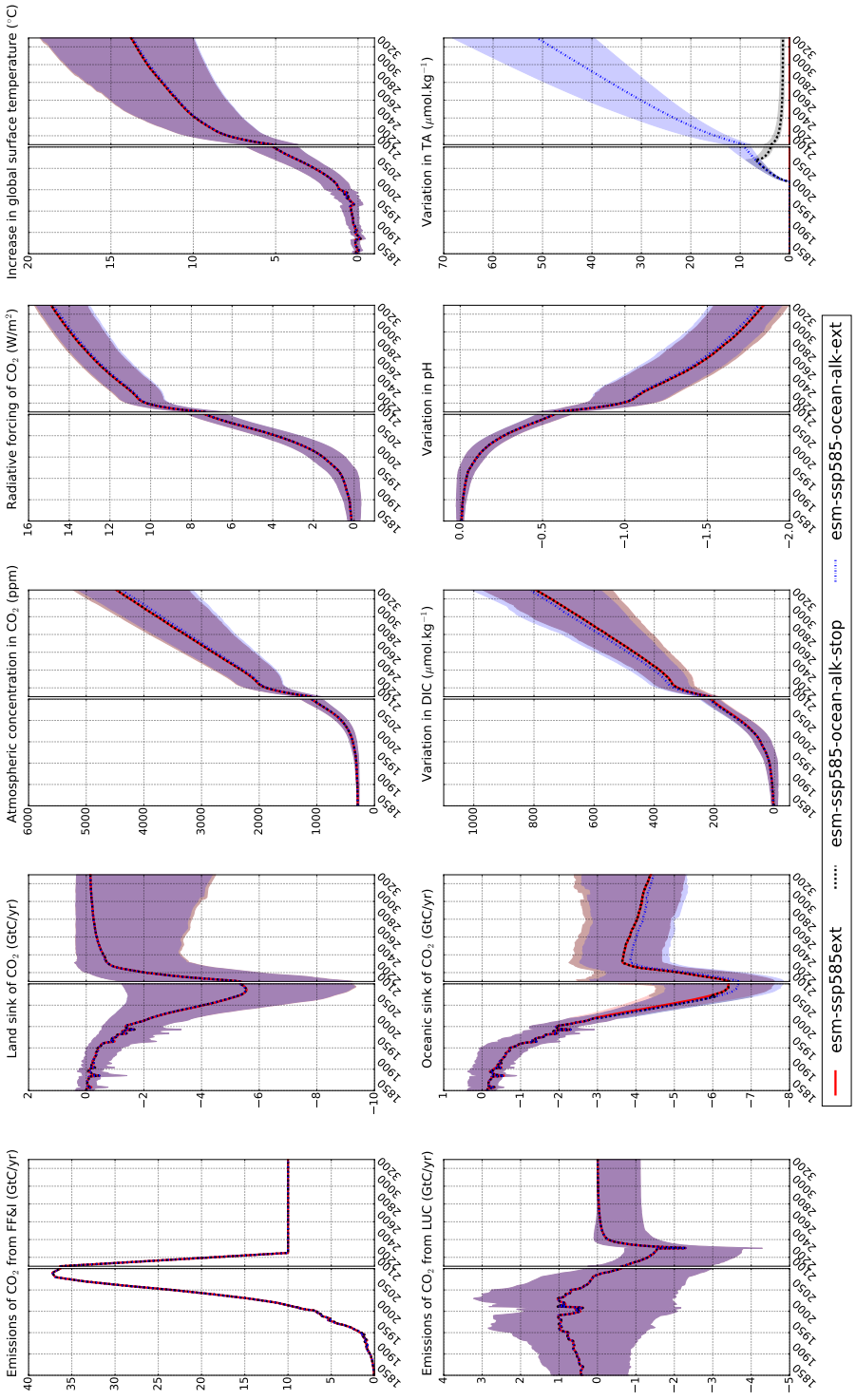

Figure 4.22: *Consequences of the scenarios esm-ssp585ext, esm-ssp585-ocean-alk-stop and esm-ssp585-ocean-alk-ext for the carbon cycle. Their median and 90% confidence interval are represented in red for the esm-ssp585ext, in black for esm-ssp585-ocean-alk-stop and in blue for the esm-ssp585-ocean-alk-ext.*

4.3.6 C4, alternative: Ocean alkalinization

Scenarios of the experiment C4 are based on the scenario SSP5-8.5. Therefore, the same reasons noted in section 4.3.4 still stand. We recall that this protocol leads to a global warming by about 14°C, and models are not meant to explore such domains. Even though this protocol has not be designed to evaluate the full extent of the potential of enhanced weathering, that high cumulative CO_2 emissions obliterate completely the effectiveness of this measure. Finally, from a geological perspective, that high CO_2 emissions for such a long time is not feasible. Then, following the principle of the alternative scenarios of section 4.3.4, we propose alternative scenarios for which the only change is that CO_2 emissions from Fossil Fuels & Industry are zero from 2100. In figure 4.23, we group the consequences of the three alternative scenarios for the carbon cycle.

- Fossil Fuels & Industry and LUC emissions are those of *esm-ssp585ext*, as in the alternative experiment C3 (section 4.3.4). The LUC emissions and the land sink remain similar in the three scenarios.
- In 2300, the ocean sink of *esm-ssp585-ocean-alk-ext* has absorbed 37.6% of the emitted carbon over 1700-2300, whereas those of *esm-ssp585-ocean-alk-stop* and *esm-ssp585ext* absorb respectively 35.7 and 35.4% of the emitted carbon. The increase in the carbon fraction absorbed by the ocean is thus due to the stopping in emissions.
- By 3300, TA has decreased to 1.14 μmol.kg^{-1} (0.95 to 1.56) in *esm-ssp585-ocean-alk-stop*, but it has increased up to 42.4 μmol.kg^{-1} (35.2 to 57.9) in *esm-ssp585-ocean-alk-ext*.
- The reduction of acidity in 3300 remains at about 0.04, just as with the original scenarios, though the relative difference is higher because of the lower emissions, and thus ocean acidification.
- The surface concentration of DIC remains relatively constant. As a remark, carbon is still being stored in the ocean, with a rate of 0.22 GtC/yr (-0.58 to 0.32) in *esm-ssp585-ocean-alk-ext*.
- In 3300, the increase of the ocean sink has decreased the atmospheric partial pressure of CO_2 from 590.2 ppm (309.0 to 780.9) to 537.3 ppm (280.3 to 694.8). It corresponds to the removal of 112 GtC over 2020-3300, that is to say about 5% of the CO_2 of the Fossil Fuels & Industry emitted over this period. For comparison, the initial protocol leads to a removal of 197 GtC from the atmosphere over 2020-3300. This is higher, but only because more CO_2 is emitted: it corresponds to about 1% of what is emitted by Fossil Fuels & Industry over 2020-3300.
- In this alternative protocol, enhanced weathering reduces by 3300 the radiative forcing by 0.51W.m^{-2} and the ΔT by 0.41°C. In this case, the cooling become

more important, because emissions have been stopped for long enough, and the atmospheric CO_2 is being reduced. This reduction of 0.41°C corresponds to about 8% of the 4.99°C of global warming by 3300, whereas the initial protocol lead to a cooling of 0.12°C, that is to say about 0.8% of the 13.8°C of global warming.

From the initial protocol (section 4.3.5) and this alternative protocol, we observe that the potential of enhanced weathering is 6 to 7 times lower than expected, because most of the TA is exported to the deeper layers of the oceans. Besides, the potential of this method is much clearer in scenarios with realistic CO_2 emissions.

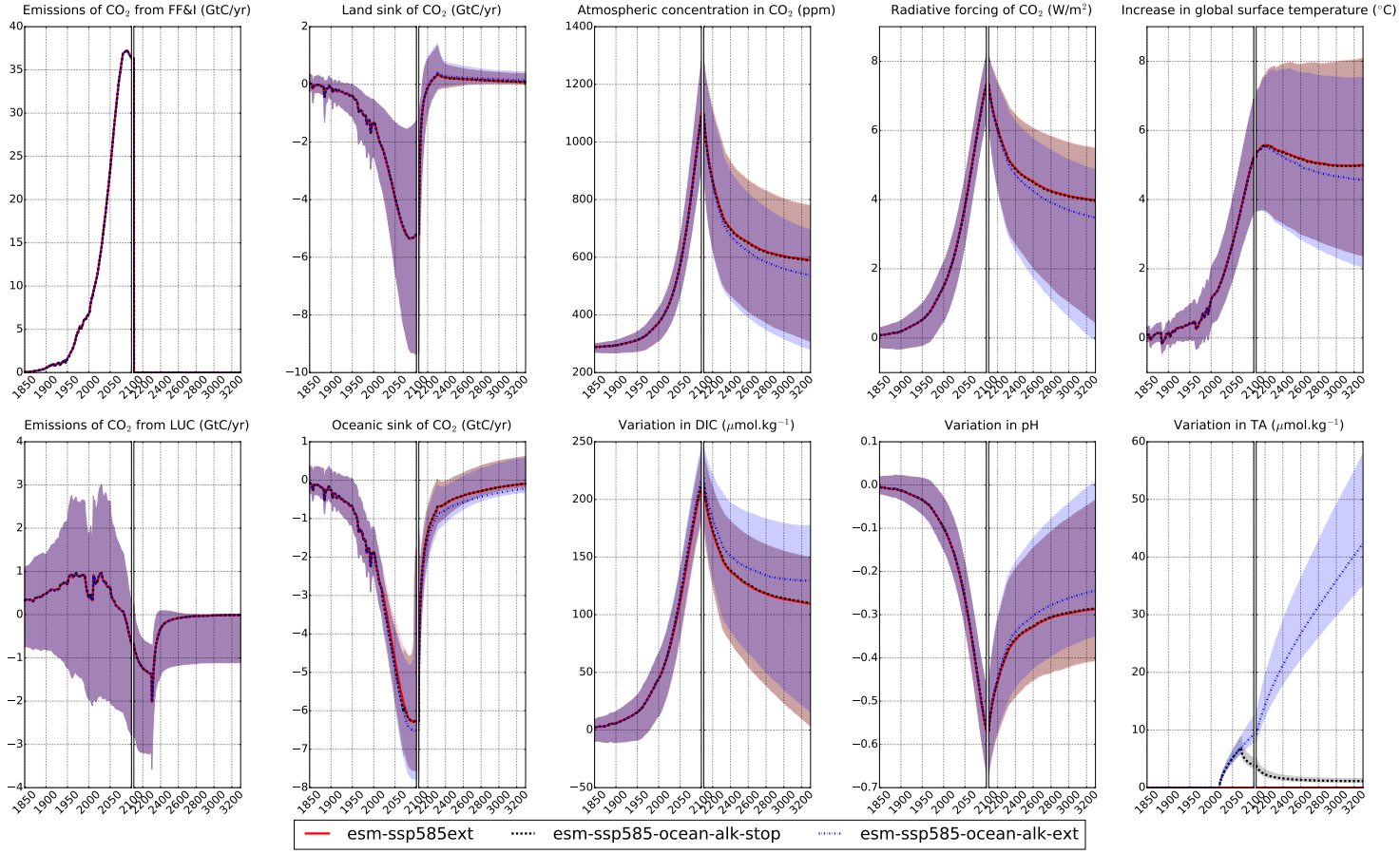

Figure 4.23: *Consequences of the alternative scenarios esm-ssp585ext, esm-ssp585-ocean-alk-stop and esm-ssp585-ocean-alk-ext for the carbon cycle. Their median and 90% confidence interval are represented in red for the esm-ssp585ext, in black for esm-ssp585-ocean-alk-stop and in blue for the esm-ssp585-ocean-alk-ext.*

4.4 Discussion

In the implementation of the protocols, several modifications have been made (section 4.2.3). Here are summarized these adjustments:

- In experiments of C2_yr2010-pulse, non-CO_2 drivers are kept constant after 2010. Concerning land use, either the land cover or the land use change transitions could be assumed constant. Assuming a constant land cover imply reductions in CO_2 emissions from LUC. Assuming constant land use changes would imply a change in the albedo, and in the carbon cycle. We have chosen to force a constant land cover from 2010, but biogenic emissions (biomass burning and wetlands) are affected. Yet, this is more representative of the objective of this experiment, that is to say the evaluation of the consequences of a CO_2 pulse over time from 2010 conditions.
- In C2_overshoot, C3 and C4, historical emissions (up to 2010) are prescribed using CDIAC emissions (Boden et al., 2013) for fossil-fuels emissions, EDGAR v4.2 (Joint Research Centre, 2011) for N_2O and halogenated compounds and ACCMIP for CH_4, NO_X, CO, VOC, SO_2, NH_3, OC and BC (Lamarque et al., 2010). This choice responds to a sake of simplicity in the preparation of the protocols, taking into account that the inventories used are relatively closed to those of *input4MIPs*.
- Emissions from SS5-3.4 (C2_overshoot) and SSP5-8.5 (C3, C4) are not yet available (ScenarioMIP). The treatment of the SSP database used in the chapter 3 is used.
- The LUC variables for SSP5-3.4 (C2_overshoot) are not yet available (ESGF, 2018; LUH2, 2018). The treatment of the land covers of the SSP database used in the chapter 3 is used.
- the extension of SSP5-3.4 (C2_overshoot) assumes a transition over 2100-2120 from its LUC emissions to the LUC emissions of SSP1-2.6. This transition has been performed instead on LUC variables.

In C2_overshoot and in C3, we have observed that the LUC emissions calculated by OSCAR are different from the LUC emissions prescribed by the IAM marker for the corresponding SSP scenarios. We acknowledge that the transformation of the land covers of SSP scenarios into net transitions reproduces imperfectly the transitions. Yet, this treatment applies here only to SSP5-3.4. The land variables for SSP1-2.6 and SSP5-8.5 are those of LUH2 (LUH2, 2018). The preparation of the LUH2 database leads to a reproduction of the land use variables (section 4.2.2) consistent with those of LUH1 (Hurtt et al., 2011). These scenarios are meant to be evaluated within ScenarioMIP (O'Neill et al., 2016) and LUMIP (Lawrence et al., 2016), which will provide an opportunity to explain these differences. These differences in LUC emissions are critical for the afforestation/reforestation experiment (C3). The

relatively low differences in LUC emissions between *esm-ssp585-ssp126Lu-ext* and *esm-ssp585ext*, especially in the face of the cumulated emissions from Fossil Fuels & Industry, leads to a weak mitigation. Although this experiment is not designed to investigate the full potential of afforestation/reforestation (but its implications), the problem of the low differences in LUC emissions diminishes the usefulness of this experiment.

The alkalinization of the experiment C4 implies a withdrawal of about 14.5 GtC over 2020-2100. The level of 0.14Pmol.yr^{-1} was established using exploratory simulations to prescribe over 2020-2100 a 100 GtC removal from the atmosphere (Keller et al., 2017). We reproduce the carbonate chemistry with a maximum relative uncertainty of 5% (section 4.2.1) for oceanic pCO_2 within 180-1120 ppm. Further improvements of these fits is still an ongoing process, because of its computation cost. We explain the observed difference in carbon withdrawal by our hypothesis of the physical transport of total alkalinity, assumed to be equivalent the physical transport of dissolved inorganic carbon. This assumption is made in the absence of more appropriate hypothesis. As a development, a upward flux for alkalinity could be introduced, as it is neglected for carbon (Joos et al., 1996). Another development would be the explicit modelling of the biological pump. Nevertheless, the 100 GtC removal over 2020-2100, and even 2010-2100, in the face of the 2295 GtC of cumulated Fossil-Fuels & Industry emissions over 2010-2100 leads to a relatively weak mitigation of climate change.

The IRFs of pulsed carbon additions/removal, and then AGWPs and AGTPs have been evaluated in section 4.3.2. We observed a reduction of the ranges in AGWPs and AGTPs by about 30 to 40% compared to Joos et al. (2013). On one hand, the 90% confidence interval of Joos et al. (2013) is constructed using a multi-model analysis. The individual models gathered in Joos et al. (2013) having their corresponding AGWPs and AGTPs, that have been gathered into a single distribution, and the method used to gather them may have an impact in Joos et al. (2013). On the other hand, the 90% confidence interval of OSCAR v2.2 is based on the combination of a set of sensitivities for each component of the Earth system. The parametrization of these sensitivities are based on an ensemble of models and on the literature. As explained in section 4.2.4, the combination of these elements through the multiple modules of OSCAR offers more degrees of freedom. In a Monte Carlo experiment, the parametrizations of OSCAR may not be represented in the literature albeit physically consistent, whereas others may not be consistent. The problem of inconsistent parametrizations can be solved by weighting the elements of the Monte Carlo using observational constraints, or simply by withdrawing unrealistic elements. For these reasons, results of OSCAR may differ in terms of median, mean or range compared to those of intercomparison exercises (Gasser et al., 2017a). Yet, some differences may remain, because some physically consistent parametrizations are kept, that are not present in the literature. This is a reason that may explain why the range in AGWPs and AGTPs are different in this study and in Joos et al. (2013). According to Gasser et al. (2017b), it is

expected to have only a limited impact. However, in this study, the strong climate changes implied by several scenarios of this project, especially with the SSP5-8.5, with its extension over 2300 and another 1000 years, are out of the domains of validity of several parametrizations. Unrealistic elements are withdrawn if land and carbon sinks exceed the unrealistic values of 20 GtC/yr (section 4.2.4). About half of the parametrizations are excluded in the Monte Carlo, for being unrealistic. That many exclusions may affect the distribution of the results from OSCAR v2.2, thus the AGWPs and AGTPs. A last explanation for the differences in the ranges of AGWPs and AGTPs between this study and Joos et al. (2013) is that we include all the feedbacks from the system in these metrics, whereas they are not in those ofJoos et al. (2013). Nevertheless, the values for AGWPs and AGTPs from positive emission pulses are consistent with the literature, thus we deem that the AGWPs and AGTPs from negative emission pulses may be used as GCPs.

Finally, the modelling of OSCAR v2.2 does not integrate yet several tipping elements (Lenton et al., 2008). Some, as permafrost thawing, will be. Yet, reversibility experiments (C1) or scenarios featuring high climate change (C3, C4) are likely to evaluate different climate consequences with their integration. The integration of these elements in ESM is still an ongoing process (Flato et al., 2013).

4.5 Conclusions

In this study, we have adapted OSCAR v2.2 for its use in the CDR-MIP project. OSCAR now integrates the evaluation of changes in total alkalinity, with new emulations of the carbonate chemistry and pH. These fits reproduce oceanic pCO_2 within 5% of relative uncertainty over a four-fold multiplication of the preindustrial CO_2. The LUH2 has also been treated for this study. The protocols of CDR-MIP have been adjusted, principally because of the lack of the required inputs for several scenarios.

Concerning the reversibility of the Earth system atfer a four-fold multiplication of the preindustrial CO_2, the system presents several hysteresis, particularly in the carbon sinks, temperatures and precipitations. Overall, we consider that the system returns to its preindustrial conditions as it is within 5% of its most perturbed state. It results to a return about 350 years after the atmospheric CO_2 has returned to its preindustrial level. The ocean sink takes the longer time (345 years), whereas the land sink equilibrates faster. The inertias in the climate system cause the ΔT to require 218 years to be within 5% (0.2°C) of the preindustrial level. The long lasting perturbation of the hydrological cycle because of climate change is partially compensated by the local desequilibriums in energy budget because of the atmospheric fraction of radiative forcing. This compensation occurs mostly while CO_2 is still higher than at preindustrial, reducing the maximal perturbation at the peak in CO_2, but making the return of global precipitations virtually last longer. Because of change in precipitations and ΔT, natural emissions are also perturbed, but in a lesser

extent, and so are aerosols. Changes in hydroxyle concentrations are also observed, mostly because of ΔT, and the relatively weak perturbation of the stratospheric chemistry still takes 200 to 300 years to return within 5% of the preindustrial.

Impulse response functions for negative and positive 100 GtC pulses from preindustrial and present-day conditions have been compared, and AGWPs and AGTPs have been deduced. In the present-day state, carbon sinks are less efficient, implying that an additional unit of CO_2 added to a present-day state warms more the Earth system than does the same unit added to the preindustrial state, but only over long term (time horizons $>$ 100 years). Over short term, because of the logarithmic relation in the radiative forcing of CO_2, an increase in the atmospheric concentration of CO_2 leads to an inferior additional radiative forcing in the present-day state compared to the preindustrial state. For the same reasons, a unit of negative emissions leads to a greater cooling than the warming induced by a unit of positive emissions, but only in the short term. In the long term, the cooling of negative emissions is inferior to the warming of positive emissions. Yet, the absolute values of AGWPs and AGTPs for positive and negative pulses are very similar. From a present-day state, the AGWP at 100 yr of negative emissions is -90.3.10^{-15} yr.W.m^{-2}.kg$CO_2{}^{-1}$ (-108.2 to -73.2), and the AGTP at 100 yr of negative emissions is -0.5.10^{-15} yr.°C.kg$CO_2{}^{-1}$ (-0.32 to -0.68). Global Cooling Potential are meant to be evaluated, and we note that they should actually be called Absolute Global Cooling Potentials. We consider our values as appropriate for this use.

We observe strong differences in CO_2 emissions from LUC calculated by the IAM and by OSCAR in the overshoot scenario SSP5-3.4. The land variables used are not those developed by LUH2, for they are not available yet, and we use our own treatment instead. Albeit our treatment has an impact on the CO_2 emissions from LUC, other factors could contribute to these differences, such as the definition of the CO_2 emissions from LUC used in the IAM or in OSCAR, as illustrated in the chapter 3. As a remark, the expected peak in ΔT is consistent to the preliminary study using MAGICCv6, but not the long term stabilization.

The evaluation of the implications of the afforestation/reforestation experiment have been hindered by the weaker than expected difference in LUC emissions between the control scenario (SSP5-8.5) and the scenario with afforestation/reforestation (SSP5-8.5 with SSP1-2.6 land use). For these scenarios, the land variables do not come from our treatment, but are those provided by LUH2. The differences in LUC emissions have still represented a problem here. These scenarios are meant to be evaluated by other models in ScenarioMIP and LUMIP. It represents an opportunity to evaluate the possible explanations for this difference. We also not that the extension of Fossil Fuels & Industry emissions from SSP5-8.5 renders the protocol almost useless to calculate the consequences of strong afforestation/reforestation measures. Besides, this extension is not consistent with available reserves. Alternative scenarios are developed, but that lead to similar conclusions: the reduction in the radiative forcing from CO_2 is more than compensated by the radiative forcing from Land Cover Change. For this reason, change in albedo may represent a limit

for the potential of this method. Yet, OSCAR may not be appropriate to answer this question, and the calculation from ESMs would represent an advantage for this project.

The ocean alkalinization experiment have also been disturbed by the lower than expected CO_2 removal by ocean. A 100 GtC removal was expected over 2010-2100, but only 14.5 GtC was actually removed. This is due to the rapid removal of TA to the deeper layer of the oceans. Our assumption regarding the similarity of the physical transports of total alkalinity and dissolved inorganic carbon may not be appropriate. Complementary exploration is required. Although the removals are different, the 100 GtC removal over 2010-2100 remains relatively weak in the face of the 2295 GtC from Fossil Fuels & Emissions over the same period. In the initial protocol, the extension represents the same problems encountered in the afforestation/reforestation experiment: the global warming is too extreme for the model to be valid, the extreme CO_2 emissions obliterate the potential of the measure, and these emissions are not feasible from a geological perspective. Alternative scenarios were also developed, showing that the potential of this method is more perceptible without high CO_2 emissions as background. In the original scenario, by 3300, this method had decreased ΔT by 0.12°C, but by 0.51°C in the alternative scenario.

Despite the difficulties shown here, more research is required to evaluate the potential and the implications of CDR technologies. Though, in the meantime, an ambitious mitigation is highly required to avoid a delayed mitigation, under a less favorable climate (Strefler et al., 2018).

Chapter 5

Conclusion

All of the work presented in this thesis has for purpose to provide insights on socio-economic scenarios from an Earth system modelling perspective. The chapter 2 analyzes the contribution of the uncertainty in emissions to the uncertainty in climate projections. The chapter 3 assesses the climate projections of the scenarios built on the matrix of Shared Socioeconomic Pathways (SSPs) and Representative Concentration Pathways (RCPs). The chapter 4 focuses on Carbon Dioxide Removal (CDR) techniques, used to calculate the negative emissions in the socio-economic scenarios. Throughout the thesis, we have used the reduced-form Earth system model (reduced-form ESM) OSCAR v2.2 (short descriptions in boxes 1.5). These insights are related to the consistencies of data, models and scenarios, but also to the development of OSCAR.

In chapter 2 of this thesis, we calculate how uncertain emission factors affect the calculation of fossil-fuel emissions. We also show how these uncertainties contribute climate projections. The use of non-conventional fuels cause the uncertainty in fossil-fuel emissions to rise, with an overall $\pm 15\%$ range in the cumulative CO_2 emissions over 2000-2300. We decompose the uncertainty in climate projections across its sources: Earth system modelling, CO_2 emissions and non-CO_2 emissions. We show that virtually all of the uncertainty in the increase in global surface temperature can still be attributed to the Earth system modelling. However, for several variables, the consequences of the uncertainties in emissions cannot be neglected in the face of the Earth system modelling. For issues related to air quality, it results that the uncertainty in emissions should be accounted for.

In chapter 3 of this thesis, we evaluate the climate projections of the socio-economic scenarios built on the SSP-RCP matrix. To do so, we have completed the SSP public database on two points. The land-use has been enhanced to provide the net transitions in land use change (LUC), the area extents of shifting cultivations and the harvested biomass. The details of the emissions of fluorinated gases and other halogenated compounds have been calculated. Using this extended database, we calculate the climate projections of the 103 SSP scenarios.

- The increases in global surface temperature are used to derive the probabilities to respect the Paris Agreement for SSP-RCPs, outlining the hypotheses of the storylines. By construction, the SSP scenarios target different levels of radiative forcings and ultimately increases in global surface temperature. Yet, only the median global surface temperature reaches this level of global warming: the temperature that is not exceeded with 90% of probability is about 0.5 to 1°C higher.

- We identify the radiative forcings of the species that are effectively reduced by climate policies. Also, scenarios that share the same targets for 2100 may have very contrasted for the late evolutions of the radiative forcings. It suggests that their climate trajectories after 2100 are likely to be very different.

- We show trade-offs in the reduction in emissions of greenhouse gases. Also, the perturbation of biomass burning and wetlands emissions may become about half of the emissions in scenarios with strong mitigation. Furthermore, we show that the CO_2 emissions from LUC of the Integrated Assessment Models (IAMs) are lower than those calculated by OSCAR v2.2, with differences as big as 268 GtC over 2010-2100.

- Analyzing the carbon cycle, we show how the carbon sinks are affected in these scenarios.

- We use a Kaya decomposition to show that the main driver of reduction in CO_2 emissions is the reduction in the carbon intensity of energy. We also extend it to other species, outlining the hypotheses regarding technology development.

- We propose a rigorous definition of carbon budgets, for exceedance and avoidance of an ensemble of thresholds in global warming. To avoid a climate change above 2°C with a probability of 66%, 1240 GtCO2 (610 to 1790) can be emitted from 2015. To exceed the same threshold, 1690 GtCO2 (940 to 2770) have to be emitted from 2015, but with temperature that would keep increasing afterwards.

Overall, this assessment provides several key features and numbers for issues relative to climate change and mitigation challenges.

The chapter 4 is a focus on the negative emissions, under the modelling of the Earth system in OSCAR v2.2. We follow the protocol of the Carbon Dioxide Removal Model Intercomparison Project (CDRMIP, Keller et al. (2017)). We identify flaws in the prescribed experiments, and we add alternative experiments as corrections. According to this version of OSCAR, we show that once the atmospherical CO_2 has returned to its preindustrial level, the Earth system has globally returned to preindustrial equilibrium 350 years later. We calculate the absolute global cooling potentials, that can be used to evaluate the potential of direct air capture techniques. According to OSCAR, afforestation/reforestation effectively decreases the radiative forcing from atmospheric CO_2, but this reduction is overcompensated by the change

in surface albedo. Under our assumptions for physical transport of surface alkalinity, the enhanced oceanic weathering removes 6-7 times less CO_2 from the atmosphere than expected.

Although relatively independents, these chapters are still connected. Because of the uncertainties in emissions shown in the chapter 2, different inventories integrated in OSCAR v2.2 (Gasser et al., 2017a) are used to account for this uncertainty in chapter 3. In chapter 3, the extension of the Kaya decomposition to non-CO_2 emissions helps us validate the use of co-emissions ratios in chapter 2. Our calculation of the SSP net land use changes performed in chapter 3 has been used for the SSP5-3.4 in the chapter 4, because this scenario was not treated yet in the LUH2 (LUH2, 2018). The SSP scenarios treated in LUH2 have been used to evaluate our methods for calculating land variables from SSP scenarios. Finally, the calculation of CO_2 cumulative emissions in chapter 2 has been used to develop the alternative scenarios in chapter 4.

From this work as a whole, several elements stand out, that we highlight here. As a first key conclusion, while producing these works, we have encountered numerous inconsistencies in the data, models and scenarios.

- First of all, databases are often incomplete. It has been critical for the chapter 3 in order to calculate the climate projections of the SSP scenarios. We have been forced to fill the gaps of the SSP public database. In this regard, the land-use is particularly important. Providing mere changes in land cover is not enough, land-use change transitions, harvested biomass and even area extents of shifting cultivations would be much better. We acknowledge that adding these variables would be difficult, but it is necessary for calculating reliable climate projections. The climate projections of these socio-economic scenarios are supporting the design of climate policies. The existing climate assessment of the SSP scenarios by the reduced-form ESM MAGICC v6 uses the CO_2 emissions from LUC calculated by the IAMs, although the IAMs do not use equivalent definitions of these emissions. Besides, forcing the CO_2 emissions from LUC in the model implies a forcing of the land sink as well, even tough their calculation of both remain uncertain. Our assessment shows that the CO_2 emissions from LUC of IAMs are globally lower than those calculated by OSCAR. Our treatment of the land-use of SSP scenarios is not enough to explain these differences, for the scenarios run under the SSP scenarios present in the LUH2 dataset still show differences. Hopefully, the upcoming calculations by models taking part in the LUMIP (Lawrence et al., 2016) and the ScenarioMIP (O'Neill et al., 2016) projects will help solve this problem.

- As a second category of inconsistencies, numerous emissions inventories coexist, but with discrepancies amongst themselves. Each inventory uses its definitions and its methods. It complicates their comparison, and when compared, they show sometimes large differences. These differences are representative of the uncertainties in their calculation, and can hardly be reduced. In scenarios,

this problem is often neglected. We have shown when it can effectively be neglected, and how to correct it when required. The chapter 3 is an example of how to integrate this uncertainty in the framework.

- As a third category, we have encountered experiments, whose design leads to useless results. For instance, under the experiments for afforestation/reforestation and enhanced alkalinization of the chapter 4, the climate changes were extreme enough to strike down any model. Yet, such extreme experiments are infeasible in terms of available fossil-fuel resources.

As a second key conclusion, all the elements of this thesis helps us identify strengths and flaws in OSCAR v2.2. On the one hand, this model is capable of accurate and efficient calculation of climate scenarios, for large datasets of scenarios and in a probabilistic framework. On the other hand, several aspects could be improved.

- First comes the datasets used in OSCAR. In most cases, the second to last versions of datasets are used, be it for emissions inventories or land-use. For instance, using the LUH2 instead of the LUH1 would represent a direct improvement through up-to-date data, but indirectly as well by improving pre-industrial maps. The work realized in chapter 4 is a step toward this objective.

- The second possibility to improve OSCAR concerns the modelling of land-use. As noticed throughout the thesis, the aggregation into broad categories of biomes introduces biases. On this point, the LUH2 has also the potential of improving the aggregation. Besides, OSCAR v2.2 does not integrate yet the nitrogen and phosphorus cycles, which are known to affect the terrestrial biosphere, and may be responsible for the differences to the CO_2 emissions from LUC calculated by IAMs. Integrating the associated processes in this model would not only improve the accuracy of OSCAR, but also help understanding their role in climate change (Peñuelas et al., 2013).

- The third aspect concerns the oceanic carbon cycle. OSCAR uses Joos et al. (1996) as basis, just like other simple climate models, albeit with modifications in OSCAR v2.2. A new approach could be proposed, that could also emulate the marine biology, using results from CMIP5. The upcoming CMIP6 would provide better data to calibrate new parameters, and not only for the oceanic carbon cycle. This aspect of OSCAR has been particularly important when dealing with enhanced alkalinization.

- A fourth aspect concerns the tipping elements. OSCAR needs other models to integrate these features, in order to emulate their behaviors. The integration of permafrost thawing in OSCAR is planned, but the modelling of other tipping elements would improve the robustness of the climate projections (Lenton et al., 2008). This is a key aspect for studies like CDR-MIP that investigate the reversibility of the Earth system.

- Fifth, local processes remain a flaw of "simple" ESMs. In this regard, the global consequences of change in the surface albedo are difficult to model, since several local processes interact with each other, all with their own seasonal variations. However, scenarios involving large increases of the area extent of forests may require such development. This aspect of OSCAR has been particularly important when dealing with afforestation/reforestation.

Keeping OSCAR up-to-date and improving its modelling is required, to ensure the robustness of its outcomes. Fulfilling all of the aforementioned points would enhance its potential to answer a larger panel of questions, with an increased quality.

The third key conclusion is somewhat different from the two others, in that it roots to the crux.

First, the transformation pathways that respect the Paris Agreement require rapid reduction in the emissions and/or strong negative emissions, be it in older scenarios or in the SSP scenarios. Using negative emissions is a risky gamble, for these technologies are not ready yet for large scale development. Secondly, the CDR techniques constitute the basis of negative emissions, the solution to mitigate climate change even after delayed climate policies. The CDR techniques are shown to be not as efficient as expected, albeit it involves several features of OSCAR that could be improved. The odds of winning this gamble are then thinner. Thirdly, even though these pathways are designed to respect the Paris Agreement, it is in terms of median: a significative probability of not respecting the Paris Agreement remains. Fourthly, the modelling of tipping elements is still very difficult, and they are not integrated in most of these assessments. As such, climate projections do not account for elements that may become significative. This is not new to say, but under current evolutions, we are likely not to respect the Paris Agreement. Going further, our work suggest that our capacity to mitigate climate change is even thinner than planned.

I believe that the research on climate change has to keep providing information on how to mitigate climate change, but also which adaptations for our societies and our environment are possible. Obviously, it means that the datasets and models have to be improved, but not only. It seems that climate sciences develop faster than its internal consistency. To ensure the robustness of the outcomes, the internal consistency of the ensemble has to be improved. Through this thesis, we have reached several boundaries in-between models, data and scenarios. These boundaries are still limiting our potential for integrated assessments and robust analyses. By careful and rigorous exchanges in-between communities, it might be possible to remove these barriers. Anyway, an efficient mitigation of climate change implies strong changes in technologies, behaviors and societies, and the urgency for these changes keeps rising. These strong developments have to start now, without waiting science to reach an ideal state of knowledge.

Chapter 6

Appendix

6.1 Appendix for chapter 2

Code	Sector CMIP5
ene	Energy production and distribution
ind	Industry (combustion and non-combustion)
air	Aviation
tra	Land transport
shp	Maritime transport
dom	Residential and commercial
slv	Solvents
agr	Agriculture
gra	Open vegetation fires in savanna and grasslands
awb	Agricultural waste burning on fields
for	Open vegetation fires in forests
wst	Waste
ooo	Other

Table 6.1: *Description of CMIP5 sectors*

Code	Sector EDGAR-HYDE
FC	Fossil-fuel combustion
FP	Fossil-fuel production, transmission, transformation
BC	Biofuel production, transformation and combustion
IN	Industrial production and consumption processes
AL	Agricultural land activities
AN	Animals
SB	Savannah burning
DF	Deforestation
AW	Agricultural waste burning
LF	Landfills
OO	Other

Table 6.2: *Description of EDGAR-HYDE sectors*

Description	IPCC Code	CMIP5 Code	E.-HYDE Code
Public Electricity Generation	**1A1a1**	**ene**	**FC**
Public Combined Heat and Power gen.	**1A1a2**	**ene**	**FC**
Public Heat Plants	**1A1a3**	**ene**	**FC**
Public Electricity Generation (own use)	**1A1a4**	**ene**	**FC**
Electricity Generation (autoproducers)	**1A1a5**	**ene**	**FC**
Combined Heat and Power gen. (autoprod.)	**1A1a6**	**ene**	**FC**
Heat Plants (autoproducers)	**1A1a7**	**ene**	**FC**
Public Electricity Generation (biomass)	1A1ax1	**ene**	**FC**
Public Combined Heat and Power gen. (biom.)	1A1ax2	**ene**	**FC**
Public Heat Plants (biomass)	1A1ax3	**ene**	**FC**
Public Electricity Gen. (own use) (biom.)	1A1ax4	**ene**	**FC**
Electricity Generation (autoproducers) (biom.)	1A1ax5	**ene**	**FC**
Combined Heat and Power gen. (autopr.) (biom.)	1A1ax6	**ene**	**FC**
Heat Plants (autoproducers) (biomass)	1A1ax7	**ene**	**FC**
Refineries	**1A1b**	**ene**	**FC**
Refineries (biomass)	1A1bx	**ene**	**FC**
Fuel combustion coke ovens	**1A1c1**	**ene**	**FC**
Blast furnaces (pig iron prod.)	**1A1c2**	**ene**	**FC**
Gas works	**1A1c3**	**ene**	**FC**
Other transformation sector (BKB, etc.)	**1A1c5**	**ene**	**FC**
Gas works (biom.)	1A1cx3	**ene**	**FC**
Fuel comb. charcoal production (biom.)	1A1cx4	**ene**	**FC**
Other transf. sector (BKB, etc.) (biom.)	1A1cx5	**ene**	**FC**
Iron and steel	**1A2a**	ind	**FC**
Iron and steel (biomass)	1A2ax	ind	**FC**
Non-ferrous metals	**1A2b**	ind	**FC**
Non-ferrous metals (biomass)	1A2bx	ind	**FC**
Chemicals	**1A2c**	ind	**FC**
Chemicals (biomass)	1A2cx	ind	**FC**
Pulp and paper	**1A2d**	ind	**FC**

Table 6.3: *List of the sectors from EDGAR v4.3.2 dataset. In bold are the sectors kept for the production of co-emission ratios. Within each of these sectors, only the emissions associated with the use of fossil fuels are kept. For all EDGAR sectors are given the matching CMIP5 sectors (table 6.1) and EDGAR-HYDE sectors (table 6.2). These sectors are in bold if they are kept as fossil-fuel related sectors. (Part 1/3)*

Description	IPCC Code	CMIP5 Code	E.-HYDE Code
Pulp and paper (biomass)	1A2dx	ind	**FC**
Food and tobacco	**1A2e**	ind	**FC**
Food and tobacco (biomass)	1A2ex	ind	**FC**
Other industries (stationary) (fos.)	**1A2f**	ind	**FC**
Off-road machinery: construction (diesel)	**1A2f1**	ind	**FC**
Off-road machinery: mining (diesel)	**1A2f2**	ind	**FC**
Other industries (stationary) (biom.)	1A2fx	ind	**FC**
Domestic air transport	**1A3a**	**air**	**FC**
Road transport (incl. evap.) (foss.)	**1A3b**	**tra**	**FC**
Road transport (incl. evap.) (biom.)	1A3bx	**tra**	**FC**
Non-road transport (rail, etc.) (fos.)	**1A3c**	**tra**	**FC**
Non-road transport (rail, etc.)(biom.)	1A3cx	**tra**	**FC**
Inland shipping (fos.)	**1A3d**	**shp**	**FC**
Inland shipping (biom.)	1A3dx	**shp**	**FC**
Non-road transport (fos.)	**1A3e**	**tra**	**FC**
Non-road transport (biom.)	1A3ex	**tra**	**FC**
Commercial and public services (fos.)	**1A4a**	**dom**	**FC**
Commercial and public services (biom.)	1A4ax	**dom**	**FC**
Residential (fos.)	**1A4b**	**dom**	**FC**
Residential (biom.)	1A4bx	**dom**	**FC**
Agriculture and forestry (fos.)	**1A4c1**	**dom**	**FC**
Agriculture and forestry (biom.)	1A4c1x	**dom**	**FC**
Off-road machinery: agric./for. (diesel)	**1A4c2**	**dom**	**FC**
Fishing (fos.)	**1A4c3**	**dom**	**FC**
Fishing (biom.)	1A4c3x	**dom**	**FC**
Non-specified other (fos.)	**1A4d**	**dom**	**FC**
Non-specified other (biom.)	1A4dx	**dom**	**FC**
Off-road machinery: mining (diesel)	**1A5b1**	**ind**	**FP**
Fuel transformation coke ovens	**1B1b1**	**ene**	**FP**
Fuel transformation in gas works	**1B1b2**	**ene**	**FP**
Fuel transformation charcoal production	1B1b3x	**ene**	**FP**
Fuel transformation of solid fuels (BKB Plants, coal liquefaction, patent fuel plants)	**1B1b4**	**ene**	**FP**
Fuel transformation of solid fuels (BKB Plants, coal liquefaction, patent fuel plants) using biofuel	1B1b4x	**ene**	**FP**
Oil production	**1B2a1**	**ene**	**FP**
Oil transmission	**1B2a2**	**ene**	**FP**
Transport by oil trucks	**1B2a4-t**	**ene**	**FP**
Fuel transformation of gaseous fuels (GTL, Blend, (re-)gasif./Liquef., NSF)	**1B2b5**	**ene**	**FP**
Fuel transformation in non-specified transformation activity	1B2b5x	**ene**	**FP**

Table 6.4: *List of the sectors from EDGAR v4.3.2 dataset. In bold are the sectors kept for the production of co-emission ratios. Within each of these sectors, only the emissions associated with the use of fossil fuels are kept. For all EDGAR sectors are given the matching CMIP5 sectors (table 6.1) and EDGAR-HYDE sectors (table 6.2). These sectors are in bold if they are kept as fossil-fuel related sectors. (Part 2/3)*

Description	IPCC Code	CMIP5 Code	E.-HYDE Code
Venting and flaring during oil and gas production	1B2c	**ene**	**FP**
International air transport	**1C1**	**air**	**FC**
International marine transport (bunkers)	**1C2**	**shp**	**FC**
International marine transport (biom.)	1C2x	**shp**	**FC**
Cement production	**2A1**	ind	IN
Lime production	**2A2**	ind	IN
Limestone and Dolomite Use	**2A3**	ind	IN
Soda ash production	**2A4a**	ind	IN
Soda ash use	**2A4b**	ind	IN
Ammonia production (gross CO2)	**2B1g**	ind	IN
CO2-ammonia stored in urea	**2B1s**	ind	IN
Silicon carbide production	**2B4a**	ind	IN
Calcium carbide production	**2B4b**	ind	IN
Carbon black production	**2B5a**	ind	IN
Ethylene production	**2B5b**	ind	IN
Methanol production	**2B5e**	ind	IN
Other bulk chemicals production	**2B5g**	ind	IN
Urea production	**2B5g1**	ind	IN
Vinyl chloride production	**2B5g2**	ind	IN
Crude steel production total	**2C1a**	ind	IN
Blast furnaces	**2C1b**	ind	IN
Ferroy Alloy production	**2C2**	ind	IN
Aluminium production (primary)	**2C3a**	ind	IN
Aluminium production (secondary)	**2C3b**	ind	IN
Lead production (primary)	**2C5lp**	ind	IN
Magnesium production (primary)	**2C5mp**	ind	IN
Zinc production (primary)	**2C5zp**	ind	IN
Non-energy use of lubricants/waxes (CO2)	**2G1**	ind	IN
Solvents in paint	**3A**	slv	IN
Degreasing and dry cleaning	**3B**	slv	IN
Chemical products	**3C**	slv	IN
Other product use	**3D**	slv	IN
CO2 from urea application	**4D4a**	agr	AL
CO2 from agricultural lime application	**4D4b**	agr	AL
Field burning of agric. res.: cereals	**4F1**	awb	AW
Field burning of agric. res.: pulses	**4F2**	awb	AW
Field burning of agric. res.: tuber and roots	**4F3**	awb	AW
Field burning of agric. res.: sugar cane	**4F4**	awb	AW
Field burning of agric. res.: other	**4F5**	awb	AW
Waste incineration - uncontrolled MSW burning	**6Cb1**	wst	LF
Waste incineration - other non-biogenic	**6Cb2**	wst	LF
Coal fires (underground)	**7A1**	ooo	OO
Oil fires (Kuwait)	**7A2**	ooo	OO

Table 6.5: *List of the sectors from EDGAR v4.3.2 dataset. In bold are the sectors kept for the production of co-emission ratios. Within each of these sectors, only the emissions associated with the use of fossil fuels are kept. For all EDGAR sectors are given the matching CMIP5 sectors (table 6.1) and EDGAR-HYDE sectors (table 6.2). These sectors are in bold if they are kept as fossil-fuel related sectors. (Part 3/3)*

6.2 Appendix for chapter 3

6.2.1 Composition of the regions

OECD countries in 1990	Includes the OECD 90 and EU member states and candidates (Albania, Australia, Austria, Belgium, Bosnia and Herzegovina, Bulgaria, Canada, Croatia, Cyprus, Czech Republic, Denmark, Estonia, Finland, France, Germany, Greece, Guam, Hungary, Iceland, Ireland, Italy, Japan, Latvia, Lithuania, Luxembourg, Malta, Montenegro, Netherlands, New Zealand, Norway, Poland, Portugal, Puerto Rico, Romania, Serbia, Slovakia, Slovenia, Spain, Sweden, Switzerland, The former Yugoslav Republic of Macedonia, Turkey, United Kingdom, United States of America)
Reforming countries	Countries from the Reforming Economies of Eastern Europe and the Former Soviet Union (Armenia, Azerbaijan, Belarus, Georgia, Kazakhstan, Kyrgyzstan, Republic of Moldova, Russian Federation, Tajikistan, Turkmenistan, Ukraine, Uzbekistan)
Asia	Most Asian countries with the exception of the Middle East, Japan and Former Soviet Union states (Afghanistan, Bangladesh, Bhutan, Brunei Darussalam, Cambodia, China (incl. Hong Kong and Macao, excl. Taiwan) Democratic People's Republic of Korea, Fiji, French Polynesia, India, Indonesia, Lao People's Democratic Republic, Malaysia, Maldives, Micronesia (Fed. States of), Mongolia, Myanmar, Nepal, New Caledonia, Pakistan, Papua New Guinea, Philippines, Republic of Korea, Samoa, Singapore, Solomon Islands, Sri Lanka, Taiwan, Thailand, Timor-Leste, Vanuatu, Viet Nam)
Middle East and Africa	Countries of the Middle East and Africa (Algeria, Angola, Bahrain, Benin, Botswana, Burkina Faso, Burundi, Cameroon, Cape Verde, Central African Republic, Chad, Comoros, Congo, Côte d'Ivoire, Democratic Republic of the Congo, Djibouti, Egypt, Equatorial Guinea, Eritrea, Ethiopia, Gabon, Gambia, Ghana, Guinea, Guinea-Bissau, Iran (Islamic Republic of), Iraq, Israel, Jordan, Kenya, Kuwait, Lebanon, Lesotho, Liberia, Libyan Arab Jamahiriya, Madagascar, Malawi, Mali, Mauritania, Mauritius, Mayotte, Morocco, Mozambique, Namibia, Niger, Nigeria, Occupied Palestinian Territory, Oman, Qatar, Rwanda, Réunion, Saudi Arabia, Senegal, Sierra Leone, Somalia, South Africa, South Sudan, Sudan, Swaziland, Syrian Arab Republic, Togo, Tunisia, Uganda, United Arab Emirates, United Republic of Tanzania, Western Sahara, Yemen, Zambia, Zimbabwe)
Latin America	Countries of Latin America and the Caribbean (Argentina, Aruba, Bahamas, Barbados, Belize, Bolivia (Plurinational State of), Brazil, Chile, Colombia, Costa Rica, Cuba, Dominican Republic, Ecuador, El Salvador, French Guiana, Grenada, Guadeloupe, Guatemala, Guyana, Haiti, Honduras, Jamaica, Martinique, Mexico, Nicaragua, Panama, Paraguay, Peru, Suriname, Trinidad and Tobago, United States Virgin Islands, Uruguay, Venezuela (Bolivarian Republic of))

Table 6.6: *Descriptions of the 5 global regions.*

6.2.2 Figures for fluorinated gases

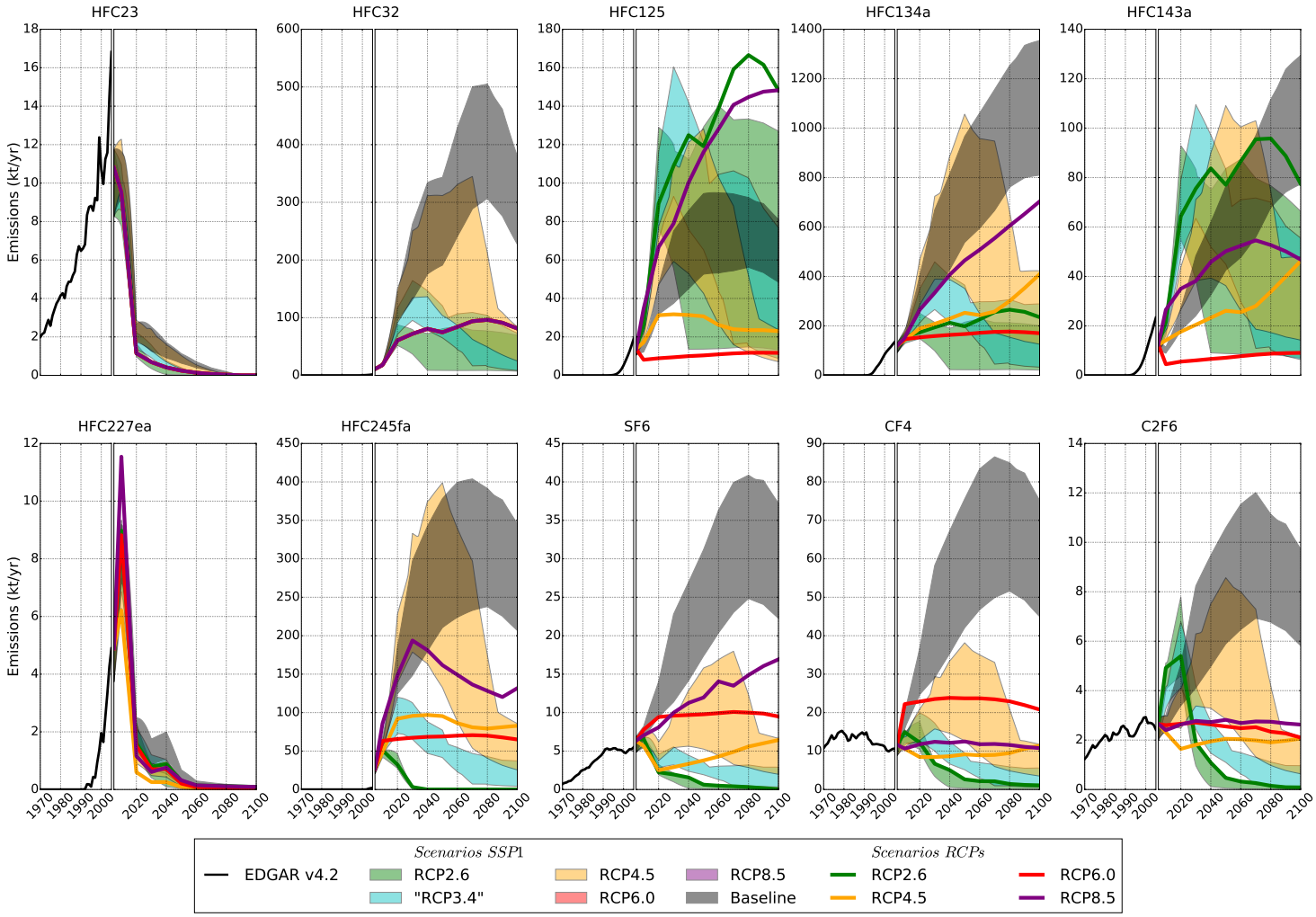

Figure 6.1: *Decomposition of the emissions of the category Fluorinated gases of the SSP scenarios illustrated with* ***SSP1*** *(section 3.2.2). For comparison, the emissions over 1970-2005 are given, prescribed by EDGAR v4.2 (Joint Research Centre (2011)). We also represent for comparison the emissions from RCPs (Meinshausen et al. (2011b)). The color of lines corresponds either to the RCP targeted in the SSP scenarios (shaded areas), or to the RCP itself (plain lines). Similar figures for the other SSPs are given in appendix.*

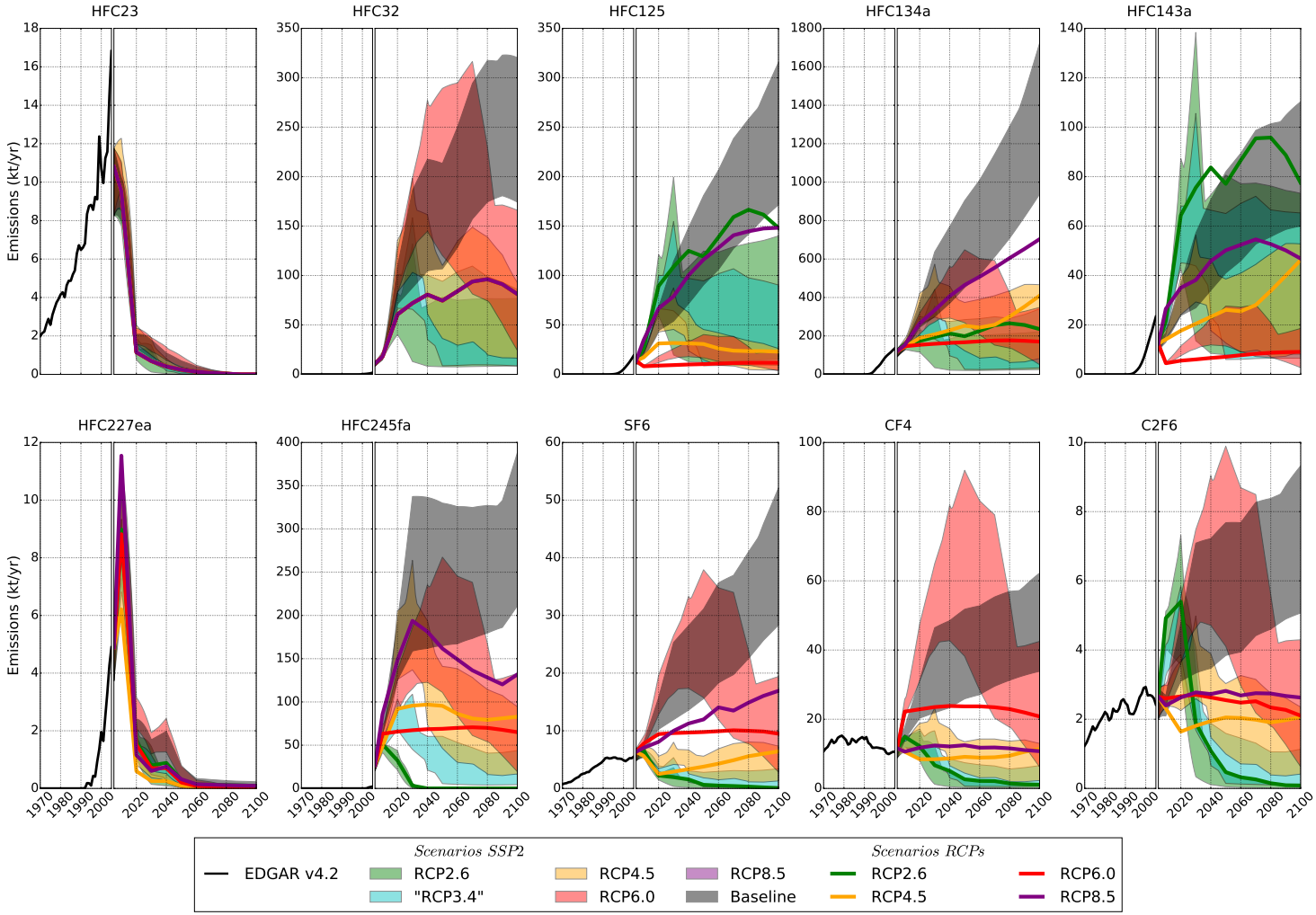

Figure 6.2: *Decomposition of the emissions of the category Fluorinated gases of the SSP scenarios illustrated with* ***SSP2*** *(section 3.2.2). For comparison, the emissions over 1970-2005 are given, prescribed by EDGAR v4.2 (Joint Research Centre (2011)). We also represent for comparison the emissions from RCPs (Meinshausen et al. (2011b)). The color of lines corresponds either to the RCP targeted in the SSP scenarios (shaded areas), or to the RCP itself (plain lines). Similar figures for the other SSPs are given in appendix.*

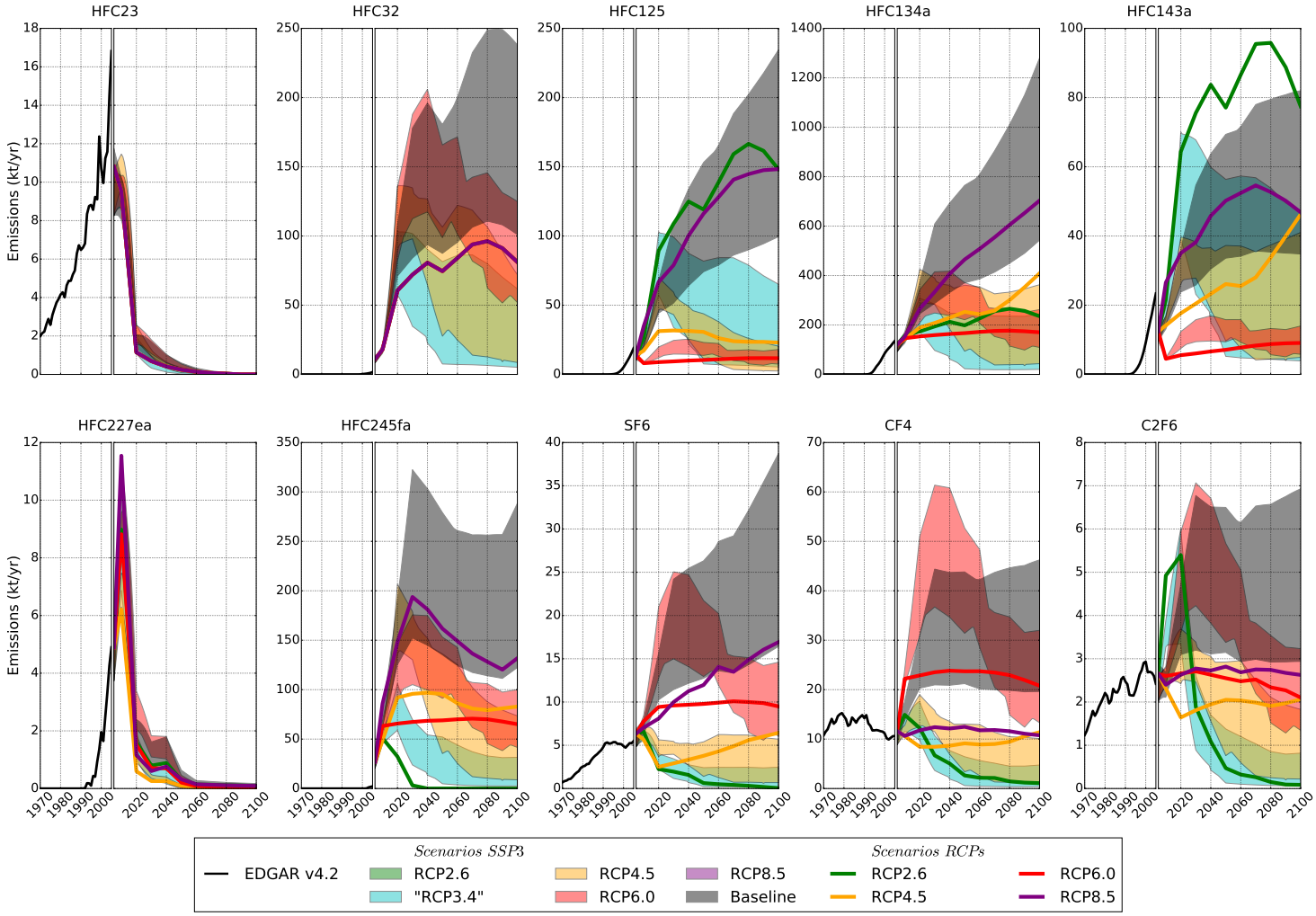

Figure 6.3: *Decomposition of the emissions of the category Fluorinated gases of the SSP scenarios illustrated with* ***SSP3*** *(section 3.2.2). For comparison, the emissions over 1970-2005 are given, prescribed by EDGAR v4.2 (Joint Research Centre (2011)). We also represent for comparison the emissions from RCPs (Meinshausen et al. (2011b)). The color of lines corresponds either to the RCP targeted in the SSP scenarios (shaded areas), or to the RCP itself (plain lines). Similar figures for the other SSPs are given in appendix.*

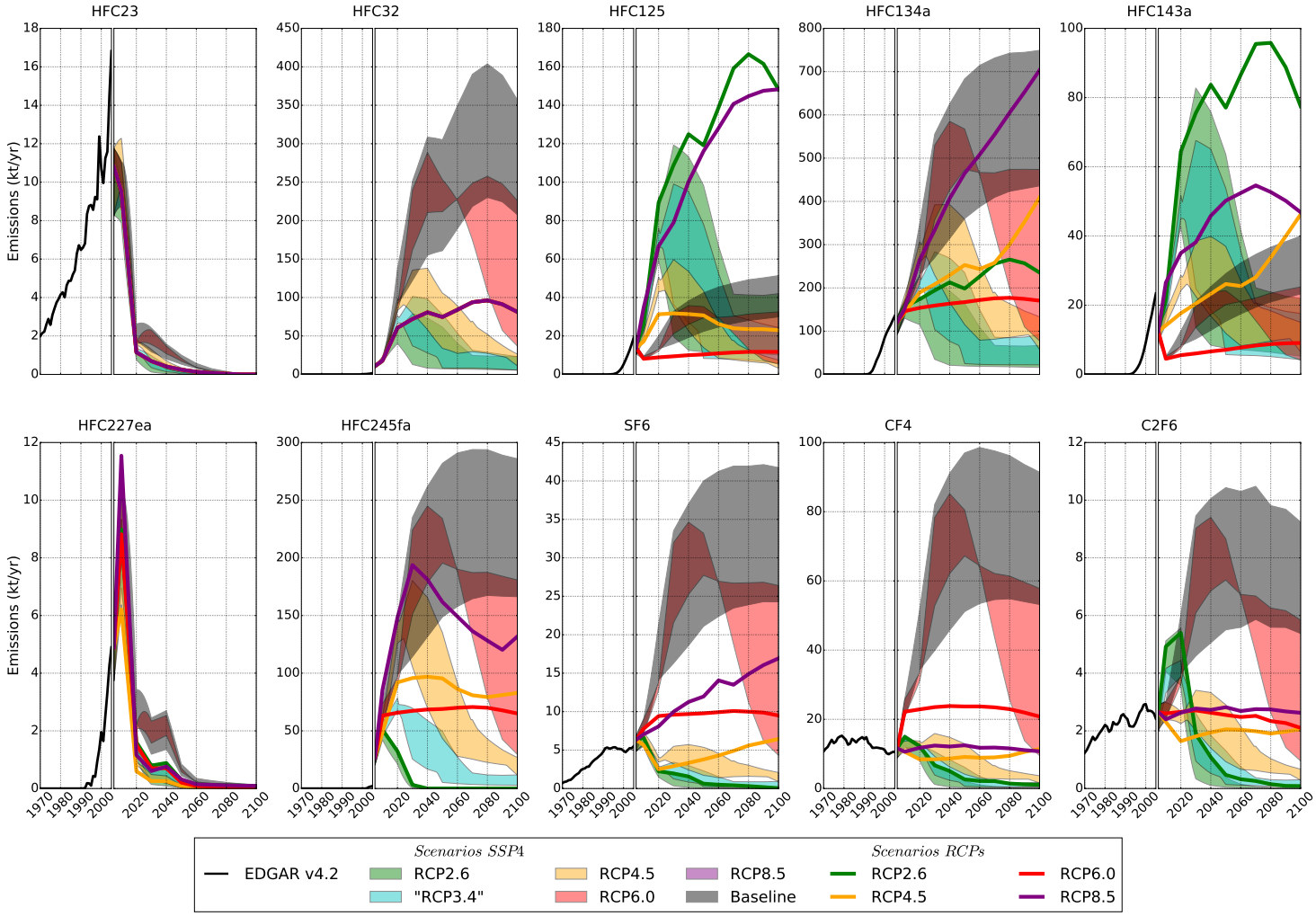

Figure 6.4: *Decomposition of the emissions of the category Fluorinated gases of the SSP scenarios illustrated with* ***SSP4*** *(section 3.2.2). For comparison, the emissions over 1970-2005 are given, prescribed by EDGAR v4.2 (Joint Research Centre (2011)). We also represent for comparison the emissions from RCPs (Meinshausen et al. (2011b)). The color of lines corresponds either to the RCP targeted in the SSP scenarios (shaded areas), or to the RCP itself (plain lines). Similar figures for the other SSPs are given in appendix.*

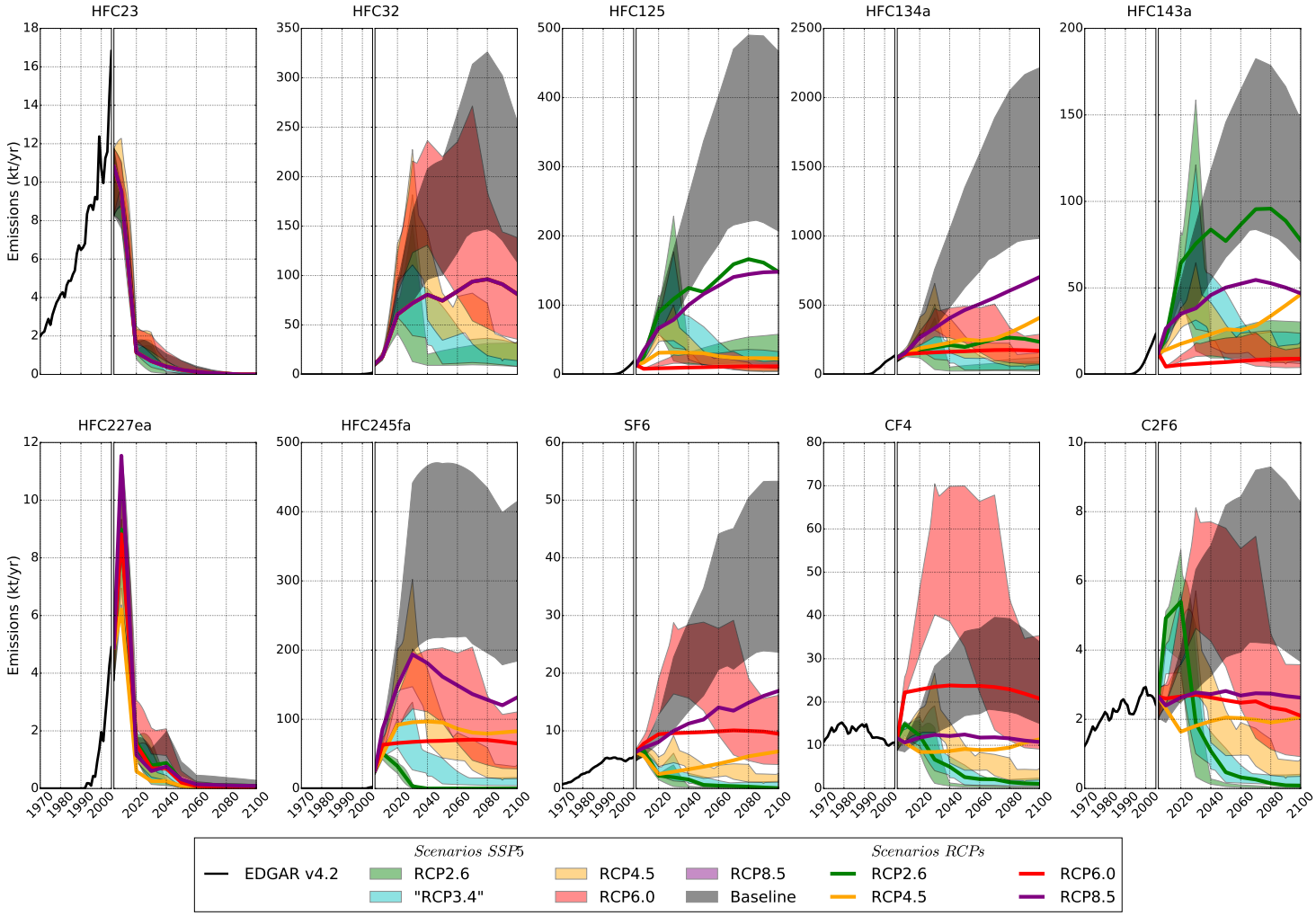

Figure 6.5: *Decomposition of the emissions of the category Fluorinated gases of the SSP scenarios illustrated with* ***SSP5*** *(section 3.2.2). For comparison, the emissions over 1970-2005 are given, prescribed by EDGAR v4.2 (Joint Research Centre (2011)). We also represent for comparison the emissions from RCPs (Meinshausen et al. (2011b)). The color of lines corresponds either to the RCP targeted in the SSP scenarios (shaded areas), or to the RCP itself (plain lines). Similar figures for the other SSPs are given in appendix.*

6.2.3 Figures for the land cover

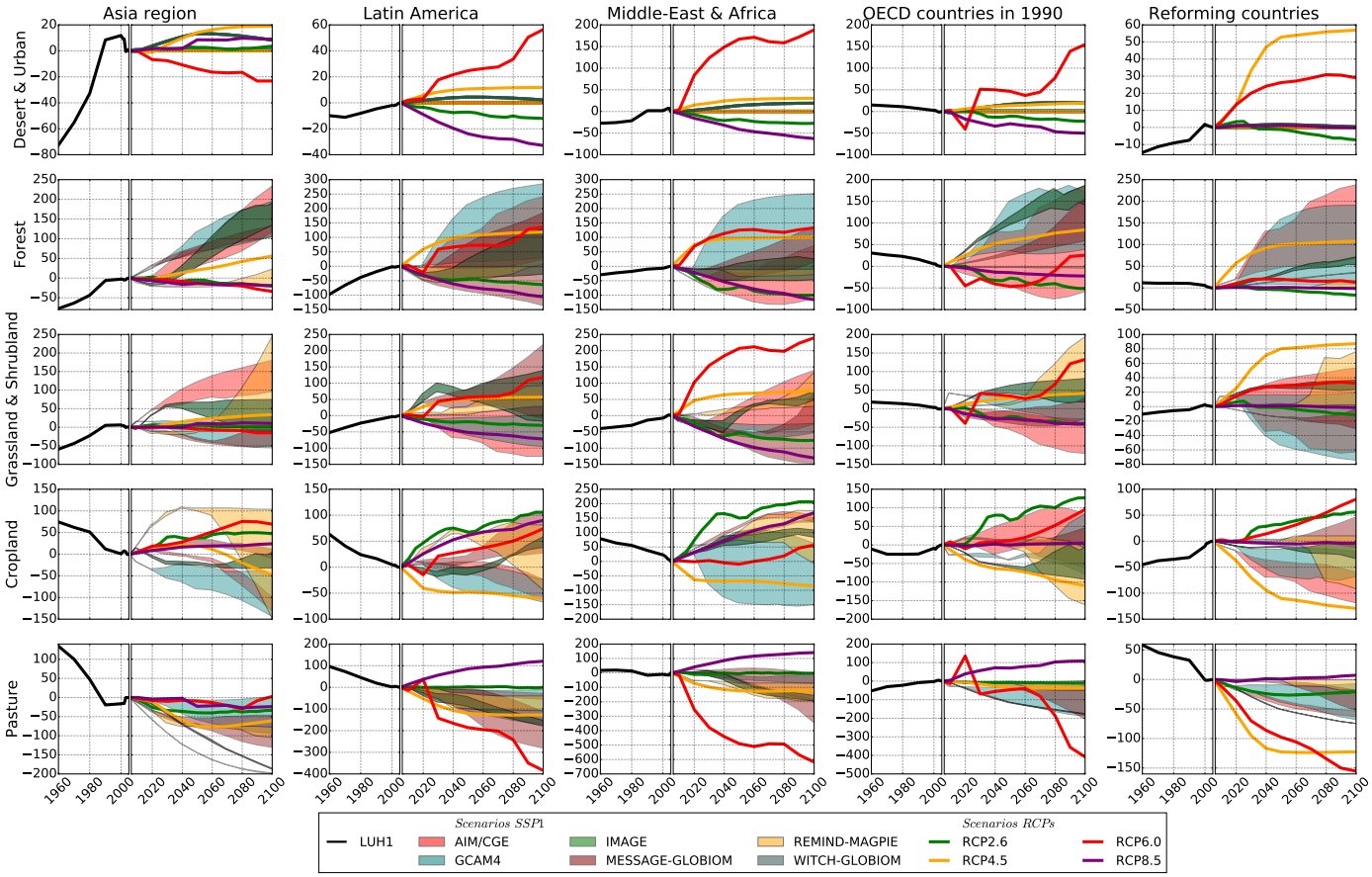

Figure 6.6: *Change in land cover (Mha) with reference to 2005 for the SSP scenarios under storyline* ***SSP1*** *over 2005-2100 (section 3.2.3.2). The land cover for 1960-2010 and for RCPs scenarios are shown for comparison, prescribed by the Land Use Harmonization dataset v1.1 (Hurtt et al. (2011)). For the SSP scenarios (shaded areas), the color corresponds to the IAM that has produced the corresponding scenario. For the RCPs scenarios (plain lines), similar colors may be used if and only if the IAM used to produce the RCP is the same: IMAGE has been used for RCP2.6, MiniCAM (now GCAM4) for RCP4.5, AIM for RCP6.0 and MESSAGE for RCP8.5 (IIASA (2018b)).*

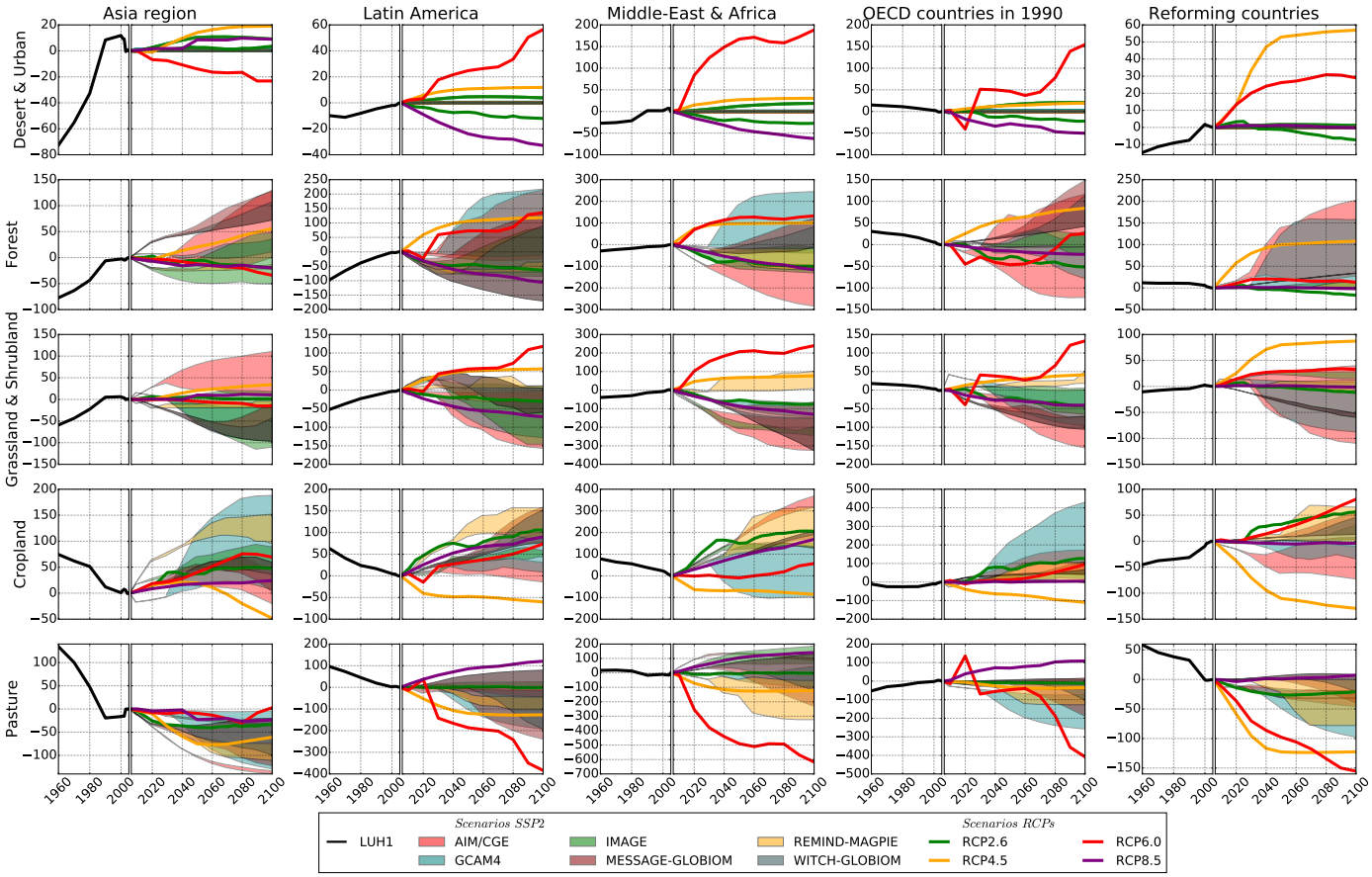

Figure 6.7: *Change in land cover (Mha) with reference to 2005 for the SSP scenarios under storyline* ***SSP2*** *over 2005-2100 (section 3.2.3.2). The land cover for 1960-2010 and for RCPs scenarios are shown for comparison, prescribed by the Land Use Harmonization dataset v1.1 (Hurtt et al. (2011)). For the SSP scenarios (shaded areas), the color corresponds to the IAM that has produced the corresponding scenario. For the RCPs scenarios (plain lines), similar colors may be used if and only if the IAM used to produce the RCP is the same: IMAGE has been used for RCP2.6, MiniCAM (now GCAM4) for RCP4.5, AIM for RCP6.0 and MESSAGE for RCP8.5 (IIASA (2018b)).*

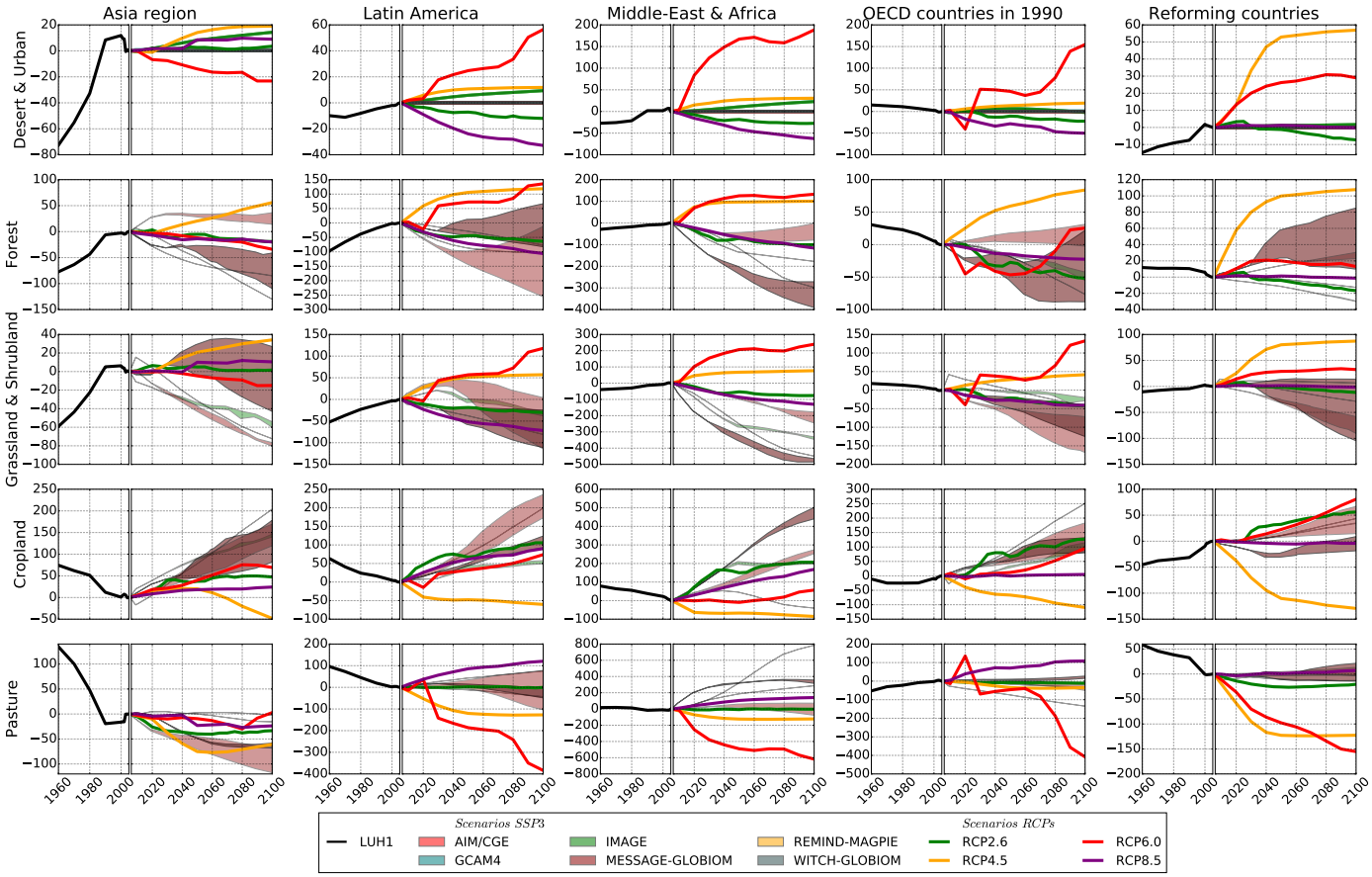

Figure 6.8: *Change in land cover (Mha) with reference to 2005 for the SSP scenarios under storyline* ***SSP3*** *over 2005-2100 (section 3.2.3.2). The land cover for 1960-2010 and for RCPs scenarios are shown for comparison, prescribed by the Land Use Harmonization dataset v1.1 (Hurtt et al. (2011)). For the SSP scenarios (shaded areas), the color corresponds to the IAM that has produced the corresponding scenario. For the RCPs scenarios (plain lines), similar colors may be used if and only if the IAM used to produce the RCP is the same: IMAGE has been used for RCP2.6, MiniCAM (now GCAM4) for RCP4.5, AIM for RCP6.0 and MESSAGE for RCP8.5 (IIASA (2018b)).*

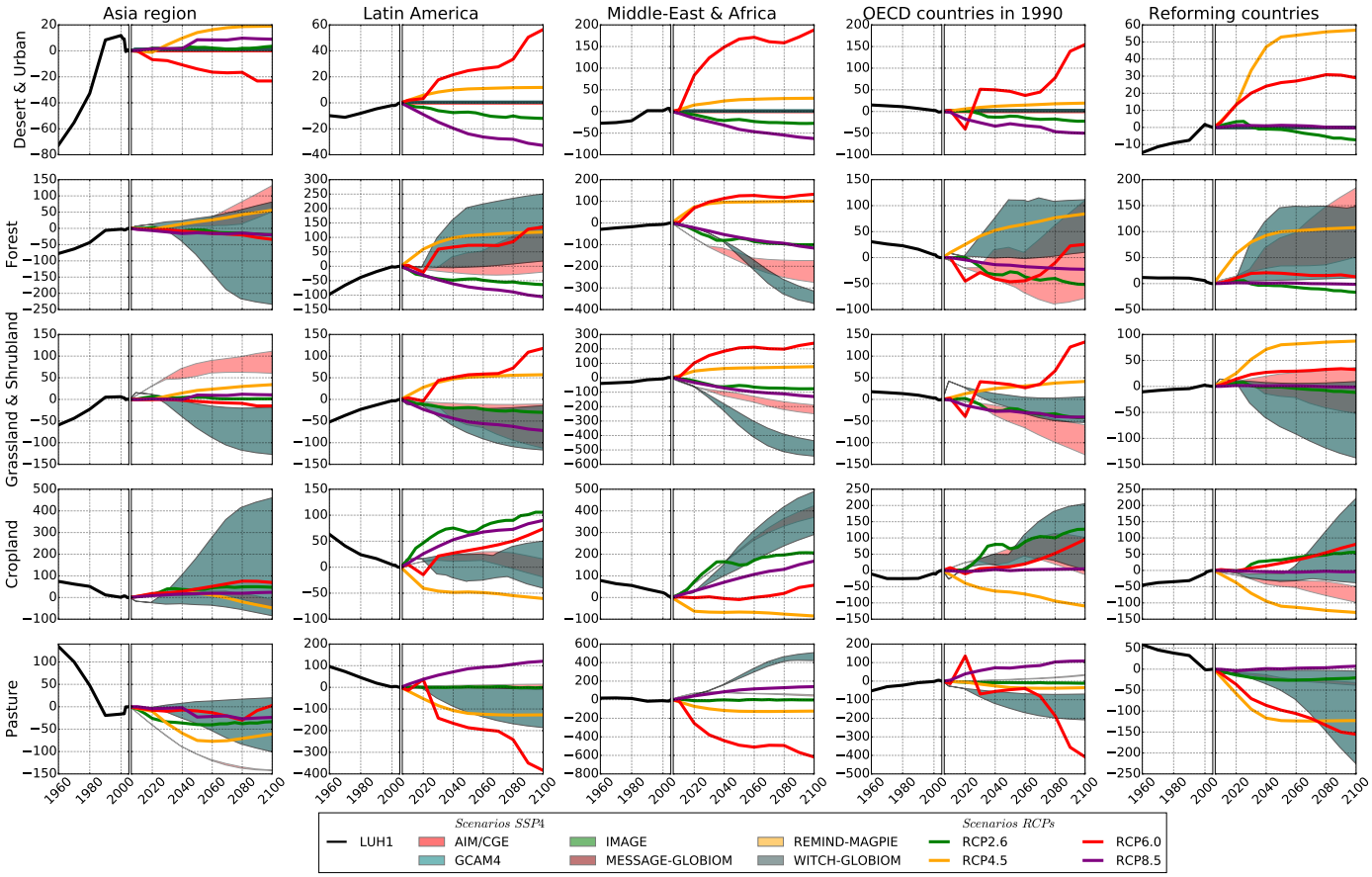

Figure 6.9: *Change in land cover (Mha) with reference to 2005 for the SSP scenarios under storyline* ***SSP4*** *over 2005-2100 (section 3.2.3.2). The land cover for 1960-2010 and for RCPs scenarios are shown for comparison, prescribed by the Land Use Harmonization dataset v1.1 (Hurtt et al. (2011)). For the SSP scenarios (shaded areas), the color corresponds to the IAM that has produced the corresponding scenario. For the RCPs scenarios (plain lines), similar colors may be used if and only if the IAM used to produce the RCP is the same: IMAGE has been used for RCP2.6, MiniCAM (now GCAM4) for RCP4.5, AIM for RCP6.0 and MESSAGE for RCP8.5 (IIASA (2018b)).*

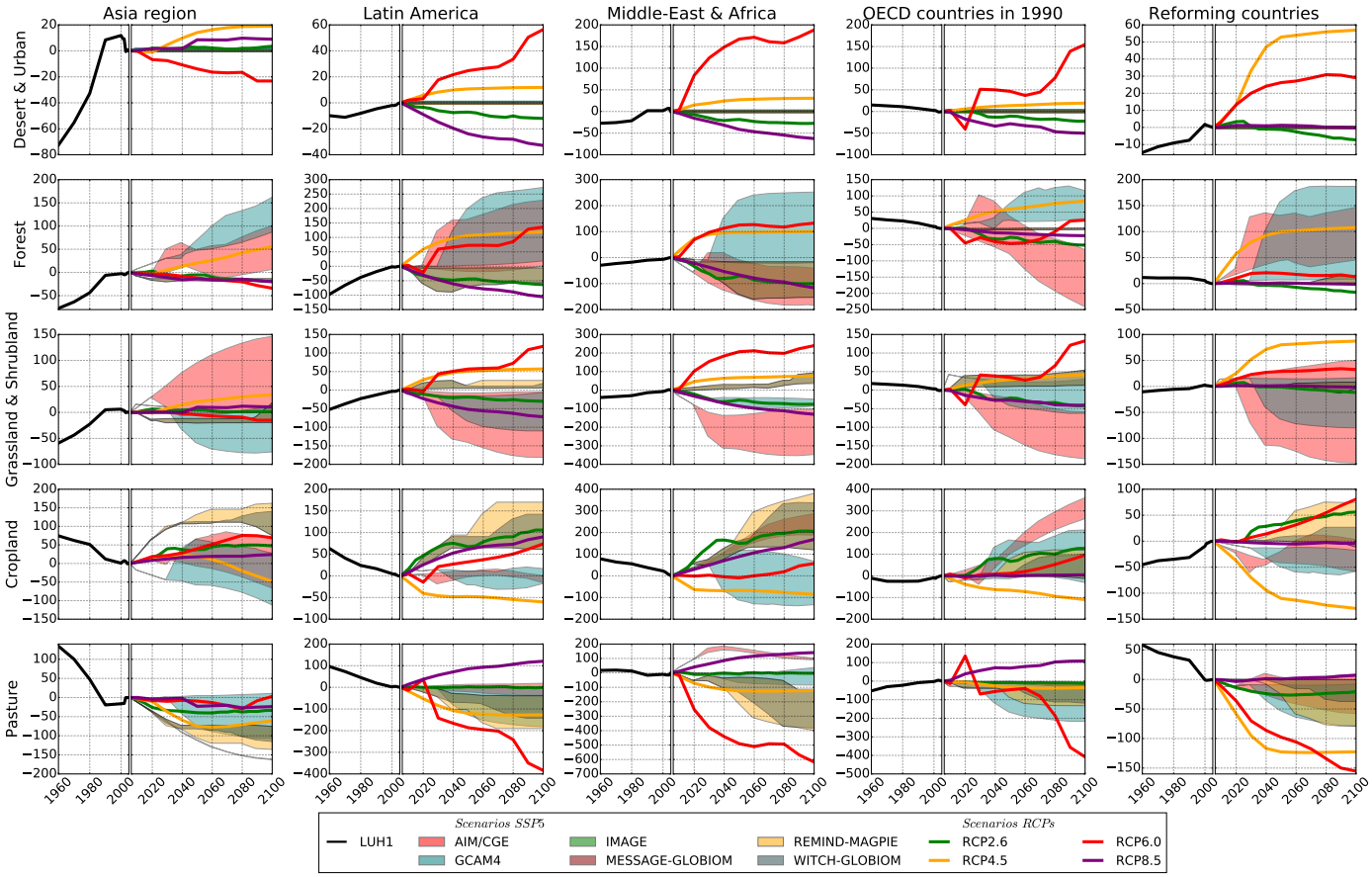

Figure 6.10: *Change in land cover (Mha) with reference to 2005 for the SSP scenarios under storyline* ***SSP5*** *over 2005-2100 (section 3.2.3.2). The land cover for 1960-2010 and for RCPs scenarios are shown for comparison, prescribed by the Land Use Harmonization dataset v1.1 (Hurtt et al. (2011)). For the SSP scenarios (plain lines), the color corresponds to the IAM that has produced the corresponding scenario. For the RCPs scenarios (dashed lines), similar colors may be used if and only if the IAM used to produce the RCP is the same: IMAGE has been used for RCP2.6, MiniCAM (now GCAM4) for RCP4.5, AIM for RCP6.0 and MESSAGE for RCP8.5 (IIASA (2018b)).*

6.2.4 Figures for the land use changes

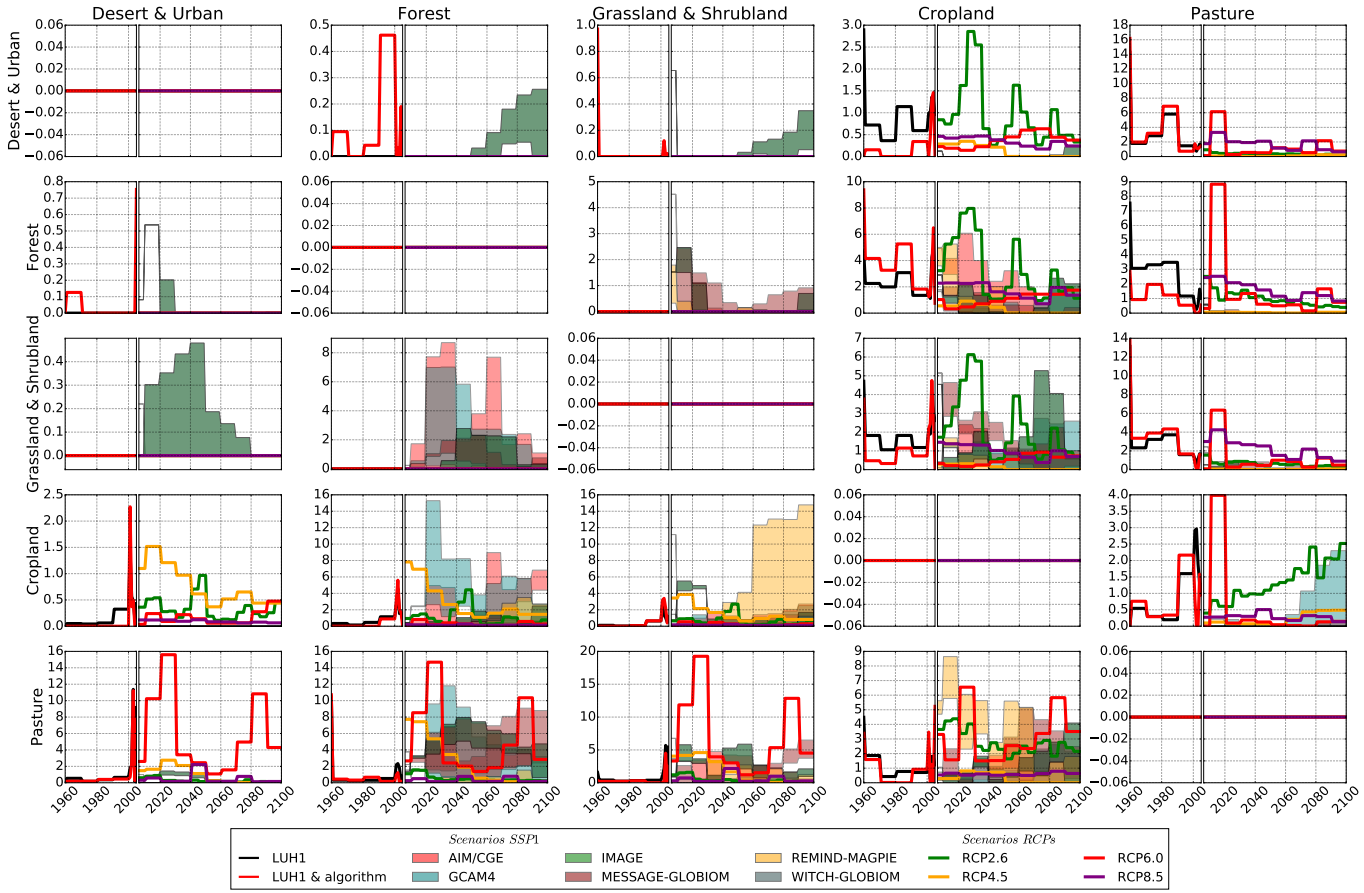

Figure 6.11: *Global annual net land use transitions (Mha/yr) for the SSP scenarios under the storyline* ***SSP1*** *over 2005-2100, and for all RCPs (section 3.2.3.2). The land use changes for 1960-2010 and for RCPs scenarios are shown for comparison, prescribed by the Land Use Harmonization dataset v1.1 (Hurtt et al. (2011)). For comparison, the reconstruction of the net transitions from LUH1 are done using its land cover changes and the algorithm from Stocker et al. (2014) (red plain line), for comparison with the original transitions of LUH1 (black plain lines). For the SSP scenarios (plain lines), the color corresponds to the IAM that has produced the corresponding scenario. For the RCPs scenarios (dashed lines), similar colors may be used if and only if the IAM used to produce the RCP is the same: IMAGE has been used for RCP2.6, MiniCAM (now GCAM4) for RCP4.5, AIM for RCP6.0 and MESSAGE for RCP8.5 (IIASA (2018b)).*

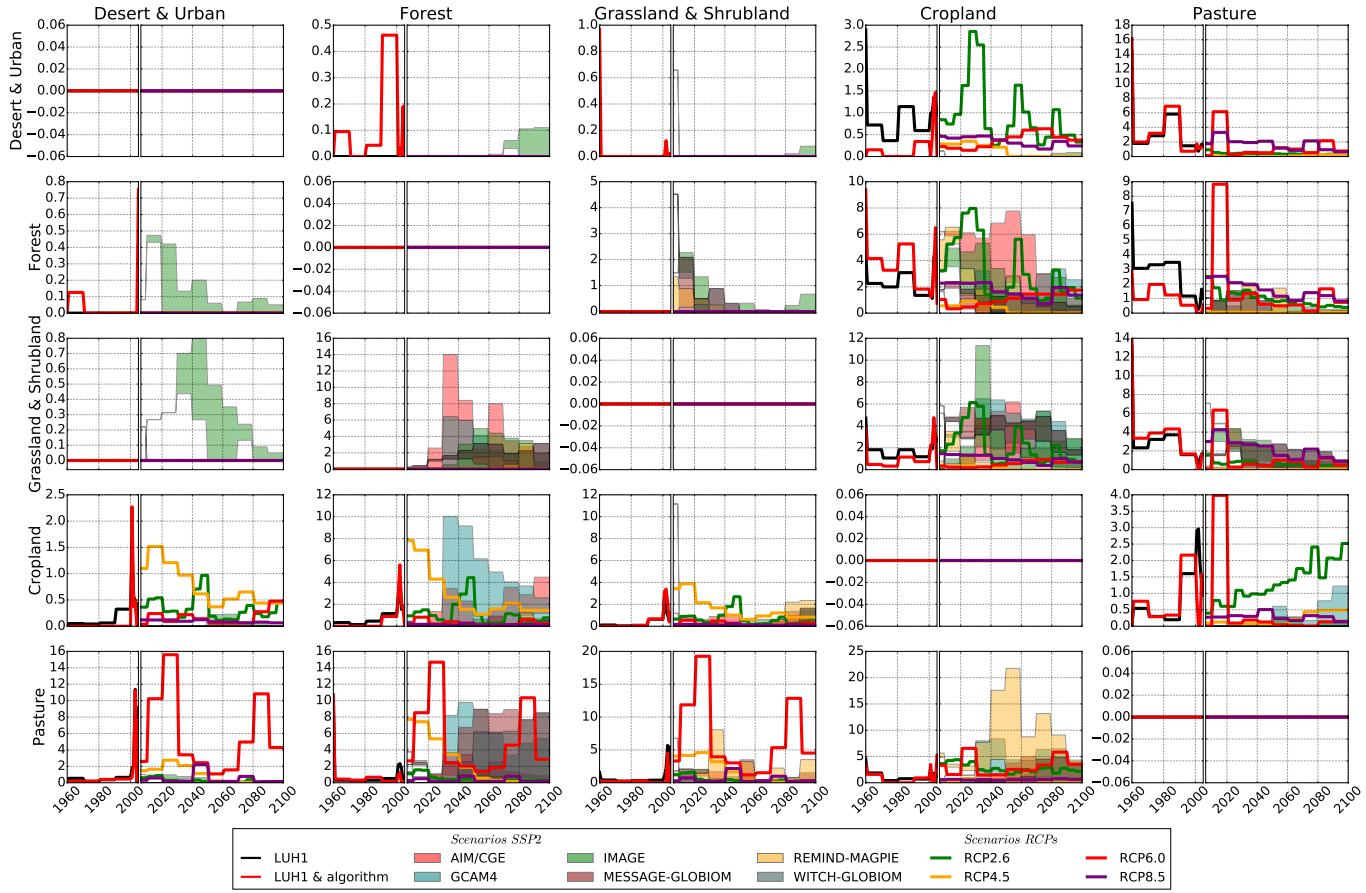

Figure 6.12: *Global annual net land use transitions (Mha/yr) for the SSP scenarios under the storyline* ***SSP2*** *over 2005-2100, and for all RCPs (section 3.2.3.2). The land use changes for 1960-2010 and for RCPs scenarios are shown for comparison, prescribed by the Land Use Harmonization dataset v1.1 (Hurtt et al. (2011)). For comparison, the reconstruction of the net transitions from LUH1 are done using its land cover changes and the algorithm from Stocker et al. (2014) (red plain line), for comparison with the original transitions of LUH1 (black plain lines). For the SSP scenarios (plain lines), the color corresponds to the IAM that has produced the corresponding scenario. For the RCPs scenarios (dashed lines), similar colors may be used if and only if the IAM used to produce the RCP is the same: IMAGE has been used for RCP2.6, MiniCAM (now GCAM4) for RCP4.5, AIM for RCP6.0 and MESSAGE for RCP8.5 (IIASA (2018b)).*

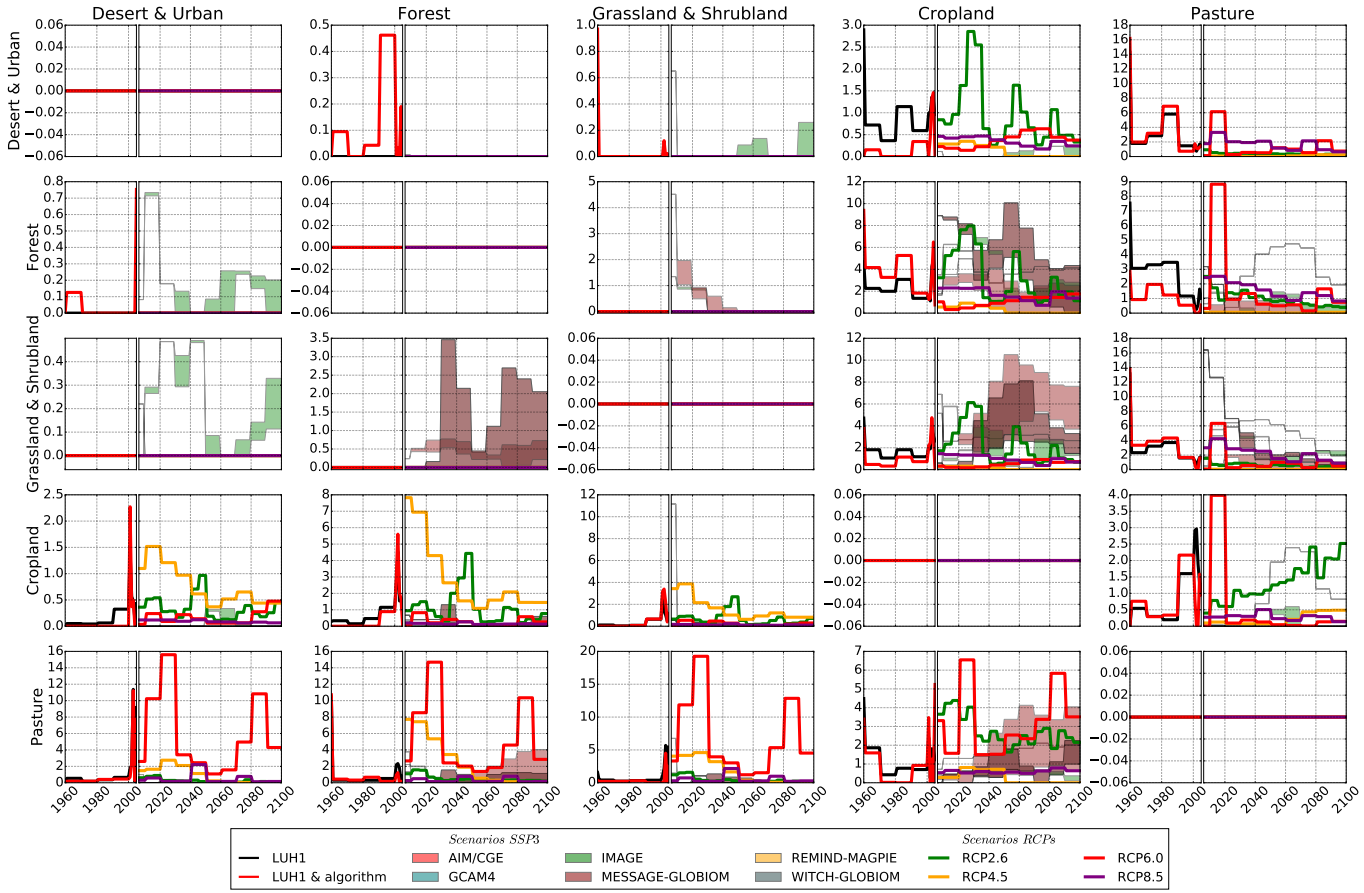

Figure 6.13: *Global annual net land use transitions (Mha/yr) for the SSP scenarios under the storyline* ***SSP3*** *over 2005-2100, and for all RCPs (section 3.2.3.2). The land use changes for 1960-2010 and for RCPs scenarios are shown for comparison, prescribed by the Land Use Harmonization dataset v1.1 (Hurtt et al. (2011)). For comparison, the reconstruction of the net transitions from LUH1 are done using its land cover changes and the algorithm from Stocker et al. (2014) (red plain line), for comparison with the original transitions of LUH1 (black plain lines). For the SSP scenarios (plain lines), the color corresponds to the IAM that has produced the corresponding scenario. For the RCPs scenarios (dashed lines), similar colors may be used if and only if the IAM used to produce the RCP is the same: IMAGE has been used for RCP2.6, MiniCAM (now GCAM4) for RCP4.5, AIM for RCP6.0 and MESSAGE for RCP8.5 (IIASA (2018b)).*

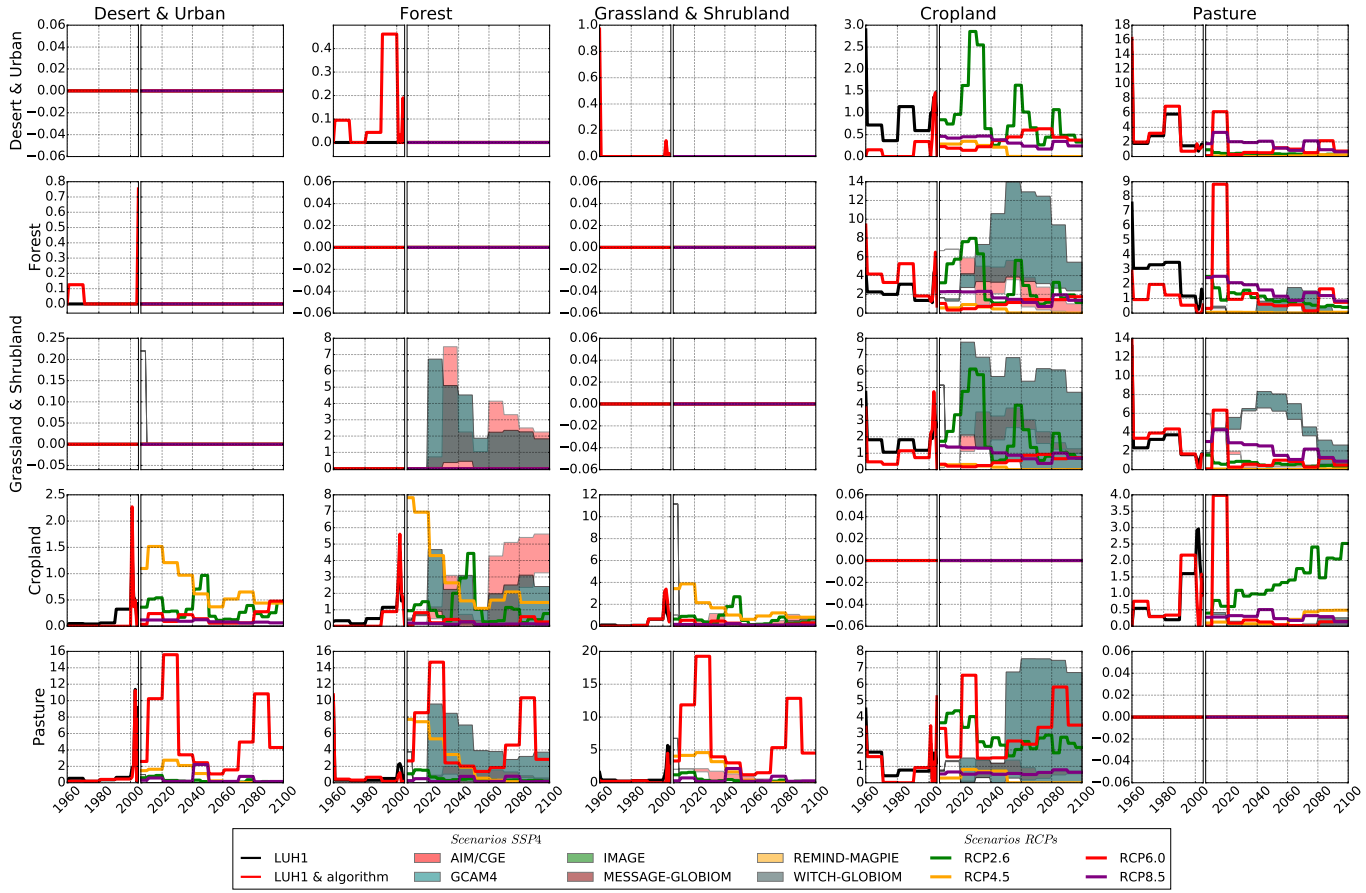

Figure 6.14: *Global annual net land use transitions (Mha/yr) for the SSP scenarios under the storyline* ***SSP4*** *over 2005-2100, and for all RCPs (section 3.2.3.2). The land use changes for 1960-2010 and for RCPs scenarios are shown for comparison, prescribed by the Land Use Harmonization dataset v1.1 (Hurtt et al. (2011)). For comparison, the reconstruction of the net transitions from LUH1 are done using its land cover changes and the algorithm from Stocker et al. (2014) (red plain line), for comparison with the original transitions of LUH1 (black plain lines). For the SSP scenarios (plain lines), the color corresponds to the IAM that has produced the corresponding scenario. For the RCPs scenarios (dashed lines), similar colors may be used if and only if the IAM used to produce the RCP is the same: IMAGE has been used for RCP2.6, MiniCAM (now GCAM4) for RCP4.5, AIM for RCP6.0 and MESSAGE for RCP8.5 (IIASA (2018b)).*

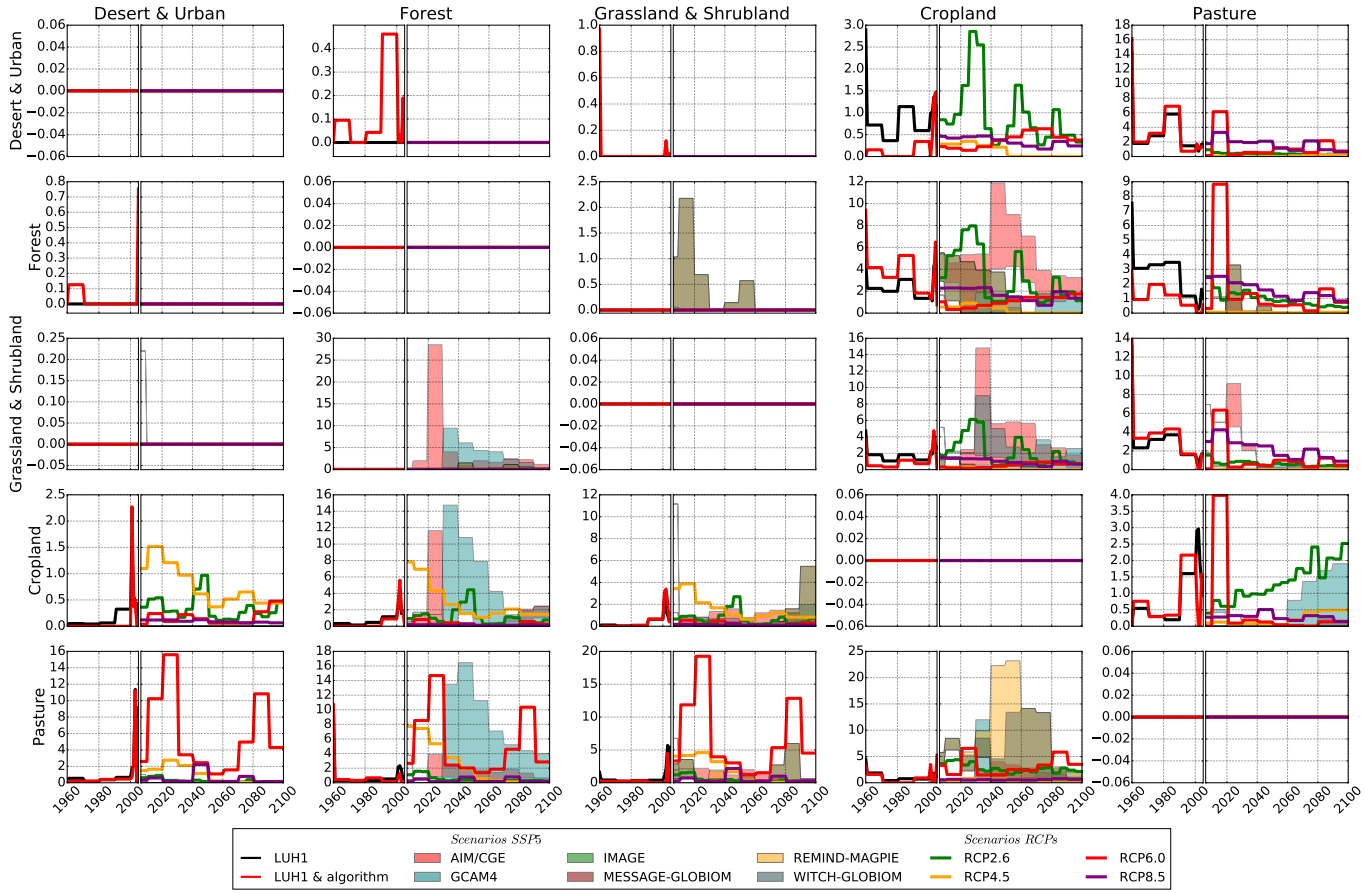

Figure 6.15: *Global annual net land use transitions (Mha/yr) for the SSP scenarios under the storyline* ***SSP5*** *over 2005-2100, and for all RCPs (section 3.2.3.2). The land use changes for 1960-2010 and for RCPs scenarios are shown for comparison, prescribed by the Land Use Harmonization dataset v1.1 (Hurtt et al. (2011)). For comparison, the reconstruction of the net transitions from LUH1 are done using its land cover changes and the algorithm from Stocker et al. (2014) (red plain line), for comparison with the original transitions of LUH1 (black plain lines). For the SSP scenarios (plain lines), the color corresponds to the IAM that has produced the corresponding scenario. For the RCPs scenarios (dashed lines), similar colors may be used if and only if the IAM used to produce the RCP is the same: IMAGE has been used for RCP2.6, MiniCAM (now GCAM4) for RCP4.5, AIM for RCP6.0 and MESSAGE for RCP8.5 (IIASA (2018b)).*

6.2.5 Figures for harvested biomass

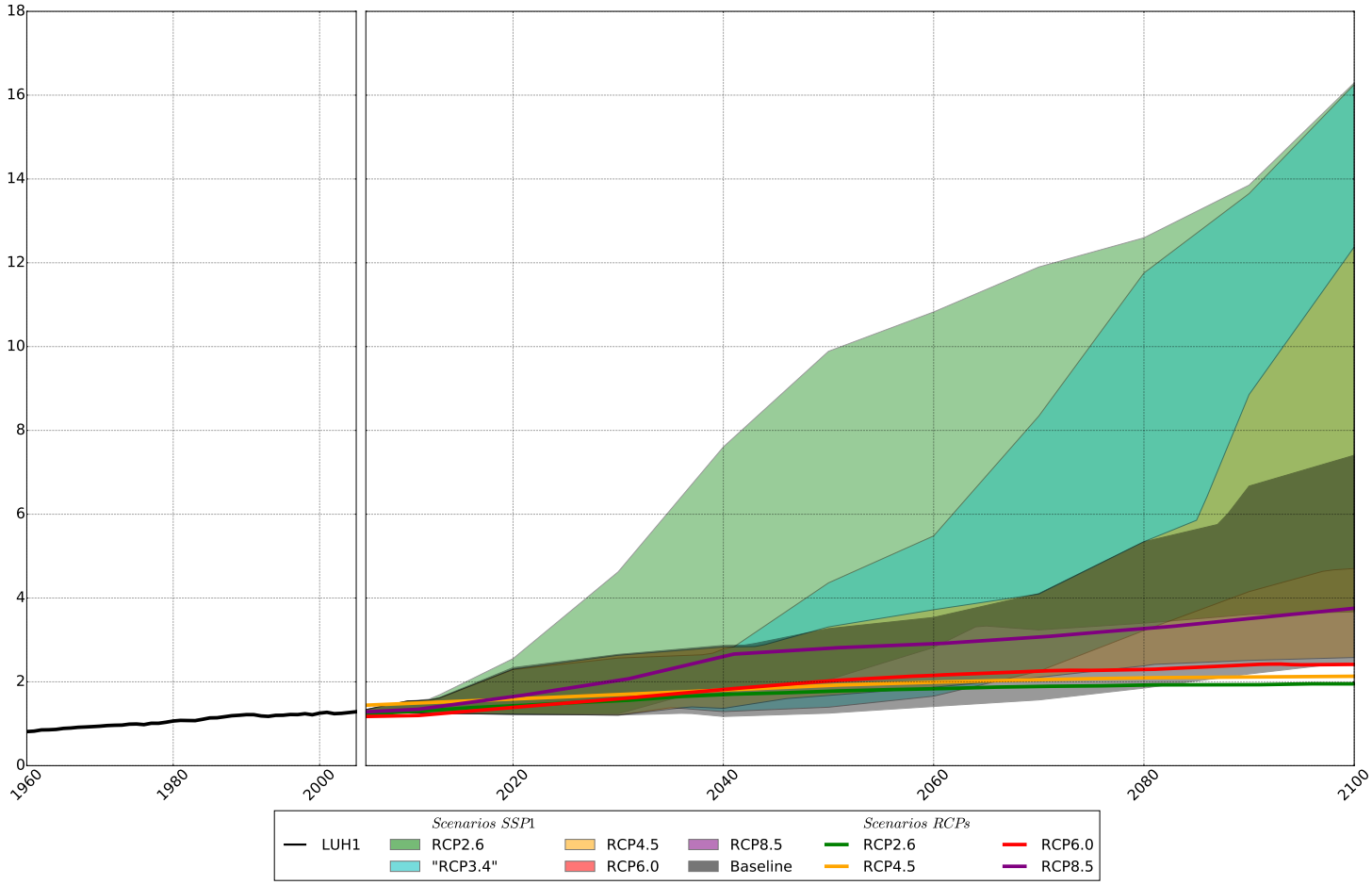

Figure 6.16: *Annual harvested biomass (**GtC/yr**) for the SSP scenarios under the storyline SSP1 over 2005-2100, summed over all regions and all biomes. The detail for all SSP scenarios can be found in appendix (section 6.2.5). The harvested biomass for 1960-2010 and for RCPs scenarios are shown for comparison, prescribed by the Land Use Harmonization dataset v1.1 (Hurtt et al., 2011). For the SSP scenarios, each color corresponds to the realizations by the ensemble of IAMs for sthis RCP under this SSP. For the RCPs scenarios (plain lines), similar colors may be used if and only if the IAM used to produce the RCP is the same: IMAGE has been used for RCP2.6, MiniCAM (now GCAM4) for RCP4.5, AIM for RCP6.0 and MESSAGE for RCP8.5 (IIASA, 2018b).*

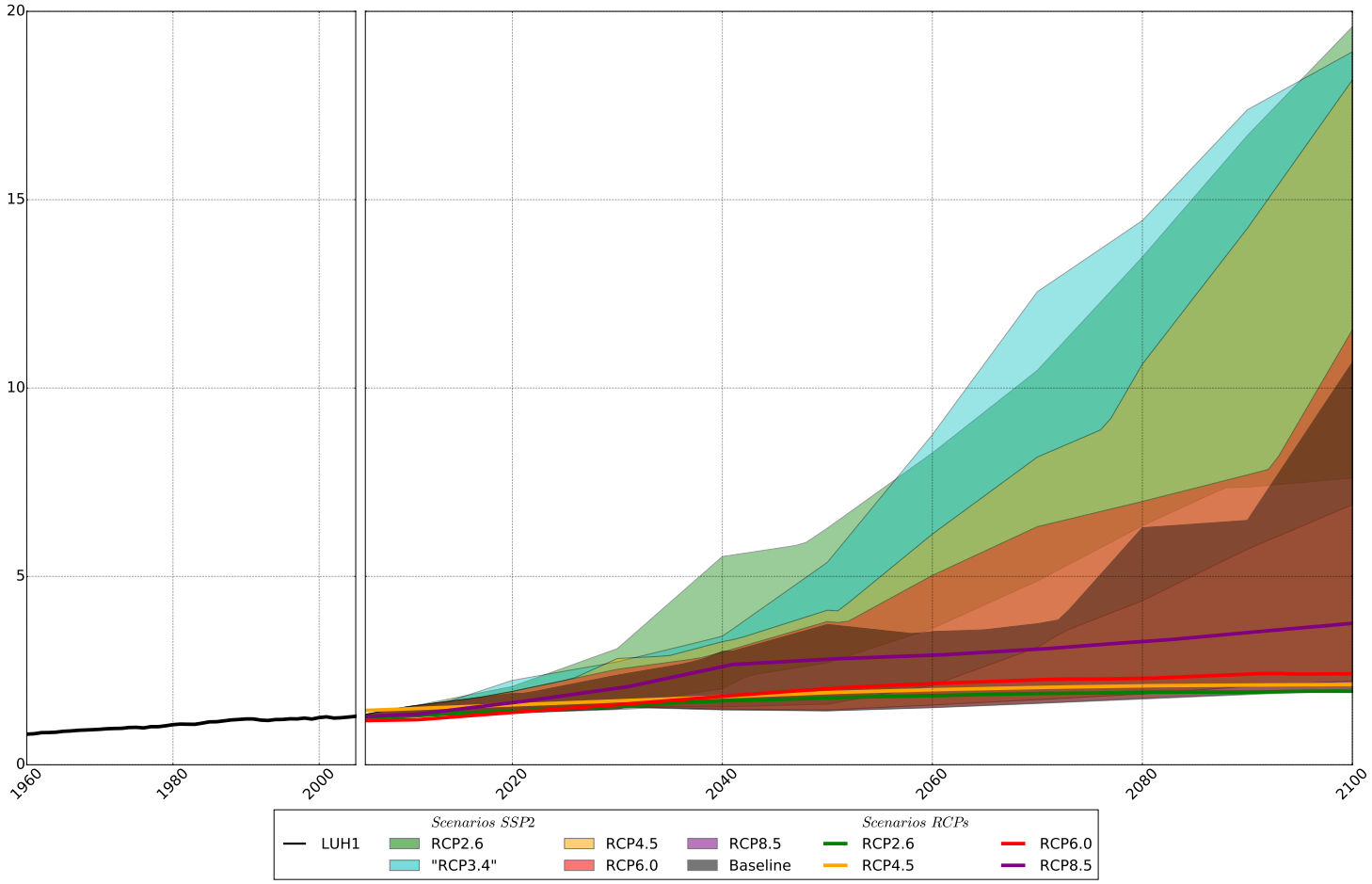

Figure 6.17: *Annual harvested biomass (**GtC/yr**) for the SSP scenarios under the storyline SSP2 over 2005-2100, summed over all regions and all biomes. The detail for all SSP scenarios can be found in appendix (section 6.2.5). The harvested biomass for 1960-2010 and for RCPs scenarios are shown for comparison, prescribed by the Land Use Harmonization dataset v1.1 (Hurtt et al., 2011). For the SSP scenarios, each color corresponds to the realizations by the ensemble of IAMs for sthis RCP under this SSP. For the RCPs scenarios (plain lines), similar colors may be used if and only if the IAM used to produce the RCP is the same: IMAGE has been used for RCP2.6, MiniCAM (now GCAM4) for RCP4.5, AIM for RCP6.0 and MESSAGE for RCP8.5 (IIASA, 2018b).*

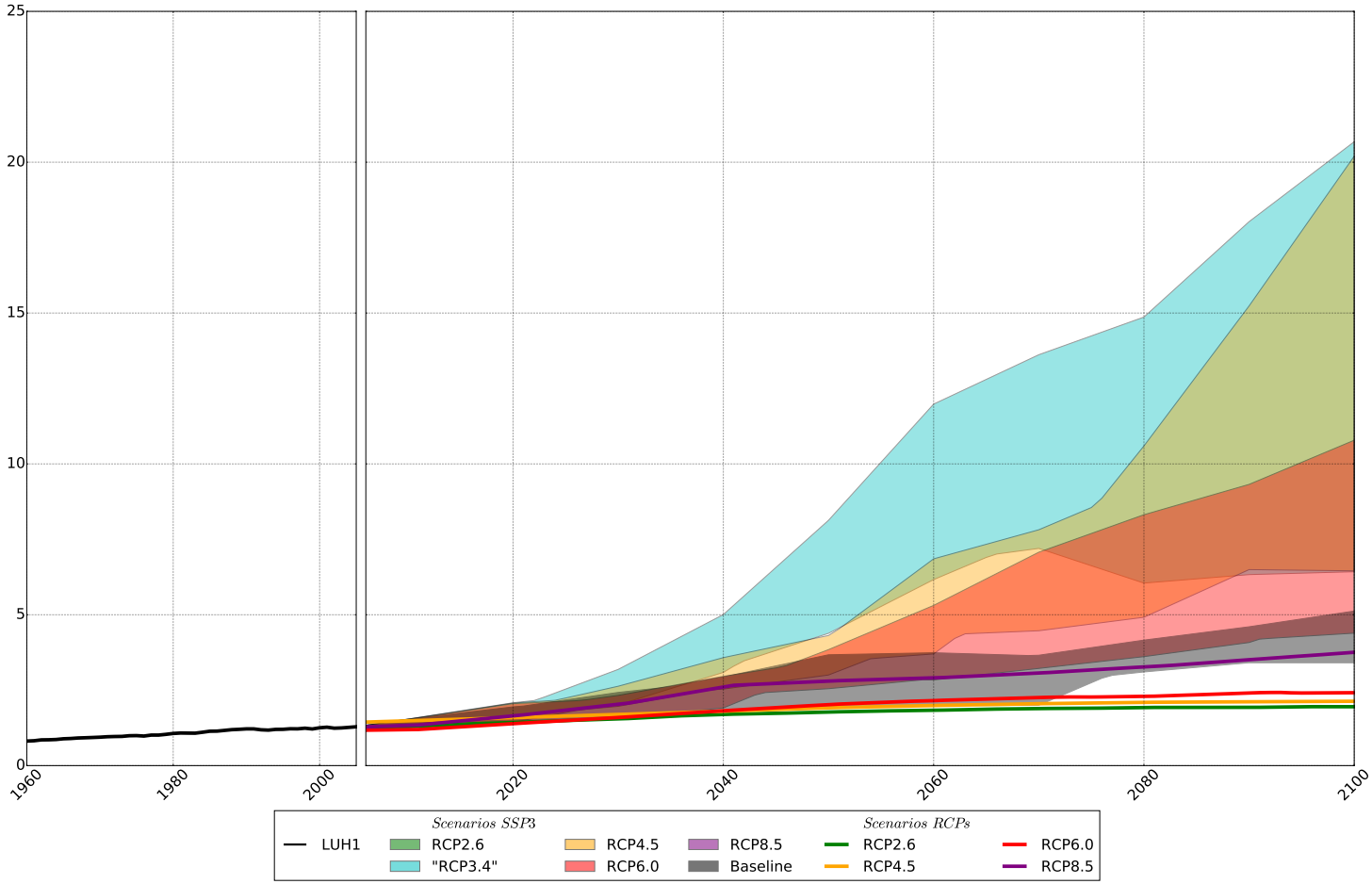

Figure 6.18: *Annual harvested biomass (**GtC/yr**) for the SSP scenarios under the storyline SSP3 over 2005-2100, summed over all regions and all biomes. The detail for all SSP scenarios can be found in appendix (section 6.2.5). The harvested biomass for 1960-2010 and for RCPs scenarios are shown for comparison, prescribed by the Land Use Harmonization dataset v1.1 (Hurtt et al., 2011). For the SSP scenarios, each color corresponds to the realizations by the ensemble of IAMs for sthis RCP under this SSP. For the RCPs scenarios (plain lines), similar colors may be used if and only if the IAM used to produce the RCP is the same: IMAGE has been used for RCP2.6, MiniCAM (now GCAM4) for RCP4.5, AIM for RCP6.0 and MESSAGE for RCP8.5 (IIASA, 2018b).*

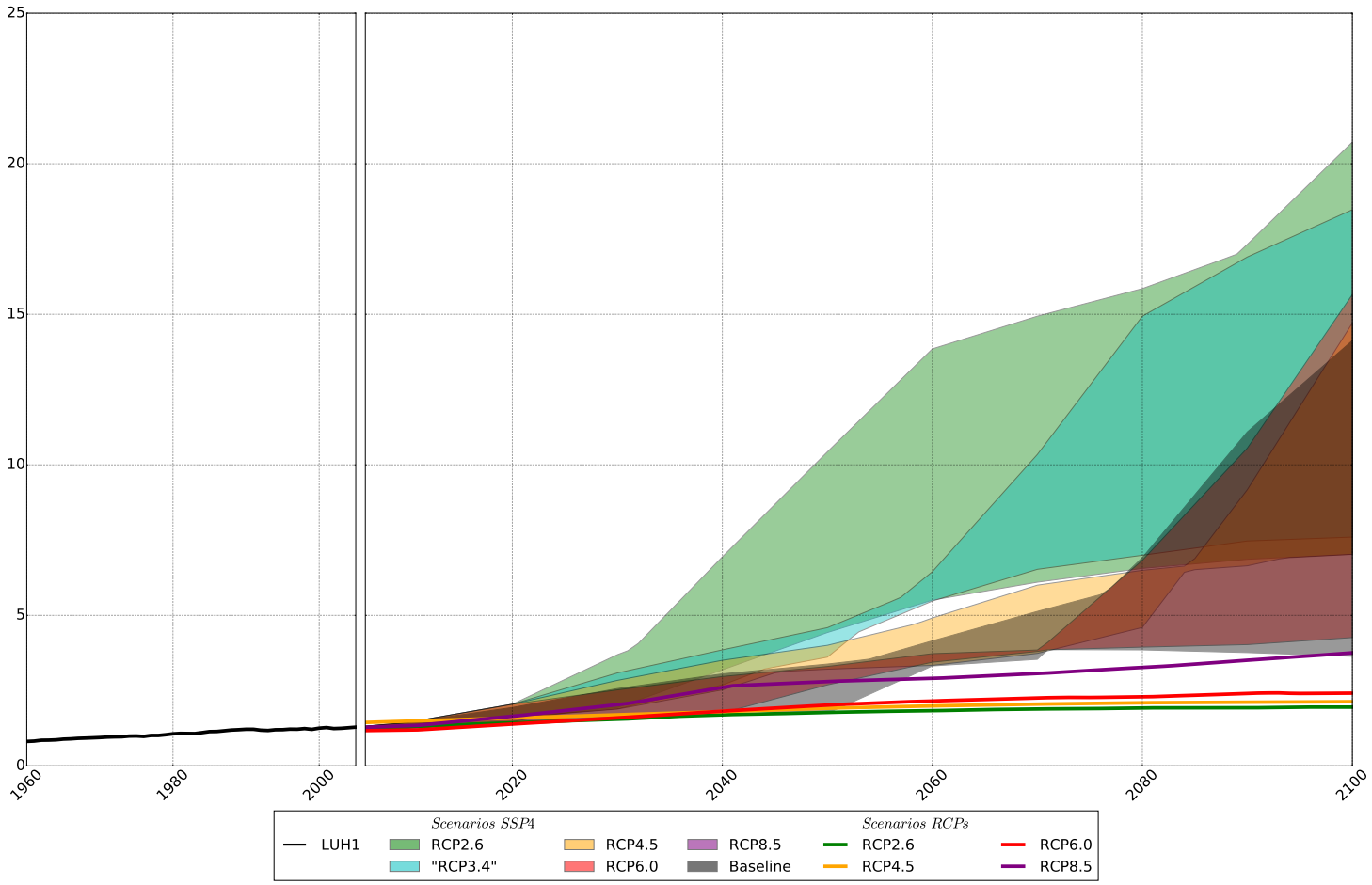

Figure 6.19: *Annual harvested biomass (**GtC/yr**) for the SSP scenarios under the storyline SSP4 over 2005-2100, summed over all regions and all biomes. The detail for all SSP scenarios can be found in appendix (section 6.2.5). The harvested biomass for 1960-2010 and for RCPs scenarios are shown for comparison, prescribed by the Land Use Harmonization dataset v1.1 (Hurtt et al., 2011). For the SSP scenarios, each color corresponds to the realizations by the ensemble of IAMs for sthis RCP under this SSP. For the RCPs scenarios (plain lines), similar colors may be used if and only if the IAM used to produce the RCP is the same: IMAGE has been used for RCP2.6, MiniCAM (now GCAM4) for RCP4.5, AIM for RCP6.0 and MESSAGE for RCP8.5 (IIASA, 2018b).*

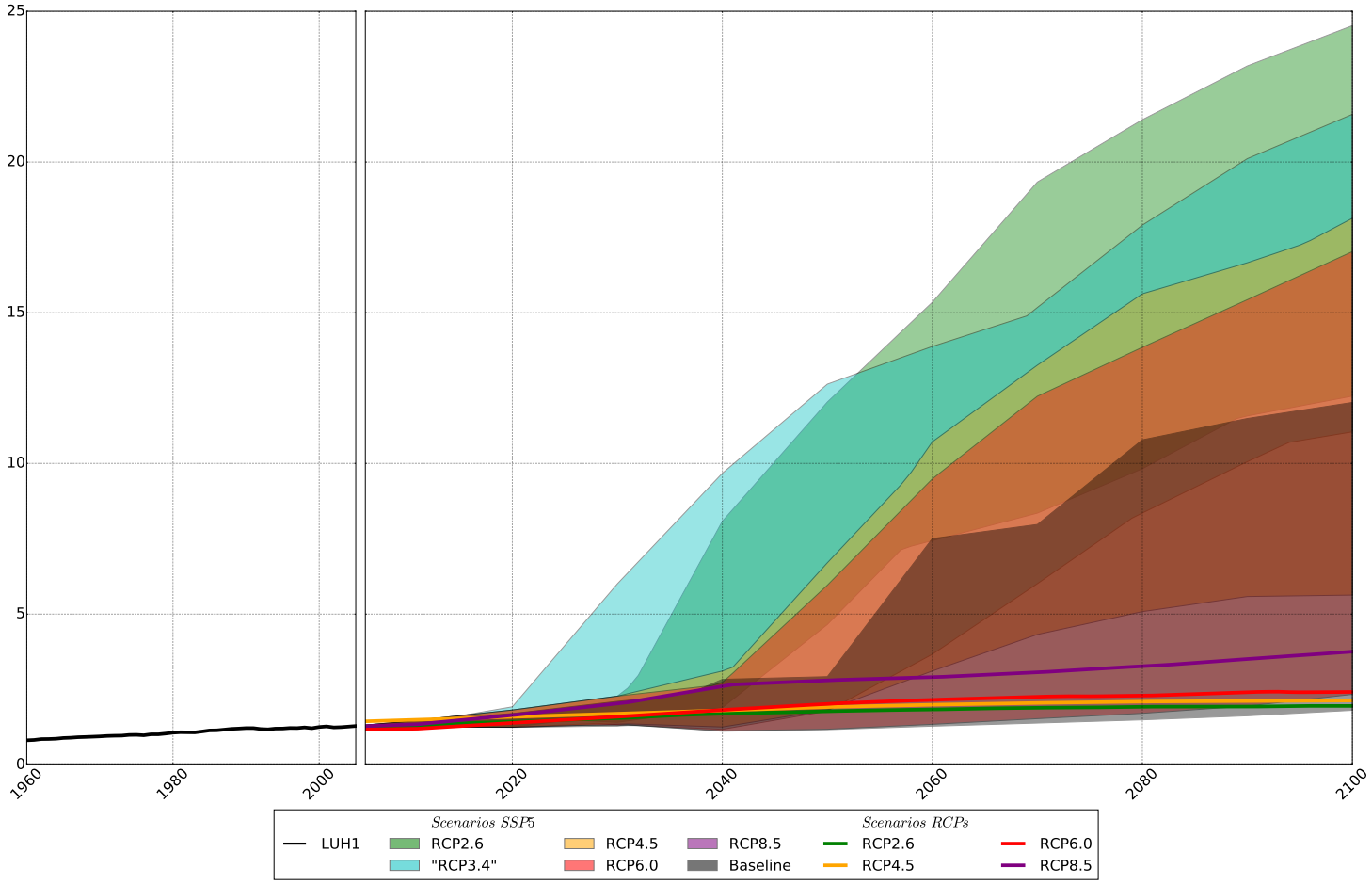

Figure 6.20: *Annual harvested biomass (**GtC/yr**) for the SSP scenarios under the storyline SSP5 over 2005-2100, summed over all regions and all biomes. The detail for all SSP scenarios can be found in appendix (section 6.2.5). The harvested biomass for 1960-2010 and for RCPs scenarios are shown for comparison, prescribed by the Land Use Harmonization dataset v1.1 (Hurtt et al., 2011). For the SSP scenarios, each color corresponds to the realizations by the ensemble of IAMs for sthis RCP under this SSP. For the RCPs scenarios (plain lines), similar colors may be used if and only if the IAM used to produce the RCP is the same: IMAGE has been used for RCP2.6, MiniCAM (now GCAM4) for RCP4.5, AIM for RCP6.0 and MESSAGE for RCP8.5 (IIASA, 2018b).*

6.2.6 Figures for shifting cultivations

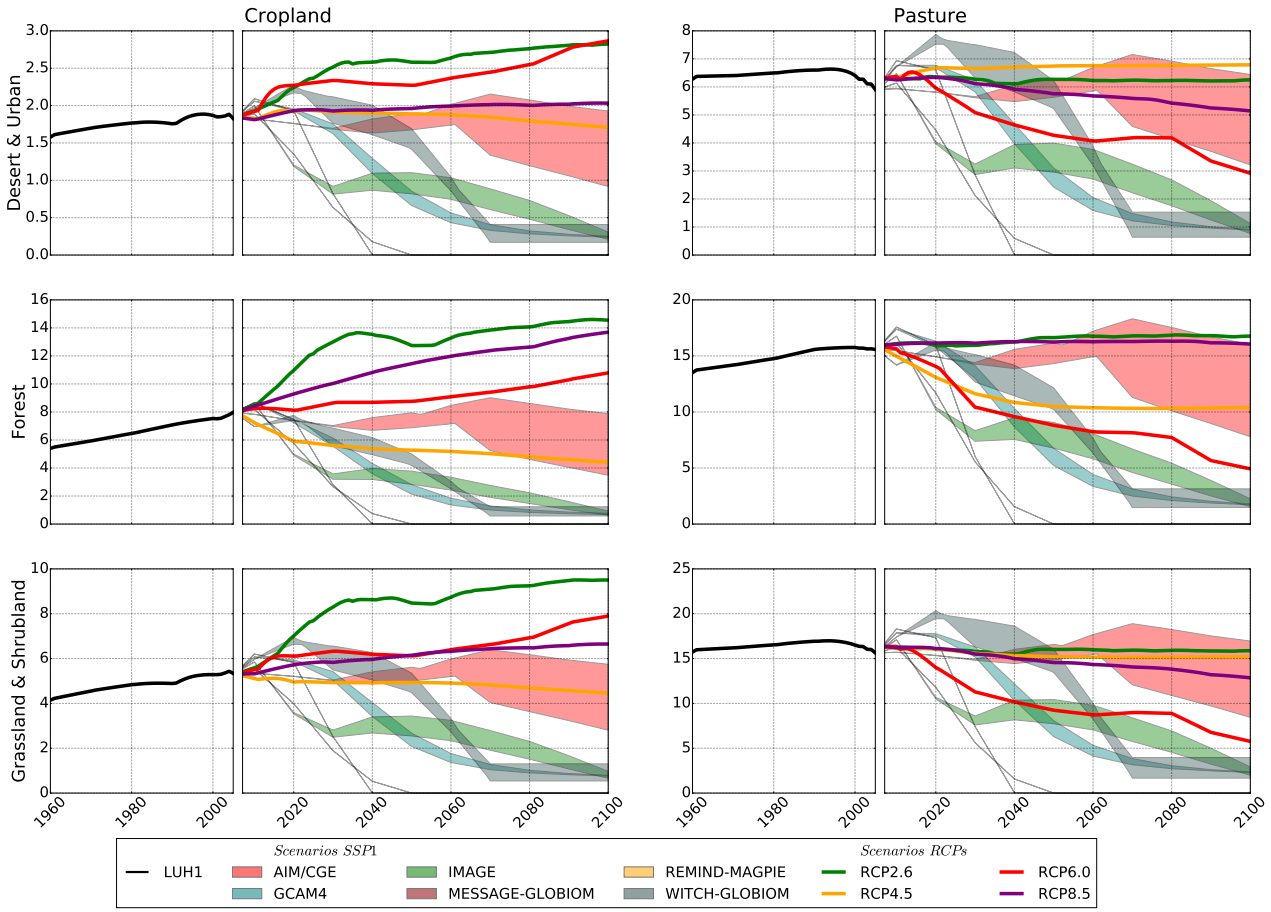

Figure 6.21: *Global annual bidirectional transitions for shifting cultivations (Mha/yr) for the SSP scenarios under the storyline* ***SSP1*** *over 2005-2100 (section 3.2.3.4). The transitions for shifting cultivations for 1960-2010 and for RCPs scenarios are shown for comparison, prescribed by the Land Use Harmonization dataset v1.1 (Hurtt et al. (2011)). For the SSP scenarios (shaded areas), the color corresponds to the IAM that has produced the corresponding scenario. For the RCPs scenarios (plain lines), similar colors may be used if and only if the IAM used to produce the RCP is the same: IMAGE has been used for RCP2.6, MiniCAM (now GCAM4) for RCP4.5, AIM for RCP6.0 and MESSAGE for RCP8.5 (IIASA (2018b)).*

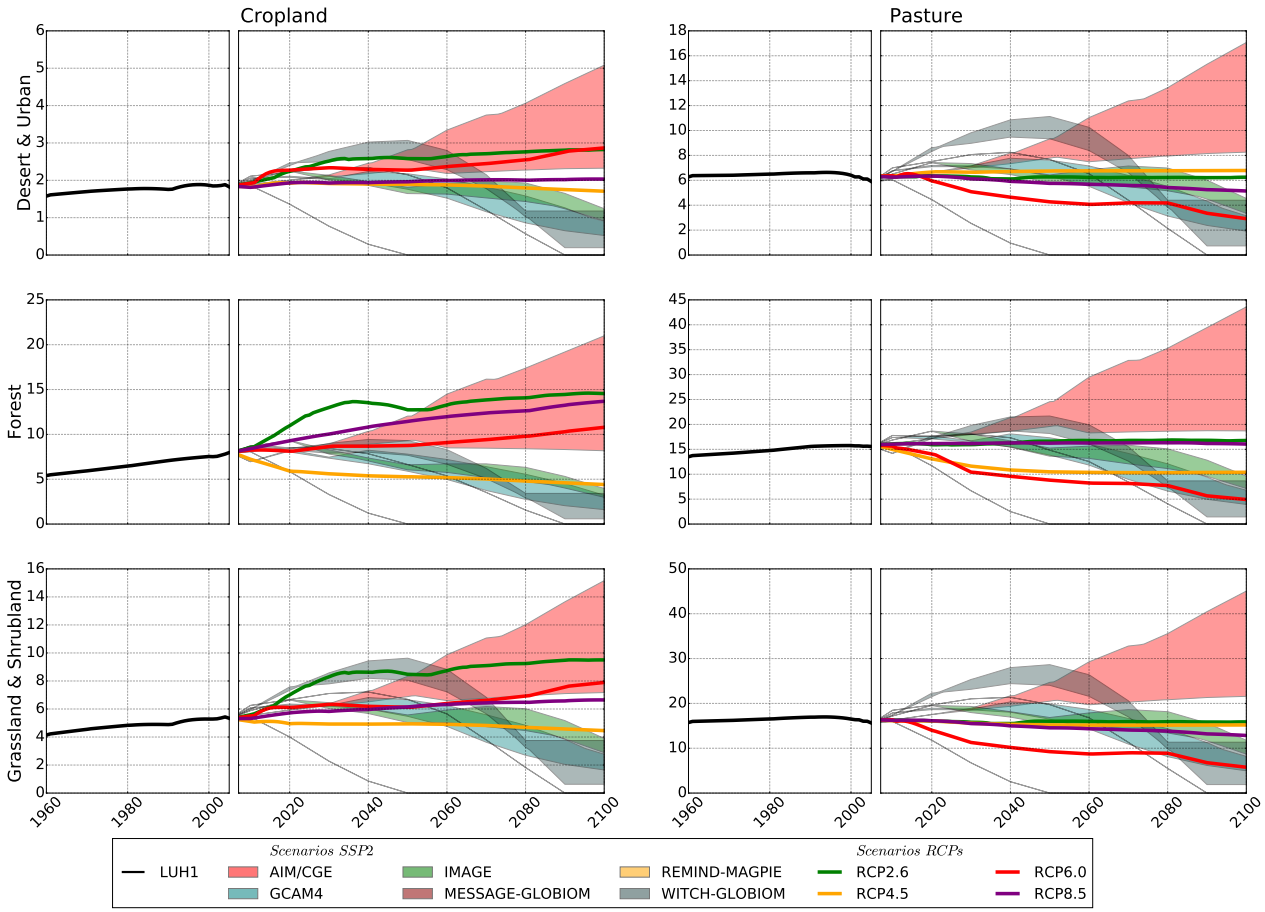

Figure 6.22: *Global annual bidirectional transitions for shifting cultivations (Mha/yr) for the SSP scenarios under the storyline* ***SSP2*** *over 2005-2100 (section 3.2.3.4). The transitions for shifting cultivations for 1960-2010 and for RCPs scenarios are shown for comparison, prescribed by the Land Use Harmonization dataset v1.1 (Hurtt et al. (2011)). For the SSP scenarios (shaded areas), the color corresponds to the IAM that has produced the corresponding scenario. For the RCPs scenarios (plain lines), similar colors may be used if and only if the IAM used to produce the RCP is the same: IMAGE has been used for RCP2.6, MiniCAM (now GCAM4) for RCP4.5, AIM for RCP6.0 and MESSAGE for RCP8.5 (IIASA (2018b)).*

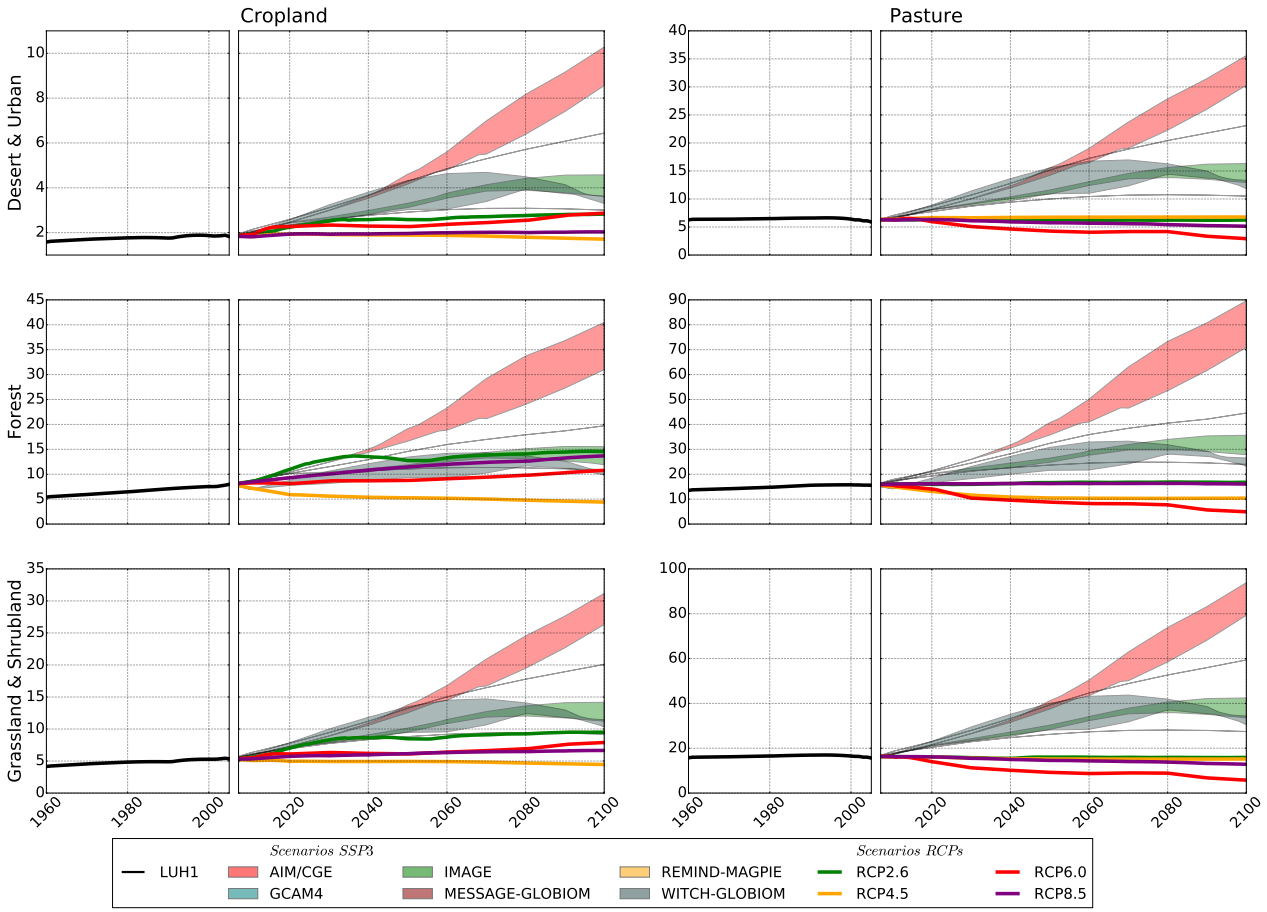

Figure 6.23: *Global annual bidirectional transitions for shifting cultivations (Mha/yr) for the SSP scenarios under the storyline* ***SSP3*** *over 2005-2100 (section 3.2.3.4). The transitions for shifting cultivations for 1960-2010 and for RCPs scenarios are shown for comparison, prescribed by the Land Use Harmonization dataset v1.1 (Hurtt et al. (2011)). For the SSP scenarios (shaded areas), the color corresponds to the IAM that has produced the corresponding scenario. For the RCPs scenarios (plain lines), similar colors may be used if and only if the IAM used to produce the RCP is the same: IMAGE has been used for RCP2.6, MiniCAM (now GCAM4) for RCP4.5, AIM for RCP6.0 and MESSAGE for RCP8.5 (IIASA (2018b)).*

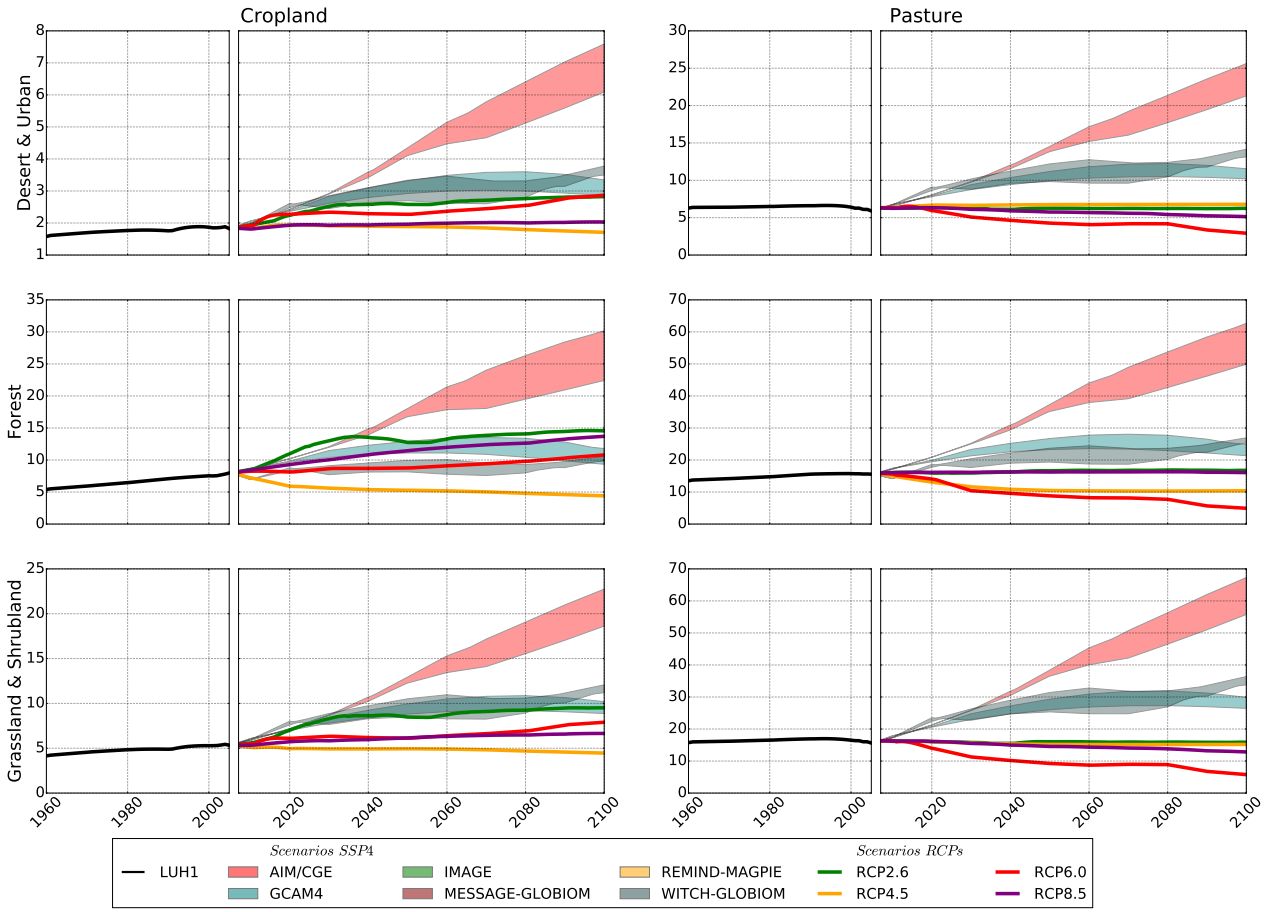

Figure 6.24: *Global annual bidirectional transitions for shifting cultivations (Mha/yr) for the SSP scenarios under the storyline* ***SSP4*** *over 2005-2100 (section 3.2.3.4). The transitions for shifting cultivations for 1960-2010 and for RCPs scenarios are shown for comparison, prescribed by the Land Use Harmonization dataset v1.1 (Hurtt et al. (2011)). For the SSP scenarios (shaded areas), the color corresponds to the IAM that has produced the corresponding scenario. For the RCPs scenarios (plain lines), similar colors may be used if and only if the IAM used to produce the RCP is the same: IMAGE has been used for RCP2.6, MiniCAM (now GCAM4) for RCP4.5, AIM for RCP6.0 and MESSAGE for RCP8.5 (IIASA (2018b)).*

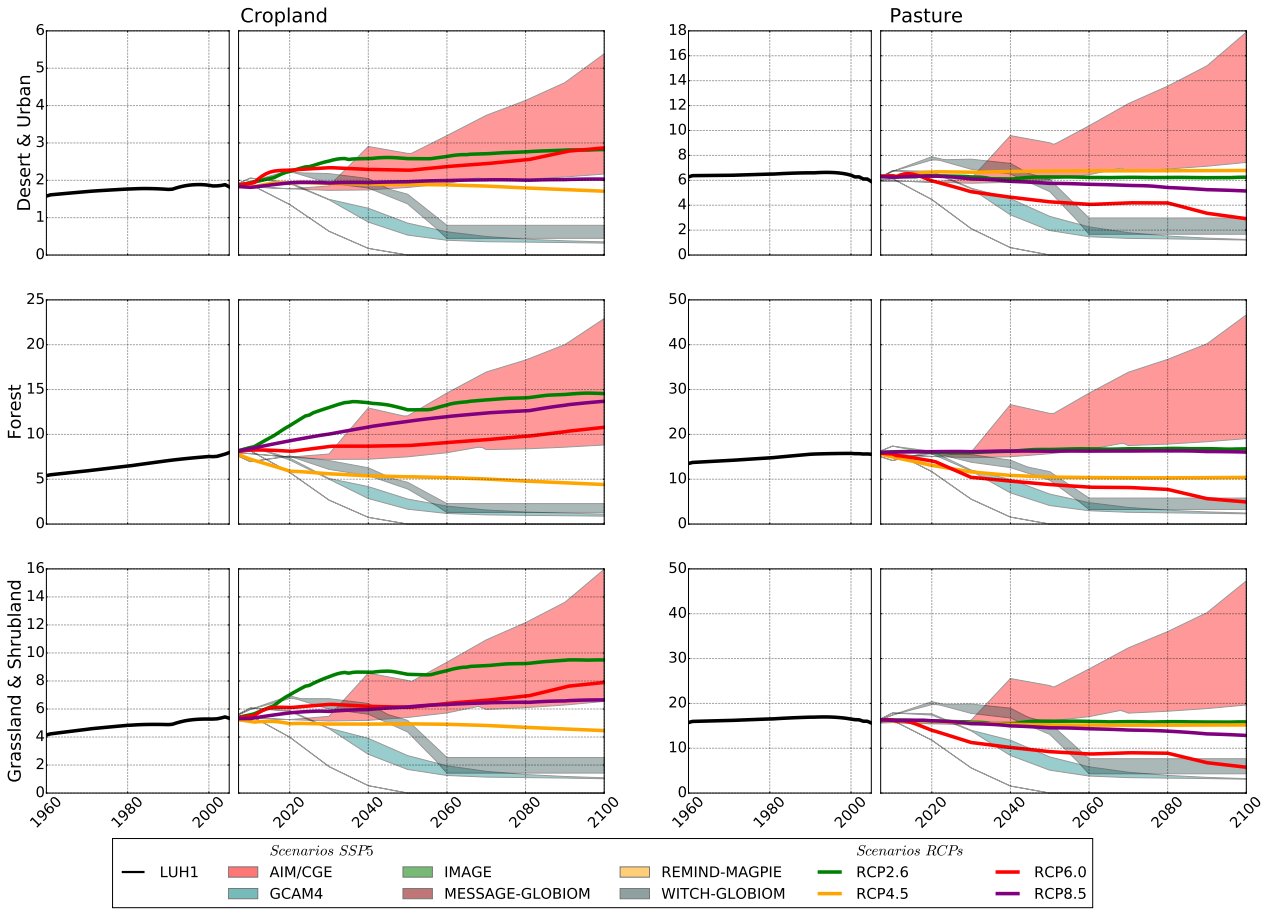

Figure 6.25: *Global annual bidirectional transitions for shifting cultivations (Mha/yr) for the SSP scenarios under the storyline* ***SSP5*** *over 2005-2100 (section 3.2.3.4). The transitions for shifting cultivations for 1960-2010 and for RCPs scenarios are shown for comparison, prescribed by the Land Use Harmonization dataset v1.1 (Hurtt et al. (2011)). For the SSP scenarios (shaded areas), the color corresponds to the IAM that has produced the corresponding scenario. For the RCPs scenarios (plain lines), similar colors may be used if and only if the IAM used to produce the RCP is the same: IMAGE has been used for RCP2.6, MiniCAM (now GCAM4) for RCP4.5, AIM for RCP6.0 and MESSAGE for RCP8.5 (IIASA (2018b)).*

6.2.7 Figures for natural CH_4 emissions

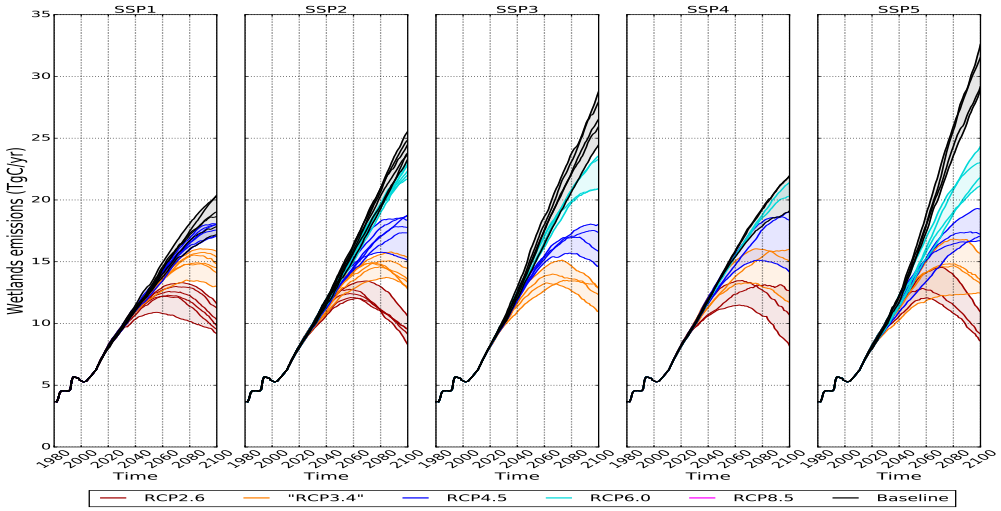

Figure 6.26: *Change in wetlands emissions since the preindustrial equilibrium from 1980 to 2100 (section 3.3.1.3). The scenarios are classified depending on the SSP and the RCP. Each line represents an IAM that has run this SSP and this climate target, and in plain color is their ensemble. Uncertainties are not represented.*

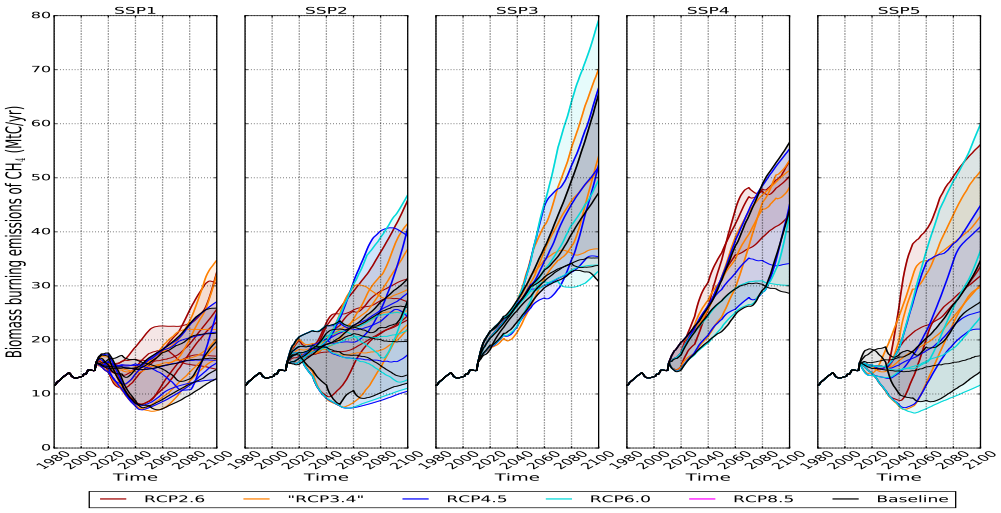

Figure 6.27: *Change in CH_4 emissions from biomass burning since the preindustrial equilibrium from 1980 to 2100 (section 3.3.1.3). The scenarios are classified depending on the SSP and the RCP. Each line represents an IAM that has run this SSP and this climate target, and in plain color is their ensemble. Uncertainties are not represented.*

6.2.8 Figures for natural N_2O emissions

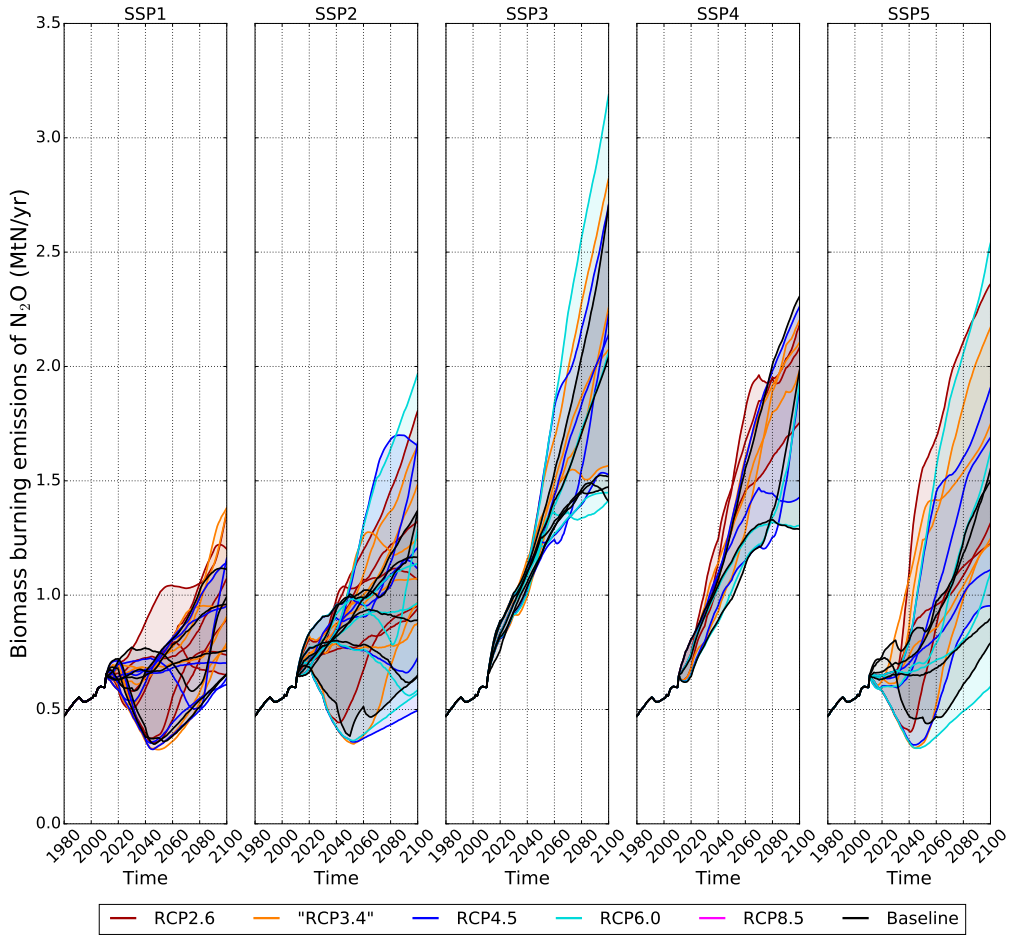

Figure 6.28: *Change in N_2O emissions from biomass burning since the preindustrial equilibrium from 1980 to 2100 (section 3.3.1.4). The transition from the historic period and the scenario happens in 2010. Each subfigure details the results for a given SSP. The scenarios are also classified depending on the climate target. Each line represents an IAM that has run this SSP and this climate target, and in plain color is their ensemble. For the sake of clarity, uncertainties are not represented here.*

6.2.9 Figures for natural SO_2 emissions

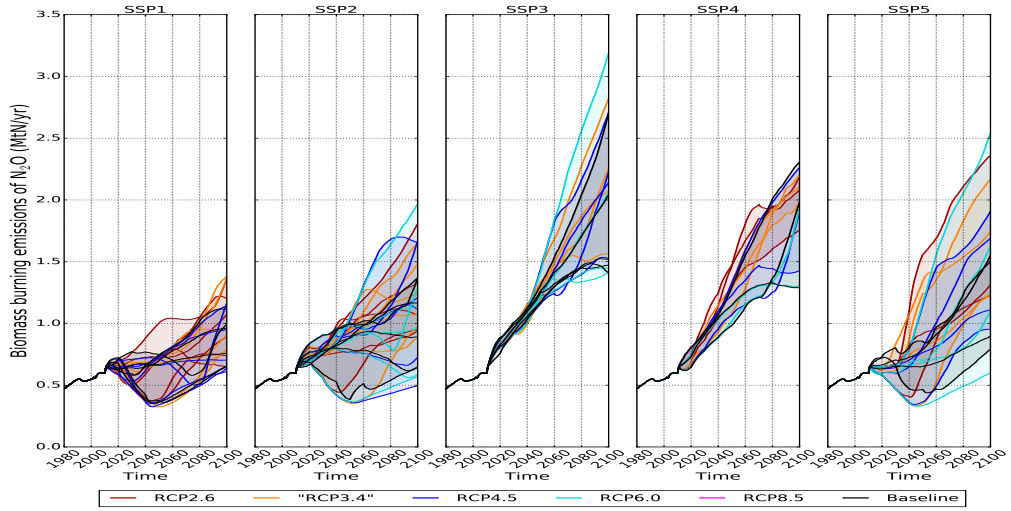

Figure 6.29: *Change in SO_2 emissions from biomass burning since the preindustrial equilibrium from 1980 to 2100 (section 3.3.1.5). The scenarios are classified depending on the SSP and the RCP. Each line represents an IAM that has run this SSP and this climate target, and in plain color is their ensemble. Uncertainties are not represented.*

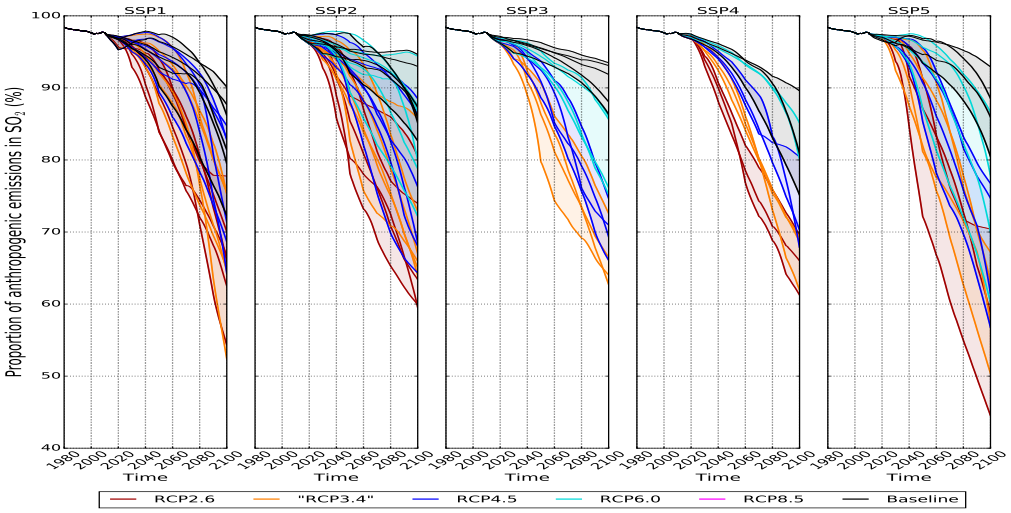

Figure 6.30: *Fraction of anthropogenic emissions in the total SO_2 emissions from 1980 to 2100 (section 3.3.1.5). The scenarios are classified depending on the SSP and the RCP. Each line represents an IAM that has run this SSP and this climate target, and in plain color is their ensemble. Uncertainties are not represented.*

6.2.10 Figures for co-emission ratios

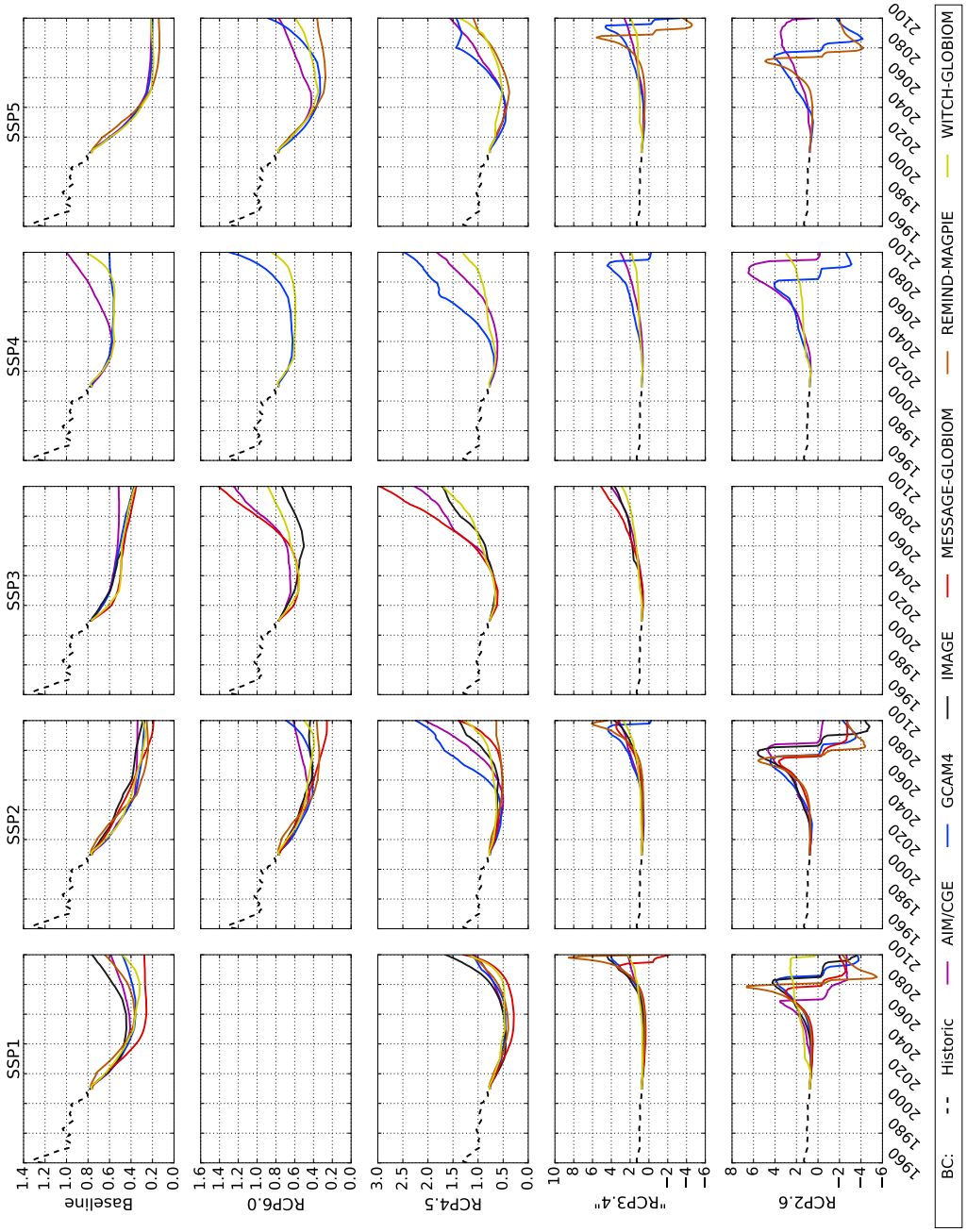

Figure 6.31: *Co-emissions ratios for BC (Tg/GtC), for extension of the Kaya decomposition in section 3.3.7. For the sake of clarity, uncertainties are not represented for the ratios.*

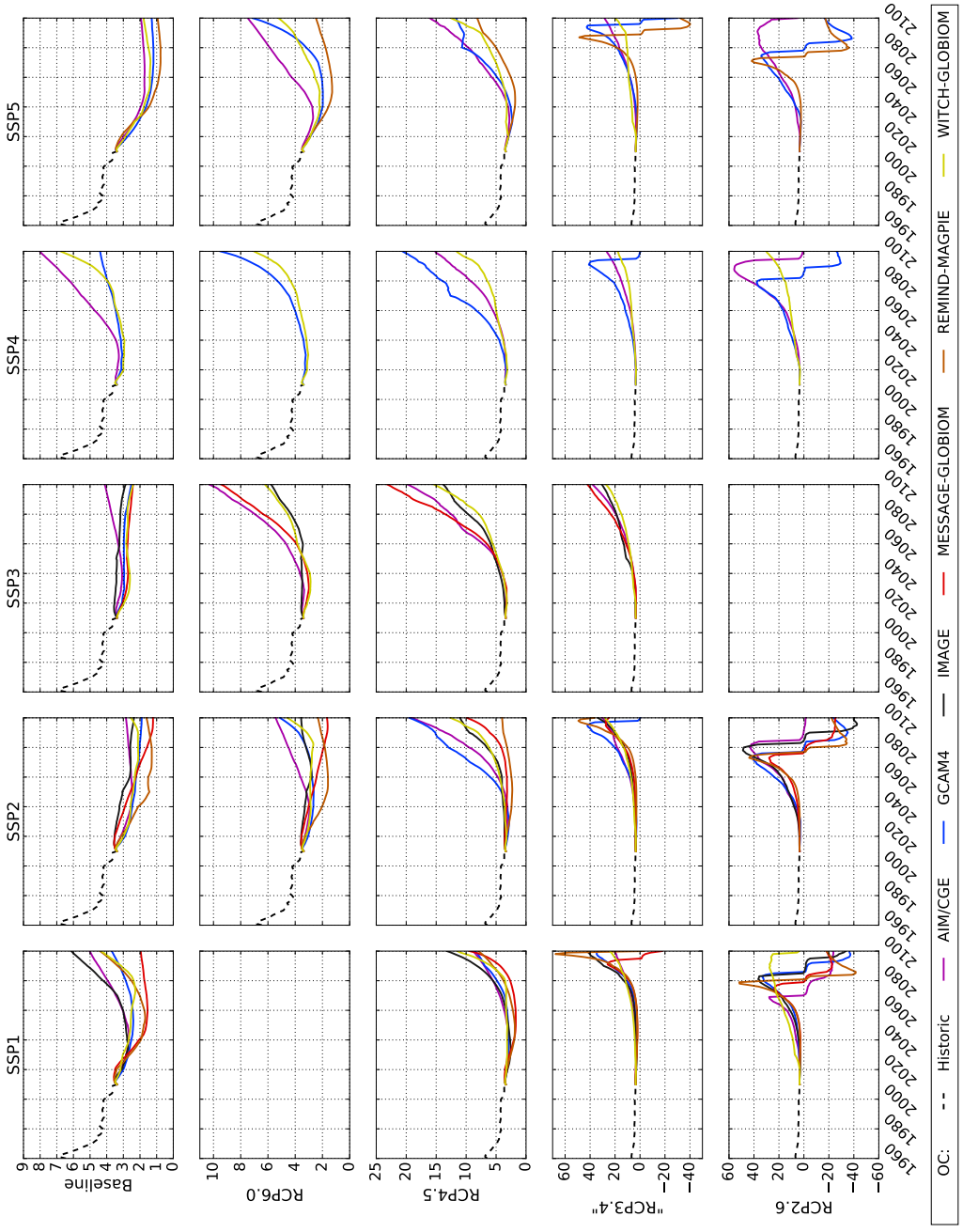

Figure 6.32: *Co-emissions ratios for OC (Tg/GtC), for extension of the Kaya decomposition in section 3.3.7. For the sake of clarity, uncertainties are not represented for the ratios.*

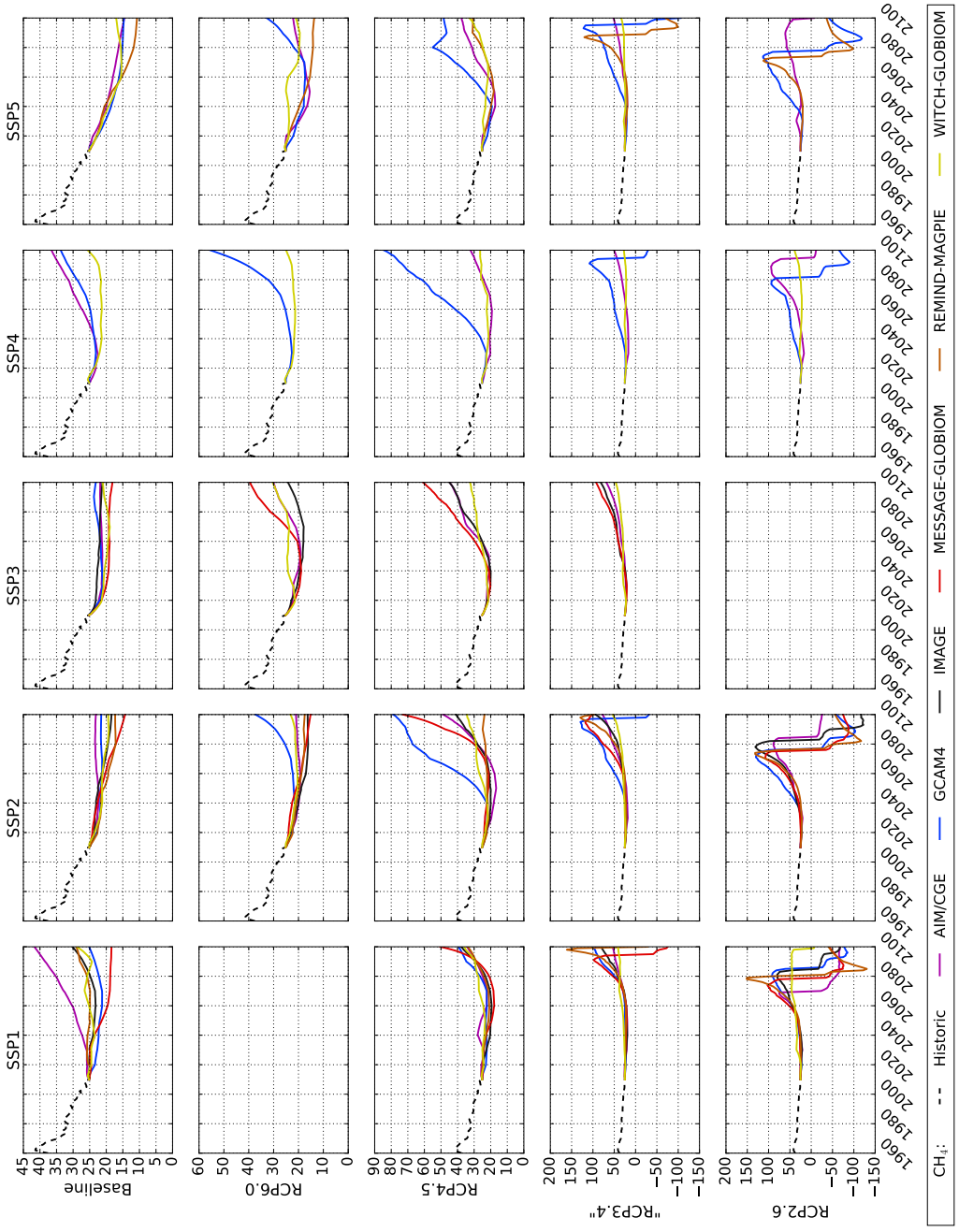

Figure 6.33: *Co-emissions ratios for CH_4 (TgC/GtC), for extension of the Kaya decomposition in section 3.3.7. For the sake of clarity, uncertainties are not represented for the ratios.*

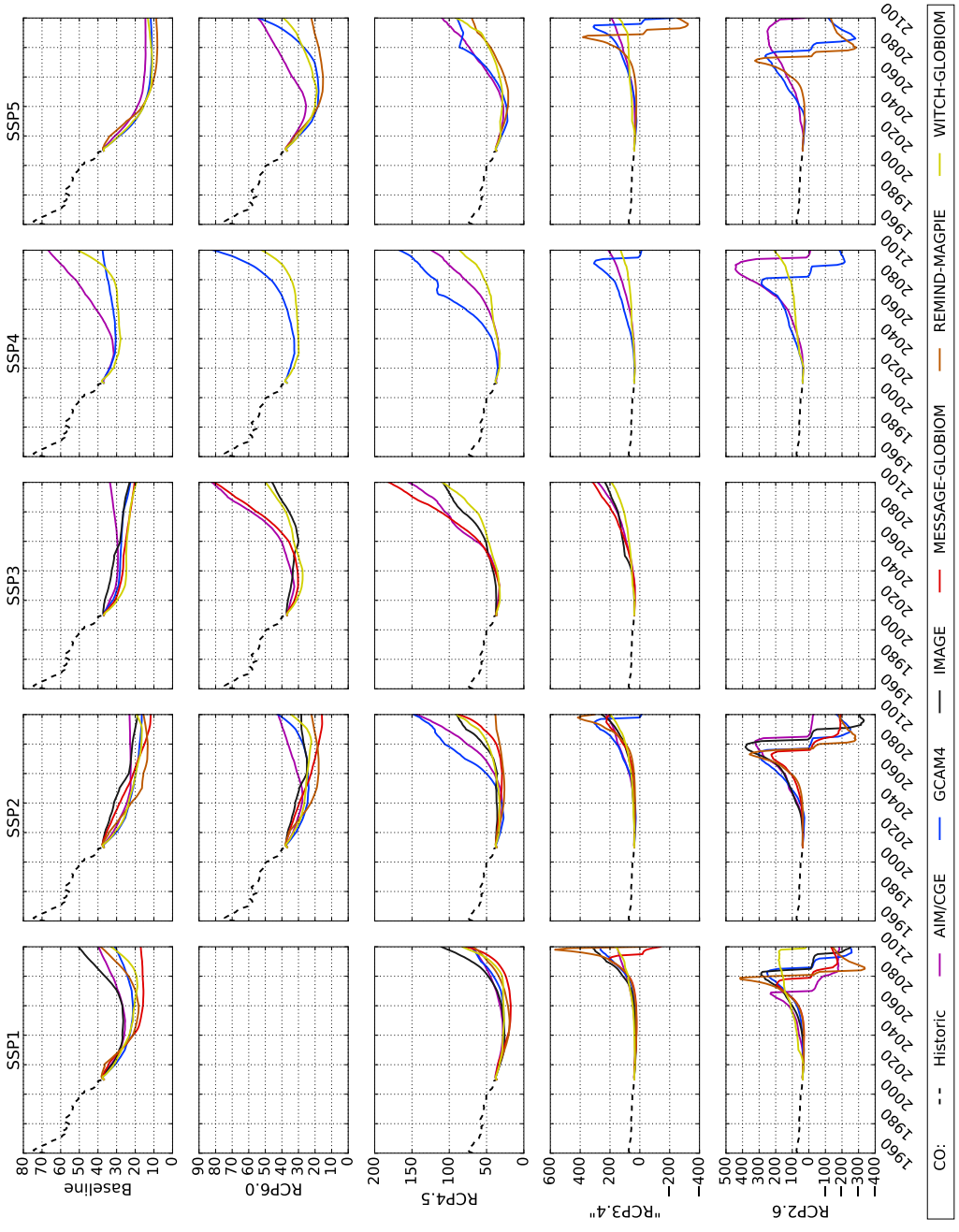

Figure 6.34: *Co-emissions ratios for CO (TgC/GtC), for extension of the Kaya decomposition in section 3.3.7. For the sake of clarity, uncertainties are not represented for the ratios.*

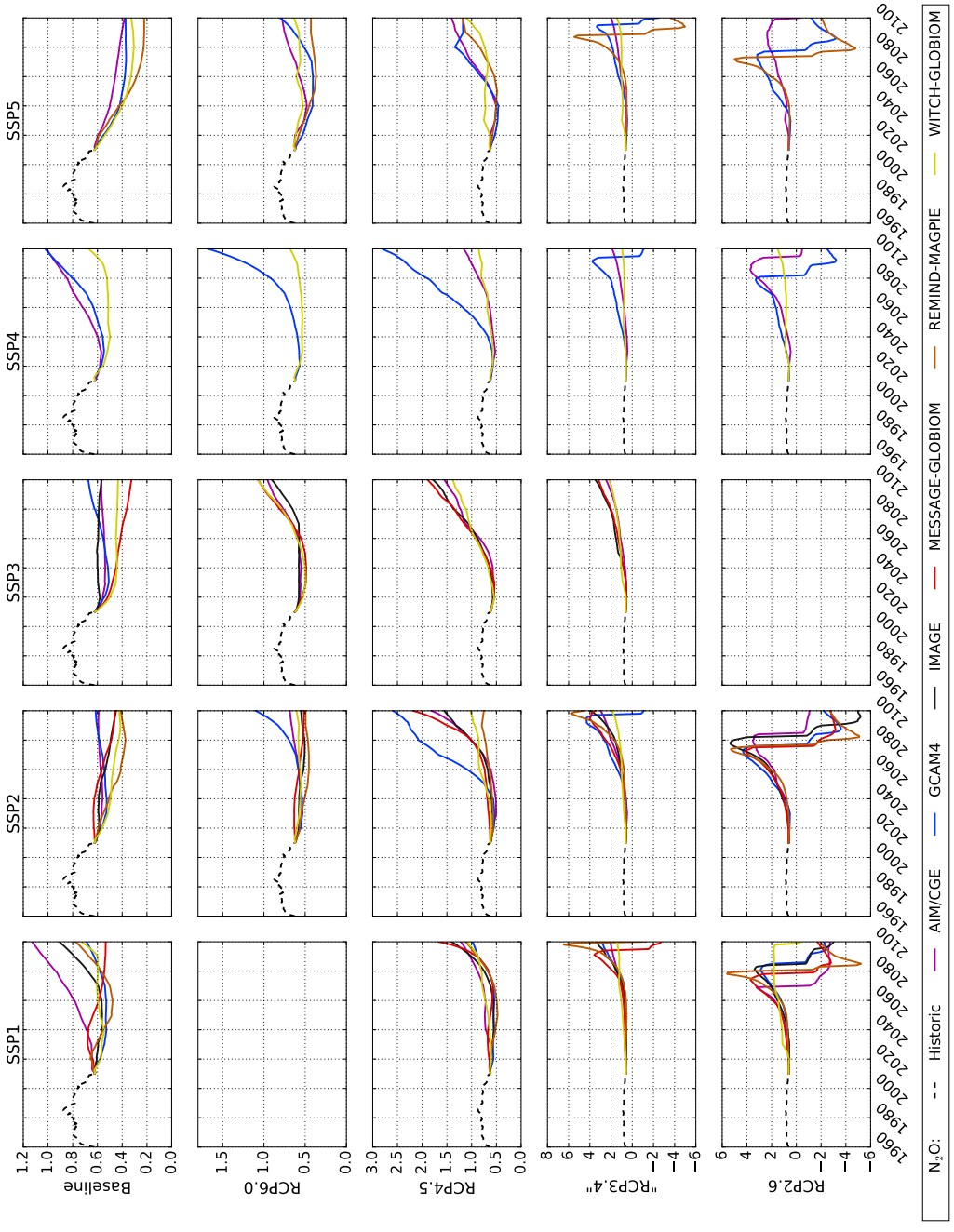

Figure 6.35: *Co-emissions ratios for N_2O (TgN/GtC), for extension of the Kaya decomposition in section 3.3.7. For the sake of clarity, uncertainties are not represented for the ratios.*

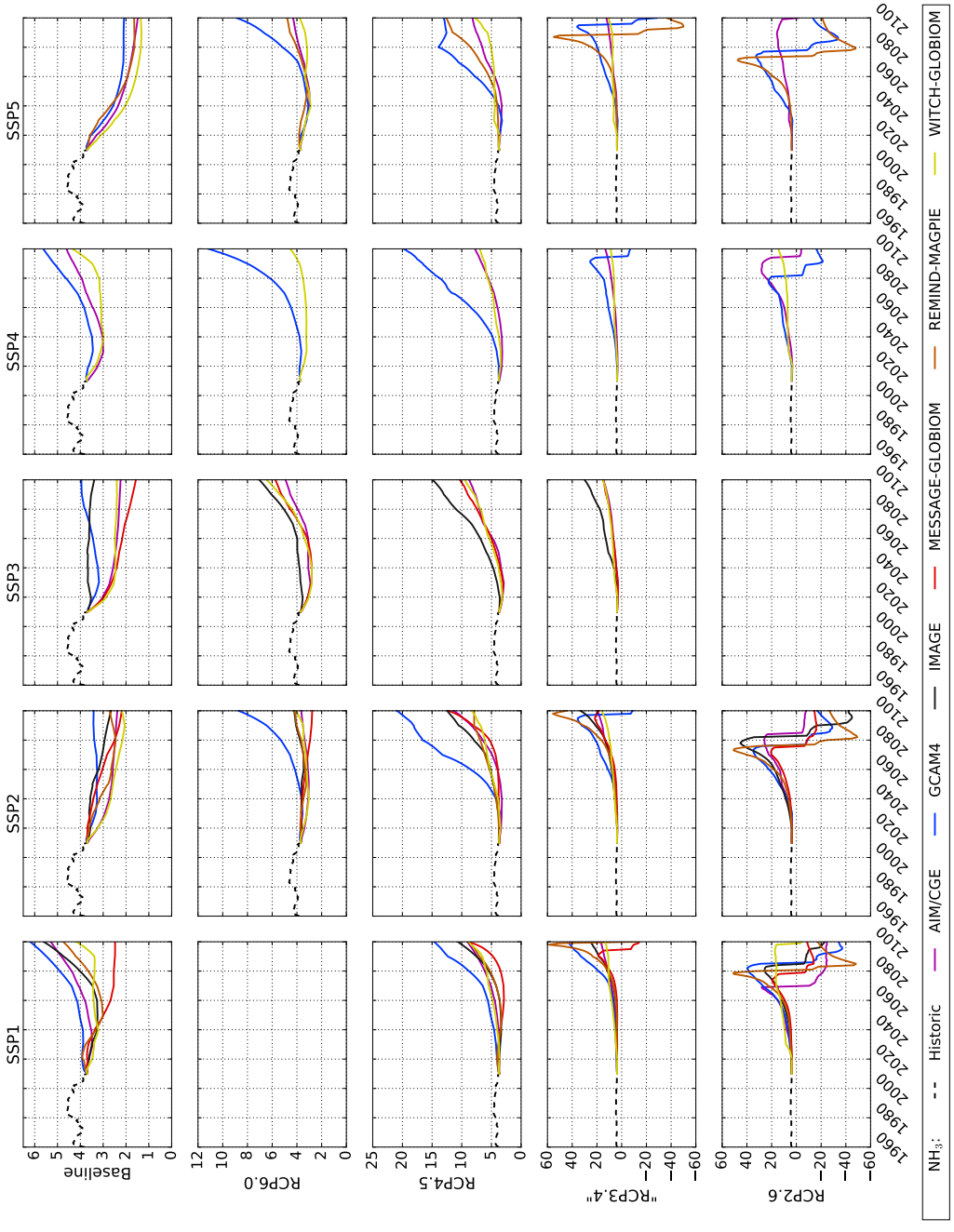

Figure 6.36: *Co-emissions ratios for NH_3 (TgN/GtC), for extension of the Kaya decomposition in section 3.3.7. For the sake of clarity, uncertainties are not represented for the ratios.*

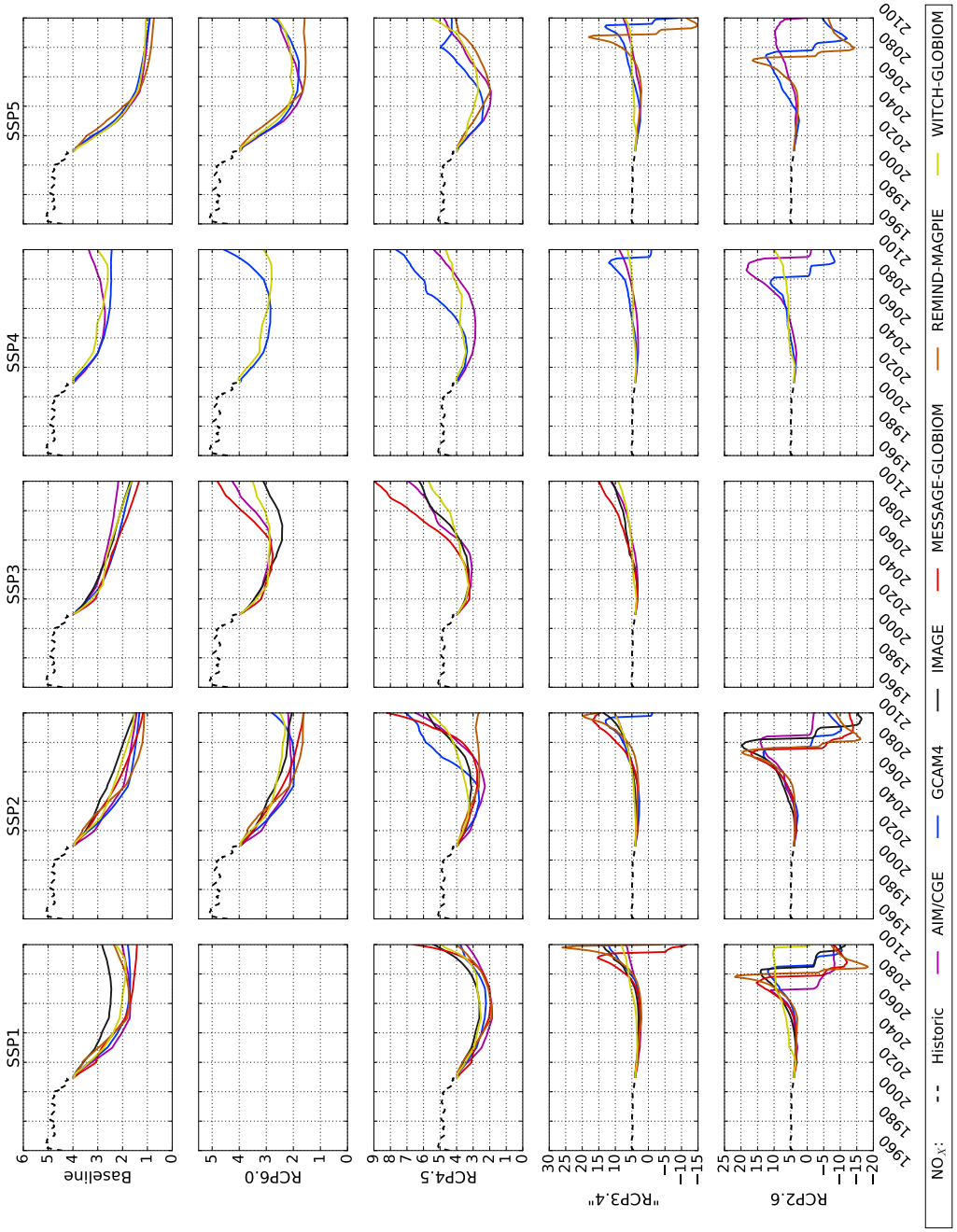

Figure 6.37: *Co-emissions ratios for NO_X (TgN/GtC), for extension of the Kaya decomposition in section 3.3.7. For the sake of clarity, uncertainties are not represented for the ratios.*

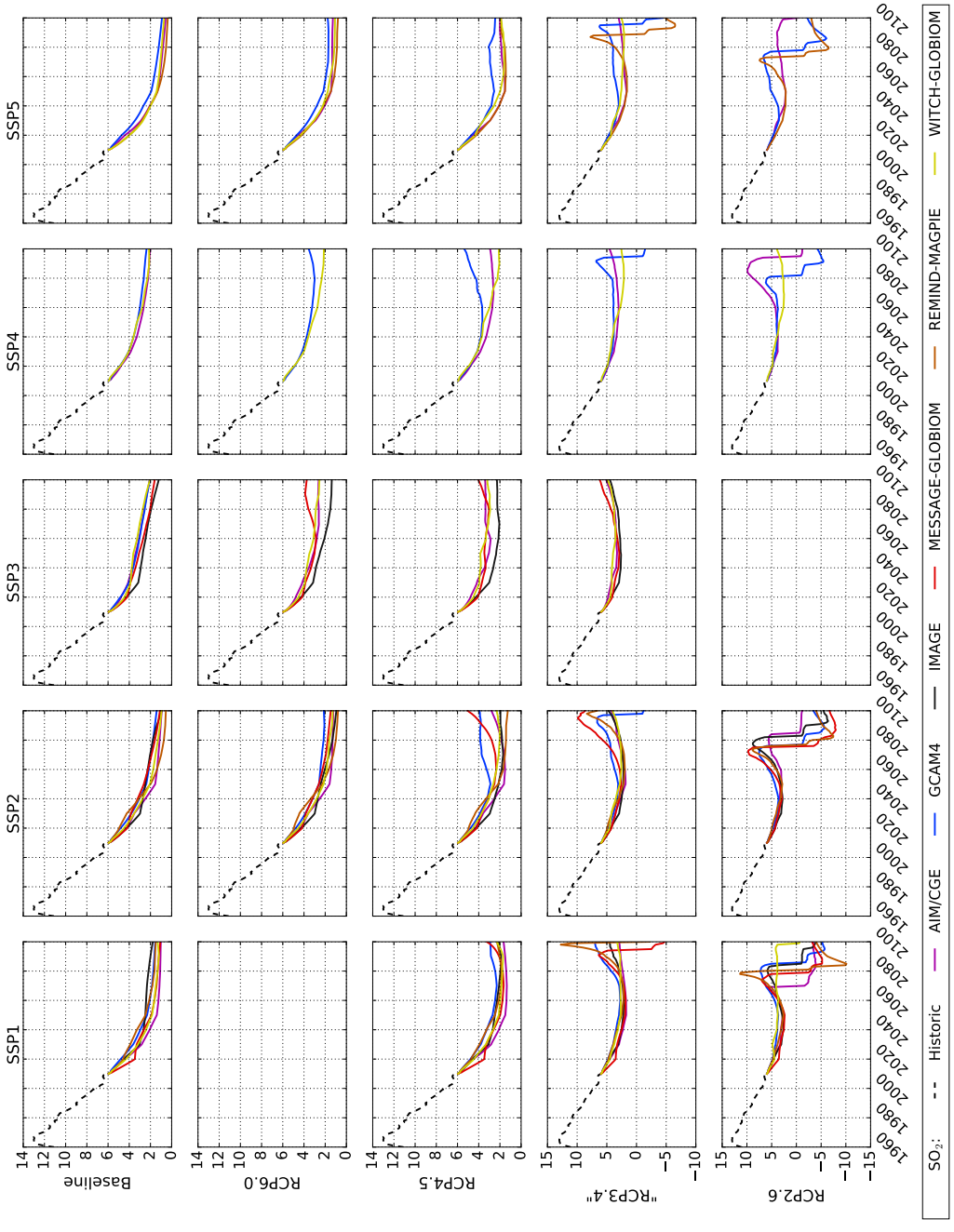

Figure 6.38: *Co-emissions ratios for SO_2 (TgS/GtC), for extension of the Kaya decomposition in section 3.3.7. For the sake of clarity, uncertainties are not represented for the ratios.*

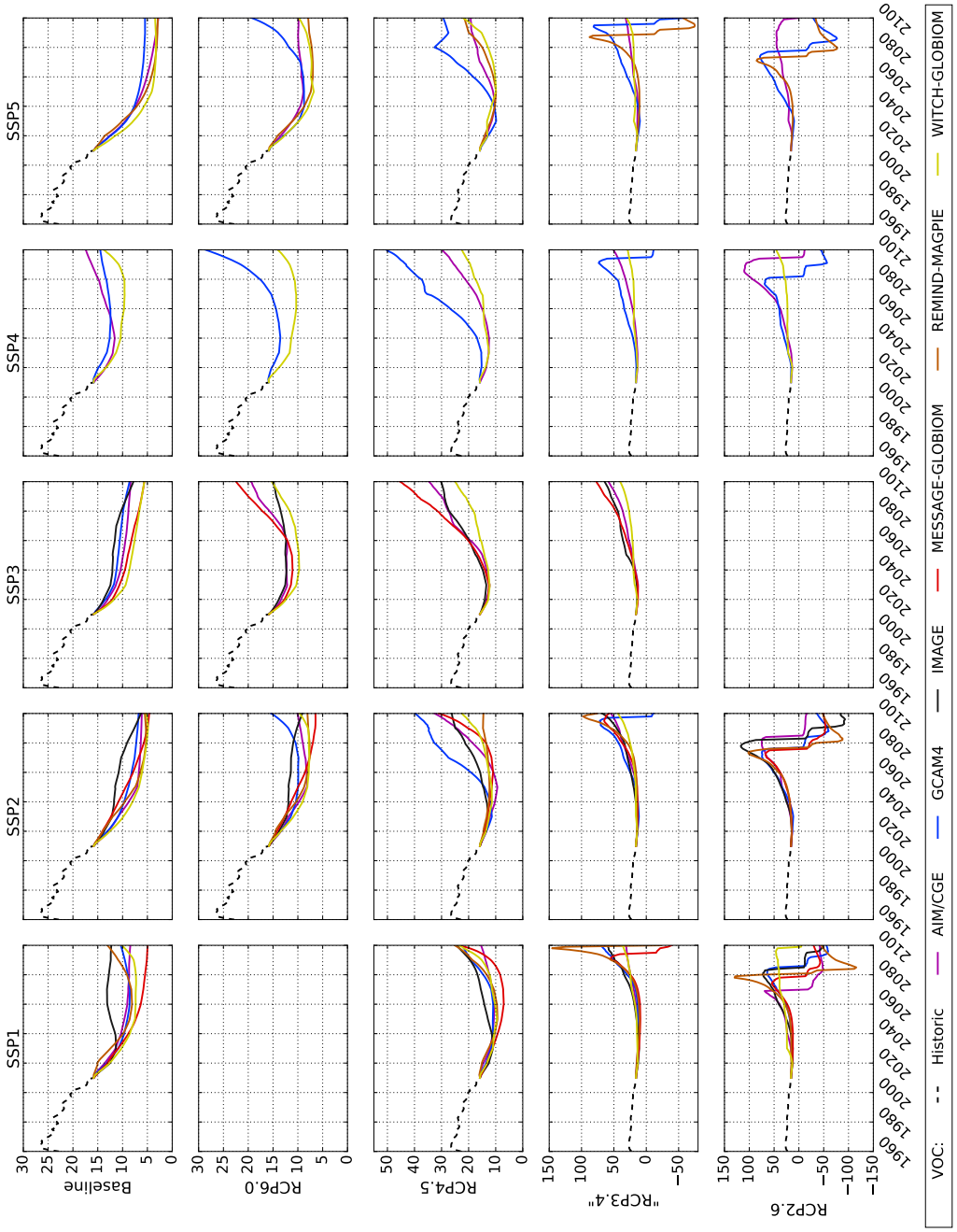

Figure 6.39: *Co-emissions ratios for VOC (Tg/GtC), for extension of the Kaya decomposition in section 3.3.7. For the sake of clarity, uncertainties are not represented for the ratios.*

6.3 Appendix for chapter 4

6.3.1 Demonstration for equations 4.10

Concerning the equation 4.10a, the expressions in equations 6.1 can be deduced from equations 4.2. Because $[H_2CO_3] <$ DIC, we deduce that $CO_2K_0 - DIC < 0$ and thus the result in equation 4.10a.

$$DIC = [H_2CO_3]\left(1 + K_1/\left[H^+\right] + K_1K_2/\left[H^+\right]^2\right) \tag{6.1a}$$

$$[H_2CO_3] = K_0CO_2 \tag{6.1b}$$

$$0 = (CO_2K_0 - DIC)\left[H^+\right]^2 + K_0K_1\left[H^+\right] + K_1K_2 \tag{6.1c}$$

Concerning the equation 4.10b, we use the expressions for DIC and CA as shown in equations 6.2.

$$DIC = [H_2CO_3]\left(1 + K_1/\left[H^+\right] + K_1K_2/\left[H^+\right]^2\right) \tag{6.2a}$$

$$CA = [H_2CO_3]\,K_1/\left[H^+\right]\left(1 + 2K_2/\left[H^+\right]\right) \tag{6.2b}$$

$$\frac{CA\left[H^+\right]^2}{DIC\left[H^+\right]^2} = \frac{K_1\left[H^+\right] + 2K_1K_2}{\left[H^+\right]^2 + K_1\left[H^+\right] + K_1K_2} \tag{6.2c}$$

$$0 = CA\left[H^+\right]^2 + (CA - DIC)\,K_1\left[H^+\right] + (CA - 2DIC)\,K_1K_2 \tag{6.2d}$$

Bibliography

AIM/CGE . Description of AIM/CGE. https://wiki.ucl.ac.uk/display/ADVIAM/AIME-CGE, 2018.

Allen , M. R., Stott , P. A., Mitchell , J. F. B., Schnur , R., and Delworth , T. L. Quantifying the uncertainty in forecasts of anthropogenic climate change. *Nature*, 407, 617, 2000. doi: 10.1038/35036559.

Anderegg , W. R., Kane , J. M., and Anderegg , L. D. Consequences of widespread tree mortality triggered by drought and temperature stress. *Nature Climate Change*, 3, 30–36, 2013. doi: 10.1038/nclimate1635.

Anderson , K. and Peters , G. The trouble with negative emissions. *Science*, 354, 182–183, 2016. doi: 10.1126/science.aah4567.

Andres , R. J., Boden , T. A., Bréon , F. M., Ciais , P., Davis , S., Erickson , D., Gregg , J. S., Jacobson , A., Marland , G., Miller , J., Oda , T., Olivier , J. G., Raupach , M. R., Rayner , P., and Treanton , K. A synthesis of carbon dioxide emissions from fossil-fuel combustion. *Biogeosciences*, 9, 1845–1871, 2012. doi: 10.5194/bg-9-1845-2012.

Arneth , A., Sitch , S., Pongratz , J., Stocker , B. D., Ciais , P., Poulter , B., Bayer , A. D., Bondeau , A., Calle , L., Chini , L. P., Gasser , T., Fader , M., Friedlingstein , P., Kato , E., Li , W., Lindeskog , M., Nabel , J. E. M. S., Pugh , T. A. M., Robertson , E., Viovy , N., Yue , C., and Zaehle , S. Historical carbon dioxide emissions caused by land-use changes are possibly larger than assumed. *Nature Geoscience*, 10, 79–84, 2017. doi: 10.1038/ngeo2882.

Arora , V. K., Boer , G. J., Friedlingstein , P., Eby , M., Jones , C. D., Christian , J. R., Bonan , G., Bopp , L., Brovkin , V., Cadule , P., Hajima , T., Ilyina , T., Lindsay , K., Tjiputra , J. F., and Wu , T. Carbon-concentration and carbon-climate feedbacks in CMIP5 earth system models. *Journal of Climate*, 26, 5289–5314, 2013. doi: 10.1175/JCLI-D-12-00494.1.

Arrhenius , S. On the influence of carbonic acid in the air upon the temperature of the ground. *Philosophical Magazine and Journal of Science*, 41, 237-276, 1896.

Azar , C. and Johansson , D. J. On the relationship between metrics to compare greenhouse gases the case of IGTP, GWP and SGTP. *Earth System Dynamics*, 3, 139–147, 2012. doi: 10.5194/esd-3-139-2012.

Bajželj , B., Richards , K. S., Allwood , J. M., Smith , P., Dennis , J. S., Curmi , E., and Gilligan , C. A. Importance of food-demand management for climate mitigation. *Nature Climate Change*, 4, 924–929, 2014. doi: 10.1038/nclimate2353.

Barbour , W. and Gillenwater , M. Estimation of emissions from road transport, 2004. doi: FCCC/SBSTA/2004/INF.3.

Bauer , N., Calvin , K., Emmerling , J., Fricko , O., Fujimori , S., Hilaire , J., Eom , J., Krey , V., Kriegler , E., Mouratiadou , I., Sytze de Boer , H., van den Berg , M., Carrara , S., Daioglou , V., Drouet , L., Edmonds , J. E., Gernaat , D., Havlik , P., Johnson , N., Klein , D., Kyle , P., Marangoni , G., Masui , T., Pietzcker , R. C., Strubegger , M., Wise , M., Riahi , K., and van Vuuren , D. P. Shared Socio-Economic Pathways of the Energy Sector – Quantifying the Narratives. *Global Environmental Change*, 42, 316–330, 2017. doi: 10.1016/j.gloenvcha.2016.07.006.

Bernie , D., Lowe , J., Tyrrell , T., and Legge , O. Influence of mitigation policy on ocean acidification. *Geophysical Research Letters*, 37, 1–5, 2010. doi: 10.1029/2010GL043181.

Blanco , G., Gerlagh , R., Suh , S., Barrett , J., de Coninck , H. C., Diaz Morejon , C. F., Mathur , R., Nakicenovic , N., Ofosu Ahenkora , A., Pan , J., Pathak , J., H. Rice, Richels , R., Smith , S. J., Stern , D. I., Toth , F. L., and Zho , P. Drivers, Trends and Mitigation. *Climate Change 2014: Mitigation of Climate Change. Contribution of Working Group III to the Fifth Assessment Report of the Intergovernmental Panel on Climate Change*, 2014.

Boden , T., Marland , G., and Andres , R. Estimates of global, regional and national annual CO2 emissions from fossil-fuel burning, hydraulic cement production and gas flaring: 1950-1992. *Tech. Rep., Carbon Dioxide Information Analysis Center, Oak Ridge National Laboratory, U.S. Department of Energy, Oak Ridge, Tenn., U.S.A*, 1995.

Boden , T., Marland , G., and Andres , R. Global, Regional, and National Fossil-Fuel CO2 Emissions. *Carbon Dioxide Information Analysis Center, Oak Ridge National Laboratory, U.S. Department of Energy, Oak Ridge, Tenn., U.S.A.*, 2013. doi: 10.3334/CDIAC/00001_V2013.

Boden , T., Marland , G., and Andres , R. Global, Regional, and National Fossil-Fuel CO2 Emissions. *Carbon Dioxide Information Analysis Center, Oak Ridge National Laboratory, U.S. Department of Energy, Oak Ridge, Tenn., U.S.A.*, 2017. doi: 10.3334/CDIAC/00001_V2017.

Bond , T. C., Streets , D. G., Yarber , K. F., Nelson , S. M., Woo , J. H., and Klimont , Z. A technology-based global inventory of black and organic carbon emissions from combustion. *Journal of Geophysical Research D: Atmospheres*, 109, 1–43, 2004. doi: 10.1029/2003JD003697.

Bondeau , A., Smith , P. C., Zaehle , S., Schaphoff , S., Lucht , W., Cramer , W., Gerten , D., Lotze-campen , H., Müller , C., Reichstein , M., and Smith , B. Modelling the role of agriculture for the 20th century global terrestrial carbon balance. *Global Change Biology*, 13, 679–706, 2007. doi: 10.1111/j.1365-2486.2006.01305.x.

Bosetti , V., Carraro , C., Galeotti , M., Massetti , E., and Tavoni , M. WITCH: A World Induced Technical Change Hybrid Model. *Energy Journal*, 27, 13-38, 2006.

Bosetti , V., Tavoni , M., Cian , E. D., and Sgobbi , A. The 2008 WITCH Model: New Model Features and Baseline. *Sustainable Development Series*, 2009. doi: http://www.feem.it/userfiles/attach/2009111910584485-09.pdf.

Boucher , O. and Reddy , M. S. Climate trade-off between black carbon and carbon dioxide emissions. *Energy Policy*, 36, 193–200, 2008. doi: 10.1016/j.enpol.2007.08.039.

Boucher , O., Halloran , P. R., Burke , E. J., Doutriaux-Boucher , M., Jones , C. D., Lowe , J., Ringer , M. A., Robertson , E., and Wu , P. Reversibility in an Earth System model in response to CO ₂ concentration changes. *Environmental Research Letters*, 7, 024013, 2012. doi: 10.1088/1748-9326/7/2/024013.

Boyer , T., Antonov , J. I., Baranova , O. K., Coleman , C., Garcia , H. E., Grodsky , A., Johnson , D. R., Locarnini , R. A., Mishonov , A. V., O'Brien , T., Paver , C., Reagan , J., Seidov , D., Smolyar , I. V., and Zweng , M. M. *NOAA Atlas NESDIS 72, S. Levitus, Ed., A. Mishonov, Technical Ed.; Silver Spring*, 2013. doi: 10.7289/V5NZ85MT.

BP . Statistical Review of World Energy. `https://www.bp.com/en/global/corporate/energy-economics/statistical-review-of-world-energy/downloads.html`, 2018.

Brown , R. The Climate of Middle Earth. *Journal of Hobbitlore*, 2013.

Calvin , K., Clarke , L., Edmonds , J., Eom , J., Hejazi , M., Kim , S., Kyle , P., Link , P., R. Luckow, and Patel , P. The global change assessment model. `https://wiki.umd.edu/gcam/`, 2011.

Calvin , K., Bond-Lamberty , B., Clarke , L., Edmonds , J., Eom , J., Hartin , C., Kim , S., Kyle , P., Link , R., Moss , R., McJeon , H., Patel , P., Smith , S., Waldhoff , S., and Wise , M. The SSP4: A world of deepening inequality. *Global Environmental Change*, 42, 284–296, 2017. doi: 10.1016/j.gloenvcha.2016.06.010.

Ciais , P., Sabine , C., Bala , G., Bopp , L., Brovkin , V., Canadell , J., Chhabra , A., DeFries , R., Galloway , J., Heimann , M., Jones , C., Le Quere , C., Myneni , R. B., Piao , S., and Thornton , P. *Carbon and Other Biogeochemical Cycles*, book section 6, pages 465–570. Cambridge University Press, Cambridge, United Kingdom and New York, NY, USA, 2013. ISBN ISBN 978-1-107-66182-0. doi: 10.1017/CBO9781107415324.015.

Clarke , L. E., Jiang , K., Akimoto , K., Babiker , M., Blanford , G., Fisher-Vanden , K., Hourcade , J.-C., Krey , V., Kriegler , E., Löschel , A., McCollum , D., Paltsev , S., Rose , S., Shukla , P., Tavoni , M., van der Zwaan , B., and van Vuuren , D. Assessing transformation pathways. *Climate Change 2014: Mitigation of Climate Change. Contribution of Working Group III to the Fifth Assessment Report of the Intergovernmental Panel on Climate Change*, 2014.

Cofala , J., Amann , M., Klimont , Z., Kupiainen , K., and Höglund-Isaksson , L. Scenarios of global anthropogenic emissions of air pollutants and methane until 2030. *Atmospheric Environment*, 41, 8486–8499, 2007. doi: 10.1016/j.atmosenv.2007.07.010.

Collins , M., Knutti , R., Arblaster , J., Dufresne , J.-L., Fichefet , T., Friedlingstein , P., Gao , X., Gutowski , W. J., Johns , T., Krinner , G., Shongwe , M., Tebaldi , C., Weaver , A. J., and Wehner , M. *Long-term Climate Change: Projections, Commitments and Irreversibility*, book section 12, pages 1029–1136. Cambridge University Press, Cambridge, United Kingdom and New York, NY, USA, 2013. ISBN ISBN 978-1-107-66182-0. doi: 10.1017/CBO9781107415324.024.

Cox , P. and Stephenson , D. A Changing Climate for Prediction. *Science*, 317, 207–208, 2007. doi: 10.1126/science.1145956.

Crippa , M., Janssens-Maenhout , G., Dentener , F., Guizzardi , D., Sindelarova , K., Muntean , M., Van Dingenen , R., and Granier , C. Forty years of improvements in European air quality: Regional policy-industry interactions with global impacts. *Atmospheric Chemistry and Physics*, 16, 3825–3841, 2016. doi: 10.5194/acp-16-3825-2016.

Cripps , G., Widdicombe , S., Spicer , J. I., and Findlay , H. S. Biological impacts of enhanced alkalinity in Carcinus maenas. *Marine Pollution Bulletin*, 71, 190–198, 2013. doi: 10.1016/j.marpolbul.2013.03.015.

Crooks , S., Herr , D., Tamelander , J., Laffoley , D., and Vandever , J. Mitigating Climate Change through Restoration and Management of Coastal Wetlands and Near-shore Marine Ecosystems: Challenges and Opportunities. *Environment Department Papers*, 121, 1–69, 2011.

Cubasch , U., Wuebbles , D., Chen , D., Facchini , M. C., Frame , D., Mahowald , N., and Winther , J.-G. *Introduction*, book section 1, pages 119–158. Cambridge

University Press, Cambridge, United Kingdom and New York, NY, USA, 2013. ISBN ISBN 978-1-107-66182-0. doi: 10.1017/CBO9781107415324.007.

Daioglou , V. *The role of biomass in climate change mitigation - Assessing the long-term dynamics of bioenergy and biochemicals in the land and energy systems*. 2016. ISBN 9789086720699.

Daioglou , V., Stehfest , E., Wicke , B., Faaij , A., and van Vuuren , D. P. Projections of the availability and cost of residues from agriculture and forestry. *GCB Bioenergy*, 8, 456–470, 2016. doi: 10.1111/gcbb.12285.

Daniel , J. S., Solomon , S., Sanford , T. J., McFarland , M., Fuglestvedt , J. S., and Friedlingstein , P. Limitations of single-basket trading: Lessons from the Montreal Protocol for climate policy. *Climatic Change*, 111, 241–248, 2012. doi: 10.1007/s10584-011-0136-3.

David , N. Summary for Policymakers, 2014.

Davis , S. J., Peters , G. P., and Caldeira , K. The supply chain of CO2 emissions. *Proceedings of the National Academy of Sciences*, 108, 18554–18559, 2011. doi: 10.1073/pnas.1107409108.

Dépoues , V., Giguet , S., Jézéquel , A., and Quilcaille , Y. Témoignage de quatre étudiants engagés pour la réussite de la COP 21. *Natures Sciences Sociétés*, 23, S122–S125, 2015. doi: 10.1051/nss/2015024.

Dickson , A. G. An exact definition of total alkalinity and a procedure for the estimation of alkalinity and total inorganic carbon from titration data. *Deep Sea Research Part A, Oceanographic Research Papers*, 28, 609–623, 1981. doi: 10.1016/0198-0149(81)90121-7.

EEA . EMEP/EEA air pollutant emission inventory guidebook 2013: Technical guidance to prepare national emission inventories. *EEA Technical report*, 2013. doi: 10.2800/92722.

EEA . *Explaining road transport emissions. A non-technical guide.* 2016. ISBN 978-92-9213-723-6. doi: 10.2800/71804.

Eggleston , S. and Galbraith , E. D. The devil's in the disequilibrium: sensitivity of ocean carbon storage to climate state and iron fertilization in a general circulation model. *Biogeosciences Discussions*, 2017. doi: 10.5194/bg-2017-328.

EIA . EIA: International Energy Statistics. `http://www.eia.gov/cfapps/ipdbproject/IEDIndex3.cfm?tid=90&pid=44&aid=8`, 2018.

EPA . US EPA 2012 National Emissions Inventory (NEI) Air Pollutant Emissions Trends Data, 1970–2012 Average Annual Emissions, All Criteria Pollutants. 2012.

ESA-CCI . ESA-CCI: Land Cover CCI Climate Research Data Package v1.4.1. http://maps.elie.ucl.ac.be/CCI/viewer/download.php, 2018.

ESGF . ESGF, input4MIPs. https://esgf-node.llnl.gov/search/input4mips/, 2018.

et al. Ramankutty , N. Estimating historical changes in global land cover. 13, 997–1027, 1999.

Eyring , V., Bony , S., Meehl , G. A., Senior , C. A., Stevens , B., Stouffer , R. J., and Taylor , K. E. Overview of the Coupled Model Intercomparison Project Phase 6 (CMIP6) experimental design and organization. *Geoscientific Model Development*, 9, 1937–1958, 2016a. doi: 10.5194/gmd-9-1937-2016.

Eyring , V., Bony , S., Meehl , G. A., Senior , C. A., Stevens , B., Stouffer , R. J., and Taylor , K. E. Overview of the Coupled Model Intercomparison Project Phase 6 (CMIP6) experimental design and organization. *Geoscientific Model Development*, 9, 1937–1958, 2016b. doi: 10.5194/gmd-9-1937-2016.

Flato , G., Marotzke , J., Abiodun , B., Braconnot , P., Chou , S. C., Collins , W., Cox , P., Driouech , F., Emori , S., Eyring , V., Forest , C., Gleckler , P., Guilyardi , E., Jakob , C., Kattsov , V., Reason , C., and Rummukainen , M. *Evaluation of Climate Models*, book section 9, pages 741–866. Cambridge University Press, Cambridge, United Kingdom and New York, NY, USA, 2013. ISBN ISBN 978-1-107-66182-0. doi: 10.1017/CBO9781107415324.020.

Fricko , O., Havlik , P., Rogelj , J., Klimont , Z., Gusti , M., Johnson , N., Kolp , P., Strubegger , M., Valin , H., Amann , M., Ermolieva , T., Forsell , N., Herrero , M., Heyes , C., Kindermann , G., Krey , V., McCollum , D. L., Obersteiner , M., Pachauri , S., Rao , S., Schmid , E., Schoepp , W., and Riahi , K. The marker quantification of the Shared Socioeconomic Pathway 2: A middle-of-the-road scenario for the 21st century. *Global Environmental Change*, 42, 251–267, 2017. doi: 10.1016/j.gloenvcha.2016.06.004.

Friedlingstein , P., Fung , I., Holland , E., John , J., Brasseur , G., Erickson , D., and Schimel , D. On the Contribution of Co2 Fertilization to the Missing Biospheric Sink. *Global Biogeochemical Cycles*, 9, 541–556, 1995. doi: Doi 10.1029/95gb02381.

Friedlingstein , P., Cox , P., Betts , R., Bopp , L., von Bloh , W., Brovkin , V., Cadule , P., Doney , S., Eby , M., Fung , I., Bala , G., John , J., Jones , C., Joos , F., Kato , T., Kawamiya , M., Knorr , W., Lindsay , K., Matthews , H. D., Raddatz , T., Rayner , P., Reick , C., Roeckner , E., Schnitzler , K.-G., Schnur , R., Strassmann , K., Weaver , A. J., Yoshikawa , C., and Zeng , N. Climate–Carbon Cycle Feedback Analysis: Results from the C 4 MIP Model Intercomparison. *Journal of Climate*, 19, 3337–3353, 2006. doi: 10.1175/JCLI3800.1.

Friedlingstein , P., Andrew , R. M., Rogelj , J., Peters , G. P., Canadell , J. G., Knutti , R., Luderer , G., Raupach , M. R., Schaeffer , M., Van Vuuren , D. P., and Le Quéré , C. Persistent growth of CO2emissions and implications for reaching climate targets. *Nature Geoscience*, 7, 709–715, 2014a. doi: 10.1038/NGEO2248.

Friedlingstein , P., Meinshausen , M., Arora , V. K., Jones , C. D., Anav , A., Liddicoat , S. K., and Knutti , R. Uncertainties in CMIP5 climate projections due to carbon cycle feedbacks. *Journal of Climate*, 27, 511–526, 2014b. doi: 10.1175/JCLI-D-12-00579.1.

Frölicher , T. L., Winton , M., and Sarmiento , J. L. Continued global warming after CO2 emissions stoppage. *Nature Climate Change*, 4, 40–44, 2014. doi: 10.1038/nclimate2060.

Fujii , M., Ikeda , M., and Yamanaka , Y. Roles of Biogeochemical Processes in the Oceanic Car- bon Cycle Described with a Simple Coupled Physical- Biogeochemical Model. *Journal of Oceanography*, 61, 803–815, 2005.

Fujimori , S., Masui , T., and Matsuoka , Y. Development of a global computable general equilibrium model coupled with detailed energy end-use technology. *Applied Energy*, 128, 296–306, 2014. doi: 10.1016/j.apenergy.2014.04.074.

Fujimori , S., Hasegawa , T., Masui , T., Takahashi , K., Herran , D. S., Dai , H., Hijioka , Y., and Kainuma , M. SSP3: AIM implementation of Shared Socioeconomic Pathways. *Global Environmental Change*, 42, 268–283, 2017. doi: 10.1016/j.gloenvcha.2016.06.009.

Fuss , S., Canadell , J. G., Peters , G. P., Tavoni , M., Andrew , R. M., Ciais , P., Jackson , R. B., Jones , C. D., Kraxner , F., Nakicenovic , N., Le Quéré , C., Raupach , M. R., Sharifi , A., Smith , P., and Yamagata , Y. COMMENTARY: Betting on negative emissions. *Nature Climate Change*, 4, 850–853, 2014. doi: 10.1038/nclimate2392.

Gasser , T. and Ciais , P. A theoretical framework for the net land-to-atmosphere CO2 flux and its implications in the definition of "emissions from land-use change". *Earth System Dynamics*, 4, 171–186, 2013. doi: 10.5194/esd-4-171-2013.

Gasser , T., Guivarch , C., Tachiiri , K., Jones , C. D., and Ciais , P. Negative emissions physically needed to keep global warming below 2°C. *Nature Communications*, 6, 1–7, 2015. doi: 10.1038/ncomms8958.

Gasser , T. Attribution régionalisée des causes anthropiques du changement climatique, Thèse de doctorat Spécialité : Sciences du climat. 2014.

Gasser , T., Ciais , P., Boucher , O., Quilcaille , Y., Tortora , M., Bopp , L., and Hauglustaine , D. The compact Earth system model OSCAR v2.2: Description and first results. *Geoscientific Model Development*, 10, 271–319, 2017a. doi: 10.5194/gmd-10-271-2017.

Gasser , T., Peters , G. P., Fuglestvedt , J. S., Collins , W. J., Shindell , D. T., and Ciais , P. Accounting for the climate–carbon feedback in emission metric. *Earth System Dynamics*, 8, 235–253, 2017b. doi: 10.5194/esd-8-235-2017.

Gauci , V., Matthews , E., Dise , N., Walter , B., Koch , D., Granberg , G., and Vile , M. Sulfur pollution suppression of the wetland methane source in the 20th and 21st centuries. *Proceedings of the National Academy of Sciences*, 101, 12583–12587, 2004. doi: 10.1073/pnas.0404412101.

GCAM . Gcam v4.4 documentation: Global change assessment model (gcam). `http://jgcri.github.io/gcam-doc/`, 2017.

Gillett , N. P., Arora , V. K., Matthews , D., and Allen , M. R. Constraining the ratio of global warming to cumulative CO2emissions using CMIP5 simulations. *Journal of Climate*, 26, 6844–6858, 2013. doi: 10.1175/JCLI-D-12-00476.1.

Goll , D. S., Brovkin , V., Parida , B. R., Reick , C. H., Kattge , J., Reich , P. B., Van Bodegom , P. M., and Niinemets , Ü. Nutrient limitation reduces land carbon uptake in simulations with a model of combined carbon, nitrogen and phosphorus cycling. *Biogeosciences*, 9, 3547–3569, 2012. doi: 10.5194/bg-9-3547-2012.

González , M. F. and Ilyina , T. Impacts of artificial ocean alkalinization on the carbon cycle and climate in Earth system simulations. *Geophysical Research Letters*, 43, 6493–6502, 2016. doi: 10.1002/2016GL068576.

Granier , C., Bessagnet , B., Bond , T., D'Angiola , A., van der Gon , H. D., Frost , G. J., Heil , A., Kaiser , J. W., Kinne , S., Klimont , Z., Kloster , S., Lamarque , J. F., Liousse , C., Masui , T., Meleux , F., Mieville , A., Ohara , T., Raut , J. C., Riahi , K., Schultz , M. G., Smith , S. J., Thompson , A., van Aardenne , J., van der Werf , G. R., and van Vuuren , D. P. Evolution of anthropogenic and biomass burning emissions of air pollutants at global and regional scales during the 1980-2010 period. *Climatic Change*, 109, 163–190, 2011. doi: 10.1007/s10584-011-0154-1.

Greenstone , M. The Impacts of Environmental Regulations on Industrial Activity: Evidence from the 1970 and 1977 Clean Air Act Amendments and the Census of Manufactures. *Journal of Political Economy*, 110, 1175–1219, 2002. doi: 10.1086/342808.

Hao , H., Liu , Z., Zhao , F., and Li , W. Natural gas as vehicle fuel in China: A review. *Renewable and Sustainable Energy Reviews*, 62, 521–533, 2016. doi: 10.1016/j.rser.2016.05.015.

Haraway , D. Anthropocene, Capitalocene, Plantationocene, Chthulucene: Making Kin. *Environmental Humanities*, 6, 159–165, 2015. doi: 10.1215/22011919-3615934.

Harman , I. N. and Al. . SCCM – the Simple Carbon-Climate Model : Technical Documentation. Technical report, CAWCR, 2011.

Hartmann , D. L., Klein Tank , A. M. G., Rusticucci , M., Alexander , L. V., Brönnimann , S., Charabi , Y., Dentener , F. J., Dlugokencky , E. J., Easterling , D. R., Kaplan , A., Soden , B. J., Thorne , P. W., Wild , M., and Zhai , P. M. *Observations: Atmosphere and Surface*, book section 2, pages 159–254. Cambridge University Press, Cambridge, United Kingdom and New York, NY, USA, 2013. ISBN ISBN 978-1-107-66182-0. doi: 10.1017/CBO9781107415324.008.

Hasegawa , T., Fujimori , S., Ito , A., Takahashi , K., and Masui , T. Global land-use allocation model linked to an integrated assessment model. *Science of the Total Environment*, 580, 787–796, 2017. doi: 10.1016/j.scitotenv.2016.12.025.

Hauck , J., Köhler , P., Wolf-Gladrow , D., and Völker , C. Iron fertilisation and century-scale effects of open ocean dissolution of olivine in a simulated CO2removal experiment. *Environmental Research Letters*, 11, 2016. doi: 10.1088/1748-9326/11/2/024007.

Havlík , P., Schneider , U. A., Schmid , E., Böttcher , H., Fritz , S., Skalský , R., Aoki , K., Cara , S. D., Kindermann , G., Kraxner , F., Leduc , S., McCallum , I., Mosnier , A., Sauer , T., and Obersteiner , M. Global land-use implications of first and second generation biofuel targets. *Energy Policy*, 39, 5690–5702, 2011. doi: 10.1016/j.enpol.2010.03.030.

Hawkins , E. and Sutton , R. The potential to narrow uncertainty in regional climate predictions. *Bulletin of the American Meteorological Society*, 90, 1095–1107, 2009. doi: 10.1175/2009BAMS2607.1.

Hawkins , E., Ortega , P., Suckling , E., Schurer , A., Hegerl , G., Jones , P., Joshi , M., Osborn , T. J., Masson-Delmotte , V., Mignot , J., Thorne , P., and Van Oldenborgh , G. J. Estimating changes in global temperature since the preindustrial period. *Bulletin of the American Meteorological Society*, 98, 1841–1856, 2017. doi: 10.1175/BAMS-D-16-0007.1.

Heinimann , A., Mertz , O., Frolking , S., Christensen , A. E., Hurni , K., Sedano , F., Chini , L. P., Sahajpal , R., Hansen , M., and Hurtt , G. A global view of shifting cultivation: Recent, current, and future extent. *PLoS ONE*, 12, 1–21, 2017. doi: 10.1371/journal.pone.0184479.

Hiç , C., Pradhan , P., Rybski , D., and Kropp , J. P. Food Surplus and Its Climate Burdens. *Environmental Science and Technology*, 50, 4269–4277, 2016. doi: 10.1021/acs.est.5b05088.

Hoesly , R. M., Smith , S. J., Feng , L., Klimont , Z., Janssens-Maenhout , G., Pitkanen , T., Seibert , J. J., Vu , L., Andres , R. J., Bolt , R. M., Bond , T. C., Dawidowski , L., Kholod , N., Kurokawa , J.-i., Li , M., Liu , L., Lu , Z., Moura , M.

C. P., O'Rourke , P. R., and Zhang , Q. Historical (1750–2014) anthropogenic emissions of reactive gases and aerosols from the Community Emission Data System (CEDS). *Geoscientific Model Development Discussions*, 2017. doi: 10.5194/gmd-2017-43.

Houghton , J. T., Jenkins , G. J., and Ephraums , J. J. Climate Change. The IPCC Scientific Assessment. *Cambridge University Press, Cambridge, United Kingdom and New York, NY, USA*, 1990.

Hurtt , G. C., Chini , L. P., Frolking , S., Betts , R. A., Feddema , J., Fischer , G., Fisk , J. P., Hibbard , K., Houghton , R. A., Janetos , A., Jones , C. D., Kindermann , G., Kinoshita , T., Klein Goldewijk , K., Riahi , K., Shevliakova , E., Smith , S., Stehfest , E., Thomson , A., Thornton , P., van Vuuren , D. P., and Wang , Y. P. Harmonization of land-use scenarios for the period 1500-2100: 600 years of global gridded annual land-use transitions, wood harvest, and resulting secondary lands. *Climatic Change*, 109, 117–161, 2011. doi: 10.1007/s10584-011-0153-2.

Hurtt , G. C., Frolking , S., Fearon , M. G., Moore , B., Shevliakova , E., Malyshev , S., Pacala , S. W., and Houghton , R. A. The underpinnings of land-use history: Three centuries of global gridded land-use transitions, wood-harvest activity, and resulting secondary lands. *Global Change Biology*, 12, 1208–1229, 2006. doi: 10.1111/j.1365-2486.2006.01150.x.

IEA . IEA: CO2 emission statistics. http://www.iea.org/statistics/topics/co2emissions/, 2018.

IIASA . AR5WG3 database. https://secure.iiasa.ac.at/web-apps/ene/AR5DB/dsd?Action=htmlpage&page=welcome, 2018a.

IIASA . RCP database. http://tntcat.iiasa.ac.at:8787/RcpDb/dsd?Action=htmlpage&page=welcome, 2018b.

IIASA . SSP database. https://tntcat.iiasa.ac.at/SspDb/dsd?Action=htmlpage&page=welcome, 2018c.

IIASA . SSP: detailed comparison of model characteristics. https://tntcat.iiasa.ac.at/SspDb/download/iam_scenario_doc/SSP_Model_Documentation.xlsx, 2018d.

IIASA . SSP study protocol. https://tntcat.iiasa.ac.at/SspDb/download/iam_scenario_doc/SSP_Study_Protocol.pdf, 2018e.

Ilyina , T., Wolf-Gladrow , D., Munhoven , G., and Heinze , C. Assessing the potential of calcium-based artificial ocean alkalinization to mitigate rising atmospheric CO2 and ocean acidification. *Geophysical Research Letters*, 40, 5909–5914, 2013. doi: 10.1002/2013GL057981.

IMS Luxembourg Magazine . Towards a civilisational change. *IMS*.

IPCC . Revised 1996 IPCC Guidelines for National Greenhouse Gas Inventories vol. 1-3. *Intergovernmental Panel on Climate Change*, 1996.

IPCC . 2006 IPCC Guidelines for National Greenhouse Gas Inventories vol. 1-5. *2006 IPCC Guidelines for National Greenhouse Gas Inventories*, 2006.

IPCC . *Annex II: Climate System Scenario Tables*, book section AII, pages 1395–1446. Cambridge University Press, Cambridge, United Kingdom and New York, NY, USA, 2013. ISBN ISBN 978-1-107-66182-0. doi: 10.1017/CBO9781107415324.030.

IPCC, Working Group I . Climate change 1990: The science of climate change. contribution of working group i to the first assessment report of the intergovernmental panel on climate change, 1990.

IPCC, Working Group I . Climate change 1995: The science of climate change, contribution of working group i to the second assessment report of the intergovernmental panel on climate change, 1996.

IPCC, Working Group I . *Climate Change 2001: The Scientific Basis. Contribution of Working Group I to the Third Assessment Report of the Intergovernmental Panel on Climate Change*. Cambridge University Press, 2001.

IPCC, Working Group I . *Climate Change 2007: The Physical Science Basis. Contribution of Working Group I to the Fourth Assessment Report of the Intergovernmental Panel on Climate Change*. Cambridge University Press, 2007.

IPCC, Working Group I . *Climate Change 2013: The Physical Science Basis. Contribution of Working Group I to the Fifth Assessment Report of the Intergovernmental Panel on Climate Change*. Cambridge University Press, 2013.

Ito , A. and Penner , J. E. Historical emissions of carbonaceous aerosols from biomass and fossil fuel burning for the period 1870-2000. *Global Biogeochemical Cycles*, 19, 1–14, 2005. doi: 10.1029/2004GB002374.

Janssens-Maenhout , G., Crippa , M., Guizzardi , D., Dentener , F., Muntean , M., Pouliot , G., Keating , T., Zhang , Q., Kurokawa , J., Wankmüller , R., Denier Van Der Gon , H., Kuenen , J. J., Klimont , Z., Frost , G., Darras , S., Koffi , B., and Li , M. HTAP-v2.2: A mosaic of regional and global emission grid maps for 2008 and 2010 to study hemispheric transport of air pollution. *Atmospheric Chemistry and Physics*, 15, 11411–11432, 2015. doi: 10.5194/acp-15-11411-2015.

Jerez , S., Tobin , I., Vautard , R., Montávez , J. P., López-Romero , J. M., Thais , F., Bartok , B., Christensen , O. B., Colette , A., Déqué , M., Nikulin , G., Kotlarski , S., van Meijgaard , E., Teichmann , C., and Wild , M. The impact of climate change on photovoltaic power generation in Europe. *Nature Communications*, 6, 10014, 2015. doi: 10.1038/ncomms10014.

Joint Research Centre . EDGAR4.2: Emission Database for Global Atmospheric Research. *Global Emissions EDGAR v4.2*, 2011. doi: 10.2904/EDGARv4.2.

Jones , C. D., Ciais , P., Davis , S. J., Friedlingstein , P., Gasser , T., Peters , G. P., Rogelj , J., van Vuuren , D. P., Canadell , J. G., Cowie , A., Jackson , R. B., Jonas , M., Kriegler , E., Littleton , E., Lowe , J. A., Milne , J., Shrestha , G., Smith , P., Torvanger , A., and Wiltshire , A. Simulating the Earth system response to negative emissions. *Environmental Research Letters*, 11, 095012, 2016a. doi: 10.1088/1748-9326/11/9/095012.

Jones , C., Lowe , J., Liddicoat , S., and Betts , R. Committed terrestrial ecosystem changes due to climate change. *Nature Geoscience*, 2, 484-487, 2009. doi: 10.1038/ngeo555.

Jones , C., Liddicoat , S., and Lowe , J. Role of terrestrial ecosystems in determining CO2stabilization and recovery behaviour. *Tellus, Series B: Chemical and Physical Meteorology*, 62, 682–699, 2010. doi: 10.1111/j.1600-0889.2010.00490.x.

Jones , C. D., Arora , V., Friedlingstein , P., Bopp , L., Brovkin , V., Dunne , J., Graven , H., Hoffman , F., Ilyina , T., John , J. G., Jung , M., Kawamiya , M., Koven , C., Pongratz , J., Raddatz , T., Randerson , J. T., and Zaehle , S. C4MIP-The Coupled Climate-Carbon Cycle Model Intercomparison Project: Experimental protocol for CMIP6. *Geoscientific Model Development*, 9, 2853–2880, 2016b. doi: 10.5194/gmd-9-2853-2016.

Joos , F., Sarmiento , J. L., and Siegenthaler , U. Estimates of the effect of Southern Ocean iron fertilization on atmospheric CO sub(2) concentrations. *Nature*, 349, 772–774, 1991. doi: 10.1038/349772a0.

Joos , F., Roth , R., Fuglestvedt , J. S., Peters , G. P., Enting , I. G., Von Bloh , W., Brovkin , V., Burke , E. J., Eby , M., Edwards , N. R., Friedrich , T., Frölicher , T. L., Halloran , P. R., Holden , P. B., Jones , C., Kleinen , T., Mackenzie , F. T., Matsumoto , K., Meinshausen , M., Plattner , G. K., Reisinger , A., Segschneider , J., Shaffer , G., Steinacher , M., Strassmann , K., Tanaka , K., Timmermann , A., and Weaver , A. J. Carbon dioxide and climate impulse response functions for the computation of greenhouse gas metrics: A multi-model analysis. *Atmospheric Chemistry and Physics*, 13, 2793–2825, 2013. doi: 10.5194/acp-13-2793-2013.

Joos , F., Bruno , M., Fink , R., Siegenthaler , U., Stocker , T. F., Le Quéré , C., and Sarmiento , J. L. An efficient and accurate representation of complex oceanic and biospheric models of anthropogenic carbon uptake. *Tellus*, 48, 397–417, 1996. doi: 10.1034/j.1600-0889.1996.t01-2-00006.x.

Junker , C. and Liousse , C. A global emission inventory of carbonaceous aerosol from historic records of fossil fuel and biofuel consumption for the period 1860–1997. *Atmospheric Chemistry and Physics Discussions*, 6, 4897–4927, 2006. doi: 10.5194/acpd-6-4897-2006.

Keeling , C. D., Adams , J. A., Ekdahl , C. a., and Guenther , P. R. Atmospheric carbon dioxide variations at the South Pole. *Tellus*, 28, 552–564, 1976a. doi: 10.1111/j.2153-3490.1976.tb00702.x.

Keeling , C. D., Bacastow , R. B., Bainbridge , A. E., Ekdahl Jr. , C. A., Guenther , P. R., Waterman , L. S., and Chin , J. F. S. Atmospheric carbon dioxide variations at Mauna Loa Observatory, Hawaii. *Tellus*, 28, 538–551, 1976b. doi: 10.3402/tellusa.v28i6.11322.

Keller , D. P., Lenton , A., Scott , V., Vaughan , N. E., Bauer , N., Ji , D., Jones , C. D., Kravitz , B., Muri , H., and Zickfeld , K. The Carbon Dioxide Removal Model Intercomparison Project (CDR-MIP): Rationale and experimental design. *Geoscientific Model Development Discussions*, 2017. doi: 10.5194/gmd-2017-168.

Kemper , J. Biomass and carbon dioxide capture and storage: A review. *International Journal of Greenhouse Gas Control*, 40, 401–430, 2015. doi: 10.1016/j.ijggc.2015.06.012.

Kheshgi , H. S. Sequestering atmospheric carbon dioxide by increasing ocean alkalinity. *Energy*, 20, 915–922, 1995. doi: 10.1016/0360-5442(95)00035-F.

Kiel Earth Institute . CDR Model Intercomparison project website. `https://www.kiel-earth-institute.de/CDR_Model_Intercomparison_Project.html`, 2018.

Kindermann , G. E., Obersteiner , M., Rametsteiner , E., and McCallum , I. Predicting the deforestation-trend under different carbon-prices. *Carbon Balance and Management*, 1, 1–17, 2006. doi: 10.1186/1750-0680-1-15.

Kirchhoff , G. On the relation between the radiating and absorbing powers of different bodies for light and heat. *The London, Edinburgh, and Dublin Philosophical Magazine and Journal of Science*, 20, 1-21, 1860. doi: 10.1080/14786446008642901.

Kirschke , S., Bousquet , P., Ciais , P., Saunois , M., Canadell , J. G., Dlugokencky , E. J., Bergamaschi , P., Bergmann , D., Blake , D. R., Bruhwiler , L., Cameron-Smith , P., Castaldi , S., Chevallier , F., Feng , L., Fraser , A., Heimann , M., Hodson , E. L., Houweling , S., Josse , B., Fraser , P. J., Krummel , P. B., Lamarque , J.-F., Langenfelds , R. L., Le Quéré , C., Naik , V., O'Doherty , S., Palmer , P. I., Pison , I., Plummer , D., Poulter , B., Prinn , R. G., Rigby , M., Ringeval , B., Santini , M., Schmidt , M., Shindell , D. T., Simpson , I. J., Spahni , R., Steele , L. P., Strode , S. A., Sudo , K., Szopa , S., van der Werf , G. R., Voulgarakis , A., van Weele , M., Weiss , R. F., Williams , J. E., and Zeng , G. Three decades of global methane sources and sinks. *Nature Geoscience*, 6, 813–823, 2013. doi: 10.1038/ngeo1955.

Knutti , R. and Sedláček , J. Robustness and uncertainties in the new CMIP5 climate model projections. *Nature Climate Change*, 3, 369–373, 2012. doi: 10.1038/nclimate1716.

Kohler , P., Hartmann , J., and Wolf-Gladrow , D. A. Geoengineering potential of artificially enhanced silicate weathering of olivine. *Proceedings of the National Academy of Sciences*, 107, 20228–20233, 2010. doi: 10.1073/pnas.1000545107.

Köhler , P., Abrams , J. F., Völker , C., Hauck , J., and Wolf-Gladrow , D. A. Geoengineering impact of open ocean dissolution of olivine on atmospheric CO2, surface ocean pH and marine biology. *Environmental Research Letters*, 8, 2013. doi: 10.1088/1748-9326/8/1/014009.

Kravitz , B., Lynch , C., Hartin , C., and Bond-Lamberty , B. Exploring precipitation pattern scaling methodologies and robustness among CMIP5 models. *Geoscientific Model Development*, 10, 1889–1902, 2017. doi: 10.5194/gmd-10-1889-2017.

Krey , V., Havlik , P., Fricko , O., Zilliacus , J., Gidden , M., Strubegger , M., Kartasasmita , G., Ermolieva , T., Forsell , N., Gusti , M., Johnson , N., Kindermann , G., Kolp , P., McCollum , D. L., Pachauri , S., Rao , S., Rogelj , J., Valin , H., Obersteiner , M., and Riahi , K. MESSAGE-GLOBIOM 1.0 Documentation. http://data.ene.iiasa.ac.at/message-globiom/, 2016.

Kriegler , E., Edmonds , J., Hallegatte , S., Ebi , K. L., Kram , T., Riahi , K., Winkler , H., and van Vuuren , D. P. A new scenario framework for climate change research: The concept of shared climate policy assumptions. *Climatic Change*, 122, 401–414, 2014. doi: 10.1007/s10584-013-0971-5.

Kriegler , E., Bauer , N., Popp , A., Humpenöder , F., Leimbach , M., Strefler , J., Baumstark , L., Bodirsky , B. L., Hilaire , J., Klein , D., Mouratiadou , I., Weindl , I., Bertram , C., Dietrich , J. P., Luderer , G., Pehl , M., Pietzcker , R., Piontek , F., Lotze-Campen , H., Biewald , A., Bonsch , M., Giannousakis , A., Kreidenweis , U., Müller , C., Rolinski , S., Schultes , A., Schwanitz , J., Stevanovic , M., Calvin , K., Emmerling , J., Fujimori , S., and Edenhofer , O. Fossil-fueled development (SSP5): An energy and resource intensive scenario for the 21st century. *Global Environmental Change*, 42, 297–315, 2017. doi: 10.1016/j.gloenvcha.2016.05.015.

Kroeker , K. J., Kordas , R. L., Crim , R., Hendriks , I. E., Ramajo , L., Singh , G. S., Duarte , C. M., and Gattuso , J. P. Impacts of ocean acidification on marine organisms: Quantifying sensitivities and interaction with warming. *Global Change Biology*, 19, 1884–1896, 2013. doi: 10.1111/gcb.12179.

Lackner , K. S., Brennan , S., Matter , J. M., Park , A.-H. A., Wright , A., and van der Zwaan , B. The urgency of the development of CO2 capture from ambient air. *Proceedings of the National Academy of Sciences*, 109, 13156–13162, 2012. doi: 10.1073/pnas.1108765109.

Lamarque , J. F., Bond , T. C., Eyring , V., Granier , C., Heil , A., Klimont , Z., Lee , D., Liousse , C., Mieville , A., Owen , B., Schultz , M. G., Shindell , D., Smith , S. J., Stehfest , E., Van Aardenne , J., Cooper , O. R., Kainuma , M., Mahowald , N., McConnell , J. R., Naik , V., Riahi , K., and Van Vuuren , D. P. Historical (1850-2000) gridded anthropogenic and biomass burning emissions of reactive gases and aerosols: Methodology and application. *Atmospheric Chemistry and Physics*, 10, 7017–7039, 2010. doi: 10.5194/acp-10-7017-2010.

Lamarque , J. F., Kyle , P. P., Meinshausen , M., Riahi , K., Smith , S. J., van Vuuren , D. P., Conley , A. J., and Vitt , F. Global and regional evolution of short-lived radiatively-active gases and aerosols in the Representative Concentration Pathways. *Climatic Change*, 109, 191–212, 2011. doi: 10.1007/s10584-011-0155-0.

Lawrence , D. M., Hurtt , G. C., Arneth , A., Brovkin , V., Calvin , K. V., Jones , A. D., Jones , C. D., Lawrence , P. J., Noblet-Ducoudré , N. D., Pongratz , J., Seneviratne , S. I., and Shevliakova , E. The Land Use Model Intercomparison Project (LUMIP) contribution to CMIP6: Rationale and experimental design. *Geoscientific Model Development*, 9, 2973–2998, 2016. doi: 10.5194/gmd-9-2973-2016.

Le Quéré , C., Moriarty , R., Andrew , R. M., Canadell , J. G., Sitch , S., Korsbakken , J. I., Friedlingstein , P., Peters , G. P., Andres , R. J., Boden , T. A., Houghton , R. A., House , J. I., Keeling , R. F., Tans , P., Arneth , A., Bakker , D. C., Barbero , L., Bopp , L., Chang , J., Chevallier , F., Chini , L. P., Ciais , P., Fader , M., Feely , R. A., Gkritzalis , T., Harris , I., Hauck , J., Ilyina , T., Jain , A. K., Kato , E., Kitidis , V., Klein Goldewijk , K., Koven , C., Landschützer , P., Lauvset , S. K., Lefèvre , N., Lenton , A., Lima , I. D., Metzl , N., Millero , F., Munro , D. R., Murata , A., S. Nabel , J. E., Nakaoka , S., Nojiri , Y., O'Brien , K., Olsen , A., Ono , T., Pérez , F. F., Pfeil , B., Pierrot , D., Poulter , B., Rehder , G., Rödenbeck , C., Saito , S., Schuster , U., Schwinger , J., Séférian , R., Steinhoff , T., Stocker , B. D., Sutton , A. J., Takahashi , T., Tilbrook , B., Van Der Laan-Luijkx , I. T., Van Der Werf , G. R., Van Heuven , S., Vandemark , D., Viovy , N., Wiltshire , A., Zaehle , S., and Zeng , N. Global Carbon Budget 2015. *Earth System Science Data*, 7, 349–396, 2015. doi: 10.5194/essd-7-349-2015.

Le Quéré , C., Andrew , R. M., Canadell , J. G., Sitch , S., Ivar Korsbakken , J., Peters , G. P., Manning , A. C., Boden , T. A., Tans , P. P., Houghton , R. A., Keeling , R. F., Alin , S., Andrews , O. D., Anthoni , P., Barbero , L., Bopp , L., Chevallier , F., Chini , L. P., Ciais , P., Currie , K., Delire , C., Doney , S. C., Friedlingstein , P., Gkritzalis , T., Harris , I., Hauck , J., Haverd , V., Hoppema , M., Klein Goldewijk , K., Jain , A. K., Kato , E., Körtzinger , A., Landschützer , P., Lefèvre , N., Lenton , A., Lienert , S., Lombardozzi , D., Melton , J. R., Metzl , N., Millero , F., Monteiro , P. M., Munro , D. R., Nabel , J. E., Nakaoka , S. I., O'Brien , K., Olsen , A., Omar , A. M., Ono , T., Pierrot , D., Poulter , B., Rödenbeck , C., Salisbury , J., Schuster , U., Schwinger , J., Séférian , R.,

Skjelvan , I., Stocker , B. D., Sutton , A. J., Takahashi , T., Tian , H., Tilbrook , B., Van Der Laan-Luijkx , I. T., Van Der Werf , G. R., Viovy , N., Walker , A. P., Wiltshire , A. J., and Zaehle , S. Global Carbon Budget 2016. *Earth System Science Data*, 8, 605–649, 2016. doi: 10.5194/essd-8-605-2016.

Lenton , T. M., Held , H., Kriegler , E., Hall , J. W., Lucht , W., Rahmstorf , S., and Schellnhuber , H. J. Tipping elements in the earth's climate system. *Proceedings of the National Academy of Sciences*, 105, 1786–1793, 2008. doi: 10.1073/pnas.0705414105.

Levavasseur , G., Vrac , M., Roche , D. M., and Paillard , D. Statistical modelling of a new global potential vegetation distribution. *Environmental Research Letters*, 7, 2012. doi: 10.1088/1748-9326/7/4/044019.

Li , B., Gasser , T., Ciais , P., Piao , S., Tao , S., Balkanski , Y., Hauglustaine , D., Boisier , J.-P., Chen , Z., Huang , M., Li , L. Z., Li , Y., Liu , H., Liu , J., Peng , S., Shen , Z., Sun , Z., Wang , R., Wang , T., Yin , G., Yin , Y., Zeng , H., Zeng , Z., and Zhou , F. The contribution of China's emissions to global climate forcing. *Nature*, 531, 357–361, 2016. doi: 10.1038/nature17165.

Li , M., Klimont , Z., Zhang , Q., Martin , R. V., Zheng , B., Heyes , C., Cofala , J., and He , K. Comparison and evaluation of anthropogenic emissions of SO₂ and NO<sub>x<\\sub> over China. *Atmospheric Chemistry and Physics Discussions*, 2017a. doi: 10.5194/acp-2017-646.

Li , W., Ciais , P., Yue , C., Gasser , T., Peng , S., and Bastos , A. Gross changes in forest area shape the future carbon balance of tropical forests. *Biogeosciences Discussions*, 2017, 1–19, 2017b. doi: 10.5194/bg-2017-291.

Lima , I. D., Lam , P. J., and Doney , S. C. Dynamics of particulate organic carbon flux in a global ocean model. *Biogeosciences*, 11, 1177–1198, 2014. doi: 10.5194/bg-11-1177-2014.

Liu , Z., Guan , D., Wei , W., Davis , S. J., Ciais , P., Bai , J., Peng , S., Zhang , Q., Hubacek , K., Marland , G., Andres , R. J., Crawford-Brown , D., Lin , J., Zhao , H., Hong , C., Boden , T. A., Feng , K., Peters , G. P., Xi , F., Liu , J., Li , Y., Zhao , Y., Zeng , N., and He , K. Reduced carbon emission estimates from fossil fuel combustion and cement production in China. *Nature*, 524, 335–338, 2015. doi: 10.1038/nature14677.

Lotze-Campen , H., Müller , C., Bondeau , A., Rost , S., Popp , A., and Lucht , W. Global food demand, productivity growth, and the scarcity of land and water resources: A spatially explicit mathematical programming approach. *Agricultural Economics*, 39, 325–338, 2008. doi: 10.1111/j.1574-0862.2008.00336.x.

Lucas , P. L., van Vuuren , D. P., Olivier , J. G., and den Elzen , M. G. Long-term reduction potential of non-CO2 greenhouse gases. *Environmental Science and Policy*, 10, 85–103, 2007. doi: 10.1016/j.envsci.2006.10.007.

Luderer , G., Leimbach , M., Bauer , N., Kriegler , E., Baumstark , L., Bertram , C., Giannousakis , A., Hilaire , J., Klein , D., Levesque , A., Mouratiadou , I., Pehl , M., Pietzcker , R., Piontek , F., Roming , N., Schultes , A. S., Jana , V., and Strefler , J. Description of the REMIND Model 1.6.

Lueker , T. J., Dickson , A. G., and Keeling , C. D. Ocean pCO2 calculated from dissolved inorganic carbon, alkalinity, and equations for K1 and K2: validation based on laboratory measurements of CO2 in gas and seawater at equilibrium. *Marine Chemistry*, 70, 105–119, 2000. doi: 10.1016/S0304-4203(00)00022-0.

LUH2 . Official LUH2 Future Scenario datasets for CMIP6. `http://luh.umd.edu/data.shtml`, 2018.

Marangoni , G., Tavoni , M., Bosetti , V., Borgonovo , E., Capros , P., Fricko , O., Gernaat , D. E. H. J., Guivarch , C., Havlik , P., Huppmann , D., Johnson , N., Karkatsoulis , P., Keppo , I., Krey , V., Ó Broin , E., Price , J., and van Vuuren , D. P. Sensitivity of projected long-term CO2 emissions across the Shared Socioeconomic Pathways. *Nature Climate Change*, 7, 113–117, 2017. doi: 10.1038/nclimate3199.

Marland , G. and Rotty , R. M. Carbon dioxide emissions from fossil fuels: a procedure for estimation and results for 1950–1982. *Tellus B*, 36 B, 232–261, 1984. doi: 10.1111/j.1600-0889.1984.tb00245.x.

Marland , G., Hamal , K., and Jonas , M. How uncertain are estimates of CO2 emissions? *Journal of Industrial Ecology*, 13, 4–7, 2009. doi: 10.1111/j.1530-9290.2009.00108.x.

Masui , T., Matsumoto , K., Hijioka , Y., Kinoshita , T., Nozawa , T., Ishiwatari , S., Kato , E., Shukla , P. R., Yamagata , Y., and Kainuma , M. An emission pathway for stabilization at 6 Wm-2 radiative forcing. *Climatic Change*, 109, 59–76, 2011. doi: 10.1007/s10584-011-0150-5.

Matthews , H. D. and Caldeira , K. Stabilizing climate requires near-zero emissions. *Geophysical Research Letters*, 35, 1–5, 2008. doi: 10.1029/2007GL032388.

Matthews , H., Weaver , A., Meissner , K., Gillett , N., and Eby , M. Natural and anthropogenic climate change: incorporating historical land cover change, vegetation dynamics and the global carbon cycle. *Climate Dynamics*, 22, 461–479, 2004. doi: 10.1007/s00382-004-0392-2.

Meinshausen , M., Raper , S. C. B., and Wigley , T. M. L. Emulating atmosphere-ocean and carbon cycle models with a simpler model, MAGICC6[mdash]Part 1: Model description and calibration. *Atmos. Chem. Phys.*, 11, 1417–1456, 2011a.

Meinshausen , M., Meinshausen , N., Hare , W., Raper , S. C. B., Frieler , K., Knutti , R., Frame , D. J., and Allen , M. R. Greenhouse-gas emission targets for limiting global warming to 2C. *Nature*, 458, 1158–1162, 2009. doi: 10.1038/nature08017.

Meinshausen , M., Smith , S. J., Calvin , K., Daniel , J. S., Kainuma , M. L., Lamarque , J., Matsumoto , K., Montzka , S. A., Raper , S. C., Riahi , K., Thomson , A., Velders , G. J., and van Vuuren , D. P. The RCP greenhouse gas concentrations and their extensions from 1765 to 2300. *Climatic Change*, 109, 213–241, 2011b. doi: 10.1007/s10584-011-0156-z.

Meinshausen , M., Vogel , E., Nauels , A., Lorbacher , K., Meinshausen , N., Etheridge , D. M., Fraser , P. J., Montzka , S. A., Rayner , P. J., Trudinger , C. M., Krummel , P. B., Beyerle , U., Canadell , J. G., Daniel , J. S., Enting , I. G., Law , R. M., Lunder , C. R., O'Doherty , S., Prinn , R. G., Reimann , S., Rubino , M., Velders , G. J., Vollmer , M. K., Wang , R. H., and Weiss , R. Historical greenhouse gas concentrations for climate modelling (CMIP6). *Geoscientific Model Development*, 10, 2057–2116, 2017. doi: 10.5194/gmd-10-2057-2017.

Melton , J. R., Wania , R., Hodson , E. L., Poulter , B., Ringeval , B., Spahni , R., Bohn , T., Avis , C. A., Beerling , D. J., Chen , G., Eliseev , A. V., Denisov , S. N., Hopcroft , P. O., Lettenmaier , D. P., Riley , W. J., Singarayer , J. S., Subin , Z. M., Tian , H., Zürcher , S., Brovkin , V., van Bodegom , P. M., Kleinen , T., Yu , Z. C., and Kaplan , J. O. Present state of global wetland extent and wetland methane modelling: conclusions from a model inter-comparison project (wetchimp). *Biogeosciences*, 10, 753–788, 2013. doi: 10.5194/bg-10-753-2013.

MESSAGE . Description of MESSAGE. `https://wiki.ucl.ac.uk/display/ADVIAM/MESSAGE`, 2018.

Milankovictch , M. *Canon of insolation and the ice-age problem (Kanon der Erdbestrahlung und seine Anwendung auf das Eiszeitenproblem) Belgrade, 1941.* 1969.

Millar , R. J., Fuglestvedt , J. S., Friedlingstein , P., Rogelj , J., Grubb , M. J., Matthews , H. D., Skeie , R. B., Forster , P. M., Frame , D. J., and Allen , M. R. Emission budgets and pathways consistent with limiting warming to 1.5C. *Nature Geoscience*, 2017. doi: 10.1038/ngeo3031.

Millero , F. J. Thermodynamics of the carbon dioxide system in the oceans. *Science*, 59, 661–677, 1995. doi: 10.1016/0016-7037(94)00354-O.

Millero , F. J. Carbonate constant for estuarine waters. *Marine and Freshwater Research*, 61, 139–142, 2010.

Millero , F. J., Pierrot , D., Lee , K., Wanninkhof , R., Feely , R., Sabine , C. L., Key , R. M., and Takahashi , T. Dissociation constants for carbonic acid determined from eld measurements. *Deep-Sea Research*, 49, 1705–1723, 2002.

MOCSY . mocsy 2.0, Fortran 95 routines to model ocean carbonate system thermodynamics. `http://ocmip5.ipsl.jussieu.fr/mocsy/`, 2018.

MODIS . Global Mosaics of the Standard MODIS Land Cover Type Data. `http://glcf.umd.edu/data/lc/`, 2018.

Mohr , S. H., Wang , J., Ellem , G., Ward , J., and Giurco , D. Projection of world fossil fuels by country. *Fuel*, 141, 120–135, 2015. doi: http://dx.doi.org/10.1016/j.fuel.2014.10.030.

Mohr , S. and Evans , P. G. M. Projection of world fossil fuel production with supply and demand interactions. *Chemical Engineering Department*, Doctor of, 783, 2010.

Molina , M. J. and Rowland , F. S. Stratospheric sink for chlorofluoromethanes: chlorine atom-catalysed destruction of ozone. *Nature*, 249, 1974. doi: 10.1038/249810a0.

Moss , R. H., Edmonds , J. A., Hibbard , K. A., Manning , M. R., Rose , S. K., van Vuuren , D. P., Carter , T. R., Emori , S., Kainuma , M., Kram , T., Meehl , G. A., Mitchell , J. F. B., Nakicenovic , N., Riahi , K., Smith , S. J., Stouffer , R. J., Thomson , A. M., Weyant , J. P., and Wilbanks , T. J. The next generation of scenarios for climate change research and assessment. *Nature*, 463, 747–756, 2010. doi: 10.1038/nature08823.

Muratori , M., Calvin , K., Wise , M., Kyle , P., and Edmonds , J. Global economic consequences of deploying bioenergy with carbon capture and storage (BECCS). *Environmental Research Letters*, 11, 2016. doi: 10.1088/1748-9326/11/9/095004.

Muri , H. The role of large—scale beccs in the pursuit of the 1.5°c target: an earth system model perspective. *Environmental Research Letters*, 13, 044010, 2018.

Murphy , J. M., Sexton , D. M. H., Barnett , D. N., Jones , G. S., Webb , M. J., Collins , M., and Stainforth , D. A. Quantification of modelling uncertainties in a large ensemble of climate change simulations. *Nature*, 430, 768–772, 2004. doi: 10.1038/nature02771.

Muzio , L. J., Quartucy , G. C., Energy , F., Pointe , C. S., and Hills , L. Implementing NOx Control : Research to Application. *Progress in Energy and Combustion Science*, 23, 233–266, 1997. doi: 10.1016/S0360-1285(97)00002-6.

Myhre , G., Shindell , D., Bréon , F.-M., Collins , W., Fuglestvedt , J., Huang , J., Koch , D., Lamarque , J.-F., Lee , D., Mendoza , B., Nakajima , T., Robock , A., Stephens , G., Takemura , T., and Zhang , H. *Anthropogenic and Natural Radiative Forcing*, book section 8, pages 659–740. Cambridge University Press, Cambridge, United Kingdom and New York, NY, USA, 2013. ISBN ISBN 978-1-107-66182-0. doi: 10.1017/ CBO9781107415324.01.

Nakicenovic , N., Alcamo , J., Davis , G., de Vries , B., Fenhann , J., Gaffin , S., Gregory , K., Grübler , A., Yong Jung , T., Kram , T., Lebre La Rovere , E., Michaelis , L., Mori , S., Morita , T., Pepper , W., Pitcher , H., Price , L., Riahi , K., Roehrl , A., Rogner , H.-H., Sankovski , A., Schlesinger , M., Shukla , P., Smith , S., Swart , R., van Rooijen , S., Victor , N., and Zhou , D. Special

Report on Emissions Scenarios: A Special Report of Working Group III of the Intergovernmental Panel on Climate Change. *Intergovernmental Panel on Climate Change*, 2000.

Narayanan , B. G. and Walmsley , T. L. Global Trade, Assistance, and Production: The GTAP 7 Data Base, Center for Global Trade Analysis. *Editors, Purdue University*, 2008.

Nemet , G. F., Holloway , T., and Meier , P. Implications of incorporating air-quality co-benefits into climate change policymaking. *Environmental Research Letters*, 5, 014007, 2010. doi: 10.1088/1748-9326/5/1/014007.

Novakov , T., Ramanathan , V., Hansen , J. E., Kirchstetter , T. W., Sato , M., Sinton , J. E., and Sathaye , J. A. Large historical changes of fossil-fuel black carbon aerosols. *Geophysical Research Letters*, 30, 1–4, 2003. doi: 10.1029/2002GL016345.

O'Connor , F. M., Boucher , O., Gedney , N., Jones , C. D., Folberth , G. A., Coppell , R., Friedlingstein , P., Collins , W. J., Chappellaz , J., Ridley , J., and Johnson , C. E. Possible role of wetlands, permafrost, and methane hydrates in the methane cycle under future climate change: A review. *Reviews of Geophysics*, 48, 1–33, 2010. doi: 10.1029/2010RG000326.

Olivier , J. and Janssens-Maenhout , G. Part III: Total greenhouse gas emissions. *CO2 emissions from fuel combustion, 2014 Edition, International Energy Agency (IEA), Paris*, 2014. doi: http://dx.doi.org/10.1787/co2_fuel-2014-enCO2.

Olivier , J., Muntean , M., and Peters , J. Trends in global CO2 emissions: 2015 report. *PBL Netherlands Environmental Assessment Agency & European Commission's Joint Research Centre (JRC)*, 2015.

Olivier , J. G. On the Quality of Global Emission Inventory. Approaches, methodologies, input data and uncertainties. *Utrecht Thesis*, 2002.

O'Neill , B. C. The jury is still out on Global Warming Potentials. *Climatic Change*, 44, 427–443, 2000. doi: 10.1023/A:1005582929198.

O'Neill , B. C., Kriegler , E., Riahi , K., Ebi , K. L., Hallegatte , S., Carter , T. R., Mathur , R., and van Vuuren , D. P. A new scenario framework for climate change research: The concept of shared socioeconomic pathways. *Climatic Change*, 122, 387–400, 2014. doi: 10.1007/s10584-013-0905-2.

O'Neill , B. C., Tebaldi , C., Van Vuuren , D. P., Eyring , V., Friedlingstein , P., Hurtt , G., Knutti , R., Kriegler , E., Lamarque , J. F., Lowe , J., Meehl , G. A., Moss , R., Riahi , K., and Sanderson , B. M. The Scenario Model Intercomparison Project (ScenarioMIP) for CMIP6. *Geoscientific Model Development*, 9, 3461–3482, 2016. doi: 10.5194/gmd-9-3461-2016.

Orr , J. C. and Epitalon , J. M. Improved routines to model the ocean carbonate system: mocsy 1.0. *Geoscientific Model Development Discussions*, 7, 2877–2902, 2014.

Peng , S., Piao , S., Bousquet , P., Ciais , P., Li , B., Lin , X., Tao , S., Wang , Z., Zhang , Y., and Zhou , F. Inventory of anthropogenic methane emissions in mainland China from 1980 to 2010. *Atmospheric Chemistry and Physics*, 16, 14545–14562, 2016. doi: 10.5194/acp-16-14545-2016.

Peñuelas , J., Poulter , B., Sardans , J., Ciais , P., Van Der Velde , M., Bopp , L., Boucher , O., Godderis , Y., Hinsinger , P., Llusia , J., Nardin , E., Vicca , S., Obersteiner , M., and Janssens , I. A. Human-induced nitrogen-phosphorus imbalances alter natural and managed ecosystems across the globe. *Nature Communications*, 4, 2013. doi: 10.1038/ncomms3934.

Peters , G. P. Beyond carbon budgets. *Nature Geoscience*, 11, 1–3, 2018. doi: 10.1038/s41561-018-0142-4.

Peters , G. P., Aamaas , B., Berntsen , T., and Fuglestvedt , J. S. The integrated global temperature change potential (iGTP) and relationships between emission metrics. *Environmental Research Letters*, 6, 044021, 2011. doi: 10.1088/1748-9326/6/4/044021.

Peters , G. P., Andrew , R. M., Boden , T., Canadell , J. G., Ciais , P., Le Quéré , C., Marland , G., Raupach , M. R., and Wilson , C. The challenge to keep global warming below 2C. *Nature Climate Change*, 3, 4–6, 2013. doi: 10.1038/nclimate1783.

Popp , A., Calvin , K., Fujimori , S., Havlik , P., Humpenöder , F., Stehfest , E., Bodirsky , B. L., Dietrich , J. P., Doelmann , J. C., Gusti , M., Hasegawa , T., Kyle , P., Obersteiner , M., Tabeau , A., Takahashi , K., Valin , H., Waldhoff , S., Weindl , I., Wise , M., Kriegler , E., Lotze-Campen , H., Fricko , O., Riahi , K., and Vuuren , D. P. Land-use futures in the shared socio-economic pathways. *Global Environmental Change*, 42, 331–345, 2017. doi: 10.1016/j.gloenvcha.2016.10.002.

Pugh , T. A. M., Arneth , A., Olin , S., Ahlström , A., Bayer , A. D., Goldewijk , K. K., Lindeskog , M., and Schurgers , G. Simulated carbon emissions from land-use change are substantially enhanced by accounting for agricultural management. *Environmental Research Letters*, 10, 124008, 2015.

Quilcaille , Y., Chavaillaz , Y., Giguet , S., Jézéquel , A., Rajaud , A., Ferron , C., Amat , A., Dépoues , V., Revelard , A., Lugen , M., Tourneville , L., Comte , A., Ranché , M., Hovsepian , M., and Sansilvestri , R. (In)certitudes et adaptation au climat futur: le regard des "acteurs de demain". *Iddri Studies*, 4, 2015.

Quilcaille , Y., Gasser , T., Ciais , P., Lecocq , F., Janssens-Maenhout , G., and Mohr , S. Uncertainty in projected climate change arising from uncertain fossil-fuel emission factors. *Environmental Research Letters*, 13, 044017, 2018.

Quilcaille , Y., Gasser , T., Ciais , P., Lecocq , F., Janssens-Maenhout , G., Mohr , S., Andres , R. J., and Bopp , L. Uncertainty in projected climate change caused by methodological discrepancy in estimating co2 emissions from fossil fuel combustion. https://meetingorganizer.copernicus.org/EGU2016/EGU2016-10549.pdf, 2016a.

Quilcaille , Y., Gasser , T., Ciais , P., Lecocq , F., and Peters , G. Analysis of the ipcc ar5 transformation pathways with a new compact earth system mode. http://www.eci.ox.ac.uk/assets/img/main/1p5d150916.pdf, 2016b.

Rachev , S. T. The Monge-Kantorovich mass transference problem and its stochastic applications. *Statistics*, 29, 647–676, 1985.

Ramankutty , N., Gibbs , H. K., Achard , F., Defries , R., Foley , J. A., and Houghton , R. A. Challenges to estimating carbon emissions from tropical deforestation. *Global Change Biology*, 13, 51–66, 2007. doi: 10.1111/j.1365-2486.2006.01272.x.

Rao , S., Klimont , Z., Smith , S. J., Dingenen , R. V., Dentener , F., Bouwman , L., Riahi , K., Amann , M., Bodirsky , B. L., van Vuuren , D. P., Reis , L. A., Calvin , K., Drouet , L., Fricko , O., Fujimori , S., Gernaat , D., Havlik , P., Harmsen , M., Hasegawa , T., Heyes , C., Hilaire , J., Luderer , G., Masui , T., Stehfest , E., Strefler , J., van der Sluis , S., and Tavoni , M. Future air pollution in the shared socio-economic pathways. *Global Environmental Change*, 42, 346 - 358, 2017. doi: https://doi.org/10.1016/j.gloenvcha.2016.05.012.

Raupach , M. R., Canadell , J. G., Ciais , P., Friedlingstein , P., Rayner , P. J., and Trudinger , C. M. The relationship between peak warming and cumulative CO2 emissions, and its use to quantify vulnerabilities in the carbon-climate-human system. *Tellus, Series B: Chemical and Physical Meteorology*, 63, 145–164, 2011. doi: 10.1111/j.1600-0889.2010.00521.x.

Riahi , K., Rao , S., Krey , V., Cho , C., Chirkov , V., Fischer , G., Kindermann , G., Nakicenovic , N., and Rafaj , P. RCP 8.5-A scenario of comparatively high greenhouse gas emissions. *Climatic Change*, 109, 33–57, 2011. doi: 10.1007/s10584-011-0149-y.

Riahi , K., van Vuuren , D. P., Kriegler , E., Edmonds , J., O'Neill , B. C., Fujimori , S., Bauer , N., Calvin , K., Dellink , R., Fricko , O., Lutz , W., Popp , A., Cuaresma , J. C., KC , S., Leimbach , M., Jiang , L., Kram , T., Rao , S., Emmerling , J., Ebi , K., Hasegawa , T., Havlik , P., Humpenöder , F., Da Silva , L. A., Smith , S., Stehfest , E., Bosetti , V., Eom , J., Gernaat , D., Masui , T., Rogelj , J., Strefler , J., Drouet , L., Krey , V., Luderer , G., Harmsen , M., Takahashi , K., Baumstark , L., Doelman , J. C., Kainuma , M., Klimont , Z., Marangoni , G., Lotze-Campen , H., Obersteiner , M., Tabeau , A., and Tavoni , M. The Shared Socioeconomic Pathways and their energy, land use, and greenhouse gas emissions implications: An overview. *Global Environmental Change*, 42, 153–168, 2017. doi: 10.1016/j.gloenvcha.2016.05.009.

Robinson , S., van Meijl , H., Willenbockel , D., Valin , H., Fujimori , S., Masui , T., Sands , R., Wise , M., Calvin , K., Havlik , P., Mason d'Croz , D., Tabeau , A., Kavallari , A., Schmitz , C., Dietrich , J. P., and von Lampe , M. Comparing supply-side specifications in models of global agriculture and the food system. *Agricultural Economics (United Kingdom)*, 45, 21–35, 2014. doi: 10.1111/agec.12087.

Rogelj , J., Hare , W., Chen , C., and Meinshausen , M. Discrepancies in historical emissions point to a wider 2020 gap between 2°c benchmarks and aggregated national mitigation pledges. *Environmental Research Letters*, 6, 024002, 2011.

Rogelj , J., Rao , S., McCollum , D. L., Pachauri , S., Klimont , Z., Krey , V., and Riahi , K. Air-pollution emission ranges consistent with the representative concentration pathways. *Nature Climate Change*, 4, 446–450, 2014. doi: 10.1038/nclimate2178.

Rogelj , J., Luderer , G., Pietzcker , R. C., Kriegler , E., Schaeffer , M., Krey , V., and Riahi , K. Energy system transformations for limiting end-of-century warming to below 1.5 °C. *Nature Climate Change*, 5, 519–527, 2015. doi: 10.1038/nclimate2572.

Rogelj , J., Den Elzen , M., Höhne , N., Fransen , T., Fekete , H., Winkler , H., Schaeffer , R., Sha , F., Riahi , K., and Meinshausen , M. Paris Agreement climate proposals need a boost to keep warming well below 2°C. *Nature*, 534, 631–639, 2016a. doi: 10.1038/nature18307.

Rogelj , J., Schaeffer , M., Friedlingstein , P., Gillett , N. P., Van Vuuren , D. P., Riahi , K., Allen , M., and Knutti , R. Differences between carbon budget estimates unravelled. *Nature Climate Change*, 6, 245–252, 2016b. doi: 10.1038/nclimate2868.

Rose , S. K., Kriegler , E., Bibas , R., Calvin , K., Popp , A., van Vuuren , D. P., and Weyant , J. Bioenergy in energy transformation and climate management. *Climatic Change*, 123, 477–493, 2014a. doi: 10.1007/s10584-013-0965-3.

Rose , S. K., Richels , R., Smith , S., Riahi , K., Strefler , J., and van Vuuren , D. P. Non-Kyoto radiative forcing in long-run greenhouse gas emissions and climate change scenarios. *Climatic Change*, 123, 511–525, 2014b. doi: 10.1007/s10584-013-0955-5.

Saikawa , E., Trail , M., Zhong , M., Wu , Q., Young , C. L., Janssens-Maenhout , G., Klimont , Z., Wagner , F., Kurokawa , J.-i., Nagpure , A. S., and Gurjar , B. R. Uncertainties in emissions estimates of greenhouse gases and air pollutants in India and their impacts on regional air quality. *Environmental Research Letters*, 12, 065002, 2017. doi: 10.1088/1748-9326/aa6cb4.

Sanderson , B. M., O'Neill , B. C., and Tebaldi , C. What would it take to achieve the Paris temperature targets? *Geophysical Research Letters*, 43, 7133–7142, 2016. doi: 10.1002/2016GL069563.

Sanz-Pérez , E. S., Murdock , C. R., Didas , S. A., and Jones , C. W. Direct Capture of CO2from Ambient Air. *Chemical Reviews*, 116, 11840–11876, 2016. doi: 10.1021/acs.chemrev.6b00173.

Sarmiento , J. and Gruber , N. Carbon Cycle. *Ocean biogeochemical dynamics*, 2006. doi: http://dx.doi.org/10.1016/B978-0-12-384719-5.00306-3.

ScenarioMIP . Timeline of ScenarioMIP.

Schaeffer , M., Gohar , L., Kriegler , E., Lowe , J., Riahi , K., and van Vuuren , D. Mid- and long-term climate projections for fragmented and delayed-action scenarios. *Technological Forecasting and Social Change*, 90, 257–268, 2015. doi: 10.1016/j.techfore.2013.09.013.

Schmitz , C., Biewald , A., Lotze-Campen , H., Popp , A., Dietrich , J. P., Bodirsky , B., Krause , M., and Weindl , I. Trading more food: Implications for land use, greenhouse gas emissions, and the food system. *Global Environmental Change*, 22, 189–209, 2012. doi: 10.1016/j.gloenvcha.2011.09.013.

Scott , V., Gilfillan , S., Markusson , N., Chalmers , H., and Haszeldine , R. S. Last chance for carbon capture and storage. *Nature Climate Change*, 3, 105–111, 2013. doi: 10.1038/nclimate1695.

Seijas-Macias , A. and Oliveira , A. An Approach to Distribution of the Product of Two Normal Variables. *Discussiones Mathematicae Probability and Statistics*, 32, 87–99, 2012. doi: 10.7151/dmps.1146.

Seitzinger , S. P., Kroeze , C., and Styles , R. V. Global distribution of N2O emissions from aquatic systems: Natural emissions and anthropogenic effects. *Chemosphere - Global Change Science*, 2, 267–279, 2000. doi: 10.1016/S1465-9972(00)00015-5.

Shine , K. P. The global warming potential-the need for an interdisciplinary retrial. *Climatic Change*, 96, 467–472, 2009. doi: 10.1007/s10584-009-9647-6.

Shine , K. P., Fuglestvedt , J. S., Hailemariam , K., and Stuber , N. Alternatives to the Global Warming Potential for comparing climate impacts of emissions of greenhouse gases. *Climatic Change*, 68, 281–302, 2005. doi: 10.1007/s10584-005-1146-9.

Sitch , S., Cox , P. M., Collins , W. J., and Huntingford , C. Indirect radiative forcing of climate change through ozone effects on the land-carbon sink. *Nature*, 448, 791–794, 2007. doi: 10.1038/nature06059.

Sitch , S., Friedlingstein , P., Gruber , N., Jones , S. D., Murray-Tortarolo , G., Ahlström , A., Doney , S. C., Graven , H., Heinze , C., Huntingford , C., Levis , S., Levy , P. E., Lomas , M., Poulter , B., Viovy , N., Zaehle , S., Zeng , N., Arneth , A., Bonan , G., Bopp , L., Canadell , J. G., Chevallier , F., Ciais , P., Ellis , R., Gloor , M., Peylin , P., Piao , S. L., Le Quéré , C., Smith , B., Zhu ,

Z., and Myneni , R. Recent trends and drivers of regional sources and sinks of carbon dioxide. *Biogeosciences*, 12, 653–679, 2015. doi: 10.5194/bg-12-653-2015.

Smith , P., Bustamante , M., Ahammad , H., Clark , H., Dong , H., Elsiddig , E. A., Haberl , R., H. Harper, House , J., Jafari , M., Masera , O., Mbow , C., Ravindranath , N. H., Rice , C. W., Robledo Abad , C., Romanovskaya , A., Sperling , F., and Tubie , F. Agriculture, Forestry and Other Land Use (AFOLU). *Climate Change 2014: Mitigation of Climate Change. Contribution of Working Group III to the Fifth Assessment Report of the Intergovernmental Panel on Climate Change*, 2014.

Smith , P., Davis , S. J., Creutzig , F., Fuss , S., Minx , J., Gabrielle , B., Kato , E., Jackson , R. B., Cowie , A., Kriegler , E., Van Vuuren , D. P., Rogelj , J., Ciais , P., Milne , J., Canadell , J. G., McCollum , D., Peters , G., Andrew , R., Krey , V., Shrestha , G., Friedlingstein , P., Gasser , T., Grübler , A., Heidug , W. K., Jonas , M., Jones , C. D., Kraxner , F., Littleton , E., Lowe , J., Moreira , J. R., Nakicenovic , N., Obersteiner , M., Patwardhan , A., Rogner , M., Rubin , E., Sharifi , A., Torvanger , A., Yamagata , Y., Edmonds , J., and Yongsung , C. Biophysical and economic limits to negative CO2emissions. *Nature Climate Change*, 6, 42–50, 2016. doi: 10.1038/nclimate2870.

Smith , S. J., Van Aardenne , J., Klimont , Z., Andres , R. J., Volke , A., and Delgado Arias , S. Anthropogenic sulfur dioxide emissions: 1850-2005. *Atmospheric Chemistry and Physics*, 11, 1101–1116, 2011. doi: 10.5194/acp-11-1101-2011.

Smith , S. and Wigley , T. M. L. Global Warming Potentials: 1. Climatic implications of emission reductions. *Climatic Change*, 44, 445–457, 2000.

Speirs , J., McGlade , C., and Slade , R. Uncertainty in the availability of natural resources: Fossil fuels, critical metals and biomass. *Energy Policy*, 87, 654–664, 2015. doi: 10.1016/j.enpol.2015.02.031.

SSP . SSP: a brief description of the models. `https://tntcat.iiasa.ac.at/SspDb/download/iam_scenario_doc/SSP_Model_Documentation.pdf`, 2018.

Stehfest , E., van Vuuren , D., Kram , T., Bouwman , L., Alkemade , R., Bakkenes , M., Biemans , H., Bouwman , A., den Elzen , M., Janse , J., Lucas , P., van Minnen , J., Müller , M., and Prins , A. *Integrated Assessment of Global Environmental Change with IMAGE 3.0: Model description and policy applications*. 2014. ISBN 9789491506710.

Stern , D. I. Reversal of the trend in global anthropogenic sulfur emissions. *Global Environmental Change*, 16, 207–220, 2006. doi: 10.1016/j.gloenvcha.2006.01.001.

Stocker , B. D., Feissli , F., Strassmann , K. M., Spahni , R., and Joos , F. Past and future carbon fluxes from land use change, shifting cultivation and wood harvest. *Tellus, Series B: Chemical and Physical Meteorology*, 66, 1–15, 2014. doi: 10.3402/tellusb.v66.23188.

Stohl , A., Aamaas , B., Amann , M., Baker , L. H., Bellouin , N., Berntsen , T. K., Boucher , O., Cherian , R., Collins , W., Daskalakis , N., Dusinska , M., Eckhardt , S., Fuglestvedt , J. S., Harju , M., Heyes , C., Hodnebrog , Hao , J., Im , U., Kanakidou , M., Klimont , Z., Kupiainen , K., Law , K. S., Lund , M. T., Maas , R., MacIntosh , C. R., Myhre , G., Myriokefalitakis , S., Olivié , D., Quaas , J., Quennehen , B., Raut , J. C., Rumbold , S. T., Samset , B. H., Schulz , M., Seland , Shine , K. P., Skeie , R. B., Wang , S., Yttri , K. E., and Zhu , T. Evaluating the climate and air quality impacts of short-lived pollutants. *Atmospheric Chemistry and Physics*, 15, 10529–10566, 2015. doi: 10.5194/acp-15-10529-2015.

Strefler , J., Amann , T., Bauer , N., Kriegler , E., and Hartmann , J. Potential and costs of carbon dioxide removal by enhanced weathering of rocks. *Environmental Research Letters*, 13, 034010, 2018. doi: 10.1088/1748-9326/aaa9c4.

Swart , R., Robinson , J., and Cohen , S. Climate change and sustainable development: expanding the options. *Climate Policy*, 3, S19 - S40, 2003. doi: https://doi.org/10.1016/j.clipol.2003.10.010. Special Supplement on Climate Change and Sustainable Development.

Takahashi , T., Sutherland , S. C., Wanninkhof , R., Sweeney , C., Feely , R. A., Chipman , D. W., Hales , B., Friederich , G., Chavez , F., Sabine , C., Watson , A., Bakker , D. C., Schuster , U., Metzl , N., Yoshikawa-Inoue , H., Ishii , M., Midorikawa , T., Nojiri , Y., Körtzinger , A., Steinhoff , T., Hoppema , M., Olafsson , J., Arnarson , T. S., Tilbrook , B., Johannessen , T., Olsen , A., Bellerby , R., Wong , C., Delille , B., Bates , N., and de Baar , H. J. Climatological mean and decadal change in surface ocean pco2, and net sea–air co2 flux over the global oceans. *Deep Sea Research Part II: Topical Studies in Oceanography*, 56, 554 - 577, 2009. doi: https://doi.org/10.1016/j.dsr2.2008.12.009. Surface Ocean CO2 Variability and Vulnerabilities.

Tans , P. An Accounting of the Observed Increase in Oceanic and Atmospheric CO2 and the Outlook for the Future. *Oceanography*, 22, 26–35, 2009. doi: 10.5670/oceanog.2009.94.

Thornton , P. E., Lamarque , J. F., Rosenbloom , N. A., and Mahowald , N. M. Influence of carbon-nitrogen cycle coupling on land model response to CO2 fertilization and climate variability. *Global Biogeochemical Cycles*, 21, 1–15, 2007. doi: 10.1029/2006GB002868.

Tuomi , M., Vanhala , P., Karhu , K., Fritze , H., and Liski , J. Heterotrophic soil respiration-Comparison of different models describing its temperature dependence. *Ecological Modelling*, 211, 182–190, 2008. doi: 10.1016/j.ecolmodel.2007.09.003.

Turetsky , M. R., Kotowska , A., Bubier , J., Dise , N. B., Crill , P., Hornibrook , E. R. C., Minkkinen , K., Moore , T. R., Myers-Smith , I. H., Nykänen , H., Olefeldt , D., Rinne , J., Saarnio , S., Shurpali , N., Tuittila , E., Waddington ,

J. M., White , J. R., Wickland , K. P., and Wilmking , M. A synthesis of methane emissions from 71 northern, temperate, and subtropical wetlands. *Global Change Biology*, 20, 2183-2197, 2014. doi: 10.1111/gcb.12580.

United States Environmental Protection Agency . Assessment of the Potential Impacts of Hydraulic Fracturing for Oil and Gas on Drinking Water Resources. *External Review*, 2015. doi: EPA/600/R-15/047a.

Van Der Werf , G. R., Randerson , J. T., Giglio , L., Collatz , G. J., Mu , M., Kasibhatla , P. S., Morton , D. C., Defries , R. S., Jin , Y., and Van Leeuwen , T. T. Global fire emissions and the contribution of deforestation, savanna, forest, agricultural, and peat fires (1997-2009). *Atmospheric Chemistry and Physics*, 10, 11707–11735, 2010. doi: 10.5194/acp-10-11707-2010.

van Vuuren , D. P. and Riahi , K. The relationship between short-term emissions and long-term concentration targets. *Climatic Change*, 104, 793–801, 2011. doi: 10.1007/s10584-010-0004-6.

van Vuuren , D. P., Edmonds , J., Kainuma , M., Riahi , K., Thomson , A., Hibbard , K., Hurtt , G. C., Kram , T., Krey , V., Lamarque , J. F., Masui , T., Meinshausen , M., Nakicenovic , N., Smith , S. J., and Rose , S. K. The representative concentration pathways: An overview. *Climatic Change*, 109, 5–31, 2011a. doi: 10.1007/s10584-011-0148-z.

van Vuuren , D. P., Stehfest , E., den Elzen , M. G., Kram , T., van Vliet , J., Deetman , S., Isaac , M., Goldewijk , K. K., Hof , A., Beltran , A. M., Oostenrijk , R., and van Ruijven , B. RCP2.6: Exploring the possibility to keep global mean temperature increase below 2°C. *Climatic Change*, 109, 95–116, 2011b. doi: 10.1007/s10584-011-0152-3.

van Vuuren , D. P., Kriegler , E., O'Neill , B. C., Ebi , K. L., Riahi , K., Carter , T. R., Edmonds , J., Hallegatte , S., Kram , T., Mathur , R., and Winkler , H. A new scenario framework for Climate Change Research: Scenario matrix architecture. *Climatic Change*, 122, 373–386, 2014. doi: 10.1007/s10584-013-0906-1.

van Vuuren , D. P., van Soest , H., Riahi , K., Clarke , L., Krey , V., Kriegler , E., Rogelj , J., Schaeffer , M., and Tavoni , M. Carbon budgets and energy transition pathways. *Environmental Research Letters*, 11, 075002, 2016.

van Vuuren , D. P., Stehfest , E., Gernaat , D. E., Doelman , J. C., van den Berg , M., Harmsen , M., de Boer , H. S., Bouwman , L. F., Daioglou , V., Edelenbosch , O. Y., Girod , B., Kram , T., Lassaletta , L., Lucas , P. L., van Meijl , H., Müller , C., van Ruijven , B. J., van der Sluis , S., and Tabeau , A. Energy, land-use and greenhouse gas emissions trajectories under a green growth paradigm. *Global Environmental Change*, 42, 237–250, 2017. doi: 10.1016/j.gloenvcha.2016.05.008.

Vaughan , N. E., Gough , C., Mander , S., Littleton , E. W., Welfle , A., Gernaat , D. E. H. J., and van Vuuren , D. P. Evaluating the use of biomass energy with carbon capture and storage in low emission scenarios. *Environmental Research Letters*, 13, 044014, 2018.

Velders , G. J. M., Fahey , D. W., Daniel , J. S., Andersen , S. O., and McFarland , M. Future atmospheric abundances and climate forcings from scenarios of global and regional hydrofluorocarbon (HFC) emissions. *Atmospheric Environment*, 123, 200–209, 2015. doi: 10.1016/j.atmosenv.2015.10.071.

Verburg , R., Stehfest , E., Woltjer , G., and Eickhout , B. The effect of agricultural trade liberalisation on land-use related greenhouse gas emissions. *Global Environmental Change*, 19, 434–446, 2009. doi: 10.1016/j.gloenvcha.2009.06.004.

Ward , J. D., Mohr , S. H., Myers , B. R., and Nel , W. P. High estimates of supply constrained emissions scenarios for long-term climate risk assessment. *Energy Policy*, 51, 598–604, 2012. doi: 10.1016/j.enpol.2012.09.003.

Weindl , I., Lotze-Campen , H., Popp , A., Müller , C., Havlík , P., Herrero , M., Schmitz , C., and Rolinski , S. Livestock in a changing climate: Production system transitions as an adaptation strategy for agriculture. *Environmental Research Letters*, 10, 2015. doi: 10.1088/1748-9326/10/9/094021.

Weiss , R. Carbon dioxide in water and seawater: the solubility of a non-ideal gas. *Marine Chemistry*, 2, 203 - 215, 1974. doi: https://doi.org/10.1016/0304-4203(74)90015-2.

West , J. J., Smith , S. J., Silva , R. A., Naik , V., Zhang , Y., Adelman , Z., Fry , M. M., Anenberg , S., Horowitz , L. W., and Lamarque , J.-F. Co-benefits of mitigating global greenhouse gas emissions for future air quality and human health. *Nature Climate Change*, 3, 885–889, 2013. doi: 10.1038/nclimate2009.

Wieder , W. R., Cleveland , C. C., Smith , W. K., and Todd-Brown , K. Future productivity and carbon storage limited by terrestrial nutrient availability. *Nature Geoscience*, 8, 441–444, 2015. doi: 10.1038/NGEO2413.

Wise , M., Calvin , K., Kyle , P., Luckow , P., and Edmonds , J. Economic and physical modeling of land use in GCAM 3.0 and an application to agricultural productivity, lLand, and terrestrial carbon. *Climate Change Economics*, 05, 1450003, 2014. doi: 10.1142/S2010007814500031.

WMO . Scientific Assessment of Ozone Depletion: 2006, Global Ozone Research and Monitoring Project. *World Meteorological Organization*, 2006.

Woltjer , G., Kavallari , A., Meijl , H. V., Powell , J., Rutten , M., and Shutes , L. The MAGNET model, 2014.

Yamanaka , Y. and Tajika , E. The role of the vertical fluxes of particulate organic matter and calcite in the oceanic carbon cycle: Studies using an ocean biogeochemical general circulation model. *Global Biogeochemical Cycles*, 10, 361–382, 1996. doi: 10.1029/96GB00634.

Yue , C., Ciais , P., and Li , W. Smaller global and regional carbon emissions from gross land use change when considering sub-grid secondary land cohorts in a global dynamic vegetation model. *Biogeosciences Discussions*, 2017. doi: 10.5194/bg-2017-329.

Zickfeld , K., MacDougall , A. H., and Matthews , H. D. On the proportionality between global temperature change and cumulative CO2 emissions during periods of net negative CO2 emissions. *Environmental Research Letters*, 11, 055006, 2016. doi: 10.1088/1748-9326/11/5/055006.

Thank you!

This thesis has been funded for three years with a grant for students of the Ecole Normale Superieure Paris-Saclay (previously ENS Cachan). This period has been extended by three months with a CEA contract under decision of Philippe Ciais.

As expected, thank you very much to the defense commitee for your work. Special acknowledgements for reading the manuscript, I value this effort, and what has ensued. I hope that we will have productive exchanges at the defense. I am particulary thankful to Glen Peters and Joeri Rogelj, who have read this manuscript in quite a short time, as a response of the French administration.

Obviously, thank you very much to all I have worked with. Thomas Gasser, Philippe Ciais and Franck Lecocq, and not forgetting Laurent Bopp. Our works have indubitably learn me *a lot*, and I think that it will keep on this way. We still have lots of ideas to develop, I do hope that we will be able to carry them out.

Obviously, again, thank you to all collaborators. Robert J. Andres, Greet Janssens-Maenhout, Steve Mohr and Joeri Rogelj. Working with you has also learn me a lot and your contributions have been of great help in our projects.

Thank you as well to my colleagues at CIRED and LSCE. A full list would be way too long, and I would forget way too many people. Thus, in very short, thank you Ruben for our coffee chats, Florian for our night talks in CIRED, Arnaud for our chocolate breaks, Cyril for our office discussions, Franck for our board exchanges (with or without Δ)... To all others, sorry not to have quoted you, but be sure that I think of you.

Indeed, thank you very much to the family and friends. Here, as well, an exhaustive list would be too long. Anyway, you have put up with me in my worse times, you have my gratefulness. Well, much more than my mere "gratefulness", but you already know it. Special thanks to Laetitia, I owe you one.

Finally, thanks to myself. It seems logic to thank me, for without Yann, this thesis would not have been written.

Works performed during the PhD

The first chapter of this thesis has been presented in an earlier version at the European Geosciences Union 2016 as an oral presentation (Quilcaille et al. (2016a)). A paper in Environmental Research Letters (Quilcaille et al. (2018)) forms the basis of this chapter.

The second chapter of this thesis has not been published yet. Though, a former version has been performed using the AR5WG3 database (IIASA (2018a)). An analysis of these scenarios has been showed at the conference "1.5 degrees: Meeting the challenges of the Paris Agreement" (Quilcaille et al. (2016b)). Several papers from the second chapter are planned.

The third chapter of this thesis has not been published yet. It is meant to be part of the model intercomparison project CDR-MIP (Keller et al. (2017)).

In the course of this thesis, different contributions have been produced, even if not directly related to the subject of this thesis.

- Quilcaille et al. (2015): synthesis and analysis of the symposium-debate for the integration of the uncertainties in the adaptation to climate change (Meudon, November 2014). I have lead the writting of this papier, thanks to the 15 others authors.
- Dépoues et al. (2015): perspective of the importance of associations for the mobilization in the mitigation of climate change.
- Courses given in the ATHENS (Advanced Technology Higher Education Network / SOCRATES) European program (intensive specialization courses) at AgroParisTech, 2016 and 2017: "Climate change, the physical aspects"
- Courses and practical works given in the Master EEET (Economy of Environnement, Energy and Transports) at AgroParisTech, 2016 and 2017: "Simple modelling of climate change"
- Round-table discussions at the festival Tropikantes, 2017, after oral presentation: "How do we study climate change?"
- IMS Luxembourg Magazine: Production of inserted pages relative to climate change in the interview of Jean Jouzel for the special edition of the IMS-Magazine, with Christophe Cassen.
- Ongoing collaboration with Vipin Veetil and Antoine Mandel for the assessment of the change of work productivity as a response to global warming in a firms network.

Yann Quilcaille
Analyse des scénarios climatiques à l'aide d'un modèle compact du système Terre

Cette thèse met en perspective un ensemble d'éléments des scénarios socio-économiques sous l'angle de la modélisation du climat. Ces éléments contribuent à améliorer la compréhension de l'état actuel des sciences du climat en ce qui concerne les scénarios. En parallèle, ces éléments montrent le potentiel du récent modèle compact du système Terre OSCAR v2.2.

Le premier élément concerne l'incertitude des émissions. Les émissions historiques sont reconstruites à l'aide de données statistiques et de modèles. Ces inventaires d'émissions sont par exemple employés par les modèles climatiques pour reconstruire les évolutions historiques du climat. Cependant, le calcul de ces émissions est incertain. Le détail des activités économiques est souvent méconnu, et parfois contient des erreurs. Par ailleurs, ce détail est requis pour utiliser les coefficients d'émissions adaptés. Néanmoins, ces coefficients sont eux aussi incertains. Par exemple, le calcul des émissions de dioxyde de carbone lors de la combustion de charbon dans des centrales thermiques nécessite d'avoir le détail de la consommation de chacun des types de charbon avec leurs compositions respectives. Cette incertitude se traduit par des différences entre les inventaires, de l'ordre de 5 à 10% pour les émissions de dioxyde de carbone par l'usage d'énergies fossiles. Pour les autres composés émis, comme pour les autres secteurs d'activités économiques, ces incertitudes sont bien supérieures. Néanmoins, ces incertitudes sont négligées dans les reconstructions climatiques. Par ailleurs, ces incertitudes devraient se retrouver aussi dans les projections d'émissions, et donc dans les projections climatiques.

Nous quantifions l'impact sur les émissions et le changement climatique qu'ont les incertitudes sur les coefficients d'émissions des énergies fossiles. Nous utilisons des scénarios détaillant les extractions pour de nombreux combustibles fossiles, conventionnels et non conventionnels. Chaque scénario suppose une absence de régulation sur leurs extractions, mais chacun scénario suppose un niveau propre de récupération d'énergies fossiles. Par ailleurs, nous utilisons un ensemble de sources pour le calcul des émissions de dioxyde de carbone, nous permettant d'obtenir un intervalle de confiance sur les reconstructions et les projections d'émissions. Les reconstructions sont cohérentes avec les autres inventaires d'émissions. Nous projetons une augmentation des incertitudes dans les émissions, s'élevant à 15% pour les émissions cumulées sur 2000-2300. L'utilisation croissante des énergies fossiles non-conventionnelles est responsable de cette augmentation, comme les coefficients sont moins bien connus.

Nous utilisons en outre une approche top-down pour le calcul des émissions des autres composés et de leurs incertitudes. Cette approche repose sur les coefficients de coémissions, chacun avec leurs incertitudes propres, qui dépendent du temps et de la catégorie du combustible. Utilisant en sus le modèle OSCAR v2.2 et plusieurs simulations Monte-Carlo, nous projetons le changement climatique sous ces scén-

arios avec trois sources d'incertitude : modélisation du système Terre, émissions de dioxyde de carbone et émissions d'autres composés. Nous identifions précisément les contributions de ces incertitudes dans chacun des aspects du système Terre. Ainsi, nous démontrons que les incertitudes sur les émissions n'augmentent pas de manière significative l'incertitude dans les projections climatiques. Ceci est vrai pour la majeure partie des variables, comme l'augmentation de la température moyenne de surface. Ceci est dû à la large incertitude dans la modélisation du système Terre. Néanmoins, pour d'autres variables telles que les concentrations d'ozone, les incertitudes sur les émissions augmentent significativement les incertitudes que présentent déjà la modélisation du système Terre. Ainsi, les études relatives à la qualité de l'air devraient considérer ces incertitudes.

Il demeure important d'améliorer notre connaissance sur les facteurs d'émissions, avec des évaluations récurrentes pour tenir compte des évolutions dans leurs utilisations. Nous nous sommes focalisés sur les énergies fossiles pour simplifier le propos. Ce secteur est la principale cause du changement climatique, mais les autres secteurs contribuent également. Bien que les émissions liées à l'agriculture sont inférieures à celles liées à l'utilisation d'énergies fossiles, les incertitudes sur les émissions de l'agriculture sont supérieures.

Le second élément est une analyse climatique des récents scénarios Shared Socio-Economic Pathways (SSP). Ces scénarios accompagnent les scénarios Representative Concentrations Pathways (RCP). Les RCP correspondent à 4 trajectoires de compositions atmosphériques, et donc d'émissions et d'utilisations des terres. Ces 4 trajectoires sont représentatives de futurs possibles. Les modèles climatiques les plus récents (Earth System Model, ESM) ont produit une évaluation détaillée des projections climatiques sous ces RCP. L'idée des RCP et des SSP est d'avoir un ensemble de trajectoires socio-économiques dont les projections climatiques pointent vers l'un ou l'autre des RCP à leur terme, soit en 2100. Cette correspondance est faite pour accélérer l'évaluation des politiques climatiques, que ça soit pour l'atténuation du ou l'adaptation au changement climatique. Chacun des 5 SSP est formé d'un ensemble d'hypothèses sur l'utilisation d'énergies fossiles, la coopération internationale, le développement démographique, la croissance économique, et bien d'autres. 6 modèles économiques (Integrated Assessment Model, IAM) ont testé différentes politiques climatiques pour tenter d'atteindre chacun des RCP sous chacun des SSP, résultant en 103 scénarios socio-économiques SSP-RCP, et donc d'émissions et d'usages des sols.

L'objectif de cet élément est d'analyser de manière aussi exhaustive que possible l'ensemble des projections climatiques sous ces scénarios. La concordance des scénarios SSP-RCP aux RCP a déjà été faite en utilisant MAGICC v6, un modèle similaire à OSCAR v2.2. Cependant, les données climatiques communiquées sont incomplètes. Par ailleurs, la méthodologie employée pour cette évaluation n'est pas fournie dans le détail, et de potentiels biais peuvent y être présents. Finalement, cet ensemble de projections climatiques est employé à d'autres fins.

Afin de faire cette analyse, nous comblons des failles dans la base de don-

nées. MAGICCv6 utilise directement les émissions de dioxyde de carbone liées à l'utilisation des terres (Land Use Change, LUC) calculées par les IAM. Or, ces émissions dépendent du changement climatique, de l'état de la biosphère terrestre, et leurs évolutions, ainsi que leurs paramètres sont incertains. Ainsi, nous faisons le choix de recalculer ces émissions avec OSCARv2.2. Pour ce faire, nous avons besoin de connaître certaines variables en rapport à l'usage des terres. Cependant, il n'est renseigné dans la base de données qu'en termes de couverture des sols. Pourtant, les transitions en LUC devraient être fournies, avec l'extraction de biomasse et l'étendue des surfaces pour l'agriculture itinérante. Le LUC est reconstruit à l'aide des couvertures des sols et d'un algorithme. Nous reconstruisons également l'extraction de biomasse et l'étendue de l'agriculture itinérante, à l'aide des évolutions des énergies primaires liées aux utilisations respectives de biomasse traditionnelle, biomasse moderne sans Capture et Stockage de Carbone (CCS), et avec CCS. Comme autre limite de la base de données des scénarios SSP-RCP, les émissions de composés halogénés est résumée en émissions agrégées pour les composés fluorés. Les émissions de cette catégorie sont donc redécomposées en émissions de composés fluorés, complétées par les autres composés halogénés. Comme synthèse des résultats sur cette base, nous obtenons :

- Les scénarios SSP-RCP atteignent dans l'ensemble les RCP en 2100, leurs évolutions autour de la cible sont très différentes. En d'autres mots, les scénarios à overshoot qui dépassent leurs cibles tendent à avoir des évolutions très différentes après 2100.

- Les augmentations dans la température globale de surface sont utilisées avec leurs densités de probabilités pour calculer les probabilités de respecter l'Accord de Paris pour chaque RCP-SSP. Globalement, les hypothèses de ces scénarios se dessinent, et montre qu'une coopération internationale est aussi nécessaire qu'une diminution de l'utilisation des énergies fossiles.

- Ces scénarios atteignent leur cible d'élévation de la température globale de surface en médiane, donc avec 50% de chance. Avec l'incertitude sur la modélisation du système Terre, nous montrons que la limite en température qui n'est pas dépassée 90% de chance est 0.5 à 1°C plus élevée.

- Nous mettons en exergue des compensations entre les réductions d'émissions des différents gaz à effet. Autrement dit, les émissions d'un gaz à effet de serre d'après un IAM sous une politique climatique donnée peuvent être inférieures à celles calculées par un autre IAM sous une politique climatique pourtant plus forte.

- Nous montrons que les émissions de dioxyde de carbone dues au LUC calculées par les IAM sont inférieures à celles calculées par OSCAR. Ces différences peuvent s'élever jusqu'à 268 GtC sur 2010-2100.

- Nous montrons un lien partiel aux hypothèses relatives à l'agriculture itinérante. Pour autant, une analyse de sensibilité révèle que des différences demeurent, et sont liées aussi à l'IAM employé. Il semblerait que les méthodes pour le calcul de ces émissions, voire même leurs définitions, ne soient pas identiques. Cela remet en question le traitement par MAGICC qui emploie directement ces émissions.

- L'analyse du cycle du carbone identifie les scénarios dans lesquels les puits sont dégradés, ou au contraire, sont restaurés.

- A l'aide d'une décomposition de Kaya, nous montrons que le moteur principal de la réduction des émissions de dioxyde de carbone est l'intensité en carbone de l'énergie, et ce pour tous les scénarios. Nous développons cette décomposition pour les autres émissions, et mettrons en avant les hypothèses sur les technologies sous-jacentes aux scénarios.

- Nous proposons des définitions mathématiques rigoureuses pour les budgets carbone, soulignons une limite des budgets actuels. Nous recalculons donc à l'aide de ces scénarios quel budget de dioxyde de carbone peut être émis pour atteindre ou excéder un ensemble de seuils, qui sont des limites en température globale de surface, avec différentes probabilités. Ainsi, pour éviter 2°C avec 66% de probabilité, 1240 $GtCO_2$ peuvent être émises depuis 2015, avec un intervalle de confiance à 90% de 610-1790 $GtCO_2$. Pour dépasser ce même seuil, 1690 $GtCO_2$ doivent être émises (940-2770), bien que les températures continueront à augmenter au-delà.

Les limites de notre étude résident principalement dans notre traitement des données relatives à l'utilisation des terres. Nous identifions les limites de l'algorithme employé pour la reconstruction du LUC, en théorie et en pratique. Cet algorithme reproduit les tendances générales, mais pas l'ensemble des transitions, que ça soit sur la période historique ou sur les 6 SSP-RCP traitées dans la base LUH2. Comme mentionné auparavant, une analyse de sensibilité montre que les hypothèses pour la récolte de biomasse et l'agriculture itinérante restent des hypothèses ad hoc, qui ont un impact sur nos calculs. Néanmoins, nous montrons que ces hypothèses gardent un impact relativement faible sur les élévations de température.

Le troisième élément concerne les émissions négatives. Cela correspond à l'emploi de techniques à large échelle pour la capture et le stockage de dioxyde de carbone (CCS). Par exemple, cela peut être obtenu à l'aide d'extraction de dioxyde de carbone directement depuis l'atmosphère, stocké dans des réservoirs géologiques, ou bien à l'aide de reforestation, éventuellement avec bioénergies et stockage en réservoir, ou encore à l'aide d'une altération de l'océan, soit par fertilisation, soit par alcalinisation. Pour respecter l'Accord de Paris, il faut une réduction rapide, forte et maintenue des émissions de gaz à effet de serre et/ou l'emploi d'émissions négatives. Bien que ces techniques ne peuvent encore être développées à large échelle, la

plupart des scénarios qui limitent le changement climatique bien en dessous de 2°C par rapport au préindustriel, utilisent des émissions négatives.

Dans cette troisième étude, nous rejoignons l'exercice d'intercomparaison de modèles CDR-MIP, dont l'objectif est d'évaluer la validité de ces techniques, et ce qu'elles impliquent pour la planète. Une version développée de OSCAR v2.2 est employée pour cette analyse. Selon cette version, nous montrons que le système Terre est réversible dans l'ensemble, avec une hystérésis de 350 ans après retour de la pression partielle de dioxyde de carbone au préindustriel. Nous calculons le potentiel de refroidissement due à l'absorption de dioxyde de carbone, en forçage radiatif et en température globale de surface, et ce au cours du temps. A 100 ans, l'absorption d'une tonne de dioxyde de carbone diminue le changement climatique de 0.5.10-15 °C. Concernant les mesures de reforestation, elles permettent effectivement de réduire la teneur atmosphérique en dioxyde de carbone, et donc son forçage radiatif. Cependant, cette diminution est sur-compensée par le changement dans l'albedo global. Vis-à-vis des mesures d'alcalinisation, nous montrons une augmentation du puits océanique de carbone, et donc une diminution de sa teneur atmosphérique. L'acidification des océans est aussi réduite, grâce à l'alcalinité. Cependant, le potentiel de cette technique est 6 fois inférieur à celui initialement prévu.

Les limites sur ces résultats sont liées au modèle OSCARv2.2. Pour l'instant, les effets de seuil ne sont pas implémentés dans le modèle, bien qu'ils interviennent dans la réversibilité du système Terre. Par nature, OSCAR représente difficilement les processus avec de multiples interactions locales, telles que les conséquences du changement d'albedo. Finalement, les hypothèses sur le transport physique de l'alcalinité sont ad hoc, faute de mieux.

De ces travaux, des éléments communs ressortent. Comme premier élément clé, nous avons rencontrés de nombreuses incohérences dans les modèles, données et scénarios.

- Les bases de données sont souvent incomplètes. Cet aspect s'est révélé critique pour les projections climatiques sous les scénarios SSP-RCP. Nous avons donc dû compléter la base de données. A cet égard, l'utilisation des terres est souvent desservie. Une évaluation rigoureuse des projections climatiques requiert les transitions en LUC, la récolte de biomasse, et sur l'évolution de l'agriculture itinérante. Les différences observées sur les émissions de dioxyde de carbone dues au LUC montrent l'importance que peuvent avoir ces données. Ces différences pourront être explorées plus en détail au travers des exercices d'intercomparaison LUMIP et ScenarioMIP.

- Comme deuxième catégorie d'incohérences, les multiples inventaires d'émissions rencontrés peuvent difficilement être comparés dans le détail. Cela est dû aux différentes définitions et méthodes employées. Ces différences révèlent les incertitudes dans le calcul de ces émissions. Pour autant, les scénarios d'émissions sont souvent prolongés depuis des émissions historiques supposées certaines. Nous avons montré ici dans quelles circonstances cette manière de faire peut

être employée avec la première étude. Avec l'étude sur les scénarios SSP-RCP, nous avons montré comment tenir compte de cette incertitude.

- Comme troisième catégorie d'incohérences, nous avons rencontrés des scénarios, dont la conception invalide tout résultat. Avec l'étude sur les émissions négatives, les expériences sur la reforestation et l'alcalinisation des océans proposaient des extensions conduisant à un changement climatique suffisamment élevé pour sortir tout modèle de son domaine de validité.

Comme deuxième conclusion clé, cette thèse permet d'identifier les forces et faiblesses d'OSCAR v2.2. D'un côté, ce modèle permet de calculer avec précision et efficacité des projections climatiques, même pour un grand nombre de scénarios, et de manière probabilistique. Pour autant, il pourrait être amélioré sur certains points :

- La modélisation de la biosphère terrestre d'OSCARv2.2 est adaptée pour la base de données LUH1. L'intégration de la récente base de données LUH2 dans OSCAR ouvre la voie à une amélioration de la représentation de la biosphère terrestre.
- Par ailleurs, l'intégration des cycles biogéochimiques de l'azote et du phosphore permettrait d'améliorer davantage la précision du modèle.
- Le cycle océanique du carbone d'OSCAR v2.2 repose sur un modèle, comme la plupart des modèles compacts du système Terre, bien qu'avec des améliorations. Une nouvelle version pour cet aspect pourrait grandement améliorer avec le modèle. Une représentation simple de la biologie marine pourrait intégrer la dépendance aux cycles biogéochimiques.
- Les effets de seuil devraient être représentés dans OSCAR. Pour autant, il existe encore trop peu de modèles complexes qui intègrent explicitement ces processus, et qu'OSCAR pourrait émuler. En ce sens, la fonte du permafrost sera intégrée prochainement au modèle. Cet élément se révélerait clé, en particulier pour la réversibilité du système Terre.
- Finalement, l'interaction des processus locaux reste un défaut des modèles de basse résolution. Une correction du modèle serait une amélioration notable, particulièrement pour les scénarios présentant de fort changements de surface.

Dans l'ensemble, ce travail rassemble de nombreux éléments en rapport aux scénarios. Les scénarios respectant l'Accord de Paris emploient des énergies négatives, qui ne sont toujours pas prête pour un développement à grande échelle. Nous montrons que leur potentiel semble inférieur à celui espéré. Ainsi, nos chances de respecter l'Accord de Paris sont encore plus minces que prévues. En outre, ce travail montre aussi que, bien que les sciences du climat s'enrichissent de scénarios, de modèles et de données, la cohérence de cet ensemble semble ne pas suivre à la même

vitesse. Des échanges rigoureux entre communautés sont requis pour assurer la robustesse des conclusions. Pour autant, l'urgence de la lutte contre le changement climatique continue à croître. Ainsi, cette lutte ne doit pas attendre que les sciences du climat atteignent une cohérence et un état des connaissances optimales.

université PARIS-SACLAY
ÉCOLE DOCTORALE
Sciences de l'environnement d'île-de-France (SEIF)

Titre : Analyse des scénarios climatiques à l'aide d'un modèle compact du système Terre

Mots clés : climate, émissions, scénarios, modélisation

Résumé : Cette thèse met en perspective un ensemble d'éléments des scénarios socio-économiques sous l'angle de la modélisation du climat. Ces éléments contribuent à améliorer la compréhension de l'état actuel des sciences du climat. En parallèle, ces éléments montrent le potentiel du récent modèle compact du système Terre OSCAR v2.2.
Le premier élément concerne l'incertitude des émissions. Bien que les inventaires d'émissions soient incertains, nous ignorons dans quelle mesure ces incertitudes affectent les projections climatiques. Nous quantifions cet impact pour les émissions des énergies fossiles, la principale cause du changement climatique. Nous montrons que ces incertitudes dans les émissions augmentent avec l'utilisation des énergies fossiles non-conventionnelles, mais qu'elles n'augmentent pas significativement l'incertitude dans les projections climatiques. Nous montrons toutefois des exceptions pour des variables d'intérêt pour la qualité de l'air.
Le second élément est une analyse climatique des récents scénarios *Shared Socio-Economic Pathways* (SSP). Nous montrons la présence des failles dans la base de données, que nous comblons. Sur cette base, nous calculons les projections climatiques des scénarios SSP. Nous identifions des incohérences dans l'utilisation des émissions CO_2 dues à l'utilisation des terres calculées par les modèles intégrés et des variables associées . Nous identifions des compromis dans les réductions d'émissions pour l'atténuation du changement climatique. Nous réévaluons de manière plus robuste les budgets carbone. Les incertitudes dans les élévations de températures sont examinées en détail.
Le troisième élément concerne les émissions négatives. La plupart des scénarios utilisent des émissions négatives pour limiter le changement climatique à 2°, et donc respecter l'Accord de Paris. A l'aide d'une version développée de OSCAR v2.2, nous calculons ce qu'impliquent ces techniques d'absorption de CO_2 pour le système Terre. Nous identifions les réversibilités des différentes parties du système terre, et évaluons le potentiel de refroidissement de ces techniques. Nous montrons aussi que la reforestation pourrait être moins apte à atténuer le changement climatique, du fait du changement dans l'albedo de surface. Par ailleurs, le potentiel des techniques d'alcalinisation des eaux de surfaces pour atténuer le changement climatique pourrait être inférieur à celui initialement estimé.
Dans l'ensemble, cette thèse identifie des défauts dans le développement actuel des scénarios. Certains ne constituent pas un problème pour les projections climatiques, comme les incertitudes dans le calcul des émissions. D'autres nécessitent une attention particulière, comme le calcul des émissions CO_2 dues au LUC par les IAMs ou l'éventuelle surestimation des capacités des techniques de CDR. Ce travail renforce l'urgence du besoin d'atténuation du changement climatique, et appelle à une meilleure cohérence interne dans les sciences du climat.

Title : Revisiting emissions and climate scenarios with a compact Earth system model

Keywords : climate, emissions, scenarios, modelling

Abstract : This thesis puts into perspective different elements of socio-economic scenarios from a climate change modelling point of view. These elements contribute at improving the comprehension of the current state of climate sciences. In the meantime, these elements demonstrate the potential of the recent reduced-form Earth System Model OSCAR v2.2.
The first element concerns the uncertainty of emissions. Although emission inventories are uncertain, we ignore what impact on climate change have these uncertainties. We quantify this impact for fossil-fuel emissions, the major contributor to climate change. We show that the uncertainties in emissions are expected to increase with the use of non-conventional fuels, but that they do not increase significantly the uncertainty from Earth system modelling in variables, such as the increase in global surface temperature.
The second element is a climate assessment of the recent Shared Socio-economic Pathways scenarios. We identify gaps in the SSP database, and we complete it to calculate the climate projections under these scenarios. Our conclusions suggest inconsistencies in CO_2 emissions from land-use change calculated by the integrated assessment models and in the associated land variables. We identify trade-offs between greenhouse gases in the mitigation of climate change. Using a robust assessment, new carbon budgets are proposed. The uncertainties in increases in global surface temperature are discussed.
The third element concerns the negative emissions. Most climate scenarios use negative emissions to limit global warming well below 2°C, thus respecting the Paris Agreement. Using a developed version of OSCAR v2.2, we calculate what imply these technologies for the Earth system. We identify the reversibility in the different components of the Earth system and calculate the cooling potential of carbon dioxide removal technologies. We also show that the potential of afforestation/reforestation techniques may be impeded by the change in albedo, and that the potential of oceanic enhanced weathering may be lower than expected.
Overall, this thesis identifies gaps in the current development of scenarios. Some do not hinder current conclusions regarding climate change, such as the uncertainties in emission inventories. Others call for further analysis, such as the inconsistencies in the use of CO_2 emissions from LUC or the eventual overestimation of the potential of some CDR technologies. It emphasizes the need for an urgent mitigation of climate change, and calls for a better internal consistency in climate sciences.

Université Paris-Saclay
Espace Technologique / Immeuble Discovery
Route de l'Orme aux Merisiers RD 128 / 91190 Saint-Aubin, France